# POLYMERISATION CATALYSTS TO MAKE POLYESTERS AND COPOLYMERS

Nattawut Yuntawattana




Trinity College

Department of Inorganic Chemistry

University of Oxford

July 2020

A thesis submitted in partial fulfilment of the requirements for the degree of Doctor of Philosophy in Chemistry

*For my parents,*

*'Until we meet again'*

**Declaration**

The work presented in this thesis was conducted between October 2016 and March 2020 at the University of Oxford. This is the work of the author unless otherwise stated.

The copyright of this thesis rests with the author and is made available under a Creative Commons Attribution Non-Commercial No Derivatives licence. Researchers are free to copy, distribute or transmit the thesis on the condition that they attribute it, that they do not use it for commercial purposes and that they do not alter, transform or build upon it. For any reuse or distribution, researchers must make clear to others the licence terms of this work.



Nattawut Yuntawattana
30 July 2020

**Abstract**

The world needs more sustainable polymers and although there are some promising front-runners, the range of degradable and renewably sourced plastics remains narrow. One issue to address is to improve the efficiency of production of aliphatic polyesters and to expand the range and properties of easily accessible degradable materials. This thesis describes new In(III), Sn(II), Ti(IV), and Zr(IV) polymerisation catalysts used to make aliphatic polyesters and copolymers. The overall objective is to develop efficient catalysis to improve upon the structures, scope and range of degradable polyesters. This is achieved by stereoselective lactide ring-opening polymerisation, by epoxide/anhydride ring-opening copolymerisation and by switch catalysis using mixtures of lactide/lactone, epoxide and anhydride.

Chapter 3 presents a series of phosphasalen In(III) complexes, with different diamine linkers and phosphorous substituents, which are highly active and iso-selective in the ring-opening polymerisation of racemic lactide. The highest performing catalyst produces isotactic polylactide (up to 92 %), *via* a chain-end control mechanism. Additionally, the complexes polymerise a range of other lactones with the activity depending strongly on both the catalyst and lactone structures.

Chapter 4 describes a series of phosphasalen Ti(IV) and Zr(IV) complexes which are active and, in some cases, highly selective for epoxide and anhydride ring-opening copolymerisations without any co-catalyst. Phosphasalen complexes show superior activity and selectivity over their salen and salalen analogues, highlighting the importance of the iminophosphorane backbone. A polymerisation mechanism is proposed, based on kinetic experiments and the polymerisation propagating intermediate isolation.

Chapter 5 describes the first report of an industrially relevant catalyst, $Sn(OMe)_2$, for both epoxide/anhydride ring-opening copolymerisation and 'Switch' catalysis using lactone, epoxide and anhydride mixtures. The switch catalysis yields new polyester-ethers with

microstructures including block-, tapered-, and gradient-copolymers. Selected copolymers are efficient toughening additives, at just 2 wt. % loading, for polylactide increasing toughness values by 400 %.

**Acknowledgements**

First and foremost, I would like to express my deep gratitude and sincere thanks to my supervisor, Professor Charlotte Williams, for the opportunity to let me work independently in her excellent research team, as well as for her help and guidance throughout my 3.5 years of PhD study. I have always been inspired and encouraged every time I talk to her and never fail to be impressed by her gifts in the field of chemistry.

I am very fortunate to have worked with an incredibly gifted postdoc team over the years. Giulia, Frank, Patrick, Georgina, Andres, Ryan, Duncan, Andy, Chris, Seb, and Caroline, I am indebted for your help and guidance over my time in the group. My special thanks goes to Leti for her help, kindness and very secret recipe “berenjenas con pisto”. I am sure you know that my life here would not be that easy without your help carrying 20 kg rice packages to my flat in the past two years. I would also like to thank Sumesh for lunches and tea breaks over my past three years with you.

I would also like to thank the Williams team members, past and present: Arnaud, Gemma, Greg, Ni, Said, Tim, Gloria, Tom, Alice, Arron, Lisa, Natalia, Wouter, Joost, Wilf, Jamie, Claire, Dan, Nathan, Seb, and, Emma. It is my pleasure to work with you all.

The research facilities team at the Department of Chemistry, University of Oxford have provided valuable assistance during my time at Oxford. Thank you to Dr. Nick Rees, Dr. Nader Amin, and Tina Jackson for their help with all NMR analyses and Dr. Kirsten Christensen for the X-ray diffraction analyses.

I would not have a chance to pursue my PhD study here in Oxford without the financial support from the Development and Promotion of Science and Technology Talents Project (DPST scholarship), under the Royal Thai government. I am sincerely thankful to them for almost a decade of support.

This thesis would have never been finished without proofreading from my friend, Dr. Thomas Samuels. I am very grateful for your patience with me and the excellent job you did proofreading my thesis. Thank you to all my friends, here in the UK and in Thailand for their support and encouragement. I am very lucky to have all of you in my life.

I am also sincerely grateful to my former supervisor, Ajarn Pimpa Hormnirun for her help and support. I must say that my leading research skills come from your excellent training. Also, thank you to her research team at the Department of Chemistry, Kasetsart University for their help and support.

Paul, I do not know how to thank you enough for your kindness and understanding throughout the whole process of my thesis writing. This thesis would have not been finished without your encouragement and support, I am very grateful for that. I also am very impressed by your patience at listening to me complaining about my writing. I do know that you do not like to talk over the phone, but you still keep putting up with it over the past few months. A huge thank you for your efforts.

My special thanks goes to my siblings, Ping and Pang and my cousin, J'Nooch and the rest of my family. I would not be able to overcome all the tough challenges which had been set during my study without their endless support. Thank you everyone for being there for me.

I would also like to thank my aunty Nong and her family for everything they have done for me since the first day I arrived here in the UK.

Last but certainly not least, I would like to thank my parents for their tireless support and unconditional love. I do not know whether you would both be able to see all these messages, but I would like to say that I am always very proud to be your child. Papa and Mama, you are always and forever my inspiration, motivation, and role models. I would not have got this far without your endless encouragement. Thank you for teaching me and shaping who I am today. This whole thesis is for both of you.

**Abbreviations**

| | |
|---|---|
| AGE | Allyl glycidyl ether |
| $^{t}$BGE | *tert*-Butyl glycidyl ether |
| *β*-BL | *β*-Butyrolactone |
| BnGE | Benzyl glycidyl ether |
| BO | Butylene oxide |
| $^{n}$Bu | *n*-Butyl |
| $^{t}$Bu | *tert*-Butyl |
| $^{t}$BuO | *tert*-Butoxide |
| °C | Degree Celsius |
| Cat. | Catalyst |
| CEC | Chain-end control |
| CHA | 1,2-Cyclohexanedicarboxylic anhydride |
| CHD | 1,2-Cyclohexanediol |
| CHE | 1,2,3,6-Tetrahydrophthalic anhydride |
| CHDO | 1,4-Cyclohexadiene oxide |
| CHO | Cyclohexene oxide |
| vCHO | 2-Vinylcyclohexene oxide |
| CPA | 1,2-cyclopentanedicarboxylic anhydride |
| *ε*-CL | *ε*-Caprolactone |
| $CO_2$ | Carbon dioxide |
| Conv. | Conversion |
| COSY | Correlated spectroscopy |
| CPO | Cyclopentene oxide |
| 1D | One-dimensional |

| | |
|---|---|
| 2D | Two-dimensional |
| 3D | Three-dimensional |
| *Đ* | Dispersities |
| *D* | Diffusion coefficient |
| *d* | Interplanar distance |
| d | Day |
| Da | Dalton |
| DABCO | 1,4-Diazabicyclo[2.2.2]octane |
| DCM | Dichloromethane |
| DGA | Diglycolic anhydride |
| *ε*-DL | *ε*-Decalactone |
| DMSO | Dimethyl sufoxide |
| DOSY | Diffusion-ordered spectroscopy |
| DSC | Differential scanning calorimetry |
| ECH | Epichlorohydrin |
| EDG | Electron donating group |
| EO | Ethylene oxide |
| EPO | 2,3-Epoxypropyl benzene |
| Equiv. | Equivalent |
| ESC | Enantiomorphic-site control |
| Et | Ethyl |
| EtO | Ethoxide |
| $Et_2O$ | Diethyl ether |
| EWG | Electron withdrawing group |
| FGE | Furfuryl glycidyl ether |

| | |
|---|---|
| g | Gram |
| GA | Glycolic anhydride |
| h | Hour |
| $\Delta H_c$ | Crystallisation enthalpy |
| $\Delta H_m$ | Melting enthalpy |
| $\delta$-HL | $\delta$-Hexalactone |
| HMBC | Heteonuclear multiple-bond coherence |
| HSQC | Heteronuclear single quantum coherence |
| K | Kelvin |
| $K_M$ | Michaelis-Menten constant |
| $k_B$ | Boltzmann constant |
| $k_{obs}$ | Observed rate constant |
| $k_p$ | Propagation rate constant |
| kg | Kilogram |
| LA | Lactide |
| LHS | Left-hand side |
| LO | Limonene oxide |
| MA | Maleic anhydride |
| M | Mol $dm^{-3}$ |
| Me | Methyl |
| min | Minute |
| MJ | Megajoule |
| mol | Mol |
| MPa | Megapascal |
| $M_n$ | Number average molecular weight |

| | |
|---|---|
| MW | Molecular weight |
| $\eta$ | Solvent viscosity |
| $N_2$ | Nitrogen |
| NBA | cis-5-Norbornene-endo-2,3-dicarboxylic anhydride |
| NMR | Nuclear magnetic resonance |
| $P_i$ | Probability of isotactic enchainment between two monomer units |
| $P_s$ | Probability of syndiotactic enchainment between two monomer units |
| PA | Phthalic anhydride |
| PBL | Polybutyrolactone |
| PCL | Polycaprolactone |
| PCP | Poly(cyclohexane phthalate) |
| PDL | Polydecalactone |
| PDLA | Poly-*D*-lactide |
| PE | Polyester |
| PEE | Poly(ester-*co*-ether) |
| PGE | Phenyl glycidyl ether |
| Ph | Phenyl |
| PHL | Polyhexalactone |
| PLA | Polylactide |
| PLLA | Poly-*L*-lactide |
| PO | Propylene oxide |
| ppm | Part per million |
| PPO | Polypropylene oxide |
| $^{i}$PrO | *iso*-Propoxide |
| PS | Polystyrene |

| | |
|---|---|
| $r$ | Solvodynamic radius |
| *rac* | Racemic |
| RHS | Right-hand side |
| ROCOP | Ring-opening copolymerisation |
| ROESY | Rotating frame nuclear overhauser effect spectroscopy |
| ROP | Ring-opening polymerisation |
| s | Second |
| SA | Succinic anhydride |
| SCXRD | Single crystal X-ray diffraction |
| SEC | Size exclusion chromatography |
| SO | Styrene oxide |
| sin | Sine |
| $\tau$ | Tau |
| T | Temperature |
| $T_c$ | Crystallisation temperature |
| $T_d$ | Degradation temperature |
| $T_{d5}$ | Degradation temperature at 5 % weight loss |
| $T_g$ | Glass transition temperature |
| $T_m$ | Melting temperature |
| TGA | Thermogravimetric analysis |
| THF | Tetrahydrofuran |
| TOCSY | Total correlation spectroscopy |
| $\chi_c$ | Percent crystallinity |

**List of Figures, Schemes, and Tables**

**Chapter 1: Introduction**


Figure 1.1. Global plastic production between 1950 and 2018 (LHS) and amount of plastic waste generation (red) and recycling (black) from1950 to 2015 and their projections (dashed lines) (RHS).

Figure 1.2. The life cycle of polylactide.

Figure 1.3. Schiff base aluminium complexes (**1**–**5**).

Figure 1.4. Structures of bis(pyrrolidine) Schiff base (**6a**–**6f**) and salan (**7a** and **7b**) aluminium complexes.

Figure 1.5. Structures of indium (**8a**–**8c** and **9**) and gallium (**10a**–**10d**) complexes.

Figure 1.6. Structures of thiolene (**11a**–**11e**) and bispyridine monophenolate (**12a**–**12d**) iron complexes.

Figure 1.7. Structures of crown ether K(I) (**13a**–**13c**) and salen Na(I) (**14a**–**14d**) complexes.

Figure 1.8. Structures of iminophosphorane group II (**15a**–**15c**) and benzoxazolyl aminophenolate Mg(II) (**16a** and **16b**) complexes.

Figure 1.9. Structures of zinc complexes bearing benzoxazolyl aminophenolate (**17**), benzylimidazolyl aminophenolate (**18a**–**18f**), and scorpionate (**19**) ligands.

Figure 1.10. Structures of hafnium salan complex (**20**) and zirconium and halfnium salalen complexes (**21a**–**21d**).

Figure 1.11. Structures of Y(III) (**22**) and Lu(III) (**23**) phosphasalen complexes and Y(III) bisphenolate complex (**24**).

Figure 1.12. Structures of N-methylated proline (**25a** and **25b**), Takemoto's (**26**), and [2]rotaxane (**27**) organo catalysts.

Figure 1.13. Structures of selected In(III), Zn(II), and Y(III) complexes exhibiting high activity and iso-selectivity for *rac*-LA polymerisations.

Figure 1.14. Structures of epoxides and anhydrides presented in this thesis.

Figure 1.15. Structures of M(III) porphyrin complexes (**28**–**30**).

Figure 1.16. Structures of corrole (**31a**–**31d**) and Zn(II) *β*-diiminate (**32a**–**32e**) complexes.

Figure 1.17. Structures of Al(III) and Co(III) salen complexes (**33a**–**33d**).

Figure 1.18. Structures of M(III) salen complexes (**34**–**36**).

Figure 1.19. Structures of Al(III) (**37a**–**37d**) and Cr(III) (**38a**–**38h**) salen complexes.

Figures 1.20. Structures of bifunctional M(III) and M(II) salen complexes.

Figure 1.21. Structures of Cr(III) Schiff base complexes (**42** and **43**).

Figure 1.22**.** Structures of homodinuclear and heterodinuclear Zn(II) and Mg(II) complexes.

Figure 1.23. Structures of mononuclear and dinuclear cationic Co(III) salen complexes.

Figure 1.24. Structures of mononuclear (**48**) and dinuclear (**49**) Cr(III) salen complexes.

Figure 1.25. Structures of mononuclear (**50**) and dinuclear (**51**) Al(III) scorpionate complexes.

Figure 1.26. Structures of dinuclear (**52**–**54**) and mononuclear (**55**) Fe(III) amino triphenolate complexes.

Figure 1.27. Structures of organocatalysts and Lewis acid and bases described in this section.

Figure 1.28. Structures of selected metal complexes showing high activity in CHO/PA ROCOP.

Figure 1.29. Structures of selected metal complexes showing high activity for PO/PA ROCOP.

Figure 1.30. Structures of proposed phosphasalen complexes.

Figure 1.31. Proposed structures of In(III) phosphsalen complexes.

Figure 1.32. Proposed phosphasalen and salen group IV complexes.

Figure 1.33. One-pot polymerisation access new copolyesters.

Scheme 1.1. Lactone ROP and epoxide/anhydride ROCOP for the production of polyesters.

Scheme 1.2. Proposed activated monomer mechanism (LHS) and coordination-insertion mechanism (RHS).

Scheme 1.3. Polylactide tacticities arising from stereocontrol polymerisation.

Scheme 1.4. Proposed ROCOP mechanisms: mononuclear, binuclear, and bicomponent mechanisms.

**Chapter 2: Methodology**

Figure 2.1. Stacks of $^{31}P\{^{1}H\}$ NMR spectra showing the formation of **3.1**.

Figure 2.2. Stacks of $^{31}P\{^{1}H\}$ NMR spectra of phosphasalen Ti(IV) and Zr(IV) complexes.

Figure 2.3. $^{1}H$ DOSY NMR spectrum of indium complex **3.5** in THF-$d_8$.

Figure 2.4. Possible geometries of penta- and hexa-coordinate compounds.

Figure 2.5. $^{1}H$ NMR of an aliquot from the CHO/PA ROCOP in $CDCl_3$ at 298 K.

Figure 2.6. $^{1}H$ NMR of isolated poly(PO-*ran*-MA) in $CDCl_3$ at 298 K.

Figure 2.7. Possible polymer microstructures obtained from *rac*-LA (i and s represent I isotactic and syndiotactic enchainments, respectively).

Figure 2.8. $^{1}H\{^{1}H\}$ NMR spectrum of isolated PLA, initiated by **3.5**.

Figure 2.9. $^{1}H$ DOSY NMR spectrum of $\mathbf{P_{LA}1}$ in $CDCl_3$ at 298 K.

Figure 2.10. $^{1}H$ DOSY NMR spectrum of PLLA and $PEE_{MA}$ blend in $CDCl_3$ at 298 K.

Figure 2.11. $^{1}H$-$^{1}H$ TOCSY NMR spectrum of $PEE_{MA}$-*b*-PLLA.

Figure 2.12. The separation mechanism for size-exclusion chromatography.

Figure 2.13. DSC thermogram of isolated PLA, initiated by complex **3.4**.

Figure 2.14. TGA thermogram of PLLA, catalysed by $Sn(OMe)_2$.

Figure 2.15. Tensile plot of PLLA, containing 2 wt. % of **P$_{LA}$1**.

Table 2.1. List of $^1$H NMR chemical shifts of monomers and polymers produced by ROP.

Table 2.2. List of $^1$H NMR chemical shifts of monomers and polymers prepared by ROCOP.

Table 2.3. List of $^1$H NMR chemical shifts of selected polyesters and polyethers.

**Chapter 3: Phosphasalen Indium Complexes Showing High Activity and Selectivity for *rac*-Lactide and Lactone Polymerisations**

Figure 3.1. Previously reported iso-selective phosphasalen Y(III), Lu(III), and In(III) catalysts.

Figure 3.2. Structures of diamine linkers used in the formation of phosphasalen ligands.

Figure 3.3. Structures of phosphine intermediates featuring different level of steric hindrance.

Figure 3.4. Stacks of the $^{31}$P{$^1$H} NMR spectra acquired during each stage of the formation of complex **3.3**.

Figure 3.5. Representation of molecular structures of a) complex **3.2**, and b) complex **3.3**.

Figure 3.6. Representation of the molecular structures of a) complex **3.4**, and b) complex **3.5**.

Figure 3.7. The $^{31}$P{$^1$H} NMR spectrum of complex **3.5** in THF-$d_8$.

Figure 3.8. The $^1$H NMR spectrum of complex **3.5** in THF-$d_8$.

Figure 3.9. The $^1$H DOSY NMR spectrum of complex **3.5** in THF-$d_8$.

Figure 3.10. Selected regions of the $^{1}$H ROESY NMR spectrum of complex **3.4** in THF-$d_8$.

Figure 3.11. Semi-logarithmic plots of $[LA]_0/[LA]_t$ against time for a) complexes **3.1**–**3.3** and b) complexes **3.4** and **3.5**.

Figure 3.12. a) Semi-logarithmic plots of $[LA]_0/[LA]_t$ against time at different concentrations of complex **3.5** and b) Linear plots of $k_{obs}$ against [In].

Figure 3.13. a) Plots of $M_n$ (●), theoretical $M_n$ (…) and $Đ$ (♦) against percentage conversion and b) overlay of SEC traces for the polymerisation of *rac*-lactide initiated by complex **3.5**.

Figure 3.14. DSC thermogram of PLA, prepared by catalyst **3.4** at 278 K (PLA3).

Figure 3.15. a) $^{1}$H{$^{1}$H} NMR spectrum of PLA, prepared by complex **3.4** (condition: [In]:[LA] = 1:500, [LA] =1 M, 298 K) and b) Semi logarithmic plot of $[LA]_0/[LA]_t$ against time of *R*,*R*-, *S*,*S*- and *rac*-LA ROP using complex **3.4**.

Figure 3.16. Molecular structure of the propagation intermediate **3.4′**.

Figure 3.17. Stacked $^{1}$H NMR spectra of complex **3.4** and the propagating intermediate **3.4′**.

Figure 3.18. Complex modification to access high catalytic activity and stereoselectivity.

Figure 3.19. Switch catalysis using epoxide, $CO_2$ and lactone.

Scheme 3.1. Synthetic routes used to make phosphasalen ligands. Reagents and conditions: i) $^{n}$BuLi (2.1 equiv.), $Et_2O$, –78 °C, 1 h; ii) $Ph_2PCl$ or ($^{t}$Bu)PhCl (1 equiv.), $Et_2O$, –78 °C, 18 h; iii) $Br_2$ (1 equiv.), DCM, –78 °C, 2 h; iv) $^{n}Bu_3N$ (0.5 equiv.), v) diamine backbone (0.5 equiv.) DCM, –78 °C, 18 h.

Scheme 3.2. Structures of phosphasalen ligands $^{P\text{-}salen}\mathbf{L^1H_2}$–$^{P\text{-}salen}\mathbf{L^4H_2}$.

Scheme 3.3. Structures of phosphasalen indium complexes **3.1**–**3.5**.

Scheme 3.4. Proposed mechanism for the formation of intermediate **3.4′**.

Table 3.1. Selected bond lengths (Å) and angles (º) of complexes **3.2**–**3.5**.

Table 3.2. *rac*-lactide polymerisation data initiated by **3.1**–**3.5**.

Table 3.3. PLA block length of resultant PLA prepared by complexes **3.4** and **3.5**.

Table 3.4. DSC analysis data of PLA, prepared by complexes **3.4** and **3.5**.

Table 3.5. Lactone polymerisation data initiated by **3.1**–**3.3** and **3.5**.

**Chapter 4: N,N,O,O-Tetradentate Group IV Catalysts for Various Epoxide/Anhydride Ring-Opening Copolymerisations and Ethylene Polymerisations**

Figure 4.1. Structures of salen and phosphasalen ligands: $^{salen}\mathbf{L^1H_2}$–$^{salen}\mathbf{L^3H_2}$ and $^{P\text{-}salen}\mathbf{L^5H_2}$, respectively and their isolated yields in brackets.

Figure 4.2. Structures of the Ti(IV) and Zr(IV) complexes, **4.1**–**4.7,** and their isolated yields in brackets.

Figure 4.3. Representative molecular structures of phosphasalen Ti(IV) complexes **4.1**–**4.3** and Zr(IV) complex **4.7**.

Figure 4.4. Representative molecular structures of salen and salalen complexes **4.4**–**4.6**.

Figure 4.5. Kinetic plots of CHO/PA ROCOP for complexes **4.1** (●), **4.4** (■), and **4.5** (▲) obtained using *in situ* IR spectroscopy.

Figure 4.6. DSC thermograms of isolated polyesters: a) from table 4.4 and b) from table 4.5, prepared by complex **4.1**.

Figure 4.7. Representative structures of intermediates: a) **4.3′** and b) **4.3′′**.

Figure 4.8. Stacked $^{1}$H NMR spectra for the formation of the cationic complex **4.3**$^{+}$.

Figure 4.9. Stacked $^{31}$P{$^{1}$H} NMR spectra for the formation of the cationic complex **4.3**$^{+}$.

Figure 4.10. Stacked $^{1}$H NMR spectra of the cationic compound **4.3**$^{+}$ following formation.

Figure 4.11. Stacked $^{31}$P{$^{1}$H} NMR spectra of the cationic compound **4.3**$^{+}$ following formation.

Figure 4.12. a) Bar chart comparing catalyst activity and productivity of complexes **4.1**–**4.7** and b) DSC thermograms of isolated polyethylenes.

Scheme 4.1. Proposed mononuclear mechanism for the ROCOP of CHO and $CO_2$ using phosphasalen In(III) catalyst.

Scheme 4.2. Proposed ROCOP mechanism of epoxide and cyclic anhydride by phosphasalen Ti(IV) complexes.

Scheme 4.3. Preparation of the cationic compound of phosphasalen Ti(IV) complex **4.3**.

Scheme 4.4. Proposed structures of phosphasalen and salen Ti(IV) complexes with various functional groups.

Scheme 4.5. 'Switch' catalysis using salen Ti complexes.

Table 4.1. Selected bond lengths (Å) and angles (º) of phosphasalen Ti(IV) complexes **4.1**–**4.3** and Zr(IV) complex **4.7**.

Table 4.2. List of selected bond lengths (Å) and angles (°) for complexes **4.4**–**4.6.**

Table 4.3. ROCOP of CHO with PA data of complexes **4.1**–**4.7**.

Table 4.4. ROCOP of PA with various epoxides results using **4.1**.

Table 4.5. ROCOP of CHO with various cyclic anhydrides data using **4.1**.

Table 4.6. List of selected bond lengths (Å) and angles (°) for propagating **4.3′′**.

Table 4.7. Ethylene polymerisation data of complexes **4.1–4.7**.

**Chapter 5: An Industrially Relevant Sn(II) Catalyst for the Production of High Performance Polyester-co-Ether**

Figure 5.1. DSC thermograms for a) $PEE_{MA}$, $PEE_{SA}$, and $PEE_{PA}$ and b) PCL and PLLA.

Figure 5.2. $^1$H NMR analysis of the one-pot polymerisation of PO, MA, and *L*-LA.

Figure 5.3. a) Plot of $M_n$ against percent conversion, b) SEC traces of selected aliquots from PO, MA, and *L*-LA one-pot polymerisation, $^1$H DOSY NMR spectra of c) $\mathbf{P_{LA}1}$, and d) $PEE_{MA}$ and PLLA blend.

Figure 5.4. *In situ* $^{1}$H NMR analysis of switch catalysis from a PO, MA, and *L*-LA monomer mixture.

Figure 5.5. a) SEC traces of selected aliquots from the formation of $PEE_{MA}$-*b*-PLLA, b) $^{1}$H-$^{1}$H TOCSY NMR spectrum of isolated $PEE_{MA}$-*b*-PLLA, $^{1}$H DOSY NMR spectra of c) $PEE_{MA}$-*b*-PLLA, and d) $PEE_{MA}$ and PLLA blend.

Figure 5.6. Stacks of DSC thermograms of a) $PEE_{MA}$-*b*-PLLA, $PEE_{MA}$-*b*-PDLA and $PEE_{MA}$-*b*-$PLA_{stereocomplex}$ and b) $PEE_{MA}$-*g*-PCL.

Figure 5.7. $^{1}$H NMR analysis of PO, MA, and $\varepsilon$-CL one-pot polymerisation.

Figure 5.8. a) Plot of $M_n$ against percent conversion, b) SEC traces of selected aliquots from the PO, MA, and $\varepsilon$-CL one-pot polymerisation, c) $^{1}$H DOSY NMR spectra of **$P_{CL}$1**, and d) the $PEE_{MA}$ and PCL blend.

Figure 5.9. Dumbbell shaped PLLA samples containing different wt. % of **$P_{LA}$1**: a) 0 wt. % b) 2 wt. %, c) 5 wt. %, d) 10 wt %, and e) 20 wt. %.

Figure 5.10. Mechanical properties of PLLA–**$P_{LA}$1** (0–20 wt. %) blends: a) elongation at break and tensile strength and b) tensile toughness.

Figure 5.11. a) Stacks of DSC thermograms of isolated uncross-linked and cross-linked $PEE_{MA}$-PLLA tapered copolymers and b) stacks of Raman spectra of **$P_{LA}$1**, **$P_{LA}$1**+SH, and **$P_{LA}$4**.

Figure 5.12. Mechanical properties of PLLA – different additives (2 wt. %) blends: a) elongation at break and tensile strength and b) tensile toughness.

Figure 5.13. Mechanical properties of high molar mass PLLA – different additives (2 wt. %) blends: a) elongation at break and tensile strength and b) tensile toughness.

Figure 5.14. Examples of potential cyclic anhydride and epoxide monomers.

Scheme 5.1. Generally proposed switch catalysis mechanism.

Scheme 5.2. Schematic diagram showing the ROP of lactones (LHS) and the ROCOP of propylene oxide and cyclic anhydride (RHS).

Scheme 5.3. One-pot polymerisation of PO, MA, and *L*-LA (RHS) or *ε*-CL (LHS) pathways.

Scheme 5.4. Synthesis of $PEE_{MA}$-*b*-PLA block copolymers and their stereocomplex formation.

Scheme 5.5. One-pot polymerisation of PO, MA, LA and CL to access better additive for PLLA.

Scheme 5.6. Proposed $PEE_{MA}$-*co*-PCL with different architecture depending on CL concentration.

Table 5.1. Polymerisation results from CAs/PO ROCOP.

Table 5.2. Polymerisation data from ROP of lactones.

Table 5.3. One-pot polymerisation data.

Table 5.4. Tensile testing data for PLLA specimens containing different amounts of **$P_{LA}$1**.

Table 5.5. Tensile testing data for PLLA, containing 2 wt. % of different additives.

Table 5.6. Tensile testing data for high molar mass PLLA, containing 2 wt. % of different additives.

**Chapter 6: Conclusion, Challenges, and Future Work**

Figure 6.1. Structures of proposed phosphasalen complexes.

Figure 6.2. Proposed phosphasalen yttrium complexes for stereoselective β-BL polymerisations.

Figure 6.3. Structures of titanium(IV) salen or phosphasalen complexes.

Figure 6.4. Switch catalyses for the synthesis of copolymers with various architectures.

**Table of Contents**

Declaration iii
Abstract iv
Acknowledgements vi
Abbreviations viii
List of Figures, Schemes, and Tables xiii

**Chapter 1: Introduction**

1.1. Introduction to biodegradable polymers 2
1.2. Aliphatic polyesters 3
1.3. Polylactide (PLA) 5
1.3.1. Synthesis of polylactide 5
1.3.2. Ring-opening polymerisation mechanisms 6
1.3.3. Stereocontrol polymerisation and polylactide microstructure 8
1.3.4. Iso-selective catalysts for *rac*-lactide polymerisations 10
1.3.4.1. Group 13 complexes 11
1.3.4.2. Iron(III) complexes 15
1.3.4.3. Group 1 complexes 16
1.3.4.4. Group 2 complexes 17
1.3.4.5. Zn(II) complexes 18
1.3.4.6. Group 4 complexes 19
1.3.4.7. Lanthanide(III) complexes 19
1.3.4.8. Organo-catalysts 21
1.3.4.9. Evaluation of highly active and iso-selective catalysts 22
1.4. Ring-opening copolymerisation of epoxide and cyclic anhydride 23
1.4.1. Polymerisation mechanisms 23
1.4.2. Polymerisation catalysts 25
1.4.2.1. Porphyrin, corrole and *β*-diiminate complexes 26
1.4.2.2. Salen and salen-like complexes 29
1.4.2.3. Dinuclear complexes 36
1.4.2.4. Organocatalysts 41
1.4.2.5. Evaluation of highly active catalysts for epoxide/anhydride ROCOP 44
1.5. Aims and objectives 46
1.6. References 50

**Chapter 2: Methodology**

2.1. General analytical techniques for ligand and complex synthesis 61
2.1.1. Nuclear Magnetic Resonance (NMR) spectroscopy 61
2.1.1.1. $^{31}P\{^{1}H\}$ NMR spectroscopy 61
2.1.1.2. $^{1}H$ Diffusion Ordered Spectroscopy (DOSY) NMR spectroscopy 63
2.1.2. Single Crystal X-ray Diffraction 65
2.2. Characterisation techniques for polymerisation 67
2.2.1. NMR spectroscopy 67
2.2.1.1. Determination of monomer conversion 67
2.2.1.2. Identification of selectivity in polymer chain 68
2.2.1.3. $^{1}H\{^{1}H\}$ NMR spectroscopy for stereocontrol degree calculation in PLA 70
2.2.1.4. Proof of formation of copolymer 72
2.2.2. Size-Exclusion Chromatography (SEC) 74
2.2.3. Differential Scanning Calorimetry (DSC) 75
2.2.4. Thermogravimetric Analysis (TGA) 77
2.2.5. Tensile Mechanical Testing 78
2.3. Kinetic Studies 79
2.3.1. LA polymerisation catalysis 79
2.4. References 81

**Chapter 3: Phosphasalen Indium Complexes Showing High Activity and Selectivity for *rac*-Lactide and Lactone Polymerisations**

3.1. Introduction 84
3.2. Design, synthesis, and characterisation of ligands 88
3.3. Synthesis and characterisation of phosphasalen indium complexes **3.1**–**3.5** 92
3.3.1. Synthesis of complexes **3.1**–**3.5** 92
3.3.2. Solid state characterisation for **3.1**–**3.5** 93
3.3.3. Solution state characterisation for **3.1**–**3.5** 96
3.4. *rac*-LA ring-opening polymerisation studies 100
3.4.1. Catalytic activity 101
3.4.2. Polymerisation control 104
3.4.3. Catalyst stereocontrol 105
3.4.4. PLA thermal properties 107
3.4.5. Stereocontrol mechanism 109

3.5. Ring-opening polymerisation of other lactones 112
3.6. Conclusion and Outlook 115
3.6.1. Conclusion 115
3.6.2. Outlook 116
3.7. References 118

**Chapter 4: N,N,O,O-Tetradentate Group IV Catalysts for Various Epoxide/Anhydride Ring-Opening Copolymerisations and Ethylene Polymerisations**
4.1. Introduction 123
4.2. Synthesis and characterisation of phosphasalen and salen ligands 126
4.3. Synthesis and characterisation of Ti(IV) and Zr(IV) complexes (**4.1**–**4.7**) 127
4.3.1. Synthesis of Ti(IV) and Zr(IV) complexes (**4.1**–**4.7**) 127
4.3.2. Solution state characterisation of Ti(IV) and Zr(IV) complexes (**4.1**–**4.7**) 128
4.3.3. Solid state characterisation of Ti(IV) and Zr(IV) complexes (**4.1**–**4.7**) 131
4.4. Polymerisation studies 136
4.4.1. Preliminary polymerisation studies of **4.1**–**4.7** in ROCOP of CHO and PA 136
4.4.1.1. Catalytic activity 138
4.4.1.2. Catalyst selectivity 141
4.4.1.3. Polymer molar mass and molar mass distribution 142
4.4.2. Monomer scoping using phosphasalen Ti(IV) complex **4.1** 143
4.4.2.1. Scope of epoxide substrate 143
4.4.2.2. Scope of cyclic anhydride substrate 145
4.5. Understanding the ROCOP mechanism 147
4.5.1. Phosphasalen Ti(IV) complex 147
4.5.2. Propagating intermediate isolation 149
4.6. Ethylene polymerisation using complexes **4.1**–**4.7** 151
4.6.1. Preliminary ethylene polymerisation study using Ti(IV) complex **4.3** 152
4.6.2. Formation and stability studies for the cationic complex 153
4.6.3. Ethylene polymerisations using *in situ* generated cationic species 156
4.7. Conclusion and Outlook 158
4.7.1. Conclusion 158
4.7.2. Outlook 159
4.8. References 162

**Chapter 5: An Industrially Relevant Sn(II) Catalyst for the Production of High Performance Polyester-*co*-Ether**

5.1. Introduction 167

5.2. PO/CAs ROCOP and lactone ROP 170

5.2.1. ROCOP of PO and CAs 170

5.2.2. ROP of Lactones 173

5.3. One-pot polymerisation for block-, tapered-, and gradient-copolymer formation 174

5.3.1. PO/MA/*L*-LA one-pot polymerisation 174

5.3.2. PO/MA/$\varepsilon$-CL one-pot polymerisation 181

5.4. Application of **$P_{LA}$1** in toughening PLLA 184

5.4.1. Effect of additive amount 184

5.4.2. Exploring the chemistry of the additive – Cross-linking through alkene groups 187

5.4.3. Effect of PLLA molar mass 190

5.5. Conclusion and Outlook 191

5.5.1. Conclusion 191

5.5.2. Outlook 192

5.6. References 195

**Chapter 6: Conclusion, Challenges, and Future Work**

6.1. Conclusion 199

6.2. Challenges and Future Work 201

6.3. References 207

**Chapter 7: Conclusion, Challenges, and Future Work**

7.1. General procedures 210

7.1.1. Material and methods 210

7.1.2. Measurements 211

7.2. Typical polymerisation procedures for Chapter 3 213

7.2.1. Lactide polymerisation 213

7.2.2. $\varepsilon$-Caprolactone polymerisation. 214

7.2.3. $\beta$-Butyrolactone polymerisation. 214

7.2.4. $\varepsilon$-Decalactone polymerisation. 214

7.2.5. $\delta$-Hexalactone polymerisation. 215

7.2.6. Polymer purification 215

7.2.7. Determination of stereocontrol degree of polymers 215
7.3. Typical polymerisation procedures for Chapter 4 216
7.3.1. Polymerisation procedure for ROCOP of epoxide and cyclic anhydride. 216
7.3.2. Polymerisation procedure for *in situ* IR study. 216
7.3.3. Ethylene polymerisation using sMAO as a co-catalyst procedure. 217
7.3.4. Ethylene polymerisation procedure by cationic complex. 217
7.3.5. Polymer purification 217
7.4. Typical polymerisation procedures for Chapter 5. 218
7.4.1. Polymerisation procedure for ROCOP of PO and cyclic anhydride. 218
7.4.2. Polymerisation procedure for ROP of *L*-LA or *ε*-CL. 218
7.4.3. One-pot polymerisation of PO, MA, and *L*-LA procedure. 219
7.4.4. PO, MA, *L*-LA one-pot polymerisation procedure: *in situ* $^{1}$H NMR study. 219
7.4.5. One-pot polymerisation of PO, MA, and *ε*-CL procedure. 219
7.4.6. Polymer purification 220
7.4.7. Preparation of polymer film for tensile testing. 220
7.5. Typical synthetic procedures for starting materials for ligand synthesis 220
7.5.1. Synthesis of 2-bromo-4,6-di-*tert*-butylphenol 220
7.5.2. Synthesis of 2-(diphenylphosphaneyl)-4,6-di-*tert*-butyl-phenol (**S2**) 221
7.5.3. Synthesis of 2-(*tert*-butyl-phenylphosphaneyl)-4,6-di-*tert*-butyl-phenol (**S3**) 222
7.6. Synthesis of phosphasalen, and salen ligands 223
7.6.1. Synthesis of phosphasalen ligand $^{\text{P-salen}}\mathbf{L^1H_2}$ 223
7.6.2. Synthesis of phosphasalen ligand $^{\text{P-salen}}\mathbf{L^2H_2}$ 224
7.6.3. Synthesis of phosphasalen ligand $^{\text{P-salen}}\mathbf{L^3H_2}$ 225
7.6.4. Synthesis of phosphasalen ligand $^{\text{P-salen}}\mathbf{L^4H_2}$ 226
7.6.5. Synthesis of phosphasalen ligand $^{\text{P-salen}}\mathbf{L^5H_2}$ 227
7.6.6. Synthesis of salen ligand $^{\text{salen}}\mathbf{L^1H_2}$ 228
7.6.7. Synthesis of salen ligand $^{\text{salen}}\mathbf{L^2H_2}$ 228
7.6.8. Synthesis of salen ligand $^{\text{salen}}\mathbf{L^3H_2}$ 229
7.7. Synthesis of Indium Complexes 230
7.7.1. Synthesis of indium complex **3.1** 230
7.7.2. Synthesis of indium complex **3.2** 231
7.7.3. Synthesis of indium complex **3.3** 231
7.7.4. Synthesis of indium complex **3.4** 232
7.7.5. Synthesis of indium complex **3.5** 233

7.8. Synthesis of phosphasalen and salen titanium complexes 234
7.8.1. Synthesis of phosphasalen titanium complex **4.1** 234
7.8.2. Synthesis of phosphasalen titanium complex **4.2** 236
7.8.3. Synthesis of phosphasalen titanium complex **4.3** 237
7.8.4. Synthesis of salen titanium complex **4.4** 238
7.8.5. Synthesis of salen titanium complex **4.5** 239
7.8.6. Synthesis of salalen titanium complex **4.6** 240
7.9. Synthesis of phosphasalen zirconium complex 241
7.9.1. Synthesis of phosphasalen zirconium complex **4.7** 241
7.10. References 242

**Appendices**

A1. Chapter 3 244
A1.1. Spectral characterisation for ligands $^{\text{P-salen}}\mathbf{L^1H_2}$–$^{\text{P-salen}}\mathbf{L^4H_2}$ 244
A1.2. Spectral characterisation for indium complexes **3.1**–**3.5** 255
A1.3. Additional crystallographic data for ligand $^{\text{P-salen}}\mathbf{L^4H_2}$ 264
A1.4. Additional crystallographic data for complexes **3.1**–**3.5** and intermediate **3.4′** 266
A1.5. Additional polymerisation data 268
A2. Chapter 4 278
A2.1. Spectral characterisation data for ligand $^{\text{P-salen}}\mathbf{L^5H_2}$ and $^{\text{salen}}\mathbf{L^1H_2}$–$^{\text{salen}}\mathbf{L3H_2}$ 278
A2.2. Additional crystallographic data for complexes **4.1**–**4.7** and intermediate **4.3′′** 294
A2.3. Additional polymerisation data 297
A3. Chapter 5 302
A3.1. Additional polymerisation data 302

# *Chapter 1*

# *Introduction*

*The happiness of your life depends upon the quality of your thoughts...*

*~ Marcus Aurelius ~*

## 1.1. Introduction to biodegradable polymers

Plastics are both cheap and durable. Their cost-effectiveness allows manufacturers to take advantage of these properties to high profitability. Plastic has become a ubiquitous material in the modern world across a range of applications, from packaging materials to electronic goods, automotive parts, and medical devices. However, this durability is also problematic.[1] As the cost of plastic has reduced, its use has exploded. Plastic production worldwide has been drastically increased from 1.5 million metric tons (Mt) in 1950 to over 350 Mt in 2018, with the increasing rate of 1.5 – 3.5 % per annum (Figure 1.1, LHS).[2] Global analysis of plastic production shows that out of the 8,300 Mt of plastic produced between 1950 and 2015, 2,500 Mt is in current use, and only 600 Mt (~ 9 % of the plastic production worldwide) have been recycled (Figure 1.1, RHS).[3] In addition, almost none of the commonly used plastics are biodegradable. As a result, the amount of plastic waste in circulation now harms our environment, in particular the oceans.[1] The development of alternative materials, which have equivalent properties to conventional plastics but with managed end-of-life pathways, is an urgent need.[4]

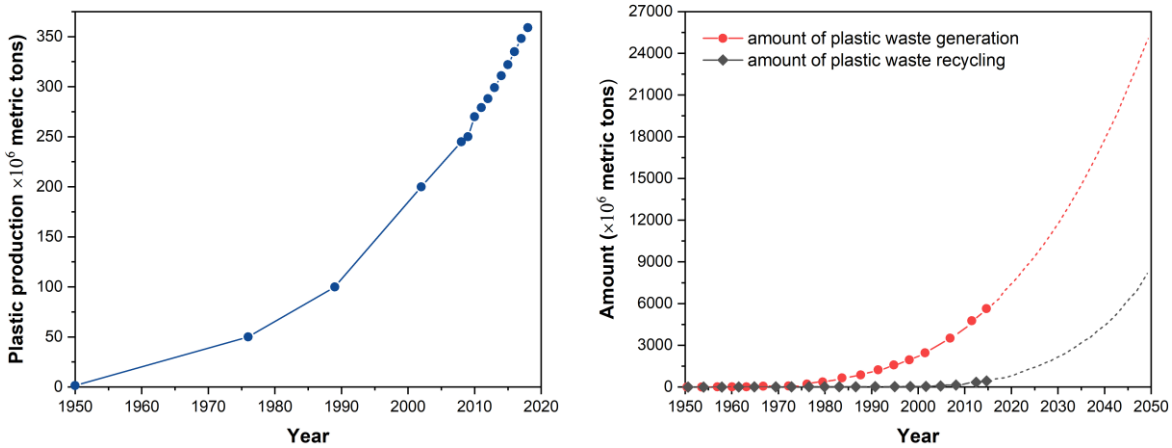


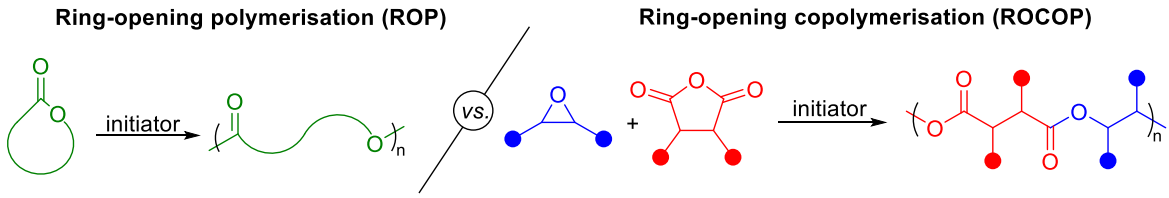

**Figure 1.1.** Global plastic production between 1950 and 2018 (LHS) and amount of plastic waste generation (red) and recycling (black) from1950 to 2015 and their projections (dashed lines) (RHS).[2, 3]

Additionally, the most commonly used plastics are obtained from non-renewable feedstocks (*e.g.* oil, gas). Although only a small proportion of oil (~ 6 % of oil produced globally) is

used in polymer manufactures, the depletion of this feedstock is encouraging the use of bio-renewable resources as alternative substrates.[4] This may improve the sustainability of polymer production.

### 1.2. Aliphatic polyesters

Aliphatic polyesters are polymers which contain ester functionalised monomer repeating units in the polymer skeleton which are susceptible to (bio)degradation after use.[5] Some of them even show similar thermal and mechanical properties to commonly used conventional polymers.[6] In addition, many aliphatic polyesters can be obtained from renewable resources. Some of these polymers are promising candidates to replace conventional polymers.[7]




**Scheme 1.1.** Lactone ROP and epoxide/anhydride ROCOP for the production of polyesters.

Polyesters are traditionally synthesised from the direct condensation of a diol and a di-acid. Although this provides a convenient route to products with a wide variety of properties and exploits a nearly unlimited choice of available diol and di-acid substrates, accessing high molar mass polyester is more difficult and requires high purity monomers, careful stoichiometry balancing and tight control over process conditions.[8] An alternative method, ring-opening polymerisation (ROP) of cyclic esters, allows access to high molar mass polyesters, with narrow molar mass distributions, under low temperature polymerisation conditions and reaches higher molar masses rapidly and controllably (Scheme 1.1).[8] To date, several different types of aliphatic polyestes have been reported in the academic literature using this route.[9, 10] For a cyclic ester to polymerise *via* ROP, the reaction must be both kinetically and thermodynamically favoured.[11] Consequently, some cyclic esters which

possess relatively low ring strain energies (*e.g.* $\gamma$-butyrolactone) are almost thermodynamically impossible to polymerise (unless polymerisation occurs at extremely low temperature and high monomer concentration to drive the monomer-polymer equilibrium toward the polymer formation and/or polymer crystallisation/precipitation is exploited to drive equilibria).[12, 13] The limited commercial availability of some cyclic esters (*e.g.* cyclic esters containing aromatic backbones or unsaturated cyclic esters) and the difficulty of polymerisation of functionalised lactones (due to reduced ring-strain) also limits this method for the production of some polyesters.[14] The sister method, ring-opening copolymerisation (ROCOP) of epoxides and anhydrides, provide access to a wider range of polyesters and there are many commercially available epoxides and anhydrides (Scheme 1.1). As a result, polyesters with a wide variety of properties are obtained using functionalised epoxides and anhydrides – *i.e.* there is no compromise on ring-strain through incorporation of substituents on the monomers, in contrast to lactone ROP.[8, 14] Additionally, some of these substrates are already made and used at scale by polymer manufacturers providing greater confidence in these new products being translated to large-scale production. These factors could also help ensure cost-competitiveness for these polyesters obtained by epoxide/anhydride ROCOP and may allow them to compete with conventional petrochemicals.[15-17]

### 1.3. Polylactide (PLA)

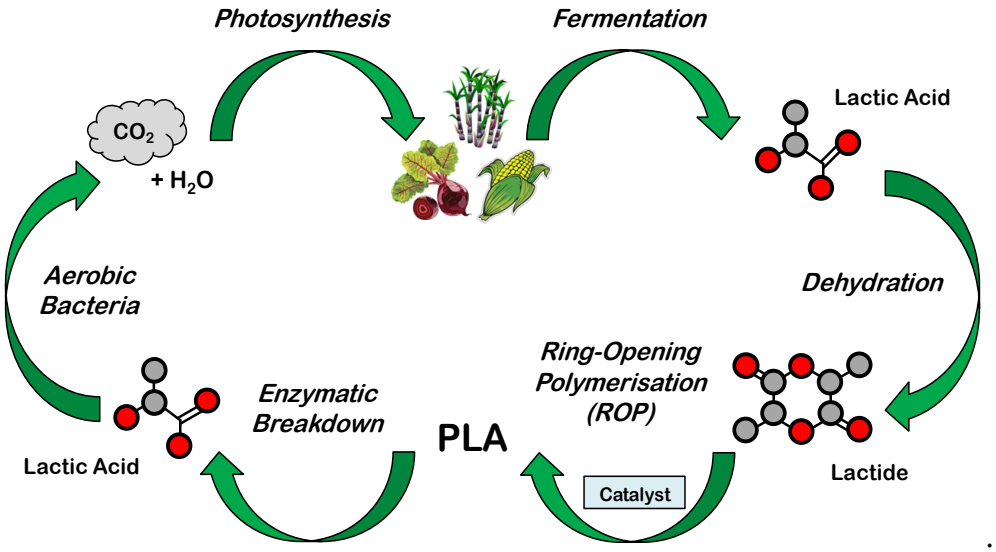



**Figure 1.2.** The life cycle of polylactide.

Polylactide (PLA), an aliphatic polyester, has received considerable attention over the last few decades due to its biodegradability and biocompatibility.[18] PLA is obtained from a bio-renewable resource, lactic acid, which can be produced from either the fermentation of high starch content plants (*e.g.* corn, potato, sugar cane etc.) or by chemical synthesis (Figure 1.2).[19] Additionally, the end-of-life by-products from PLAs are environmentally benign since they slowly hydrolyse to lactic acid which is a metabolite. PLA provides comparable mechanical and thermal properties to a range of commercially available fossil-based polymers such as polypropylene, polyethylene phthalate, and polystyrene. As a result, its use is expanding in a number of applications. (*e.g.* fibres, textiles, packaging containers).[6] In addition, it is also a promising candidate for biomedical uses such as surgical sutures, medical devices, and implants due to its high biocompatibility.[20]

#### 1.3.1. Synthesis of polylactide

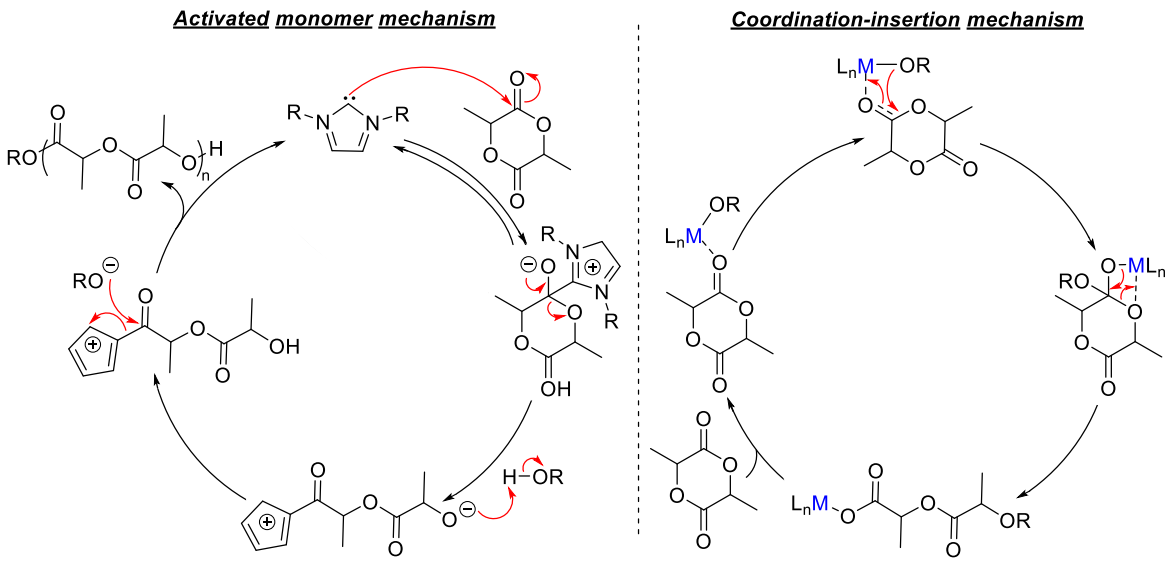
There are two general routes used to prepare PLA from lactic acid. The first route, direct polycondensation, involves the use of high pressure and temperature for the production of

polymer since water by-product needs to be removed from the reaction and drive polymerisation equilibrium toward the formation of PLA. Removal of water by-product at high conversions to prepare high molar mass PLA is the main challenge for this method.[21] However, the obtained oligomer which can be controlled by the use of different catalysts or polymerisation conditions can be further used as intermediates for the synthesis of polyurethane.[21] It should be noted that recently, high molar mass PLA has been successfully achieved by azeotropic polycondensation. In this method, the polymerisation was carried out in azeotropic solvents which allowed for the removal of water by-product more easily than in direct polycondensation. This allowed for the production of high molar mass polymer.[22]

Carothers *et al.* were the first to demonstrate the ring-opening polymerisation as an efficient method to produce high molar mass PLA with narrow dispersities.[23] The first step was the synthesis of low molar mass lactide (LA) oligomer from lactic acid. The oligomer was then depolymerised through internal transesterification to yield LA, a cyclic diester of lactic acid. PLA can be obtained from the ring-opening of LA using catalysts. ROP is generally the preferred method for the synthesis of high molar mass PLA since it provides a better polymerisation control and can be carried out at mild polymerisation conditions.[24] It is widely used in industrial PLA production and has been used by leading PLA companies such as NatureWorks and Total-Corbion.[25]

### 1.3.2. Ring-opening polymerisation mechanisms

Ring-opening polymerisation (ROP) is proposed to occur *via* either activated monomer or coordination-insertion mechanisms, depending on the nature of the initiator. Cationic complexes and organocatalysts are proposed to operate *via* an activated monomer mechanism whilst neutral metal complexes generally operate through a coordination-insertion mechanism (Scheme 1.2).[26, 27]



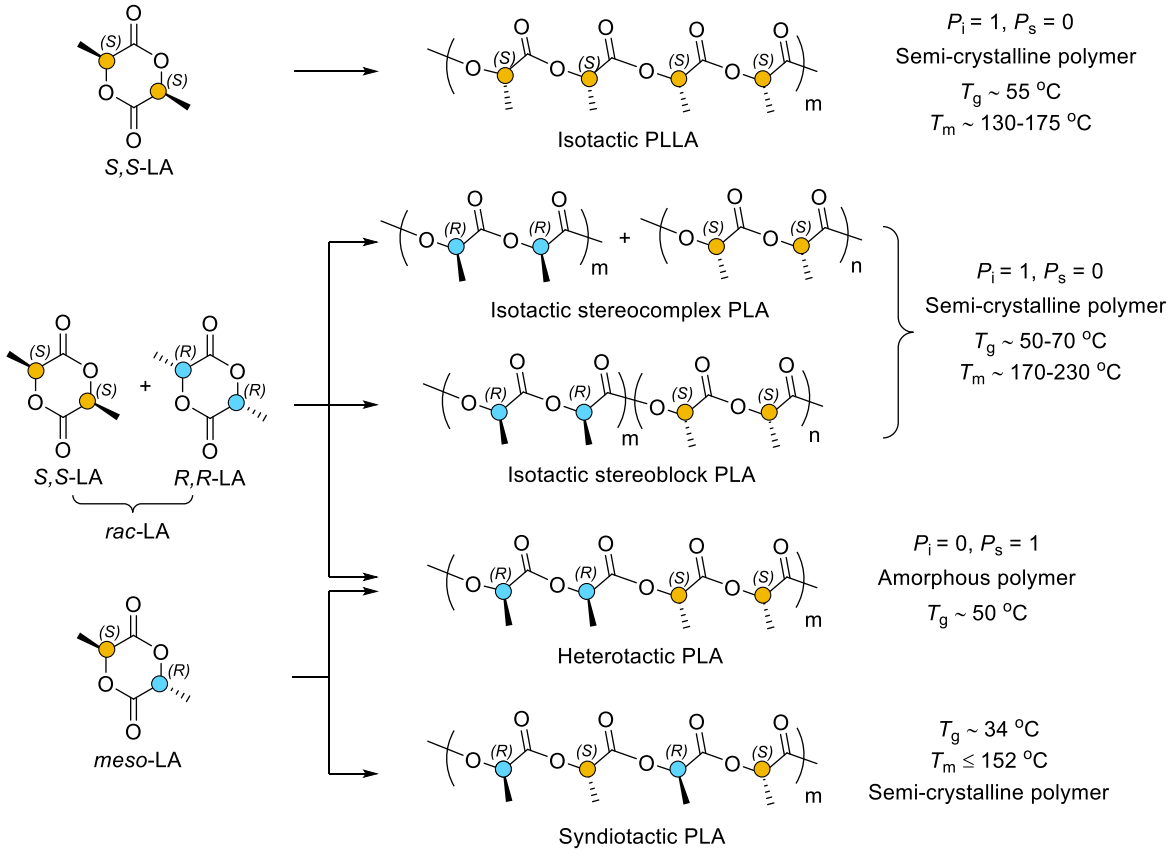

**Scheme 1.2.** Proposed activated monomer mechanism (LHS) and coordination-insertion mechanism (RHS).[28]

For the activated monomer mechanism, LA monomer is first activated *via* attack of the catalyst at the carbonyl carbon. The activation can occur using a variety of substrates, including Brønsted acids,[29] and nucleophiles (*e.g.* N-heterocyclic carbenes).[30] Polymerisation initiation is proposed to occur following the attack of the LA by the exogenous alcohol, leading to ring-opening of LA *via* acyl-oxygen cleavage. The growing polymer chain consists of the α-chain end, possessing an ester functional group, and the secondary alcohol ω-chain end which further serves as a nucleophile for further chain propagation.

Dittrich and Schulz were the first to demonstrate the three step coordination-insertion mechanism for cyclic esters.[31] After that, Kricheldorf and Teyssie showed that $Al(O^iPr)_3$ initiated polymerisations of various lactones also involved such a mechanism.[32, 33] The coordination-insertion mechanism consists of four main steps (Scheme 1.2). LA monomer first coordinates to the Lewis acid metal center, followed by the insertion of the LA monomer into the metal-alkoxide bond *via* a nucleophilic addition reaction. Then, the ring

of LA monomer is opened through acyl-oxygen cleavage and finally, LA monomer is continuously inserted to make PLA.[24, 32, 33]

### 1.3.3. Stereocontrol polymerisation and polylactide microstructure




**Scheme 1.3.** Polylactide tacticities arising from stereocontrol polymerisation.[34-37]

The presence of two stereogenic centres in LA enables the formation of PLA with different polymer microstructures, depending on catalyst selectivity (Scheme 1.3). The different polymer tacticities can be identified from two parameters: $P_i$ and $P_s$ (further details in Chapter 2). Perfectly isotactic PLA exhibits $P_i = 1$ and $P_s = 0$, whereas heterotactic PLA exhibits $P_i = 0$ and $P_s = 1$. Values of $P_i = P_s = 0.5$ are observed for atactic PLA.[38]

By using different LA stereochemistries in the feedstock, it is possible to produce PLA with different tacticities, which significantly influences the thermal and mechanical properties. For example, starting from enantiomeric *L*-LA, polymerisation (without epimerisation) leads

to the formation of isotactic PLLA. Ring-opening polymerisation of *rac*-LA (a mixture of 50:50 of *R,R*-LA and *S,S*-LA) produces PLA with a range of polymer microstructures, including isotactic stereoblock (a block of two different LA stereoisomers, *R,R*-LA and *S,S*-LA, in the same polymer chain), heterotactic (alternating incorporation of *R,R*-LA and *S,S*-LA), and atactic (random configuration of stereocentres) polymers. Syndiotactic and heterotactic PLA can be obtained from the polymerisation of *meso*-LA.

Isotactic PLA provides certain advantages over all the other congeners since it is semi-crystalline allowing access to a polymer melt. This can offer practical advantages, such as the intrinsic resistance towards melt deformation.[39] In addition, isotactic polymer can have a longer shelf life than the atactic form since crystalline regions hydrolyse more slowly than amorphous ones.[40] Isotactic PLLA often exhibits only a moderate melting temperature ($T_m$) ($T_m$ = 130 °C–175 °C). The formation of stereoblock or stereocomplex PLA allows access to polymer with a higher $T_m$ ($T_m$ = 170 °C–230 °C).[21, 39, 41-43] The production of stereocomplex PLA was first demonstrated by Tsuji and co-workers.[44-46] They showed that blending the optically pure poly-*L*-lactide (PLLA) and poly-*D*-lactide (PDLA), prepared separately, in an equal ratio improves polymer melting temperatures. Changes in the powder X-ray diffraction pattern revealed a new crystalline structure, arising from intermolecular co-crystallisation of the two opposite chirality polymer chains, through dipole-dipole van der Waals interactions. It was also proposed that the stereocomplex polymer possesses a helical structure which is consistent with the discovery of De Santis and Kovac, who showed that the optically pure polylactide will adopt a left- or right-handed structure, depending on its chirality.[47] Stereoblock PLA is of interest as it provides a range of property advantages. For example, blending stereoblock PLA into isotactic PLLA increases crystallite nucleation rates and the resulting materials have a higher Young's modulus and tensile strength than

PLLA.[41] Blending it into mixtures of PLLA/PDLA increases stereocomplex crystallisation and increases the high temperature stability of the product.[48, 49]

Although stereocomplex polylactide with a high polymer melting temperature can be obtained from polymer blends, this method requires multiple purifications and is sub-optimal in terms of scale-up and yield. Alternatively, considerable attention has been paid to developing new initiators, especially those active with *rac*-LA and showing iso-selectivity as a means to directly access stereoblock/stereocomplex PLA.

### 1.3.4. Iso-selective catalysts for *rac*-lactide polymerisations

The early development of metal-based catalysts for LA polymerisations related to the use of simple homoleptic metal complexes.[32, 33] Typically, industry relevant Sn(II) bis(2-ethylhexanoate), Zn(II) lactate, or Al($O^iPr$)$_3$ was used.[7, 50] Although these complexes have proved to be convenient for the production of PLA, and many other aliphatic polyesters, their multi-nuclearity limits control and prevents rationale design of better catalysts. Also, these catalysts undergo quite significant transesterification side reactions which results in broad molar mass distributions. The chance for stereocontrolled polymerisation using these species is also limited. The development of heteroleptic complexes, coordinated by ancillary ligands, allows for structural control, better polymerisation activities and for stereoselectivities.[24]

This section describes the early discovery of iso-selective catalysts for *rac*-LA polymerisations. Examples of some of these catalysts are presented. To date many highly iso-selective catalysts have been reported, including metal-based and organo- catalysts. In the case of metal complexes, a wide range of metal centres including Al(III), Ga(III), In(III), Y(III), Lu(III), Zn(II), Mg(II), Fe(II), K(I), Na(I), Ca(II), etc. and many types of ligand scaffolds were explored. This section aims to summarise some of the highly iso-selective

catalysts reported in recent years. The degree of iso-selectivity of each catalyst described in this section can be categorised into three main groups, depending on the $P_i$ value. Iso-selective catalysts exhibit $P_i$ = 70 % – 79 %, good iso-selectivity catalysts show $P_i$ = 80 % – 89 % and highly iso-selective catalysts possesses $P_i \geq 90$ %.

### 1.3.4.1. Group 13 complexes

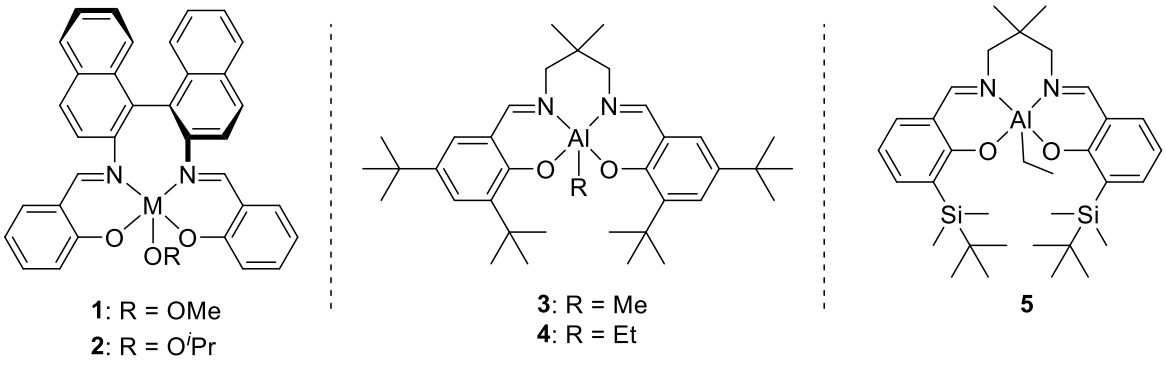



**Figure 1.3.** Schiff base aluminium complexes (**1**–**5**).[51-55]

In 1996, Spassky and co-workers reported a chiral aluminium Schiff base catalyst (**1**, Figure 1.3) and showed for the first time that this catalyst produced gradient stereoblocks between PDLA and PLLA chains from *rac*-LA in toluene at 70 °C.[51] The resultant PLA showed molar mass closed to the theoretical values and narrow dispersity (*Đ*) (*Đ* ≤ 1.15). In addition, it has an elevated melting temperature ($T_m \geq 187$ °C) than homochiral PLLA ($T_m$ = 162 °C), suggesting the formation of a stereocomplex between the two polymer chains.

After this discovery, aluminium salen complexes received a great deal of interests from many research groups.[52-55] In 2002, Coates and co-workers also reported a similar chiral aluminium salen complex with an iso-propoxide co-ligand (**2**, Figure 1.3).[53] The iso-propoxide co-ligand was selected due to its high steric hindrance which prevented the formation of a dimeric complex. They showed that enantiomerically pure complex **2** produced highly syndiotactic PLA from *meso*-LA whilst the *rac*-complex **2** polymerised *meso*- and *rac*-LA to heterotactic and isotactic stereoblock PLA, respectively using similar

polymerisation conditions to those reported by Spassky. They suggested that a chain exchange mechanism was responsible for the production of either heterotactic or isotactic stereoblock PLA. Polymer molar masses of the resultant PLAs in all cases were close to the theoretical values and narrow $Đ$ were observed ($Đ \leq 1.07$). In addition, inspection of $^{1}H\{^{1}H\}$ NMR spectra of all polymers suggested high stereoselectivity of the catalyst **2** arises from the enantiomorphic site control (ESC) mechanism.

Soon after, Nomura and Gibson independently reported a range of achiral aluminium salen complexes.[52, 54] In the presence of benzyl alcohol (BnOH), all complexes were active catalysts for *rac*-LA polymerisations in toluene at 70 °C with different degrees of activity and iso-selectivity, depending on the nature of diamine linker and phenoxide substituents. Using a 2,2-dimethyl propylene diamine bridge ($C_3Me_2$) (**3** and **4**, Figure 1.3) resulted in a drastic increase in polymerisation activity. Though bulky *tert*-butyl substituents at the *ortho*-position of phenoxide rings lead to a catalyst with slower polymerisation rate but produces PLA with a good isotacticity ($P_i \geq 0.88$ ([LA]:[cat.] = 100:1, [LA] = 0.8 M, T = 70 °C)). In all cases, polymerisations were well controlled as evidenced by the production of predictable molar mass PLA with narrow $Đ$ over the course of polymerisations. Nomura and co-workers also showed that by changing the *ortho* phenoxide substituents from *tert*-butyl groups to more sterically hindered $^{t}BuSi(CH_3)_2$ groups (complex **5**, Figure 1.3) resulted in a significant enhancement in catalyst iso-selectivity and produced PLA with $P_i$ as high as 0.98 ([LA]:[cat.] = 100:1, [LA] = 1 M, T = 70 °C).[55] This is one of the highest $P_i$ values reported to date. Additionally, complex **5** was able to polymerise *rac*-LA in bulk conditions and maintain its high iso-selectivity even at elevated temperature, producing isotactic PLA with the $P_i$ of 0.84 ([LA]:[cat.] = 300:1, bulk, T = 180 °C).

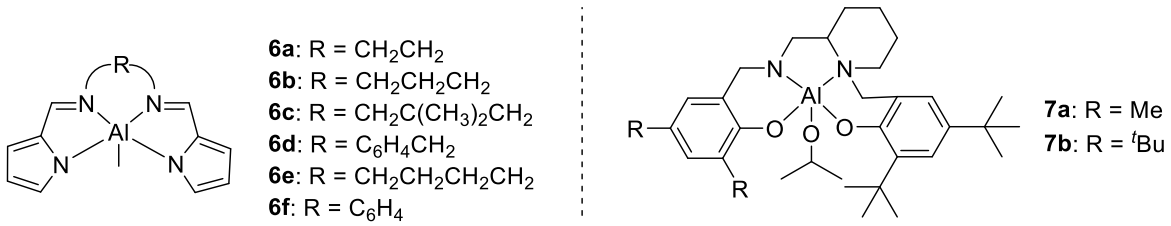



**Figure 1.4.** Structures of bis(pyrrolidine) Schiff base (**6a**–**6f**) and salan (**7a** and **7b**) aluminium complexes.[56, 57]

Aluminium complexes with different ligand scaffolds were also reported as iso-selective catalysts for *rac*-LA ROP. Hormnirun and co-workers presented a series of aluminium bis(pyrrolidine) Schiff base complexes with a variety of diamine bridges (**6a**–**6f**, Figure 1.4) which were active for LA polymerisations in the presence of BnOH in toluene at 70 °C.[56] They showed that the nature of the diamine linker played a key role in controlling catalyst activities and iso-selectivities with complex **6c**, containing a $C_3Me_2$ backbone, being the most iso-selective catalyst and producing PLA with $P_i$ of 0.80 ([LA]:[cat.] = 100:1, [LA] = 0.4 M, T = 70 °C). Davidson and Jones presented two aluminium salan complexes (**7a** and **7b**, Figure 1.4) which were active for polymerisation in both solution and bulk conditions.[57] Complex **7b** was found to be the most iso-selective catalyst and produced PLA with a $P_i$ value of 0.83 ([LA]:[cat.] = 100:1, [LA] = 0.69, T = 25 °C). It should be noted that the high iso-selectivity of **7b** was maintained at elevated temperature ($P_i$ up to 0.81 ([LA]:[cat.] = 300:1, bulk, T = 130 °C)).

The major drawback of aluminium systems is their low catalytic activity. Substitution of aluminium with heavier indium(III) or gallium(III) metals was found to improve catalyst activity.

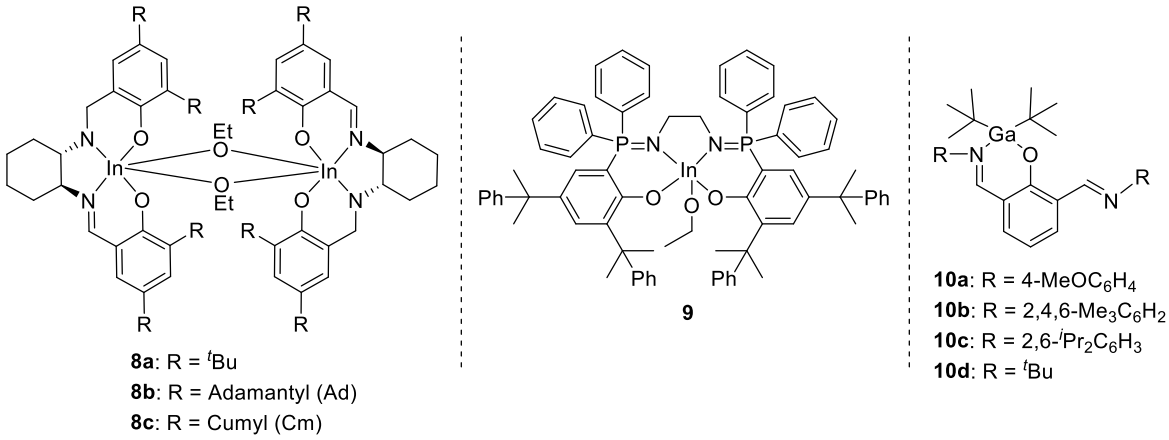



**Figure 1.5.** Structures of indium (**8a**–**8c** and **9**) and gallium (**10a**–**10d**) complexes.[58-60]

Mehrkhodavandi and co-workers reported a range of indium salen complexes containing different phenoxide substituents (**8a**–**8c**, Figure 1.5) which were highly active for *rac*-LA polymerisations at room temperature.[58] They showed that the introduction of bulky phenoxide substituents ($^t$Bu, Ad, and Cm) resulted in an increase in catalyst iso-selectivity, and complexes **8a**–**8c** produced PLA with $P_i$ in the range of 0.73–0.77 ([LA]:[cat.] = 200:1, [LA] = 0.45 M, T = 25 °C). Recently, Williams and co-workers reported an indium phosphasalen complex **9** (Figure 1.5) which was highly active and iso-selective for *rac*-LA polymerisation.[60] Complex **9** was able to achieve a full conversion of 500 equivalents of *rac*-LA at ambient temperature in an hour and produced PLA with a $P_i$ of 0.87 ([LA]:[cat.] = 500:1, [LA] = 1 M, T = 25 °C). The iso-selectivity of the complex was improved further by operating the polymerisation at low temperature (T = –15 °C) and PLA with a $P_i$ as high as 0.92 ([LA]:[cat.] = 500:1, [LA] = 0.75 M, T = –15 °C) was obtained. This complex is among the most iso-selective indium complexes reported to date. Chakraborty and co-workers reported a series of gallium phenoxy-imine complexes with different amine substituents (**10a**–**10d**, Figure 1.5).[59] All complexes were highly active catalysts for *rac*-LA polymerisations in bulk conditions at 140 °C and produced isotactic PLA with $P_i$ in the range of 0.78–0.84 ([LA]:[cat.] = 200:1, bulk, T = 140 °C).

### 1.3.4.2. Iron(III) complexes

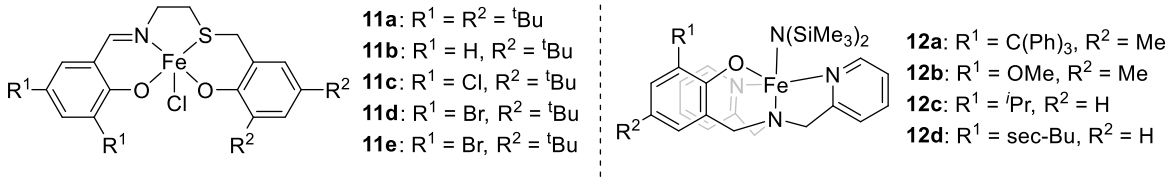



**Figure 1.6.** Structures of thiolene (**11a**–**11e**) and bispyridine monophenolate (**12a**–**12d**) iron complexes.[61, 62]

Iron complexes were also found to be promising candidates for the stereoselective polymerisation of *rac*-LA. Recently, Jones and co-workers reported a series of iron thiolen complexes (**11a**–**11e**, Figure 1.6).[62] In the presence of BnOH and $Et_3N$, all complexes were active catalysts for *rac*-LA polymerisations with different degrees of activity and iso-selectivity. Complex **11d**, possessing Br substituents on the $R^1$ of the phenoxide rings showed the highest activity and produced PLA with moderate isotacticity. Changing $R^1$ substituents to bulkier $^t$Bu substituents (complex **11a**) resulted in an increased catalyst iso-selectivity and complex **11a** produced PLA with good isotacticity ($P_i$ = 0.81 ([LA]:[cat.] = 100:1, [LA] = 1.4 M, T = 80 °C)). Manipulating the polymerisation using **11a** at lower temperature (T = 40 °C) led to further enhancement in catalyst iso-selectivty and PLA with $P_i$ of 0.85 ([LA]:[cat.] = 100:1, [LA] = 1.4 M, T = 40 °C) was obtained. Thomas and Venditto also presented a range of iron bispyridine monophenolate complexes with a variety of phenoxide substituents (**12a**–**12d**, Figure 1.6).[61] All complexes were active catalysts for *rac*-LA polymerisations, showing different degrees of activity and similar levels of iso-selectivity depending on the phenoxide substituents. Complex **12c**, containing *iso*-propyl substituents on the $R^1$ position of the phenoxide ring showed the highest activity and polymerised 800 equivalents of LA to full conversion in a few minutes at ambient temperature. All complexes produced PLA with good degrees of isotacticity ($P_i$ ~ 0.80 ([LA:[cat.] = 200:1, [LA] = 1 M, T = 25 °C)). Operating the polymerisations at low

temperature resulted in an increase in catalyst iso-selectivity and at –10 °C, complex **12a** produced PLA with $P_i$ up to 0.92 ([LA]:[cat.] = 100:1, [LA] = 1 M, T = –10 °C). The resultant PLA showed a high $T_m$ of 195 °C.

### 1.3.4.3. Group 1 complexes

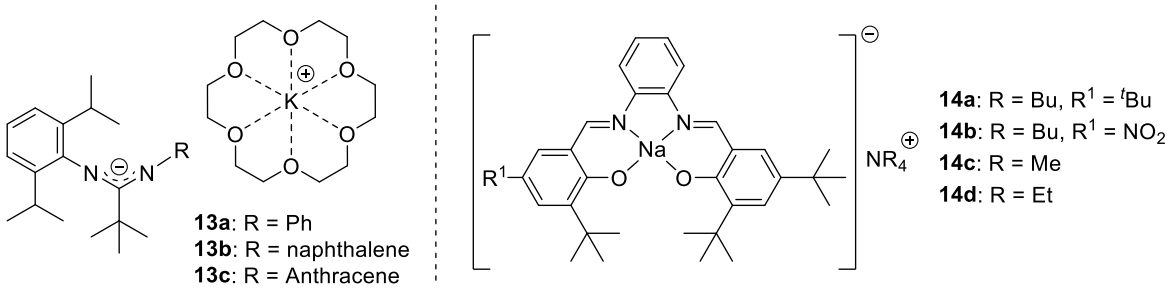



**Figure 1.7.** Structures of crown ether K(I) (**13a**–**13c**) and salen Na(I) (**14a**–**14d**) complexes.[63, 64]

In addition, Wu and co-workers reported a range of K(I) ion pair catalysts supported by a variety of crown ether ligand scaffolds (**13a**–**13c**, Figure 1.7).[63] All complexes were active catalysts for *rac*-LA polymerisations at –70 °C. Polymerisation rates of all catalysts were found to follow anti-Arrhenius polymerisation behaviours, meaning operating the polymerisation at higher temperature led to a reduction in polymerisation rate. This finding is in contrast to other reported catalysts which showed higher activities at elevated temperature.[55, 60] At –70 °C, both catalysts **13b** and **13c** produced isotactic PLA with $P_i$ ~ 0.85 ([LA]:[cat.] = 100:1, [LA] 0.2 M, T = –70 °C). Wu also presented a series of mononuclear ion pair Na(I) salen complexes (**14a**–**14d**, Figure 1.7) which were active for *rac*-LA polymerisations.[64] All complexes produced isotactic PLA with $P_i$ = 0.76–0.82 ([LA]:[cat.] = 500:1, [LA] = 0.5 M, T = –70 °C). The catalyst iso-selectivity reduced with an increase in polymerisation temperature and all complexes produced atactic PLA at ambient temperature.

### 1.3.4.4. Group 2 complexes

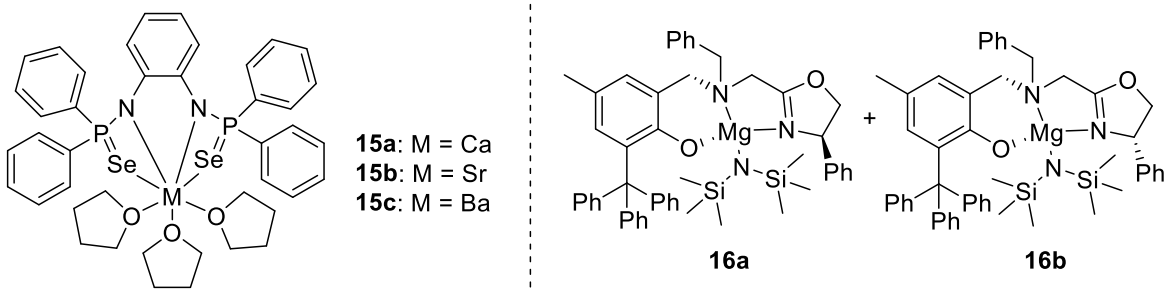



**Figure 1.8.** Structures of iminophosphorane group II (**15a**–**15c**) and benzoxazolyl aminophenolate Mg(II) (**16a** and **16b**) complexes.[65, 66]

Recently, some examples of group II catalysts, showing good iso-selectivity toward the ROP of *rac*-LA were reported. For example, Panda and co-workers reported a range of group II (Ca(II), Sr(II), Ba(II)) iminophosphorane complexes (**15a**–**15c**, Figure 1.8) which were active for *rac*-LA polymerisations at room temperature.[65] The activity order of complexes was enhanced by an increase in the metal centre radii such that Ba(II) > Sr(II) > Ca(II). Conversely, catalyst iso-selectivity decreased with an increase in metal radii with the calcium complex **15a** being the most iso-selective catalyst which produced isotactic PLA with $P_i$ up to 0.83 ([LA]:[cat.] = 100:1, [LA] = 0.1 M, T = 25 °C). In 2018, Ma and Wang presented a range of Mg(II) benzoxazolyl aminophenolate complexes with variety of amino and oxazolinyl substituents.[66] They showed that by using a racemic mixture of complexes **16a** and **16b** (Figure 1.8) in the presence of $^{i}$PrOH, hyper activity was observed. *rac*-Complex **16** polymerised 5000 equivalents of *rac*-LA to full conversion within 5 min and gave an impressive TOF of 54,000 $h^{-1}$ ([LA]:[cat.] = 5000:1, [LA] = 1 M, T = 25 °C). In addition, the resultant PLA obtained from *rac*-complex **16** showed high molar mass ($M_n$ = 461,000 g $mol^{-1}$) and isotacticity with $P_i$ of 0.80.

### 1.3.4.5. Zn(II) complexes

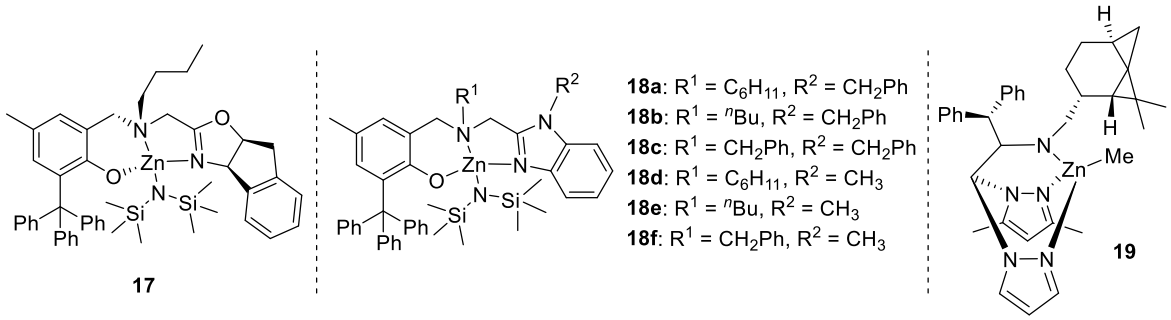



**Figure 1.9.** Structures of zinc complexes bearing benzoxazolyl aminophenolate (**17**), benzylimidazolyl aminophenolate (**18a**–**18f**), and scorpionate (**19**) ligands.[67-69]

Ma and Wang also reported a range of Zn(II) benzoxazolyl aminophenolate complexes.[67] Compared to Mg(II) complexes bearing the same class of ligand, Zn(II) complexes showed lower catalytic activities. Nonetheless, in the presence of $^{i}$PrOH, Zn(II) complex **17** (Figure 1.9) produced isotactic PLA with $P_i$ of 0.83 ([LA]:[cat.] = 500:1, [LA] = 1 M, T = 25 °C). Operating polymerisation at lower temperature resulted in an improvement in PLA isotacticity ($P_i$ = 0.91 ([lA]:[cat.] = 200:1, [LA] = 1 M, T = –20 °C)). Very recently, Ma and co-workers reported a series of Zn(II) benzylimidazolyl aminophenolate with a variety of amino and phenoxide substituents (**18a**–**18f**, Figure 1.9).[68] They were active and highly iso-selective catalysts for *rac*-LA polymerisations. Addition of an equivalent of $^{i}$PrOH to the polymerisation reactions led to better polymerisation controls, as observed by the narrow dispersities of the resultant PLA ($Đ \leq 1.34$). All complexes produced PLA with high degrees of isotacticity with $P_i$ around 0.90 ([LA]:[cat.] = 200:1, [LA] = 1 M, T = 25 °C). Using complex **18e** at –40 °C further improved the PLA isotacticity and PLA with $P_i$ exceeding 0.90 ($P_i$ = 0.93 ([LA]:[cat.] = 200:1, [LA] = 1 M, T = –40 °C)) was obtained. Fernandez-Baeza and Sanchez-Barba reported a Zn(II) scorpionate complex (**19**, Figure 1.9).[69] The zinc complex showed low activity, but exhibited good iso-selectivity for *rac*-LA polymerisation and produced PLA with $P_i$ of 0.88 ([LA]:[cat.] = 100:1, [LA] = 0.9 M, T = 50 °C).

### 1.3.4.6. Group 4 complexes

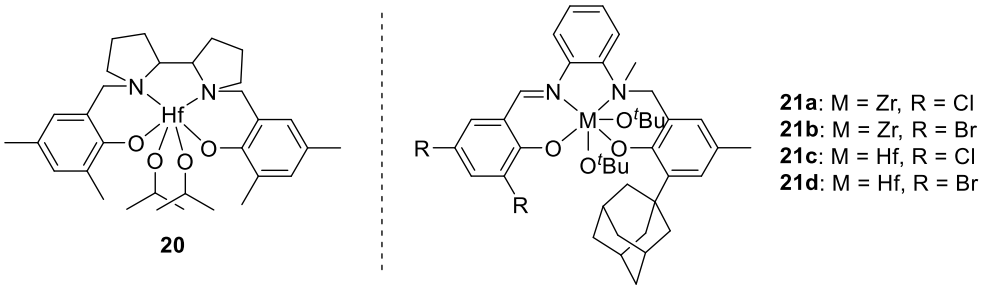



**Figure 1.10.** Structures of hafnium salan complex (**20**) and zirconium and hafnium salalen complexes (**21a**–**21d**).[70, 71]

Jones *et al*. reported a Hf(IV) salan complex (**20**, Figure 1.10) which was active and iso-selective for *rac*-LA ROP.[70] Using complex **20** in toluene at 50 °C, isotactic PLA with a $P_i$ of 0.84 ([LA]:[cat.] = 100:1, T = 50 °C) was obtained. Operating polymerisation in the bulk condition at 130 °C led to the production of moderately isotactic PLA ($P_i$ = 0.68 ([LA]:[cat.] = 300:1, bulk, T = 130 °C)). Kol and co-workers presented Zr(IV) and Hf(IV) salalen complexes with a wide range of phenoxide substituents (**21a**–**21d**, Figure 1.10).[71] Complexes **21a**–**21c**, containing an adamantane group at the *ortho*-position of the amine-side phenoxide ring showed the highest iso-selectivities and produced PLA with the $P_i$ around 0.90 ([LA]:[cat.] = 300:1, [LA] = 0.6 M, T = 50 °C). For catalytic activities, Zr(IV) complexes were found to show higher catalytic activities than their Hf(IV) analogues.

### 1.3.4.7. Lanthanide(III) complexes

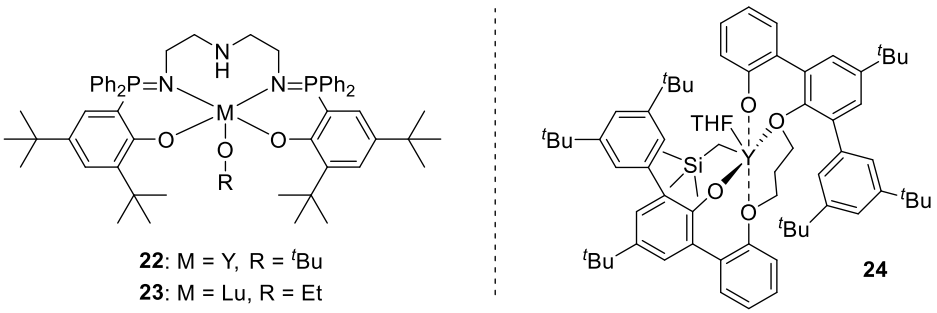



**Figure 1.11.** Structures of Y(III) (**22**) and Lu(III) (**23**) phosphasalen complexes and Y(III) bisphenolate complex (**24**).[72-74]

Williams and Auffrant reported a range of lanthanide (Lu(III), Y(III), and La(III)) phosphasalen complexes, containing different diamine backbones and phenoxide substituents.[72, 73] They showed that the nature of diamine played a key role in controlling catalyst activity and iso-selectivity. Complex **22** (Figure 1.11), possessing a nitrogen containing diamine linker showed moderate iso-selectivity at room temperature and produced PLA with $P_i$ of 0.77 ([LA]:[cat.] = 500:1, [LA] = 1 M, T = 25 °C). Lowering the polymerisation temperature to –15 °C resulted in an increase in catalyst iso-selectivity and PLA with good isotacticity ($P_i$ = 0.84 ([lA]:[cat.] = 100:1, [LA] = 0.5 M, T = –15 °C)) was obtained. By switching the diamine linker to ethylene diamine, a heterotactic PLA was produced.

Additionally, Williams and co-workers showed that the size of the metal centre had an influence on controlling catalyst activity and iso-selectivity.[73] Using a larger radii La(III) centre with phosphasalen ligands led to the production of heterotactic PLA. Conversely, smaller Lu(III) (complex **23**, Figure 1.11) yielded isotactic PLA ($P_i$ = 0.84 ([LA]:[cat.] = 500:1, [LA] = 1 M, T = 25 °C). The isotactic degree of PLA was further improved by manipulating polymerisation temperature ($P_i$ = 0.89 ([LA]:[cat.] = 500:1, [LA] = 0.75 M, T = –15 °C)). It should be noted that this is the first example of iso-selective Lu(III) complex. Lu and co-workers presented a series of Y(III) bisphenolate complexes which were active for *rac*-LA polymerisations.[74] Y(III) complex **24** (Figure 1.11) was found to show the highest catalytic activity and iso-selectivity and produced PLA with $P_i$ of 0.84 ([LA]:[cat.] = 200:1, [LA] = 1 M, T = 25 °C). Changing the polarity of the polymerisation solvent from DCM to toluene was found to decrease catalytic activity but did not effect catalyst iso-selectivity. In contrast, using coordinating THF as a polymerisation solvent resulted in a drastic decrease in catalyst selectivity and led to the formation of atactic PLA.

### 1.3.4.8. Organo-catalysts

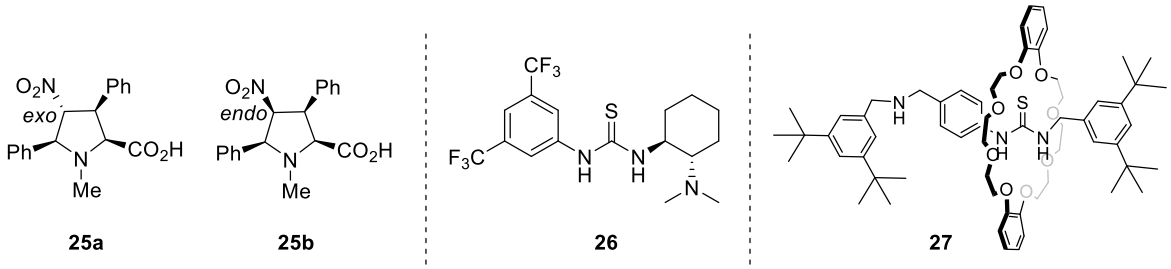



**Figure 1.12.** Structures of N-methylated proline (**25a** and **25b**), Takemoto's (**26**), and [2]rotaxane (**27**) organo catalysts.[75-77]

Mercerreyes and Cossio reported chiral N-methylate proline catalysts (**25a** and **25b**, Figure 1.12) which were found to be highly iso-selective for *rac*-LA polymerisations in the presence of 1,8-diazabicyclo[5.4.0]undec-7-ene (DBU) co-catalyst and BnOH initiator.[75] *exo*-Proline catalyst **25a** was found to preferentially ring open *L*-LA over *D*-LA in contrast to *endo*-proline **25b** which prefered to polymerise *D*-LA over *L*-LA. Due to the high ability of the catalysts to discriminate between the two monomer enantiomers, using them with *rac*-LA monomer resulted in the formation of highly isotactic PLA. *exo*-Proline **25a** showed higher iso-selectivity and produced PLA with $P_i$ of 0.96 ([LA]:[cat.] = 50:1, [LA] = 1 M, T = 25 °C), whilst a PLA with slightly lower isotacticity ($P_i$ = 0.90 ([LA]:[cat.] = 50:1, [LA] = 1 M, T = 25 °C)) was obtained from *endo*-proline **25b**. Dove, Taton and Coulembier presented the use of chiral Takemoto's catalyst (**26**, Figure 1.12) as an iso-selective catalyst for *rac*-LA polymerisations.[76] In the presence of BnOH, *S,S*-Takemoto's catalyst **26** produced isotactic PLA with good $P_i$ of 0.88 ([LA]:[cat.] = 200:1, [LA] = 1 M, T = 25 °C). Additionally, the catalyst can maintain its high iso-selectivity at high temperature and isotactic PLA with $P_i$ of 0.85 was obtained at 85 °C ([LA]:[cat.] = 200:1, [LA] = 0.8 M). Williams and Beer reported a series of [2]rotaxanes and their uses as catalysts for *rac*-LA polymersations.[77] In the presence of $KN(Si(CH_3)_3)_2$ and BnOH , all catalysts were active catalysts with catalyst **27** showing the highest iso-selectivity. Rotaxane **27** (Figure 1.12)

produced isotactic PLA with $P_i$ of 0.81 ([LA]:[cat.] = 50:1, [LA] = 1 M, T = 25 °C). In addition, they showed that the rate of macrocycle shuttling is responsible for the high iso-selectivity of catalyst **27**. This means that the macrocycle of catalyst **27** preferentially occupied the thiourea active site in contrast to other catalysts where the macrocycle prefer to occupy the amine site. The occupation of macrocycle on the thiourea active site resulted further in an increase in steric congestion which led to an improvement in catalyst iso-selectivity.

### 1.3.4.9. Evaluation of highly active and iso-selective catalysts

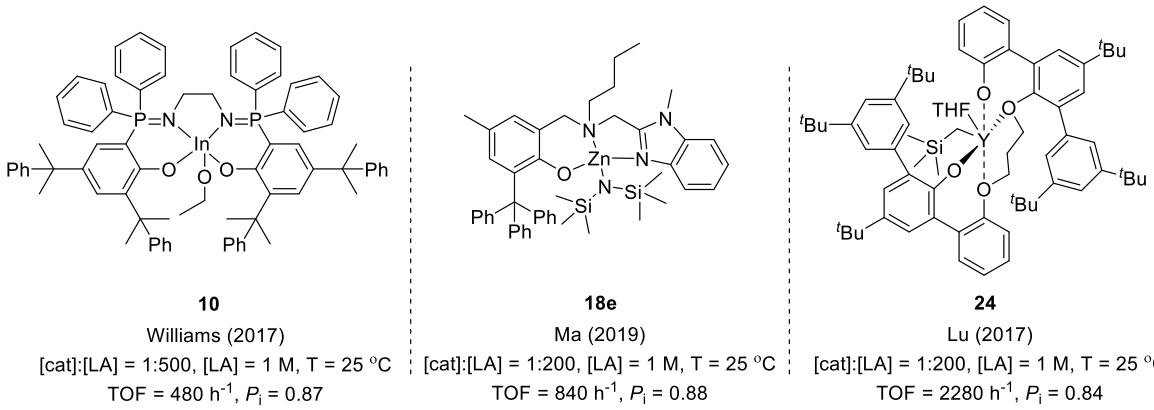



**Figure 1.13.** Structures of selected In(III), Zn(II), and Y(III) complexes exhibiting high activity and iso-selectivity for *rac*-LA polymerisations.[60, 68, 74]

In order to compare catalyst activity and iso-selectivity data, turn-over-frequencies (determined from conversion-time point kinetic data) are compared under conditions close to polymerisation conditions used in this thesis ([LA]:[cat.] = 500:1, [LA] = 1 M, T = 25 °C). At the upper end of this performance metric are three different catalysts: 1) The phosphasalen indium(III) alkoxide complexes (reported by our group, **10**);[60] 2) The benzoimidazolyl aminophenolate zinc(II) alkoxide complexes (reported by Ma and co-workers, **18e**);[68] and 3) The bis(phenolate)ether yttrium(III) alkoxide complexes (reported by Lu and co-workers, **24**)[74] (Figure 1.13). The first class (phosphasalens) is represented by an indium(III) phosphasalen alkoxide complex (**10**), reported by our group, which shows $P_i$

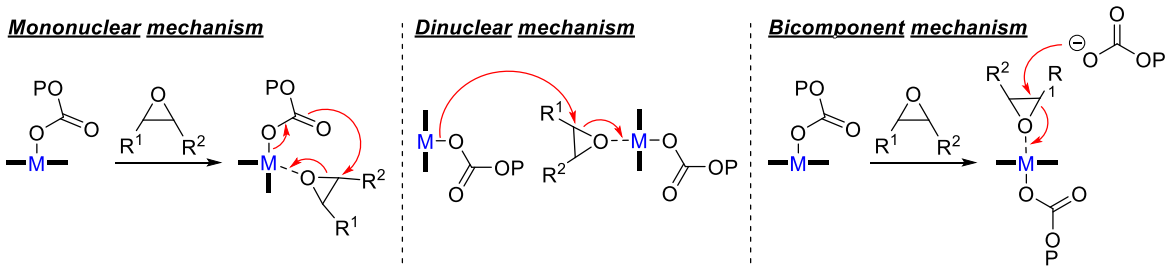
= 0.87 and TOF = 480 $h^{-1}$ ([LA]:[cat.] = 500:1, [LA] = 1 M, T = 25 °C).[60] Ma and co-workers have also pioneered over several years a series of high-performance chiral oxazolinyl aminophenolate zinc complexes.[66, 67, 78, 79] The authors, however, point out that achiral ligands are more beneficial and in 2019, an outstanding achiral benzoimidazolyl zinc complex (**18e**) was reported which shows $P_i$ = 0.88 and TOF = 840 $h^{-1}$ ([LA]:[cat.] = 200:1, [LA]= 1 M, T = 25 °C).[68] The third class of high-performance catalysts, reported by Lu and co-workers, is represented by the bis(phenolate)ether yttrium alkoxide (**24**) which shows $P_i$ = 0.84 and TOF = 2280 $h^{-1}$ ([LA]:[cat.] = 200:1, [LA] =1 M, T = 25 °C).[74] Other good catalysts, in some cases also showing excellent stereoselectivity, comprise complexes of Zn(II), Ca(II) or Fe(III).[61, 65, 80-83] Several organocatalysts are also highly iso-selective but their lower activities and the need for very high organocatalyst loadings mean they cannot compete against the best metal based catalysts.[75-77]

### 1.4. Ring-opening copolymerisation of epoxide and cyclic anhydride

Ring-opening copolymerisation (ROCOP) of epoxide and anhydride is a useful tool for the production of polyesters with a variety of polymer backbones. As a result, polyesters with various mechanical and thermal properties can be obtained.[14] In addition, the ester or ether content can be tuned *via* catalyst selectivity. This allows access to an even wider range of polymer properties.[14]

#### 1.4.1. Polymerisation mechanisms

The polymerisation mechanisms of the epoxide/anhydride or $CO_2$ ROCOP have been far less studied than that of lactone ROP. However, based on the kinetic studies and evidences proposed by previous works, the proposed mechanisms for epoxide/anhydride or $CO_2$ ROCOP can be categorised into three types: I) mononuclear pathway, II) bimetallic process, and III) bicomponent mechanism (Scheme 1.4). It should be noted that the proposed mechanism often uses epoxide and $CO_2$ as model substrates.[84-87]




**Scheme 1.4.** Proposed ROCOP mechanisms: mononuclear, binuclear, and bicomponent mechanisms.[84-88]

In the case of the monometallic mechanism, the metal centre plays two roles, coordinating an epoxide and providing a nucleophile (carboxylate or carbonate) to ring open the epoxide to form alternating polymers. This mechanism is typified by a first order in catalyst concentration. It previously was believed to be unlikely to occur for first row transition metal and small main group ions and in any case, these species generally require co-catalysts which complicate mechanisms. Very recently, Williams and co-workers established the mononuclear pathway was feasible for indium catalysts in epoxide/$CO_2$ ROCOP.[87] The mechanism was supported by kinetic studies (first order in catalyst concentration) and isolation of intermediates which occur during polymerisation. It is proposed to depend upon the *cis*-insertion of the monomers at the metal centre and requires a larger ionic radius metal, such as indium, to proceed.

The dinuclear mechanism is observed for bimetallic or dinuclear catalysts. In this case, it is proposed that the two metal centers play a different roles in polymerisation, where one metal coordinates to epoxide and the other provides the nucleophile (carbonate or carboxylate) to activate and ring open the epoxide to form an alternating polymer. For catalysts which are monometallic under the conditions of catalysis, rates often show more complex orders on catalyst concentration - typically between 1–2. For deliberately dinuclear catalysts, the

rates are first order in catalyst concentration since the catalyst already comprises two metals in close proximity and is, essentially, designed to operate by this mechanism.[85]

The bicomponent mechanism is proposed for binary systems which comprise a mononuclear catalyst + co-catalyst. In this mechanism, the polymerisation occurs by formation of metal-co-catalyst ion pairs but the precise roles for metals/ions are complex and not yet fully elucidated.[88]

### 1.4.2. Polymerisation catalysts

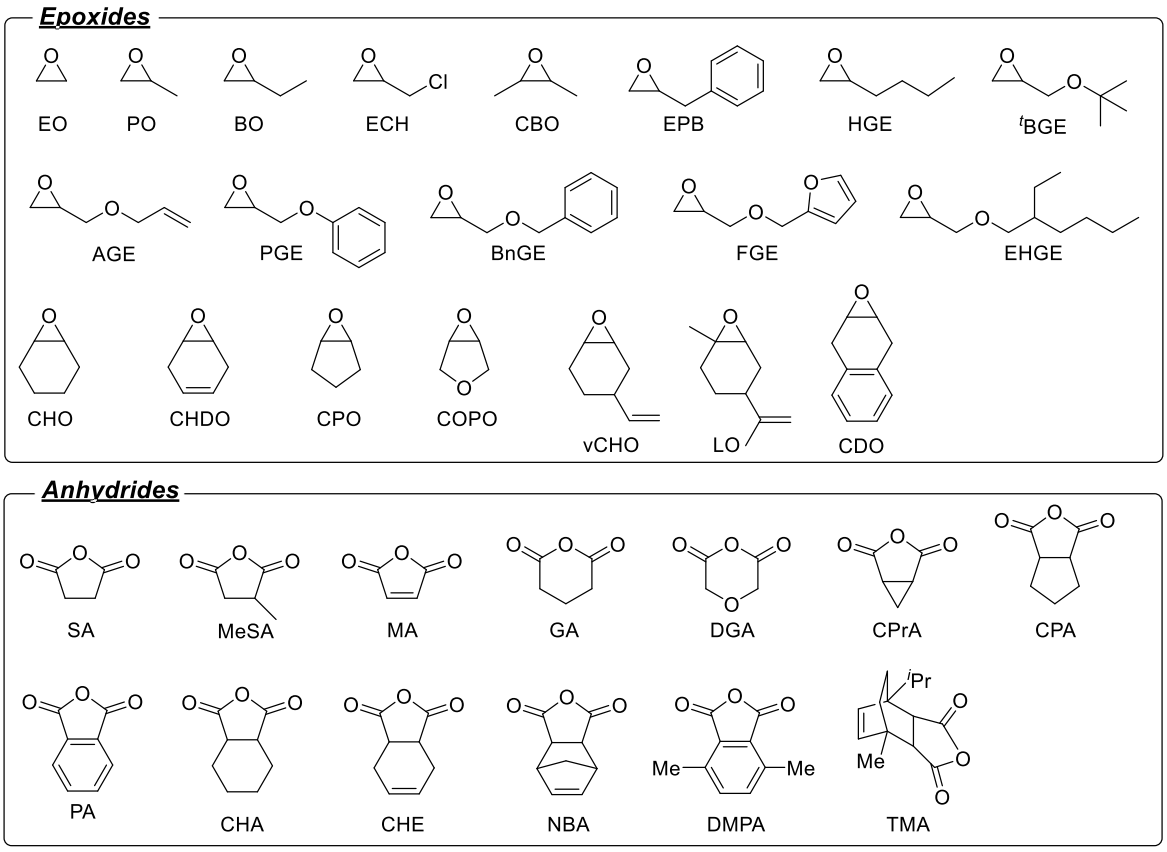


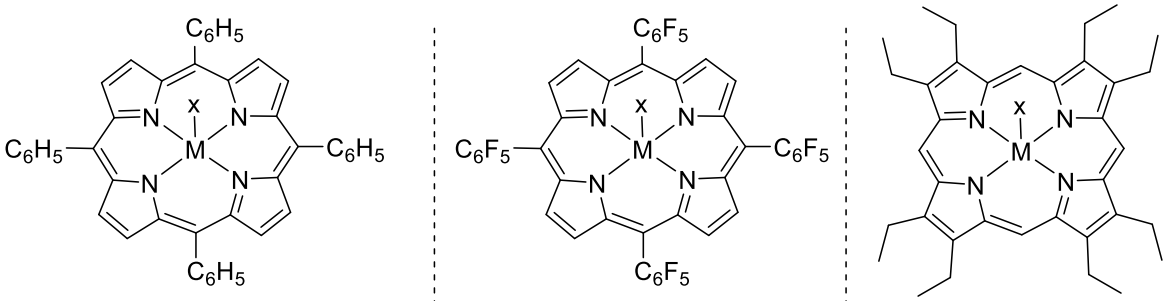

**Figure 1.14.** Structures of epoxides and anhydrides presented in this thesis.

This section presents the early discovery of catalysts as well as the development of single site catalysts, reported to date, used in the ROCOP of epoxides and cyclic anhydrides to make alternating polyesters. The abbreviations of both substrates, epoxides and anhydrides

will often be used. Hence, the key structures of these two substrates with their abbreviations are illustrated in Figure 1.14.

### 1.4.2.1. Porphyrin, corrole and *β*-diiminate complexes

The first reports of alternating ring-opening copolymerisation of epoxide and anhydride for the production of polyesters were in the 1960s.[89] Early discoveries of catalysts for this polymerisation concern the use inorganic salts, tertiary amines, or metal alkyl initiators.[90-94] However, copolymerisations were hampered by poor performance characteristics, including low catalytic activity, poor polymerisation control, and production of low molar mass polymers. In addition, in some cases, they showed low levels of selectivity, resulting in the formation of high ether linkages in the polymer backbone.




**28a**: M = Al, x = Cl
**28b**: M = Al, x = $OCOC(CH_3)_3$
**28c**: M = Cr, x = Cl
**28d**: M = Co, x = Cl
**28e**: M = Mn, x = Cl

**29a**: M = Al, x = Cl
**29b**: M = Cr, x = Cl
**29c**: M = Co, x = Cl

**30a**: M = Al, x = Cl
**30b**: M = Cr, x = Cl
**30c**: M = Co, x = Cl

**Figure 1.15.** Structures of M(III) porphyrin complexes (**28**–**30**).[95-100]

In 1985, Inoue and co-workers reported Al(III) porphyrin complexes (**28a** and **28b**, Figure 1.15) as the first examples of single site catalysts for the ROCOP of PO and PA.[95] They showed that in the presence of quaternary ammonium or phosphonium salts as co-catalysts, Al(III) porphyrin catalysts were active and produced highly alternating poly(propylene phthalate). It should be noted that the combination of Al(III) catalysts and quaternary organic salt co-catalysts were necessary to activate the polymerisation since using the Al(III) catalyst

or co-catalyst alone did not result in polymerisations. Slow polymerisation rate was observed and the catalysts required several days to achieve full conversion at room temperature. The resultant polyester showed low molar mass ($M_n \leq 3{,}000$ g mol$^{-1}$) and relatively narrow dispersity ($Đ \leq 1.1$). They suggested that the polymer chains grew from both sides of the porphyrin planar ring since the observed polymer molar mass was found to be half of the theoretical value. In the same year, Inoue also showed that catalyst **28a** with quaternary phosphonium salt as a co-catalyst was active for ROCOP of PA and a range of epoxides, including EO, SO, BO, and CHO.[96] In all cases, highly alternating polyesters were prepared and the resultant polymers showed low molar masses ($M_n \leq 4{,}000$ g mol$^{-1}$) and narrow dispersities. In addition, they showed that the formation of block copolymer by sequential monomer addition was possible, suggesting the living nature of polymerisations using this catalyst. Coates and co-workers also reported the use of catalyst **28a** without any co-catalyst for ROCOP of PO and MA.[97] Catalyst **28a** showed low selectivity and produced polyester with a high percentage of ether linkages (50 % ether linkages). The resultant polymer had high molar mass ($M_n \geq 14{,}000$ g mol$^{-1}$) and narrow molar mass distribution ($Đ \leq 1.1$).

Soon after, Duchateau and co-workers reported a porphyrin chromium(III) catalyst (**28c**, Figure 1.15).[98] Catalyst **28c** alone only showed a very poor activity and selectivity in the CHO/SA ROCOP and produced a polymer with low ester content (14 % ester linkages). However, using a molar equivalent of 4-N,N-dimethylamino-pyridine (DMAP) co-catalyst in combination with **28c** resulted in an acceleration of both activity and selectivity, perfectly alternating poly(CHO-*alt*-SA) was obtained. The scope of anhydride was also explored. They showed that using catalyst **28c**/DMAP binary catalyst produced perfectly alternating polyesters from ROCOP of CHO and a range of anhydrides, including CPrA, CPA, and PA. In 2012, Duchateau and co-workers also presented a range of porphyrin complexes with different metal centres, including Cr(III), Co(III), and Mn(III) (**28c**–**28e**, Figure 1.15).[99]

They showed that in the presence of DMAP co-catalyst, all catalysts were active and highly selective for SO/PA ROCOP and produced perfectly alternating polyesters. The activity order followed **28c** > **28d** > **28e**.

In 2013, Chisholm and co-workers reported a series of M(III) porphyrin complexes (**28a**, **28c**, **28d**, **29a**–**29c**, and **30a**–**30c**, Figure 1.15) which were active and highly selective for ROCOP of PO and MeSA in the presence of bis(triphenylphosphine) iminium chloride (PPNCl) as a co-catalyst.[100] Using the catalyst alone resulted in a very low catalytic activity and selectivity (15–20 % ester linkages). It should be noted that 1 molar equivalent of PPNCl co-catalyst was needed to achieve perfectly alternating polyester formation since using 0.5 equivalent of the co-catalyst led to the formation of polymer with low ester content. The catalytic activity was found to depend upon the porphyrin structure and metal centre with Cr(III) complexes (**28c**, **29b**, and **30b**) being the most active catalysts in each ligand type. Catalyst **28c** also worked with a range of anhydride substrates. In the presence of PPNCl, catalyst **28c** produced alternating polyesters from the ROCOP of PO and a variety of anhydrides (*i.e.* SA, MA, PA).

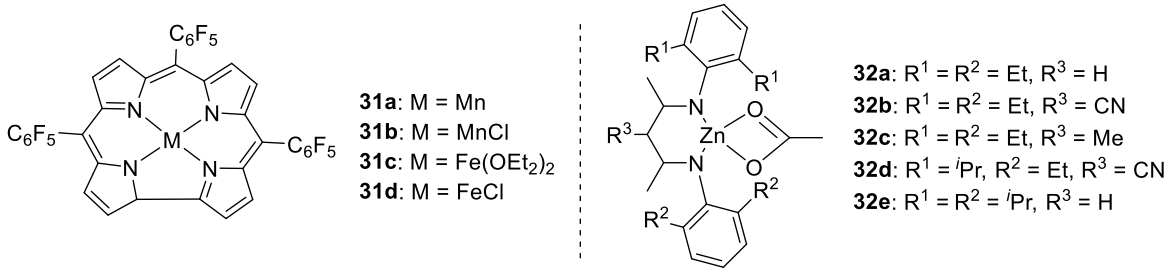


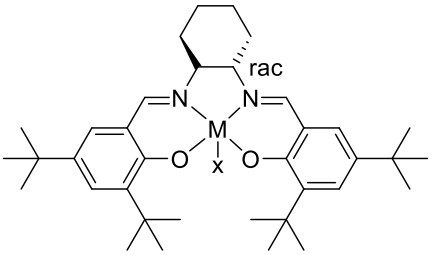

**Figure 1.16.** Structures of corrole (**31a**–**31d**) and Zn(II) *β*-diiminate (**32a**–**32e**) complexes.[101, 102]

Nozaki and co-workers reported a series of corrole complexes with different metal centres (**31a**–**31d**, Figure 1.16) as catalysts for ROCOP of epoxide and anhydride.[102] They found that all complexes, in the presence of PPNOBz$F_5$ (where PPN = bis(triphenylphosphoranylidene) ammonium and OBz$F_5$ = pentafluorobenzoate) co-

catalysts, were active and selective catalysts for CHO/GA ROCOP, with complex **31d** showing the highest activity in neat CHO. In all cases, perfectly alternating polyester was produced. Operating polymerisations using complex **31a**/PPNOBz$F_5$ in toluene resulted in a reduction of catalyst selectivity and polyester with some ether content (32 % ether linkages) was produced. Furthermore, catalyst **31a**/PPNOBz$F_5$ showed no activity when polymerisation was carried out in THF, suggesting competition between THF and epoxide for coordination at the metal centre. Complex **31a**/PPNOBz$F_5$ was effective for various epoxides (PO, SO, ECH) and anhydrides (SA, MA). In all cases, perfectly alternating polyesters were obtained.

Coates and co-workers presented a range of Zn(II) *β*-diiminate complexes (**32a**–**32e**, Figure 1.16).[101] They showed that catalysts **32b**, **32d**, and **32e** were active for CHO/DGA ROCOP without the need for any co-catalysts, with catalyst **32d** being the most active catalyst. Catalyst **32a** and **32c** were unable to show any polymer conversion and found to decompose during the polymerisation. Complex **32d** also worked with a range of other epoxides and anhydrides. They found that catalyst **32d** was highly selective and produced perfectly alternating polyesters from a wide range of epoxides (*i.e.* vCHO, LO, PO, CBO, IBO) and anhydrides (*i.e.* SA, MA).

### 1.4.2.2. Salen and salen-like complexes




**33a**: M = Al, x = Cl
**33b**: M = Cr, x = Cl
**33c**: M = Co, x = Cl
**33d**: M = Co, x = O-$COC_6F_5$

**Figure 1.17.** Structures of Al(III) and Co(III) salen complexes (**33a**–**33d**).[97, 103]

Coates and co-workers presented Cr(III) and Co(III) salen complexes (**33b** and **33d**, Figure 1.17) for PO/MA ROCOP.[97] The polymerisations were carried out without using any co-catalysts. Both complexes produced perfectly alternating poly(propylene malate) from PO and MA with Cr(III) showing higher catalytic activity. They also showed that solvent used in polymerisation had a dramatic effect on the catalyst activity. Thus, changing the polymerisation solvent form toluene to hexane boosted the activity of **33b** whilst maintaining its high selectivity. In addition, catalyst **33b** was used to investigate the epoxide substrate scope. Catalyst **33b** was highly active and selective for a range of PO derivatives (*e.g.* BO, EPC, AGE, PGE) and MA and produced perfectly alternating polyesters. The resultant polymers showed high molar masses ($M_n \geq 21$ kg mol$^{-1}$). Darensbourg *et al.* reported a Cr(III) salen catalyst (**33b**) for the ROCOP of various epoxides and bicyclic anhydrides.[103] They found that in the presence of onium salt (PPNX where X = Cl or $N_3$) co-catalysts, catalyst **33b** was an active and selective catalyst for ROCOP of a range of epoxides (PO, SO, CHO) and anhydrides (PA, CHE, CHA). When CHO was used as an epoxide, the activity order was CHA > PA > CHE, whilst the order of activity followed PO > CHO ≥ SO when PA was used as an anhydride. Kinetic studies of CHO/PA ROCOP using this catalyst were also carried out. They revealed that CHO ring opening was likely to be the rate determining step, whilst the insertion of PA into the metal alkoxide bond is a fast process.

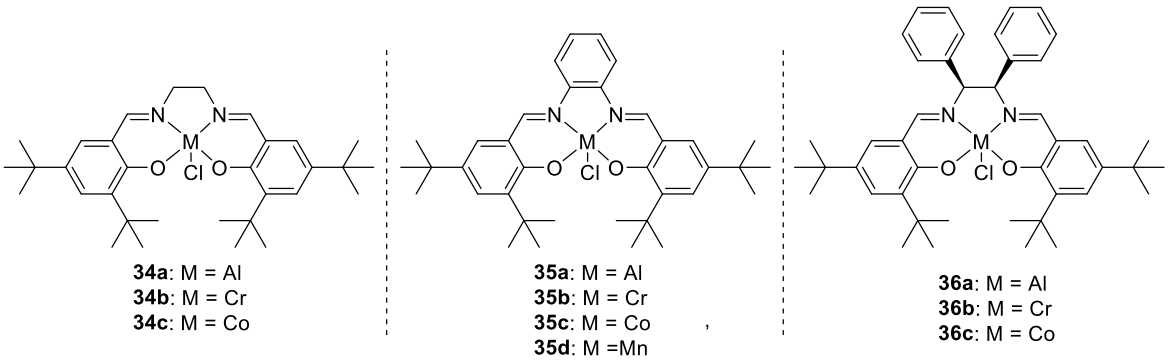



**Figure 1.18.** Structures of M(III) salen complexes (**34**–**36**).[98, 104-106]

Duchateau and co-workers presented a range of Al(III), Cr(III), and Co(III) salen complexes with different diamine backbones (**33**–**36**, Figures 1.17 and 1.18).[104] The influences of diamine backbone as well as metal centre were examined in CHO/SA ROCOP. All complexes were active and selective catalysts with DMAP as a co-catalyst. Using the catalyst alone resulted in the formation of polymers with low ester contents. Cr(III) complexes were the most active for each ligand type and using a phenylene backbone resulted in an increase in activity. Overall, catalyst **35b** was the most active of the series. The influence of co-catalyst type was also studied using complexes **33b** and **35b**. Among the reported co-catalysts (DMAP, N-methyllimidazole (N-Melem), 1,5,7-triazabicyclododecene (TBD), PPNCl), the highest activity was achieved when using PPNCl. In addition, they found that the amount of PPNCl used had an influence on the polymer molar masses but not catalyst activity, meaning that polymer molar masses decreased with an increasing PPNCl. Duchateau also showed that **35b**/DMAP was an active and selective catalyst for ROCOP of CHO and various bicyclic anhydrides, including CPA, CPrA, and PA.[98] The catalytic activity of **35b**/DMAP was higher than that of Cr(III) porphyrin catalyst **28c**. Duchateau also reported a range of M(III) salen complexes (**35a**–**35d**, Figure 1.18) as catalysts for LO/PA ROCOP.[105] Complexes **35a**–**35d**/DMAP were active and selective and produced highly alternating polyesters. The choice of metal centre greatly influenced activity and it followed Cr(III) ~ Al(III) > Co(III) ~ Mn(III). The addition of diol or di-acid as chain transfer agents resulted in the reduction of polymer molar masses and the narrowing of molar mass distributions. Coates and co-workers presented a range of Cr(III), Al(III), and CO(III) salen catalysts (**35a**–**35c**, Figure 1.18).[106] Complexes **35a**–**35c**/PPNCl binary systems were active and selective catalysts for PO and tricyclic anhydride, derived from terpene. The catalytic activity depended strongly on the metal centre and the activity order followed Cr(III) (**35b**) ~ Al(III) (**35a**) > Co(III) (**35c**). The best

performing Cr(III) catalyst **35b** was successful using a range of tricyclic anhydrides and in all cases, perfectly alternating polyesters were produced.

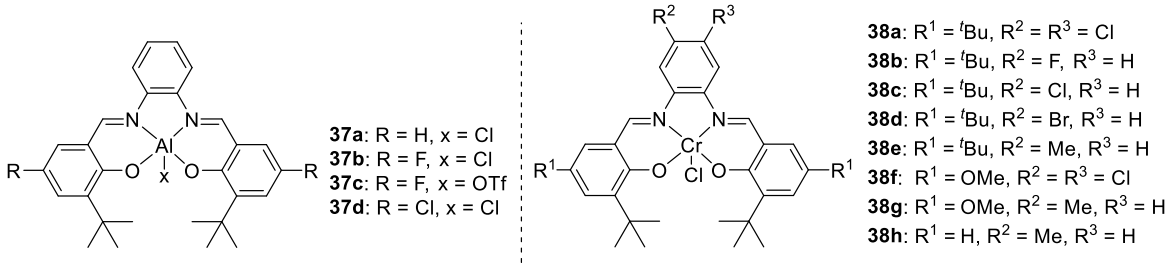


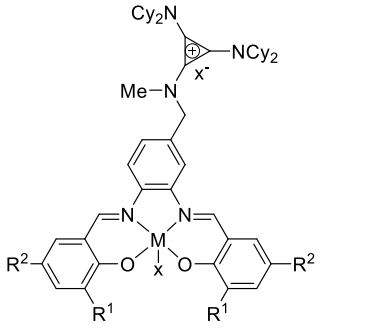

**Figure 1.19.** Structures of Al(III) (**37a**–**37d**) and Cr(III) (**38a**–**38h**) salen complexes.[107-110]

Coates and co-workers presented a range of Al(III) salen complexes with different *para*-phenoxide substituents (**35a** and **37a**–**37b**, Figures 1.18 and 1.19).[108] In the presence of PPNCl co-catalyst, all complexes were active and selective catalysts for ROCOP of PO and various tricyclic anhydrides. Although complex **35a**, bearing $^{t}$Bu para-phenoxide substituents showed the highest activity (TOF = 88 $h^{-1}$, [cat.]:[PPNCl]:[PO]:[NBA] = 1:0.9:500:100, 60 °C), it also suffered from side reactions including transesterification, and epimerisation, especially at the end of polymerisation. These reactions were attributed to cause an increase in molar mass distributions of the resultant polymers. Nonetheless, the introduction of an electron withdrawing group (EWG), F, onto the *para*-positions of phenoxide rings (complex **37b**) suppressed these side reactions and produced polymers with better dispersity controls. Coates and Kleij also showed that complexes **35a** and **37d** were active catalysts for CHO and a range of tricyclic anhydrides, in the presence of PPNCl as a co-catalyst.[107] Complexes **35a** and **37d**/PPNCl produced perfectly alternating polyesters from each combination and the resultant polymers showed very high $T_g$ values ($T_g$ = 124–184 °C). Again, complex **37d**, containing Cl EWG *para*-phenoxide substituents, showed some side reactions at the end of polymerisation. Recently, a salen Al(III) non-initiating catalyst (complex **37c**) formed by replacing Cl initiating group of complex **37b** with a triflate

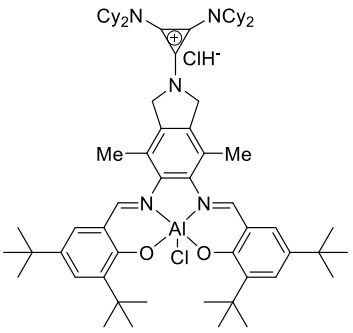
(OTf) co-ligand was presented by Coates and co-workers.[110] This non-initiating group was found to deliver an active and selective catalyst in the presence of $[PPN]_2$[1,3-adamantane dicarboxylate] ($[PPN]_2$[ADC]) as co-catalyst. Complex **37c**/($[PPN]_2$[ADC], under immortal polymerisation conditions, produced perfectly alternating polyesters with high molar masses and narrow *Đ* from ROCOP of PO and a range of tricyclic anhydrides. The polymerisation was proposed to occur *via* reversible-deactivation ROCOP. In addition, block polymers with predictable molar masses and narrow dispersities were prepared by sequential anhydride monomer additions.

Bester and co-workers presented a range of Cr(III) salen catalysts with different substituents on the phenylene diamine backbones and phenoxide rings (**38a**–**38h**, Figure 1.19).[109] All catalysts, in the presence of DMAP, were active and selective for CHO/PA ROCOP. Using catalyst alone resulted in a drastic decrease in activity and selectivity and polymers with low ester contents. The introduction of either F or Me groups on the phenylene backbones led to better activity. Conversely, the addition of OMe groups on phenoxide rings resulted in a reduced activity. The ROCOP of various epoxides (vCHO, SO, PGE, PO, BO, ECH) and PA were examined with complex **38h**/DMAP. In all cases, highly alternating polyesters were obtained.

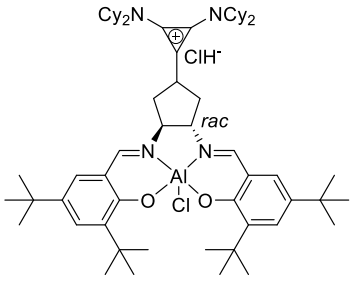
Very recently, Coates and co-workers presented a series of bifuncional M(III) and M(II) catalysts (**39**–**41**, Figure 1.20).[111] The co-catalysts were incorporated into the diamine linkers of metal salen complexes. All catalysts were active and highly selective for the ROCOP of PO and NBA, without needing any additional co-catalyst. Investigation of the ligand structure-activity relationships, using the Al complexes **39a**, **40**, and **41,** found that **39a** was most active. The reduction in activity of **40** was proposed to be due to its lower planarity, arising from twisted C=N moieties. The effect of the phenoxide substituents on the best performing Al(III) catalyst was examined (complexes **39b**–**39e**).



**39a**: M = Al, $R^1 = R^2 = {}^t$Bu, x = Cl
**39b**: M = Al, $R^1 = {}^t$Bu, $R^2$ = F, x = Cl
**39c**: M = Al, $R^1 = {}^t$Bu, $R^2$ = OMe, x = Cl
**39d**: M = Al, $R^1$ = Ad, $R^2 = {}^t$Bu, x = Cl
**39e**: M = Al, $R^1$ = Me, $R^2 = {}^t$Bu, x = Cl
**39f**: M = Cr, $R^1 = R^2 = {}^t$Bu, x = Cl
**39g**: M = Co, $R^1 = R^2 = {}^t$Bu, x= $OCOCH_3$
**39h**: M = Mn, $R^1 = R^2 = {}^t$Bu, x = Cl
**39i**: M = Fe, $R^1 = R^2 = {}^t$Bu, x = Cl
**39j**: M = Zn, $R^1 = R^2 = {}^t$Bu, x = Cl
**39k**: M = Cr, $R^1 = R^2 = {}^t$Bu, x = Cl
**39l**: $R^1$ = H, $R^2$ = Me, $R^3$ = H



**40**



**41**

**Figures 1.20.** Structures of bifunctional M(III) and M(II) salen complexes.[111]

The introduction of either F (complex **39b**) or OMe (complex **39c**) substituents on the *para*-position of phenoxide rings led to lower activity. Replacing *ortho* $^t$Bu groups of phenoxide rings with adamantane (Ad) (complex **39d**) or Me (complex **39e**) also decreased activity. The Lewis acidity of the metal centre also influenced activity. Al(III), Cr(III), and Co(III) complexes (**39a**, **39f**, and **39g**) showed higher activities than that of Mn(III), Fe(III), and Zn(II) complexes (**39h**–**39j**). Co(III) complex **39g** was the most active catalyst (TOF = 376 $h^{-1}$, [cat.]:[TCA]:[PO] = 1:400:2000, 60 °C) in the series. Complex **39a** also copolymerised a range of epoxides (PO, BO, CHO, EPB, $^t$BGE, AGE) and anhydrides (PA, DMPA, NBA, TMA). In all cases, complex **39a** produced perfectly alternating polyesters with moderate to high molar masses (5.5–23.4 kg $mol^{-1}$) and relatively narrow $Đ$ ($Đ \leq 1.24$). Kinetic studies of catalyst **39a** revealed a first order dependence on catalyst concentration and the catalytic activity of **39a** remained high at very low catalyst loading (0.025 mol %) unlike the binary system (salen Al(III) catalyst **35a** + PPNCl) where the activity drastically reduced with decrease catalyst loading.

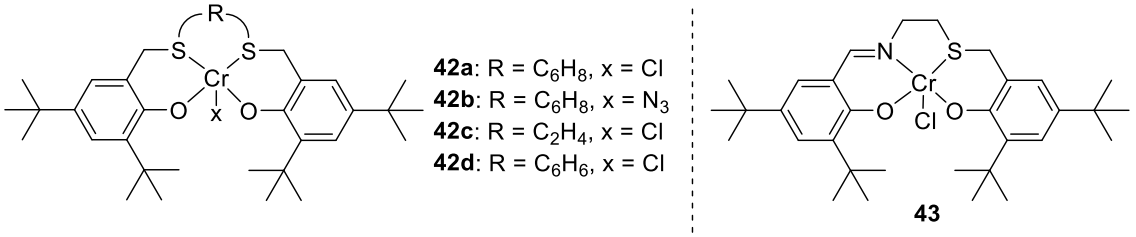
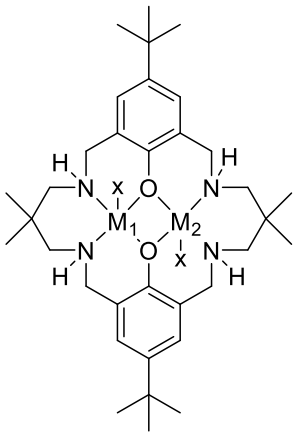



**Figure 1.21.** Structures of Cr(III) Schiff base complexes (**42** and **43**).[112, 113]

Given the promising catalytic activities and selectivities of the salen Cr(III) complexes, Liu and Li modified the ligand by replacing the two imine protons with sulfur atoms, giving four Cr(III) [OSSO] bisphenolate complexes (**42a**–**42d**, Figure 1.21).[112] It is worth noting that this ligand framework, coordinated to a range of transition metals and lanthanides, was brought to fame by Okuda and co-workers for lactone and stereoselective lactide ROP.[114, 115] A variety of ligand backbones, as well as co-catalysts, were symmetrically studied. All the complexes were active and selective for vCHO/PA ROCOP, in the presence of different types of co-catalysts triphenyl phosphine ($PPh_3$), 1,8-diazabicyclo (5,4,0)-undec-ene (DBU), DMAP, TBD, N-Melm. The co-catalysts influenced activity, with catalyst **42a**/DMAP being the most active. The diamine backbone also influenced catalyst activity. Catalyst **42a**, containing a cyclohexylene diamine linker, exhibited the highest activity followed by **42c** possessing ethylene backbone and **42d** with a phenylene bridge. The observed activity order was in contrast to the salen Cr(III) system where the complexes with phenylene backbones were the most active. Catalyst **42a**/DMAP copolymerised a range of epoxides (*i.e.* SO, ECH, CHO, AGE, $^t$BGE) and PA to give perfectly alternating polyesters. Liu and Theato also presented a Cr(III) [ONSO] Schiff base complex (**43**, Figure 1.21) which was active and highly selective for CHO/NBA ROCOP with different co-catalysts.[113] As expected, the co-catalysts affected activity, with complex **43**/PPNCl being the most active. The anhydride isomer type also affected activity. When *endo*-NBA was used a lower polymerisation rate was observed. Conversely, a higher rate was seen when *exo*-NBA was utilised. The

production of *cis*-(*endo*, *endo*), c*is*-(*exo*, *exo*), or *trans*-(*endo*, *exo*) polyesters could be achieved by adjusting the polymerisation conditions.

### 1.4.2.3. Dinuclear complexes




**44a**: $M_1 = M_2 = Mg$, $x = OCOCH_3$
**44b**: $M_1 = M_2 = Mg$, $x = Br$
**44c**: $M_1 = M_2 = Zn$, $x = OCOCH_3$
**44d**: $M_1 = M_2 = Zn$, $x = Br$
**44e**: $M_1 = Mg$, $M_2 = Zn$, $x = Br$

**Figure 1.22.** Structures of homodinuclear and heterodinuclear Zn(II) and Mg(II) complexes.[116-118]

In 2015, Williams and co-workers presented a series of homodinuclear Mg(II) and Zn(II) complexes (**44a** and **44c**, Figure 1.22) as catalysts for CHO/PA ROCOP without the need for co-catalyst.[116] In neat CHO, both catalysts were active and highly selective for the production of alternating polyesters. When operating polymerisations in toluene, **44a** and **44c** showed reduced activity and selectivity, polyesters with some ether contents (around 20 % ether linkages) was produced. The choice of metal centre played a crucial in controlling catalyst activity. The di Mg(II) complex **44a** showed about four times greater activity than that of di Zn(II) analogue **44c** (TOF = 97 $h^{-1}$ for **44a** and TOF = 24 $h^{-1}$ for **44b**, [cat.]:[PA]:[CHO] = 1:100:800, 100 °C). Williams and Meier also showed that homodinuclear Mg(II) **44a** copolymerised bio-derived epoxide CHDO and PA to give unsaturated polyesters.[118] Using the homodinuclear Zn(II) complex **44c** under identical polymerisation conditions showed no activity. The Williams group presented a range of homodinuclear Mg(II) and Zn(II) and heterodinuclear Mg(II)/Zn(II) complexes for epoxide/$CO_2$ ROCOP (**44b**, **44d**, and **44e**, Figure 1.22).[117] Theses catalysts were active at 1

bar $CO_2$, with heterodinuclear complex **44e** showing greater activity than their homodinuclear Mg(II) and Zn(II) congeners or than an equimolar mixture of both homodinuclear catalysts – *i.e.* it was synergic. A similar synergic polymerisation activity trend was observed for CHO/PA ROCOP, meaning heterodinuclear catalyst **44e** showed 20 times greater activity than homodinuclear Mg(II) complex (**44b**) and was 10 times faster than homodinuclear Zn(II) (**44d**). Complex **44e** also showed 40 times higher activity than an equimolar mixture of **44b** and **44d**.

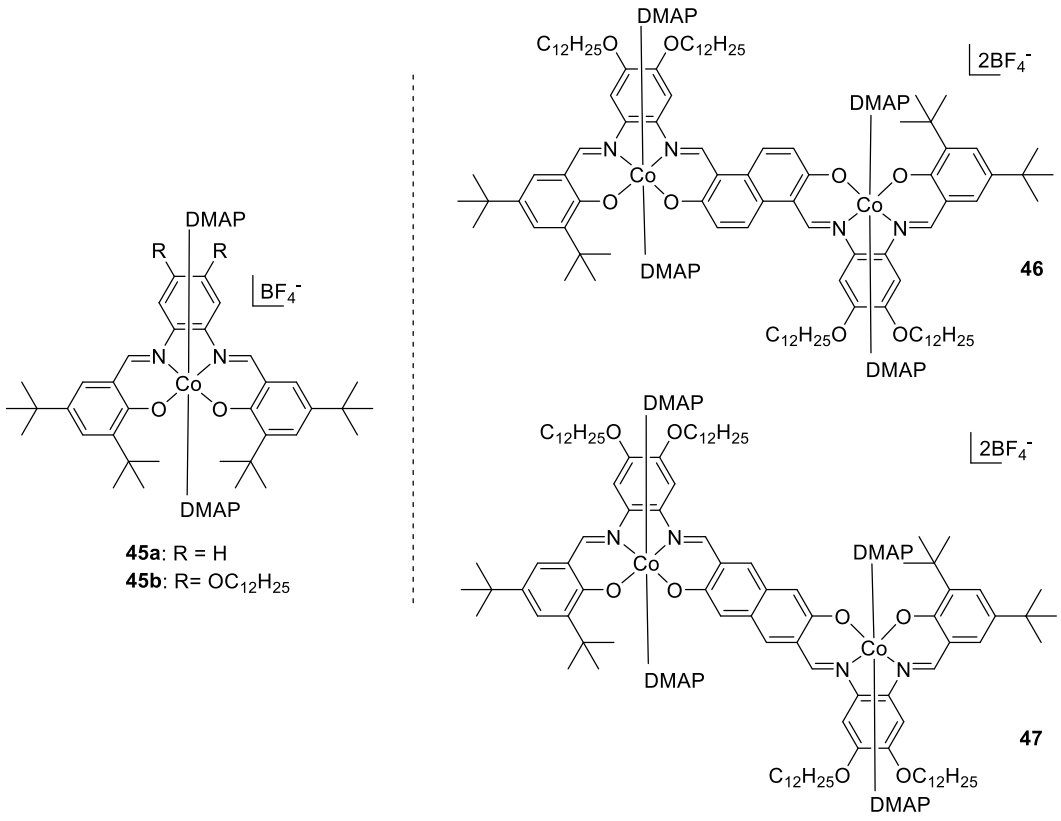



**Figure 1.23.** Structures of mononuclear and dinuclear cationic Co(III) salen complexes.[119]

Nozaki and Houjou reported mononuclear (**45**) and dinuclear (**46** and **47**) cationic Co(III) complexes (Figure 1.23) which were active and selective for CHO/PA ROCOP.[119] Under identical polymerisation conditions, cationic complex 4**5a** was both more active and selective than the neutral Co(III) salen/DMAP system (TOF = 282 $h^{-1}$ for **45a** and TOF = 203 $h^{-1}$ for CO(III) salen/DMAP, [cat.]:[PA]:[CHO] = 1:500:500, 100 °C). Bimetallic

complex **46** showed further improvement in catalytic activity than the mononuclear analogue (**45b**) (TOF = 274 $h^{-1}$ for **46** *vs.* TOF = 266 $h^{-1}$ for **45b**, [cat.]:[PA]:[CHO] = 1:500:500, 100 °C). Conversely, complex **47** showed lower activity than that of **45b**. This could be due to the lack of metal cooperation/interaction arising from the greater Co-Co distance. Bimetallic complex **46** also performed well under more dilute polymerisation conditions (0.025 mol %) and again showed higher catalytic activity than **45b**. Overall, complex **46** was the most active catalyst, showing the TOF of 303 $h^{-1}$ ([cat.]:[PA]:[CHO] = 1:500:4000, 100 °C).

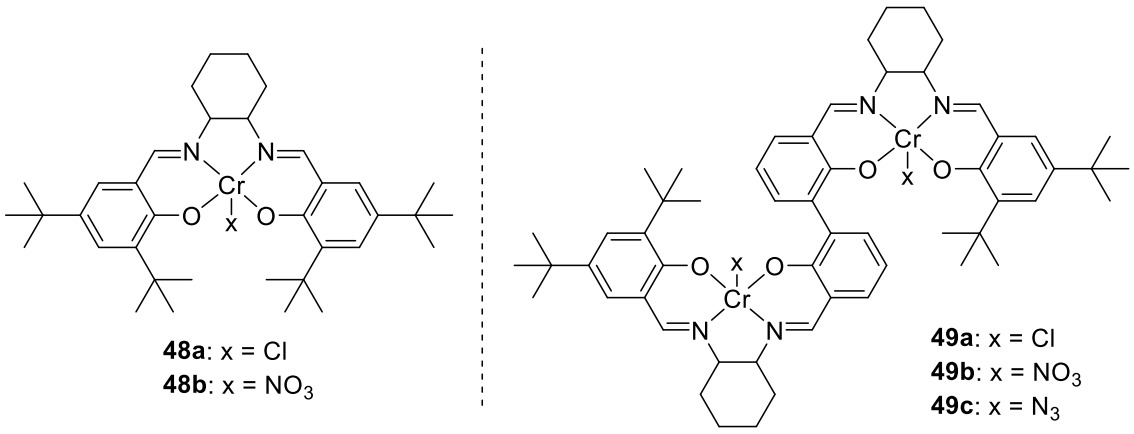



**Figure 1.24.** Structures of mononuclear (**48**) and dinuclear (**49**) Cr(III) salen complexes.[120]

Lu and Liu presented a range of mononuclear and dinuclear Cr(III) salen complexes (**48** and **49**, Figure 1.24).[120] In the presence of an onium salt (PPNX where X = Cl, $NO_3$, $N_3$) co-catalysts, all complexes were active for CHO/SA, with dinuclear complexes showing higher activities than the mononuclear analogues. The resultant polyesters exhibited highly alternating structures (~ 80 % ester linkages) and the selectivity was improved by manipulating the conditions. Dinuclear Cr(II) complex **49b**/$PPNNO_3$ copolymerised CPO and various anhydrides, including SA, DGA, GA, PA, and MA. The resultant polyesters showed different degrees of ester contents. By using SA, GA, and PA, perfectly alternating polyesters were produced whilst highly alternating polyesters were prepared with DGA. The

polymer with a low ester content was obtained when MA was used (15 % ester linkages). Complex **49b**/$PPNNO_3$ could also copolymerise SA with a variety of epoxides, including PO, SO, COPO, vCHO, CBO, CDO. In all cases, perfectly alternating polyesters were obtained.

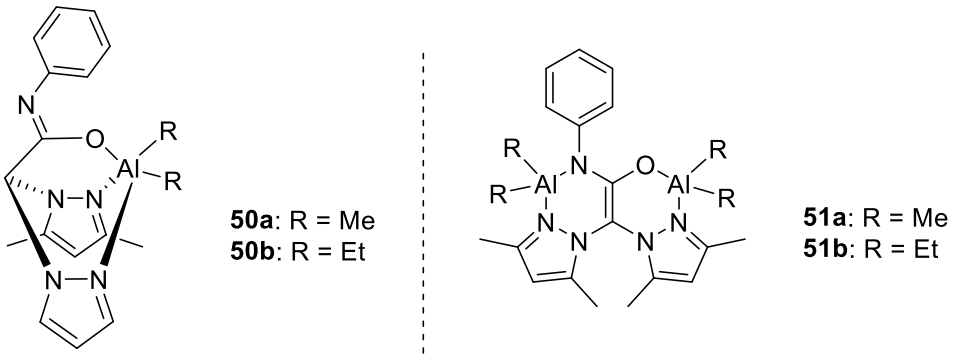



**Figure 1.25.** Structures of mononuclear (**50**) and dinuclear (**51**) Al(III) scorpionate complexes.[121]

In 2018, Castro-Osma, Otero, and Lara-Sanchez reported scorpionate Al(III) complexes (**50** and **51**, Figure 1.25).[121] **50** and **51**/tetrabutylammonium bromine (TBAB) systems were active and selective for CHO/SA ROCOP, with dinuclear complex **51** showing slightly higher activity than the mononuclear analogue (**50**). The resultant polyesters exhibited high ester contents (85–91 % ester linkages). Using the metal catalyst alone led to only a low percentages of ester linkages (43–52 % ester linkages). Complex **51b**/TBAB copolymerised SA with CHO and LO. ROCOP of CHO and SA, MA, PA were also achieved by **51b**/TBAB. In all cases, the resultant polymers showed high ester contents.

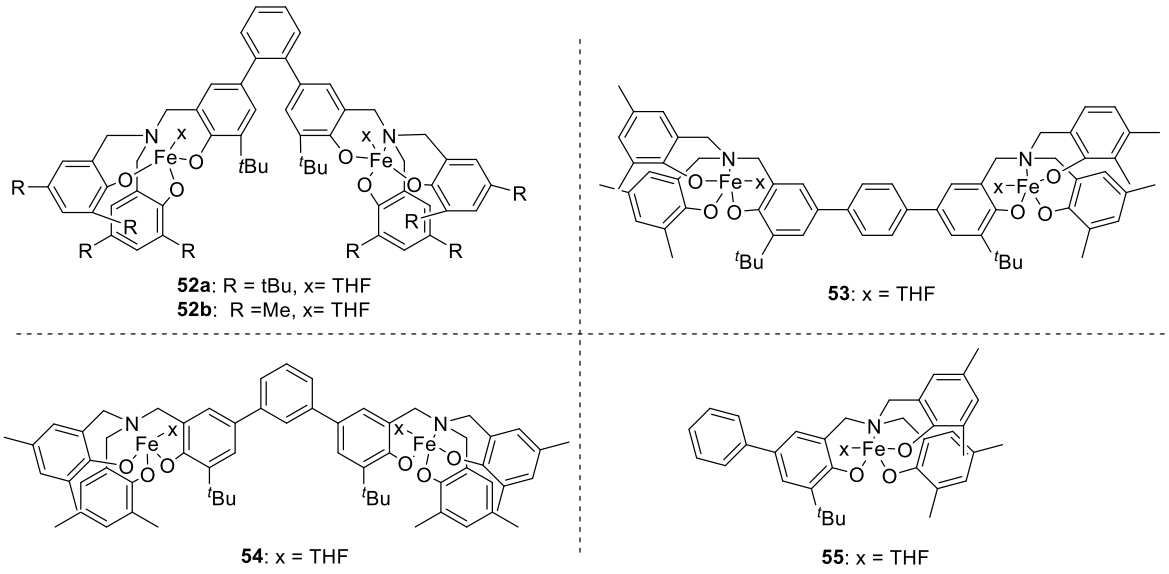



**Figure 1.26.** Structures of dinuclear (**52**–**54**) and mononuclear (**55**) Fe(III) amino trisphenolate complexes.[122]

Jiang and co-workers presented a range of mononuclear and dinuclear amino trisphenolate Fe(III) complexes (**52**–**55**, Figure 1.26).[122] The dinuclear complexes were connected through a phenylene bridge at different positions: *ortho*- (1,2) (complex **52**), *meta*- (1,3) (complex **54**), and *para*- (1,4) (complex **53**). The catalytic activities toward CHO/$CO_2$ and CHO/PA ROCOP were studied in the presence of PPNCl. Although binuclear complexes showed higher activity than mononuclear analogues for CHO/$CO_2$ ROCOP, similar activities were observed in CHO/PA ROCOP. In toluene, the **52b**/PPNCl showed the highest activity with a TOF of 165 $h^{-1}$ ([cat.]:[PPNCl]:[PA]:[CHO] = 1:1:500:550, 100 °C) which was the same as its mononuclear congener. The activity reduced with an increase in the Fe–Fe bond distance, **54**/PPNCl showed the second highest activity whilst **53**/PPNCl was the least active (activity order follows **52b** > **54** > **53**). The activity of the best performing binary catalysts, **52b**/PPNCl and **55**/PPNCl, were improved by operating in neat CHO and both complexes showed good values for TOF of 1200 $h^{-1}$ under these conditions ([cat.]:[PPNCl]:[PA]:[CHO] = 1:1:500:2500, 100 °C).

### 1.4.2.4. Organocatalysts

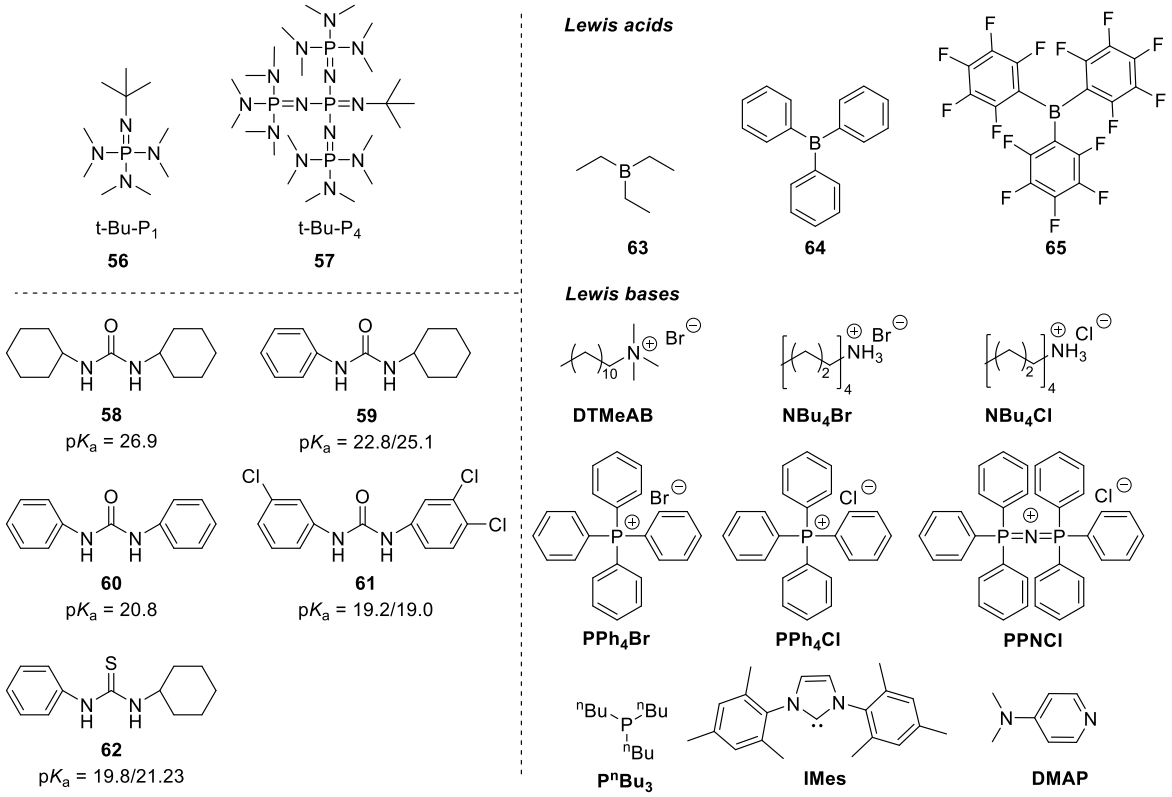



**Figure 1.27.** Structures of organocatalysts and Lewis acid and bases described in this section.[123-128]

Zhao and co-workers presented the use of commercially available phosphazene base *t*-Bu-$P_1$ (**56**) and *t*-Bu-$P_4$ (**57**) (Figure 1.27) in the presence of an alcohol initiator for EO/PA ROCOP.[123] Phosphazene base **57,** in the presence of BnOH, produced perfectly alternating polyester from EO and PA, with a broad molar mass distribution caused by transesterification side reactions. Nonetheless, under identical conditions, *t*-Bu-$P_1$ (**56**)/BnOH led to the formation of perfectly alternating polymers with predictable molar masses and narrow $Đ$ ($Đ \leq 1.08$). The homopolymerisation of BO over a prolonged period (24 h) led to incomplete consumption of PA when **56** was used. The difference in pKa is responsible for the high polymerisation control of the phosphazene base **56**. Polymerisations were proposed to occur *via* a self-buffering reaction in which the catalyst alternatively acts as an activator for carboxyls (anhydride) and deactivator for hydroxyls (epoxide). 4-Armed star polyesters can be achieved using **56** and pentaerythritol initiator. Block copolymers

between poly(BO-*alt*-PA) and poly(PO-*alt*-PA) or PLLA can also be synthesised by sequential monomer addition of epoxide, and *L*-LA, respectively. Recently, the versatility of the phosphazene base **56** was studied by the same research group.[127] They revealed that in the presence of an alcohol initiator, catalyst **56** copolymerised PA with a wide range of epoxides, including PO, BO, SO, $^{t}$BGE, AGE, CHO, vCHO, and LO. Perfectly alternating polyesters were obtained in all cases, with predictable molar masses and relatively narrow $Đ$ ($Đ \leq 1.15$). Again, block copolymers can be prepared by sequential addition of epoxide monomers. Conversely, mixtures of two different epoxides and PA in a one-pot polymerisation resulted in the formation of statistical copolymers.

Very recently, Xiao and Meng used commercially available thioureas (**58**–**52**, Figure 1.27) and various organic bases as binary catalysts for ROCOP of epoxide and anhydride.[128] First the structure-activity relationships of the binary catalysts (**58**–**52**/PPNCl) in CHO/PA ROCOP were examined. The thioureas with high basicity paired with a quaternary onium salt showed highest activity, such that **58**/PPNCl was the most active (TOF = 456 $h^{-1}$, [cat.]:[PPNCl]:[PA]:[CHO] = 1:1:100:200, 110 °C). The catalytic activity order followed **58**/PPNCl > **59**/PPNCl > **62**/PPNCl > **60**/PPNCl > **61**/PPNCl. Perfectly alternating polyesters with narrow dispersities were produced in all cases. NMR analysis of **58**/PPNCl suggested that the thiourea acts as a bifunctional catalyst, activating both the initiating chain end and monomer. The choice of organic base influences activity, with activity increasing with base nucleophilicity.

Zhong and co-workers reported a range of organic Lewis acid-base pairs as catalysts for ROCOP of epoxide and anhydride.[124] Organoboranes with different degrees of Lewis acidity and steric hindrance were used (**63**–**65**, Figure 1.27), whilst onium salts with bromide and chloride anions were Lewis bases. **63**/DTMeAB, **64**/DTMeAB, and **65**/DTMeAB were active for PO/MA ROCOP, in the presence of 2 mol % of water. Under identical conditions,

using Lewis acid alone yielded no polymer. Using Lewis base DTMeAB showed some degree of polymerisation, but it was lower than that of Lewis acid-base pairs. The catalyst activity and selectivity depended strongly on Lewis acidity and steric hindrance of the Lewis acid. Catalyst activity decreased with an increase in Lewis acidity and steric hindrance, following the trend **63** > **64** > **65**. Catalysts **63**/DTMeAB and **64**/DTMeAB produced perfectly alternating polyesters, whilst polymer with low ester content (3 % ester linkages) was obtained from **65**/DTeAB. Using the best performing Lewis acid **63** with various Lewis bases resulted in catalysts with different activities. In general Lewis bases containing the bromide anion were more active than those with a chloride anion. The activity order follows **63**/$PPh_4Br$ > **63**/$PPh_4Cl$ > **63**/$NBu_4Br$ > **63**/$NBu_4Cl$. **63**/DTMeAB produced perfectly alternating polyesters from a range of epoxides (PO, PGE, ECH) and anhydrides (SA, DGA, MA). Organoborane **63**–**65**/organic base combinations were active for PO and NBA ROCOP.[125] **63**/PPNCl binary catalyst showed the highest activity and a reduction of activity was observed when replacing **63** with the higher Lewis acidity borane **64**. Perfectly alternating polyesters were produced in both cases. Using the highest Lewis acidity borane **65**/PPNCl resulted in a complete loss of catalyst selectivity and only polyether was obtained. Once again, PPNCl was the most active and selective base pair for **63** compared against alternatives (*t*-Bu-$P_1$, $P^nBu_3$, IMes, DMAP). Unsurprisingly, varying the molar ratios of PPNCl to triethylborane had a great influence on catalyst activity and selectivity. Reducing the ratio of PPNCl:**63** from 1:1 to 1:2 reduced activity and selectivity, whilst using PPNCl:**63** = 2:1 increased activity but decreased the selectivity. **63**/PPNCl produced perfectly alternating polymers from NBA and a wide variety of epoxides, including PO, BO, HO, SO, ECH, AGE, PGE, FGE, BnGE. Chakraborty and co-workers also showed that **63**/PPNCl was active and highly selective for ROCOP of PA and various epoxides, including CHO, BO, $^t$BGE.[126] Perfectly alternating polyesters were obtained in all cases.

### 1.4.2.5. Evaluation of highly active catalysts for epoxide/anhydride ROCOP

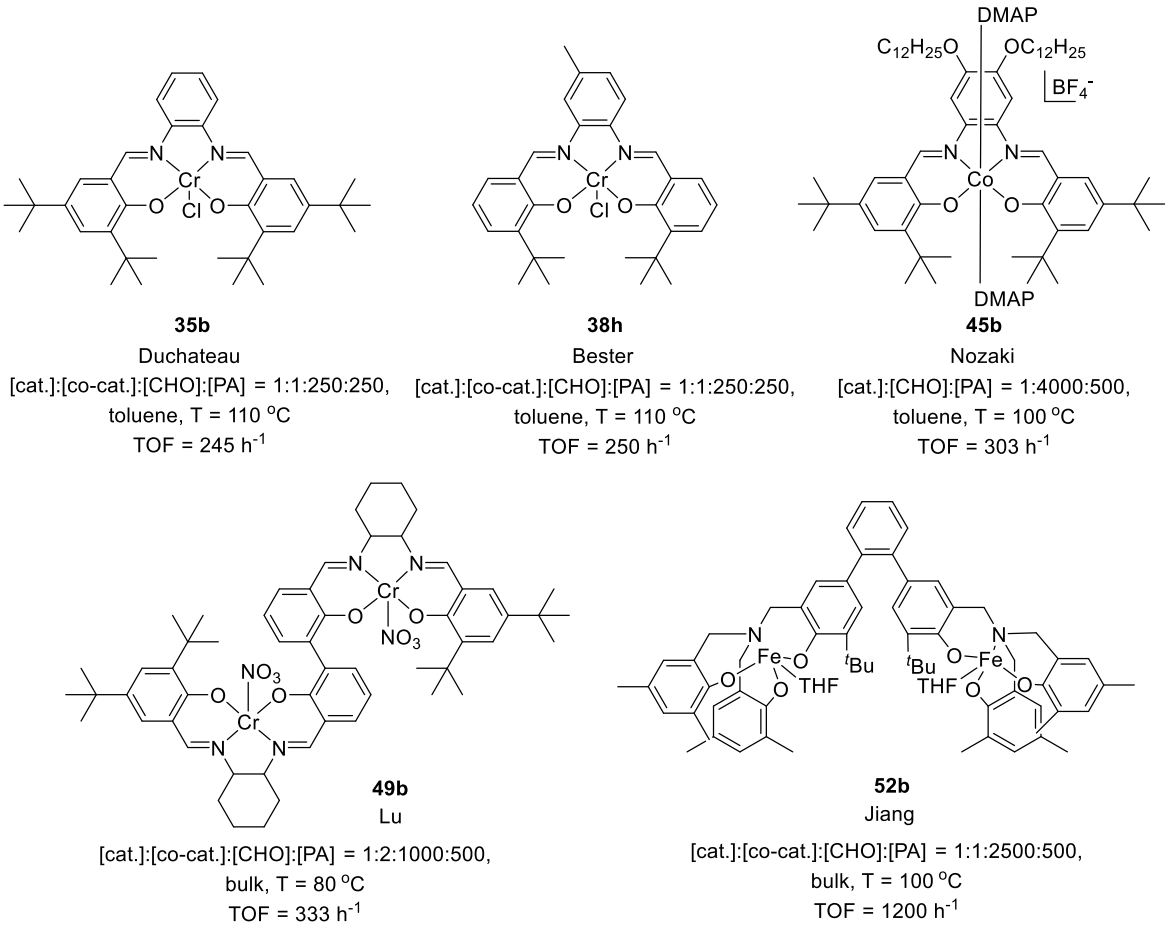



**Figure 1.28.** Structures of selected metal complexes showing high activity in CHO/PA ROCOP.[104, 109, 111, 119, 120, 122]

To date, catalysts with a variety of metal centres and ligand scaffolds have been reported for epoxide/anhydride ROCOP (see above). Each catalyst was tested under a different set of polymerisation conditions. This clearly causes difficulties when comparing catalyst performances. In addition, a range of different epoxides and anhydrides were used. This will show also a dramatic effect on the catalyst activities and selectivities. In order to draw a proper comparison between these catalysts, only those showing high selectivity for ester linkages (> 95 % selectivity) will be considered and turn over frequencies are compared under conditions as close as possible to those used in this thesis ([cat.]:[anhydride]:[epoxide] = 1:100:125, [anhydride] = 5 M, T = 80 °C). Additionally, CHO and PO will be used as

epoxide models and PA will be used as a representative anhydride for comparison since they are the most widely studied substrates.

For CHO/PA ROCOP, a range of catalysts were highly active under various conditions. For solution polymerisations, Cr(III) salen catalysts, reported by Duchateau and co-workers (**35b**) and Bester and co-workers (**38h**), are at the upper end of performances (Figure 1.28).[104, 109] Both catalysts showed impressive TOFs of 245 $h^{-1}$ and 250 $h^{-1}$ for **35b** and **38h**, respectively ([cat.]:[co-catalyst]:[CHO]:[PA] = 1:1:250:250, T = 110 °C). Under solvent free conditions most catalysts possessed higher activities (since most rates are first order in epoxide concentration). Neat conditions also allow for a higher loading of PA to be used. Under similar solvent free conditions, there are three classes of high performance catalysts. The dinuclear Fe(III) amino phenolate complex **52b** (reported by Jiang and co-workers)[122], the cationic Co(III) salen complex **45b** (reported by Nozaki and co-workers) and the dinuclear Cr(III) salen complex (**49b**) (reported by Lu and co-workers) (Figure 1.28).[119, 120] For dinuclear Fe(III) ammino phenolate complex **52b**, a TOF of 1200 $h^{-1}$ was observed ([cat.]:[co-catalyst]:[CHO]:[PA] = 1:1:2500:500, T = 100 °C).[122] Cationic Co(III) salen complex **45b**, also exhibited an impressive TOF of 303 $h^{-1}$ without the need for co-catalyst ([cat.]:[CHO]:[PA] = 1:4000:500, T = 100 °C).[119] A similar TOF was also feasible for the dinuclear Cr(III) salen complex **49b** (TOF = 333 $h^{-1}$, [cat.]:[co-catalyst]:[CHO]]:[PA] = 1:2:1000:500, T = 80 °C).[120]

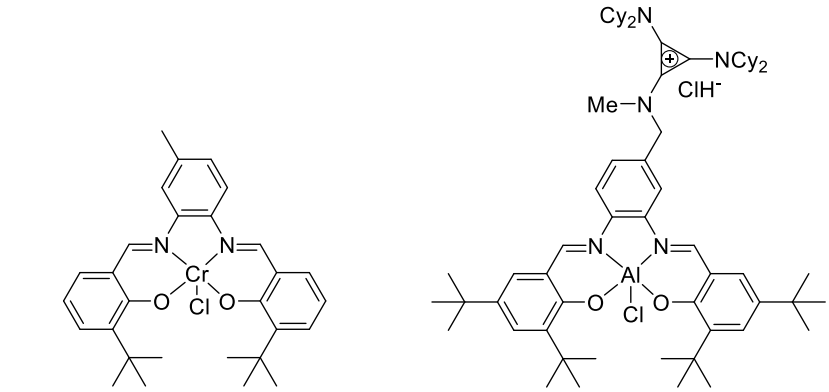



**Figure 1.29.** Structures of selected metal complexes showing high activity for PO/PA ROCOP.[109, 111]

In the case of PO/PA ROCOP, only a handful of catalysts have been studied. More diverse polymerisation conditions compared to CHO/PA ROCOP were presented. Among the reported catalysts, Cr(III) salen catalyst **38h**, reported by Bester and co-workers, is at the forefront (Figure 1.29). Cr(III) salen complex **38h** shows a TOF of 250 $h^{-1}$ ([cat.]:[co-catalyst]:[PO]:[PA] = 1:1:250:250, T = 110 °C).[109] Under bulk polymerisation conditions, Al(III) salen complex **39a**, reported by Coates and co-workers is at the upper end (Figure 1.29). A TOF of 100 $h^{-1}$ was achieved by complex **39a** ([cat.]:[PO]:[PA] = 1:2000:400, T = 60 °C).[111] It is worth mentioning that the bulk polymerisations are usually performed at lower temperatures due to the low boiling point of PO.

### 1.5. Aims and objectives

This thesis aims to explore the chemistry of novel phosphasalen group 4 and 13 complexes as well as industry relevant Sn(II) complexes as polymerisation catalysts for the production of a variety of polyesters and their copolymers. The use of target copolymers as a toughening

agent for the well-known biodegradable polymer, polylactide, will also be examined. The general objectives of this thesis can be summarised as follow:

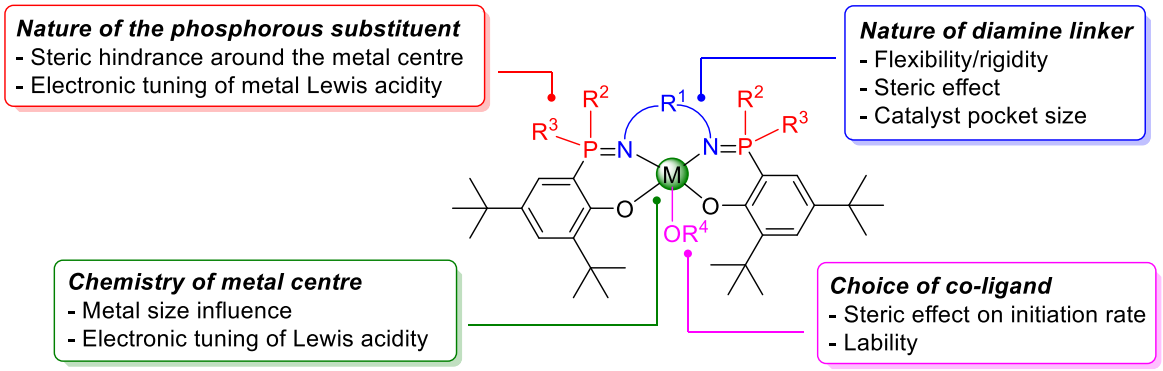



**Figure 1.30.** Structures of proposed phosphasalen complexes.

Given the success of phosphasalen In(III) catalysts for $CO_2$/epoxide ROCOP and the very high rates and iso-selectivity of In(III) and Ln(III) catalysts for LA ROP [60, 72, 73, 87], this ligand class needs further exploration in catalysis. Firstly, it is important to establish the generality of these ligands in catalysis. To do this their coordination chemistry will be explored with metal centres with precedent for Lewis acidity, labile alkoxide and carboxylate bonds – since these features underpin both LA ROP and epoxide/anhydride ROCOP. Therefore, the first target is to understand the coordination chemistry of the phosphasalen ligands with Group 4 and Group 13 metals, specifically In(III) (Figure 1.30). Group 4 and 13 metal catalysts would be attractive based on their elemental abundance, cost, and lack of colour. There is also good precedent for their use at scale in industrial polymerisations. In terms of the phosphasalen ligand targets, studies need to benchmark against previous successes and so a ligand featuring diphenyl phosphorus substituents and an ethylene diamine backbone is targeted.[60] After that, changes to both the diamine backbone and the phosphorus substituents will be explored to understand the impact on coordination chemistry (both in solid and solution state) and on catalysis.

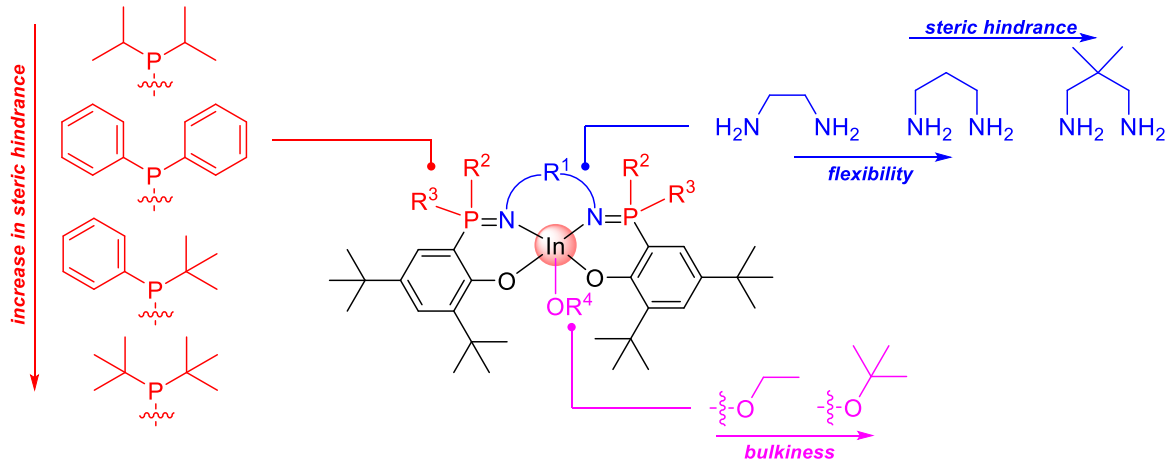



**Figure 1.31.** Proposed structures of In(III) phosphsalen complexes.

For lactone ROP, the goal is to prepare highly active and iso-selective catalysts. Combining both features into one catalyst requires careful ligand and metal selection (Figure 1.31). To help understand the parameters underpinning the performances, a series of phosphasalen In(III) complexes will be explored using the ancillary ligands proposed above. The structure-activity and -selectivity relationships will be explored using both an understanding of ground state structure, chemical kinetics, and attempts to isolate catalytic intermediates.

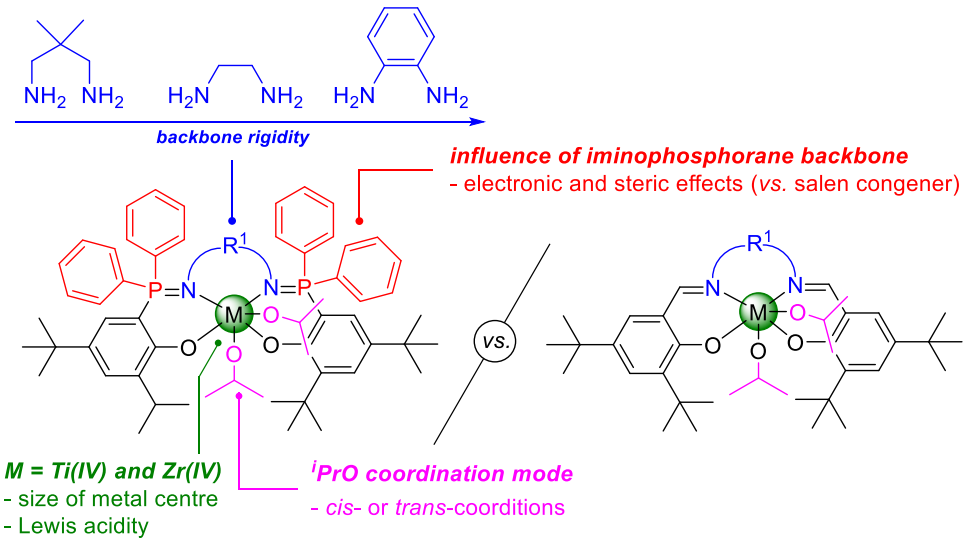



**Figure 1.32**. Proposed phosphasalen and salen group IV complexes.

For epoxide/anhydride ROCOP, a range of catalysts are already known but there is still a generally ill-defined understanding of how to design better catalysts – particularly how to

avoid salt systems featuring catalyst + co-catalysts or Lewis acid + base systems. These ion pair catalysts should be replaced since they generally fail at applicable loadings (due to obvious entropy limitations) and because the salts are expensive and corrosive. Therefore, our goal is to design colourless, active, and selective catalysts using Group IV metal centres (Figure 1.32). These complexes are also designed to test the *cis*-mononuclear mechanistic hypothesis and to understand how the ligand substituents affect the coordination geometry.

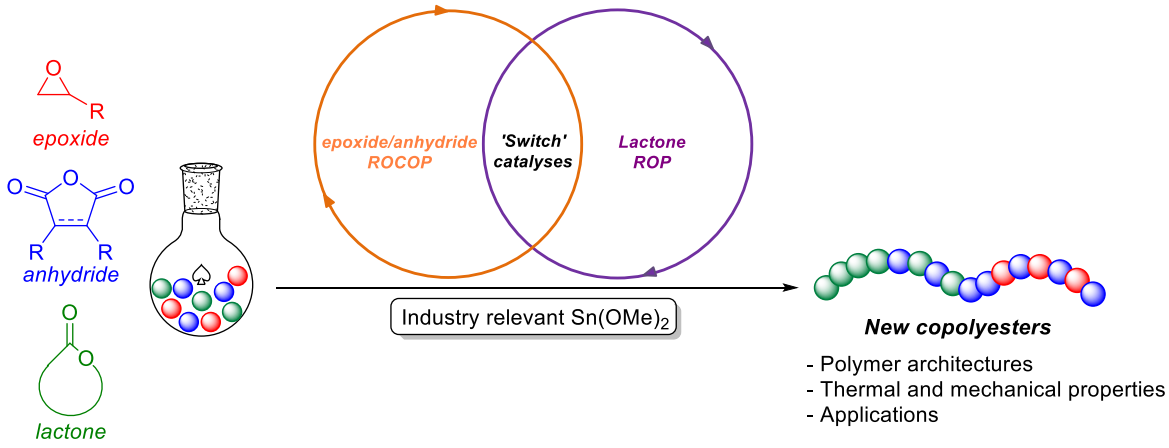



**Figure 1.33.** One-pot polymerisation access new copolyesters.

A final target is to investigate the use of an industrially applied Sn(II) catalyst system for epoxide/anhydride ROCOP (Figure 1.33). Tin alkoxides are used today in large-scale, industrial lactide polymerisation.[7] It is not yet reported how they might perform in epoxide/anhydride ROCOP or in switch catalyses combining lactone ROP and epoxide/anhydride ROCOP. It is important to understand whether the same catalysts and reactor types could be used to deliver alternating polyesters and copolyesters using these alternate monomers. A goal of this thesis is to evaluate the performance of tin methoxide and to assess the polyester formed. Another aim is to understand the composition of switch catalysis products and to assess their properties.

## 1.6. References


(1) Coates, G. W.; Getzler, Y. D. Y. L., Chemical recycling to monomer for an ideal, circular polymer economy. *Nat. Rev. Mater.* **2020,** *5*, 501–516.

(2) https://www.statista.com/statistics/282732/global-production-of-plastics-since-1950/ (accessed 29 June 2020).

(3) Geyer, R.; Jambeck, J. R.; Law, K. L., Production, use, and fate of all plastics ever made. *Sci. Adv.* **2017,** *3* (7), e1700782.

(4) Zhu, Y.; Romain, C.; Williams, C. K., Sustainable polymers from renewable resources. *Nature* **2016,** *540* (7633), 354362.

(5) Woodard, L. N.; Grunlan, M. A., Hydrolytic Degradation and Erosion of Polyester Biomaterials. *ACS Macro Lett.* **2018,** *7* (8), 976–982.

(6) Auras, R.; Harte, B.; Selke, S., An overview of polylactides as packaging materials. *Macromol. biosci.* **2004,** *4* (9), 835–864.

(7) Drumright, R. E.; Gruber, P. R.; Henton, D. E., Polylactic Acid Technology. *Adv. Mater.* **2000,** *12* (23), 1841–1846.

(8) Robert, C.; de Montigny, F.; Thomas, C. M., Tandem synthesis of alternating polyesters from renewable resources. *Nat. Commun.* **2011,** *2* (1), 586.

(9) Albertsson, A.-C.; Varma, I. K., Recent Developments in Ring Opening Polymerization of Lactones for Biomedical Applications. *Biomacromolecules* **2003,** *4* (6), 1466–1486.

(10) Hillmyer, M. A.; Tolman, W. B., Aliphatic Polyester Block Polymers: Renewable, Degradable, and Sustainable. *Acc. Chem. Res.* **2014,** *47* (8), 2390–2396.

(11) Thermodynamics and Kinetics of Ring-Opening Polymerization. In *Handbook of Ring-Opening Polymerization*, pp 1–51.

(12) Hong, M.; Chen, E. Y. X., Completely recyclable biopolymers with linear and cyclic topologies via ring-opening polymerization of γ-butyrolactone. *Nat. Chem.* **2016,** *8* (1), 42–49.

(13) Song, Q.; Zhao, J.; Zhang, G.; Peruch, F.; Carlotti, S., Ring-opening (co)polymerization of γ-butyrolactone: a review. *Polym. J.* **2020,** *52* (1), 3–11.

(14) Paul, S.; Zhu, Y.; Romain, C.; Brooks, R.; Saini, P. K.; Williams, C. K., Ring-opening copolymerization (ROCOP): synthesis and properties of polyesters and polycarbonates. *Chem. Commun.* **2015,** *51* (30), 6459–6479.

(15) Nijhuis, T. A.; Makkee, M.; Moulijn, J. A.; Weckhuysen, B. M., The Production of Propene Oxide: Catalytic Processes and Recent Developments. *Ind. Eng. Chem. Res.* **2006,** *45* (10), 3447–3459.

(16) Mahmoud, E.; Watson, D. A.; Lobo, R. F., Renewable production of phthalic anhydride from biomass-derived furan and maleic anhydride. *Green Chem.* **2014,** *16* (1), 167–175.

(17) Stößer, T.; Mulryan, D.; Williams, C. K., Switch Catalysis To Deliver Multi-Block Polyesters from Mixtures of Propene Oxide, Lactide, and Phthalic Anhydride. *Angew. Chem. Int. Ed.* **2018,** *57* (51), 16893–16897.

(18) Madhavan Nampoothiri, K.; Nair, N. R.; John, R. P., An overview of the recent developments in polylactide (PLA) research. *Bioresour. Technol.* **2010,** *101* (22), 8493–8501.

(19) Datta, R.; Henry, M., Lactic acid: recent advances in products, processes and technologies — a review. *J. Chem. Technol. Biotechnol.* **2006,** *81* (7), 1119–1129.

(20) Castro-Aguirre, E.; Iñiguez-Franco, F.; Samsudin, H.; Fang, X.; Auras, R., Poly(lactic acid)—Mass production, processing, industrial applications, and end of life. *Adv. Drug Deliv. Rev.* **2016,** *107*, 333–366.

(21) Mehta, R.; Kumar, V.; Bhunia, H.; Upadhyay, S. N., Synthesis of Poly(Lactic Acid): A Review. *J. Macromol. Sci. C.* **2005,** *45* (4), 325–349.

(22) Gupta, A. P.; Kumar, V., New emerging trends in synthetic biodegradable polymers – Polylactide: A critique. *Eur. Polym. J.* **2007**, 4053–4074.

(23) Carothers, W. H.; Dorough, G. L.; Natta, F. J. v., Studies of polymerization and ring formation. x. the reversible polymerization of six-membered cyclic esters. *J. Am. Chem. Soc.* **1932,** *54* (2), 761–772.

(24) Thomas, C. M., Stereocontrolled ring-opening polymerization of cyclic esters: synthesis of new polyester microstructures. *Chem. Soc. Rev.* **2010,** *39* (1), 165–173.

(25) Hu, Y.; Daoud, W. A.; Cheuk, K. K. L.; Lin, C. S. K., Newly Developed Techniques on Polycondensation, Ring-Opening Polymerization and Polymer Modification: Focus on Poly(Lactic Acid). *Materials.* **2016,** *9* (3).

(26) Dechy-Cabaret, O.; Martin-Vaca, B.; Bourissou, D., Controlled Ring-Opening Polymerization of Lactide and Glycolide. *Chem. Rev.* **2004,** *104* (12), 6147–6176.

(27) Kamber, N. E.; Jeong, W.; Waymouth, R. M.; Pratt, R. C.; Lohmeijer, B. G. G.; Hedrick, J. L., Organocatalytic Ring-Opening Polymerization. *Chem. Rev.* **2007,** *107* (12), 5813–5840.

(28) Platel, R. H.; Hodgson, L. M.; Williams, C. K., Biocompatible Initiators for Lactide Polymerization. *Polym. Rev.* **2008,** *48* (1), 11–63.

(29) Bourissou, D.; Martin-Vaca, B.; Dumitrescu, A.; Graullier, M.; Lacombe, F., Controlled Cationic Polymerization of Lactide. *Macromolecules* **2005,** *38* (24), 9993–9998.

(30) Connor, E. F.; Nyce, G. W.; Myers, M.; Möck, A.; Hedrick, J. L., First Example of N-Heterocyclic Carbenes as Catalysts for Living Polymerization: Organocatalytic Ring-Opening Polymerization of Cyclic Esters. *J. Am. Chem. Soc.* **2002,** *124* (6), 914–915.

(31) Dittrich, V. W.; Schulz, R. C., Kinetik und Mechanismus der ringöffnenden Polymerisation von L(—)-Lactid. *Angew. Makromol. Chem.* **1971,** *15* (1), 109–126.

(32) Dubois, P.; Jérŏme, R.; Teyssié, P., Aluminium alkoxides: A family of versatile initiators for the ring-opening polymerization of lactones and lactides. *Makromol. Chem. Macromol. Symp.* **1991,** *42-43* (1), 103–116.

(33) Kricheldorf, H. R.; Berl, M.; Scharnagl, N., Poly(lactones). 9. Polymerization mechanism of metal alkoxide initiated polymerizations of lactide and various lactones. *Macromolecules* **1988,** *21* (2), 286–293.

(34) Cheng, M.; Attygalle, A. B.; Lobkovsky, E. B.; Coates, G. W., Single-Site Catalysts for Ring-Opening Polymerization: Synthesis of Heterotactic Poly(lactic acid) from *rac*-Lactide. *J. Am. Chem. Soc.* **1999,** *121* (49), 11583–11584.

(35) Ovitt, T. M.; Coates, G. W., Stereoselective Ring-Opening Polymerization of *meso*-Lactide: Synthesis of Syndiotactic Poly(lactic acid). *J. Am. Chem. Soc.* **1999,** *121* (16), 4072–4073.

(36) Tsuji, H., Poly(lactide) Stereocomplexes: Formation, Structure, Properties, Degradation, and Applications. *Macromol. Biosci.* **2005,** *5* (7), 569–597.

(37) Chile, L.-E.; Mehrkhodavandi, P.; Hatzikiriakos, S. G., A Comparison of the Rheological and Mechanical Properties of Isotactic, Syndiotactic, and Heterotactic Poly(lactide). *Macromolecules* **2016,** *49* (3), 909–919.

(38) Coudane, J.; Ustariz-Peyret, C.; Schwach, G.; Vert, M., More about the stereodependence of DD and LL pair linkages during the ring-opening polymerization of racemic lactide. *J. Polym. Sci., Part A: Polym. Chem.* **1997,** *35* (9), 1651–1658.

(39) Tsuji, H., Poly(lactic acid) stereocomplexes: A decade of progress. *Adv. Drug Deliv. Rev.* **2016,** *107*, 97–135.

(40) Ahmed, J.; Varshney, S. K., Polylactides—Chemistry, Properties and Green Packaging Technology: A Review. *Int. J. Food Prop.* **2011,** *14* (1), 37–58.

(41) Schmidt, S. C.; Hillmyer, M. A., Polylactide stereocomplex crystallites as nucleating agents for isotactic polylactide. *J. Polym. Sci., Part B: Polym. Phys.* **2001,** *39* (3), 300–313.

(42) Li, Z.; Tan, B. H.; Lin, T.; He, C., Recent advances in stereocomplexation of enantiomeric PLA-based copolymers and applications. *Prog. Polym. Sci.* **2016,** *62*, 22–72.

(43) Worch, J. C.; Prydderch, H.; Jimaja, S.; Bexis, P.; Becker, M. L.; Dove, A. P., Stereochemical enhancement of polymer properties. *Nat. Rev. Chem.* **2019,** *3* (9), 514–535.

(44) Ikada, Y.; Jamshidi, K.; Tsuji, H.; Hyon, S. H., Stereocomplex formation between enantiomeric poly(lactides). *Macromolecules* **1987,** *20* (4), 904–906.

(45) Tsuji, H.; Ikada, Y., Stereocomplex formation between enantiomeric poly(lactic acid)s. XI. Mechanical properties and morphology of solution-cast films. *Polymer* **1999,** *40* (24), 6699–6708.

(46) Tsuji, H.; Fukui, I., Enhanced thermal stability of poly(lactide)s in the melt by enantiomeric polymer blending. *Polymer* **2003,** *44* (10), 2891–2896.

(47) De Santis, P.; Kovacs, A. J., Molecular conformation of poly(*S*-lactic acid). *Biopolymers* **1968,** *6* (3), 299–306.

(48) Fukushima, K.; Chang, Y.-H.; Kimura, Y., Enhanced Stereocomplex Formation of Poly(*L*-lactic acid) and Poly(*D*-lactic acid) in the Presence of Stereoblock Poly(lactic acid). *Macromol. Biosci.* **2007,** *7* (6), 829–835.

(49) Hirata, M.; Kimura, Y., Thermomechanical properties of stereoblock poly(lactic acid)s with different PLLA/PDLA block compositions. *Polymer* **2008,** *49* (11), 2656–2661.

(50) Wang, C.; Li, H.; Zhao, X., Ring opening polymerization of *L*-lactide initiated by creatinine. *Biomaterials* **2004,** *25* (27), 5797–801.

(51) Spassky, N.; Wisniewski, M.; Pluta, C.; Le Borgne, A., Highly stereoelective polymerization of *rac*-(*D,L*)-lactide with a chiral schiff's base/aluminium alkoxide initiator. *Macromol. Chem. Phys.* **1996,** *197* (9), 2627–2637.

(52) Nomura, N.; Ishii, R.; Akakura, M.; Aoi, K., Stereoselective Ring-Opening Polymerization of Racemic Lactide Using Aluminum-Achiral Ligand Complexes: Exploration of a Chain-End Control Mechanism. *J. Am. Chem. Soc.* **2002,** *124* (21), 5938–5939.

(53) Ovitt, T. M.; Coates, G. W., Stereochemistry of Lactide Polymerization with Chiral Catalysts: New Opportunities for Stereocontrol Using Polymer Exchange Mechanisms. *J. Am. Chem. Soc.* **2002,** *124* (7), 1316–1326.

(54) Hormnirun, P.; Marshall, E. L.; Gibson, V. C.; Pugh, R. I.; White, A. J. P., Study of ligand substituent effects on the rate and stereoselectivity of lactide polymerization using aluminum salen-type initiators. *Proc. Natl. Acad. Sci.* **2006,** *103* (42), 15343–15348.

(55) Nomura, N.; Ishii, R.; Yamamoto, Y.; Kondo, T., Stereoselective Ring-Opening Polymerization of a Racemic Lactide by Using Achiral Salen– and Homosalen–Aluminum Complexes. *Chem. Eur. J.* **2007,** *13* (16), 4433–4451.

(56) Tabthong, S.; Nanok, T.; Sumrit, P.; Kongsaeree, P.; Prabpai, S.; Chuawong, P.; Hormnirun, P., Bis(pyrrolidene) Schiff Base Aluminum Complexes as Isoselective-Biased Initiators for the Controlled Ring-Opening Polymerization of *rac*-Lactide: Experimental and Theoretical Studies. *Macromolecules* **2015,** *48* (19), 6846–6861.

(57) McKeown, P.; Davidson, M. G.; Kociok-Köhn, G.; Jones, M. D., Aluminium salalens vs. salans: "Initiator Design" for the isoselective polymerisation of *rac*-lactide. *Chem. Commu.* **2016,** *52* (68), 10431–10434.

(58) Aluthge, D. C.; Ahn, J. M.; Mehrkhodavandi, P., Overcoming aggregation in indium salen catalysts for isoselective lactide polymerization. *Chem. Sci.* **2015,** *6* (9), 5284–5292.

(59) Ghosh, S.; Gowda, R. R.; Jagan, R.; Chakraborty, D., Gallium and indium complexes containing the bis(imino)phenoxide ligand: synthesis, structural characterization and polymerization studies. *Dalton Trans.* **2015,** *44* (22), 10410–10422.

(60) Myers, D.; White, A. J. P.; Forsyth, C. M.; Bown, M.; Williams, C. K., Phosphasalen Indium Complexes Showing High Rates and Isoselectivities in *rac*-Lactide Polymerizations. *Angew. Chem. Int. Ed.* **2017,** *56* (19), 5277–5282.

(61) Marin, P.; Tschan, M. J.-L.; Isnard, F.; Robert, C.; Haquette, P.; Trivelli, X.; Chamoreau, L.-M.; Guérineau, V.; del Rosal, I.; Maron, L.; Venditto, V.; Thomas, C. M., Polymerization of *rac*-Lactide Using Achiral Iron Complexes: Access to Thermally Stable Stereocomplexes. *Angew. Chem. Int. Ed.* **2019,** *58* (36), 12585–12589.

(62) Stewart, J. A.; McKeown, P.; Driscoll, O. J.; Mahon, M. F.; Ward, B. D.; Jones, M. D., Tuning the Thiolen: Al(III) and Fe(III) Thiolen Complexes for the Isoselective ROP of *rac*-Lactide. *Macromolecules* **2019,** *52* (15), 5977–5984.

(63) Chen, C.; Jiang, J.; Mao, X.; Cong, Y.; Cui, Y.; Pan, X.; Wu, J., Isoselective Polymerization of *rac*-Lactide Catalyzed by Ion-Paired Potassium Amidinate Complexes. *Inorg. Chem.* **2018,** *57* (6), 3158–3168.

(64) Cui, Y.; Jiang, J.; Mao, X.; Wu, J., Mononuclear Salen–Sodium Ion Pairs as Catalysts for Isoselective Polymerization of *rac*-Lactide. *Inorg. Chem.* **2019,** *58* (1), 218–227.

(65) Bhattacharjee, J.; Harinath, A.; Nayek, H. P.; Sarkar, A.; Panda, T. K., Highly Active and Iso-Selective Catalysts for the Ring-Opening Polymerization of Cyclic Esters using Group 2 Metal Initiators. *Chem. Eur. J.* **2017,** *23* (39), 9319–9331.

(66) Hu, J.; Kan, C.; Wang, H.; Ma, H., Highly Active Chiral Oxazolinyl Aminophenolate Magnesium Initiators for Isoselective Ring-Opening Polymerization of *rac*-Lactide: Dinuclearity Induced Enantiomorphic Site Control. *Macromolecules* **2018,** *51* (14), 5304–5312.

(67) Kan, C.; Hu, J.; Huang, Y.; Wang, H.; Ma, H., Highly Isoselective and Active Zinc Catalysts for *rac*-Lactide Polymerization: Effect of Pendant Groups of Aminophenolate Ligands. *Macromolecules* **2017,** *50* (20), 7911–7919.

(68) Gong, Y.; Ma, H., High performance benzoimidazolyl-based aminophenolate zinc complexes for isoselective polymerization of *rac*-lactide. *Chem. Commun.* **2019,** *55* (68), 10112–10115.

(69) Honrado, M.; Sobrino, S.; Fernández-Baeza, J.; Sánchez-Barba, L. F.; Garcés, A.; Lara-Sánchez, A.; Rodríguez, A. M., Synthesis of an enantiopure scorpionate ligand by a nucleophilic addition to a ketenimine and a zinc initiator for the isoselective ROP of *rac*-lactide. *Chem. Commun.* **2019,** *55* (61), 8947–8950.

(70) Jones, M. D.; Brady, L.; McKeown, P.; Buchard, A.; Schäfer, P. M.; Thomas, L. H.; Mahon, M. F.; Woodman, T. J.; Lowe, J. P., Metal influence on the iso- and hetero-selectivity of complexes of bipyrrolidine derived salan ligands for the polymerisation of *rac*-lactide. *Chem. Sci.* **2015,** *6* (8), 5034–5039.

(71) Stopper, A.; Rosen, T.; Venditto, V.; Goldberg, I.; Kol, M., Group 4 Metal Complexes of Phenylene–Salalen Ligands in *rac*-Lactide Polymerization Giving High Molecular Weight Stereoblock Poly(lactic acid). *Chem. Eur. J.* **2017,** *23* (48), 11540–11548.

(72) Bakewell, C.; Cao, T.-P.-A.; Long, N.; Le Goff, X. F.; Auffrant, A.; Williams, C. K., Yttrium Phosphasalen Initiators for *rac*-Lactide Polymerization: Excellent Rates and High Iso-Selectivities. *J. Am. Chem. Soc.* **2012,** *134* (51), 20577–20580.

(73) Bakewell, C.; White, A. J. P.; Long, N. J.; Williams, C. K., Metal-Size Influence in Iso-Selective Lactide Polymerization. *Angew. Chem. Int. Ed.* **2014,** *53* (35), 9226–9230.

(74) Xu, T.-Q.; Yang, G.-W.; Liu, C.; Lu, X.-B., Highly Robust Yttrium Bis(phenolate) Ether Catalysts for Excellent Isoselective Ring-Opening Polymerization of Racemic Lactide. *Macromolecules* **2017,** *50* (2), 515–522.

(75) Sanchez-Sanchez, A.; Rivilla, I.; Agirre, M.; Basterretxea, A.; Etxeberria, A.; Veloso, A.; Sardon, H.; Mecerreyes, D.; Cossío, F. P., Enantioselective Ring-Opening Polymerization of *rac*-Lactide Dictated by Densely Substituted Amino Acids. *J. Am. Chem. Soc.* **2017,** *139* (13), 4805–4814.

(76) Orhan, B.; Tschan, M. J. L.; Wirotius, A.-L.; Dove, A. P.; Coulembier, O.; Taton, D., Isoselective Ring-Opening Polymerization of *rac*-Lactide from Chiral Takemoto's Organocatalysts: Elucidation of Stereocontrol. *ACS Macro Lett.* **2018,** *7* (12), 1413–1419.

(77) Lim, J. Y. C.; Yuntawattana, N.; Beer, P. D.; Williams, C. K., Isoselective Lactide Ring Opening Polymerisation using [2]Rotaxane Catalysts. *Angew. Chem. Int. Ed.* **2019,** *58* (18), 6007–6011.

(78) Wang, H.; Ma, H., Highly diastereoselective synthesis of chiral aminophenolate zinc complexes and isoselective polymerization of *rac*-lactide. *Chem. Commun.* **2013,** *49* (77), 8686–8688.

(79) Wang, H.; Yang, Y.; Ma, H., Exploring Steric Effects in Diastereoselective Synthesis of Chiral Aminophenolate Zinc Complexes and Stereoselective Ring-Opening Polymerization of *rac*-Lactide. *Inorg. Chem.* **2016,** *55* (15), 7356–7372.

(80) Abbina, S.; Du, G., Zinc-Catalyzed Highly Isoselective Ring Opening Polymerization of *rac*-Lactide. *ACS Macro Lett.* **2014,** *3* (7), 689–692.

(81) Mou, Z.; Liu, B.; Wang, M.; Xie, H.; Li, P.; Li, L.; Li, S.; Cui, D., Isoselective ring-opening polymerization of *rac*-lactide initiated by achiral heteroscorpionate zwitterionic zinc complexes. *Chem. Commun.* **2014,** *50* (77), 11411–11414.

(82) Rosen, T.; Popowski, Y.; Goldberg, I.; Kol, M., Zinc Complexes of Sequential Tetradentate Monoanionic Ligands in the Isoselective Polymerization of *rac*-Lactide. *Chem. Eur. J.* **2016,** *22* (33), 11533–11536.

(83) Stasiw, D. E.; Luke, A. M.; Rosen, T.; League, A. B.; Mandal, M.; Neisen, B. D.; Cramer, C. J.; Kol, M.; Tolman, W. B., Mechanism of the Polymerization of *rac*-Lactide by Fast Zinc Alkoxide Catalysts. *Inorg. Chem.* **2017,** *56* (22), 14366–14372.

(84) Darensbourg, D. J.; Yarbrough, J. C., Mechanistic Aspects of the Copolymerization Reaction of Carbon Dioxide and Epoxides, Using a Chiral Salen Chromium Chloride Catalyst. *J. Am. Chem. Soc.* **2002,** *124* (22), 6335–6342.

(85) Klaus, S.; Lehenmeier, M. W.; Anderson, C. E.; Rieger, B., Recent advances in $CO_2$/epoxide copolymerization—New strategies and cooperative mechanisms. *Coord. Chem. Rev.* **2011,** *255* (13), 1460–1479.

(86) Qin, Z.; Thomas, C. M.; Lee, S.; Coates, G. W., Cobalt-Based Complexes for the Copolymerization of Propylene Oxide and $CO_2$: Active and Selective Catalysts for Polycarbonate Synthesis. *Angew. Chem. Int. Ed.* **2003,** *42* (44), 5484–5487.

(87) Thevenon, A.; Cyriac, A.; Myers, D.; White, A. J. P.; Durr, C. B.; Williams, C. K., Indium Catalysts for Low-Pressure $CO_2$/Epoxide Ring-Opening Copolymerization: Evidence for a Mononuclear Mechanism? *J. Am. Chem. Soc.* **2018,** *140* (22), 6893–6903.

(88) Fieser, M. E.; Sanford, M. J.; Mitchell, L. A.; Dunbar, C. R.; Mandal, M.; Van Zee, N. J.; Urness, D. M.; Cramer, C. J.; Coates, G. W.; Tolman, W. B., Mechanistic Insights into the Alternating Copolymerization of Epoxides and Cyclic Anhydrides Using a (Salph)AlCl and Iminium Salt Catalytic System. *J. Am. Chem. Soc.* **2017,** *139* (42), 15222–15231.

(89) Fischer, R. F., Polyesters from expoxides and anhydrides. *J. Polym. Sci.* **1960,** *44* (143), 155–172.

(90) Tsuruta, T.; Matsuura, K.; Inoue, S., Preparation of some polyesters by organometallic-catalyzed ring opening polymerization. *Macromol. Chem. Phys.* **1964,** *75* (1), 211–214.

(91) Matsuura, K.; Tsuruta, T.; Terada, Y.; Inoue, S., Asymmetric-induced copolymerization of propylene oxide with cyclic anhydride. *Macromol. Chem. Phys.* **1965,** *81* (1), 258-260.

(92) Schaefer, J.; Katnik, R. J.; Kern, R. J., The monomer distributions of propylene oxide-maleic anhydride copolymers. *J. Am. Chem. Soc.* **1968,** *90* (10), 2476–2480.

(93) Inoue, S.; Kitamura, K.; Tsuruta, T., Alternating copolymerization of phthalic anhydride and propylene oxide by dialkylzinc. *Macromol. Chem. Phys.* **1969,** *126* (1), 250–265.

(94) Hsieh, H. L., Terpolymerization of Cyclic Ethers with Cyclic Anhydride. *J. Macromol. Sci., Part A: Chem.* **1973,** *7* (7), 1525–1535.

(95) Aida, T.; Inoue, S., Catalytic reaction on both sides of a metalloporphyrin plane. Alternating copolymerization of phthalic anhydride and epoxypropane with an aluminum porphyrin-quaternary salt system. *J. Am. Chem. Soc.* **1985,** *107* (5), 1358–1364.

(96) Aida, T.; Sanuki, K.; Inoue, S., Well-controlled polymerization by metalloporphyrin. Synthesis of copolymer with alternating sequence and regulated molecular weight from cyclic acid anhydride and epoxide catalyzed by the system of aluminum porphyrin coupled with quaternary organic salt. *Macromolecules* **1985,** *18* (6), 1049–1055.

(97) DiCiccio, A. M.; Coates, G. W., Ring-Opening Copolymerization of Maleic Anhydride with Epoxides: A Chain-Growth Approach to Unsaturated Polyesters. *J. Am. Chem. Soc.* **2011,** *133* (28), 10724–10727.

(98) Huijser, S.; HosseiniNejad, E.; Sablong, R.; de Jong, C.; Koning, C. E.; Duchateau, R., Ring-Opening Co- and Terpolymerization of an Alicyclic Oxirane with Carboxylic Acid Anhydrides and $CO_2$ in the Presence of Chromium Porphyrinato and Salen Catalysts. *Macromolecules* **2011,** *44* (5), 1132–1139.

(99) Hosseini Nejad, E.; Paoniasari, A.; Koning, C. E.; Duchateau, R., Semi-aromatic polyesters by alternating ring-opening copolymerisation of styrene oxide and anhydrides. *Polym. Chem.* **2012,** *3* (5), 1308–1313.

(100) Bernard, A.; Chatterjee, C.; Chisholm, M. H., The influence of the metal (Al, Cr and Co) and the substituents of the porphyrin in controlling the reactions involved in the copolymerization of propylene oxide and cyclic anhydrides by porphyrin metal(III) complexes. *Polymer* **2013,** *54* (11), 2639–2646.

(101) Jeske, R. C.; DiCiccio, A. M.; Coates, G. W., Alternating Copolymerization of Epoxides and Cyclic Anhydrides: An Improved Route to Aliphatic Polyesters. *J. Am. Chem. Soc.* **2007,** *129* (37), 11330–11331.

(102) Robert, C.; Ohkawara, T.; Nozaki, K., Manganese-Corrole Complexes as Versatile Catalysts for the Ring-Opening Homo- and Co-Polymerization of Epoxide. *Chem. Eur. J.* **2014,** *20* (16), 4789–4795.

(103) Darensbourg, D. J.; Poland, R. R.; Escobedo, C., Kinetic Studies of the Alternating Copolymerization of Cyclic Acid Anhydrides and Epoxides, and the

Terpolymerization of Cyclic Acid Anhydrides, Epoxides, and $CO_2$ Catalyzed by (salen)CrIIICl. *Macromolecules* **2012,** *45* (5), 2242–2248.

(104) Hosseini Nejad, E.; van Melis, C. G. W.; Vermeer, T. J.; Koning, C. E.; Duchateau, R., Alternating Ring-Opening Polymerization of Cyclohexene Oxide and Anhydrides: Effect of Catalyst, Cocatalyst, and Anhydride Structure. *Macromolecules* **2012,** *45* (4), 1770–1776.

(105) Nejad, E. H.; Paoniasari, A.; van Melis, C. G. W.; Koning, C. E.; Duchateau, R., Catalytic Ring-Opening Copolymerization of Limonene Oxide and Phthalic Anhydride: Toward Partially Renewable Polyesters. *Macromolecules* **2013,** *46* (3), 631–637.

(106) Van Zee, N. J.; Coates, G. W., Alternating Copolymerization of Propylene Oxide with Biorenewable Terpene-Based Cyclic Anhydrides: A Sustainable Route to Aliphatic Polyesters with High Glass Transition Temperatures. *Angew. Chem. Int. Ed.* **2015,** *54* (9), 2665–2668.

(107) Sanford, M. J.; Peña Carrodeguas, L.; Van Zee, N. J.; Kleij, A. W.; Coates, G. W., Alternating Copolymerization of Propylene Oxide and Cyclohexene Oxide with Tricyclic Anhydrides: Access to Partially Renewable Aliphatic Polyesters with High Glass Transition Temperatures. *Macromolecules* **2016,** *49* (17), 6394–6400.

(108) Van Zee, N. J.; Sanford, M. J.; Coates, G. W., Electronic Effects of Aluminum Complexes in the Copolymerization of Propylene Oxide with Tricyclic Anhydrides: Access to Well-Defined, Functionalizable Aliphatic Polyesters. *J. Am. Chem. Soc.* **2016,** *138* (8), 2755–2761.

(109) Bester, K.; Bukowska, A.; Myśliwiec, B.; Hus, K.; Tomczyk, D.; Urbaniak, P.; Bukowski, W., Alternating ring-opening copolymerization of phthalic anhydride with epoxides catalysed by salophen chromium(iii) complexes. An effect of substituents in salophen ligands. *Polym. Chem.* **2018,** *9* (16), 2147–2156.

(110) Sanford, M. J.; Van Zee, N. J.; Coates, Geoffrey W., Reversible-deactivation anionic alternating ring-opening copolymerization of epoxides and cyclic anhydrides: access to orthogonally functionalizable multiblock aliphatic polyesters. *Chem. Sci.* **2018,** *9* (1), 134–142.

(111) Abel, B. A.; Lidston, C. A. L.; Coates, G. W., Mechanism-Inspired Design of Bifunctional Catalysts for the Alternating Ring-Opening Copolymerization of Epoxides and Cyclic Anhydrides. *J. Am. Chem. Soc.* **2019,** *141* (32), 12760–12769.

(112) Si, G.; Zhang, L.; Han, B.; Duan, Z.; Li, B.; Dong, J.; Li, X.; Liu, B., Novel chromium complexes with a [OSSO]-type bis(phenolato) dianionic ligand mediate the alternating ring-opening copolymerization of epoxides and phthalic anhydride. *Polym. Chem.* **2015,** *6* (35), 6372–6377.

(113) Han, B.; Zhang, L.; Yang, M.; Liu, B.; Dong, X.; Theato, P., Highly Cis/Trans-Stereoselective (ONSO)CrCl-Catalyzed Ring-Opening Copolymerization of Norbornene Anhydrides and Epoxides. *Macromolecules* **2016,** *49* (17), 6232–6239.

(114) Ma, H.; Spaniol, T. P.; Okuda, J., Highly Heteroselective Ring-Opening Polymerization of *rac*-Lactide Initiated by Bis(phenolato)scandium Complexes. *Angew. Chem. Int. Ed.* **2006,** *45* (46), 7818–7821.

(115) Buffet, J.-C.; Martin, A. N.; Kol, M.; Okuda, J., Controlled stereoselective polymerization of lactide monomers by group 4 metal initiators that contain an (OSSO)-type tetradentate bis(phenolate) ligand. *Polym. Chem.* **2011,** *2* (10), 2378–2384.

(116) Saini, P. K.; Romain, C.; Zhu, Y.; Williams, C. K., Di-magnesium and zinc catalysts for the copolymerization of phthalic anhydride and cyclohexene oxide. *Polym. Chem.* **2014,** *5* (20), 6068–6075.

(117) Garden, J. A.; Saini, P. K.; Williams, C. K., Greater than the Sum of Its Parts: A Heterodinuclear Polymerization Catalyst. *J. Am. Chem. Soc.* **2015,** *137* (48), 15078–15081.

(118) Winkler, M.; Romain, C.; Meier, M. A. R.; Williams, C. K., Renewable polycarbonates and polyesters from 1,4-cyclohexadiene. *Green Chem.* **2015,** *17* (1), 300–306.

(119) Hatazawa, M.; Takahashi, R.; Deng, J.; Houjou, H.; Nozaki, K., Cationic Co–Salphen Complexes Bisligated by DMAP as Catalysts for the Copolymerization of Cyclohexene Oxide with Phthalic Anhydride or Carbon Dioxide. *Macromolecules* **2017,** *50* (20), 7895–7900.

(120) Liu, Y.; Guo, J.-Z.; Lu, H.-W.; Wang, H.-B.; Lu, X.-B., Making Various Degradable Polymers from Epoxides Using a Versatile Dinuclear Chromium Catalyst. *Macromolecules* **2018,** *51* (3), 771–778.

(121) Martínez de Sarasa Buchaca, M.; de la Cruz-Martínez, F.; Martínez, J.; Alonso-Moreno, C.; Fernández-Baeza, J.; Tejeda, J.; Niza, E.; Castro-Osma, J. A.; Otero, A.; Lara-Sánchez, A., Alternating Copolymerization of Epoxides and Anhydrides Catalyzed by Aluminum Complexes. *ACS Omega* **2018,** *3* (12), 17581–17589.

(122) Shi, Z.; Jiang, Q.; Song, Z.; Wang, Z.; Gao, C., Dinuclear iron(iii) complexes bearing phenylene-bridged bis(amino triphenolate) ligands as catalysts for the copolymerization of cyclohexene oxide with carbon dioxide or phthalic anhydride. *Polym. Chem.* **2018,** *9* (38), 4733–4743.

(123) Li, H.; Zhao, J.; Zhang, G., Self-Buffering Organocatalysis Tailoring Alternating Polyester. *ACS Macro Lett.* **2017,** *6* (10), 1094–1098.

(124) Hu, L.-F.; Zhang, C.-J.; Wu, H.-L.; Yang, J.-L.; Liu, B.; Duan, H.-Y.; Zhang, X.-H., Highly Active Organic Lewis Pairs for the Copolymerization of Epoxides with Cyclic Anhydrides: Metal-Free Access to Well-Defined Aliphatic Polyesters. *Macromolecules* **2018,** *51* (8), 3126–3134.

(125) Ji, H.-Y.; Chen, X.-L.; Wang, B.; Pan, L.; Li, Y.-S., Metal-free, regioselective and stereoregular alternating copolymerization of monosubstituted epoxides and tricyclic anhydrides. *Green Chem.* **2018,** *20* (17), 3963–3973.

(126) Kummari, A.; Pappuru, S.; Chakraborty, D., Fully alternating and regioselective ring-opening copolymerization of phthalic anhydride with epoxides using highly active metal-free Lewis pairs as a catalyst. *Polym. Chem.* **2018,** *9* (29), 4052–4062.

(127) Li, H.; Luo, H.; Zhao, J.; Zhang, G., Well-Defined and Structurally Diverse Aromatic Alternating Polyesters Synthesized by Simple Phosphazene Catalysis. *Macromolecules* **2018,** *51* (6), 2247–2257.

(128) Lin, L.; Liang, J.; Xu, Y.; Wang, S.; Xiao, M.; Sun, L.; Meng, Y., Fully alternating sustainable polyesters from epoxides and cyclic anhydrides: economical and metal-free dual catalysis. *Green Chem.* **2019,** *21* (9), 2469–2477.

# *Chapter 2*

# *Methodology*

*If the plan doesn't work, change the plan but never the goal...*

*~ Unknown ~*

## 2.1. General analytical techniques for ligand and complex synthesis

### 2.1.1. Nuclear Magnetic Resonance (NMR) spectroscopy

1D (*e.g.* $^{1}H$, $^{13}C\{^{1}H\}$, $^{31}P\{^{1}H\}$) and 2D (*e.g.* $^{1}H$-COSY, HSQC, HMBC) multinuclear NMR spectroscopies were routinely used to characterise the synthesised ligands and complexes reported in this thesis.

#### 2.1.1.1. $^{31}P\{^{1}H\}$ NMR spectroscopy

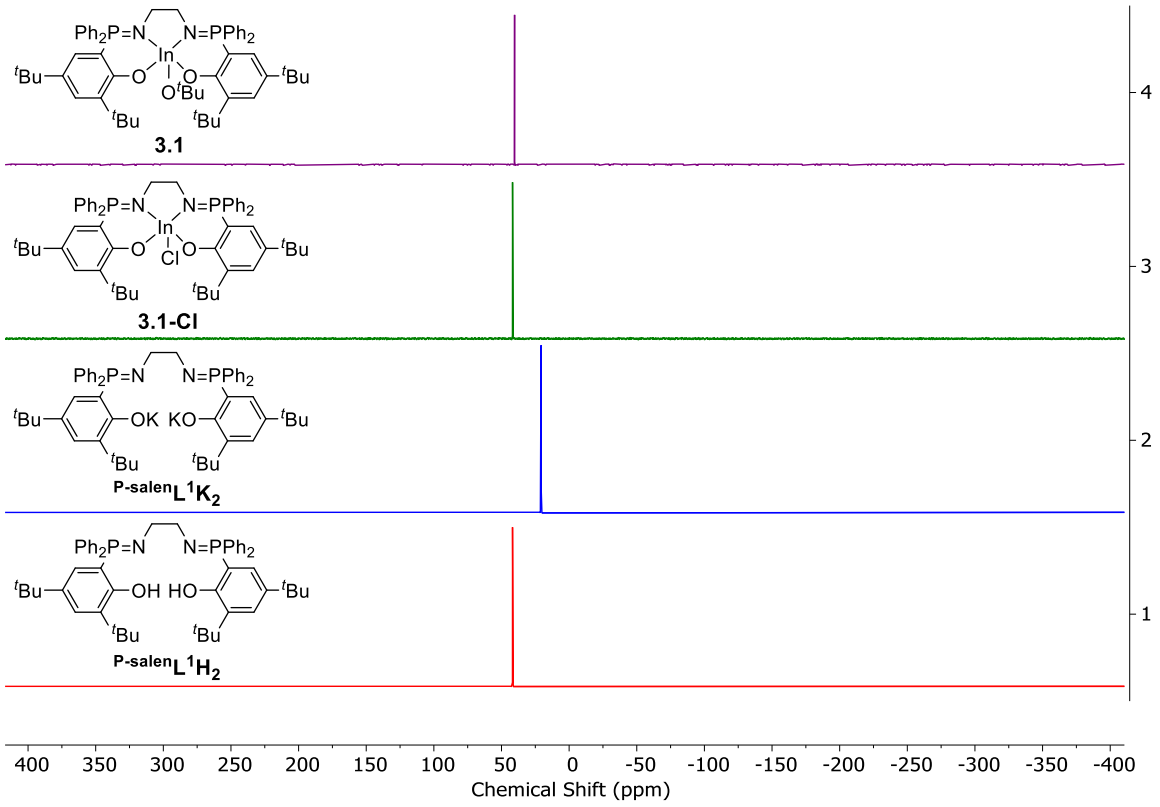



**Figure 2.1.** Stacks of $^{31}P\{^{1}H\}$ NMR spectra showing the formation of **3.1**.

Due to the presence of phosphine moiety on the ancillary ligands of the complexes reported in chapters 3 and 4, *in situ* $^{31}P\{^{1}H\}$ NMR spectroscopy can be used to monitor the complexation reactions without the need to isolate intermediates formed during the reaction.[1-5] In the synthesis of indium complex **3.1**, the phosphorous signals change chemical shift and split during the complexation process (Figure 2.1). Successful formation of the individual compounds can be seen by the shift of phosphorous signal. For example, ligand

$^{P\text{-salen}}\mathbf{L}^{1}\mathbf{H}_2$ exhibits a single phosphorous signal at 41.8 ppm (red line) which shifts upfield to 20.7 ppm ($^{P\text{-salen}}\mathbf{L}^{1}\mathbf{K}_2$, blue line) following deprotonation with potassium bis(trimethylsilyl) amide. When the chloro indium complex (**3.1-Cl**) was formed, the phosphorous resonance shifts downfield to 41.8 ppm (green line). A lower chemical shift (40.3 ppm, purple line) is observed when the indium alkoxide complex **3.1** was generated.

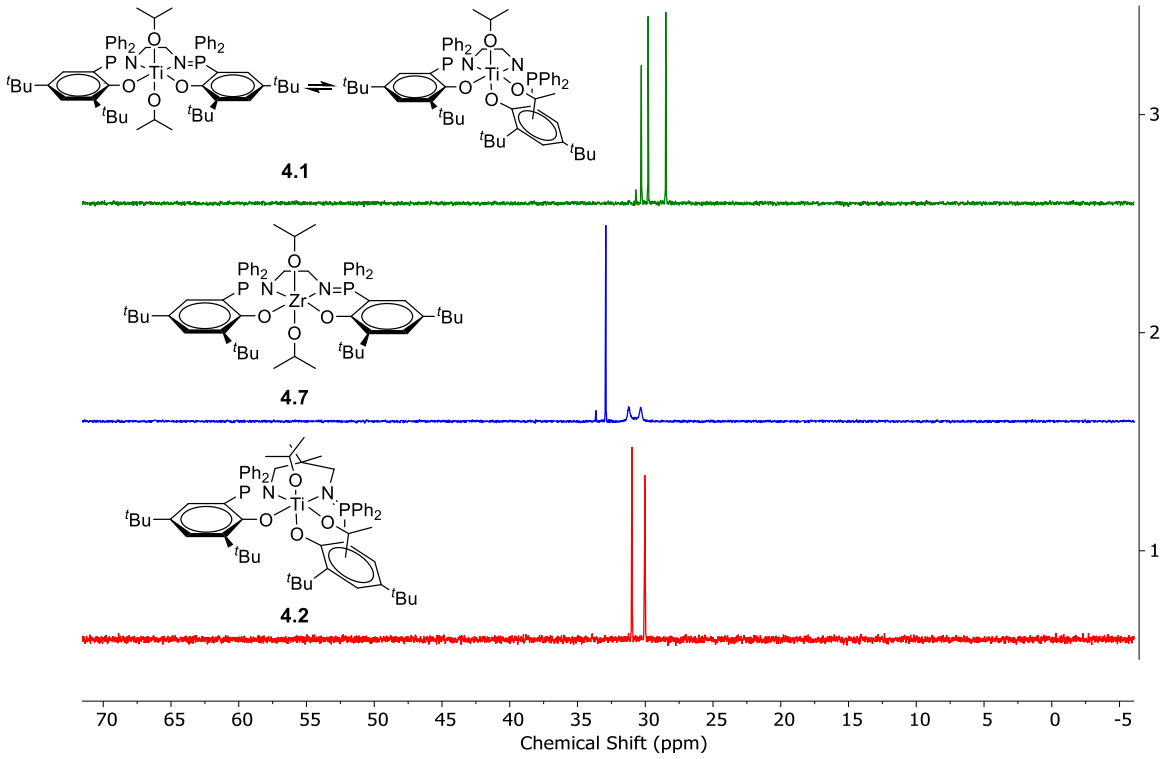



**Figure 2.2.** Stacks of $^{31}P\{^{1}H\}$ NMR spectra of phosphasalen Ti(IV) and Zr(IV) complexes.

In chapter 4, $^{31}P\{^{1}H\}$ NMR spectroscopy was used to identify the nature of the *iso*-propoxide coordination mode to the metal centre. The $^{i}$PrO co-ligand configurations and complex geometries of phosphasalen complexes were determined by the different splitting patterns of $^{31}P$ signals (Figure 2.2). In the case of **4.2**, two different phosphorous resonances at 31.0 and 30.0 ppm are observed and this suggests the *cis*-coordination of the $^{i}$PrO co-ligands (red trace). In contrast, **4.7** shows a singlet phosphorous signal at 32.9 ppm, suggesting the *trans*-coordination of the $^{i}$PrO groups (blue line). For **4.1**, three distinct signals are obtained,

suggesting that *cis*- and *trans*- $^{i}$PrO co-ligand coordination modes are present perhaps due to different complexes being in equilibrium (green spectrum).

### 2.1.1.2. $^{1}$H Diffusion Ordered Spectroscopy (DOSY) NMR spectroscopy

$^{1}$H DOSY NMR spectroscopy, a 2D NMR spectroscopic technique, is a useful technique for probing the solution state nuclearity of organometallic complexes based on their different diffusion coefficients. It provides information on compound aggregation, solvent phenomena, and multicomponent solutions. As the diffusion coefficient is directly related to the solvodynamic radius of the compound *via* the Stokes-Einstein equation (see below), the aggregation state can then be identified from the DOSY analysis.[6, 7]

*Stokes-Einstein equation*

$$D = \frac{k_B T}{6\pi\eta r}$$

*Where D ($cm^2\ s^{-1}$) is diffusion coefficient, $k_B$ ($J\ K^{-1}$) is Boltzmann constant, T is absolute temperature in Kelvin, η (Pa·s) is solvent viscosity, and r (cm) is solvodynamic radius*

By assuming that each component in solution can be spherical and are highly diluted, a linear correlation between the logarithm of the diffusion coefficient (log(D)) and the logarithm of the molecular weight (log(MW)) can be obtained. The compound molecular weights can then be estimated using a calibration plot.

$$D = A(MW)^{\alpha}$$

$$log(D) = \alpha\, log(MW) + log(A)$$

*Where A and α are intrinsic constants of the used deuterated solvent.*

It should be noted that in this thesis, DOSY was only used to approximate the MW of the synthesised complexes and to help identify the complex nuclearity in solution (mononuclear

or dinuclear). Other analytical techniques (*e.g.* 1D and 2D NMR spectroscopy, elemental analysis, single X-ray crystallography (solid state) were also used to confirm the complex aggregation state. $^{1}$H DOSY NMR spectrum of complex **3.5** in THF-$d_8$ shows a single diffusion coefficient (log(D)) of –9.164 (Figure 2.3) and the following equations are an example of MW calculation of **3.5**.

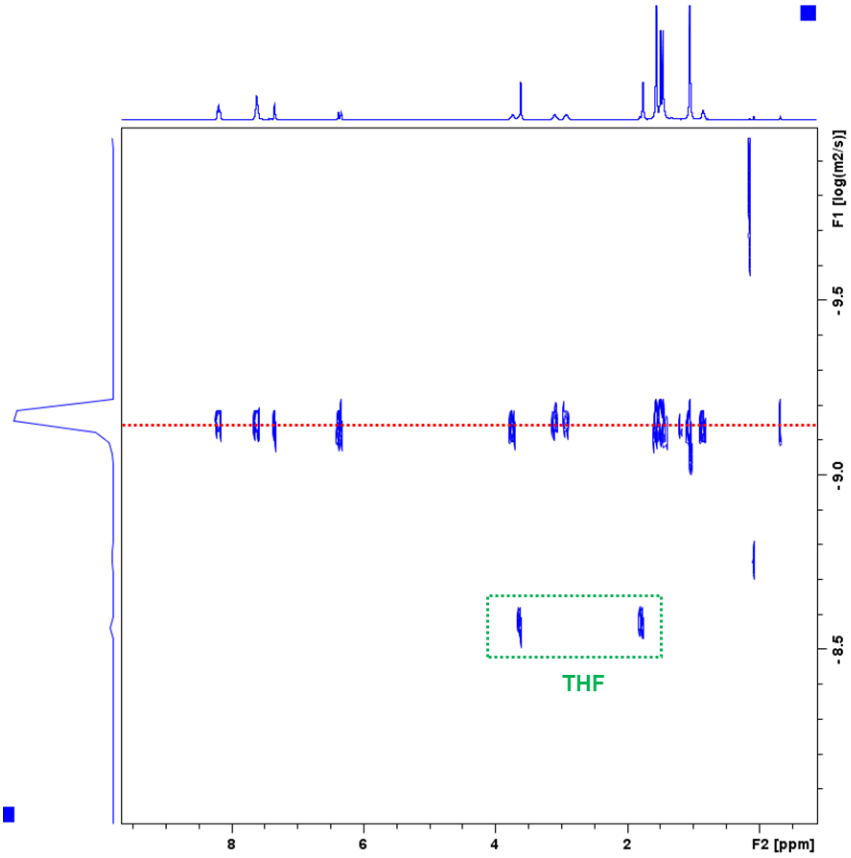



**Figure 2.3.** $^{1}$H DOSY NMR spectrum of indium complex **3.5** in THF-$d_8$.

The linear calibration obtained in THF-$d_8$ gives α = –0.5626 and log(A) = –7.505

In the case of **3.5**, a log(D) of –9.164 was obtained from DOSY analysis.

$$log(D) = -7.505 - 0.5626 \times log(MW)$$

$$MW = 10^{\left(\frac{7.505+log(D)}{-0.5626}\right)}$$

$$MW(DOSY) = 10^{\left(\frac{7.505-9.164}{-0.5626}\right)} = 888.81\ gmol^{-1}$$

### 2.1.2. Single Crystal X-ray Diffraction

Single crystal X-ray diffraction (SCXRD) is a non-destructive analytical technique which is commonly used to characterise the crystal structures and interatomic distances of crystalline compounds. It provides detailed information about unit cell dimensions, bond lengths, and bond angles of crystalline materials.

SCXRD is based on the constructive interference of the monochromatic X-rays and a crystalline sample. The monochromatic X-rays can be generated from a cathode ray tube, filtered and concentrated to give monochromatic radiation. The interaction of the incident X-rays with the sample results in diffraction when conditions satisfy Bragg′s Law. The diffracted radiation is detected and processed. The crystal structures of the measured samples can be then characterised from the collected data.

$$Bragg's\ Law: \qquad n\lambda = 2dsin\theta$$

*Where n is a positive integer, λ (nm) is incident ray wavelength, d (nm) is interplanar distance, and θ is the angle between incident ray and surface of crystal units.*

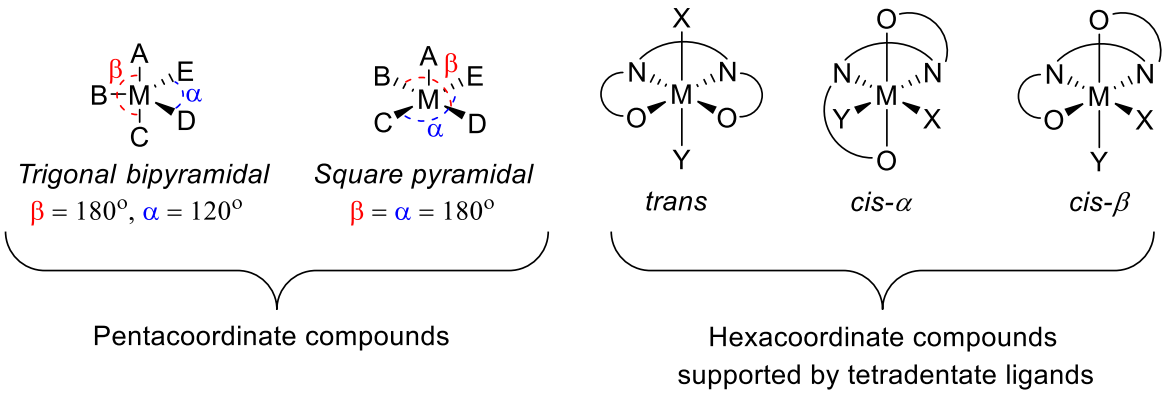



**Figure 2.4.** Possible geometries of penta- and hexa-coordinate compounds

Individual single crystals which were isolated by either a slow diffusion of non-polar hexane to higher polar solvents (*e.g.* THF, toluene etc.) or a layer-by-layer of two solvents were characterised by single X-ray crystallography. In the case of a slow diffusion crystallisation,

the target compounds were dissolved in either THF or toluene and placed into a small vial. The small vial was then put into a bigger vial containing hexane and left at ambient temperature to allow non-polar solvent slowly diffuse into the solution mixture until single crystals were formed. In contrast, layer-by-layer crystallisation only requires a single vial. The crystallisation was carried out by dissolving the target compound in a small amount of polar solvent (*e.g.* THF, toluene). About 3–4 times the amount used for polar solvent of hexane was then added on the top layer and left to crystallise at –20 °C. The reported catalysts and intermediates in this thesis exhibit either penta- or hexa-coordinate metal-centres. In the case of penta-coordination, two different geometries (trigonal bipyramidal and square pyramidal) are observed (Figure 2.4). The particular geometries can be identified using the geometry index for penta-coordinated compound ($\tau_5$) value which can be calculated according to the following equation.[8]

$$\tau_5 = \frac{\beta - \alpha}{60^o}$$

*Where β and α are the two greatest valence angles on the coordination centre and β > α.*

In the case of a perfect square pyramidal structure, a $\tau_5$ of 0 will be obtained. Conversely, a τ5 of 1 suggests an ideal trigonal bipyramidal geometry at the metal centre. In the case of hexacoordinated complexes, only octahedral geometries can be seen. However, the ligand and co-ligand coordination modes can rearrange and this results in three different configurations; *trans*, *cis-α,* and *cis-β* (Figure 2.4). For the *trans* configuration, the coordination of the two monodentate co-ligands (x and y) are in the *trans* configuration. In the case of *cis-α,* the two co-ligands are *cis* to one another and the two O atoms of the [N,N,O,O] ancillary ligand are in a *trans* configuration. Finally, for *cis-β,* both the two co-ligands and the two O atoms of the [N,N,O,O] tetradentate ligand are in a *cis* configuration.

## 2.2. Characterisation techniques for polymerisation

### 2.2.1. NMR spectroscopy

#### 2.2.1.1. Determination of monomer conversion

$^1$H NMR spectroscopy was used to determine the monomer conversion during polymerisation reactions (see Figure 2.5). Tables 2.1 and 2.2 summarise the key chemical shifts of the monomers and polymers reported in this thesis. The conversion was calculated based on the following equation.

$$Conversion\ (\%) = \frac{\int H_{polymer}}{\int H_{polymer} + \int H_{monomer}} \times 100\ \%$$

**Table 2.1.** List of $^1$H NMR chemical shifts of monomers and polymers produced by ROP.[a]

| | PCL | PLA | PBL | PDL | PHL |
|---|---|---|---|---|---|
| **Monomer chemical shift (ppm)** | $\delta$ 4.17-4.12 | $\delta$ 5.06-4.98 | $\delta$ 4.59-4.48 | $\delta$ 4.18-4.03 | $\delta$ 4.43-4.27 |
| **Polymer chemical shift (ppm)** | $\delta$ 4.02-3.92 | $\delta$ 5.22-5.08 | $\delta$ 5.18-5.01 | $\delta$ 4.80-4.63 | $\delta$ 4.91-4.68 |

[a] All $^1$H NMR spectra were recorded in $CDCl_3$.

**Table 2.2.** List of $^1$H NMR chemical shifts of monomers and polymers prepared by ROCOP.[a]

| | Epoxide/PA | CHO/SA | CHO/GA | CHO/DGA | CHO/NBA |
|---|---|---|---|---|---|
| **Cyclic anhydride chemical shift (ppm)** | $\delta$ 7.99-7.80 | $\delta$ 2.95-2.87 | $\delta$ 2.75-2.54 | $\delta$ 4.41-4.27 | $\delta$ 3.58-3.41 |
| **Polymer chemical shift (ppm)** | $\delta$ 7.63-7.26 | $\delta$ 2.68-2.35 | $\delta$ 2.40-2.17 | $\delta$ 4.23-3.99 | $\delta$ 3.41-2.89 |

[a] All $^1$H NMR spectra were recorded in $CDCl_3$.

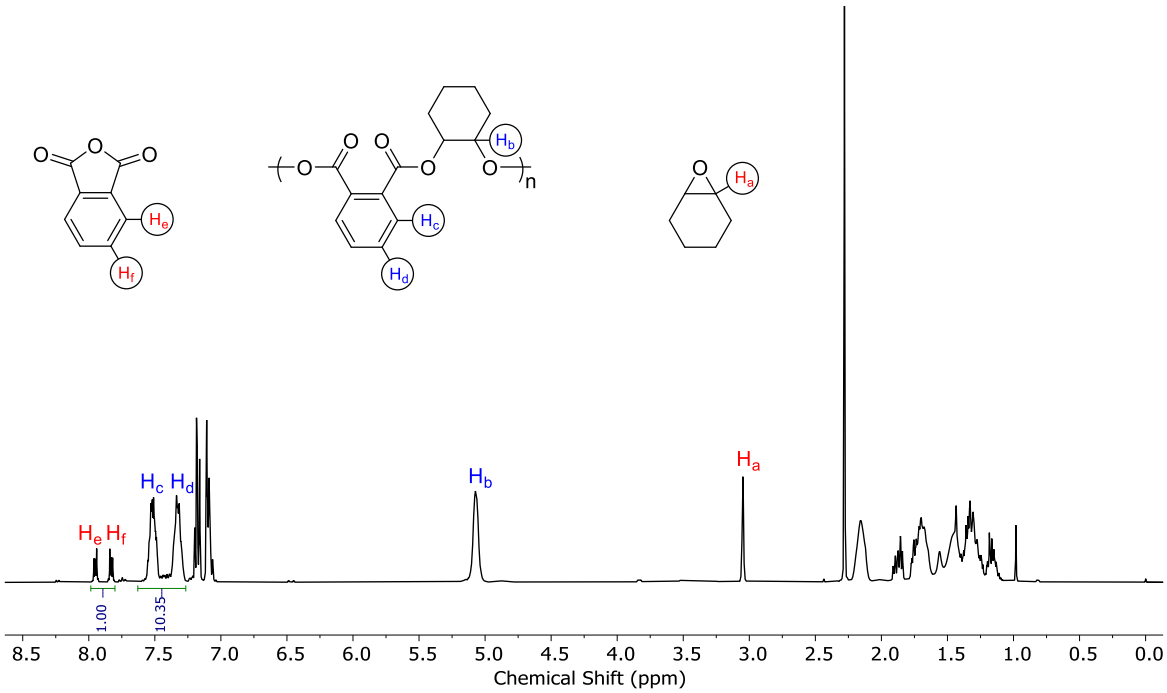



**Figure 2.5.** $^{1}$H NMR of an aliquot from the CHO/PA ROCOP in $CDCl_3$ at 298 K.

The peak area of monomer and polymer can be determined by the integration of monomer and polymer signals in the $^{1}$H NMR spectrum, respectively. In the case of Figure 2.5, the conversion of phthalic anhydride is

$$Conversion\ (\%) = \frac{10.35}{10.35 + 1} \times 100 = 91\ \%$$

### 2.2.1.2. Identification of selectivity in polymer chain

In chapters 4 and 5, the ROCOP of epoxide and anhydride moieties was carried out. In this particular polymerisation, when the catalyst is less selective, the homopolymerisation of epoxide groups can also occur to form ether linkages in the polymer chain. $^{1}$H NMR spectroscopy was used to quantify the percentage of ether linkages incorporated into polyester chains (see Figure 2.6). Table 2.3 lists the chemical shifts of polyether and polyester signals presented in this thesis. The calculations were carried out according to the following equation. The calculation of the percentage ether linkages in poly(propylene

maleate), reported in chapter 5 was used as an example (Figure 2.6). In this case, 66 % ether linkages were observed (see more details in following equations).

$$ether\ linkages\ (\%) = \frac{\int H_{polyether}}{\int H_{polyether} + \int H_{polyester}} \times 100$$

$$ether\ linkages\ (\%) = \frac{5.95}{5.95+3} \times 100 = 66\ \%$$

**Table 2.3.** List of $^{1}$H NMR chemical shifts of selected polyesters and polyethers.

| | **CHO/Anhydride** [a] | **PO/Anhydride** [b] |
|---|---|---|
| **Chemical shift (polyester) (ppm)** | $\delta$ 5.23-4.51 | $\delta$ 5.20-5.03 (methine H)<br>$\delta$ 4.31-3.95 (methylene H) |
| **Chemical shift (polyether) (ppm)** | $\delta$ 3.90-2.78 | $\delta$ 3.93-3.17 |

[a] $^{1}$H NMR spectra were recorded in DMSO-$d_6$ at 298 K. [b] $^{1}$H NMR spectra were measured in $CDCl_3$ at 298 K.

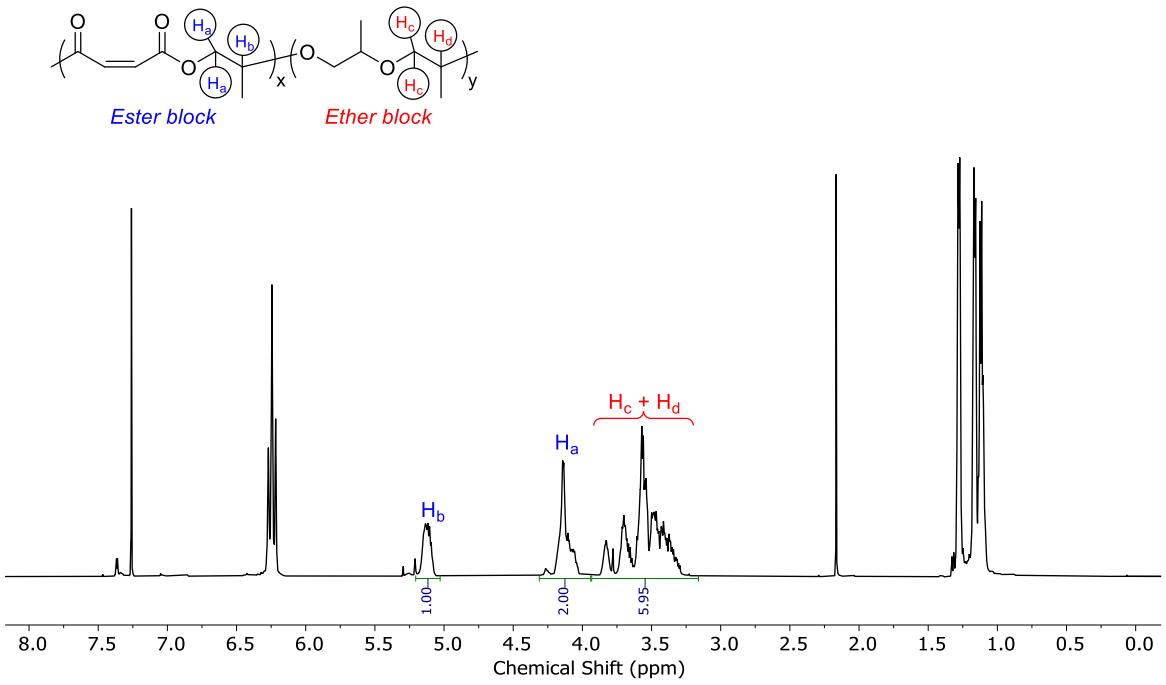



**Figure 2.6.** $^{1}$H NMR of isolated poly(PO-*ran*-MA) in $CDCl_3$ at 298 K.

### 2.2.1.3. $^{1}H\{^{1}H\}$ NMR spectroscopy for stereocontrol degree calculation in PLA

Owing to the presence of stereogenic centres on LA monomers, there are three different LA isomers namely *D*-LA (*R*,*R*), *L*-LA (*S*,*S*), and *meso*-LA (*R*,*S*). Chapter 3 focuses on the polymerisation of *rac*-LA, a 50:50 mixture of both *D*- and *L*-LA. Various types of PLA microstructures can be obtained from this mixture, depending on the selectivity of the catalyst (Figure 2.7). Individual microstructures can be identified by two parameters, $P_i$ and $P_s$ where $P_i$ is probability of isotactic enchainment and $P_s$ is probability of syndiotactic enchainment between two monomer units. This means that if the catalyst has a higher rate of ring-opening for one enantiomer, isotactic PLA will be obtained ($P_i \leq 1$). Heterotactic PLA will be formed if the catalyst ring-opens both enantiomers alternatively ($P_s \leq 1$). In the case of poor catalyst selectivity both enantiomers are ring-opened randomly and atactic PLA will be prepared ($P_i = P_s = 0.5$).

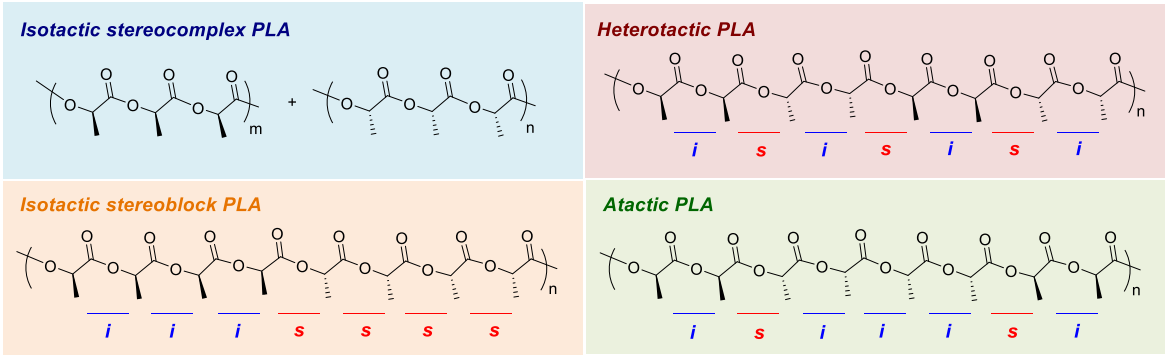



**Figure 2.7.** Possible polymer microstructures obtained from *rac*-LA (i and s represent isotactic and syndiotactic enchainments, respectively).

$P_i$ and $P_s$ can be determined from $^{1}H\{^{1}H\}$ NMR spectroscopy using the Bernoulli statistical model. A $^{1}H\{^{1}H\}$ NMR spectrum of isolated PLA prepared from **3.5** shows five different resonances (Figure 2.8). Each resonance represents an individual tetrad probability which was identified following the literature.[9, 10] The deconvoluted spectrum was analysed with MestReNova v.11.0.2 using the Global Spectral Deconvolution (GSD) algorithm (level 2) with 5 fitting cycles, and the peak areas of the deconvoluted peaks were used to calculate

the normalised tetrad integrals. $P_i$ and $P_s$ were then calculated from each tetrad level following Bernoulli statistical equations (see the equations below).[11]

$$[iii] = P_i^2 + P_iP_s/2 \quad (1)$$

$$[iis] = P_iP_s/2 \quad (2)$$

$$[sii] = P_iP_s/2 \quad (3)$$

$$[sis] = P_s^2/2 \quad (4)$$

$$[isi] = (P_s^2 + P_iP_s)/2 \quad (5)$$

The reported $P_i$ and $P_s$ values are all obtained from the average values from five different tetrad integrals. The errors associated with each $P_i$ were determined by calculating standard of the mean, which is described in the following equation. σ is standard deviation and N is the number of $P_i$ or $P_s$ values used to calculate an average $P_i$ or $P_s$.

$$\text{Standard error} = \frac{\sigma}{\sqrt{N}}$$

| Tetrad | Integration | $P_i$ |
|---|---|---|
| sis | 0.02 | 0.77 |
| sii/iis | 0.02 | 0.95 |
| iis/sii | 0.03 | 0.93 |
| iii | 0.88 | 0.92 |
| isi | 0.04 | 0.92 |
| **Average** | | **0.90 ± 0.05** |

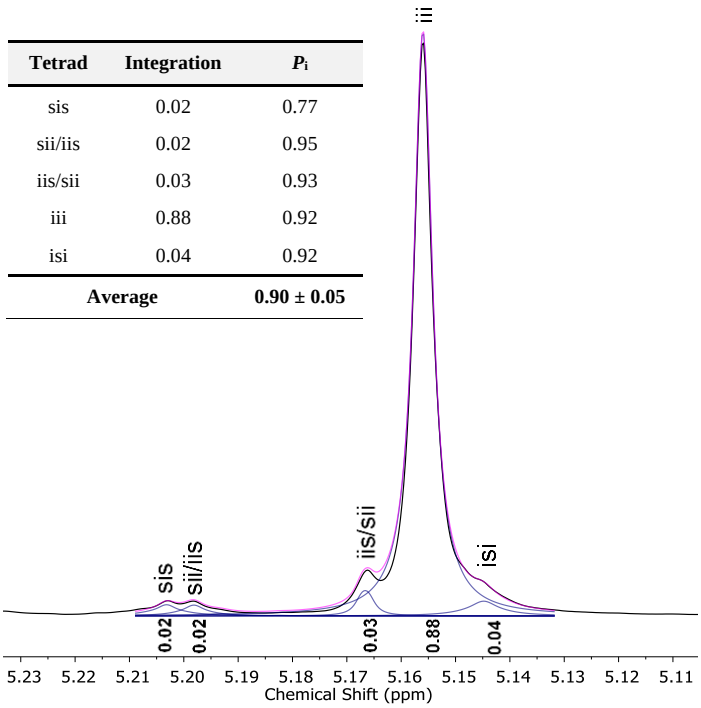



**Figure 2.8.** $^1H\{^1H\}$ NMR spectrum of isolated PLA, initiated by **3.5**.

Additionally, the mechanism of polymerisation (which determines the selectivity), can be determined by the ratio of individual tetrads. In the case of chain-end control (CEC) mechanism, the ratio of tetrads is iis:isi:sii = 1:1:1.[1, 2, 4] In contrast, if the catalyst operates using an enantiomorphic site control (ESC) mechanism, the tetrads ratio observed is iis:isi:sis:sii = 1:2:1:1. In the case of isolated PLA, prepared by **3.5**, a ratio of iis:isi:sii = 0.031:0.039:0.022 ≈ 1:1:1 was seen, thus suggested the CEC mechanism is more predominant in this In(III) system.[1]

### 2.2.1.4. Proof of formation of copolymer

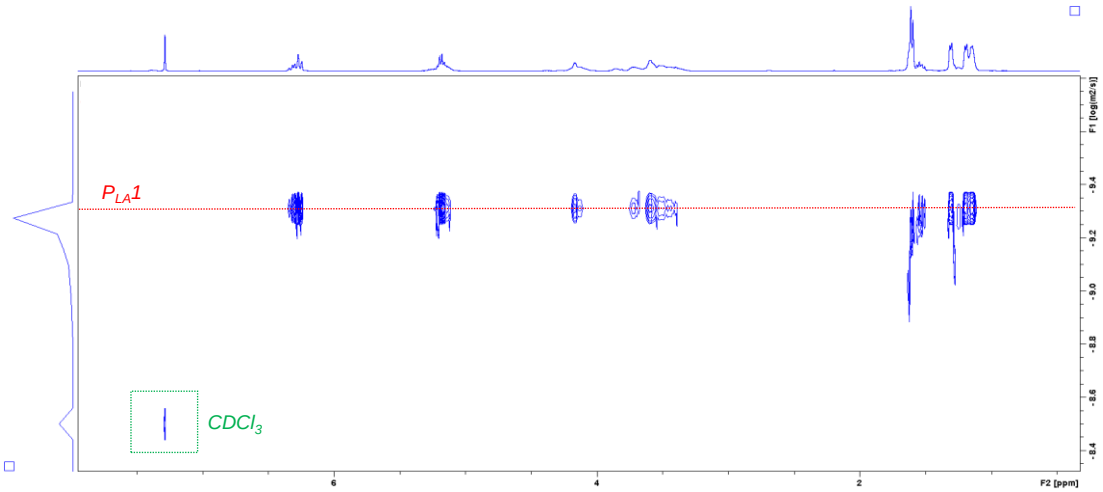



**Figure 2.9.** $^1$H DOSY NMR spectrum of **$P_{LA}1$** in $CDCl_3$ at 298 K.

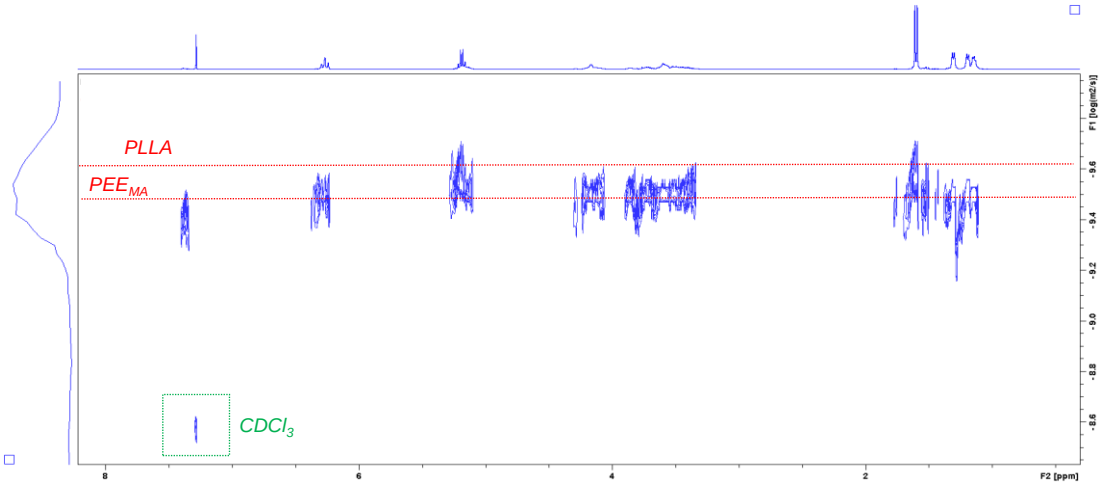



**Figure 2.10.** $^1$H DOSY NMR spectrum of PLLA and $PEE_{MA}$ blend in $CDCl_3$ at 298 K.

A variety of two-dimensional NMR spectroscopic techniques were used to characterise the architectures of the reported polymers. $^{1}$H DOSY NMR spectroscopy was used to confirm the formation of the copolymer. $^{1}$H DOSY NMR experiments resolve the different compounds based on their differing diffusion coefficients. The formation of copolymer is indicated by comparing the $^{1}$H DOSY NMR spectrum of a copolymer to a blend of the respectively homopolymers.[12] A single chain copolymer should exhibit a single diffusion coefficient whereas two different diffusion coefficients should be observed in a polymer blend. It should be noted that it is important for the blended homopolymers to have comparable molar masses as their blocks in the copolymer. $^{1}$H DOSY NMR spectrum shows a single diffusion coefficient for **$P_{LA}$1** copolymer whereas two different diffusion coefficients were seen in the case of blend PLLA and $PEE_{MA}$ (Figures 2.9 and 2.10).

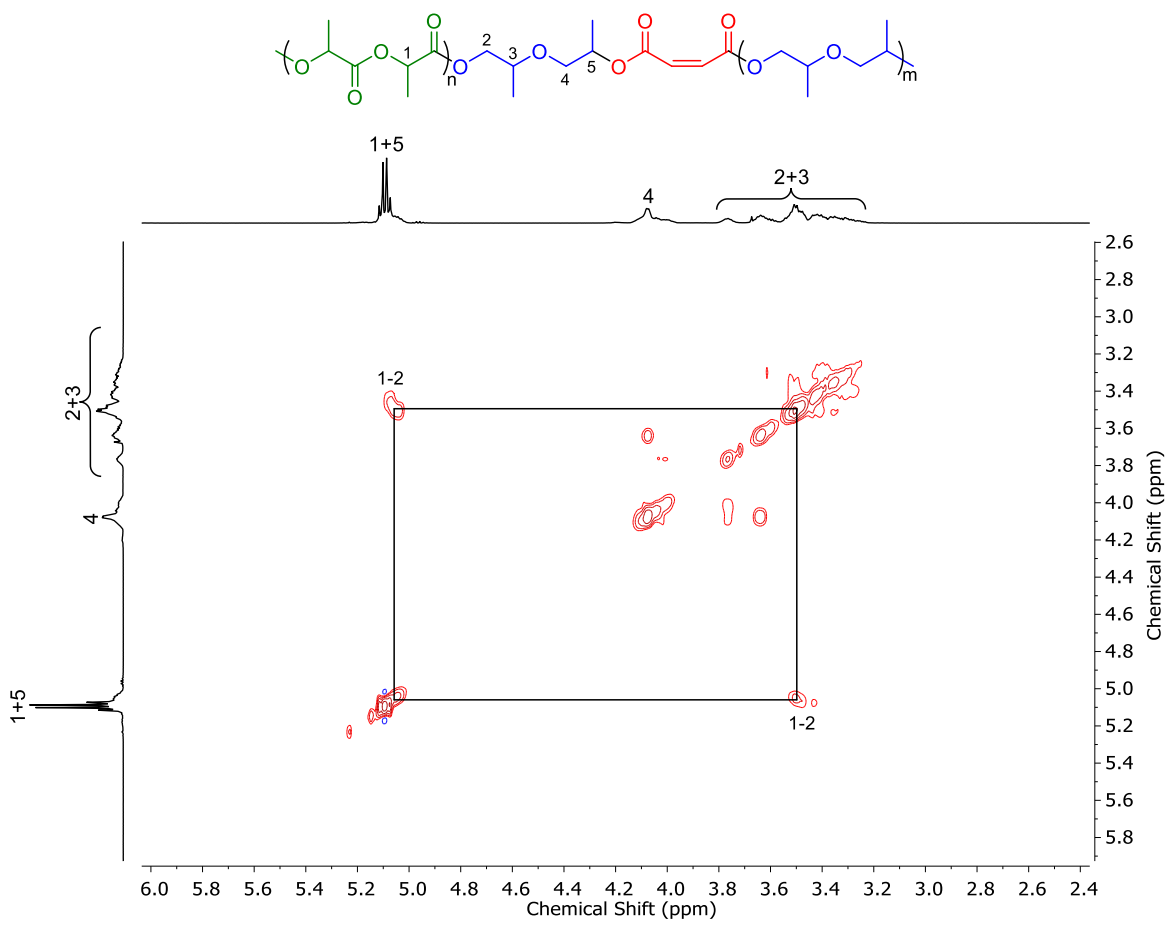



**Figure 2.11.** $^{1}$H-$^{1}$H TOCSY NMR spectrum of $PEE_{MA}$-*b*-PLLA.

$^{1}$H-$^{1}$H Total Correlation Spectroscopy (TOCSY) NMR experiments are often used to study the correlation in large molecules (*e.g.* proteins, oligosaccharides) where complicated couplings are seen. In this thesis, $^{1}$H-$^{1}$H TOCSY NMR spectroscopy was used to study the $^{1}$H correlations in the two polymer chains of block copolymers.[12] The $^{1}$H-$^{1}$H TOCSY NMR spectrum shows the proton correlation of PEE$_{MA}$-*b*-PLLA (Figure 2.11). The correlation between the methylene proton of the PO units in polyester-ether block (2) and the methine protons of PLLA (1) is observed, confirming the junction between two polymer blocks.

### 2.2.2. Size-Exclusion Chromatography (SEC)

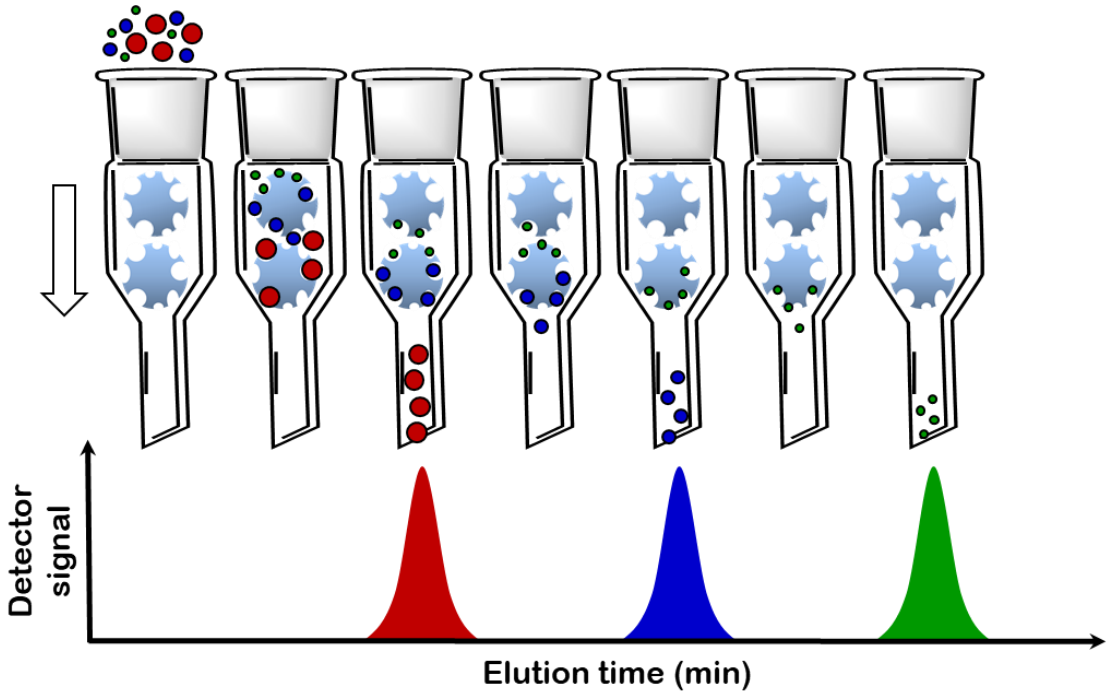



**Figure**. **2.12.** The separation mechanism for size-exclusion chromatography.

Size exclusion chromatography (SEC), a liquid chromatography technique, has been widely used to determine the size of macromolecules including proteins and polymers. SEC employs beads as a stationary phase and various solvents are used as a mobile phase. The liquid mobile phase can flow around or in and out of the bead pores. After the polymers are dissolved in the organic solvent, they are assumed to adopt a random coil conformation

(represented by spheres with different colours in Figure 2.12). High molar mass polymers form spheres with larger radii than shorter chain polymers. The separation mechanism is based on the solvodynamic volume of the macromolecule. After the polymer solution is injected to the column, they elute through the column beads *via* the flow of mobile phase. In the case of high molar mass polymers, the solvodynamic radii may be greater than the pore sizes in which case they elute quickly from the column and show a shorter retention time. In contrast, the lower molar mass polymers have smaller solvodynamic radii and can enter the pores (only entering pores of larger radii) and as such take longer to elute and show longer retention times (see Figure 2.12). Polymer molar masses reported in this thesis were determined against polystyrene standards. In the case of PLA, a correction factor of 0.58 was applied.[13] A correction factor of 0.56 was used to correct PCL molar mass.[14] Other polyester and polyether molar masses were reported as obtained.

### 2.2.3. Differential Scanning Calorimetry (DSC)

Glass transition temperature ($T_g$), crystallisation temperature ($T_c$) and melting temperature ($T_m$) of the isolated polymers reported in the thesis were determined using DSC. DSC is a thermoanalytical technique which measures heat flow changes between the sample and an empty reference crucible resulting from physical or chemical transformations of materials as a function of time or temperature. A DSC thermogram of isolated PLA, prepared by the indium complex **3.4** showed three different transitions, including $T_g$, $T_m$, and $T_c$ (Figure 2.13). $T_g$, the temperature where polymer changes from a rigid glassy state to a viscous rubbery form, may occur in an amorphous or semi-crystalline polymer. This transition can be observed as a 'step' on the DSC thermogram base line. $T_c$, a temperature where material crystallises in the heating cycle and is usually observed when there are barriers to crystallisation that annealing (holding at a higher temperature) or the heating cycle can reveal, and $T_m$, a temperature where the material begins to melt, are only seen in (semi-)

crystalline materials. Crystallisation is an exothermic process while melting is endothermic. Both transitions can be observed as peaks in the DSC thermogram. The percentage crystallinity of a material can be calculated from peak areas of melting/crystallisation peaks compared to a reference sample which has 100 % crystallinity.

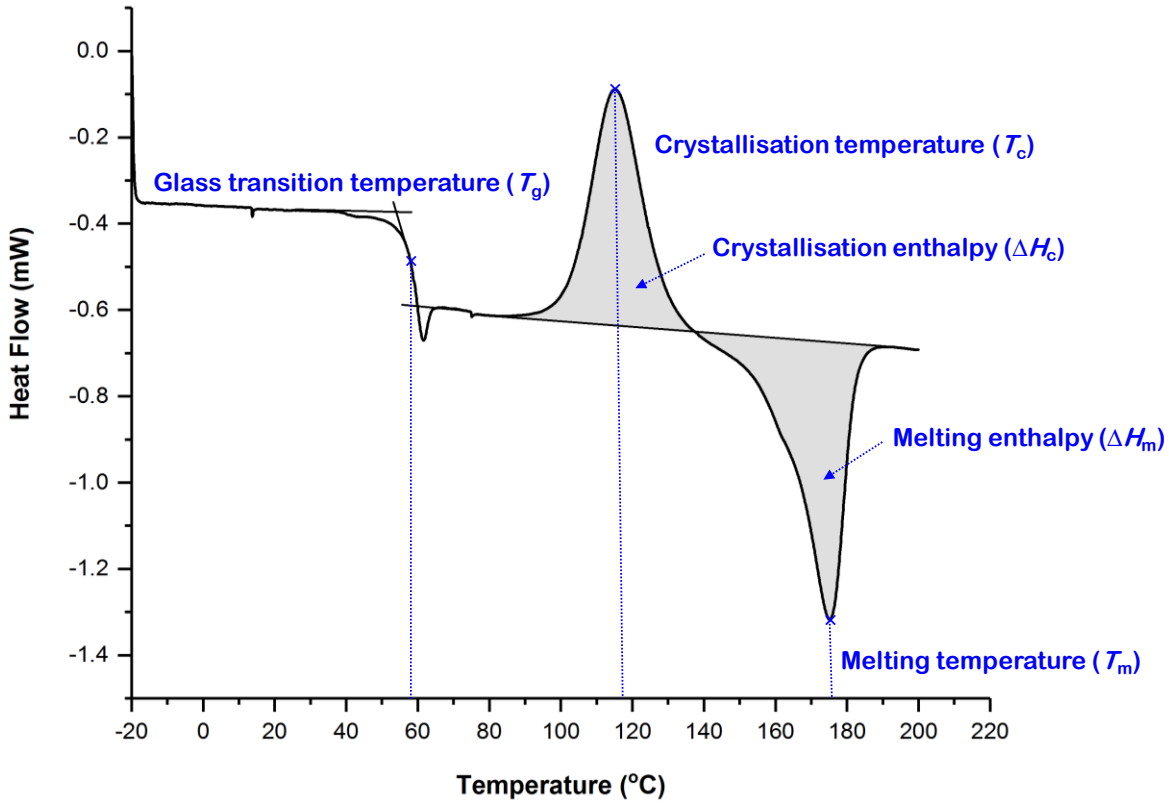



**Figure 2.13.** DSC thermogram of isolated PLA, initiated by complex **3.4**.

*Percentage crystallinity calculation:*

$$Crystallinity\ (\%) = \frac{\Delta H_m}{\Delta H_m^0} \times 100\%$$

*Where $\Delta H_m^0$ is a melting enthalpy of 100 % crystalline material.*

In the case of the DSC thermogram showed in Figure 2.13 ($\Delta H_m^0$ of PLA = 93 J g$^{-1}$)[15]

$$Crystallinity\ (\%) = \frac{25.68}{93} \times 100\ \%$$

$$Crystallinity\ (\%) = \ 28\ \%$$

### 2.2.4. Thermogravimetric Analysis (TGA)

Thermal degradation temperatures ($T_d$) of the polymers presented in this thesis were determined by TGA. TGA is a thermal analysis method which measures the mass changes for a material function of temperature or time. In this thesis, a dynamic thermogravimetric method, where a weight loss of sample was measured while continuously increasing temperature at constant rate is employed. The heating rate was usually kept constant at 5 °C $min^{-1}$ and the experiments were typically performed from 25 °C to 500 °C. An example TGA thermogram of PLLA, catalysed by $Sn(OMe)_2$ is displayed in Figure 2.14. $T_d$ can be obtained by analysing the curve and is generally reported at 5 % weight loss ($T_{d5}$). In the case of Figure 2.14, a $T_{d5}$ of 230 °C was observed.

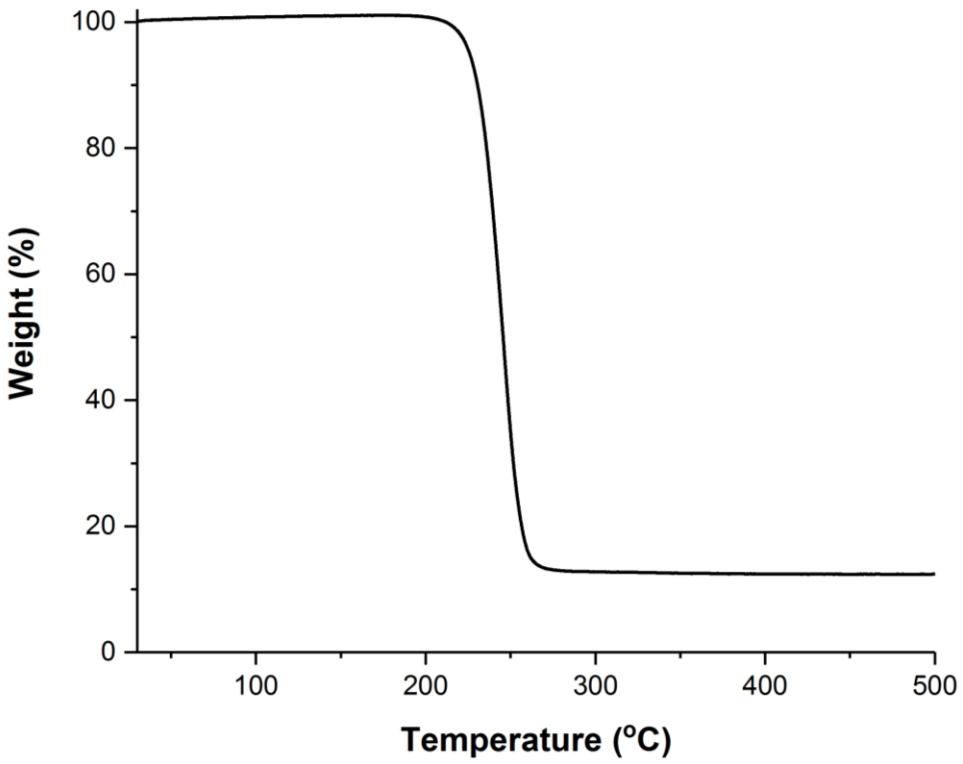



**Figure 2.14.** TGA thermogram of PLLA, catalysed by $Sn(OMe)_2$.

### 2.2.5. Tensile Mechanical Testing

Mechanical properties (*e.g.* strength, percent elongation, toughness *etc.*) of the polymeric materials presented in chapter 5 were determined using tensile measurements. Tensile analysis is an analytical technique which helps to determine the behavior of a material under strain. After the tensile (pulling) stress is applied to the material, the equipment will measure the response of the specimen. As a result, tensile tests can determine how strong a material is and how much it can elastically deform. The tensile curve of PLLA, containing 2 wt. % of **PLA1** is illustrated in Figure 2.15.

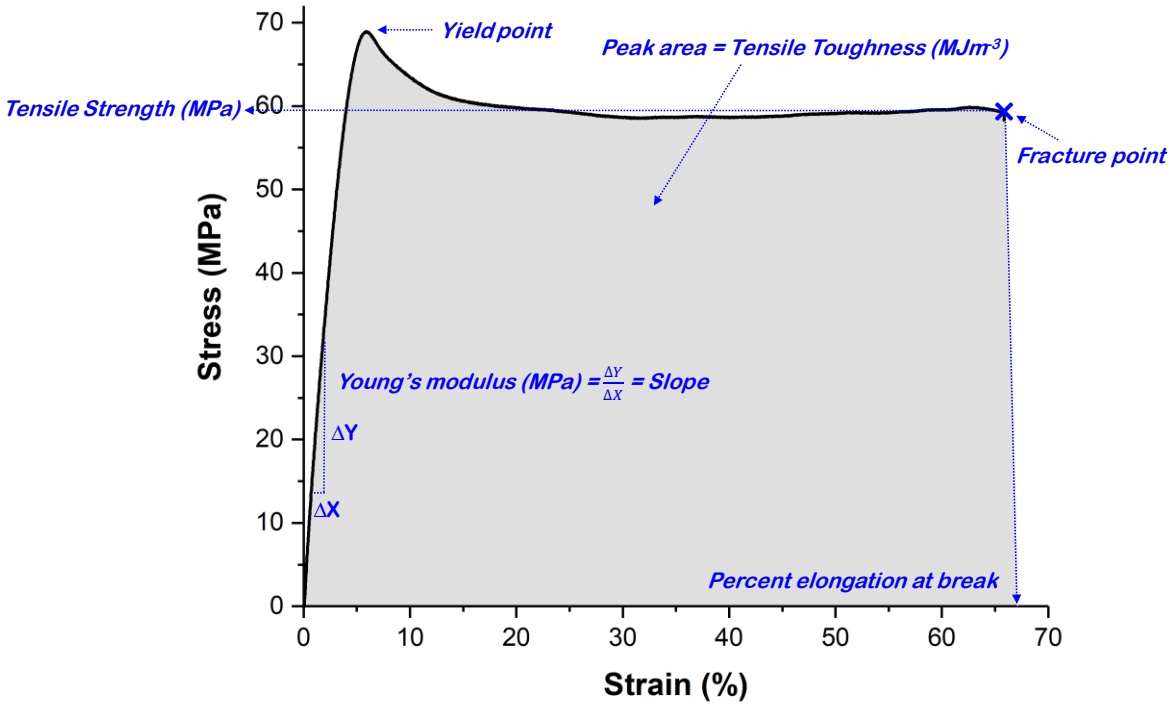



**Figure 2.15.** Tensile plot of PLLA, containing 2 wt. % of **PLA1**.

The Young's modulus can be identified from the slope at low strain of the plot between stress and strain (Figure 2.15). Additionally, a peak area under stress *vs.* strain curve can further determine the material's tensile toughness (Figure 2.15).

## 2.3. Kinetic Studies

### 2.3.1. LA polymerisation catalysis

In chapter 3, the integrated rate law method was used to determine polymerisation order in both LA and catalyst concentrations and determine the rate law, which can be simplified as:

$$Rate = k_{obs}[LA]^x$$

*where* $k_{obs} = k_p[catalyst]^x$ and $k_p$ = propagation rate constant

$$Rate = k_p[catalsyt]^x[LA]^y$$

The kinetic investigation was studied using the Michaelis-Menten model. This model has been widely used in enzyme-catalysed reactions and has been extensively used as a model in LA polymerisation kinetic studies. The model can be exemplified by the following equation.[9] This model starts with the reversible reaction between the catalyst $L_nM(OR)$ and LA monomer to form the intermediate $L_nM(OR)\cdot LA$ complex which then reacts irreversibly to form PLA as the polymer product.

$$[L_nM(OR)] + [LA] \underset{k_{-1}}{\overset{k_1}{\rightleftharpoons}} [L_nM(OR)\cdot LA] \xrightarrow{k_2} [L_nM(OR)] + [PLA]$$

The polymerisation rate can then be calculated from:

$$\frac{d[PLA]}{dt} = k_2[L_nM(OR)\cdot LA]$$

A steady state approximation is used to determine the concentration of $L_nM(OR)\cdot LA$. In this case, the reactive intermediate concentration is present at low concentrations and constant throughout polymerisation thus, its concentration is negligible.

$$\frac{d[L_nM(OR)\cdot LA]}{dt} = k_1[L_nM(OR)][LA] - k_{-1}[L_nM(OR)\cdot LA] - k_2[L_nM(OR)\cdot LA] = 0$$

$$[L_nM(OR)\cdot LA] = \frac{k_1[L_nM(OR)][LA]}{k_{-1}+k_2}$$

Additionally, the total concentration of the catalyst is $[L_nM(OR)]_0$, thus, the amount of free catalyst ($[L_nM(OR)]$) should be $[L_nM(OR)]_0 - [L_nM(OR)\cdot LA]$ and this is substituted into the previous equation to give:

$$[L_nM(OR)\cdot LA] = \frac{k_1[[L_nM(OR)]_0 - [L_nM(OR)\cdot LA]][LA]}{k_{-1}+k_2}$$

Which further rearranges to give

$$[L_nM(OR)\cdot LA] + k_1[L_nM(OR)\cdot LA][LA] = \frac{k_1[L_nM(OR)]_0[LA]}{k_{-1}+k_2}$$

$$[L_nM(OR)\cdot LA] = \frac{k_1[L_nM(OR)]_0[LA]}{k_{-1}+k_2+k_1[LA]} = \frac{[L_nM(OR)]_0[LA]}{K_M+[LA]}$$

*Where $K_M$ is Michaelis-Menten constant and* $K_M = \frac{k_1}{k_{-1}+k_2}$

The overall polymerisation rate can therefore be rearranged to:

$$\frac{d[PLA]}{dt} = k_2\frac{[L_nM(OR)]_0[LA]}{K_M+[LA]}$$

In the case of [LA] >> $K_M$, the LA concentration is assumed to be in excess and constant throughout the polymerisation. The overall polymerisation rate depends on [LA]. The catalysts should always be saturated with monomer and therefore the polymerisation rate obtained under these conditions is maximised.

## 2.4. References


(1) Bakewell, C.; Cao, T.-P.-A.; Long, N.; Le Goff, X. F.; Auffrant, A.; Williams, C. K., Yttrium Phosphasalen Initiators for *rac*-Lactide Polymerization: Excellent Rates and High Iso-Selectivities. *J. Am. Chem. Soc.* **2012,** *134* (51), 20577–20580.

(2) Bakewell, C.; White, A. J. P.; Long, N. J.; Williams, C. K., Metal-Size Influence in Iso-Selective Lactide Polymerization. *Angew. Chem. Int. Ed.,* **2014,** *53* (35), 9226–9230.

(3) Cao, T.-P.-A.; Buchard, A.; Le Goff, X. F.; Auffrant, A.; Williams, C. K., Phosphasalen Yttrium Complexes: Highly Active and Stereoselective Initiators for Lactide Polymerization. *Inorg. Chem.* **2012,** *51* (4), 2157–2169.

(4) Myers, D.; White, A. J. P.; Forsyth, C. M.; Bown, M.; Williams, C. K., Phosphasalen Indium Complexes Showing High Rates and Isoselectivities in *rac*-Lactide Polymerizations. *Angew. Chem. Int. Ed.,* **2017,** *56* (19), 5277–5282.

(5) Thevenon, A.; Cyriac, A.; Myers, D.; White, A. J. P.; Durr, C. B.; Williams, C. K., Indium Catalysts for Low-Pressure CO2/Epoxide Ring-Opening Copolymerization: Evidence for a Mononuclear Mechanism? *J. Am. Chem. Soc.,* **2018,** *140* (22), 6893–6903.

(6) Garden, J. A.; Saini, P. K.; Williams, C. K., Greater than the Sum of Its Parts: A Heterodinuclear Polymerization Catalyst. *J. Am. Chem. Soc.,* **2015,** *137* (48), 15078–15081.

(7) Thevenon, A.; Garden, J. A.; White, A. J. P.; Williams, C. K., Dinuclear Zinc Salen Catalysts for the Ring Opening Copolymerization of Epoxides and Carbon Dioxide or Anhydrides. *Inorg. Chem.* **2015,** *54* (24), 11906–11915.

(8) Addison, A. W.; Rao, T. N.; Reedijk, J.; van Rijn, J.; Verschoor, G. C., Synthesis, structure, and spectroscopic properties of copper(II) compounds containing nitrogen–sulphur donor ligands; the crystal and molecular structure of aqua[1,7-bis(N-methylbenzimidazol-2′-yl)-2,6-dithiaheptane]copper(II) perchlorate. *J. Chem. Soc. Dalton Trans.,* **1984,** (7), 1349–1356.

(9) Hormnirun, P.; Marshall, E. L.; Gibson, V. C.; Pugh, R. I.; White, A. J. P., Study of ligand substituent effects on the rate and stereoselectivity of lactide polymerization using aluminum salen-type initiators. *Proc. Natl. Acad. Sci.,* **2006,** *103* (42), 15343–15348.

(10) Nomura, N.; Ishii, R.; Akakura, M.; Aoi, K., Stereoselective Ring-Opening Polymerization of Racemic Lactide Using Aluminum-Achiral Ligand Complexes: Exploration of a Chain-End Control Mechanism. *J. Am. Chem. Soc.,* **2002,** *124* (21), 5938–5939.

(11) Coudane, J.; Ustariz-Peyret, C.; Schwach, G.; Vert, M., More about the stereodependence of DD and LL pair linkages during the ring-opening polymerization of racemic lactide. *J. Polym. Sci., Part A: Polym. Chem.,* **1997,** *35* (9), 1651–1658.

(12) Stößer, T.; Mulryan, D.; Williams, C. K., Switch Catalysis To Deliver Multi-Block Polyesters from Mixtures of Propene Oxide, Lactide, and Phthalic Anhydride. *Angew. Chem. Int. Ed.,* **2018,** *57* (51), 16893–16897.

(13) Baran, J.; Duda, A.; Kowalski, A.; Szymanski, R.; Penczek, S., Intermolecular chain transfer to polymer with chain scission: general treatment and determination of $k_p/k_{tr}$ in *L,L*-lactide polymerization. *Marcomol. Rapid Commun.,* **1997,** *18* (4), 325–333.

(14) Barakat, I.; Dubois, P.; Jérôme, R.; Teyssié, P., Macromolecular engineering of polylactones and polylactides. X. Selective end-functionalization of poly(*D,L*)-lactide. *J. Polym. Sci., Part A: Polym. Chem.,* **1993,** *31* (2), 505-514.

(15) Ray, S. S.; Okamoto, M., Biodegradable Polylactide and Its Nanocomposites: Opening a New Dimension for Plastics and Composites. *Marcomol. Rapid Commun.,* **2003,** *24* (14), 815-840.

# *Chapter 3*

## *Phosphasalen Indium Complexes Showing High Activity and Selectivity for rac-Lactide and Lactone Polymerisations*

*An expert is a man who has made all the mistakes which can be made, in a narrow field...*

*~ Niels Bohr ~*

**Overview**

This chapter presents a novel series of phosphasalen indium complexes, **3.1**–**3.5,** and their uses in ring-opening polymerisation catalysis for various lactones. The synthesis and characterisation of all complexes in both solution and solid states are described. The structure-activity and structure-stereoselectivity relationships are examined. These include the importance of the diamine linkers, the effect of phosphorous substituents, and the influence of alkoxide co-ligands. Furthermore, the scope of monomer substrates is explored with a range of the target complexes and, where relevant, stereocontrol mechanisms are investigated. The experimental findings are used to discuss the structures of key propagating species.

## 3.1. Introduction

Aliphatic polyesters, an interesting class of (bio)degradable polymers, comprise ester repeat units which are susceptible to degradation following use. Some of these polymers have the potential to substitute pervasive petroleum based polymers.[1-3] Conventionally, polyesters are obtained from the direct condensation of diols and diacids.[4] The preparation of high molar mass polymer using this method is limited by the need for the precise quantity control of diol and diacid substrates. Without quality control, materials with less attractive properties are obtained.[4] Ring-opening polymerisation (ROP) of cyclic esters, utilising catalysts, allows the production of high molar mass aliphatic polyesters with narrow molar mass distributions, and polymers with more uniform properties can be obtained.[5]

There are several catalysts reported to date for the ROP of cyclic esters to make various aliphatic polyesters.[5-8] Some of these are already used for plastic manufacture and comprise commercial products. For example, $Sn(oct)_2$, in the presence of an alcohol initiator, is widely used in the production of polylactide (PLA).[9] PLA, an aliphatic polyester, has

received considerable attention in both academia and industry in the past decades due to its biodegradability and biocompatibility.[1] In addition, the starting monomer, lactide (LA), is obtained from biorenewable resources and its degradation products are environmental friendly.[1] In 2019, approximately 190 000 tons of PLA were produced worldwide making it one of the highest volume biodegradable polymers produced globally.[10] Its thermal and mechanical properties depend strongly on its microstructure. For example, isotactic PLA is a semi-crystalline polymer whilst, heterotactic and atactic PLAs are amorphous materials.[11] In addition, the shelf life of semi-crystalline PLA is generally longer than that of amorphous polymers. Therefore, isotactic PLA is suitable for use as a high strength material, for durable goods and/or for other applications requiring longer degradation time (*e.g.* long-lasting packaging materials, 3D printing objects etc.).[1, 11] Isotactic PLA can be prepared from either: I) the polymerisation of enantiopure LA monomer using catalyst; or II) polymerisation of *rac*-LA using an iso-selective catalyst.[12] The polymer obtained from the first route generally exhibits only a moderate melting temperature ($T_m$) around 130–175 °C. In contrast, the production of stereoblock/complex PLA from *rac*-LA allows access to materials with much higher $T_m$ ($T_m \geq 230$ °C).[12]

Additionally, stereoblock PLA can be prepared in one-step by the iso-selective ring-opening polymerisation (ROP) of *rac*-LA. The process stereoselectivity, rate and control is highly dependent upon the nature of the ROP catalyst and by its mode of operation.[8, 13, 14] Generally, there are two stereocontrol mechanisms: 1) Enantiomorphic site control (ESC) occurs when chiral catalysts react faster with one LA enantiomer and 2) Chain-end control (CEC) occurs using achiral catalysts and with stereocontrol being induced by interactions between the catalyst and the growing polymer chain end group.[12] Currently, the highest iso-selectivity catalysts usually operate by enantiomorphic site control mechanisms and the stand-out examples are chiral salen aluminium catalysts (Al-salen).[15-18] After optimisation,

the most selective chiral Al-salen catalyst show probability of isotactic diad formation, $P_i$, values exceeding 0.95 (where $P_i = 1$ corresponds to a fully isotactic, stereoblock polymer).[19] The high performance of these Al-salen catalysts arises from very low rates of transesterification, and, hence, limited loss of stereo-sequences through scrambling side-reactions, but it comes with a significant down-side since rates of forward polymerisation, which are also a form of intermolecular transesterification, are also very slow.[12, 13, 15-21] Because of their low rates, most Al-salen complexes are applied at unacceptably high catalyst loadings (~1 mol %).[12, 13, 15-21] Enantiomorphic site control mechanisms inherently result in even slower polymerisation of the 'wrong' enantiomer which further limits their application in stereoblock PLA production. Pioneering work by Nomura and co-workers established that achiral Al-salen catalysts also showed outstanding iso-selectivity and operate by chain-end control mechanisms ($P_i$ = 0.92–0.98).[19, 20] Nomura's ground-breaking stereoselectivity discovery is unfortunately still limited by low activity values.[19]

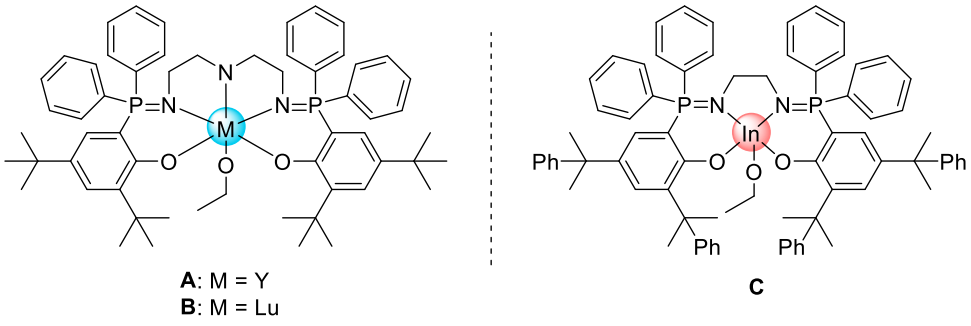



**Figure 3.1.** Previously reported iso-selective phosphasalen Y(III), Lu(III), and In(III) catalysts.[22-24]

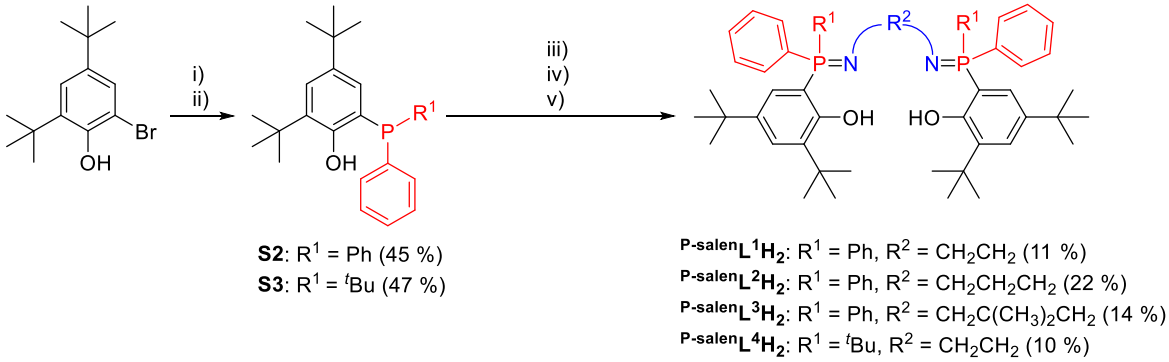
Our group has reported stereoselective phosphasalen metal catalysts, featuring yttrium(III), lutetium(III) and indium(III) (Figure 3.1).[22-25] The phosphasalen ligand is important in conferring high rates and stereocontrol and generally significantly out-performs when compared with analogous salen ligands.[22, 24-33] Phosphasalen ligands are both σ and π-donors and, so, are considerably more electron donating than salens. It is proposed that the

enhanced electron donation increases the lability of the metal alkoxide propagating bond and accelerates monomer insertion reactions.[26-28, 30-33] In addition to increasing polymerisation rates, phosphasalen ligands feature two phosphorus atoms and their substituents may enhance steric shielding and direct lactone coordination at the active site thereby enabling monomer stereoselectivity.[22-25, 27, 28, 34] The first iso-selective catalyst of this class was a pentadentate phosphasalen yttrium complex (**A**, Figure 3.1), showing $P_i$ = 0.72 ([LA]:[cat.] = 500:1, [LA] = 1 M, T = 25 °C).[22] Comparing a series of pentadentate phosphasalen lanthanide complexes revealed that the lutetium complex (**B**, Figure 1) showed the highest iso-selectivity with $P_i$ = 0.82 ([LA]:[cat.] = 500:1, [LA] = 1 M, T = 25 °C).[23] A tetradentate phosphasalen indium (**C**, Figure 1) catalyst showed even higher iso-selectivity $P_i$ = 0.87 ([LA]:[cat.] = 500:1, [LA] = 1 M, T = 25 °C) and better rate.[24] The highest performing catalysts were able to achieve full conversion of 500 equivalents of monomer in less than an hour and this is considerably faster and more iso-selective than many other reported complexes of indium and other metals featuring tetradentate ligands.[9] Notably, the same tetradentate ligand coordinated to yttrium resulted in a highly *heteroselective* catalyst, a finding whose explanation is not obvious and which underscores the need for detailed insight into structure-stereoselectivity mechanisms.[27, 28] Both isoselective yttrium and indium phosphasalen catalysts operate by chain-end control mechanisms and the continued development of this type of catalyst is desirable since it obviates expensive chiral ligands and allows for high rates throughout polymerisation reactions.

Given the promising polymerisation data using In(III) phosphasalen catalysts, it was relevant to conduct a more detailed study of structure-activity and structure-stereoselectivity relationships. Specifically, changes to the diamine linker chemistry were targeted as prior work on phosphasalen yttrium and lanthanide complexes revealed this site influenced rate

and stereocontrol. Additionally, all prior studies on phosphasalen metal catalysts applied symmetric diphenyl iminophosphoranes and so a second target was to understand the influence, if any, of asymmetric phosphorus on stereocontrol. The key objectives are: a) To synthesise and characterise a series of new phosphasalen indium complexes featuring different diamine linkers, as well as asymmetric phosphorous substituents. b) To investigate the structure-activity and structure-stereoselectivity relationships in lactide ROP catalysis. c) To better understand the mechanisms underpinning stereocontrol using these complexes. d) To understand the applicability of these complexes in the ROP of other lactone monomers.

### 3.2. Design, synthesis, and characterisation of ligands




**Scheme 3.1.** Synthetic routes used to make phosphasalen ligands. Reagents and conditions: i) $^{n}$BuLi (2.1 equiv.), $Et_2O$, –78 °C, 1 h; ii) $Ph_2PCl$ or ($^{t}$Bu)PhCl (1 equiv.), $Et_2O$, –78 °C, 18 h; iii) $Br_2$ (1 equiv.), DCM, –78 °C, 2 h; iv) $^{n}Bu_3N$ (0.5 equiv.), v) diamine backbone (0.5 equiv.) DCM, –78 °C, 18 h.

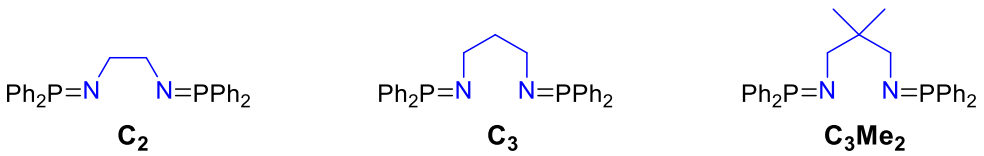



**Figure 3.2.** Structures of diamine linkers used in the formation of phosphasalen ligands.

The synthesis of all the target phosphasalen ligands is based on a modified Kirsanov reaction (Scheme 3.1).[22] First, a series of phosphasalen ligands featuring di-phenyl substituents on the phosphorous atoms and a range of diamine linkers were synthesised. A series of diamine

backbones with different degrees of flexibility, including ethylene diamine ($C_2$), propylene diamine ($C_3$), and 2,2-di-methyl-propyleanediamine ($C_3Me_2$) were used (Figure 3.2). Phosphasalen ligands $^{P\text{-salen}}\mathbf{L^1H_2}$–$^{P\text{-salen}}\mathbf{L^3H_2}$ were obtained, after purification by column chromatography ($Al_2O_3$, DCM:EtOH = 40:1), in 11–22 % yield. The ligands were fully characterised by multinuclear NMR spectroscopy and the purity was confirmed by elemental analysis. The $^1$H NMR spectra of ligands $^{P\text{-salen}}\mathbf{L^1H_2}$–$^{P\text{-salen}}\mathbf{L^3H_2}$ each show one set of resonances corresponding to all the expected environments in the ligand structures (Figures A1.8, A1.11, A1.14). The integrals of all the peaks also match expected values. A singlet phosphorous signal, around δ 41.6 ppm, was observed for each of the ligands in the $^{31}$P{$^1$H} NMR spectra, suggesting that both phosphorous atoms are in an identical environment, on an NMR time scale (Figures A1.10, A1.13, A1.16).

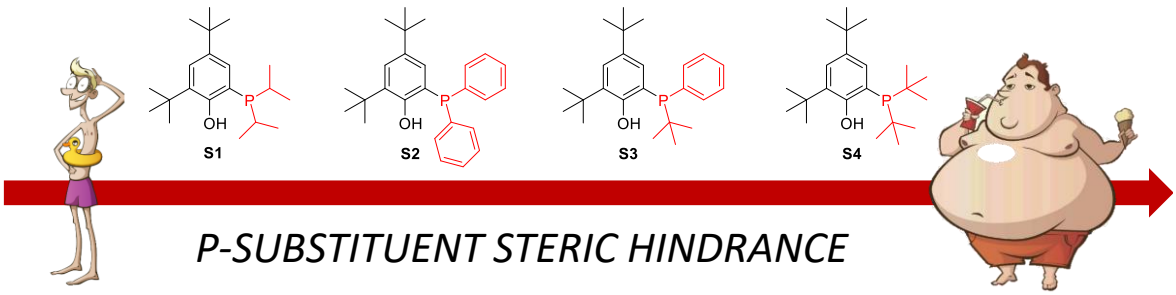
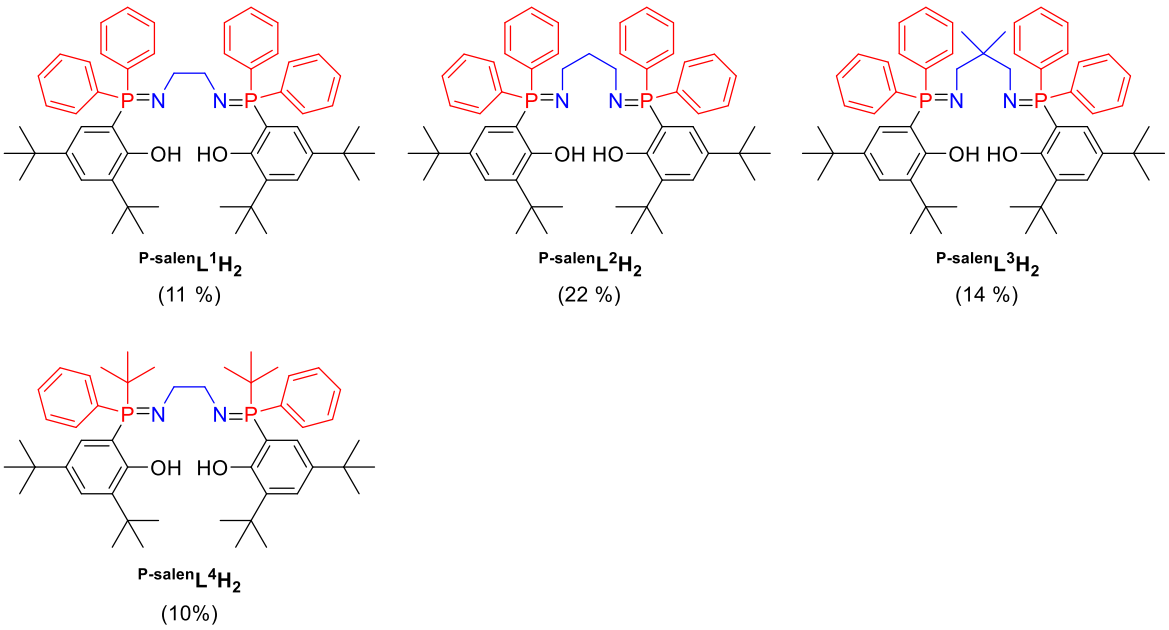



**Figure 3.3.** Structures of phosphine intermediates featuring different level of steric hindrance.

The best performing ligand backbone was further used to explore the effect of phosphorous substituents. Regarding the lactide polymerisation results, it was observed that the indium complex featuring the ethylene linker showed the highest polymerisation activity and second highest iso-selectivity (see more details in section 3.4). Therefore, the ethylene backbone was used to further explore the influence of the phosphorous substituents in this ligand system. A range of di-substituted phosphines, with different phosphorous substituents, were targeted. The selection of substituents based on steric hindrance and commercial availability (Figure 3.3). For example, using a di-isopropyl substituted phosphine could allow

understanding of reducing steric hindrance at the active site (compared to the usual diphenyl substituted ligand). Using a phosphine featuring asymmetric phenyl and *tert*-butyl groups or di-*tert*-butyl substituents could allow insight into increase steric congestion. Intermediates **S1**–**S3** were successfully synthesised and isolated as colourless crystals in 45–55 % yield.[35] **S1**–**S3** were characterised using multinuclear NMR spectroscopies and purity was authenticated by either elemental analysis or high resolution mass spectroscopy (Figures A1.2–A1.7). The $^{1}$H NMR spectra of all intermediates reveal one set of resonances assigned to the expected protons for each intermediate. In all cases, a singlet phosphorous signal, around –19.2 to –30.0 ppm, was observed. In the case of **S4**, $^{1}$H and $^{31}$P{$^{1}$H} NMR spectra suggested the formation of a mixture of products despite repeat synthesis attempts and this material was not progressed further. The pure phosphine intermediates (**S1**–**S3**) were then reacted with the ethylene diamine linker, *via* a modified Kirsanov reaction, to form the desired ligands (Scheme 3.1). Unfortunately, it was not possible to isolate the pure ligand from **S1** despite several attempts using solvent extractions, chromatography and selective crystallisation. A range of ligands, with different diamine linkers, were isolated from intermediate **S2** (see previous section). The reaction of **S3** with ethylene diamine led to the formation of $^{\text{P-salen}}\mathbf{L^{4}H_{2}}$ which was then characterised by multinuclear NMR spectroscopic techniques and its purity was assessed by elemental analysis (Figures A1.17–A1.21). Its $^{1}$H NMR spectrum showed the expected single set of resonances and a single phosphorous signal, at 55.9 ppm, indicate both phosphorous atoms are in equivalent environments. The structures of ligands $^{\text{P-salen}}\mathbf{L^{1}H_{2}}$–$^{\text{P-salen}}\mathbf{L^{4}H_{2}}$ are summarised in Scheme 3.2.

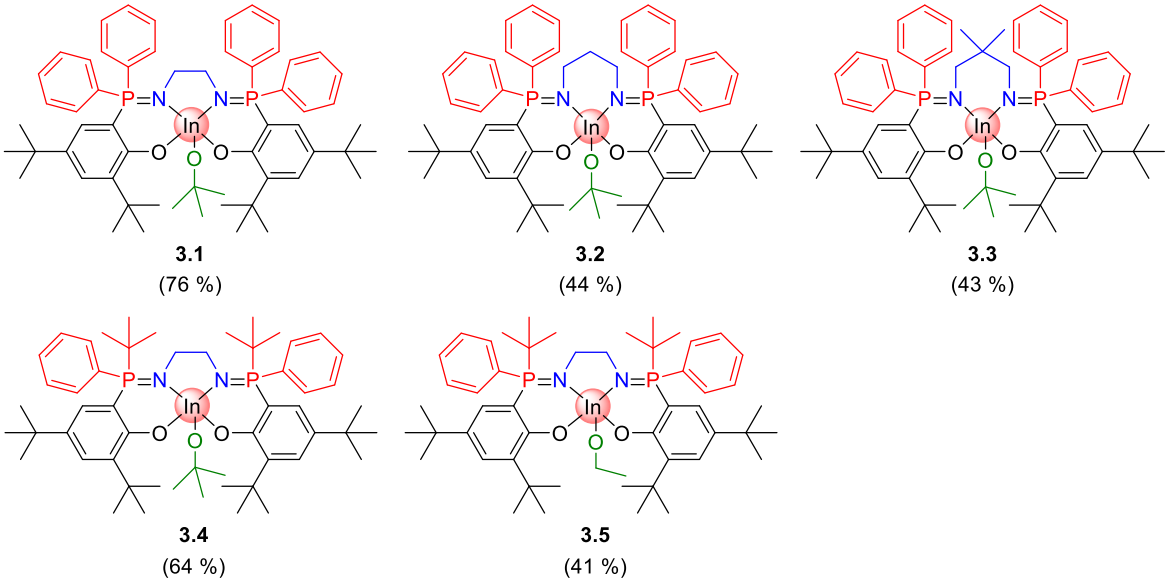



**Scheme 3.2.** Structures of phosphasalen ligands $^{P\text{-salen}}\mathbf{L^1H_2}$–$^{P\text{-salen}}\mathbf{L^4H_2}$.

Since ligand $^{P\text{-salen}}\mathbf{L^4H_2}$ possesses asymmetric phosphorous substituents and therefore, chiral phosphorous atoms, it was decided to gain further understanding of the ligand configuration in the solid state. Suitable single crystals of $^{P\text{-salen}}\mathbf{L^4H_2}$ were isolated by layer-by-layer crystallisation, with $CHCl_3$ and hexane, the molecular structure was determined by single crystal X-ray diffraction (SCXRD). SCXRD revealed $^{P\text{-salen}}\mathbf{L^4H_2}$ exists as a single diastereoisomeric pair (with *R*,*S* and *S*,*R* stereochemistry at each phosphorus atom) (Figure A1.40 and Tables A1.1 and A1.2). As the crystals were isolated from a sample which had been purified by column chromatography, it was important to establish whether the other set of diastereoisomers (*R*,*R* and *S*,*S*) also formed. Thus, the crude reaction product (*i.e.* prior to any purification by column chromatography) was analysed by $^1$H NMR spectroscopy (Figure A1.18). The $^1$H NMR spectrum of the crude product showed identical signals to the purified fraction after column chromatography and identical signals to the NMR of the isolated crystals (Figure A1.17). This data is consistent with the synthesis of only the *R*,*S*/*S*,*R* ligand diastereoisomers.

## 3.3. Synthesis and characterisation of phosphasalen indium complexes 3.1–3.5

### 3.3.1. Synthesis of complexes 3.1–3.5




**Scheme 3.3.** Structures of phosphasalen indium complexes **3.1**–**3.5**.

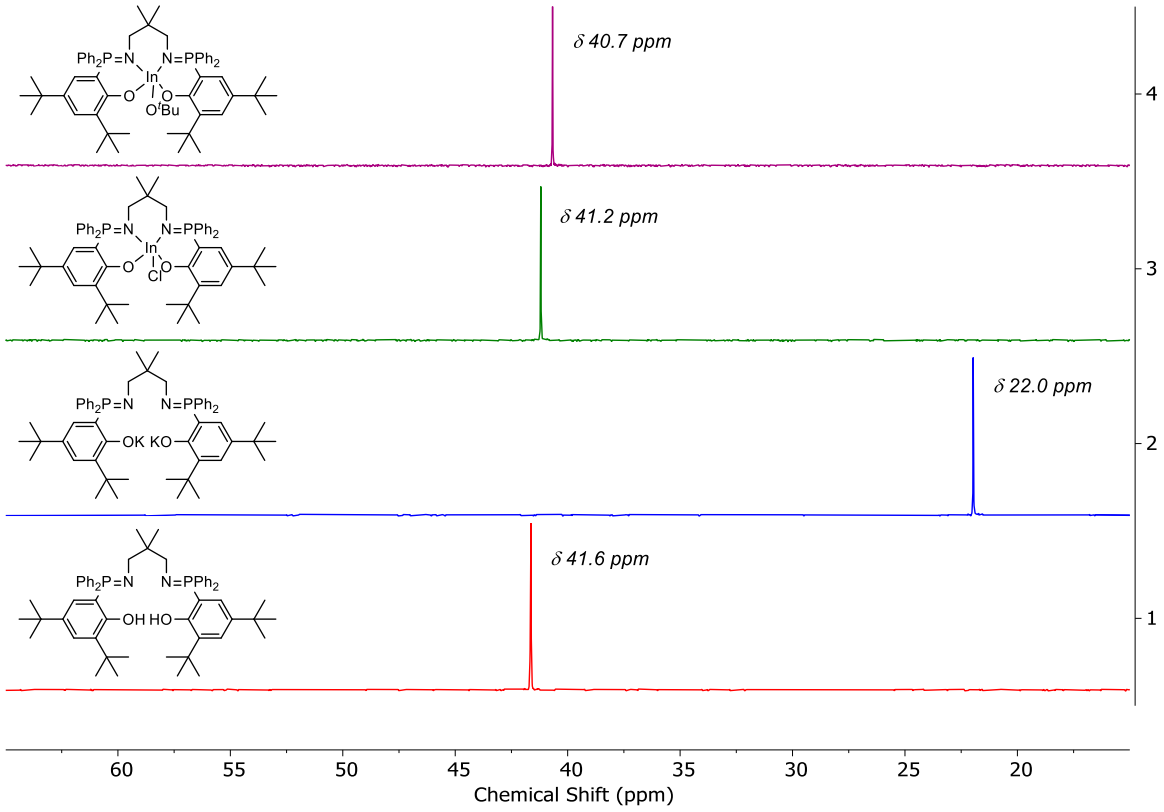



**Figure 3.4.** Stacks of the $^{31}P\{^{1}H\}$ NMR spectra acquired during each stage of the formation of complex **3.3**.

A range of indium alkoxide complexes, **3.1**–**3.5,** were isolated in moderate yield (41–64 %) after three step sequential reactions (Scheme 3.3). Each step of the complexation process was monitored by *in situ* $^{31}P\{^{1}H\}$ NMR spectroscopy and the three reactions were conducted without intermediate isolation (see the example of the $^{31}P\{^{1}H\}$ NMR spectra of the formation of complex **3.3** in Figure 3.4).

For example, in the synthesis of indium complex **3.3**, the appropriate ligand was first deprotonated, using $KN(Si(CH_3)_3)_2$ as the base, to from the di-potassium salt intermediate and, in this step, the phosphorous resonance shifts from δ 41.6 ppm to δ 22.0 ppm. The di-potassium salt intermediate was then reacted, *in situ*, with $InCl_3$ to yield the chloro indium complex. The phosphorous signal shifts from δ 22.0 ppm to δ 41.2 ppm. The chloro indium intermediate was further reacted with either KO$^t$Bu or KOEt to generate the indium alkoxide complex *in situ* and only a slight change in the chemical shift of phosphorous was observed in this case.

### 3.3.2. Solid state characterisation for 3.1–3.5

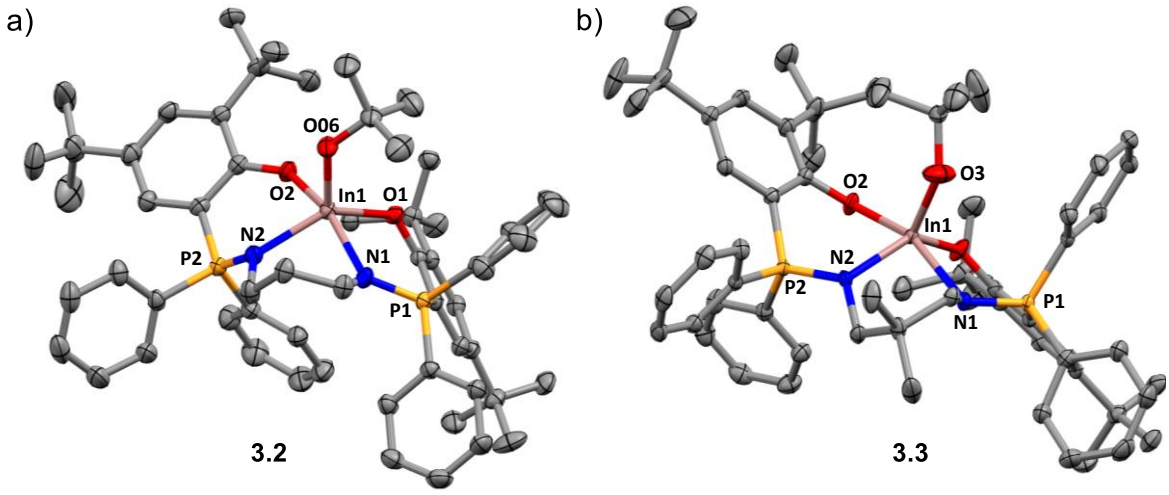



**Figure 3.5.** Representation of molecular structures of a) complex **3.2**, and b) complex **3.3**.

**Table 3.1.** Selected bond lengths (Å) and angles (º) of complexes **3.2**–**3.5**.

| Bond length (Å) | | Angle (º) | | | |
|---|---|---|---|---|---|
| **Complex 3.2** | | | | | |
| In(1)-N(1) | 2.218(1) | N(1)-In(1)-N(2) | 84.64(5) | N(2)-In(1)-O(2) | 85.25(5) |
| In(1)-N(2) | 2.176(1) | N(1)-In(1)-O(1) | 86.41(5) | N(2)-In(1)-O(06) | 109.12(5) |
| In(1)-O(1) | 2.106(1) | N(1)-In(1)-O(2) | 157.09(5) | O(1)-In(1)-O(2) | 86.43(5) |
| In(1)-O(2) | 2.127(1) | N(1)-In(1)-O(06) | 106.54(5) | O(1)-In(1)-O(06) | 115.38(5) |
| In(1)-O(3) | 2.025(1) | N(2)-In(1)-O(1) | 135.34(5) | O(2)-In(1)-O(06) | 96.18(5) |
| **Complex 3.3** | | | | | |
| In(1)-N(1) | 2.250(3) | N(1)-In(1)-N(2) | 83.2(1) | N(2)-In(1)-O(2) | 88.0(1) |
| In(1)-N(2) | 2.168(3) | N(1)-In(1)-O(1) | 87.4(1) | N(2)-In(1)-O(3) | 107.1(1) |
| In(1)-O(1) | 2.090(3) | N(1)-In(1)-O(2) | 157.0(1) | O(1)-In(1)-O(2) | 84.7(1) |
| In(1)-O(2) | 2.152(2) | N(1)-In(1)-O(3) | 91.5(1) | O(1)-In(1)-O(3) | 115.0(1) |
| In(1)-O(3) | 2.002(4) | N(2)-In(1)-O(1) | 137.1(1) | O(2)-In(1)-O(3) | 111.4(1) |
| **Complex 3.4** | | | | | |
| In(1)-N(1) | 2.178(4) | N(1)-In(1)-N(2) | 77.2(1) | N(2)-In(1)-O(2) | 85.9(1) |
| In(1)-N(2) | 2.190(4) | N(1)-In(1)-O(1) | 88.4(1) | N(2)-In(1)-O(3) | 99.8(1) |
| In(1)-O(1) | 2.100(3) | N(1)-In(1)-O(2) | 146.5(1) | O(1)-In(1)-O(2) | 90.2(1) |
| In(1)-O(2) | 2.094(3) | N(1)-In(1)-O(3) | 108.2(1) | O(1)-In(1)-O(3) | 117.2(1) |
| In(1)-O(3) | 2.025(4) | N(2)-In(1)-O(1) | 142.9(1) | O(2)-In(1)-O(3) | 103.0(1) |
| **Complex 3.5** | | | | | |
| In(1)-N(1) | 2.173(5) | N(1)-In(1)-N(2) | 76.9(2) | N(2)-In(1)-O(2) | 86.6(2) |
| In(1)-N(2) | 2.171(4) | N(1)-In(1)-O(1) | 87.2(2) | N(2)-In(1)-O(3) | 109.2(2) |
| In(1)-O(1) | 2.111(3) | N(1)-In(1)-O(2) | 145.5(2) | O(1)-In(1)-O(2) | 90.2(2) |
| In(1)-O(2) | 2.116(4) | N(1)-In(1)-O(3) | 109.2(2) | O(1)-In(1)-O(3) | 104.4(2) |
| In(1)-O(3) | 2.051(6) | N(2)-In(1)-O(1) | 146.0(1) | O(2)-In(1)-O(3) | 104.7(2) |

The single crystals of complexes **3.2**–**3.5** were isolated from a layer-by-layer crystallisation with a THF and hexane (1:3) solvent mixture (see more details in Chapter 2), the solid state structures of all complexes were determined using SCXRD (Figures 3.5 and 3.6). Selected bond lengths and angles of each isolated complex are listed in Table 3.1. The single crystal structure of **3.1,** was reported previously by us, is included to allow for comparison of the, the structural data.[24] SCXRD suggested that all complexes were mononuclear and adopted pentacoordinate structures. The indium centers showed a distorted square pyramidal geometry with the alkoxide initiating group occupying in the axial position. As discussed in chapter 2, pentacoordinate compounds can adopt two different geometries at the metal:

trigonal bipyramidal or square pyramidal and the propensity towards either is assessed by the $\tau_5$ values. In the case of complexes **3.2** and **3.3**, $\tau_5$ values of 0.36 and 0.33 were observed, suggesting distorted square pyramidal geometries ($\tau_5$ = 0 for perfect square pyramidal geometry).[36] These are comparable to the value obtained for complex **3.1** where $\tau_5$ of 0.33 was observed.[24] This suggests that the diamine linker has a small effect on the metal geometry. Complex **3.2** shows a similar bond distance between indium and the *tert*-butoxide co-ligand to that of **3.1** (In1–O3 = 2.025(1) Å for **3.2** *vs.* In1–O3 = 2.017(6) Å for **3.1**) (Table 3.1).[24] A significantly shorter indium alkoxide bond length was observed for complex **3.3,** compared to **3.1** or **3.2** (In1–O3 = 2.002(4) Å). This indicates a stronger interaction in complex **3.3** and might explain the dramatically lower catalytic activity of **3.3** compared to **3.1** and **3.2** (see more details in polymerisation catalysis section 3.4).

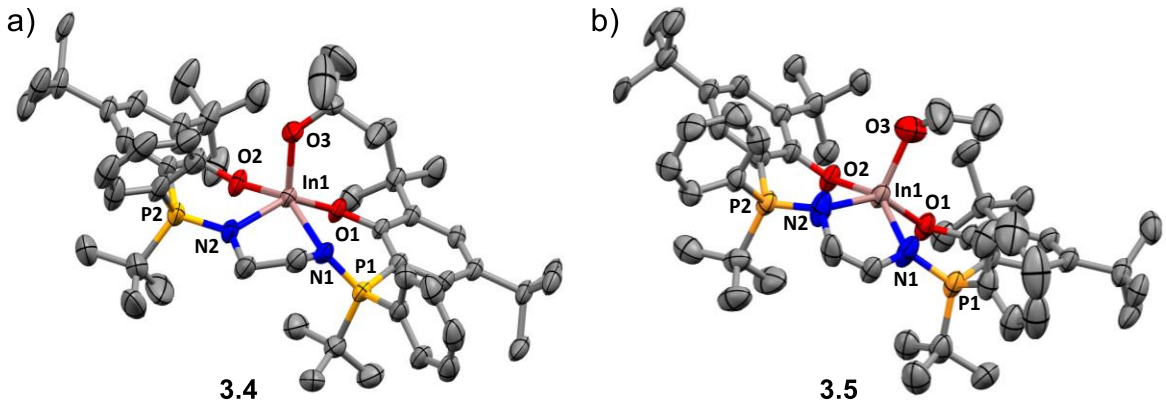



**Figure 3.6.** Representation of the molecular structures of a) complex **3.4**, and b) complex **3.5**.

Complex **3.4** showed a less distorted square pyramidal geometry compared to **3.1** ($\tau_5$ for complex **3.5** = 0.06), whilst the In–O$^t$Bu bond lengths are comparable (In1-O3 = 2.017(6) Å for **3.1** *vs.* In1-O3 = 2.025(4) for **3.4**). Complex **3.5**, possessing a less encumbered EtO co-ligand, adopts an almost perfect square pyramid geometry with $\tau_5$ = 0.01 ($\tau_5$ = 0 for perfect square pyramid geometry).[36] The In1-O3 bond length in **3.5** is slightly longer than that of complex **3.4** (In1-O3 for **3.4** = 2.051(6)). This is inconsistent with a faster rate of

polymerisation for **3.5** relative to **3.4** (see more details in polymerisation section 3.4). Both complexes **3.4** and **3.5** are *meso*-isomers, with the ligands exhibiting an *R,S*-configuration at each phosphorous atom. In addition, the two phosphorous *tert*-butyl substituents of both structures are in a *cis* arrangement to one another and both are on the opposite face to the alkoxide co-ligand (*trans*-configuration to alkoxide co-ligands). It is worth noting that the single crystals from different synthetic batches always showed the same structures and other configurations of the two phosphorous atoms (*e.g. R,R, S,S, S,R*-configurations) were not observed.

### 3.3.3. Solution state characterisation for 3.1–3.5

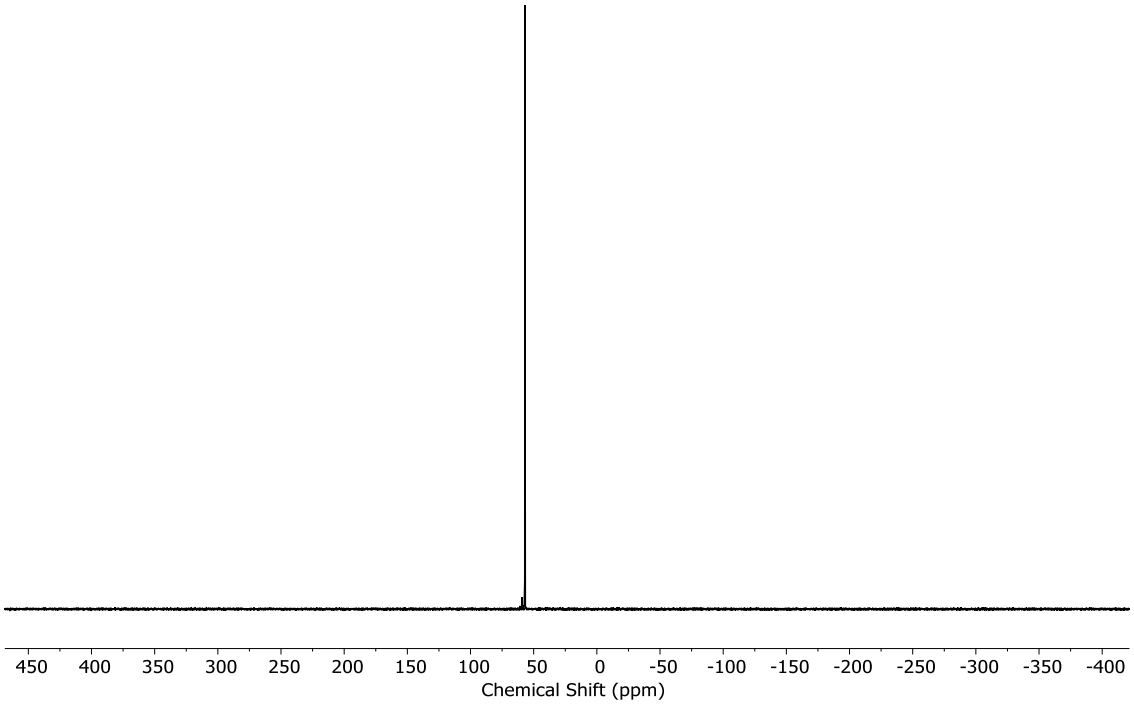



**Figure 3.7.** The $^{31}P\{^{1}H\}$ NMR spectrum of complex **3.5** in THF-$d_8$.

All the indium complexes were characterised by multinuclear NMR spectroscopy (Figures 3.7, 3.8, and A1.22–A1.35). In THF-$d_8$ solution, complexes **3.1**–**3.3** show a single resonance in the $^{31}P\{^{1}H\}$ NMR spectra, around δ 40.0 ppm, whilst a single phosphorous signal at higher chemical shift, around δ 56.0 ppm, was observed for complexes **3.4** and **3.5**. This is

indicative of the symmetric structures of all complexes and indicates complexes have identical phosphorus environments, on the NMR timescale.

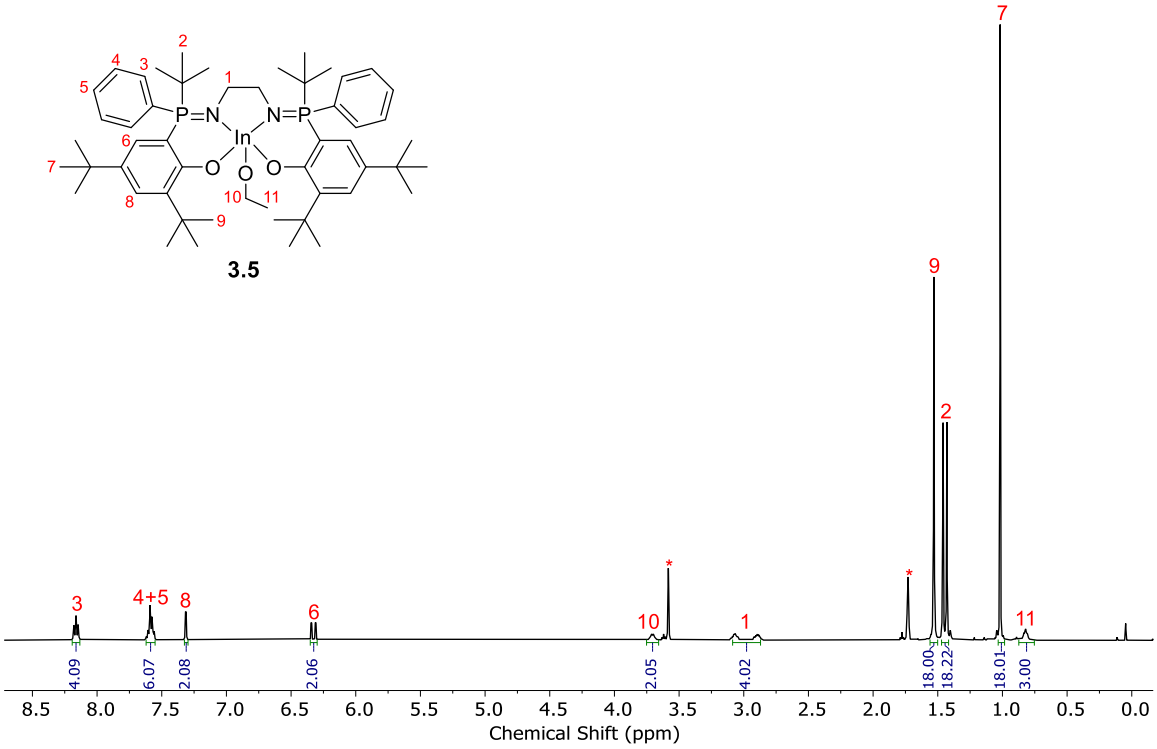



**Figure 3.8.** The $^{1}$H NMR spectrum of complex **3.5** in THF-$d_8$.

The $^{1}$H NMR spectra also show resonances and integrals consistent with symmetrical complex geometries (Figures 3.8, A1.22, A1.25, A1.28, ad A1.31). The spectra are also fully consistent with the selective formation of indium alkoxide complexes. The successful formation of the indium complexes was confirmed by the appearance of alkoxide proton resonance, at 1.00 ppm (OC(C***H***$_3$)$_3$) for **3.1–3.4**, or at δ 3.71 (OC***H***$_2$) and δ 0.82 (OCH$_2$C***H***$_3$) ppm for **3.5** (Figures 3.8, A1.22, A1.25, A1.28, ad A1.31), with the appropriate relative integrals to the ligand resonances. In the case of proton resonances on the diamine backbone, complex **3.2** showed a broad singlet signal, at δ 3.35 ppm, suggesting high fluxionality of the C$_3$ diamine linker. Conversely, two sets of methylene protons and gem-methyl protons of the C$_3$Me$_2$ backbone were observed for complex **3.3**. This revealed the asymmetric nature of the C$_3$Me$_2$ linker on the NMR time scale. It is worth mentioning that the characterisation

data for complex **3.1** was fully consistent with previously reported results from Myers *et al.*[24]

For the $^{1}$H NMR spectra of both catalysts **3.4** and **3.5**, a doublet signal for the *tert*-butyl phosphorous substituents was observed (Figures 3.8 and A1.31). This is due to $^{1}$H-$^{31}$P coupling and is confirmed by a singlet signal being observed in the $^{1}$H{$^{31}$P} NMR spectrum (Figure A1.33).

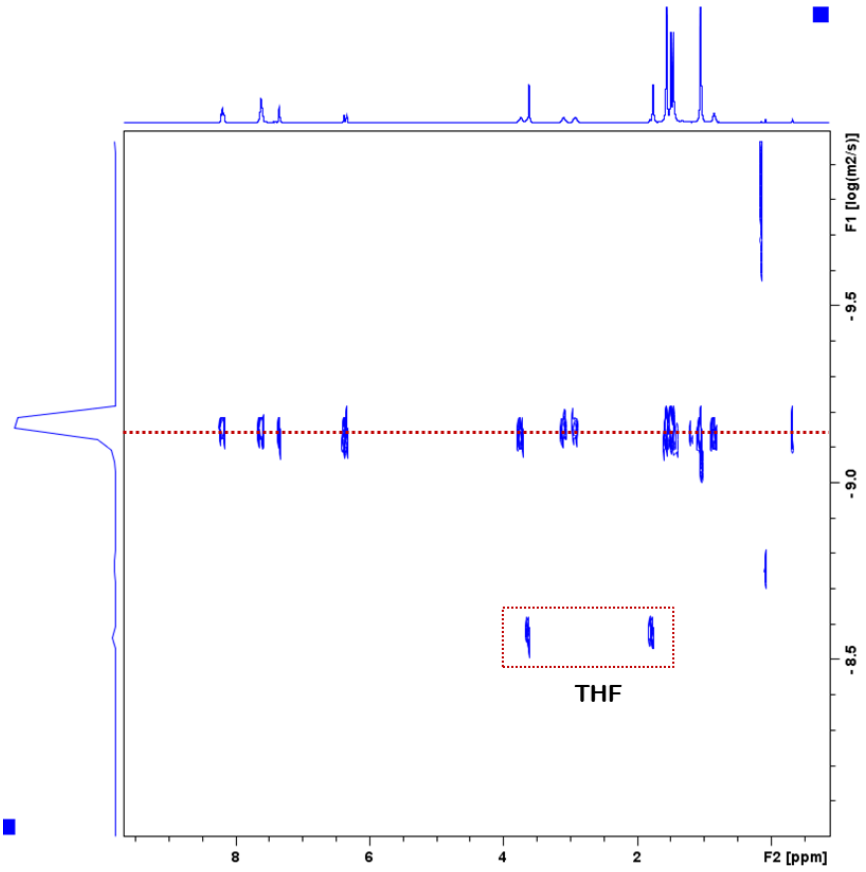



**Figure 3.9.** The $^{1}$H DOSY NMR spectrum of complex **3.5** in THF-$d_8$.

$^{1}$H diffusion ordered spectroscopy (DOSY) enabled understanding of the solution state nuclearity of all complexes (Figures 3.9 and A1.36–A1.39). The $^{1}$H DOSY NMR spectra of all complexes were determined in THF-$d_8$. THF was chosen for the measurements because of it is expected to show similar Lewis basicity to the monomer lactide and therefore improves the understanding of speciation of the complex under conditions relevant to those

used in catalysis. All complexes show a single diffusion coefficient in the $^{1}$H DOSY NMR spectra, with diffusion rates correlating with mononuclear complexes of related molar mass.

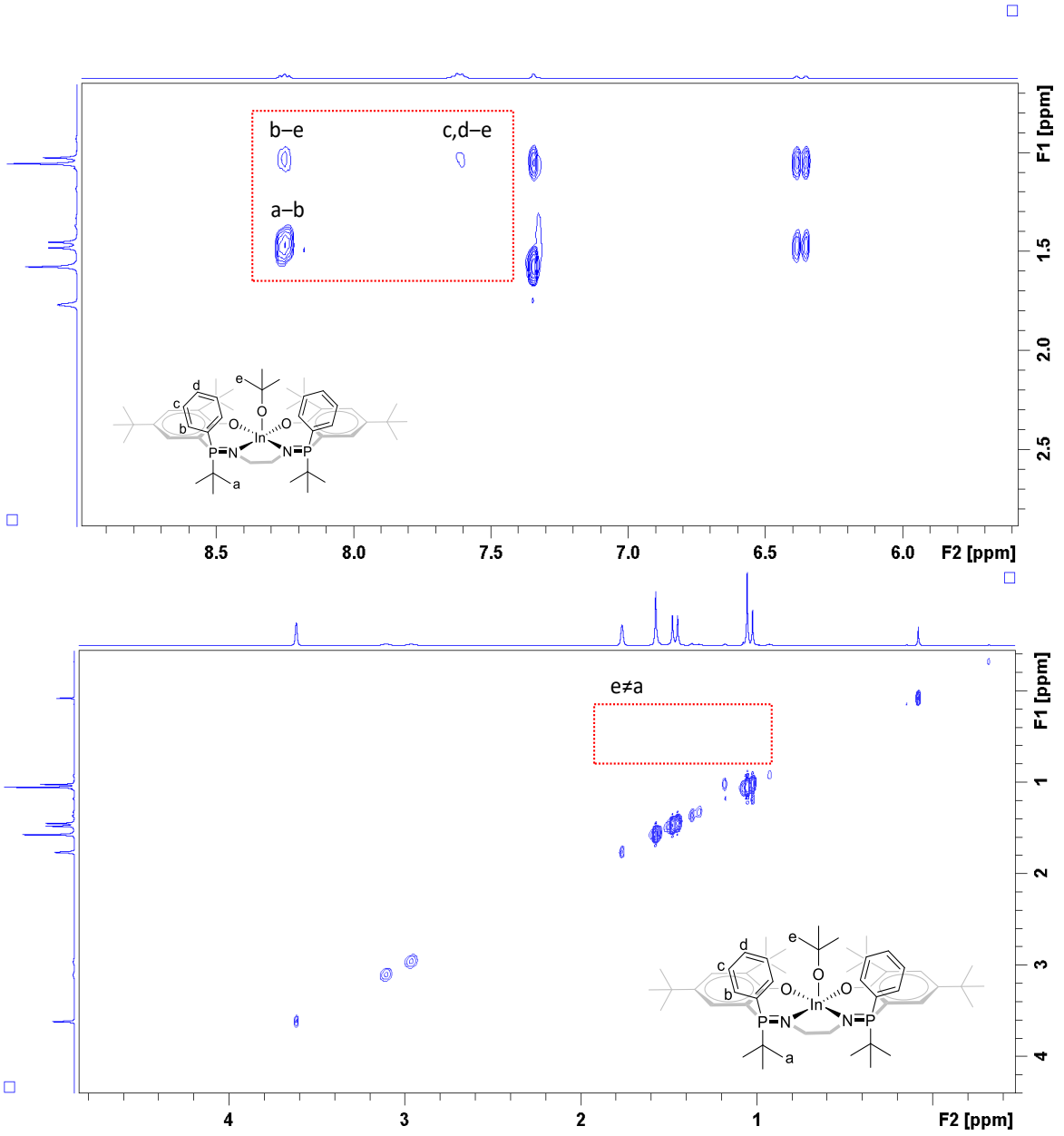



**Figure 3.10.** Selected regions of the $^{1}$H ROESY NMR spectrum of complex **3.4** in THF-$d_8$.

To gain further understanding of the catalyst solution structures, $^{1}$H Rotating Frame Nuclear Overhauser Effect Spectroscopy (ROESY) was conducted using complex **3.4**, in THF-$d_8$ (Figure 3.10). The ROESY NMR spectrum shows a correlation peak between the two phosphorus phenyl substituents and there is a correlation between the phosphorus phenyl

and *tert*-butoxide groups. There is no correlation between the phosphorus *tert*-butyl substituents and the *tert*-butoxide groups, but there is a correlation between the two phosphorus *tert*-butyl groups. Overall, the data is fully consistent with the solid state structure being retained in solution, *i.e.* the *R,S* meso isomer is present where the phenyl phosphorous substituents are orientated *cis* to the alkoxide co-ligand.

### 3.4. *rac*-LA ring-opening polymerisation studies

**Table 3.2.** *rac*-lactide polymerisation data initiated by **3.1**–**3.5**.[a]

| Entry | Cat. | Time (h) | Conv. (%) [d] | $M_{n,SEC}$ (kg mol$^{-1}$)[e] | $M_{n,calc.}$ (kg mol$^{-1}$) | $Đ$ [e] | $P_i$ [f] | $k_{obs}$ [g] (×10$^6$ s$^{-1}$) |
|---|---|---|---|---|---|---|---|---|
| 1 | **3.1** | 1.5 | 88 | 57.1 | 63.2 | 1.01 | 0.75 ± 0.04 | 391 ± 3.20 |
| 2 | **3.2** | 8 | 81 | 36.1 | 58.4 | 1.19 | 0.69 ± 0.02 | 56.5 ± 0.58 |
| 3 | **3.3** | 74 | 61 | 29.4 | 44.0 | 1.18 | 0.84 ± 0.04 | 3.55 ± 0.08 |
| 4 | **3.4** | 8 | 88 | 90.4 | 63.4 | 1.26 | 0.91 ± 0.05 | 77.8 ± 1.77 |
| 5[b] | **3.4** | 14.5 | 80 | 108.7 | 57.7 | 1.15 | 0.92 ± 0.04 | NA |
| 6 | **3.5** | 4.5 | 90 | 57.0 | 64.9 | 1.17 | 0.90 ± 0.05 | 134 ± 2.99 |
| 7[c] | **3.5** | 46 | 63 | 157.8 | 136.2 | 1.25 | 0.92 ± 0.04 | NA |

[a] Polymerisation conditions: [In]:[LA] = 1:500, [LA] = 1 M, [In] = 2 mM, THF, 298 K. [b] The polymerisation was conducted at 278 K. [c] Polymerisation run by 3 sequential additions of *rac*-LA [3×500 equiv. of 1 M LA, (LA = 2 mol in 2 mL THF)], thus, the total ratio of [In]:[LA] = 1:1500 and the addition of LA was done once the previous polymerisation reached high percent conversion (> 80 %). [d] Determined by comparison of the normalised integrals of methine proton signals at $\delta$ 5.06-4.98 ppm (LA) and $\delta$ 5.22-5.08 ppm (PLA) in the $^1$H NMR spectrum. [e] Determined by SEC analysis, calibrated using narrow MW polystyrene standards, in THF or $CHCl_3$ (Figures. A1.41-A1.46). Values are corrected for the different Mark Houwink parameter of PLA *vs.* PS, by multiplying the raw data by 0.58.[37] [f] Determined by integration of PLA methine tetrads at $\delta$ 5.22-5.11 ppm in the $^1$H{$^1$H} NMR spectrum using values predicted according to Bernoullian statistics (Figures A1.50-A1.55). [g] $k_{obs}$ obtained from the gradient of semi-logarithmic plots between LA conversion and time (s) and errors are calculated based on a linear fit of individual plots.

The series of indium complexes **3.1**–**3.5** were first studied as catalysts for LA polymerisations using a standard set of polymerisation conditions ([In]:[LA] = 1:500, [LA] = 1 M, [In] = 2 mM, THF, 298 K).[22-24] In one experiment, the polymerisation temperature was also reduced (T = 278 K) (Table 3.2). Performances were evaluated by the catalytic activity, catalyst stereocontrol, and polymerisation control. Polymerisation kinetics were

studied *via* glovebox aliquot removal techniques, whereby percent conversions of each individual aliquot were analysed by $^{1}$H NMR spectroscopy. A pseudo first order rate constant, $k_{obs,}$ was obtained from the gradient to the linear fits of the semi-logarithmic plots of $[LA]_0/[LA]_t$ against time. The propagation rate constant ($k_p$) was determined from the gradient of a linear plot of $k_{obs}$ against catalyst concentration. Polymer molar mass and molar mass distribution were determined by SEC, in THF solvent, except for samples showing high isotacticity, in which case $CHCl_3$ was used. Reported PLA molar mass values were corrected by multiplying them by 0.58.[37] Microstructures of the resultant PLAs were determined from the two parameters $P_i$ and $P_s$, which were identified from the integration of $^{1}$H{$^{1}$H}NMR spectra and calculated using Bernoulli statistical equations.[38]

### 3.4.1. Catalytic activity

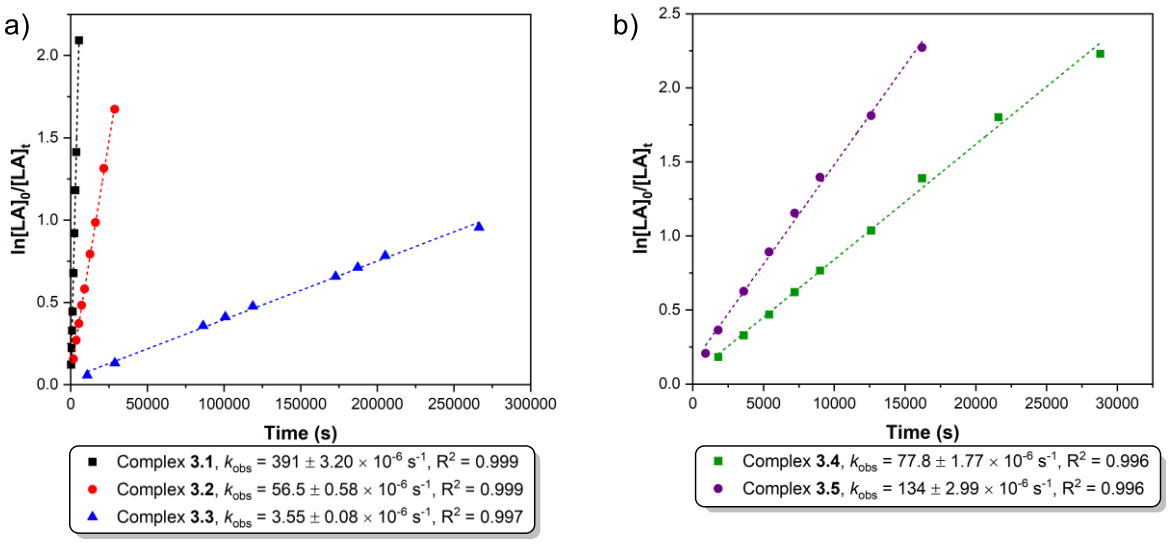



**Figure 3.11.** Semi-logarithmic plots of $[LA]_0/[LA]_t$ against time for a) complexes **3.1**–**3.3** and b) complexes **3.4** and **3.5**.

The series of indium complexes **3.1**–**3.5** were active catalysts for *rac*-LA polymerisations and able to polymerise 500 equivalents of LA in times ranging from hours to days. Comparing indium complexes, **3.1**–**3.3**, which differ in the diamine linker, it was found that complex **3.1**, featuring a $C_2$ backbone, showed the highest activity and took 1.5 h to achieve

88 % conversion. By using a more flexible $C_3$ linker (complex **3.2**), a reduction in activity was seen and it required 8 h to achieve similar conversion. The introduction of two geminal methyl groups onto the $C_3$ backbone (complex **3.3**) resulted further in a drastic decrease in activity, complex **3.3** needed more than 3 d to achieve 61 % conversion. This might be due to a shorter bond distance between the indium centre and *tert*-butoxide co-ligand in complex **3.3** which was observed from the solid state structure (see section 3.3.2 for more details). The polymerisation kinetics of each catalyst were examined to identify $k_{obs}$ (Figures 3.11). In the case of **3.1**, a $k_{obs}$ of 391 ± 3.20× $10^{-6}$ $s^{-1}$ was obtained. For **3.2** and **3.3**, as expected, smaller $k_{obs}$ values of 56.5 ± 0.06 × $10^{-6}$ $s^{-1}$ and 3.55 ± 0.08 × $10^{-6}$ $s^{-1}$ were observed, respectively. In all cases, a linear relationship between $\ln[LA]_0/[LA]_t$ *vs.* time was seen, suggesting the reaction was first order dependence on LA concentration and thus the polymerisation rate law can be simplified as: Rate = $k_{obs}[LA]^1$ where $k_{obs} = k_p[In]^x$. The polymerisation activity trends obtained by comparing either the relative percent conversions or the rate coefficient, $k_{obs}$ are highly consistent.

Comparing catalysts **3.1** and **3.4** which differ in the phosphorous substituents, **3.4** showed lower polymerisation activity and required 8 h to achieve 88 % conversion, whilst 1.5 h is needed for **3.1** to reach the same conversion (88 %) under identical conditions. In addition, about 5 fold lower $k_{obs}$ was observed in the case of **3.4** ($k_{obs}$ of 77.8 ± 0.18 × $10^{-6}$ $s^{-1}$). This is perhaps due to the steric hindrance of the *tert*-butyl substituents on the phosphorous atoms of **3.4**.

In comparing **3.4** and **3.5**, differing in the alkoxide co-ligands, as expected, **3.5**, featuring a less encumbered EtO co-ligand exhibited slightly higher polymerisation activity than that of **3.5**, possessing $^t$BuO co-ligand. Under the same polymerisation conditions, **3.4** took 8 h to reach 88 % conversion, whereas **3.5** took 4.5 h to reach a similar conversion (90 %). As expected, kinetic studies gave a smaller $k_{obs}$ for **3.4** ($k_{obs}$ of 77.8 ± 0.18 × $10^{-6}$ $s^{-1}$) than that

of **3.5** (134 ± 0.03 × $10^{-6}$ $s^{-1}$). This observation is in line with other reported phosphasalen catalysts.[22]

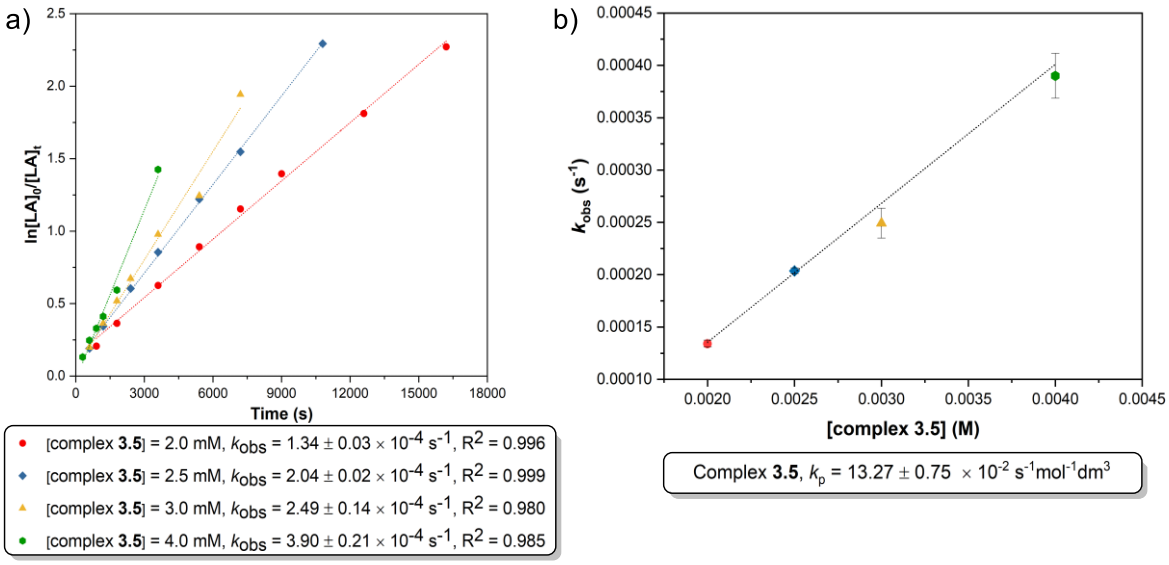



**Figure 3.12.** a) Semi-logarithmic plots of $[LA]_0/[LA]_t$ against time at different concentrations of complex **3.5** and b) Linear plots of $k_{obs}$ against [In].

The order in catalyst concentration (x) was determined using complex **3.5**. A linear relationship between $k_{obs}$ and catalyst concentration suggested a first order dependence on [In] and the gradient provided a $k_p$ of 13.27 ± 0.07× $10^{-2}$ $s^{-1}mol^{-1}dm^3$ (Figure 3.12). Therefore, the full rate law of this particular polymerisation system can be written as rate = $k_p[In]^1[LA]^1$.

### 3.4.2. Polymerisation control

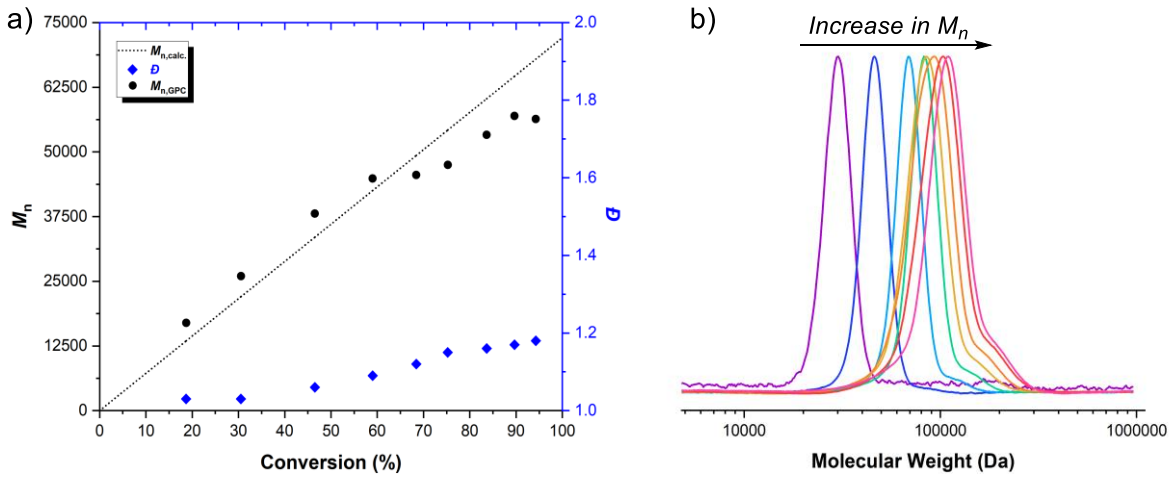



**Figure 3.13.** a) Plots of $M_n$ (●), theoretical $M_n$ (…) and $Đ$ (♦) against percentage conversion and b) overlay of SEC traces for the polymerisation of *rac*-lactide initiated by complex **3.5**.

In general, **3.1**–**3.5** produced PLA with good polymerisation control since a continuous increase in polymer molar mass against percent conversion and narrow molar mass distributions over the course of polymerisations were observed (Figures 3.13 and A1.41–A1.46). In the case of **3.1**, polymer molar masses, obtained from SEC analysis were very close to the theoretical values. In contrast, **3.2** and **3.3** produced PLA with lower molar masses than those of calculated values. The explanation for this is unclear since the complexes are analytically pure and the findings are reproducible using stock solutions of different batches of pure LA and catalysts (*i.e.* a weighing error is unlikely to be responsible). Complex **3.4** produced higher molar mass polymers than the theoretical values. This likely arises from the slow initiation step since the *tert*-butoxide is sterically hindered.[22] This is consistent with the fact that for complex **3.5**, featuring less encumbered EtO co-ligands compared to **3.4**, produced predictable molar mass PLA and a slightly higher overall polymerisation rate was obtained.

To understand the limitations of **3.5**, a polymerisation using lower catalyst loading ([In]:[LA] = 1:1000) was performed but complex **3.5** failed to progress the polymerisation

to above approximately 20 % conversion. Complex **3.5** is susceptible to decompose when using more dilute conditions and this might be due to the increased water contamination. Nonetheless, high molar mass PLA can be produced by exploiting the ability of the controlled polymerisation to undergo re-initiation upon addition of more monomer. Therefore, reacting **3.5** with 3 successive batches of LA whilst maintaining the catalyst loading of **3.5** at 0.2 mol %, it was possible to produce PLA with polymer molar mass of 160 kg $mol^{-1}$ (Table 3.2, Entry 7). The latter finding is fully consistent with the high polymerisation control of **3.5**.

### 3.4.3. Catalyst stereocontrol

All indium complexes (**3.1**–**3.5**) produced isotactic-enriched PLA with different degree of tacticity, ranging from moderate ($P_i$ = 0.69 ± 0.02) to high ($P_i$ = 0.91 ± 0.05) isotacticity (Table 3.2). This resulted in different thermal properties for the different PLA samples. The nature of the diamine group plays a key role in controlling catalyst selectivity. Catalyst **3.1**, possessing a $C_2$ backbone, produced PLA with a higher iso-selectivity ($P_i$ = 0.75 ± 0.04) than that of **3.2**, which has a $C_3$ backbone ($P_i$ = 0.69 ± 0.02). The low degree of iso-selectivity in complex **3.2** is likely related to the high flexibility of $C_3$ linker. Conversely, by utilising complex **3.3**, a higher isotactic PLA was prepared ($P_i$ = 0.84 ± 0.04). This could be due to the higher rigidity or the steric hindrance arise from two geminal methyl on $C_3Me_2$ diamine linker of complex **3.3**.

In comparing catalysts **3.1** and **3.4**, which differ in the phosphorous substituents, **3.4** showed a significant improvement in iso-selectivity and produced highly isotactic PLA with $P_i$ of 0.91 ± 0.05. This is likely due to steric congestion at the metal centre, arising from the bulky *tert*-butyl substituents on phosphorous atoms. As expected, both **3.4** and **3.5**, which differ in the alkoxide co-ligand, exhibited a similar level of iso-selectivity ($P_i$ for **3.5** = 0.90 ± 0.05).

Previous reports suggested that the iso-selectivity could be improved by carrying out polymerisations at a lower temperature.[22-24] By operating catalyst **3.4** at 278 K, PLA with a slightly increased $P_i$ was obtained ($P_i$ =0.92 ± 0.04). Indeed, the iso-selectivity becomes hard to determine at such high values, due to poor resolution of stereo-error peaks. Although the deconvolution method was used to integrate and calculate the peak area of each tetrad, in some cases peak intensity is low and overlap with neighboring signals makes values less certain than for lower selectivity samples. Nonetheless, an improvement in catalyst iso-selectivity is evidenced by a significant increase in $T_m$ of the PLA samples, as the iso-selectivity directly relates to the PLA microstructure and its thermal properties (see section 3.4.4 for more details).

**Table 3.3.** PLA block length of resultant PLA prepared by complexes **3.4** and **3.5**.

| PLA Sample | Integration of *iso*-rich hexad [a] | Integration of *racemic*-rich hexad [a] | $P_i$ [b] | $P_s$ [b] | Average block length [c] |
|---|---|---|---|---|---|
| PLA2 | 0.8234 | 0.1766 | 0.9289 | 0.0711 | 14 |
| PLA3 | 0.8796 | 0.1200 | 0.9582 | 0.0418 | 24 |
| PLA4 | 0.8490 | 0.1486 | 0.9468 | 0.0531 | 19 |

[a] Determined from the normalised integration of the carbonyl signal in the $^{13}C\{^1H\}$ NMR spectra at: δ 169.8 ppm for iso-rich hexad and δ 169.6–169.4 ppm for racemic-rich hexad (Figures A1.47–A1.49).[39] [b] Calculated from the normalised peak area of the carbonyl region in the $^{13}C\{^1H\}$ spectra using Bernoullian statistics and $P_i + P_s = 1$.[40] [c] Identified from $P_i$ and $P_s$ values and average polymer block length = $1/P_s$.[40]

To gain further an understanding the block length of prepared PLA, the $^{13}C\{^1H\}$ NMR spectroscopy of isotactic stereoblock PLA samples was performed (Table 3.3). Average polymer block lengths were determined by the method reported previously by Tsuji and co-workers.[40] The block lengths were calculated based on $P_i$ and $P_s$ parameters using Bernoullian statistics. $P_i$ and $P_s$ values were obtained from integration of the carbonyl resonances (δ 169.8 ppm for iso-rich hexad and δ 169.6-169.4 ppm for racemic-rich hexad) in the $^{13}C\{^1H\}$ NMR spectra at hexad level (Figures A1.47–A1.49).[39] It is worth highlighting that the $P_i$ and $P_s$ values that are used to identify the block length are different to those used

to identify the catalysts iso-selectivity, which are obtained from fitting of the $^{1}H\{^{1}H\}$ NMR spectra at tetrad level. The analysis indicates a block length of 14 LA units for PLA2 (prepared by **3.5**, 298 K). A slightly longer block length of 19 monomer units was observed for PLA4 (prepared by **3.4**, [In]:[LA] = 1:1500, 298 K). As expected, PLA3 (prepared by **3.4**, 278 K) exhibited the longest block length of 24 LA units.

### 3.4.4. PLA thermal properties

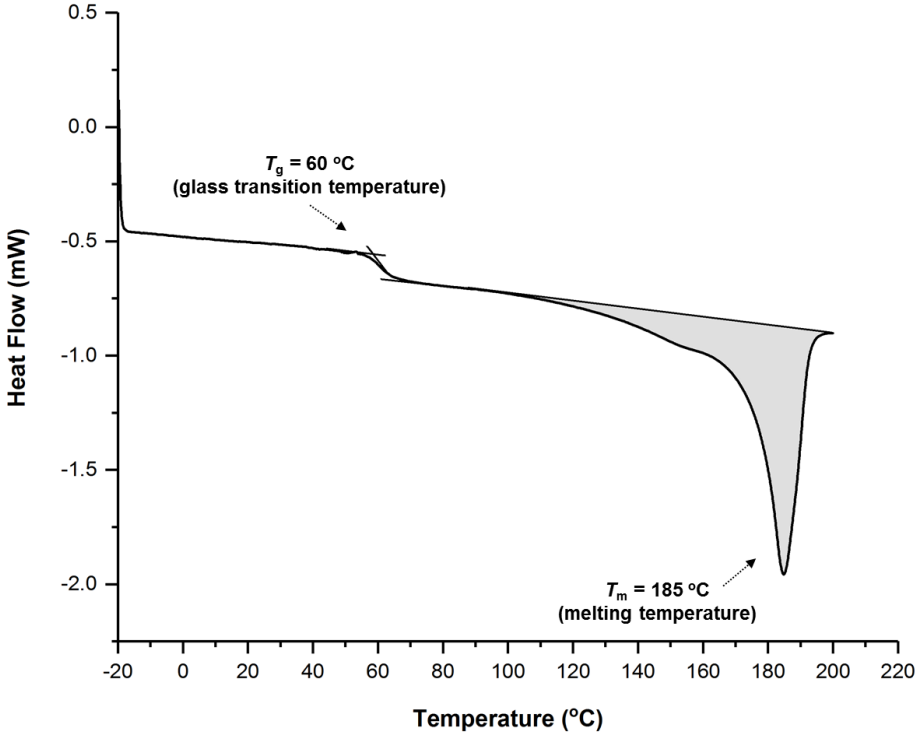



**Figure 3.14.** DSC thermogram of PLA, prepared by catalyst **3.4** at 278 K (PLA3).

**Table 3.4.** DSC analysis data of PLA, prepared by complexes **3.4** and **3.5**.[a]

| Sample | $M_{n,SEC}$ (kg mol$^{-1}$)[b] | $P_i$ [c] | $T_g$ (°C) | $T_m$ (°C) | $\Delta H_m^0$ | $\chi_c$ (%) [d] |
|---|---|---|---|---|---|---|
| PLA1 | 90.4 | 0.91 ± 0.05 | 58 | 175 | 25.68 | 28 |
| PLA2 | 57.0 | 0.90 ± 0.05 | 58 | 177 | 28.19 | 30 |
| PLA3 | 108.7 | 0.92 ± 0.04 | 60 | 185 | 36.04 | 39 |
| PLA4 | 157.8 | 0.92 ± 0.04 | 59 | 173 | 23.89 | 26 |

[a] DSC analysis using heating rate of 5 °C min$^{-1}$,the data were reported from the second heating cycle. [b] Determined by SEC analysis, calibrated using narrow MW polystyrene standards, in $CHCl_3$. Values are corrected by a correction factor of 0.58.[37] [c] Determined by integration of PLA methine tetrads at $\delta$ 5.22-5.11 ppm in the $^{1}H\{^{1}H\}$ NMR spectrum using values predicted according to Bernoullian statistics. [d] Degree of crystallinity calculated against the enthalpy of 100 % crystallinity PLA ($\Delta H_m^0$ = 93 J g$^{-1}$).[41]

In addition, the thermal properties and percent crystallinity of highly isotactic PLA samples ($P_i \geq 0.90$) were analysed by DSC (Figures 3.14 and A1.56–A1.60 and Table 3.4). Prior to the measurements, the trace indium catalyst in the PLA samples was removed by passing a solution of PLA, in $CHCl_3$, through a pad of silica. The samples were then precipitated in methanol three times to remove any residual LA monomer and then dried under vacuum in an oven at 40 °C for 48 h.

PLA, prepared from both **3.4** (PLA1) and **3.5** (PLA2) shows a well-defined $T_g$ at 58 °C, corresponding to the amorphous segment and $T_m$ values of 175 °C, and 177 °C, respectively for the crystalline domains. The peak areas obtained from the $T_m$ transitions suggest crystallinities of 28 % and 30 % for PLA1 and PLA2, respectively. Additionally, relative to PLA1, PLA3 (prepared by **3.4** at 278 K) shows a low intensity $T_g$, at 60 °C and a significantly higher $T_m$ at 185 °C. Its crystallinity increased to 39 %. This is consistent with a higher degree of isotacticity in PLA3. It should be noted that the effect of polymer molar mass on the thermal properties was not observed as high molar mass PLA4 showed comparable $T_g$ and $T_m$ values to those of lower molar mass PLA, possessing a similar level of isotacticity. ($T_g$ = 59 °C, $T_m$ = 173 °C, $\chi_c$ = 26 %). In all cases, the $T_m$ of the PLA samples was higher than that obtained for enantiopure PLLA and PDLA ($T_m$ = 160 °C–170 °C).[12] This latter finding suggests the successful formation of stereoblock PLA.

Compared to PLA with a similar level of isotacticity ($P_i$ = 0.92), previously reported by Myers *et al*., all isolated PLAs, except PLA3, show a comparable $T_m$ and degree of crystallinity ($T_m$ = 179 °C and $\chi_c$ = 25 %).[24] For PLA3, both higher $T_m$ and percent crystallinity were observed, consistent with its higher isotacticity.

### 3.4.5. Stereocontrol mechanism

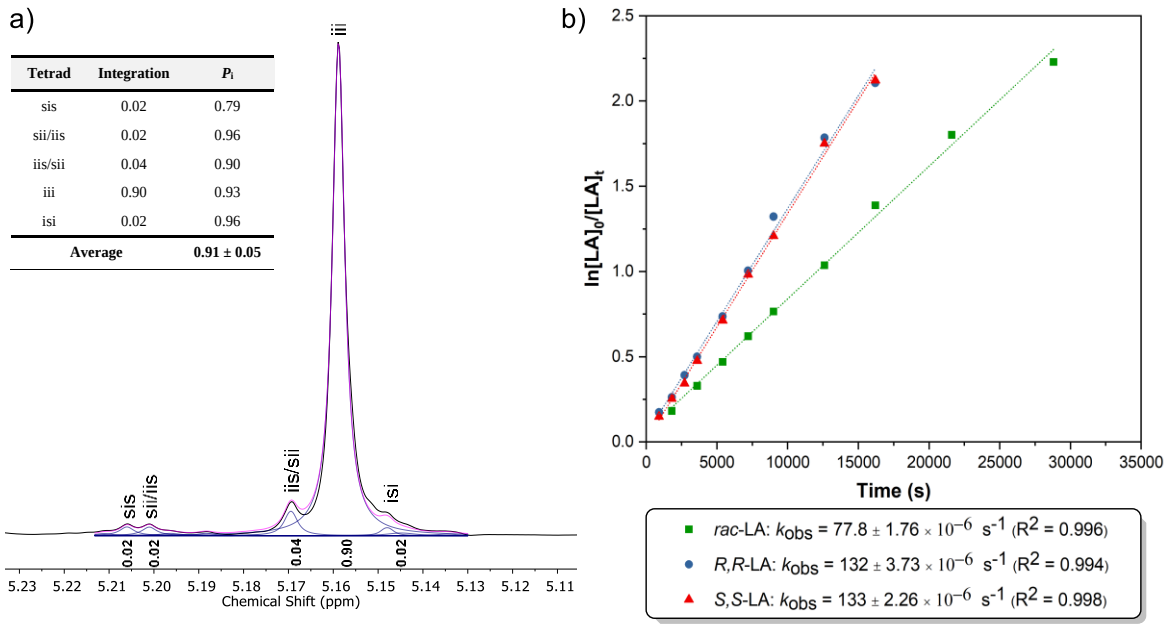
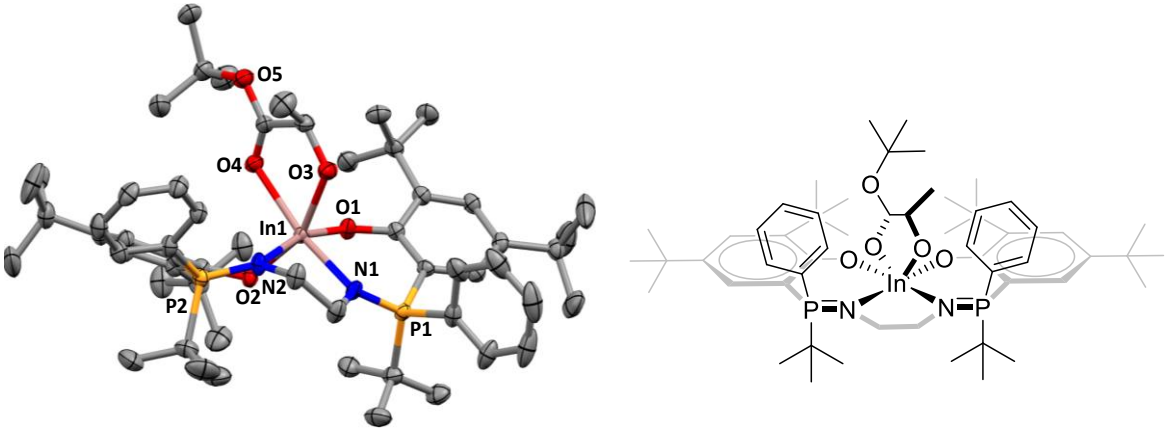



**Figure 3.15.** a) $^{1}H\{^{1}H\}$ NMR spectrum of PLA, prepared by complex **3.4** (condition: [In]:[LA] = 1:500, [LA] =1 M, 298 K) and b) Semi logarithmic plot of $[LA]_0/[LA]_t$ against time of *R,R*-, *S,S*- and *rac*-LA ROP using complex **3.4**.

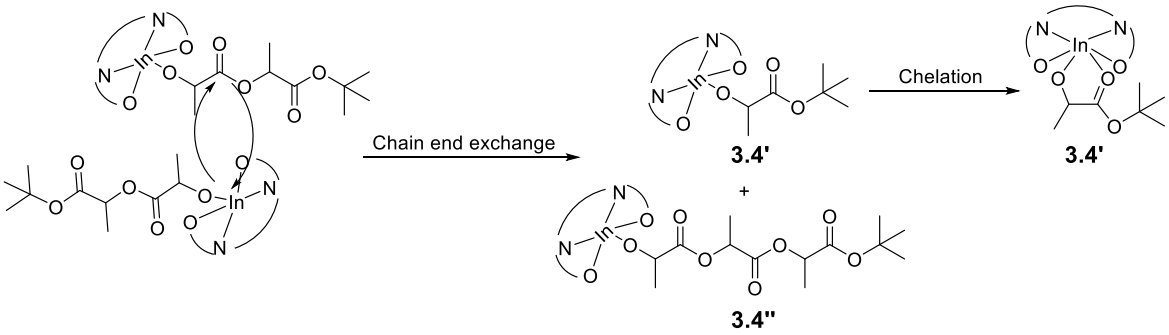
Given the very high iso-selectivity of complexes **3.4** and **3.5**, it is necessary to understand the origin of the stereocontrol. As explained in the introduction, iso-selectivity can arise from either chain-end control (CEC) or enantiomorphic site control (ESC) mechanisms.[12] One method to identify whether CEC or ESC is more dominant is to compare the integrals of stereo-errors observed in the $^{1}H\{^{1}H\}$ NMR spectrum. CEC mechanisms are expected to show an sii:iis:isi ratio of 1:1:1 whereas, the ratio for sis:sii:iis:isi of 1:1:1:2 is expected for ESC.[22, 24] In the case of the highly iso-selective catalysts **3.4**, and **3.5,** the ratio of sii:iis:isi tetrads was close to 1:1:1 suggesting a CEC mechanism is dominant (Figure 3.15a). Comparing the polymerisation rate of enantiopure monomers *R,R*-LA and *S,S*-LA to *rac*-LA also allows an understanding of the sterecontrol mechanism. In the case of a CEC mechanism, it is expected that the rate of polymerisation would be comparable for the enantiopure monomers (*R,R*-LA and *S,S*-LA), which should be faster than that of *rac*-LA.[19]

Conversely, for the ESC pathway, different polymerisation rates between enantiomers would be expected as the catalyst reacts faster with one enantiomer over the other.[21] For **3.4**, a comparable polymerisation rate of *R,R*-LA and *S,S*-LA ROP was observed ($k_{obs}$ for *R,R*-LA = 132 ± 3.73 × $10^{-6}$ $s^{-1}$ and $k_{obs}$ for *S,S*-LA = 133 ± 2.26 × $10^{-6}$ $s^{-1}$) and both are faster than *rac*-LA ($k_{obs}$ = 77.8 ± 1.76 × $10^{-6}$ $s^{-1}$) (Figure 3.15b). This reveals that the catalyst shows no discrimination between the enantiomers. The slower polymerisation rate for *rac*-LA is likely due to polymeryl exchange processes which are also fully consistent with the CEC mechanism.[19]




**3.4'**

**Figure 3.16.** Molecular structure of the propagation intermediate **3.4′**.




**Scheme 3.4.** Proposed mechanism for the formation of intermediate **3.4′**.

As part of attempts to understand the structure of the propagating intermediate species, complex **3.4** was reacted with one equivalent of *R,R*-LA in THF. A slow diffusion of hexane

in saturated THF solution of the intermediate allowed the isolation of single crystals of the intermediate complex **3.4′**. The solid state structure was analysed by SCXRD (Figure 3.16). The structure reveals that the indium center adopts an octahedral geometry with both phosphasalen ligand and *R*-*tert*-butyl lactate coordinated in a *cis*-*β* configuration. The lactate adopts a κ2 coordination mode at the indium center. The precise mechanism of the formation of this intermediate is unclear, especially because only half the LA molecule is coordinated at the metal. Nonetheless, its formation is consistent with a polymeryl chain end exchange process occurring (see proposed mechanism in Scheme 3.4). It should be noted that only intermediate **3.4′** was isolated and intermediate **3.4′′** was not observed (by SCXRD). It is proposed that intermediate **3.4′** crystallises more readily and, hence, it is isolable.

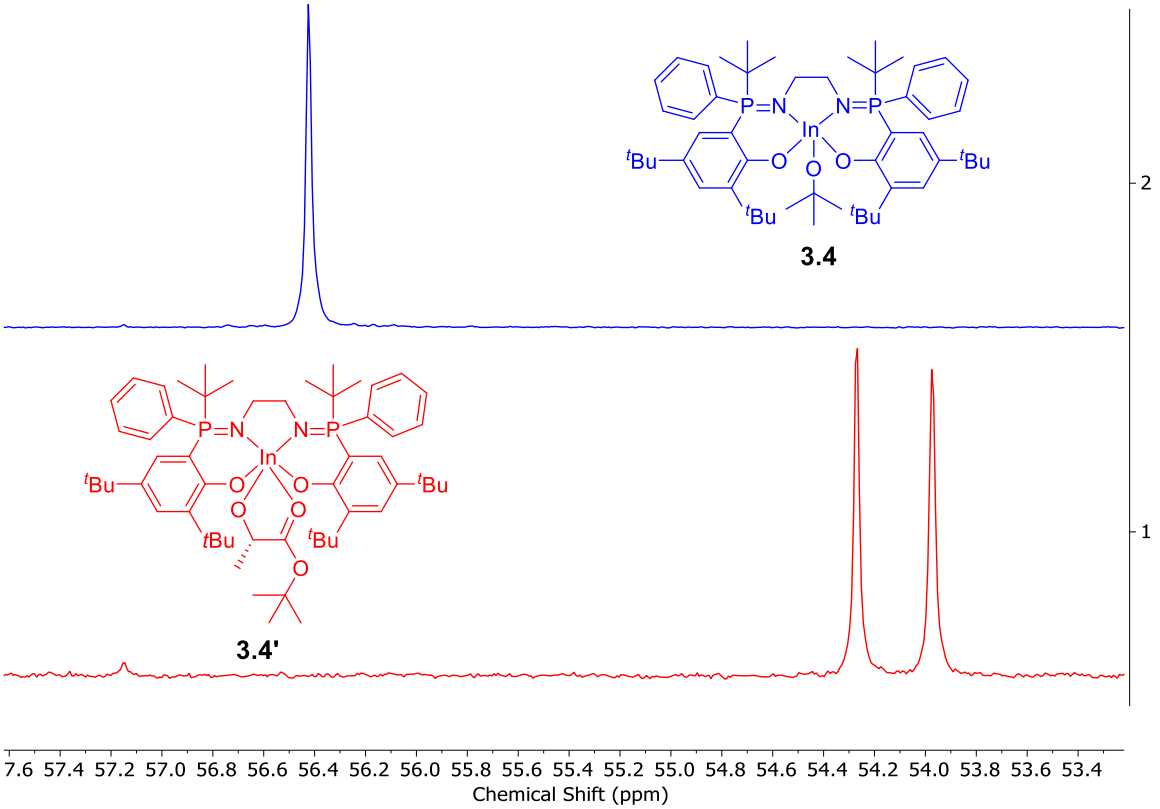



**Figure 3.17.** Stacked $^{31}P\{^{1}H\}$ NMR spectra of complex **3.4** and the propagating intermediate **3.4′**.

$^{31}P\{^{1}H\}$ NMR spectroscopy of the single crystals, in THF-$d_8$, was used to examine the environments of the phosphorous atoms in **3.4′** (Figure 3.17). Two phosphorous signals with

similar intensity, at 54.3 and 54.0 ppm, were observed, suggesting both phosphorous atoms are in different environments which might be expected from the solid state structure. A similar ligand coordination effect was observed for an Al-salen catalyst system, reported by Nomura and co-workers.[27] They observed two distinct imine proton resonances for the salen ligand, in the $^{1}$H NMR spectrum, when the Al-salen catalyst was reacted with *S*-methyl-lactate, suggesting a homochiral complex.

### 3.5. Ring-opening polymerisation of other lactones

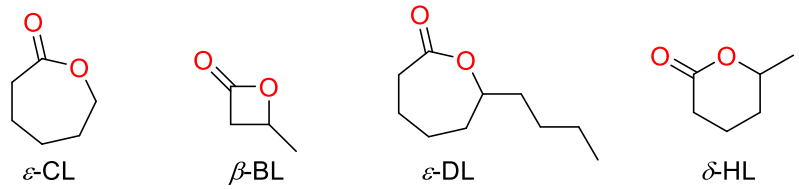



**Table 3.5.** Lactone polymerisation data initiated by **3.1**–**3.3** and **3.5**.[a]

| Entry | Monomer | Cat. | Time (h) | Conv. (%) [e] | $M_{n,SEC}$ [f] (kg mol$^{-1}$) | $Đ$ [f] |
|---|---|---|---|---|---|---|
| 1 | ε-CL[a] | **3.1** | 6.5 min | 82 | 105.3 | 1.43 |
| 2 | | **3.2** | 4.8 min | 99 | 117.9 | 1.19 |
| 3 | | **3.3** | 55 min | 95 | 63.8 | 1.09 |
| 4 | | **3.5** | 5 min | 90 | 60.8 | 1.53 |
| 5 | β-BL[b] | **3.1** | 7 | 81 | 25.9 | 1.16 |
| 6 | | **3.2** | 4 | 99 | 27.0 | 1.21 |
| 7 | | **3.3** | 48 | trace | NA | NA |
| 8 | | **3.5** | 33 | 82 | 11.9 | 1.13 |
| 9 | ε-DL[b] | **3.1** | 24 | 97 | 34.4 | 1.14 |
| 10 | | **3.2** | 120 | 99 | 28.2 | 1.13 |
| 11 | | **3.3** | 120 | 6 | NA | NA |
| 12 | | **3.5** | 80 | 70 | 18.0 | 1.17 |
| 13 | δ-HL[c] | **3.1** | 30 | 87 | 86.0 | 1.48 |
| 14 | | **3.2** | 120 | 30 | 25.8 | 1.29 |
| 15 | | **3.3** | 120 | trace | NA | NA |

[a] Conditions: [In]:[monomer] = 1:500, [monomer] = 1 M, [In] = 2 mM, THF. [b] Conditions: [In]:[monomer = 1:200, [monomer] = 1 M, [In] = 5 mM, THF. [c] Conditions: [In]: [δ-HL] = 1:500, [δ-HL] = 5 M, [In] = 10 mM, THF. [e] Determined by integration of the methine or methylene region of the $^{1}$H NMR spectrum (ε-CL: δ 4.17–4.12 ppm, PCL: δ 4.02–3.92 ppm, β-BL: δ 4.59–4.48 ppm, PBL: δ 5.18–5.01 ppm, ε-DL: δ 4.18–4.03 ppm, PDL: δ 4.80–4.63 ppm, δ-HL: δ 4.43–4.27 ppm, PHL: δ 4.91–4.68 ppm). [f] Determined by SEC analysis against polystyrene standards in THF, a correction factor of 0.56 was used to correct $M_n$ for PCL.

Given the promising results of all the indium complexes in LA ROP, polymerisations of other cyclic esters were investigated (Table 3.5). Identical polymerisation conditions to LA ROP were used to investigate polymerisation of $\varepsilon$-caprolactone ($\varepsilon$-CL) ([In]:[$\varepsilon$-CL] = 1: 500, [$\varepsilon$-CL] = 1 M, [In] = 2 mM, THF, 298 K). In the case of $\beta$-butyrolactone ($\beta$-BL) and $\varepsilon$-decalactone ($\varepsilon$-DL) ROP, a higher loading of catalyst was used since the rate is typically slower than LA polymerisation ([In]:[monomer] = 1: 200, [$\varepsilon$-DL] = 1 M, [In] = 5 mM, THF, 298 K).[42, 43] For $\delta$-hexalactone ($\delta$-HL) ROP was investigated using **3.1** (0.2 mol %) but only reached 20 % conversion (over 20 h). It was hypothesised that the low conversion may arise from the high equilibrium monomer conversion, due to a reduced polymerisation enthalpy for $\delta$-HL (given the enthalpy and entropy reported by Hillmyer and coworkers for $\delta$-HL, $\delta$-HL equilibrium concentration = 0.72 M at 25 °C can be determined).[44] Therefore, polymerisations were conducted at higher [$\delta$-HL] ([In]:[$\delta$-HL] = 1: 500, [$\delta$-HL] = 5 M, [In] = 10 mM, THF, 298 K). The catalytic activity of all catalysts was investigated by single point kinetic measurements. The integration of the carbonyl signal, in the $^{13}C\{^{1}H\}$ NMR spectra at diad level, was analysed using Bernoullian statistics to determine the polybutyrolatone (PBL) microstructure.[45] Polymer molar masses were determined by SEC, in THF using narrow MW polystyrene standards. The reported polycaprolactone molar masses were corrected by multiplying values by 0.56.[37] In the case of polybutyrolatone (PBL), polydecalactone (PDL), and polyhexalactone (PHL), polymer molar masses are presented as received.

The $\varepsilon$-CL ROP was first examined (Table 3.5, Entries 1–4). Comparing complexes **3.1**–**3.3**, both complexes **3.1** and **3.2** showed extremely fast polymerisation rates and were able to reach almost full conversion within minutes, whilst a slower rate was observed for **3.3**. Comparing catalysts **3.1** and **3.5**, which differ in phosphorous substituents, complex **3.5** showed a slightly higher rate than **3.1**. Overall, the activity order follows **3.2** > **3.5** > **3.1** >>

**3.3**. The resultant PCL obtained from **3.1** and **3.2** showed higher polymer molar masses than the theoretical values. This is likely due to slow polymerisation initiation relative to the propagation. On the contrary, a predictable molar mass PCL, with a narrow *Đ*, was obtained by complex **3.3**, whilst **3.5** prepared predictable molar mass PCL, with broad *Đ*. This suggests there is some degree of transesterification for complex **3.5**.

In the case of *β*-BL ROP (Table 3.5, Entries 5-8), complexes **3.1** and **3.2** both showed high polymerisation activities, with **3.2** reaching full conversion in 4 h. Complex **3.3** was extremely slow and only trace amount of polymer was observed after 2 d. Complex **3.5** required 33 h to reach more than 80 % conversion. Therefore, the activity order is **3.2** > **3.1** > **3.5** >> **3.3**. ROP only occurs through acyl bond cleavage and no crotonyl or alkyl chain end groups were observed by $^{1}$H NMR spectroscopy (Figure A1.61). All complexes produced atactic PBL, with $P_i$ = 0.49–0.53 (Figure A1.62 and 1.63). The PBL shows narrow *Đ* and molar masses (uncorrected by SEC) were reasonably close to the calculated values ($M_{n,calc}$ = 18 kg mol$^{-1}$ at 100% conversion).

For DL ROP (Table 3.5, Entries 9–12), complex **3.1** showed a high polymerisation rate and required 24 h to achieve the full conversion. Complexes **3.2** and **3.5** showed similar but lower polymerisation rates and full conversion was reached after 5 d by complex **3.2**. Complex **3.3** was extremely slow and only trace conversion was seen after 5 d. Overall, the order of activity is **3.1** > **3.2** ~ **3.5** >> **3.3**. All these catalysts operate at ambient temperature, which is in contrast to many other reported catalysts where high temperature is needed to achieve DL polymerisation.[43, 46, 47] All polymerisations showed good control, with $M_n$ (uncorrected by SEC) values which are close to the theoretical values ($M_{n,calc}$ = 34 kg mol$^{-1}$ at 100% conversion) and narrow *Đ*.

For $\delta$-HL ROP (Table 3.5, Entries 13–15), complex **3.1** took 30 h to reach 87 % conversion, whilst complexes **3.2** and **3.3** were extremely slow and needed days to achieve low percent conversion. The PHL, prepared by **3.1**, showed $M_n$ values (uncorrected by SEC) in a reasonable agreement with the calculated values ($M_{n,calc}$ = 50 kg mol$^{-1}$ at 85% conversion), although $Đ$ is broad.

## 3.6. Conclusion and Outlook

### 3.6.1. Conclusion

In conclusion, this chapter presents a range of new phosphasalen indium complexes **3.1**–**3.5,** all characterised in both solution and solid states. The series differ in terms of the diamine linker and the phosphorus atom substituents. For LA ROP, all are highly active and in some cases highly iso-selective. By using a $C_2$ backbone, the highest polymerisation rate with moderate iso-selectivity was observed. Although the lowest catalytic activity was seen by complex **3.3**, containing the $C_3Me_2$ linker, a highly isotactic PLA was produced. The asymmetric phenyl and *tert*-butyl phosphorus substituents significantly increase in catalyst iso-selectivity, with $P_i$ as high as 0.92 (278 K). Kinetic studies of all complexes suggested rates dependent, to the first order, on both catalyst and monomer concentrations. Average polymer block lengths for the highly isotactic PLAs are in the range of 14–24 LA units, depending on the degree of isotacticity and polymer molar mass. DSC analysis of highly isotactic PLA revealed reasonable $T_m$ values of 173–185 °C and percent crystallinity values of 26–39 %.

All complexes showed well-controlled polymerisations, with linear evolution of molar mass values against conversion. The origin of high catalyst iso-selectivity was studied by comparing the integration of the $^1H\{^1H\}$ NMR spectra in tetrad level, kinetic studies, and isolation of the propagating intermediate; all data are consistent with a chain-end control

mechanism. The complexes were also active for various lactones, including *ε*-CL, *β*-BL, *ε*-DL, and *δ*-HL.

### 3.6.2. Outlook

Further work can be separated into two main areas: I) Improving phosphasalen catalysts to access even higher catalytic activity whilst maintaining high catalyst stereoselectivity and II) Explorations in other polymerisation catalyses.

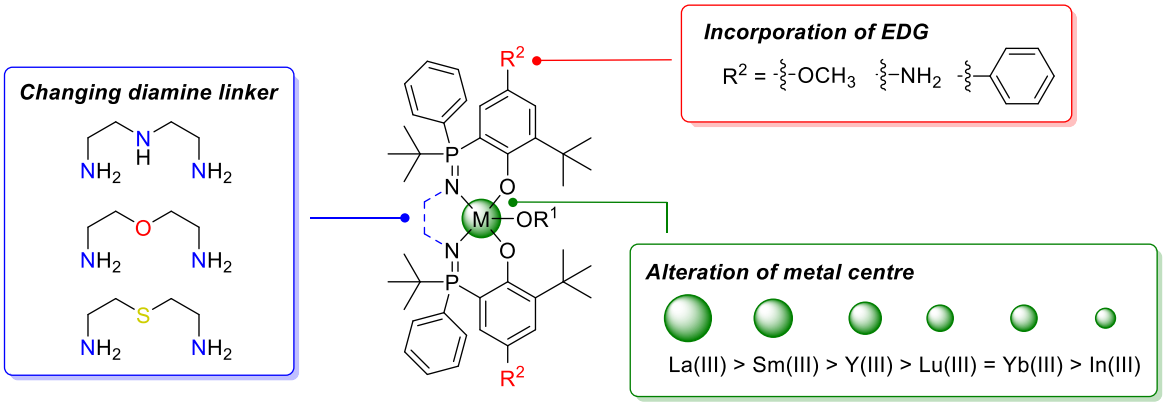



**Figure 3.18.** Complex modification to access high catalytic activity and stereoselectivity.

Given the promising stereoselectivity of complexes **3.4** and **3.5**, possessing sterically hindered asymmetric Ph and $^{t}$Bu phosphorous substituents, further improvements could result from metal center and ligand modification. Previous reports suggest that larger radii metal centres, coordinated by phosphasalen ligands, achieve higher lactone ROP activities.[23] One future direction is to apply the most stereoselective same ligand scaffold as in complexes **3.4** and **3.5** and to substitute indium with metals with lager ionic radii such as Lu(III), Y(III), La(III) etc. (Figure 3.18). The chosen metal centres should have sufficient Lewis acidity to ensure rapid monomer coordination, balanced with an alkoxide bond which is labile for substitution.

In addition, the modification of the ligand scaffold by either introducing a heteroatom on the ligand backbone or by incorporating an electron donating group (EDG) onto the phenoxide

rings would be interesting targets (Figure 3.18). Introducing a hetero atom onto the ligand backbone may stabilise the metal centre and weaken the metal-alkoxide initiating group. Likewise, incorporating EDG onto the phenolate portion may show the same effect and allow access to catalysts with higher activity. It is important to keep the *ortho* substituents of the phenoxide rings for steric hindrance and to prevent aggregation and maintain high stereoselectivity.

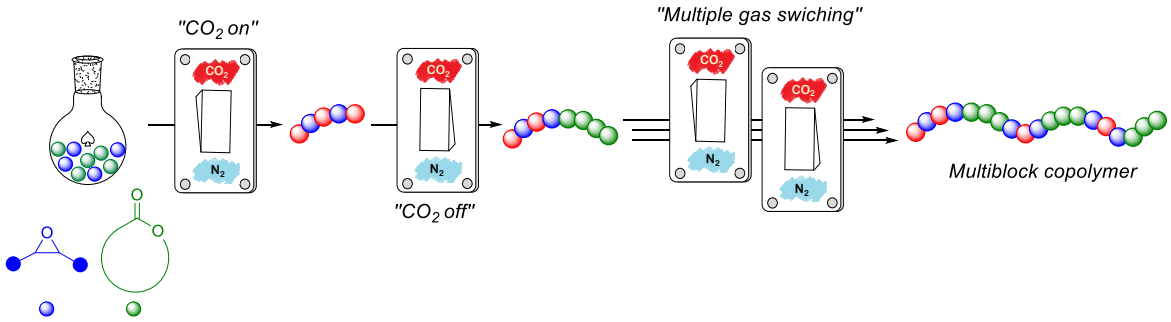



**Figure 3.19.** Switch catalysis using epoxide, $CO_2$ and lactone.

Previous work from our group showed that phosphasalen indium complexes were active ROCOP of CHO and $CO_2$.[34] Given this finding, it would be interesting to investigate switch catalysis, using indium catalysts and exposed to epoxide/$CO_2$ ROCOP and lactone ROP (Figure 3.19). Such a selective catalytic process may form copolymers, by switching between the two polymerisation mechanisms. It is predicted that under a $CO_2$ atmosphere, the catalysts should perform epoxide/$CO_2$ ROCOP. In contrast, ROP of lactone should occur under a $N_2$ atmosphere. By controlling the gas flow (presence/absence) of $CO_2$ in the reaction vessel, it may be possible to control the copolymer structure and composition. If this was successful, multiblock copolymers could be obtained by repeated switching between $CO_2$/$N_2$ atmospheres. This approach would allow access to materials with more complex structures and tunable properties.

## 3.7. References


(1) Farah, S.; Anderson, D. G.; Langer, R., Physical and mechanical properties of PLA, and their functions in widespread applications — A comprehensive review. *Adv. Drug Deliv. Rev.* **2016,** *107*, 367–392.

(2) Tang, X.; Westlie, A. H.; Caporaso, L.; Cavallo, L.; Falivene, L.; Chen, E. Y.-X., Biodegradable Polyhydroxyalkanoates by Stereoselective Copolymeriza–tion of Racemic Diolides: Stereocontrol and Polyolefin-Like Properties. *Angew. Chem. Int. Ed.* **2020,** *59* (20), 7881–7890.

(3) Zhong, Y.; Godwin, P.; Jin, Y.; Xiao, H., Biodegradable polymers and green-based antimicrobial packaging materials: A mini-review. *Adv. Ind. Eng. Polym. Res.* **2020,** *3* (1), 27–35.

(4) Robert, C.; de Montigny, F.; Thomas, C. M., Tandem synthesis of alternating polyesters from renewable resources. *Nat. Commun.* **2011,** *2* (1), 586.

(5) Jérôme, C.; Lecomte, P., Recent advances in the synthesis of aliphatic polyesters by ring-opening polymerization. *Adv. Drug Deliv. Rev.* **2008,** *60* (9), 1056–1076.

(6) Dove, A. P., Organic Catalysis for Ring-Opening Polymerization. *ACS Macro Lett.* **2012,** *1* (12), 1409–1412.

(7) Lyubov, D. M.; Tolpygin, A. O.; Trifonov, A. A., Rare-earth metal complexes as catalysts for ring-opening polymerization of cyclic esters. *Coord. Chem. Rev.* **2019,** *392*, 83–145.

(8) Thomas, C. M., Stereocontrolled ring-opening polymerization of cyclic esters: synthesis of new polyester microstructures. *Chem. Soc. Rev.* **2010,** *39* (1), 165–173.

(9) Kremer, A. B.; Mehrkhodavandi, P., Dinuclear catalysts for the ring opening polymerization of lactide. *Coord. Chem. Rev.* **2019,** *380*, 35–57.

(10) Jem, K. J.; Tan, B., The development and challenges of poly (lactic acid) and poly (glycolic acid). *Adv. Ind. Eng. Polym. Res.* **2020,** *3* (2), 60–70.

(11) Ahmed, J.; Varshney, S. K., Polylactides—Chemistry, Properties and Green Packaging Technology: A Review. *Int. J. Food Prop.* **2011,** *14* (1), 37–58.

(12) Stanford, M. J.; Dove, A. P., Stereocontrolled ring-opening polymerisation of lactide. *Chem. Soc. Rev.* **2010,** *39* (2), 486–494.

(13) Dijkstra, P. J.; Du, H.; Feijen, J., Single site catalysts for stereoselective ring-opening polymerization of lactides. *Polym. Chem.* **2011,** *2* (3), 520–527.

(14) Guillaume, S. M.; Kirillov, E.; Sarazin, Y.; Carpentier, J.-F., Beyond Stereoselectivity, Switchable Catalysis: Some of the Last Frontier Challenges in Ring-Opening Polymerization of Cyclic Esters. *Chem. Eur. J.* **2015,** *21* (22), 7988–8003.

(15) Ovitt, T. M.; Coates, G. W., Stereochemistry of Lactide Polymerization with Chiral Catalysts: New Opportunities for Stereocontrol Using Polymer Exchange Mechanisms. *J. Am. Chem. Soc.* **2002,** *124* (7), 1316–1326.

(16) Zhong, Z.; Dijkstra, P. J.; Feijen, J., [(salen)Al]-Mediated, controlled and stereoselective ring-opening polymerization of lactide in solution and without solvent: synthesis of highly isotactic polylactide stereocopolymers from racemic D,L-lactide. *Angew. Chem. Int. Ed.* **2002,** *41* (23), 4510–4513.

(17) Majerska, K.; Duda, A., Stereocontrolled Polymerization of Racemic Lactide with Chiral Initiator: Combining Stereoelection and Chiral Ligand-Exchange Mechanism. *J. Am. Chem. Soc.* **2004,** *126* (4), 1026–1027.

(18) Hormnirun, P.; Marshall, E. L.; Gibson, V. C.; Pugh, R. I.; White, A. J. P., Study of ligand substituent effects on the rate and stereoselectivity of lactide polymerization using aluminum salen-type initiators. *Proc. Natl. Acad. Sci.* **2006,** *103* (42), 15343–15348.

(19) Nomura, N.; Ishii, R.; Yamamoto, Y.; Kondo, T., Stereoselective Ring-Opening Polymerization of a Racemic Lactide by Using Achiral Salen– and Homosalen–Aluminum Complexes. *Chem. Eur. J.* **2007,** *13* (16), 4433–4451.

(20) Nomura, N.; Ishii, R.; Akakura, M.; Aoi, K., Stereoselective Ring-Opening Polymerization of Racemic Lactide Using Aluminum-Achiral Ligand Complexes: Exploration of a Chain-End Control Mechanism. *J. Am. Chem. Soc.* **2002,** *124* (21), 5938–5939.

(21) Pilone, A.; Press, K.; Goldberg, I.; Kol, M.; Mazzeo, M.; Lamberti, M., Gradient Isotactic Multiblock Polylactides from Aluminum Complexes of Chiral Salalen Ligands. *J. Am. Chem. Soc.* **2014,** *136* (8), 2940–2943.

(22) Bakewell, C.; Cao, T.-P.-A.; Long, N.; Le Goff, X. F.; Auffrant, A.; Williams, C. K., Yttrium Phosphasalen Initiators for *rac*-Lactide Polymerization: Excellent Rates and High Iso-Selectivities. *J. Am. Chem. Soc.* **2012,** *134* (51), 20577–20580.

(23) Bakewell, C.; White, A. J. P.; Long, N. J.; Williams, C. K., Metal-Size Influence in Iso-Selective Lactide Polymerization. *Angew. Chem. Int. Ed.* **2014,** *53* (35), 9226–9230.

(24) Myers, D.; White, A. J. P.; Forsyth, C. M.; Bown, M.; Williams, C. K., Phosphasalen Indium Complexes Showing High Rates and Isoselectivities in *rac*-Lactide Polymerizations. *Angew. Chem. Int. Ed.* **2017,** *56* (19), 5277–5282.

(25) Bakewell, C.; White, A. J. P.; Long, N. J.; Williams, C. K., Scandium and Yttrium Phosphasalen Complexes as Initiators for Ring-Opening Polymerization of Cyclic Esters. *Inorg. Chem.* **2015,** *54* (5), 2204–2212.

(26) Cao, T.-P.-A.; Labouille, S.; Auffrant, A.; Jean, Y.; Le Goff, X. F.; Le Floch, P., Pd(ii) and Ni(ii) complexes featuring a "phosphasalen" ligand: synthesis and DFT study. *Dalton Trans.* **2011,** *40* (39), 10029–10037.

(27) Cao, T.-P.-A.; Buchard, A.; Le Goff, X. F.; Auffrant, A.; Williams, C. K., Phosphasalen Yttrium Complexes: Highly Active and Stereoselective Initiators for Lactide Polymerization. *Inorg. Chem.* **2012,** *51* (4), 2157–2169.

(28) Bakewell, C.; Cao, T.-P.-A.; Le Goff, X. F.; Long, N. J.; Auffrant, A.; Williams, C. K., Yttrium Phosphasalen Initiators for *rac*-Lactide Polymerization. *Organometallics* **2013,** *32* (5), 1475–1483.

(29) Bouyahyi, M.; Duchateau, R., Metal-Based Catalysts for Controlled Ring-Opening Polymerization of Macrolactones: High Molecular Weight and Well-Defined Copolymer Architectures. *Macromolecules* **2014,** *47* (2), 517–524.

(30) Cao, T.-P.-A.; Nocton, G.; Ricard, L.; Le Goff, X. F.; Auffrant, A., A Tetracoordinated Phosphasalen Nickel(III) Complex. *Angew. Chem. Int. Ed.* **2014,** *53* (5), 1368–1372.

(31) Cheisson, T.; Cao, T.-P.-A.; Le Goff, X. F.; Auffrant, A., Nickel Complexes Featuring Iminophosphorane–Phenoxide Ligands for Catalytic Ethylene Dimerization. *Organometallics* **2014,** *33* (21), 6193–6199.

(32) Mustieles Marín, I.; Cheisson, T.; Singh-Chauhan, R.; Herrero, C.; Cordier, M.; Clavaguéra, C.; Nocton, G.; Auffrant, A., Electronic Structures of Mono-Oxidized Copper and Nickel Phosphasalen Complexes. *Chem. Eur. J.* **2017,** *23* (71), 17940–17953.

(33) Marín, I. M.; Auffrant, A., Phosphasalen vs. Salen Ligands: What Does the Phosphorus Change? *Eur. J. Inorg. Chem.* **2018,** *2018* (15), 1634–1644.

(34) Thevenon, A.; Cyriac, A.; Myers, D.; White, A. J. P.; Durr, C. B.; Williams, C. K., Indium Catalysts for Low-Pressure $CO_2$/Epoxide Ring-Opening Copolymerization: Evidence for a Mononuclear Mechanism? *J. Am. Chem. Soc.* **2018,** *140* (22), 6893–6903.

(35) He, L.-P.; Hong, M.; Li, B.-X.; Liu, J.-Y.; Li, Y.-S., Ethylene/hexene living copolymerization and ethylene/methyl 10-undecenoate copolymerization by titanium complexes bearing phenoxy-phosphine or thiophenoxy-phosphine ligands. *Polymer* **2010,** *51* (19), 4336–4339.

(36) Addison, A. W.; Rao, T. N.; Reedijk, J.; van Rijn, J.; Verschoor, G. C., Synthesis, structure, and spectroscopic properties of copper(II) compounds containing nitrogen–sulphur donor ligands; the crystal and molecular structure of aqua[1,7-bis(N-methylbenzimidazol-2′-yl)-2,6-dithiaheptane]copper(II) perchlorate. *J. Chem. Soc., Dalton Trans.* **1984,** (7), 1349–1356.

(37) Kowalski, A.; Duda, A.; Penczek, S., Polymerization of l,l-Lactide Initiated by Aluminum Isopropoxide Trimer or Tetramer. *Macromolecules* **1998,** *31* (7), 2114–2122.

(38) Coudane, J.; Ustariz-Peyret, C.; Schwach, G.; Vert, M., More about the stereodependence of DD and LL pair linkages during the ring-opening polymerization of racemic lactide. *J. Polym. Sci. Part A: Polym. Chem.* **1997,** *35* (9), 1651–1658.

(39) Chabot, F.; Vert, M.; Chapelle, S.; Granger, P., Configurational structures of lactic acid stereocopolymers as determined by $^{13}C\{^{1}H\}$ n.m.r. *Polymer* **1983,** *24* (1), 53–59.

(40) Rahaman, M. H.; Tsuji, H., Hydrolytic degradation behavior of stereo multiblock and diblock poly(lactic acid)s: Effects of block lengths. *Polym. Degrad. Stab.* **2013,** *98* (3), 709–719.

(41) Ray, S. S.; Okamoto, M., Biodegradable Polylactide and Its Nanocomposites: Opening a New Dimension for Plastics and Composites. *Macrolmol. Rapid Commun.* **2003,** *24* (14), 815–840.

(42) Klitzke, J. S.; Roisnel, T.; Kirillov, E.; Casagrande, O. d. L.; Carpentier, J.-F., Yttrium– and Aluminum–Bis(phenolate)pyridine Complexes: Catalysts and Model Compounds of the Intermediates for the Stereoselective Ring-Opening Polymerization of Racemic Lactide and *β*-Butyrolactone. *Organometallics* **2014,** *33* (1), 309–321.

(43) Pepels, M. P. F.; Bouyahyi, M.; Heise, A.; Duchateau, R., Kinetic Investigation on the Catalytic Ring-Opening (Co)Polymerization of (Macro)Lactones Using Aluminum Salen Catalysts. *Macromolecules* **2013,** *46* (11), 4324–4334.

(44) Schneiderman, D. K.; Hillmyer, M. A., Aliphatic Polyester Block Polymer Design. *Macromolecules* **2016,** *49* (7), 2419–2428.

(45) Ajellal, N.; Bouyahyi, M.; Amgoune, A.; Thomas, C. M.; Bondon, A.; Pillin, I.; Grohens, Y.; Carpentier, J.-F., Syndiotactic-Enriched Poly(3-hydroxybutyrate)s via Stereoselective Ring-Opening Polymerization of Racemic *β*-Butyrolactone with Discrete Yttrium Catalysts. *Macromolecules* **2009,** *42* (4), 987–993.

(46) Olsén, P.; Borke, T.; Odelius, K.; Albertsson, A.-C., *ε*-Decalactone: A Thermoresilient and Toughening Comonomer to Poly(l-lactide). *Biomacromolecules* **2013,** *14* (8), 2883–2890.

(47) Zhu, Y.; Romain, C.; Williams, C. K., Selective Polymerization Catalysis: Controlling the Metal Chain End Group to Prepare Block Copolyesters. *J. Am. Chem. Soc.* **2015,** *137* (38), 12179–12182.

# *Chapter 4*

***N,N,O,O-Tetradentate Group IV Catalysts for Various Epoxide/Anhydride Ring-Opening Copolymerisations and Ethylene Polymerisations***

*Success is the ability to go from one failure to another with no loss of enthusiasm...*

*~ Winston Churchill ~*

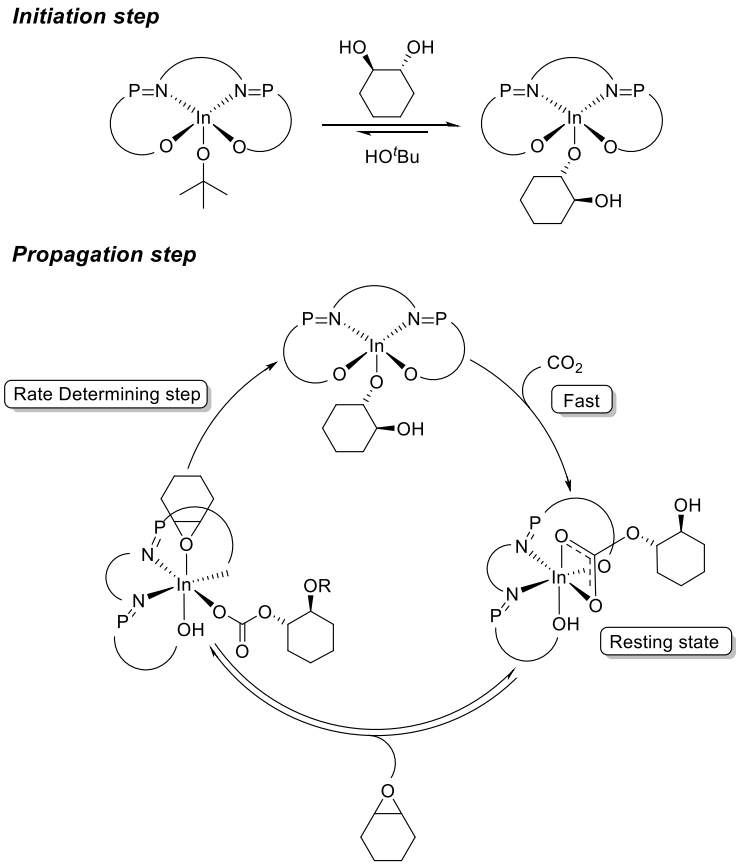
**Overview**

This chapter presents a novel series of phosphasalen group IV (Ti and Zr) complexes. The synthesis and characterisation, both in solution and the solid states, for all complexes are detailed and discussed. Catalytic activities for the ROCOP of various epoxide and anhydride and ethylene polymerisations for all complexes are studied. The structure-activity and structure-selectivity relationships are illustrated and compared with their metal salen or salalen analogues. Kinetic studies, using *in situ* IR spectroscopy for representative complexes, are demonstrated. The proposed ROCOP mechanism is presented and the solid structure of a key propagating intermediate is illustrated.

## 4.1. Introduction

Ring-opening copolymerisation (ROCOP) is a useful tool for producing polycarbonates (from epoxides and $CO_2$) and polyesters (epoxides and cyclic anhydrides) with a wide variety of polymer backbones.[1, 2] Catalysts are required to lower the reaction barrier and enable polymer selectivity. To date there are several reported catalysts for ROCOP and most of them involve binuclear complexes and bicomponent compounds (mononuclear complex + co-catalyst or mononuclear catalyst with co-catalysts tethered on the ligand moiety).[1-5] Therefore, ROCOP is proposed to occur *via* bimetallic or binuclear mechanisms, where each metal centre/component plays a different role: one binds the epoxide and the other provides the nucleophile (cyclic anhydride in the case of polyester formation or $CO_2$ for polycarbonate production) to attack and ring open the epoxide (see proposed mechanisms in Chapter 1).[4, 6-8] It should be noted that generally bimetallic complexes do not require co-catalysts to achieve high catalytic activity and selectivity, whilst co-catalysts are needed for most of the mononuclear complexes.[1, 2] The presence of the co-catalyst in the polymerisation system often leads to the formation of a polymer with a lower fidelity of end groups and a

complex polymerisation mechanism which further complicates the design of new high performance catalysts.[4, 5]




**Scheme 4.1.** Proposed mononuclear mechanism for the ROCOP of CHO and $CO_2$ using phosphasalen In(III) catalyst.[9]

Recently, Williams and co-workers reported a series of phosphasalen indium(III) complexes for the ROCOP of cyclohexene oxide (CHO) and $CO_2$.[9] Surprisingly, theses complexes were active catalysts and produced highly alternating polycarbonates without the need for co-catalysts, in contrast to other mononuclear catalysts where co-catalysts were required to achieve polymers with highly alternating structures.[2] This is proposed to be due to an unexpected mononuclear mechanism where the indium(III) centre plays both roles: coordination of CHO and providing the $CO_2$ nucleophile to ring open CHO to form alternating polycyclohexene carbonate (Scheme 4.1). The evidence of this mechanism is provided by the isolation of key intermediate structures, kinetic studies, and NMR studies.

In addition, they showed that phosphasalen ligand played a key role in directing the *cis* coordination of the monomer, which allowed the unexpected mechanism to occur (note: metal salen complexes generally show a *trans* disposition of monomer and growing polymer chain). The proposed mononuclear mechanism in this case is somewhat similar to the coordination insertion mechanism proposed for lactone ring-opening polymerisation (ROP). It consists of two main steps where the initiation occurs *via* coordination of cyclohexane diol (CHD) to form an indium(III) alkoxide. In the propagation step, $CO_2$ undergoes fast insertion to the indium(III) alkoxide complex to generate a metal carbonate intermediate and this intermediate then reacts with *cis*-coordinated epoxide (CHO). The process continues by the repeated reaction of the two monomers to form polycarbonate.

The production of polyesters *via* epoxide/anhydride ROCOP is proposed to follow a similar polymerisation mechanism, except cyclic anhydride is used instead of $CO_2$ to produce a metal carboxylate intermediate in the propagation step. We reasoned that phosphasalen metal complexes of other metals than indium(III) could also show potential in the mononuclear mechanism, particularly if they showed a sufficient large ionic radius to allow for reverse side attack at the epoxide by a *cis*-coordinated ligand. .

Although group IV complexes have been extensively investigated in the ROP of various lactones, their performances for ROCOP are under-explored.[10-16] Indeed, so far there is no report of their use for the ROCOP of epoxides and cyclic anhydrides, although reports for carbon dioxide/epoxide ROCOP are relevant.[12, 15-20] Additionally, their abundance in the Earth and their low toxicity make them very attractive metals for use in industrial catalysis. Because they have high coordination numbers, particularly in the case of zirconium(IV) where greater than 6-corodination is feasible, they are promising polymerisation catalyst candidates and their oxophilicity should allow for efficient epoxide coordination.

In this chapter, the coordination chemistry of Group IV complexes of a series of different tetradentate ligands is explored and applications in polymerisation catalysis are investigated. The main aims of this chapter include: a) To design, synthesise, and characterise a novel series of phosphasalen, salen, and salalen group IV complexes, b) To investigate the structure-activity and structure-selectivity relationships of the target complexes in the ROCOP of epoxide and cyclic anhydride and ethylene polymerisation, and c) To understand the ROCOP mechanism, operating with these catalysts.

## 4.2. Synthesis and characterisation of phosphasalen and salen ligands

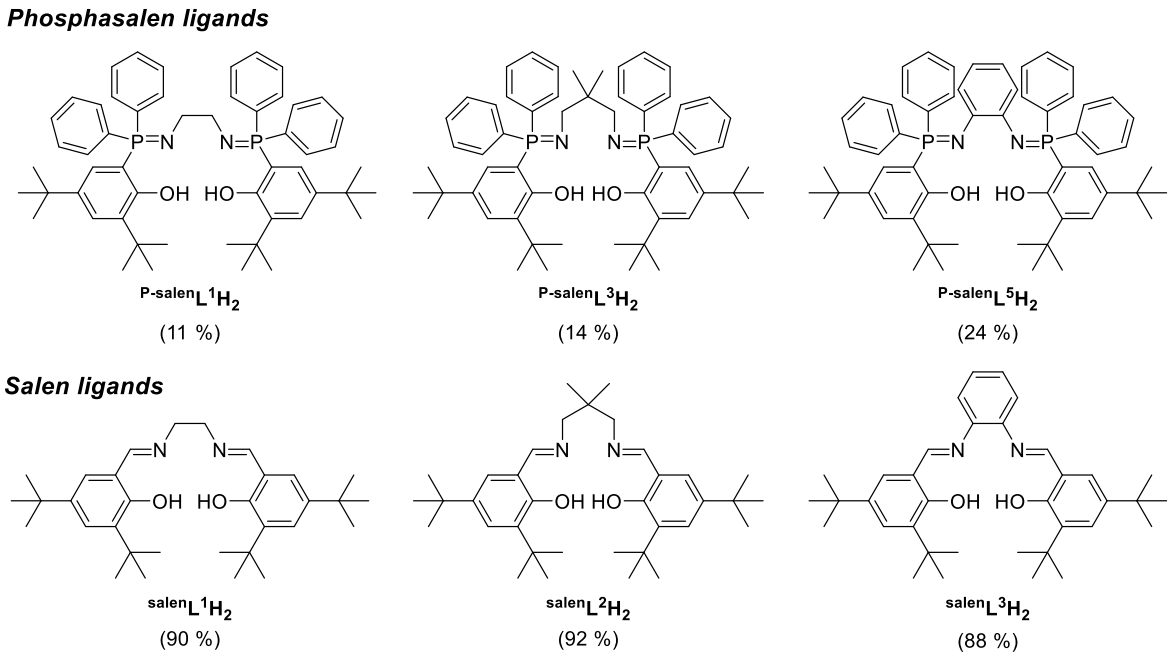



**Figure 4.1.** Structures of salen and phosphasalen ligands: $^{salen}L^1H_2$–$^{salen}L^3H_2$ and $^{P\text{-}salen}L^1H_2$, $^{P\text{-}salen}L^3H_2$, and $^{P\text{-}salen}L^5H_2$, respectively and their isolated yields in brackets.

The synthetic procedures and full characterisation details for phosphasalen ligands $^{P\text{-}salen}L^1H2$ and $^{P\text{-}salen}L^3H_2$ are described in chapter 3. In the case of $^{P\text{-}salen}L^5H_2$, a similar synthetic approach to other phosphasalen ligand, $^{P\text{-}salen}L^1H_2$, was used (see Chapter 3 for synthetic pathway).[21, 22] The difference is that 1,4-diazabicyclo[2.2.2]octane (DABCO) was used as a base, instead of $^nBu_3N$, in the final step of the ligand formation and $^{P\text{-}salen}L^5H_2$ was isolated as a yellow powder after purification by column chromatography ($Al_2O_3$,

DCM:EtOH = 40:1) in a reasonable yield (24 %). The formation of $^{P\text{-salen}}\mathbf{L^5H_2}$ was followed by *in situ* $^{31}P\{^1H\}$ NMR spectroscopy and a shift of the singlet phosphorous signal from –30.0 ppm for di-phenyl phosphine phenol to 19.2 ppm for $^{P\text{-salen}}\mathbf{L^5H_2}$ was observed. In addition, the $^1H$ NMR spectrum is fully consistent with the successful formation of $^{P\text{-salen}}\mathbf{L^5H_2}$ (Figure A2.1). One set of resonances was observed and the integrals of each resonance are fully consistent with the number of protons on the ligand structure, suggesting the successful formation of $^{P\text{-salen}}\mathbf{L^5H_2}$. This ligand has a fully symmetric structure in the solution state, over the experiment time scale.

Salen ligands $^{salen}\mathbf{L^1H_2}$–$^{salen}\mathbf{L^3H_2}$ were synthesised according to the literature procedure.[11, 12] 3,5-Di-*tert*-butyl-2-hydroxy-benzaldehyde was reacted with the desired diamine *via* a Schiff-base condensation reaction conducted under reflux for 6 h. All ligands were isolated as yellow crystals, after slowly cooling the reaction mixture to ambient temperature, in high yields (88–92 %). The formation of salen ligands $^{salen}\mathbf{L^1H_2}$–$^{salen}\mathbf{L^3H_2}$ was confirmed by the appearance of the imine protons, at δ 8.37–8.67 ppm, and the absence of the aldehyde proton of the salicylaldehyde substrate, at δ 9.86 ppm, in the $^1H$ NMR spectra (Figures A2.4, A2.6, and A2.8). The integrals of each resonance matched the number of protons on the ligand structures. This again suggested the successful formation of salen ligands $^{salen}\mathbf{L^1H_2}$–$^{salen}\mathbf{L^3H_2}$.

### 4.3. Synthesis and characterisation of Ti(IV) and Zr(IV) complexes (4.1–4.7)

#### 4.3.1. Synthesis of Ti(IV) and Zr(IV) complexes (4.1–4.7)

Ti(IV) isopropoxide complexes **4.1**–**4.6** were synthesised by the treatment of the phosphasalen ligands, $^{P\text{-salen}}\mathbf{L^1H_2}$, $^{P\text{-salen}}\mathbf{L^3H_2}$, and $^{P\text{-salen}}\mathbf{L^5H_2}$ (for **4.1**–**4.3**) and $^{salen}\mathbf{L^1H_2}$–$^{salen}\mathbf{L^3H_2}$ (for **4.4**–**4.6**), with one equivalent of $Ti(O^iPr)_4$. In the case of complex **4.7**, an equivalent of $[Zr(O^iPr)_4{\cdot}^iPrOH]$ was used to deliver desired Zr(IV) catalyst (Figure 4.2). All complexes were left to react overnight and isolated as pale yellow or yellow crystals (for

Ti(IV) complexes **4.1–4.6**) or as a white powder (for Zr(IV) complex **4.7**), in good to almost quantitative yields (72–96 %). In the case of the phosphasalen complexes, **4.1**–**4.3** and **4.7**, the formation of complexes was monitored by *in situ* $^{31}P\{^{1}H\}$ NMR spectroscopy, whilst the disappearance of the OH of the phenoxide ligand, at δ 13.58–13.82 ppm, in $^{1}H$ NMR spectra was used to follow the preparation of **4.4**–**4.6**. This synthetic work was carried out prior to the very recent publication, from the Auffrant group, which is the first report of a phosphasalen group IV complex.[23]

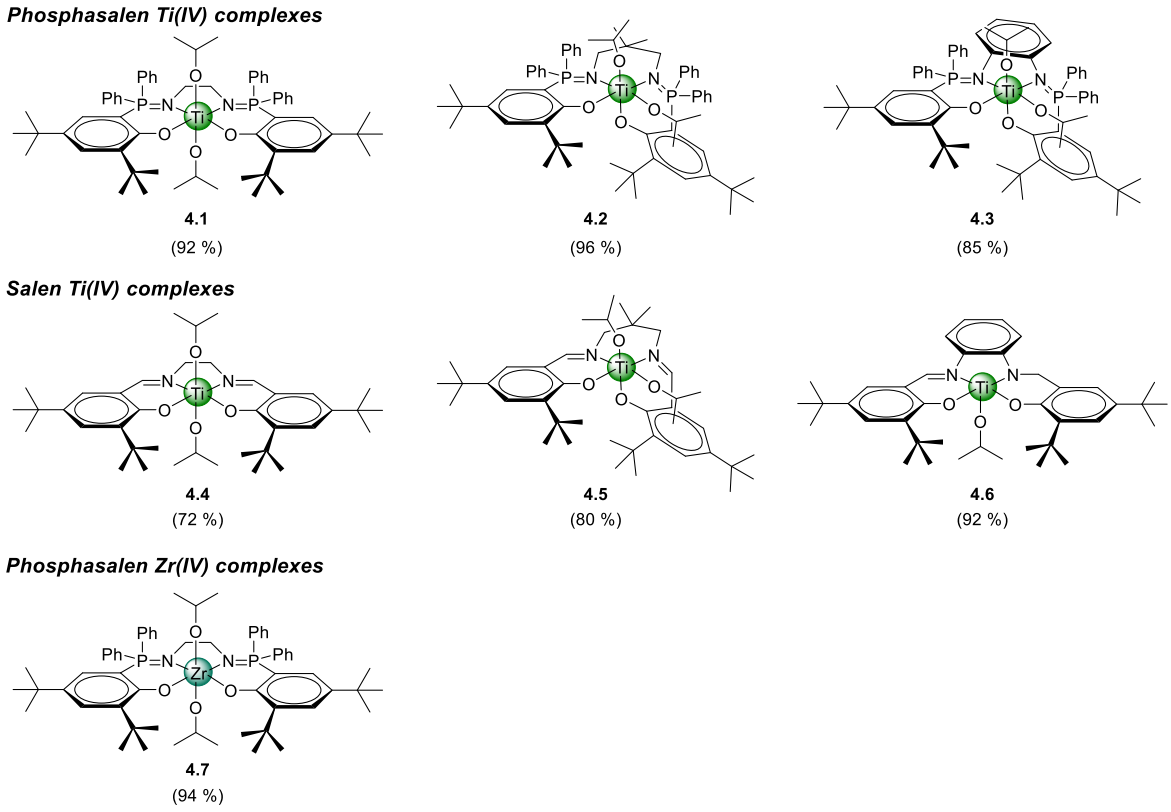



**Figure 4.2.** Structures of the Ti(IV) and Zr(IV) complexes, **4.1**–**4.7,** and their isolated yields in brackets.

### 4.3.2. Solution state characterisation of Ti(IV) and Zr(IV) complexes (4.1–4.7)

The reactions between the phosphasalen or salen ligands with $Ti(O^{i}Pr)_4$ or $[Zr(O^{i}Pr)_4{\cdot}^{i}PrOH]$ led to the formation of complexes with different metal centre geometries and $^{i}PrO$ coordination modes, depending on the nature of diamine linker of the ligand moiety. In the solution state, the different coordination modes of the $^{i}PrO$ ligand to the metal centre can be

identified by NMR spectroscopy. For the complex with a *trans* coordination of $^{i}$PrO co-ligands, it is expected that one set of $^{i}$PrO signals and a singlet phosphorous signal (for phosphasalen complexes) would be observed, since the two $^{i}$PrO co-ligands are in equivalent environments and the complexes are symmetric. Conversely, multiple sets of $^{i}$PrO resonances and/or two different phosphorous signals (for phosphasalen complexes) are expected from complexes where the $^{i}$PrO is coordinated in a *cis* fashion.

All Ti(IV) and Zr(IV) complexes **4.1**–**4.7** were characterised by multinuclear NMR spectroscopy (Figures A2.10–A2.27). The obtained NMR data enabled the identification of complex coordination geometries and also coordination modes of $^{i}$PrO co-ligands. The formation of all the phosphasalen Ti(IV) complexes were confirmed by the presence of the $^{i}$PrO signals in $^{1}$H NMR spectra. Phosphorous signals of all complexes were slightly shifted upfield from the phosphorous resonances of the ligands and split depending on the complex configuration. The $^{1}$H NMR spectrum of complex **4.1** showed two different sets of proton resonances where one set belongs to the Ti(IV) complex with a *trans* conformation and the other belongs to the complex in a *cis* configuration (Figure A2.10). This is in line with the observation of three different phosphosrous signals, at δ 30.3, 29.8, and 28.5 ppm (one and two signals represent *trans* and *cis* configuration complexes, respectively), in the $^{31}$P{$^{1}$H} NMR spectrum compared to the singlet resonance, at δ 41.8 ppm, for the free ligand $^{\mathbf{P\text{-}salen}}\mathbf{L}^{\mathbf{1}}\mathbf{H_2}$ (Figure A2.12). This suggested complex **4.1** exists in an equilibrium between *trans* and *cis* configurations and the rate of exchange between these two configurations is slower than the NMR time scale.

In the case of complexes **4.2** and **4.3**, two different sets of proton signals were observed in the $^{1}$H NMR spectra, suggesting the complexes were asymmetric in solution on the experiment time scale (Figures A2.13 and A2.16). Two sets of methine and methyl protons of $^{i}$PrO co-ligands were seen. This further indicates the different environments of both $^{i}$PrO

co-ligands. Additionally, two different phosphorous signals, at δ 31.0 and 30.0 ppm, for complex **4.2** and at δ 24.8 and 19.9 ppm, for complex **4.3** were observed, suggesting both phosphorous atoms are inequivalent (Figures A2.15 and A2.18). The observed results suggested both complexes **4.2** and **4.3** possess the *cis-β* configurations and that the $^{i}$PrO co-ligands are coordinated *cis* to one another. As a result, complexes with asymmetric structures were obtained.

The characterisation data for salen Ti(IV) complexes **4.4** and **4.5** are fully consistent with the previous reports by Gibson, Long, and Pang.[11, 12] The formation of both Ti(IV) complexes were confirmed by the disappearance of the OH signal and the presence of $^{i}$PrO co-ligands signals (Figures A2.19 and A2.21). In the case of **4.4**, one set of $^{1}$H NMR resonances and a singlet for the imine proton, at δ 8.27 ppm, was observed, suggesting a symmetric complex in solution. The observation of one set of methine and methyl resonances of the $^{i}$PrO co-ligands, at δ 4.13 ppm and δ 0.66 ppm, respectively, suggests that both $^{i}$PrO groups are in an identical environment. As a result, both $^{i}$PrO co-ligands are coordinated in a *trans* configuration to Ti(IV). In contrast, two sets of proton resonances and two different imine proton signals, at δ 7.98 ppm and δ 7.93 ppm, were seen for complex **4.5**, suggesting that complex **4.5** is asymmetric. Additionally, two sets of methine and methyl signals for the $^{i}$PrO ligands were seen. This suggested two different environments for the $^{i}$PrO co-ligands and that they are coordinated to the Ti(IV) centre in a *cis*-fashion, resulting in a complex with a *cis-β* tetradentate ligand configuration. These results highlight the importance of the diamine linker in the ligand moiety. The rigidity of the diamine backbone directs the different complex geometries and coordination modes of the $^{i}$PrO co-ligands.

The formation of complex **4.6** is confirmed by the presence of the methine and methyl proton resonances of the $^{i}$PrO co-ligands, at δ 4.17 ppm and δ 0.80 ppm, respectively, in the $^{1}$H

NMR spectrum (Figure A2.23). Surprisingly, the integrations for all resonances are consistent with the presence of a single $^{i}$PrO co-ligand and the Ti(IV) complex possesses a five coordinate structure, in contrast to the other salen Ti(IV) complexes **4.4** and **4.5** which are six-coordinate (and with the expected octahedral structures). One possible explanation for this structural difference is that one of the $^{i}$PrO co-ligands was deprotonated by the imine group to form an amine and this hypothesis is supported by the presence of the methylene proton signal of $H_2C$–N at δ 4.79 ppm in the $^{1}$H NMR spectrum. In an attempt to inhibit the proton abstraction reaction, the complexation reaction was carried out at 195 K with the slow addition of the salen ligand, $^{\mathbf{salen}}\mathbf{L}^{3}\mathbf{H}_2$, to a stirred solution of Ti($O^{i}$Pr)$_4$. However, the same product was isolated under these conditions.

In the case of the phosphasalen Zr(IV) complex **4.7**, the integrations of all the proton signals are fully consistent with the expected number of protons, suggesting the successful formation of **4.7**. One set of proton resonances, in the $^{1}$H NMR spectrum (Figure A2.25), and a singlet phosphorous signal on $^{31}$P{$^{1}$H}NMR spectrum (Figure A2.27) were observed, suggesting a symmetric complex in solution where both phosphorous atoms are in an identical environment. The appearance of one set of methine (δ 4.11 ppm) and methyl (δ 0.90 ppm) signals for the $^{i}$PrO co-ligands, suggests a *trans* coordination of $^{i}$PrO co-ligands at the Zr(IV) centre. All complexes show a single diffusion coefficient, with diffusion rates correlating with mononuclear structures, in the $^{1}$H DOSY NMR spectra (Figures A2.28–A2.34).

### 4.3.3. Solid state characterisation of Ti(IV) and Zr(IV) complexes (4.1–4.7)

The solid state structures of all the new Ti(IV) and Zr(IV) complexes were characterised by SCXRD. Single crystals of Ti(IV) complexes, **4.1**–**4.3**, and Zr catalyst, **4.7**, were grown from a layer-by-layer approach using hexane and saturated solutions of complexes in toluene whilst, suitable single crystals of complexes **4.4**–**4.6** were obtained from slow cooling of

saturated solutions of each complex in hexane. SCXRD revealed that all complexes adopt mononuclear structures with octahedral geometries at the metal centres, except complex **4.6** where a distorted square pyramidal geometry was observed. The obtained structures are fully consistent with the solution state characterisation data in all cases. It should be noted that, in the case of complex **4.1**, only the complex with a *trans* configuration was isolated in the solid state, whilst an equilibrium between *trans* and *cis-β* configurations was observed in solution state. The observed structures support the notion that using 2,2-dimethyl propylene and phenylene diamine backbones directs complexes to adopt a *cis* coordination of $^{i}$PrO co-ligands, whilst complexes with a *trans* configuration of $^{i}$PrO co-ligands were seen when an ethylene diamine linker was introduced.

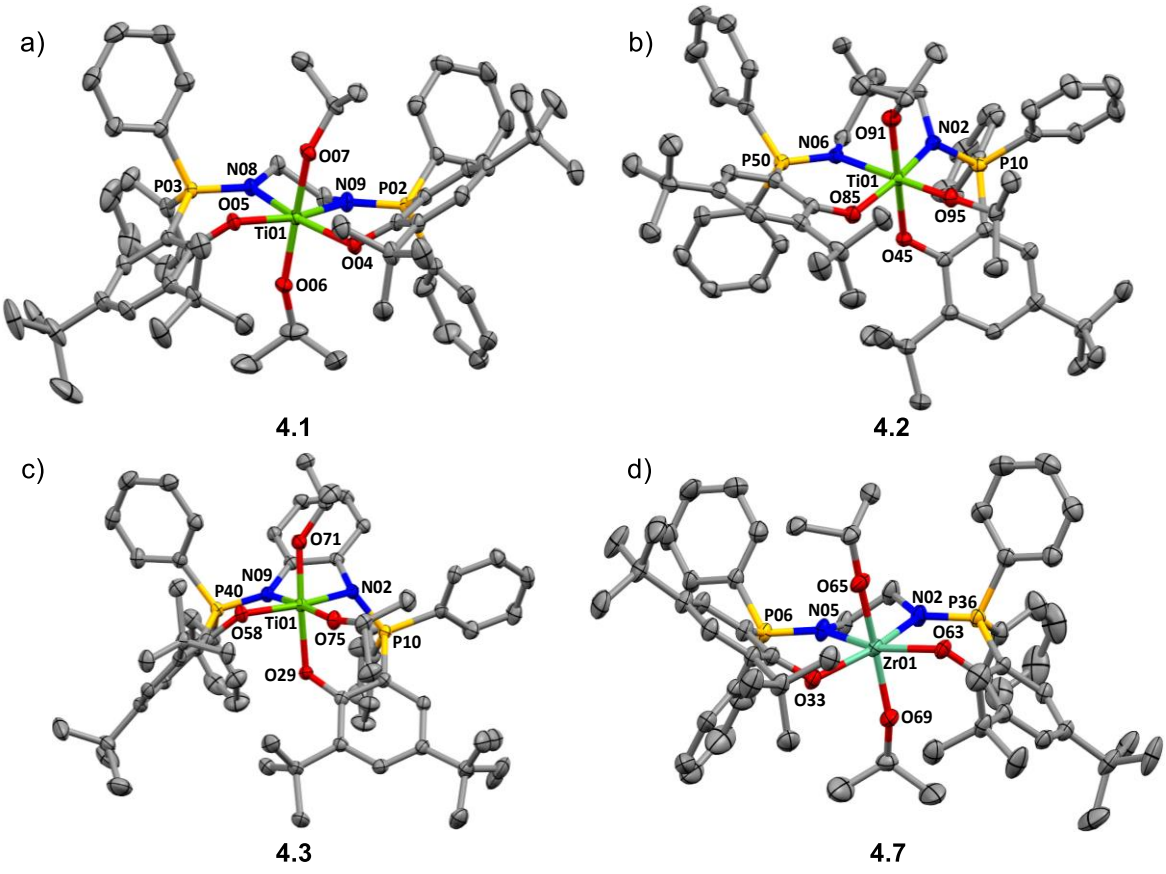



**Figure 4.3.** Representative molecular structures of phosphasalen Ti(IV) complexes **4.1**–**4.3** and Zr(IV) complex **4.7**.

**Table 4.1.** Selected bond lengths (Å) and angles (º) of phosphasalen Ti(IV) complexes **4.1**–**4.3** and Zr(IV) complex **4.7**.

| Bond length (Å) | | Angle (º) | |
|---|---|---|---|
| **Complex 4.1** | | | |
| Ti(01)-N(08) | 2.134(2) | N(08)-Ti(01)-N(09) | 74.70 |
| Ti(01)-N(09) | 2.149(2) | N(08)-Ti(01)-O(05) | 86.18 |
| Ti(01)-O(04) | 1.963(1) | N(09)-Ti(01)-O(04) | 86.67 |
| Ti(01)-O(05) | 1.982(2) | O(04)-Ti(01)-O(05) | 112.52 |
| Ti(01)-O(06) | 1.860(2) | O(06)-Ti(01)-O(07) | 174.19 |
| Ti(01)-O(07) | 1.842(2) | | |
| **Complex 4.2** | | | |
| Ti(01)-N(02) | 2.117(3) | N(02)-Ti(01)-N(06) | 81.12 |
| Ti(01)-N(06) | 2.179(1) | N(02)-Ti(01)-O(45) | 81.84 |
| Ti(01)-O(45) | 2.061(9) | N(06)-Ti(01)-O(85) | 85.64 |
| Ti(01)-O(85) | 1.954(7) | O(45)-Ti(01)-O(85) | 90.99 |
| Ti(01)-O(91) | 1.859(6) | O(91)-Ti(01)-O(95) | 95.31 |
| Ti(01)-O(95) | 1.804(9) | | |
| **Complex 4.3** | | | |
| Ti(01)-N(02) | 2.124(5) | N(02)-Ti(01)-N(09) | 74.14 |
| Ti(01)-N(09) | 2.201(8) | N(02)-Ti(01)-O(29) | 85.16 |
| Ti(01)-O(29) | 2.061(3) | N(09)-Ti(01)-O(58) | 84.13 |
| Ti(01)-O(58) | 1.931(8) | O(29)-Ti(01)-O(58) | 92.77 |
| Ti(01)-O(71) | 1.830(8) | O(71)-Ti(01)-O(75) | 98.85 |
| Ti(01)-O(75) | 1.796(8) | | |
| **Complex 4.7** | | | |
| Zr(01)-N(02) | 2.249(2) | N(02)-Zr(01)-N(05) | 72.87 |
| Zr(01)-N(05) | 2.242(8) | N(02)-Zr(01)-O(63) | 83.40 |
| Zr(01)-O(33) | 2.090(4) | N(05)-Zr(01)-O(33) | 83.07 |
| Zr(01)-O(63) | 2.099(5) | O(33)-Zr(01)-O(63) | 120.82 |
| Zr(01)-O(65) | 1.985(0) | O(65)-Zr(01)-O(69) | 169.81 |
| Zr(01)-O(69) | 1.971(2) | | |

All phosphasalen Ti(IV) and Zr(IV) complexes, **4.1**–**4.3** and **4.7**, show mononuclear structures and metal centres adopting octahedral geometries with different configurations of $^{i}$PrO co-ligands, depending on the nature of the diamine linker (Figure 4.3 and Tables 4.1). For Ti(IV) complex **4.1**, possessing ethylene ($C_2$) backbone, a *trans* coordination of $^{i}$PrO co-ligands was observed. A similar structure was observed for Zr(IV) complex **4.7** where the complex adopts a *trans* geometry. A *trans* configuration of the two $^{i}$PrO co-ligands for

both complexes **4.1** and **4.7** is in line with the bond angles between the two $^{i}$PrO groups which are very close to 180° (O(06)-Ti(01)-O(07) = 174.2° for **4.1** and O(65)-Zr(01)-O(69) = 169.8° for **4.7**) (Table 4. 1).

Conversely, when 2,2-dimethyl propylene ($C_3Me_2$) or phenylene (Ph) diamine linkers were applied, Ti(IV) complexes with *cis-β* ligand geometries were obtained. This means that the $^{i}$PrO co-ligands are coordinated to the Ti(IV) centre in a mutually *cis* arrangement. The bond angles between the two $^{i}$PrO co-ligands in both complexes **4.2** and **4.3** were closed to 90° (O(91)-Ti(01)-O(95) = 95.3° for **4.2** and O(71)-Ti(01)-O(75) = 98.8° for **4.3** ) (Table 4.1).

Complexes **4.1**–**4.3** showed comparable Ti–$^{i}$PrO bond distances and they are in the range of 1.796(8)–1.860(2) Å. Comparing between phosphasalen Ti(IV) complex **4.1** and Zr(IV) complex **4.7**, a significant longer bond length between metal centre and $^{i}$PrO was observed for the Zr(IV) complex: (Ti–$^{i}$PrO = 1.842(2)–1.860(2) Å for **4.1** and Zr–$^{i}$PrO = 1.971(2)–1.985(0) Å for **4.7**). This is in line with the larger metal radii of Zr(IV) compared with Ti(IV).

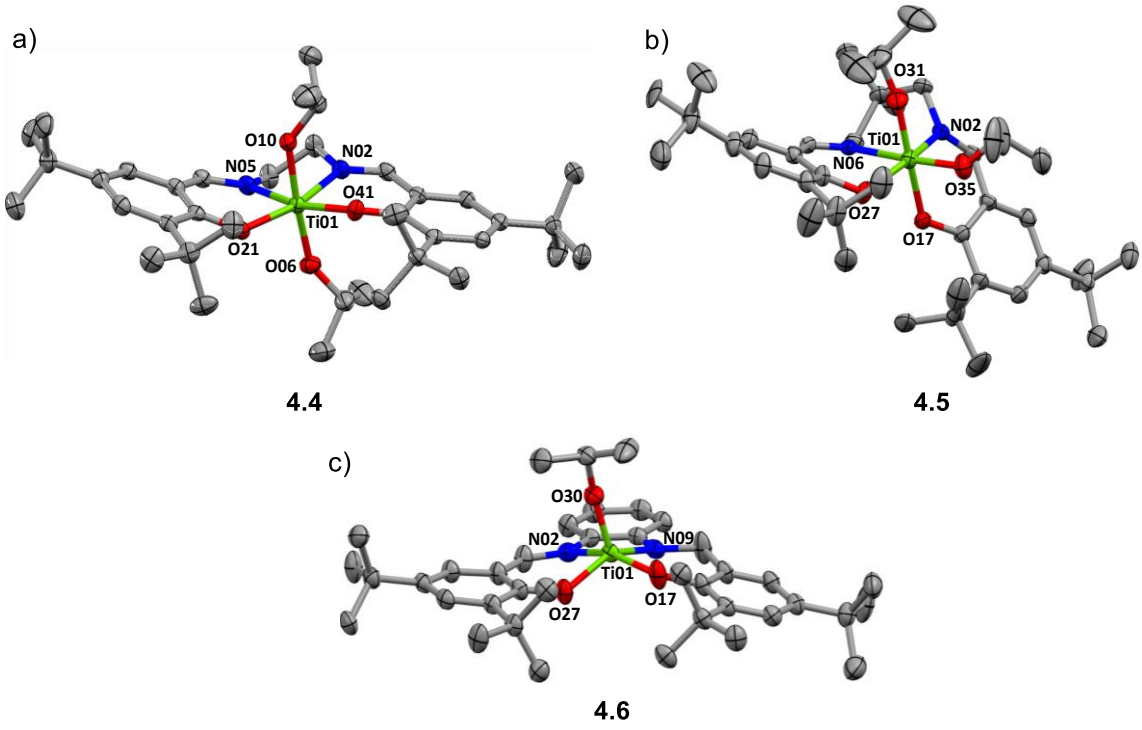



**Figure 4.4.** Representative molecular structures of salen and salalen complexes **4.4**–**4.6**.

**Table 4.2.** List of selected bond lengths (Å) and angles (°) for complexes **4.4**–**4.6.**

| Bond length (Å) | | Angle (º) | |
|---|---|---|---|
| **Complex 4.4** | | | |
| Ti(01)-N(02) | 2.141(4) | N(02)-Ti(01)-N(05) | 75.98 |
| Ti(01)-N(05) | 2.160(7) | N(02)-Ti(01)-O(41) | 83.32 |
| Ti(01)-O(06) | 1.861(5) | N(05)-Ti(01)-O(21) | 84.76 |
| Ti(01)-O(10) | 1.851(9) | O(06)-Ti(01)-O(10) | 174.54 |
| Ti(01)-O(21) | 1.907(5) | O(21)-Ti(01)-O(41) | 115.91 |
| Ti(01)-O(41) | 1.909(2) | | |
| **Complex 4.5** | | | |
| Ti(01)-N(02) | 2.177(4) | N(02)-Ti(01)-N(06) | 77.16 |
| Ti(01)-N(06) | 2.240(2) | N(02)-Ti(01)-O(17) | 80.50 |
| Ti(01)-O(17) | 1.983(8) | N(06)-Ti(01)-O(27) | 82.35 |
| Ti(01)-O(27) | 1.914(2) | O(17)-Ti(01)-O(27) | 89.16 |
| Ti(01)-O(31) | 1.809(7) | O(31)-Ti(01)-O(35) | 97.51 |
| Ti(01)-O(35) | 1.810(8) | | |
| **Complex 4.6** | | | |
| Ti(01)-N(02) | 2.128(2) | N(02)-Ti(01)-O(17) | 153.48 |
| Ti(01)-N(09) | 2.039(1) | N(02)-Ti(01)-O(30) | 94.47 |
| Ti(01)-O(17) | 1.823(1) | N(09)-Ti(01)-O(27) | 141.36 |
| Ti(01)-O(27) | 1.886(0) | N(09)-Ti(01)-O(30) | 111.09 |
| Ti(01)-O(30) | 1.772(7) | O(17)-Ti(01)-O(30) | 110.65 |
| | | O(27)-Ti(01)-O(30) | 102.70 |

Both salen complexes **4.4** and **4.5** showed mononuclear structures and Ti(IV) centres adopting octahedral geometries, with the $^{i}$PrO co-ligands coordinated in different configurations (Figure 4.4 and Table 4.2). It should be highlighted that the observed molecular structures of both **4.4** and **4.5** are fully consistent with previously reports by Long, Gibson and Peng.[11, 12] Utilising a $C_2$ backbone, complex **4.4** adopts a *trans* geometry at the Ti(IV) centre. The bond angle between the two $^{i}$PrO groups is 174.5° and this is similar to those in phosphasalen Ti(IV) complex **4.1**, possessing the same $C_2$ diamine backbone. The latter finding suggests a *trans* coordination of $^{i}$PrO co-ligands at the Ti(IV) centre. In contrast to complex **4.3**, which possesses a $C_3Me_2$ diamine linker, a *cis* $^{i}$PrO co-ligand coordination was seen. As a result, a complex with *cis-β* ligand geometry was obtained. The

bond angle analysis shows a bond angle of 97.5° between the two $^{i}$PrO co-ligands and this is comparable to those in complex **4.2** (O(91)-Ti(01)-O(95) = 95.3° for **4.2**) (Tables 4.1 and 4.2).

Comparable Ti–O$^{i}$Pr bond distances are observed in the two salen Ti(IV) complexes **4.4** and **4.5** and they are in the range 1.809(7)–1.861(5) Å (Table 4.2). In comparing the Ti–O$^{i}$Pr bond lengths of complexes **4.4** and **4.5** to their phosphasalen analogues, comparable bond distances were seen.

In the case of complex **4.6**, a mononuclear structure with pentadentate coordination of co-ligands was observed. This is fully consistent with the NMR spectroscopic data in the solution state. The $\tau_5$ value of 0.20 suggests a distorted square pyramidal geometry at the Ti(IV) centre.[24] Structure analysis indicates a bond length between the Ti(IV) centre and $^{i}$PrO co-ligand of 1.772(7) Å which is shorter than that of both salen complexes **4.4** and **4.5**. Comparing to phosphasalen complex **4.3**, possessing a similar phenylene backbone, complex **4.6** shows a shorter Ti–O$^{i}$Pr bond, suggesting a stronger binding at the Ti(IV) centre. This is perhaps due to the higher Lewis acidity Ti(IV) centre in **4.6**.

### 4.4. Polymerisation studies

#### 4.4.1. Preliminary polymerisation studies of 4.1–4.7 in ROCOP of CHO and PA

The series of Ti(IV) and Zr(IV) complexes (**4.1**–**4.7**) were first studied as polymerisation catalysts for ROCOP of CHO and PA, with a common set of polymerisation conditions ([PA] = 5 M, [CHO] = 6.25 M, [cat.] = 0.05 M, [cat.]:[PA]:[CHO] = 1:100:125, toluene, 353 K) (Table 4.3). All polymerisations were carried out without utilising any co-catalysts. ROCOP of CHO and PA was used to investigate the structure-reactivity and structure-selectivity relationships of the series of catalysts. The catalytic activity and selectivity of all complexes were compared against the Ti(O$^{i}$Pr)$_4$ precursor. The best performing catalyst **4.1**

was then used to scope a range of substrates, including different epoxides and cyclic anhydrides. The performance of the catalyst was investigated in terms of catalytic activity, polyester selectivity, and polymerisation control. In preliminary polymerisation studies, the catalytic activity of different catalysts was investigated by comparing a single time point kinetic measure for each catalyst at high PA conversions (≥ 85 % conversion), unless catalysts showed low selectivity. In such cases, polymerisations were quenched at high conversions of CHO (≥ 85 % conversion). The activity of **4.1** in the substrate scope study was investigated based on only anhydride conversion since the catalyst showed very high selectivity for ester linkage formation (*i.e.* near-perfect alternation). Kinetic studies of complexes **4.1**, **4.4**, and **4.5** were conducted using *in situ* IR spectroscopy to gain insight into the rates of representative catalysts and to understand the empirical rate laws in terms of anhydride concentration. For catalyst selectivity, the formation of ester linkages compared to ether linkages in polymer backbones were quantified by comparing appropriate integrals for selected resonances in the $^{1}$H NMR spectra of withdrawn aliquots or isolated polymers. Additionally, the thermal properties of isolated polymers were analysed using DSC measurements. All polymer molar masses were obtained from SEC measurements, conducted in THF solvent and using polystyrene standards to calibrate the instrument –molar mass values are reported as detected.

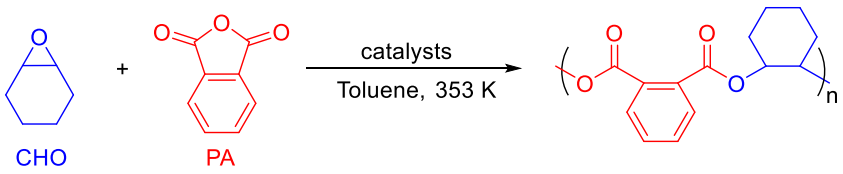



**Table 4.3.** ROCOP of CHO with PA data of complexes **4.1**–**4.7**.[a]

| Cat. | t (h) | % Conv. (CHO)[b] | % Conv. (PA)[c] | % Ester linkages[d] | $M_{n,SEC}$ (kg mol$^{-1}$)[e] | $Đ$ [e] |
|---|---|---|---|---|---|---|
| **Ti(O$^i$Pr)$_4$** | 3 | 99 | 46 | 19 | 3.7 | 2.07 |
| **4.1** | 22 | 76 | 92 | 99 | 13.2, 6.0 | 1.03, 1.07 |
| **4.2** | 78 | 91 | 78 | 63 | 8.8 | 1.28 |
| **4.3** | 46 | 98 | 60 | 36 | 5.7 | 1.43 |
| **4.4** | 27 | 78 | 89 | 90 | 8.0 | 1.13 |
| **4.5** | 166 | 83 | 59 | 52 | 6.0 | 1.43 |
| **4.6** | 27 | 92 | 74 | 60 | 18.5, 6.6 | 1.07, 1.20 |
| **4.7** | 168 | 85 | 53 | 45 | 14.5, 5.0, 1.6 | 1.19, 1.08, 1.07 |

[a] Polymerisations were conducted using [CHO] = 6.25 M, [PA] = 5 M, [cat.]:[PA]:[CHO] = 1:100:125 in toluene at 353 K. [b] Determined by comparing the integration of the methine proton of CHO in the $^1$H NMR spectra ($CDCl_3$): monomer (δ 3.0 2ppm), polyester (δ 5.22–4.70 ppm), polyether (δ 3.64–3.08 ppm). [c] Determined from comparing the integration of the aromatic proton signal of PA in the $^1$H NMR spectra ($CDCl_3$): monomer (δ 7.99–7.80 ppm) to polymer (δ 7.63–7.26 ppm). [d] Determined from the integration of the methylene proton resonance of CHO units in the $^1$H NMR spectra (DMSO-$d_6$): polyester (δ 5.23–4.51 ppm) against polyether (δ 3.90–2.78 ppm). [e] Determined by SEC analysis using THF as an eluent with a flow rate of 1 mL min$^{-1}$ at 30 °C against a polystyrene standard.

#### 4.4.1.1. Catalytic activity

The series of complexes **4.1**–**4.7** were active catalysts for ROCOP of CHO and PA and in some cases, perfectly alternating polyesters were obtained (Table 4.3). Comparing all complexes with Ti(O$^i$Pr)$_4$ shows that all complexes were slower but all show significantly higher selectivites than Ti(O$^i$Pr)$_4$ . For example, Ti(O$^i$Pr)$_4$ took 3 h to reach full CHO conversion , thereafter no further conversion of PA was observed. The resulting polymer showed just 19 % ester linkages with the remaining linkages being ethers, which is much lower than the polymers produced from all the complexes. This results underscores the importance of the ligand moiety in improving the ester linkage selectivity and moderating the Lewis acidity at Ti(IV).

Comparing phosphasalen Ti(IV) complexes **4.1**–**4.3,** which differ in the nature of diamine linker, complex **4.1**, possessing an ethylene diamine backbone showed the highest activity and needed 22 h to reach full conversion. The introduction of 2,2-dimethyl propylene (for complex **4.2**) and phenylene (for complex **4.3**) diamine bridges resulted in a drastic decrease in catalytic activity. Overall, the catalytic activity order follows **4.1** >> **4.2** ~ **4.3**. It is worth highlighting that the coordination modes of the $^{i}$PrO initiating groups of both complexes **4.2** and **4.3** were in a mutually *cis* arrangement in contrast to complex **4.1** where a *trans* coordination mode was observed. A similar polymerisation trend was also observed in the case of the salen Ti(IV) analogues, where complex **4.4**, containing a $C_2$ backbone was significantly faster than **4.5**, which possesses a $C_3Me_2$ linker. It is worth mentioning that complex **4.4** also possessed a *trans* coordination of $^{i}$PrO co-ligands and a *cis* coordination in complex **4.5**. In the case of the five coordinate Ti(IV) complex **4.6**, a slightly lower polymerisation rate compared to **4.4** was observed. The precise phenomena controlling the different catalytic activities are not yet clear, but rates may depend upon the coordination geometry of the alkoxide ligands and also upon the rigidity of the diamine linker group. For the complexes, possessing a $C_2$ backbone might generate a sterically more accessible active site and thus, enable higher polymerisation activity.

Comparing phosphasalen Ti(IV) complexes **4.1** and **4.2** with their salen analogues **4.3** and **4.4**, shows that both **4.1** and **4.2** have higher polymerisation rates than those of Ti(IV) salen complexes **4.3** and **4.4**, respectively. The weakening of the Ti–O$^{i}$Pr bond due to the high donating ability of phosphorous atoms through σ and π donation maybe responsible for the higher catalytic activities of phosphasalen complexes **4.1** and **4.2**. In comparing phosphasalen complexes **4.1** and **4.7**, which differ in the metal centre, Ti(IV) complex **4.1** showed a much higher catalytic activity than that of Zr(IV) complex **4.7**, although the Zr–O$^{i}$Pr bond distance is longer than that of Ti–O$^{i}$Pr. This is in contrast to other reported

phosphasalen complexes in which the larger metal centre showed higher catalytic activity.[25] However, it should be mentioned that these previous reports concern only the ROP of LA. We tentatively propose that either steric factors and/or stabilisation of a key carboxylate intermediate at Zr(IV) may be responsible for the lower activity of complex **4.7** for ROCOP of CHO and PA.

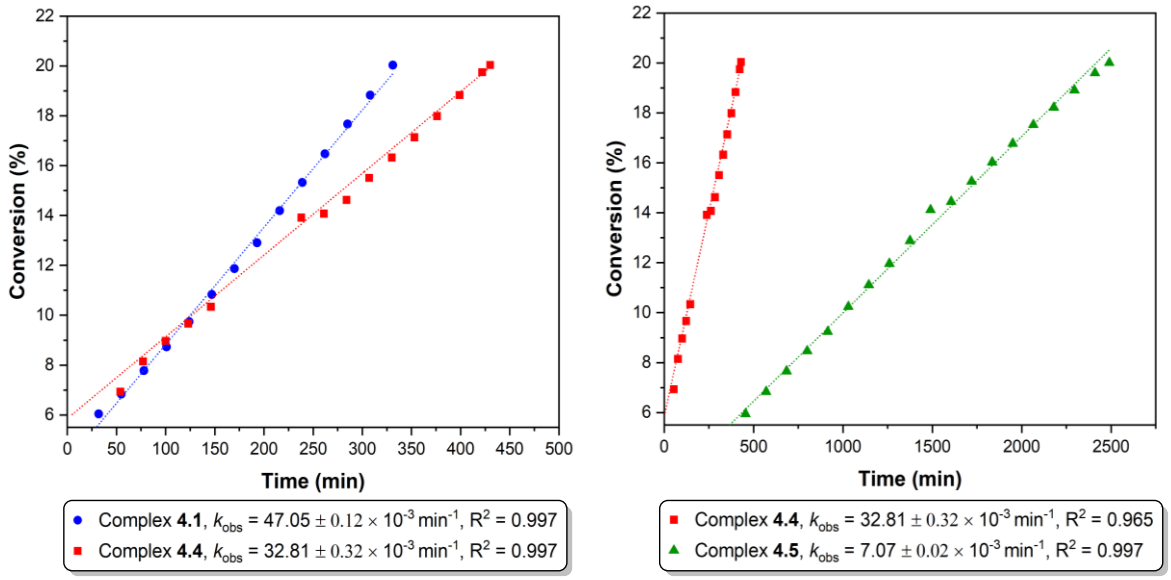



**Figure 4.5.** Kinetic plots of CHO/PA ROCOP for complexes **4.1** (●), **4.4** (■), and **4.5** (▲) obtained using *in situ* IR spectroscopy.

To gain insight into the polymerisation rates of the complexes, kinetic studies using *in situ* IR spectroscopy were conducted, using complexes **4.1**, **4.4**, and **4.5**. Complexes **4.1** and **4.4** were selected as representative catalysts since they showed the highest catalytic activities for each ligand type (Figure 4.5). Complex **4.5** was chosen to compare its catalytic activity with complex **4.4**, bearing the same class of ligand but differing in diamine linker and binding mode of the $^{i}$PrO co-ligands. The reactions were carried out using similar polymerisation conditions to those used in the preliminary polymerisation studies, except a lower concentration of PA was used as its solubility in toluene is poor ([CHO] = 3.75 M, [PA] = 3 M, [Ti] = 0.03 M, [Ti]:[PA]:[CHO] = 1:100:125, toluene, 353 K). The initial rate method was used to determine the $k_{obs}$ of each reaction and values were determined over the

5–20 % conversion range. The rate coefficient, $k_{obs}$ was obtained as the gradient of linear fit of the plots of conversion *vs.* time. Comparing complexes **4.1** and **4.4** which differ in the type of ligand, complex **4.1** showed a slightly higher $k_{obs}$ than that of complex **4.4** ($k_{obs}$ = 47.05 ± 0.12 × $10^{-3}$ $min^{-1}$ for **4.1** *vs.* $k_{obs}$ = 32.81 ± 0.32 × $10^{-3}$ $min^{-1}$ for **4.4**), which is fully consistent with the point kinetic-measurements in the preliminary studies. In comparing salen Ti(IV) complexes **4.4** and **4.5**, which differ in diamine linker and coordination mode of $^{i}$PrO co-ligands, complex **4.4** showed an almost 5 times larger $k_{obs}$ than that of complex **4.5** ($k_{obs}$ = 32.81 ± 0.32 × $10^{-3}$ $min^{-1}$ for **4.4** *vs.* $k_{obs}$ = 7.07 ± 0.02 × $10^{-3}$ $min^{-1}$ for **4.5**). This is again fully in line with the point-kinetic studies. In all cases, linear relationships between percent conversion and time was observed, suggesting a zero order in [PA]. The latter finding implicates fast insertion of the PA into the metal alkoxide bond which is fully consistent with previous work using other catalysts.[5]

#### 4.4.1.2. Catalyst selectivity

The catalytic selectivity relates to the formation of highly alternating polyesters, in contrast to Chapter 3 where the catalyst selectivity focuses on polymer microstructures (Table 4.3). The selectivities were calculated from the integration of specific protons for polyester compared to polyether units in the polymer chain (see calculation method in Chapter 2). Comparing phosphasalen Ti(IV) complexes **4.1**–**4.3**, which differ in the diamine linkers, complex **4.1** showed the highest selectivity and produced perfectly alternating poly(cyclohexene phthalate) (PCP). Complex **4.2** produced a polymer with only a moderate proportion of ester linkages (63 % ester linkages), whilst a low ester content polymer (36 % ester linkages) was prepared by complex **4.3**. A similar trend was observed for salen Ti(IV). Complex **4.4**, possessing a $C_2$ diamine linker, produced a highly alternating PCP with 90 % ester linkages. This selectivity was significantly higher than that of **4.5**, containing $C_3Me_2$ backbone, which produced a polymer with moderate ester content (52 % ester linkages).

Complex **4.6**, possessing a rigid Ph backbone, produced a polymer with 60 % ester linkages, slightly higher than **4.5**. These differences in selectivity may relate to the differences in the complex structures, active pocket sizes, and Lewis acidity of the Ti(IV) centres, since complex **4.6** features pentadentate coordination in contrast to both salen complexes **4.4** and **4.5** which possess hexadentate coordination.

Comparing complexes **4.1** and **4.4**, which differ in the type of the ligand moiety, phosphasalen Ti(IV) complex **4.1** showed higher selectivity for the formation of PCP (> 99 % ester linkages) than that of salen Ti(IV) catalyst **4.4** (90 % ester content) . It could be that the steric congestion of the phosphorous substituents improve the reaction selectivity using complex **4.1**. In addition, a reduction in the selectivity of the catalyst was observed when larger radii Zr(IV) was used and complex **4.7** produced a polymer with lower ester content (45 % ester linkages) than complex **4.1**.

#### 4.4.1.3. Polymer molar mass and molar mass distribution

Complexes **4.1**–**4.7** produced moderate molar mass polymers with narrow molar mass distributions ($Đ \leq 1.43$), except in a few cases where multimodal SEC traces were observed. In contrast, polymer chains obtained from $Ti(O^iPr)_4$ exhibited low molar mass and a broad molar mass distribution ($Đ \leq 2.07$). This shows the good polymerisation control of complexes **4.1**–**4.7** compared to the ill-controlled polymerisation using $Ti(O^iPr)_4$. The observation of multimodal SEC traces might relate to the presence of trace amounts of water which could act as a chain transfer agent during polymerisation. In addition, the hydrolysis of either the epoxide or cyclic anhydride monomers to form diol or diacid species which can further initiate polymerisations might account for the different molar mass distributions.

### 4.4.2. Monomer scoping using phosphasalen Ti(IV) complex 4.1

#### 4.4.2.1. Scope of epoxide substrate

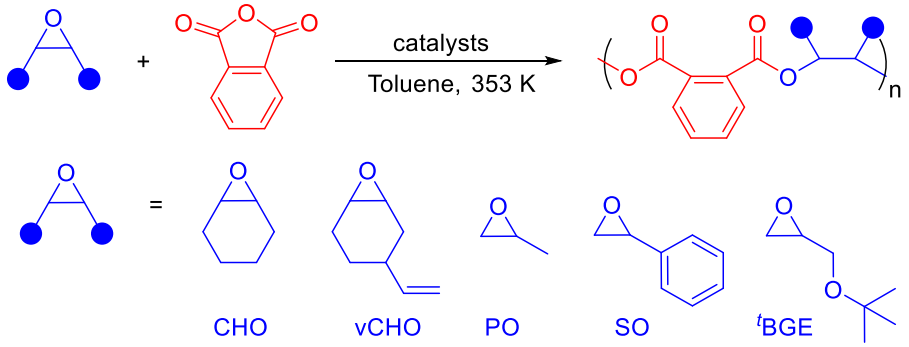



**Table 4.4.** ROCOP of PA with various epoxides results using **4.1**.[a]

| Epoxides | t (h) | Conv. (%) [b] | Ester linkages (%) [c] | $M_{n,SEC}$ (kg mol$^{-1}$) [d] | $Đ$ [d] | $T_g$ (°C) [e] |
|---|---|---|---|---|---|---|
| CHO | 22 | 91 | 99 | 13.2, 6.0 | 1.03, 1.07 | 123 |
| vCHO | 31 | 90 | 99 | 13.5 | 1.17 | 109 |
| PO | 23 | 99 | 99 | 11.2 | 1.08 | 59 |
| SO | 21 | 94 | 99 | 4.4 | 1.21 | 80 |
| $^t$BGE | 76 | 91 | 99 | 24.8, 11.8 | 1.02, 1.05 | 54 |

[a] Polymerisations were conducted using [epoxide] = 6.25 M, [PA] = 5.0 M, [Ti] = 0.05 M, [Ti]:[PA]:[epoxide] = 1:100:125, in toluene at 353 K. [b] Determined by comparing the integration of the aromatic proton signal of PA in the $^1$H NMR spectra ($CDCl_3$): monomer (δ 7.99–7.80 ppm) to polymer (δ 7.63–7.26 ppm). [c] Determined from the absence of polyether linkages in the $^1$H NMR spectra. [d] Determined by SEC analysis using THF as an eluent with a flow rate of 1 mLmin$^{-1}$ at 30 °C against a polystyrene standard. [e] Determined using DSC analysis with a heating rate of 10 °C min$^{-1}$ and $T_g$ values are reported from second heating cycle.

Given the promising catalytic activity and selectivity of the phosphasalen complex **4.1** in the ROCOP of CHO and PA, the scope of both substrates, epoxide and anhydride, were explored (Tables 4.4 and 4.5). Similar polymerisation conditions to the preliminary reactions were used ([epoxide] = 6.25 M, [anhydride] = 5.0 M, [Ti] = 0.05 M, [Ti]:[anhydride]:[epoxide] = 1:100:125, toluene, 353 K). First, ROCOP using various epoxides, from functional cyclohexene oxide to propylene oxide and its derivatives, with PA were studied (Table 4.4). Complex **4.1** showed high selectivity and produced perfectly alternating polyesters (> 99 % ester linkages) using all the epoxides as evidenced by the

absence of any polyether resonances in $^{1}$H NMR spectra of all crude polymers (Figures A2.35–A2.39).

For catalytic activity, by using 2-vinylcyclohexene oxide (vCHO), a slightly lower catalytic activity compared to CHO was observed and catalyst **4.1** required 31 h to achieve 90 % conversion. In contrast, a faster polymerisation rate for propylene oxide (PO) and styrene oxide (SO) compared to CHO was seen and both polymerisations reached full conversion within about 20 h. Complex **4.1** showed a sluggish polymerisation rate when using *tert*-butyl glycidyl ether ($^{t}$BGE) and almost 3 days was needed to achieve full conversion. All resultant polyesters showed predictable molar masses and narrow molar mass distributions ($Đ \leq 1.21$), except in some cases where a bimodal polymer was obtained. This might relate to the presence of trace amounts of diol in the polymersation system. A low molar mass polyester with monomodal distribution was obtained when SO was used.

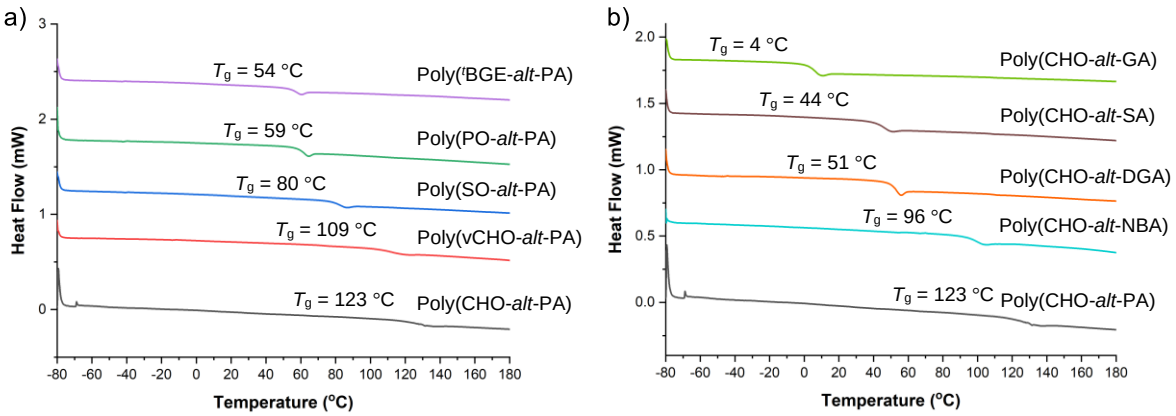



**Figure 4.6.** DSC thermograms of isolated polyesters: a) from table 4.4 and b) from table 4.5, prepared by complex **4.1**.

The thermal properties of the isolated polyesters were studied by DSC (Figure 4.6a). Polyesters with different $T_g$ values were obtained, depending on the epoxide used, highlighting the difference in the flexibility of the polymer backbones. In addition, the absence of any $T_m$ in all DSC thermograms suggests all the resultant polyesters are amorphous. Polyesters derived from CHO and its derivative vCHO, with PA, showed high

$T_g$ values ($T_g$ = 123 °C for poly(CHO-*alt*-PA) and $T_g$ = 109 °C for poly(vCHO-*alt*-PA)). This finding is attributed to the greater rigidity of the polymer backbone enforced by the cyclohexane ring. A slightly lower $T_g$ value was obtained for the polymer produced using SO ($T_g$ = 80 °C). In the case of PO and $^t$BGE, polyesters possessing lower $T_g$ values ($T_g$ = 59 °C for poly(PO-*alt*-PA) and $T_g$ = 54 °C for poly($^t$BGE-*alt*-PA)) were obtained, consistent with the greater flexibility of these polymer backbones. It is worth highlighting that all the isolated polyesters showed $T_g$ values higher than room temperature, and thus solid polymers were isolated in all cases.

### 4.4.2.2. Scope of cyclic anhydride substrate

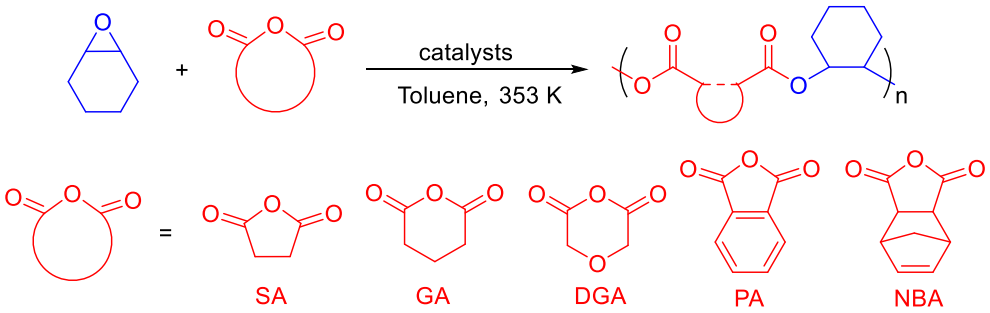



**Table 4.5.** ROCOP of CHO with various cyclic anhydrides data using **4.1**.[a]

| Anhydrides | t (h) | Conv. (%) [b] | Ester linkages (%) [c] | $M_{n,SEC}$ (kg mol$^{-1}$) [d] | $Đ$ [d] | $T_g$ (°C) [e] |
|---|---|---|---|---|---|---|
| PA | 22 | 91 | 99 | 13.2, 6.0 | 1.03,1.07 | 123 |
| NBA | 31 | 87 | 99 | 1.4 | 1.12 | 96 |
| SA | 6 | 92 | 99 | 1.7 | 1.34 | 44 |
| GA | 21 | 99 | 94 | 1.1 | 1.13 | 4 |
| DGA | 21 | 99 | 81 | 8.1, 2.5 | 1.36, 1.11 | 51 |

[a] Polymerisations were conducted using [CHO] = 6.25 M, [anhydride] = 5.0 M, [Ti] = 0.05 M, [Ti]:[anhydride]:[CHO] = 1:100:125, in toluene at 353 K. [b] Determined by comparing the integration of selected proton signal of anhydride monomer in the $^1$H NMR spectra ($CDCl_3$): PA (δ 7.99–7.80 ppm), NBA (δ 3.58–3.41 ppm), SA (δ 2.95–2.87 ppm), GA (δ 2.75–2.54 ppm), DGA (δ 4.41–4.27 ppm) to poly(CHO-PA) (δ 7.63–7.26 ppm), poly(CHO-NBA) (δ 3.41–2.89 ppm), poly(CHO-SA) (δ 2.68–2.35 ppm), poly(CHO-GA) (δ 2.40–2.17 ppm), poly(CHO-DGA) (δ 4.23–3.99 ppm). [c] Determined from the integration of the methylene proton resonance of CHO units in the $^1$H NMR spectra (DMSO-$d_6$): polyester (δ 5.23–4.51 ppm) against polyether (δ 3.90–2.78 ppm). [d] Determined by SEC analysis using THF as an eluent with a flow rate of 1 mL min$^{-1}$ at 30 °C against a polystyrene standard. [e] Determined using DSC analysis with a heating rate of 10 °C min$^{-1}$ and $T_g$ were reported from second heating cycle.

Complex **4.1** was able to copolymerise CHO with a variety of cyclic anhydrides, ranging from mono-, bi-, and tri-cyclic anhydrides (Table 4.5). Complex **4.1** produced polyesters with perfectly alternating structures and, in some cases, with high ester contents. In the case of NBA and SA, polyesters with more than 99 % ester linkages were obtained. Polymers with slightly lower ester content were observed when GA (94 % ester linkages) or DGA (81 % ester linkages) were utilised (Figures A2.40–A2.43).

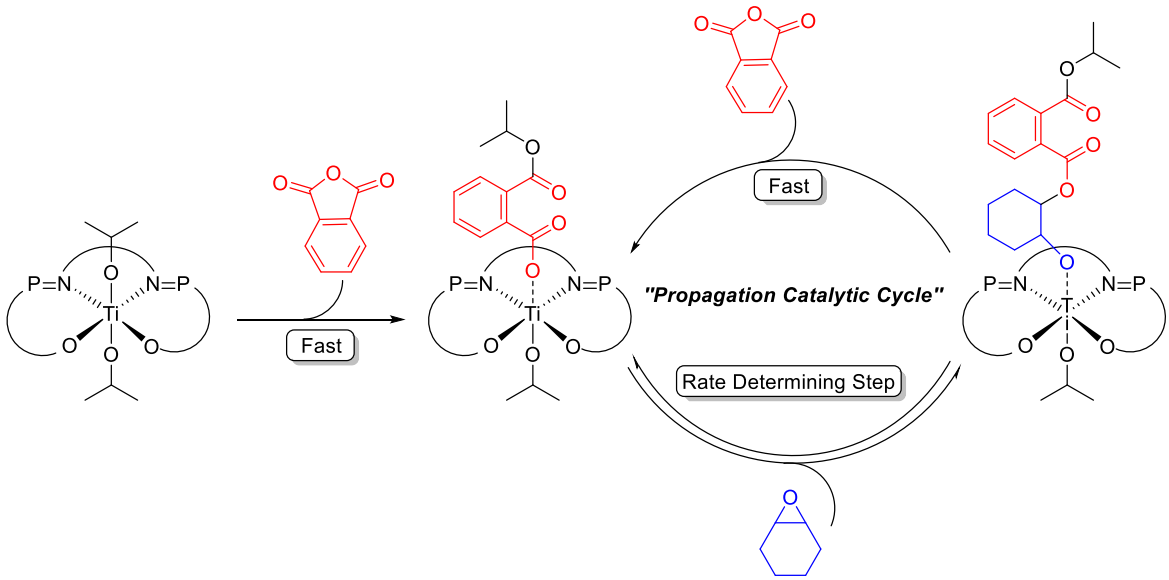
For catalytic activity, when using succinic anhydride (SA), a faster polymerisation rate compared to that of PA was seen. Complex **4.1** took 6 h to reach 92 % conversion when SA was used whilst using PA, 22 h is required to reach a similar conversion. Comparable polymerisation rates to CHO and PA ROCOP were observed when glutaric anhydride (GA) and diglycolic anhydride (DGA) were used as anhydrides. Full conversions were achieved by complex **4.1** after 21 h in both cases. In the case of norbornene anhydride (NBA), a slower polymerisation rate compared to PA was seen and complex **4.1** needed 31 h to reach 87 % conversion. Moderate to low molar mass polyesters with narrow molar mass distributions ($Đ \leq 1.36$) were produced in all cases, except DGA, where a bimodal SEC trace was seen.

DSC was used to study the thermal properties of the polymers (Figure 4.6b). Isolated polyesters showed different $T_g$ values depending on the type of cyclic anhydride. This is again consistent with the different flexibilities of the polymer backbones. All polyesters were amorphous materials, indicated by the lack of $T_m$ in all cases. Polyesters obtaining from mono cyclic anhydrides showed lower $T_g$ values than those containing bi and tri cyclic anhydrides. The lowest $T_g$ value of 4 °C was obtained from poly(CHO-GA). An increase in $T_g$ value was observed when SA and DGA were used ($T_g$ = 44 °C for poly(CHO-*alt*-SA) and $T_g$ = 51 °C for poly(CHO-DGA)). Significantly higher $T_g$ values were observed for polymers containing bi and tri cyclic anhydrides in line with the increased polymer backbone rigidity.

A $T_g$ value of 96 °C was observed for poly(CHO-*alt*-NBA) whilst, poly(CHO-*alt*-PA) showed a slightly higher $T_g$ value of 123 °C.

## 4.5. Understanding the ROCOP mechanism

### 4.5.1. Phosphasalen Ti(IV) complex




**Scheme 4.2.** Proposed ROCOP mechanism of epoxide and cyclic anhydride by phosphasalen Ti(IV) complexes.

Given the promising activity and selectivity of the phosphasalen Ti(IV) catalyst **4.1** toward the formation of highly alternating polyester without the need of using any co-catalysts, the mechanism warrants investigation. This section presents the proposed ROCOP mechanism, operating by phosphasalen Ti(IV) complexes (Scheme 4.2). CHO and PA were used as model epoxide and anhydride, respectively. Kinetic studies, using *in situ* IR spectroscopy, were used to identify the polymerisation order in anhydride concentration and predict the propagating step of ROCOP. The ROCOP mechanism involves two steps: I) Fast insertion of PA to the Ti–O$^i$Pr bond to form a carboxylate species and II) Insertion of CHO into the metal carboxylate to form an ester linkage and regenerate the titanium(IV) alkoxide intermediate.

The linear relationship between percent conversion and time, obtained from *in situ* IR spectroscopic kinetic analysis, suggests a zeroth order dependence on PA concentration (Figure 4.5). This is consistent with fast insertion of PA into the Ti-isopropoxide bond to form a propagating carboxylate intermediate. This intermediate then reacts with CHO to form the cyclohexene phthalate end group and regenerate the titanium-alkoxide intermediate. This alkoxide intermediate reacts with PA and the series of reactions are repeated to form the polyester. The polymerisation order with respect to epoxide concentration is expected to be first order, consistent with other complexes and with epoxide ring-opening being rate-determining.[5, 26] Full kinetic studies should be carried out to elucidate the full rate law and assess the polymerisation mechanism. Due to time constraints and unforeseen circumstances, the full kinetic details for this system have not been investigated. Nonetheless, these preliminary results are consistent with the proposed mechanism.

### 4.5.2. Propagating intermediate isolation

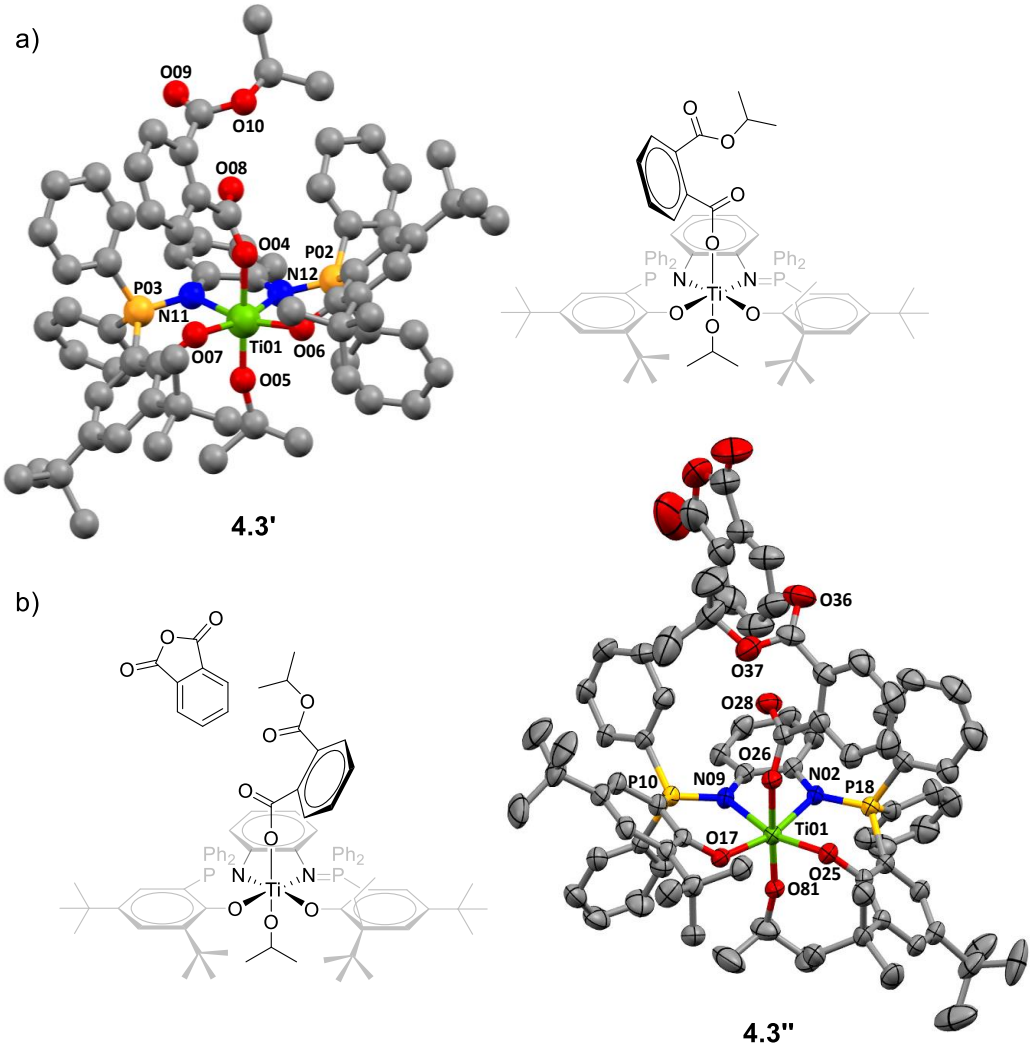



**Figure 4.7.** Representative structures of intermediates: a) **4.3′** and b) **4.3′′**.

**Table 4.6.** List of selected bond lengths (Å) and angles (°) for propagating **4.3′′**.

| Bond length (Å) | | Angle (º) | |
|---|---|---|---|
| Ti(01)-N(02) | 2.136(4) | N(02)-Ti(01)-N(09) | 75.36 |
| Ti(01)-N(09) | 2.132(6) | N(02)-Ti(01)-O(25) | 87.79 |
| Ti(01)-O(17) | 1.914(6) | N(09)-Ti(01)-O(17) | 88.34 |
| Ti(01)-O(25) | 1.943(9) | O(17)-Ti(01)-O(25) | 107.87 |
| Ti(01)-O(26) | 2.015(1) | O(26)-Ti(01)-O(81) | 173.21 |
| Ti(01)-O(81) | 1.789(2) | | |

Additionally, attempts were made to characterise the solid-state structures of propagating intermediates, by reacting complex **4.1** with a single equivalent of PA. Several crystallisation methods were attempted to grow a suitable crystal for single X-ray crystallography (SCXRD). Unfortunately, this approach was unsuccessful due to the high solubility of **4.1**. Nonetheless, reaction between the highly rigid backbone phosphasalen Ti(IV) complex **4.3** with an equivalent of PA led to the formation of single crystals of the propagating species **4.3′** (Figure 4.7a). The solid state structure of **4.3′** was characterised by SCXRD. It should be noted that the characterisation data only allows an understanding of the connection between atoms in the intermediate structure. Exact bond length and angles could not be determined due to the low quality of the obtained data due to the small single crystals and the low angle SCXRD measurements. The data obtained suggest that intermediate **4.3′** adopts a mononuclear structure, with octahedral geometry at the Ti(IV) centre. The structure has involved the PA insertion into the Ti–O$^{i}$Pr bond to form the Ti(IV)-carboxylate species which shows a *trans* arrangement of the two co-ligands.

Due to the presence of the two $^{i}$PrO co-ligands in complex **4.3**, two polymer chains could grow from one metal centre. To gain further understanding of the metal active site and number of growing polymer chains per metal centre, the reaction between **4.3** and two equivalents of PA was carried out. Suitable single crystals of propagating intermediate **4.3′′** were obtained by a slow cooling of a toluene/hexane solution and the molecular structure of this intermediate was analysed by SCXRD (Figure 4.7b and Table 4.). SCXRD revealed that intermediate **4.3′′** possesses a similar structure to that of **4.3′**, except with excess PA being observed in the lattice and showing no interaction with the Ti(IV) centre. As expected, the Ti(IV) centre adopts an octahedral geometry, where only one PA molecule is coordinated at the Ti(IV) centre and in a *trans* arrangement to the $^{i}$PrO co-ligand. This is evidenced by the close agreement of bond angles between the carboxylate and $^{i}$PrO co-ligand to 180° (O(26)-

Ti(01)-O(81) = 173.2°). The bond length between the Ti(IV) centre and O atom of the carboxylate end group (O26) is significant longer than that between the Ti(IV) centre and $^{i}$PrO co-ligand (O81) (Ti(01)-O(26) = 2.015(1) Å *vs.* Ti-O(81) = 1.789(2) Å). This reflects the increased lability of the carboxylate ligand and is consistent with its reactivity towards epoxide insertion to form an alternating polymer chain (see Scheme 4.2). This data tentatively indicates that the polymerisation may only occur with a single polymer chain growing per metal centre.

### 4.6. Ethylene polymerisation using complexes 4.1–4.7

Polyethylene, the most commonly used plastic, is a thermoplastic polymer. The production of polyethylene is predicted to account for more than one third of overall plastic produced worldwide.[27] Polyethylene possesses low strength and hardness whilst exhibiting high ductility and good impact strength. As a result, it is a very durable material.[28, 29] There are many examples of catalysts reported for the production of polyethylene and they can be categorised into the three main categories: I) Heterogeneous Ziegler-Natta catalysts, II) Metallocene catalysts and III) Post-metallocene compounds.[28] The production of broad molar mass distribution polyolefins, with a lack of stereocontrol for monomers beyond ethylene, are drawbacks of the traditional heterogeneous Ziegler-Natta system.[28] In contrast, homogeneous metallocene catalysts produce polyethylene with high control over the molar mass distribution and with more uniform properties.[28, 30] In addition, stereocontrolled propylene polymerisations have been achieved by metallocene catalysts.[28, 30] It should be stressed that the high catalytic activities of metallocene catalysts were achieved only after activation with an excess of methylaluminoxane (MAO). Brookhart and co-workers reported diamine nickel catalysts as the first post-metallocene catalysts in 1995.[31] After this ground breaking discovery, the development of post-metallocene catalysts garnered considerable attention from many research groups.[30, 32-35] As a result, many post-metallocene catalysts

have been reported to date. Among them, group IV metals (Ti, Zr, and Hf) have often been employed.[27, 34, 36-38] A wide variety of ligand moieties ranging from bi-, tri- and tetra-dentate ligands were investigated. However, phenoxy-imine and salen type ligands have been the most frequently investigated systems since some of them have shown high activity and stereoselectivity toward ethylene and propylene polymerisations.[12, 28, 33, 35, 39-42]

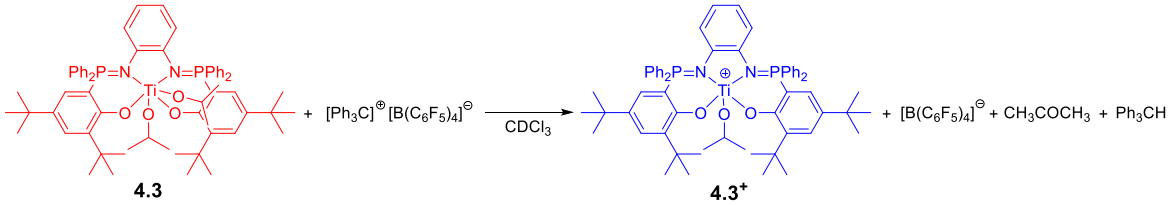
### 4.6.1. Preliminary ethylene polymerisation study using Ti(IV) complex 4.3

In this section we explored the catalytic activity of complexes **4.1**–**4.7** for ethylene polymerisation. It is worth highlighting that, these are the first phosphasalen group IV catalysts for ethylene polymerisations. All ethylene polymerisations were performed using a common set of conditions, with reactions conducted under 2 bar ethylene pressure, at 40 °C or 80 °C, in hexane or toluene. Complex **4.3** was first studied as a catalyst for ethylene polymerisation, using a standard set of conditions (activated catalyst 10 mg, TIBAL 150 mg, hexane 40 mL, 2 bar ethylene, at 80 °C).[43] Complex **4.3** was first activated by solid methylaluminoxane (sMAO) in toluene at 60 °C. The mixture was then dried, under vacuum, to give a pre-activated complex. The pre-activated complex was treated with TIBAL, *in situ* at room temperature, and the complex mixture was then used as a catalyst for ethylene polymerisation. In hexane at 80 °C, complex **4.3** was an active catalyst and produced polyethylene with activity and productivity of 12.6 $kg_{polymer}\ mol_{cat.}^{-1}h^{-1}bar^{-1}$ and 0.002 $kg_{polymer}\ g_{cat.}^{-1}h^{-1}$, respectively. SEC analysis indicated the formation of ultrahigh molar mass polyethylene, with molar mass values up to $4.49 \times 10^6$ g $mol^{-1}$ and $Đ \leq 4.19$. DSC measurement revealed the formation of highly crystalline polyethylene, with a $T_m$ of 133 °C.

Recently, the group of Klosin, Loht and Marks reported a new methodology for ethylene polymerisation without the need for the highly flammable MAO co-catalyst.[32] The polymerisation was carried out by akylation of the catalysts using trimethyl aluminium

(TMA), followed by the formation of cationic species using $[Ph_3C]^+[B(C_6F_5)_4]^-$. Ethylene polymerisations using this activation method were also studied.

### 4.6.2. Formation and stability studies for the cationic complex




**Scheme 4.3**. Preparation of the cationic compound of phosphasalen Ti(IV) complex **4.3**.

First, complex **4.3** was used as a representative catalyst to study the cationic complex formation. The formation of the cationic complex $\mathbf{4.3}^+$ was carried out in an NMR experiment, using $CDCl_3$ as the solvent (Scheme 4.3). Complex **4.3** was reacted with $[Ph_3C]^+[B(C_6F_5)_4]^-$ *in situ* and the formation of the cationic complex $\mathbf{4.3}^+$ was monitored using $^1H$ and $^{31}P\{^1H\}$ NMR spectroscopies (Figures 4.8 and 4.9).

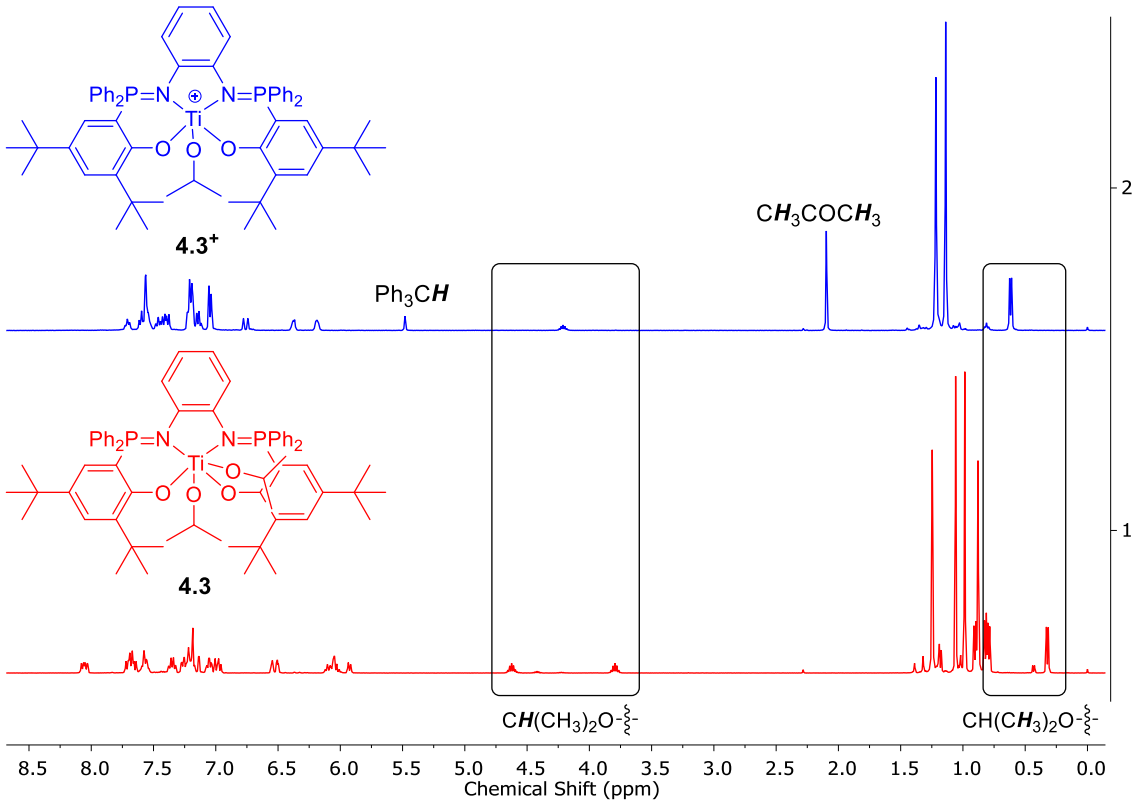



**Figure 4.8.** Stacked $^1H$ NMR spectra for the formation of the cationic complex $\mathbf{4.3}^+$.

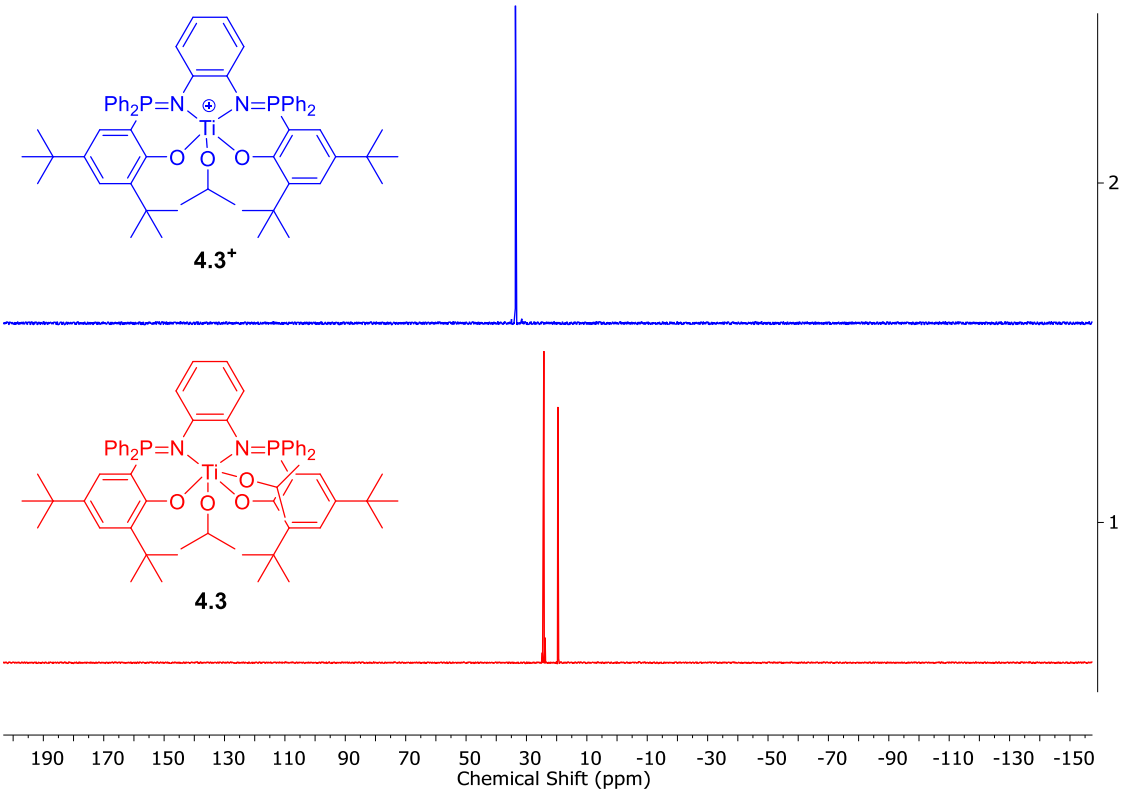



**Figure 4.9.** Stacked $^{31}P\{^{1}H\}$ NMR spectra for the formation of the cationic complex **4.3**$^{+}$.

The formation of the cationic complex occurs *via* the abstraction of the methine proton from one of the $^{i}$PrO co-ligands, by $[Ph_3C]^{+}$, to form acetone and $Ph_3CH$ as by-products. The presence of acetone and $Ph_3CH$ signals in the $^{1}H$ NMR spectrum with an integration ratio of 1:6 at δ 5.48 and 2.10 ppm, respectively, suggests the successful formation of the cationic complex **4.3**$^{+}$ (Figure 4.8). The $^{1}H$ NMR spectrum also shows the presence of one $^{i}$PrO co-ligand, consistent with the expected structure. The $^{31}P\{^{1}H\}$ NMR spectrum of the cationic compound shows a singlet resonance, in contrast to the neutral precursor compound where two different phosphorous signals were observed (Figure 4.9). The former finding suggests an identical environment for the two phosphorous atoms on the ligand backbone and is fully consistent with a complex where only one $^{i}$PrO is present as a cationic compound.

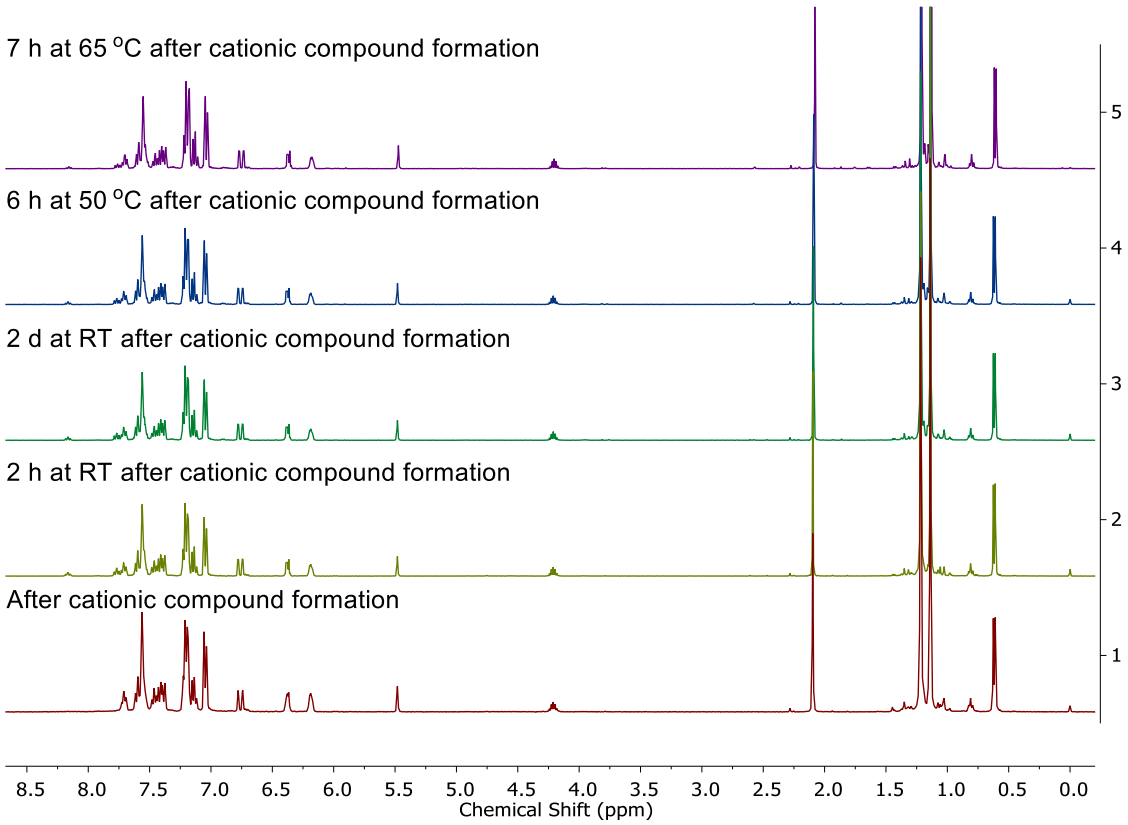



**Figure 4.10.** Stacked $^{1}H$ NMR spectra of the cationic compound **4.3**$^{+}$ following formation.

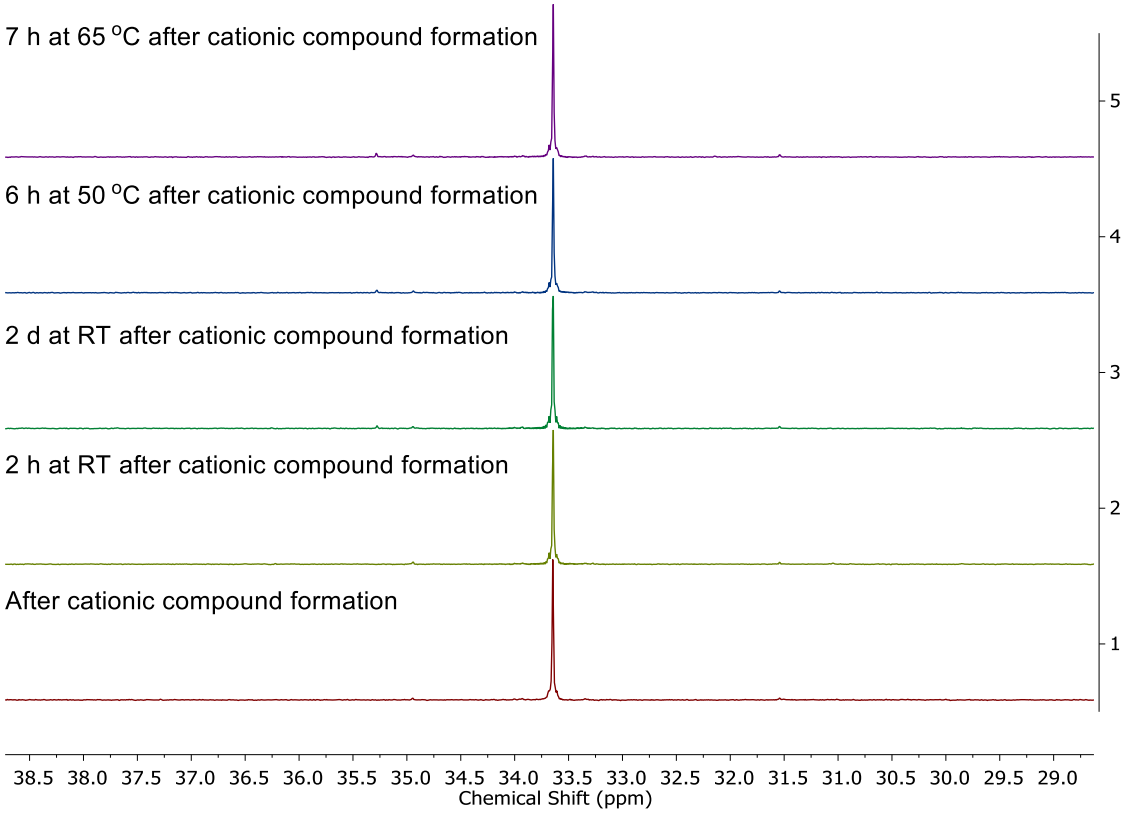



**Figure 4.11.** Stacked $^{31}P\{^{1}H\}$ NMR spectra of the cationic compound **4.3**$^{+}$ following formation.

The stability of the cationic compound was monitored by $^{1}H$ and $^{31}P\{^{1}H\}$ NMR spectroscopies (Figures 4.10 and 4.11). Surprisingly, NMR spectroscopy analysis suggests a high stability for **4.3**$^{+}$. Although the complex was left in halogenated solvent at room temperature for several days or heated to elevated temperatures, the $^{1}H$ and $^{31}P\{^{1}H\}$ NMR spectra remain unchanged. This could be due to the high electron donation of the phosphasalen which helps to stabilise the cationic species.

### 4.6.3. Ethylene polymerisations using *in situ* generated cationic species

**Table 4.7.** Ethylene polymerisation data of complexes **4.1**–**4.7**.[a]

| Catalysts | Activity (kg mol$^{-1}$h$^{-1}$bar$^{-1}$)[b] | Productivity (kg g$^{-1}$h$^{-1}$)[c] | $M_{n,SEC}$ (kg mol$^{-1}$)[d] | $Đ$ [d] | $T_m$ (°C) [e] |
|---|---|---|---|---|---|
| **4.1** | 1.82 | 0.004 | 396.09, 14.53 | 1.56, 3.07 | 136 |
| **4.2** | 0.35 | 0.0006 | NA | NA | 136 |
| **4.3** | 4.07 | 0.008 | NA | NA | 138 |
| **4.4** | 1.68 | 0.005 | NA | NA | 136 |
| **4.5** | 0.40 | 0.001 | 109.88, 2.10 | 2.73, 2.94 | 134 |
| **4.6** | 0.65 | 0.002 | NA | NA | 134 |
| **4.7** | No polymerisation was observed | | | | |

[a] Polymerisations were conducted in toluene at 40 °C for 1 h under the continuous ethylene pressure of 2 bars. [b] Calculated by comparing the amount of the produced polyethylene (kg) to the amount of the catalyst (mol), polymerisation time (h), and ethylene pressures (bar). [c] Determined by comparing the amount of produced polyethylene (kg) to the amount of catalyst (g) and polymerisation time (h). [d] Determined from SEC using 1,2-dichlorobenzene as an eluent, at 160 °C and with a flow rate of 1 ml min$^{-1}$. [e] Identified using DSC with a heating rate of 10 °C min$^{-1}$ and all $T_m$ are reported from the third heating cycle.

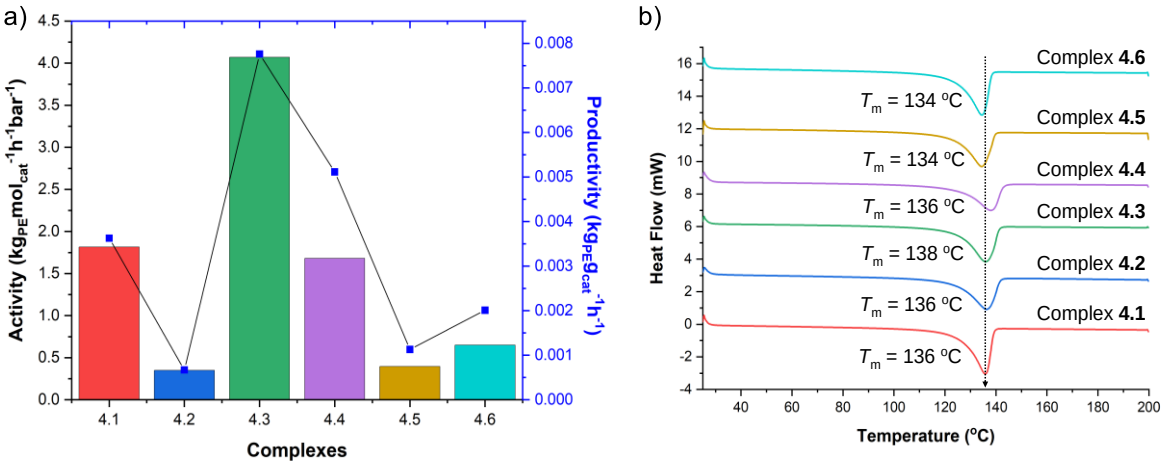



**Figure 4.12.** a) Bar chart comparing catalyst activity and productivity of complexes **4.1**–**4.7** and b) DSC thermograms of isolated polyethylenes.

Due to the high stability of the cationic compound **4.3**$^{+}$, it could be used in ethylene polymerisations utilising the procedure reported by the group of Klosin, Loht and Marks.[32] Firstly, the complexes **4.1**–**4.7** were each alkylated by reaction with TIBAL, in toluene at ambient temperature, for 30 minutes, followed by activation with $[Ph_3C]^+[B(C_6F_5)_4]^-$. All polymerisations were carried out in toluene at 40 °C, for 1 h, and with continuous 2 bar pressure of ethylene (Table 4.7 and Figure 4.12). The catalytic activity and productivity of all complexes were determined based on the amount of polymer produced against the amount of catalyst and the polymerisation time.

Phosphasalen Ti(IV) complex **4.1** showed similar activity and productivity to its salen analogue, **4.4**. In addition, phosphasalen Ti(IV) complex **4.2** and its salen analogue **4.5** showed similar behavior (Table 4.7 and Figure 4.12a). Phosphasalen complex **4.3** showed the highest activity and productivity and this is 10 times higher than that of salalen Ti complex **4.5**, containing the same phenylene diamine linker. Comparing **4.3** with other Ti(IV) phosphasalen complexes, complex **4.3** showed 2.5 times and 12 times faster than that of **4.1** and **4.2**, respectively. The overall polymerisation rate follows **4.3** > **4.1** ≈ **4.4** > **4.6** > **4.2** ≈ **4.5**. Using identical polymerisation conditions, complex **4.7** showed no activity. The molar masses of representative polyethylene samples, produced by phosphasalen complex **4.1** and salen complex **4.5** were determined by SEC using 1,2-dichlorobenzene as a solvent, at 160 °C. SEC measurement indicate the formation of ultrahigh molar mass polyethylene in both cases and a polymer molar mass of up 4 million g mol$^{-1}$ was observed. In both cases, bimodal SEC traces with narrow $Đ$ were observed. Thermal properties of the isolated polyethylenes were characterised by DSC (Figure 4.12b). DSC thermograms showed a high $T_m$ in the range of 134–138 °C, consistent with the formation of ultrahigh molar mass polyethylene. In addition, all polyethylenes were highly crystalline materials as indicated by the observation of a clear melting transition.

## 4.7. Conclusion and Outlook

### 4.7.1. Conclusion

In conclusion, this chapter presents a novel series of phosphasalen Ti(IV) and Zr(IV) complexes. Complexes show different binding modes for the two isopropoxide co-ligands, depending on the nature of the diamine backbone present in the ancillary ligand. Ligands featuring ethylene diamine linkers result in the formation of $^{i}$PrO *trans*-coordination complexes. The exception is complex **4.1**, containing an ethylene diamine linker, where the structure exists in equilibrium between *cis*- and *trans*- forms in solution. A *cis*-coordination was observed when 2,2-dimethyl propylene and phenylene diamine backbones were used. The Ti(IV) complex **4.6** with a salalen ligand containing a phenylene backbone was the only complex to adopt a pentadentate structure. All catalyst were active and in some cases highly selective for polyester formation in epoxide/anhydride ROCOP using a wide range of commercially available epoxides and cyclic anhydrides, without the need for any co-catalyst. The catalytic activities and selectivities of all complexes were compared against their salen and salalen Ti(IV) analogues. All the phosphasalen Ti(IV) catalysts are more active and more selective than salen and salalen analogues. The increased electron donating ability of the phosphasalen moiety, *via* both σ and π donations and the increased steric hindrance from the phosphorous substituents appear to correlate with increased activity and selectivity, respectively. Isolated polyesters show a range of different $T_g$ values, depending on both the epoxide and cyclic anhydride used, and as such represent a useful class of degradable/recyclable polymers for future exploration.

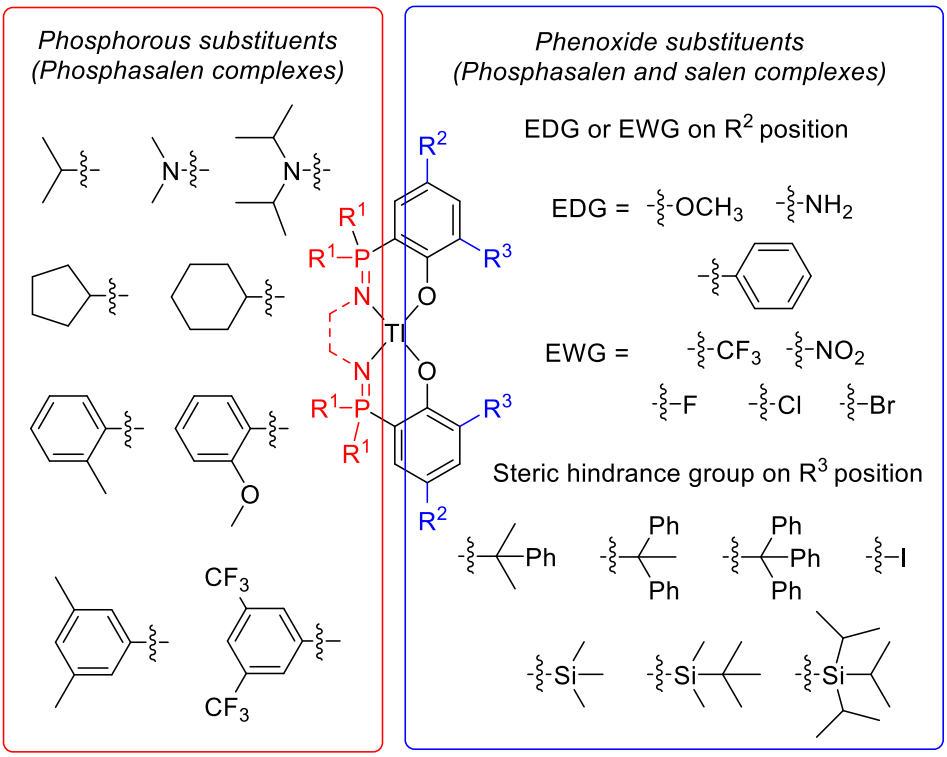
Kinetic studies using *in situ* IR spectroscopy suggest that the polymerisation rate of phosphasalen Ti(IV) complex **4.1** is comparable to its salen analogue **4.4**. Conversely, complex **4.4**, possessing ethylene backbone was significantly faster than that of complex **4.5**, containing 2,2-dimethyl propylene linker. Additionally, a proposed ROCOP mechanism

was presented and the structure of a possible propagating intermediate was isolated and its solid state structure was characterised by X-ray diffraction experiments.

Furthermore, all Ti(IV) complexes were active for ethylene polymerisations without the need for MAO. Although the catalytic activity and productivity were lower compared to other benchmark catalysts, ultrahigh molar mass polyethylenes with high $T_m$ were produced.

### 4.7.2. Outlook

Potential future research can be categorised into three main areas, including I) Development of the ROCOP catalysts to achieve higher catalytic activity, whilst maintaining the high selectivity, II) Kinetic investigations to gain more understanding of the ROCOP mechanism, and III) Utilisation of these complexes with different polymerisations to access new materials with more complex structures (*i.e.* copolymerisations).




**Scheme 4.4**. Proposed structures of phosphasalen and salen Ti(IV) complexes with various functional groups.

The tetradentate Ti(IV) complexes investigated in this chapter are interesting as catalysts for epoxide/anhydride ROCOP because they operate without the need for any toxic co-catalysts. Although the structure-reactivity or structure-stereoselectivity relationships for some of these complexes were fully optimised in lactone ROP, there is no such information relevant to the ROCOP of epoxides and anhydrides.[11-13] The presented data in this chapter represents the beginning of the discovery of group IV catalyst systems for ROCOP of epoxide and anhydride. Although some of them showed very promising selectivity for the formation of polyesters from ROCOP of various epoxides and anhydrides, their activities were lower than more optimised catalyst systems.[1, 2] One way to improve the catalytic activity would be to optimise the catalyst structure by introducing electron donating (EDG) or electron withdrawing (EWG) groups onto the ligand moiety. In the case of EDG substituents, these might weaken the metal-alkoxide bond and thus accelerate monomer insertion. The EWG substituents, could increase the Lewis acidity of the metal centre and accelerate epoxide coordination. Due to the presence of phenoxide rings or phosphorous atoms on phosphasalen and salen ligands, it is possible to introduce various functional groups (Scheme 4.4). Some possible substituent positions and EDG and EWG which could be used are shown.

II) Kinetic studies to investigate full empirical rate law.

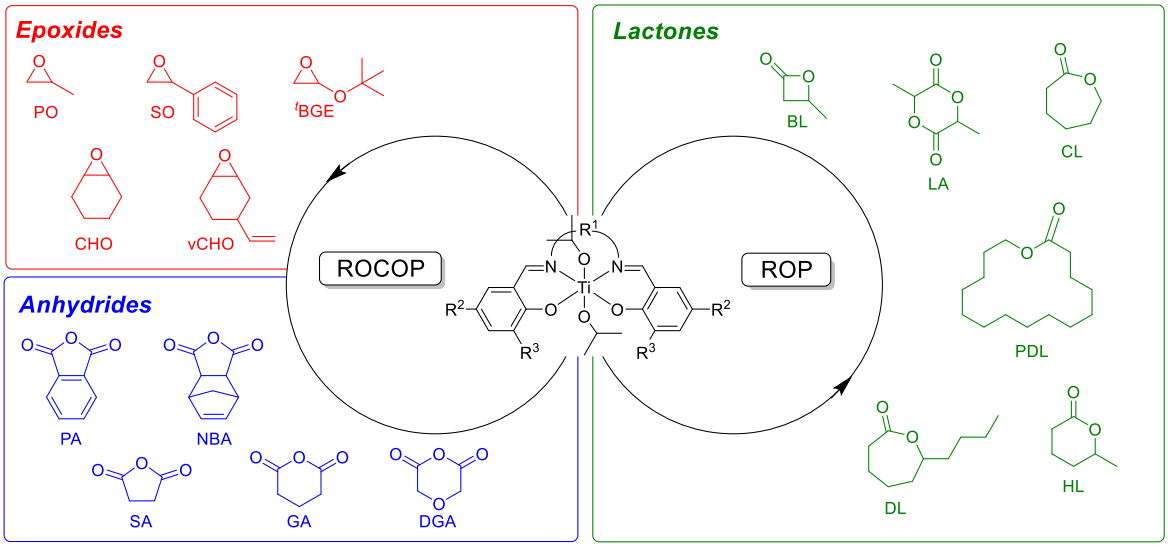
$$Rate = k_{obs}[anhydride]^0[epoxide]^x$$

$$Rate = k_p[anhydride]^0[epoxide]^x[catalyst]^y$$

Further polymerisation kinetic studies should be undertaken to gain a greater understanding of the polymerisation mechanism. This would allow determination of polymerisation orders in each component and the full rate law. Kinetic studies could be carried out using various methods (*i.e. in situ* NMR or IR spectroscopies or by taking regular aliquots etc.) As discuss

earlier, *in situ* IR spectroscopy suggested the polymerisation was zeroth order in anhydride concentration. The order in epoxide and catalyst concentrations should be determined next.

III) 'Switch' catalysis to allow the synthesis of new copolymers:




**Scheme 4.5**. 'Switch' catalysis using salen Ti(IV) complexes.

Salen Ti(IV) complexes were extensively studied for ROP of various lactones and in some cases impressive polymerisation activity and stereoselectivity were observed.[11, 12, 44] In this chapter, we presented the use of these catalyst in epoxide/anhydride ROCOP and some of them show promising results in terms of activity and selectivity. It would be interesting to investigate the combination of these two different polymerisation mechanisms using these Ti(IV) salen catalysts. If successful, the catalysts might allow formation of various copolymers *via* 'Switch' catalysis.

## 4.8. References


(1) Longo, J. M.; Sanford, M. J.; Coates, G. W., Ring-Opening Copolymerization of Epoxides and Cyclic Anhydrides with Discrete Metal Complexes: Structure–Property Relationships. *Chem. Rev.* **2016,** *116* (24), 15167–15197.

(2) Paul, S.; Zhu, Y.; Romain, C.; Brooks, R.; Saini, P. K.; Williams, C. K., Ring-opening copolymerization (ROCOP): synthesis and properties of polyesters and polycarbonates. *Chem. Commun.* **2015,** *51* (30), 6459–6479.

(3) Abel, B. A.; Lidston, C. A. L.; Coates, G. W., Mechanism-Inspired Design of Bifunctional Catalysts for the Alternating Ring-Opening Copolymerization of Epoxides and Cyclic Anhydrides. *J. Am. Chem. Soc.* **2019,** *141* (32), 12760–12769.

(4) Deacy, A. C.; Kilpatrick, A. F. R.; Regoutz, A.; Williams, C. K., Understanding metal synergy in heterodinuclear catalysts for the copolymerization of $CO_2$ and epoxides. *Nat. Chem.* **2020,** *12* (4), 372–380.

(5) Fieser, M. E.; Sanford, M. J.; Mitchell, L. A.; Dunbar, C. R.; Mandal, M.; Van Zee, N. J.; Urness, D. M.; Cramer, C. J.; Coates, G. W.; Tolman, W. B., Mechanistic Insights into the Alternating Copolymerization of Epoxides and Cyclic Anhydrides Using a (Salph)AlCl and Iminium Salt Catalytic System. *J. Am. Chem. Soc.* **2017,** *139* (42), 15222–15231.

(6) Darensbourg, D. J.; Yarbrough, J. C., Mechanistic Aspects of the Copolymerization Reaction of Carbon Dioxide and Epoxides, Using a Chiral Salen Chromium Chloride Catalyst. *J. Am. Chem. Soc.* **2002,** *124* (22), 6335–6342.

(7) Moore, D. R.; Cheng, M.; Lobkovsky, E. B.; Coates, G. W., Mechanism of the Alternating Copolymerization of Epoxides and $CO_2$ Using *β*-Diiminate Zinc Catalysts: Evidence for a Bimetallic Epoxide Enchainment. *J. Am. Chem. Soc.* **2003,** *125* (39), 11911–11924.

(8) Nakano, K.; Hashimoto, S.; Nozaki, K., Bimetallic mechanism operating in the copolymerization of propylene oxide with carbon dioxide catalyzed by cobalt–salen complexes. *Chem. Sci.* **2010,** *1* (3), 369–373.

(9) Thevenon, A.; Cyriac, A.; Myers, D.; White, A. J. P.; Durr, C. B.; Williams, C. K., Indium Catalysts for Low-Pressure CO/Epoxide Ring-Opening Copolymerization: Evidence for a Mononuclear Mechanism? *J. Am. Chem. Soc.* **2018,** *140* (22), 6893–6903.

10. Chmura, A. J.; Davidson, M. G.; Frankis, C. J.; Jones, M. D.; Lunn, M. D., Highly active and stereoselective zirconium and hafnium alkoxide initiators for solvent-free ring-opening polymerization of *rac*-lactide. *Chem. Commun.* **2008,** (11), 1293–1295.

(11) Gao, B.; Li, X.; Duan, R.; Pang, X., Titanium complexes with octahedral geometry chelated by salen ligands adopting *β*-cis configuration for the ring-opening polymerisation of lactide. *New J. Chem.* **2015,** *39* (4), 2404–2408.

(12) Gregson, C. K. A.; Blackmore, I. J.; Gibson, V. C.; Long, N. J.; Marshall, E. L.; White, A. J. P., Titanium–salen complexes as initiators for the ring opening polymerisation of rac-lactide. *Dalton Trans.* **2006,** (25), 3134–3140.

(13) Jeffery, B. J.; Whitelaw, E. L.; Garcia-Vivo, D.; Stewart, J. A.; Mahon, M. F.; Davidson, M. G.; Jones, M. D., Group 4 initiators for the stereoselective ROP of *rac*-*β*-butyrolactone and its copolymerization with rac-lactide. *Chem. Commun.* **2011,** *47* (45), 12328–12330.

(14) Nakano, K.; Kobayashi, K.; Nozaki, K., Tetravalent Metal Complexes as a New Family of Catalysts for Copolymerization of Epoxides with Carbon Dioxide. *J. Am. Chem. Soc.* **2011,** *133* (28), 10720–10723.

(15) Raman, S. K.; Deacy, A. C.; Pena Carrodeguas, L.; Reis, N. V.; Kerr, R. W. F.; Phanopoulos, A.; Morton, S.; Davidson, M. G.; Williams, C. K., Ti(IV)–Tris(phenolate) Catalyst Systems for the Ring-Opening Copolymerization of Cyclohexene Oxide and Carbon Dioxide. *Organometallics* **2020,** *39* (9), 1619–1627.

(16) Wang, Y.; Qin, Y.; Wang, X.; Wang, F., Trivalent Titanium Salen Complex: Thermally Robust and Highly Active Catalyst for Copolymerization of $CO_2$ and Cyclohexene Oxide. *ACS Catal.* **2015,** *5* (1), 393–396.

(17) Quadri, C. C.; Le Roux, E., Copolymerization of cyclohexene oxide with $CO_2$ catalyzed by tridentate N-heterocyclic carbene titanium(iv) complexes. *Dalton Trans.* **2014,** *43* (11), 4242–4246.

(18) Garden, J. A.; White, A. J. P.; Williams, C. K., Heterodinuclear titanium/zinc catalysis: synthesis, characterization and activity for $CO_2$/epoxide copolymerization and cyclic ester polymerization. *Dalton Trans.* **2017,** *46* (8), 2532–2541.

(19) Lalrempuia, R.; Breivik, F.; Törnroos, K. W.; Le Roux, E., Coordination behavior of bis-phenolate saturated and unsaturated N-heterocyclic carbene ligands to zirconium: reactivity and activity in the copolymerization of cyclohexene oxide with $CO_2$. *Dalton Trans.* **2017,** *46* (25), 8065–8076.

(20) Quadri, C. C.; Lalrempuia, R.; Hessevik, J.; Törnroos, K. W.; Le Roux, E., Structural Characterization of Tridentate N-Heterocyclic Carbene Titanium(IV) Benzyloxide, Silyloxide, Acetate, and Azide Complexes and Assessment of Their Efficacies for Catalyzing the Copolymerization of Cyclohexene Oxide with $CO_2$. *Organometallics* **2017,** *36* (22), 4477–4489.

(21) Bakewell, C.; Cao, T.-P.-A.; Le Goff, X. F.; Long, N. J.; Auffrant, A.; Williams, C. K., Yttrium Phosphasalen Initiators for *rac*-Lactide Polymerization. *Organometallics* **2013,** *32* (5), 1475–1483.

(22) Bakewell, C.; Cao, T.-P.-A.; Long, N.; Le Goff, X. F.; Auffrant, A.; Williams, C. K., Yttrium Phosphasalen Initiators for *rac*-Lactide Polymerization: Excellent Rates and High Iso-Selectivities. *J. Am. Chem. Soc.* **2012,** *134* (51), 20577–20580.

(23) Normand, A. T.; Malacea-Kabbara, R.; Lapenta, R.; Dajnak, A.; Richard, P.; Cattey, H.; Bolley, A.; Grassi, A.; Milione, S.; Auffrant, A.; Dagorne, S.; Le Gendre, P., Phosphasalen group IV metal complexes: synthesis, characterization and ring opening polymerization of lactide. *Dalton Trans.* **2020,** *49* (21), 6989–7004.

(24) Addison, A. W.; Rao, T. N.; Reedijk, J.; van Rijn, J.; Verschoor, G. C., Synthesis, structure, and spectroscopic properties of copper(II) compounds containing nitrogen–sulphur donor ligands; the crystal and molecular structure of aqua[1,7-bis(N-methylbenzimidazol-2′-yl)-2,6-dithiaheptane]copper(II) perchlorate. *J. Chem. Soc. Dalton Trans.* **1984,** (7), 1349–1356.

(25) Bakewell, C.; White, A. J. P.; Long, N. J.; Williams, C. K., Metal-Size Influence in Iso-Selective Lactide Polymerization. *Angew. Chem. Int. Ed.* **2014,** *53* (35), 9226–9230.

(26) Darensbourg, D. J.; Poland, R. R.; Escobedo, C., Kinetic Studies of the Alternating Copolymerization of Cyclic Acid Anhydrides and Epoxides, and the Terpolymerization of Cyclic Acid Anhydrides, Epoxides, and $CO_2$ Catalyzed by (salen)CrIIICl. *Macromolecules* **2012,** *45* (5), 2242–2248.

(27) Yuan, S.-F.; Yan, Y.; Solan, G. A.; Ma, Y.; Sun, W.-H., Recent advancements in N-ligated group 4 molecular catalysts for the (co)polymerization of ethylene. *Coord. Chemi. Rev.* **2020,** *411*, 213254.

(28) Białek, M.; Czaja, K., Metal salen complexes as ethylene polymerization catalysts - Effect of catalytic system composition on its activity and properties of polymerization products. *Polimery -Warsaw-* **2008,** *53*, 364–370.

(29) Khanam, P. N.; AlMaadeed, M. A. A., Processing and characterization of polyethylene-based composites. *Adv. Manuf. Polym. Compos. Sci.* **2015,** *1* (2), 63–79.

(30) Ittel, S. D.; Johnson, L. K.; Brookhart, M., Late-Metal Catalysts for Ethylene Homo- and Copolymerization. *Chem. Rev.* **2000,** *100* (4), 1169–1204.

(31) Johnson, L. K.; Killian, C. M.; Brookhart, M., New Pd(II)- and Ni(II)-Based Catalysts for Polymerization of Ethylene and .alpha.-Olefins. *J. Am. Chem. Soc.* **1995,** *117* (23), 6414–6415.

(32) Gao, Y.; Christianson, M. D.; Wang, Y.; Chen, J.; Marshall, S.; Klosin, J.; Lohr, T. L.; Marks, T. J., Unexpected Precatalyst σ-Ligand Effects in Phenoxyimine Zr-Catalyzed Ethylene/1-Octene Copolymerizations. *J. Am. Chem. Soc.* **2019,** *141* (19), 7822–7830.

(33) Iwashita, A.; Chan, M. C. W.; Makio, H.; Fujita, T., Attractive interactions in olefin polymerization mediated by post-metallocene catalysts with fluorine-containing ancillary ligands. *Catal. Sci. Technol.* **2014,** *4* (3), 599–610.

(34) Liu, C.-C.; Liu, Q.; Lo, P.-K.; Lau, K.-C.; Yiu, S.-M.; Chan, M. C. W., Olefin Polymerization Reactivity of Group 4 Post-Metallocene Catalysts Bearing a Four-Membered C($sp^3$)-Donor Chelate Ring. ChemCatChem **2019,** *11* (1), 628–635.

(35) Makio, H.; Terao, H.; Iwashita, A.; Fujita, T., FI Catalysts for Olefin Polymerization—A Comprehensive Treatment. *Chem. Rev.* **2011,** *111* (3), 2363–2449.

(36) Alt, H. G.; Köppl, A., Effect of the Nature of Metallocene Complexes of Group IV Metals on Their Performance in Catalytic Ethylene and Propylene Polymerization. *Chem. Rev.* **2000,** *100* (4), 1205–1222.

(37) Collins, R. A.; Russell, A. F.; Mountford, P., Group 4 metal complexes for homogeneous olefin polymerisation: a short tutorial review. *Appl. Petrochem. Res.* **2015,** *5* (3), 153–171.

(38) Klosin, J.; Fontaine, P. P.; Figueroa, R., Development of Group IV Molecular Catalysts for High Temperature Ethylene-α-Olefin Copolymerization Reactions. *Acc. Chem. Res.* **2015,** *48* (7), 2004–2016.

(39) Białek, M., Effect of catalyst composition on chain-end-group of polyethylene produced by salen-type complexes of titanium, zirconium, and vanadium. *J. Polym. Sci. A. Polym. Chem.* **2010,** *48* (14), 3209–3214.

(40) Białek, M.; Czaja, K., Dichlorovanadium (IV) complexes with salen-type ligands for ethylene polymerization. *J. Polym. Sci. A. Polym. Chem.* **2008,** *46* (20), 6940–6949.

(41) Białek, M.; Czaja, K.; Szydło, E., Transition metal complexes of tetradentate and bidentate Schiff bases as catalysts for ethylene polymerization: Effect of transition metal and cocatalyst. *J. Polym. Sci. A. Polym. Chem.* **2009,** *47* (2), 565–575.

(42) Białek, M.; Leksza, A.; Piechota, A.; Kurzak, K.; Koprek, K., Oxovanadium(IV) complexes with [ONNO]-chelating ligands as catalysts for ethylene homo- and copolymerization. *J. Polym. Res.* **2014,** *21* (4), 389.

(43) Kilpatrick, A. F. R.; Buffet, J.-C.; Nørby, P.; Rees, N. H.; Funnell, N. P.; Sripothongnak, S.; O'Hare, D., Synthesis and Characterization of Solid Polymethylaluminoxane: A Bifunctional Activator and Support for Slurry-Phase Ethylene Polymerization. *Chem. Mater.* **2016,** *28* (20), 7444–7450.

(44) Tsai, C.-Y.; Du, H.-C.; Chang, J.-C.; Huang, B.-H.; Ko, B.-T.; Lin, C.-C., Ring-opening polymerization of cyclic esters initiated by zirconium, titanium and yttrium complexes. *RSC Adv.* **2014,** *4* (28), 14527–14537.

# *Chapter 5*

## *An Industrially Relevant Sn(II) Catalyst for the Production of High Performance Polyester-co-Ether*

*Your value doesn't decrease based on someone's inability to see your worth...*

*~ Unknown ~*

## Overview

‘Switch’ catalysis is a useful tool for producing a wide variety of new materials from monomer mixtures and is typically applied using epoxides, anhydrides and lactones. Previous studies do not always apply the most industrially relevant monomers, which include propylene oxide, maleic anhydride and lactide. This chapter presents the use of an industrially relevant Sn(II) catalyst and its application in ‘Switch’ catalysis using those commercially significant monomers. It succeeds in making a new type of polyester-*co*-ether *via* an efficient one-pot polymerisation. Depending on the monomer selection, structures span block-, tapered-, and gradient-copolymers. *In situ* NMR spectroscopy, polymer molar mass determination, and thermal analysis measurements confirm the different structures. The isolated tapered polyester-*co*-ether copolymer was used as an additive to improve the mechanical properties of polylactide films. The influence of the additive loading as well as its chemical structure, either cross-linked or not, on the properties of the resulting PLLA plastic are discussed – with the correct conditions allowing significant improvements to elongation at break, tensile toughness without compromise over the ultimate tensile strength. Further using these copolymers allows for good plastic performances at very low additive loadings – a benefit for future applications which require bio-based/degradable additives and property enhancement of PLLA.

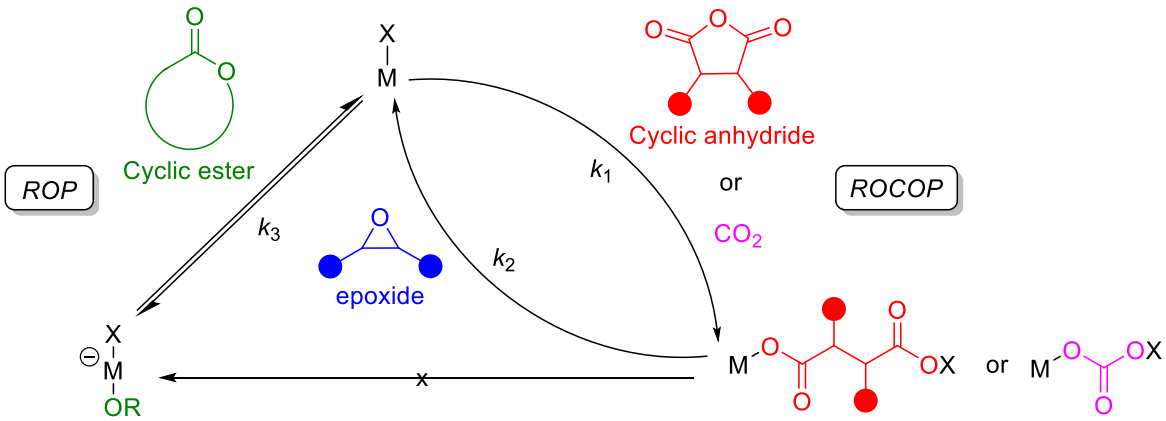
## 5.1. Introduction

Lactone/Carbonate ring-opening polymerisation (ROP) has been extensively studied in the past few decades because it allows for the controlled synthesis of a range of aliphatic polyesters and polycarbonates. Under the right conditions, ROP can be used to deliver polymers showing high molar masses and controllable molar mass distributions.[1-3] One limitation has been to expand the properties for these polymers because there is still a very limited range of commercially relevant (*i.e.* produced at scale and cost) monomers. Another

challenges has been to access aromatic polyesters as routes to aromatic lactones/cyclic carbonates tend to apply rather specialised monomer syntheses which are not yet scaled.[4] Ring-opening copolymerisation (ROCOP) of epoxides and anhydrides is an alternative polymerisation method which allows the production of a broad range of new polyesters.[5, 6] It is of interest since there are a wide variety of commercially available epoxides and cyclic anhydrides (CAs) and many of these are used already at scale in the polymer industry (*i.e.* users are familiar with these monomers and plant is equipped to use them). Further, the copolymerisation can easily deliver semi-aromatic (*e.g.* from phthalic anhydride) or rigid polyester backbones (*e.g.* from cyclohexene oxide) – both are hard to access by lactone ROP.[5, 6] Finally, epoxide/anhydride ROCOP allows the use of functionalised monomers, notably vinyl-propene oxide and maleic anhydride, without any compromise in the polymerisation thermodynamics. Installing regular alkene functional groups along the polymer backbone provides a site for efficient post-functionalisation reactions, like the thiol-ene process, which can change the properties of the polyesters – *e.g.* providing hydrophilicity or providing networked resins or providing binding sites for particular substrates.[7-9]

Another important strategy to fine tune material properties is to exploit copolymerisation and terpolymerisations.[10] 'Switch' catalysis, a useful polymerisation strategy, allows preparation of various multi-block polymers and has been applied to lactone ROP and epoxide/anhydride ROCOP.[11] By using the one-pot switch catalysis, it has been possible to access new triblock and more complex, *e.g.* 27-block, polyesters either as low molar mass polyols (hydroxyl end-capped) or as high molar mass plastics.[12] Our group, and others, have previously reported this strategy to make block polymers including polyester-*b*-polyester, polyether-*b*-polyester, and polycarbonate-*b*-polyester.[7, 12-15] In 2018, the group reported a combination of four monomers to make pentablock copolymers with a predictable and

ordered sequence.[7] Scheme 5.1 shows the generally proposed switch catalysis mechanism. Generally, epoxide/anhydride or $CO_2$ ROCOP occurs first due to the fast insertion of CA or $CO_2$ molecules into the key catalytic intermediate (the metal-alkoxide species). This rapid reaction of these monomers is evidenced by the zero order kinetics with respect to CA or $CO_2$. After CA or $CO_2$ is fully consumed, lactone ROP can occur to form block polymers.[11]

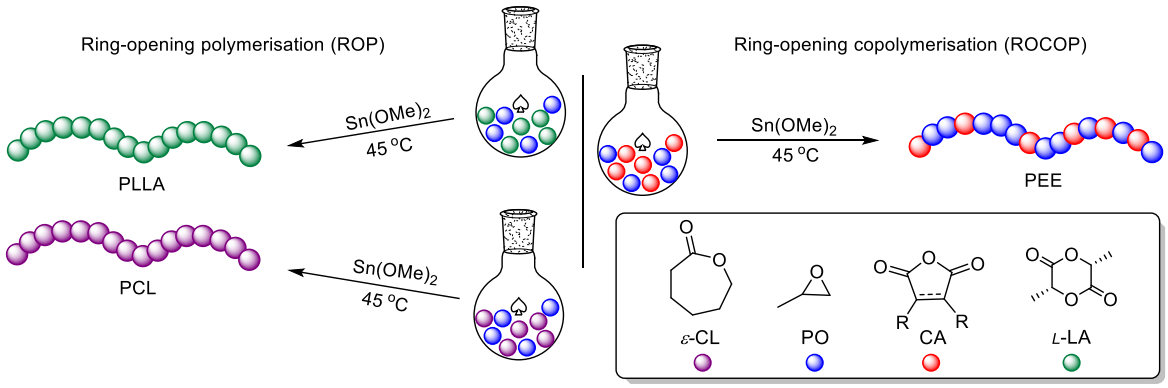



**Scheme 5.1.** Generally proposed switch catalysis mechanism.

Most of the reported catalysts for switch catalysis require complex synthesis and only a few of them are commercially available.[13, 15] On the other hand, in the field of lactone ROP the classical Sn(II)$(OR)_2$ catalysts have been extensively studied and already are used industrially for PLA production.[16] So far, there have been no investigations of how these simple and commercially relevant Sn(II) catalysts might perform in epoxide/anhydride ROCOP. It is clear that the tin catalysts can form the reactive alkoxide intermediates necessary for switch catalysis, indeed this is a pre-requisite for their outstanding performances in lactide production.[17-19] It is also therefore important to establish whether such tin-alkoxide intermediates are reactive towards cyclic anhydride monomers. Assuming this insertion succeeds, it is also not clear whether such a tin carboxylate would react with an epoxide to re-generate the alkoxide intermediate necessary for alternating copolymerisation.[20] The main objectives of this chapter are: a) To investigate the

performance of $Sn(OMe)_2$, an industrially relevant catalyst, in the epoxide/anhydride ROCOP and in 'Switch' catalysis for the production of polyesters and their copolymers, b) To assess the composition, thermal properties, and mechanical properties of the target polyesters and their copolymers, and c) To evaluate the use of the synthesised copolymers as toughening additives for PLLA.

## 5.2. PO/CAs ROCOP and lactone ROP




**Scheme 5.2.** Schematic diagram showing the ROP of lactones (LHS) and the ROCOP of propylene oxide and cyclic anhydride (RHS).

### 5.2.1. ROCOP of PO and CAs

**Table 5.1.** Polymerisation results from CAs/PO ROCOP. [a]

| CA | Time (h) | TOF ($h^{-1}$) [b] | Ether linkages (%) | $M_{n,SEC}$ (g $mol^{-1}$) [c] | $M_{n,\ calc.}$ (g $mol^{-1}$) [d] | $Đ$ [c] | $T_g$ (°C) [e] |
|---|---|---|---|---|---|---|---|
| MA | 5 | 19 | 67 | 5 600 | 5 100 | 1.25 | –19 |
| SA | 74 | 1.25 | 69 | 4 600 | 5 000 | 1.28 | –33 |
| PA | 14 | 7 | 70 | 7 100 | 6 500 | 1.16 | –1 |

[a] Conditions: polymerisations were conducted at 45 °C in neat PO and [Sn]:[BnOH]:[CA]:[PO] = 1:2:100:1000 where [CA] = 1.43 M, [Sn] = 14.3 mM. [b] TOF = (number of moles of anhydride consumed per mole of catalyst)/time (h). [c] Determined by SEC analysis against narrow MW polystyrene standards in $CHCl_3$. [d] Calculated from [((2×58.08) + CA MW) × TOF × Time)]/4 [e] Determined by DSC using heating rate of 10 °C $min^{-1}$ and $T_g$ reported from the second heating cycle.

As a starting point, PO/CA ROCOP (Table 5.1) and lactone ROP (Table 5.2) were separately investigated using $Sn(OMe)_2$ as a catalyst (Scheme 5.2). The particular polymerisation conditions used for ROCOP were $[Sn(OMe)_2]$:[BnOH]:[CA]:[PO] = 1:2:100:1000 and

[$Sn(OMe)_2$] = 14.3 mM. In the case of PO/MA ROCOP, it was observed that $Sn(OMe)_2$ was able to copolymerise PO with MA and produced the polyester-*ran*-ether ($PEE_{MA}$) with ≈ 67 % ether linkages. TOF was used to identify the activity of the tin catalyst and in the case of PO/MA ROCOP, a moderate TOF of 19 $h^{-1}$ was obtained. For PO/SA ROCOP, $PEE_{SA}$ with a similar percentage of ether linkages (≈ 69 %) was produced. In contrast, a much lower TOF of 1.25 $h^{-1}$ was observed. This might be due to the lower ring strain in SA compared to MA, which possesses an olefin functional group inside the ring. In addition, the bicyclic anhydride PA was studied. $PEE_{PA}$ with comparable level of ether linkages (≈ 70 %) was obtained with a TOF of 7 $h^{-1}$, lower than that seen with MA. The isolated PEEs were then characterised by NMR spectroscopy (Figures A3.1–A3.12) and polymer molar mass was analysed by SEC. All PEEs showed predictable molar masses and narrow dispersities ($Đ \leq$ 1.28), suggesting a well-controlled polymerisation. For $PEE_{MA}$, the methylene proton resonances in the $^1H$ NMR spectrum suggests a random regioselectivity of PO insertion with the ratio of head to head (HH): head to tail (HT): tail to tail (TT) of 1:2:1 (Figure A3.1). Similar regioselectivities of the PO units in $PEE_{SA}$ and $PEE_{PA}$ were observed from $^{13}C\{^1H\}$ NMR spectra (Figures A3.6 and A3.10).

In the comparison to catalyst **4.1** presented in chapter 4, polyester with a relatively higher percentage of ether linkages was produced by $Sn(OMe)_2$ (poly(propylene phthalate) with > 99 % ester linkage was produced by **4.1**). This suggests that the ancillary ligands used to form the complex play a role. Both ligand steric and electronic effects are expected to increase the propagation of alternating linkages and decrease ether linkage formation (*i.e.* electron donation decreases metal centre Lewis acidity and hence disfavours epoxide ROP – *i.e.* ether linkage formation).

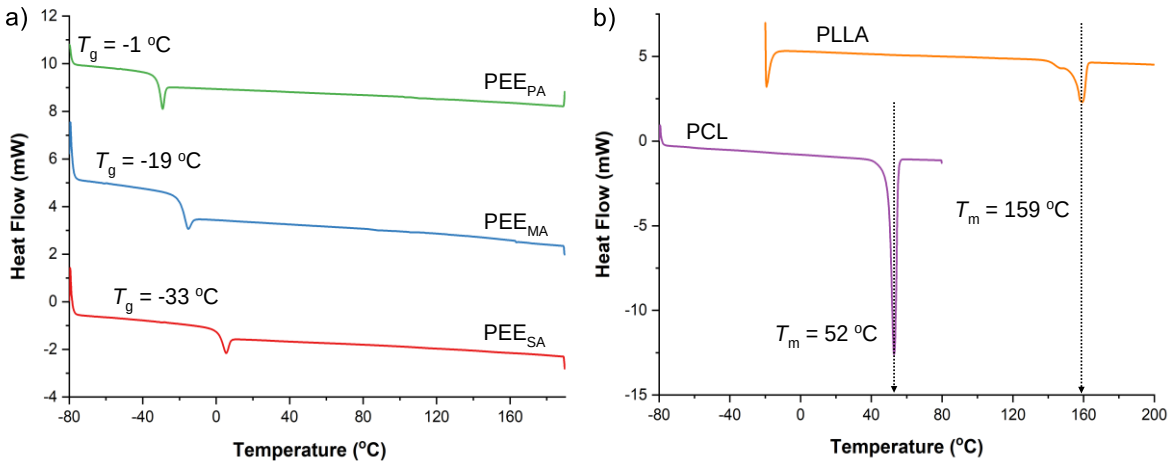



**Figure 5.1.** DSC thermograms for a) PEE$_{MA}$, PEE$_{SA}$, and PEE$_{PA}$ and b) PCL and PLLA.

The thermal properties of all purified PEEs were then characterised. Materials with tunable $T_g$ can be obtained which depends strongly on the CA incorporated in the polymer backbone. In the case of PEE$_{MA}$, DSC analysis suggested a $T_g$ of –19 °C, whilst a lower $T_g$ value was obtained for PEE$_{SA}$ ($T_g$ = –33 °C). This is due to a more flexible polymer backbone for PEE$_{SA}$. In the case of PEE$_{PA}$, which consists of highly rigid aromatic substituents on the polymer backbone, a $T_g$ of –1 °C was seen, higher than both PEE$_{MA}$ and PEE$_{SA}$ (Figure 5.1a). It is worth noting that all materials showed a $T_g$ lower than room temperature due to the presence of soft ether linkages and this would be beneficial of their use as elastomers.[21] The thermal decomposition of all polymers was identified using TGA (Figure A3.38). The decomposition temperatures at 5 % weight loss ($T_{d5}$) of PEE$_{MA}$, PEE$_{SA}$ and PEE$_{PA}$ were measured as 298 °C, 329 °C, and 307 °C respectively.

### 5.2.2. ROP of Lactones

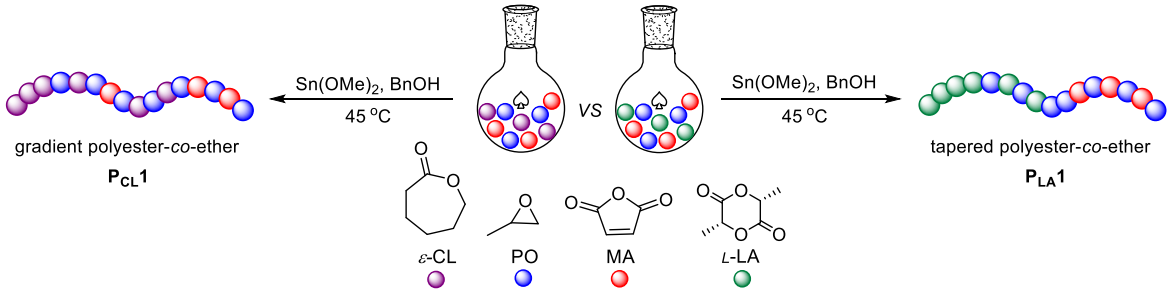
**Table 5.2.** Polymerisation data from ROP of lactones. [a]

| Lactone | Time (h) | TOF ($h^{-1}$) [b] | $M_{n,SEC}$ (g $mol^{-1}$) [c] | $M_{n,calc.}$ (g $mol^{-1}$) [d] | $Đ$ [c] | $T_m$ (°C) [e] |
|---|---|---|---|---|---|---|
| *L*-LA | 3 | 31 | 4 100 | 3 400 | 1.36 | 159 |
| ε-CL | 3 | 24 | 2 900 | 2 050 | 1.33 | 52 |

[a] Conditions: polymerisations were conducted at 45 °C in neat PO and [Sn]:[BnOH]:[lactone]:[PO] = 1:2:100:1000 where [*L*-LA] = 1.43 M, [*ε*-CL] = 1.23. [b] TOF = (number of moles of lactone consumed per mole of catalyst)/time (h). [c] Determined by SEC analysis against polystyrene standards in $CHCl_3$ and correction factors of 0.58 and 0.56 were used to correct the molar mass of PLLA and PCL, respectively.[22] [d] Calculated from (Lactone MW × TOF × Time)/4 [e] Determined by DSC using heating rate of 10 °C $min^{-1}$ and $T_m$ reported from the second heating cycle.

The same polymerisation conditions for PO/CA ROCOP were used. As expected, in the presence of BnOH, $Sn(OMe)_2$ produced PLLA with a predictable molar mass and narrow polydispersity index ($Đ \leq 1.25$). A similar result was observed for *ε*-CL ROP. The TOF of *L*-LA ROP is slightly higher than that of *ε*-CL and both are almost twice as fast as the PO/MA ROCOP (TOF = 31 $h^{-1}$ for *L*-LA and TOF = 24 $h^{-1}$ for *ε*-CL). It should be noted that, the formation of polyether during lactone ROP was not observed as evidenced by a lack of a polypropylene oxide (PPO) signal in $^1$H NMR spectra (Figures A3.13 and A3.14). We reasoned that this is due to fast insertion of lactone monomer into the Sn-alkoxide bond. DSC analysis suggested that both PLLA and PCL are semi-crystalline materials and possess $T_m$ values of 159 °C and 52 °C, respectively (Figure 5.1, right). TGA studied showed $T_{d5}$ for PLLA and PCL of 226 °C and 219 °C, respectively (Figures A3.39a and A3.40a).

## 5.3. One-pot polymerisation for block-, tapered-, and gradient-copolymer formation




**Scheme 5.3.** One-pot polymerisation of PO, MA, and *L*-LA (RHS) or ε-CL (LHS) pathways.

**Table 5.3.** One-pot polymerisation data. [a]

| Lactone | t (h) | % Conv. (MA)[b] | % Conv. (lactone)[c] | $M_{n,SEC}$ (g mol$^{-1}$)[d] | $M_{n,calc.}$ (g mol$^{-1}$)[e] | $Đ$[d] | $T_g$ (°C)[f] | $T_m$ (°C)[f] |
|---|---|---|---|---|---|---|---|---|
| *L*-LA | 105 | > 99 | 93 | 12 000 | 8 700 | 1.25 | –6 | - |
| ε-CL | 48 | > 99 | 90 | 3 200 | 7 900 | 1.44 | –37 | 38 |

[a] Conditions: polymerisations were conducted at 45 °C in neat PO and [Sn(OMe)$_2$]:[BnOH]:[MA]:[lactone]:[PO] = 1:2:100:100:1000. [b] calculated by integration of the methine proton of the $^1$H NMR spectrum (MA, δ 7.57-7.48 ppm; polymer, δ 6.88-6.63 ppm). [c] Determined by the integration of the methyl or methylene proton of the $^1$H NMR spectrum of lactone against mesitylene internal standard (*L*-LA, δ 2.16-2.05 ppm; ε-CL, δ 3.16-3.06 ppm; mesitylene, δ 2.79-2.70 ppm). [d] Determined by SEC analysis against polystyrene standards in THF. [d] Calculated from [((2×58.08)+98.08)×(% conv. of MA))+((144.14 (*L*-LA) or 114.14 (ε-CL)×(% conv. of lactone))]/4. [f] Determined by DSC using heating rate of 10 °C min$^{-1}$ and $T_g$ and $T_m$ reported from second heating cycle.

### 5.3.1. PO/MA/*L*-LA one-pot polymerisation

Given the promising results for both PO/CA ROCOP and lactone ROP, we reasoned that combining all monomers in one pot might allow for the formation of copolymers from the monomer mixture. We first examined the one-pot polymerisation of PO, MA and *L*-LA (Scheme 5.3 and Table 5.3). The same polymerisation conditions as those used in the homopolymerisations were used ([Sn(OMe)$_2$]:[BnOH]:[MA]:[*L*-LA]:[PO] = 1:2:100:100:1000 and [Sn(OMe)$_2$] = 14.3 mM).

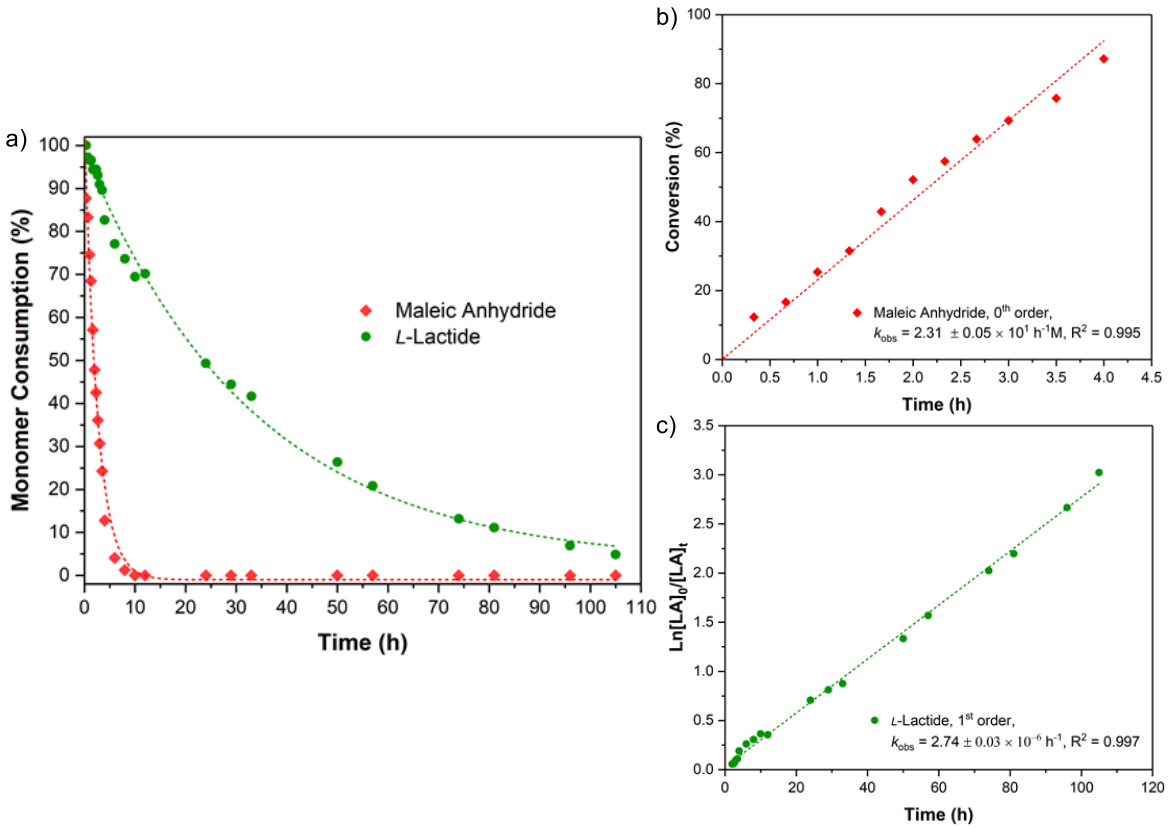



**Figure 5.2.** $^{1}$H NMR analysis of the one-pot polymerisation of PO, MA, and *L*-LA.

$Sn(OMe)_2$ was able to copolymerise three monomers, PO, MA, and *L*-LA by switching between the two different polymerisation mechanisms, ROCOP and ROP, and produce **P$_{LA}$1** copolymer. Several analytical techniques were utilised in accordance with previous studies of switch catalysis.[12-15] The polymerisation was first monitored by $^{1}$H NMR spectroscopy (Figure 5.2a). $^{1}$H NMR spectroscopic analysis suggested the PO/MA ROCOP was zero order dependent on the MA concentration and a $k_{obs}$ of 2.16 ± 0.07 × $10^{1}$ $h^{-1}M$, obtained from plot gradient, was observed (Figure 5.2b). In contrast, a first order in *L*-LA concentration was seen in LA ROP and a $k_{obs}$ of 2.65 ± 0.04 × $10^{-6}$ $h^{-1}$ was determined from the gradient (Figure 5.2c). Individual aliquots withdrawn from the reaction mixture were analysed by SEC. It was seen that polymer molar mass increases continuously with percent conversion whilst the molar mass distribution remains narrow over the course of polymerisation ($Đ \leq 1.37$) (Figures 5.3a and b), suggesting the formation of copolymer

rather than mixture of homopolymers. The isolated polymer showed a moderate $M_n$ of 12,000 g mol$^{-1}$ (uncorrected from SEC) which is in a reasonable agreement with a theoretical value, suggesting a well-controlled polymerisation. Additionally, the isolated polymer was studied by $^1$H DOSY NMR analysis. A single diffusion coefficient was observed in the case of **PLA1** unlike the blend of the respective homopolymers where two distinct diffusion coefficients were observed (Figures 5.3c and d). This again confirmed copolymer production.

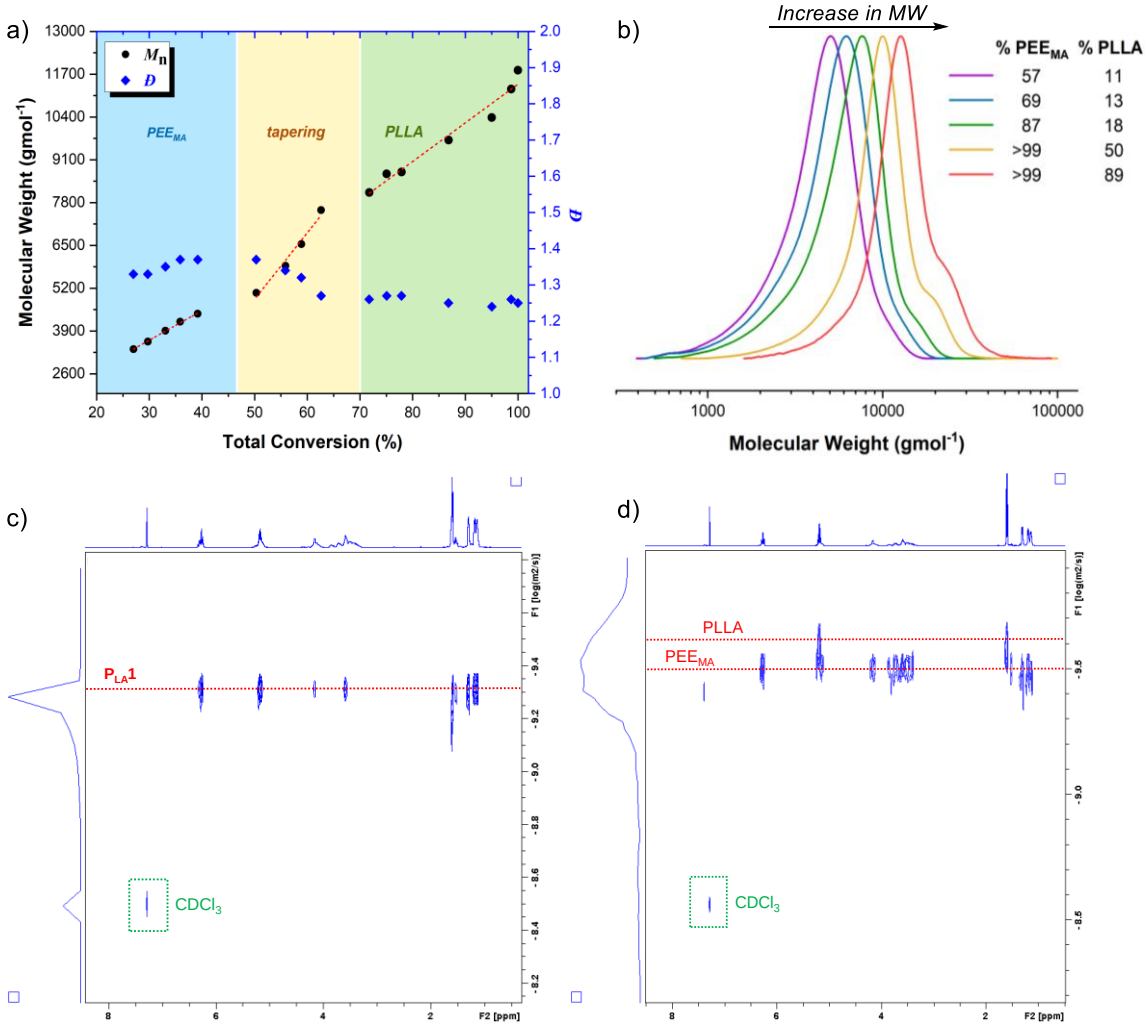



**Figure 5.3.** a) Plot of $M_n$ against percent conversion, b) SEC traces of selected aliquots from PO, MA, and *L*-LA one-pot polymerisation, $^1$H DOSY NMR spectra of c) **PLA1**, and d) $PEE_{MA}$ and PLLA blend.

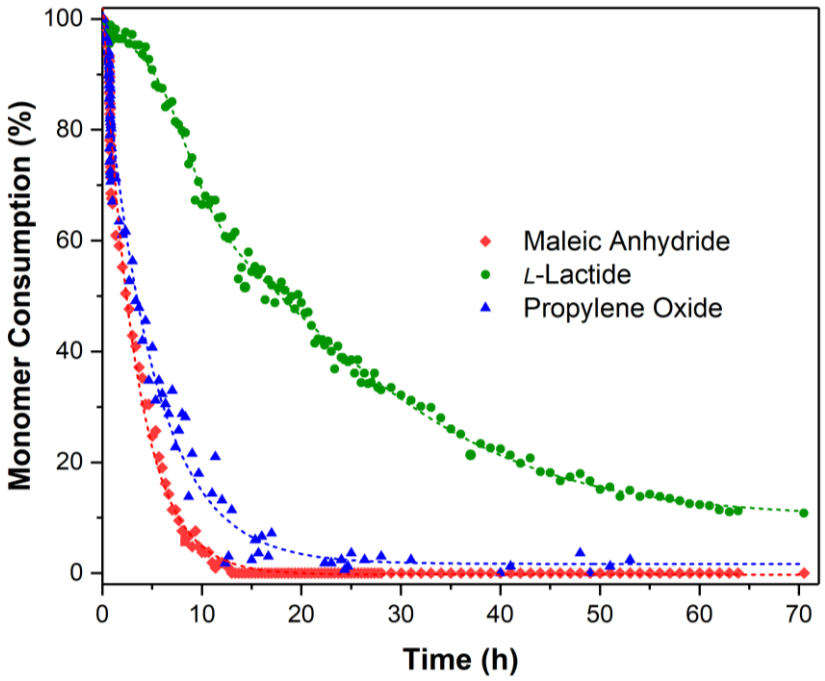
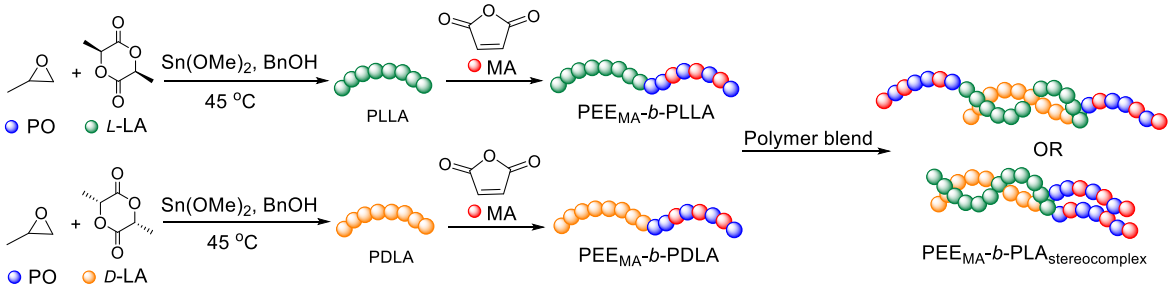



**Figure 5.4.** *In situ* $^{1}$H NMR analysis of switch catalysis from a PO, MA, and *L*-LA monomer mixture.

To gain a greater understanding of the switch mechanism in this catalyst system and to understand the polymer architectures produced, an *in situ* $^{1}$H NMR study was performed (Figure 5.4). It suggested the formation of a tapered block polymer through the initial ROCOP of PO/MA followed by the ROP of *L*-LA when around 55% of the MA was consumed. These results suggest that the insertion of MA into the Sn-alkoxide bond occurs faster than *L*-LA insertion. Such a difference in rates for anhydride *vs.* lactide insertion would be in-line with previous result using other metal-alkoxide catalyst, although in that case a much cleaner rate difference was observed as tapered copolymers are rarely produced in switchable catalysis systems.[12] Once around 55 % MA has been consumed the total concentration of MA in the polymerisation is less than that of *L*-LA. *L*-LA is then incorporated into the polymer backbone to form the tapered copolymer **P$_{LA}$1**. It is worth mentioning that after MA was consumed, the consumption of PO was completely shut down (*vide infra*) and only LA ROP occurred during the remaining reaction. It should also be noted that this observation is in contrast to other reported switch catalysts where a switch

only occurs, from ROCOP to ROP, once the CA is fully consumed.[11-15] The thermal properties of the resultant polymer were then studied. The DSC thermogram shows a single $T_g$ at –5 °C which is almost 15 °C higher than those obtained from pure $PEE_{MA}$. This suggests there is some block miscibility between the two polymers (Figure 5.11a). The TGA showed a two-step degradation profile: the onset of the first step occurring at 249 °C and the second at 326 °C. For comparison, the decomposition temperatures of the parent polymers occur at 226 °C and 291 °C for $PEE_{MA}$ and PLLA, respectively, consistent with the formation of a block (or tapered block) structure. The $T_{d5}$ of the isolated polymer is 238 °C (Figure A3.39b).




**Scheme 5.4.** Synthesis of $PEE_{MA}$-*b*-PLA block copolymers and their stereocomplex formation.

One potential way to obtain a block copolymer is by sequential addition of the monomers into the polymerisation reaction (Scheme 5.4).[23, 24] Accordingly, the ROP of *L*-LA was first carried out, with PO as a solvent. After 3 h, MA was then added to the reaction mixture and the polymerisation was carried out for another 5.5 h before reaching ~ 85% MA conversion and allowing access to the desired block polymer $PEE_{MA}$-*b*-PLLA. The entire polymerisation was monitored by $^1$H NMR spectroscopy and the polymer molar mass evolution was determined by SEC. This analysis shows a continuous increase in polymer $M_n$ with monomer percent conversion, whilst dispersities remain narrow ($Đ \leq 1.29$) throughout (Figure 5.5a). A moderate molar mass of 8,200 g mol$^{-1}$ was obtained for the isolated $PEE_{MA}$-*b*-PLLA. It should be noted that formation of $PEE_{MA}$-*b*-PLLA can also be

achieved using the inverse monomer addition order. However, in the case of polymerisations starting with the ROCOP of PO/MA, a much slower polymerisation rate was observed and when *L*-LA was added, in the second step, around 80 h of reaction time was required to complete consumption of both *L*-LA and MA.

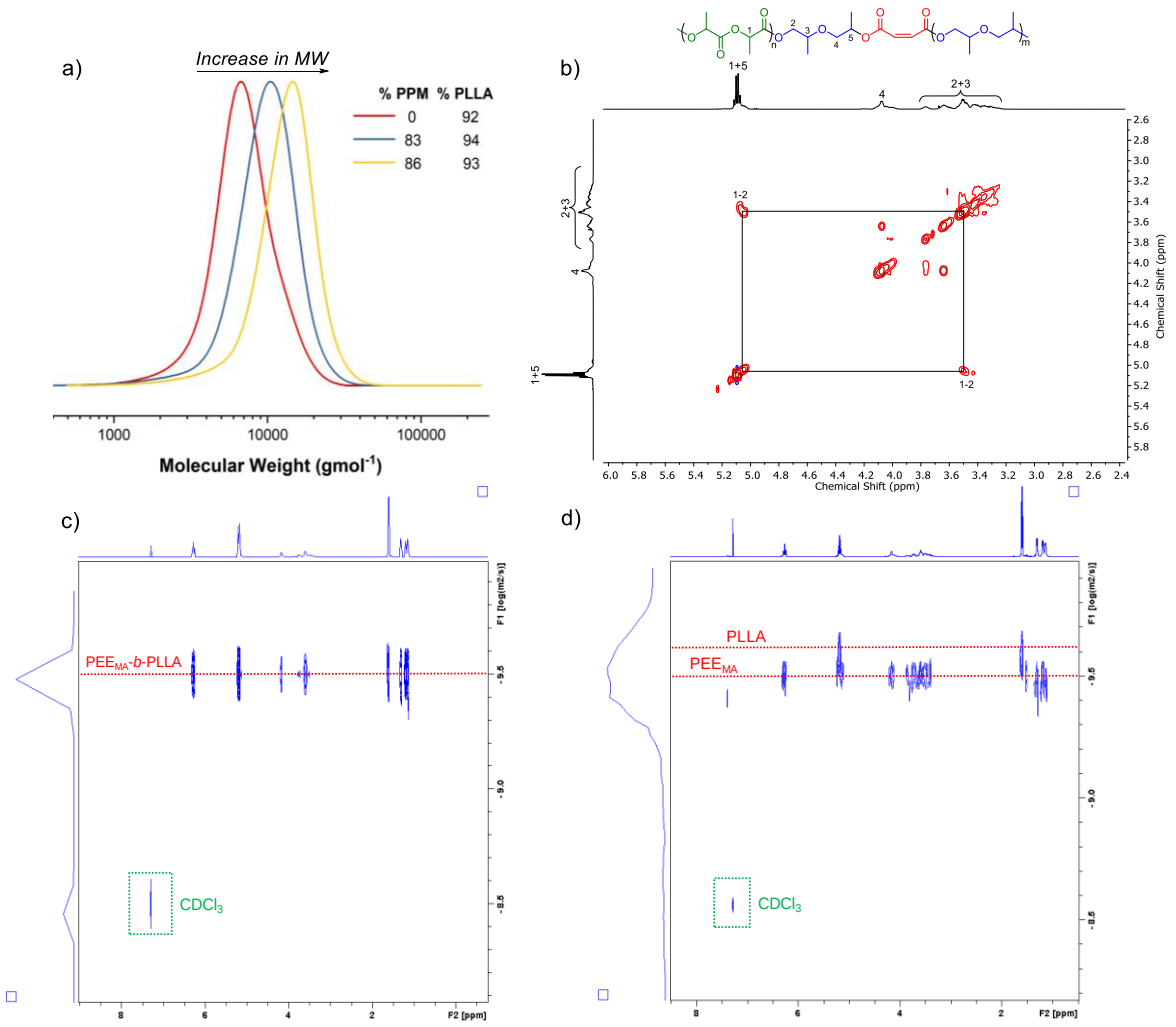



**Figure 5.5.** a) SEC traces of selected aliquots from the formation of $PEE_{MA}$-*b*-PLLA, b) $^{1}$H-$^{1}$H TOCSY NMR spectrum of isolated $PEE_{MA}$-*b*-PLLA, $^{1}$H DOSY NMR spectra of c) $PEE_{MA}$-*b*-PLLA, and d) $PEE_{MA}$ and PLLA blend.

The formation of $PEE_{MA}$-*b*-PLLA was confirmed by various NMR spectroscopic analyses (Figure 5.5). First, an interaction between the methylene protons in $PEE_{MA}$ unit and the methine protons in the PLLA block was observed in the $^{1}$H-$^{1}$H TOCSY NMR spectrum (Figure 5.5b), suggesting there is a junction between the two polymer blocks. Additionally,

a single diffusion coefficient for $PEE_{MA}$-*b*-PLLA was seen in the $^1$H DOSY NMR spectrum, unlike in the blended polymers where two different signals were observed (Figure 5.5c and d). The thermal properties of the isolated polymers were analysed by DSC and TGA. The DSC suggested the polymer adopted a microphase separated structure, since a $T_g$ was observed at similar value to the soft segment, $PEE_{MA}$ at –17 °C, and the $T_m$ of semi-crystalline PLLA at 143 °C corresponds to values for pure PLLA at equivalent molar mass (Figure 5.6a). This finding of phase separation is in contrast to the tapered block polymer **P$_{LA}$1** where only a single $T_g$ at –5 °C was observed. The TGA measurements for the block polymer sample showed two distinct decomposition steps (the onset of the first step occurring at 237 °C and the second at 322 °C), with $T_{d5}$ values of 229 °C (Figure A3.39c).

Additionally, a block polymer comprising PDLA and $PEE_{MA}$ ($PEE_{MA}$-*b*-PDLA) was formed using a similar polymerisation procedure to that for $PEE_{MA}$-*b*-PLLA (Scheme 5.4). The same level of analysis to confirm the block formation as $PEE_{MA}$-*b*-PLLA was carried out. Similar results, including a continuous increase in polymer molar mass, a single diffusion coefficient in the $^1$H DOSY NMR spectrum and the observation of clear signals corresponding to block junction units were observed, all confirming the formation of $PEE_{MA}$-*b*-PDLA (Figures A3.23–A3.26). In the past, other researchers have observed that blending equimolar quantities of PLLA and PDLA, can lead to the formation of a stereocomplex and this further improves the thermal property by raising the $T_m$.[25] To date, the highest $T_m$ of 230 °C was achieved for a high molar mass PLA stereocomplex.[26] We reasoned that the blending of the two block copolymers, $PEE_{MA}$-*b*-PLLA and $PEE_{MA}$-*b*-PDLA might allow the formation of a stereocomplex between the semi-crystalline segments of PLA (Scheme 5.4). Therefore, blending of these two block copolymers was investigated by dissolving the two block copolymers ($PEE_{MA}$-*b*-PLLA and $PEE_{MA}$-*b*-PDLA) in $CH_2Cl_2$. The reaction mixture was heated to 60 °C and allowed to stir for 3 h. The solution was then

allowed to slowly cool to ambient temperature, during which time the $CH_2Cl_2$ slowly evaporated. The resultant polymer was obtained as a white solid and stereocomplexation was confirmed by DSC measurements. The stereocomplex product showed a higher $T_m$ of 202 °C compared to the value of 143 °C for the separate enantiomers. As expected, the $T_g$ of the soft $PEE_{MA}$ segments remained similar to the constituent enantiomeric polymers, at –18 °C (Figure 5.6a). The formation of the stereocomplex also led to an increased percentage crystallinity of the PLA block, from 22 % (For $PEE_{MA}$-*b*-PLLA or $PEE_{MA}$-*b*-PDLA) to 36 % ($PEE_{MA}$-*b*-$PLA_{stereocomplex}$). TGA analysis suggested a similar $T_{d5}$ of 233 °C for the $PEE_{MA}$-*b*-$PLA_{stereocomplex}$ as for the constituent copolymers (Figure A3.39d).

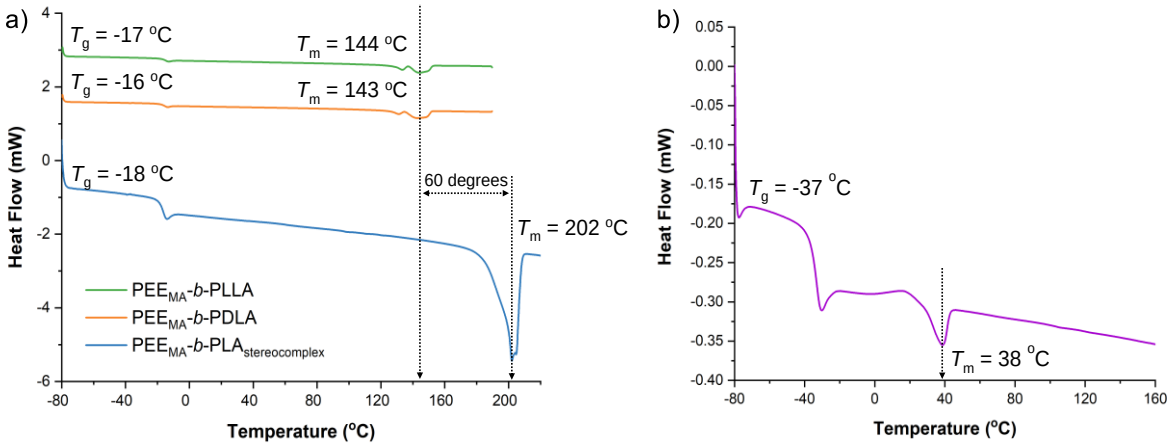



**Figure 5.6.** Stacks of DSC thermograms of a) $PEE_{MA}$-*b*-PLLA, $PEE_{MA}$-*b*-PDLA and $PEE_{MA}$-*b*-$PLA_{stereocomplex}$ and b) $PEE_{MA}$-*g*-PCL.

### 5.3.2. PO/MA/ε-CL one-pot polymerisation

The one-pot polymerisation of PO, MA, and ε-CL was also studied. Similar polymerisation conditions as used for the one-pot polymerisation of PO, MA, and *L*-LA were used ($[Sn(OMe)_2]$:[BnOH]:[MA]:[ε-CL]:[PO] = 1:2:100:100:1000 and $[Sn(OMe)_2]$ = 12.3 mM). The polymerisations were monitored using $^1$H NMR spectroscopy and individual polymer conversions were calculated against mesitylene as an internal standard (Figure 5.7).

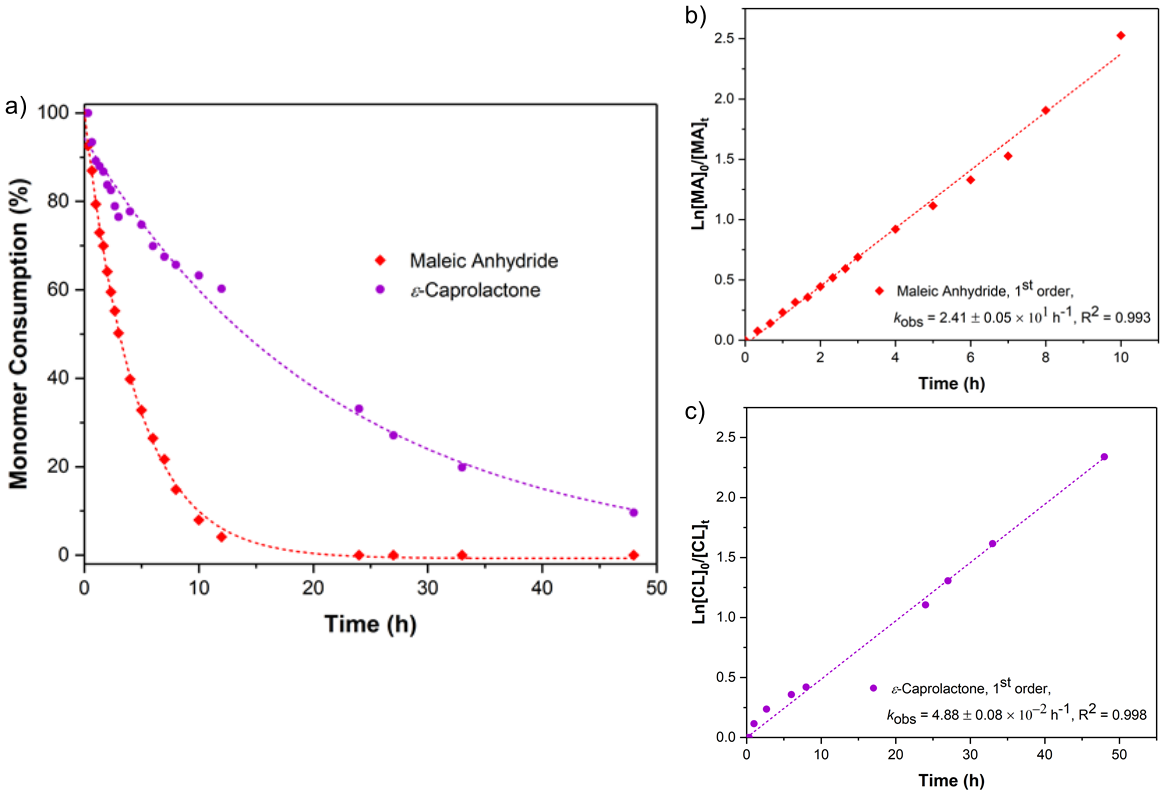



**Figure 5.7.** $^{1}$H NMR analysis of PO, MA, and ε-CL one-pot polymerisation.

Surprisingly, the $^{1}$H NMR spectroscopic analysis suggested the formation of a gradient copolymer between $PEE_{MA}$ and PCL (**$P_{CL}$1**), in contrast to the tapered copolymer formed with LA. In the case of the polymerisation using PO/MA/CL, the formation of PCL started during the PO/MA ROCOP. However, the polymerisation rate using ε-CL is slower than that for PO/MA, as evidenced by the smaller $k_{obs}$. Kinetic studies revealed a first order dependence on each of the concentrations of MA and ε-CL monomers with $k_{obs}$ values of $4.88 \pm 0.08 \times 10^{-2}$ $h^{-1}$ (ε-CL) and $2.41 \pm 0.05 \times 10^{1}$ $h^{-1}$ (MA), respectively (Figure 5.7b and c). As expected, a polymerisation rate almost 500 times faster was observed for MA than ε-CL. It should be noted that the polymerisation order in MA concentration is different to the PO, MA, and *L*-LA one-pot polymerisation where the reaction was zero order in MA concentration. This change in monomer order allows more obviously for the formation of a gradient copolymer, as the insertion of the two monomers are competitive.

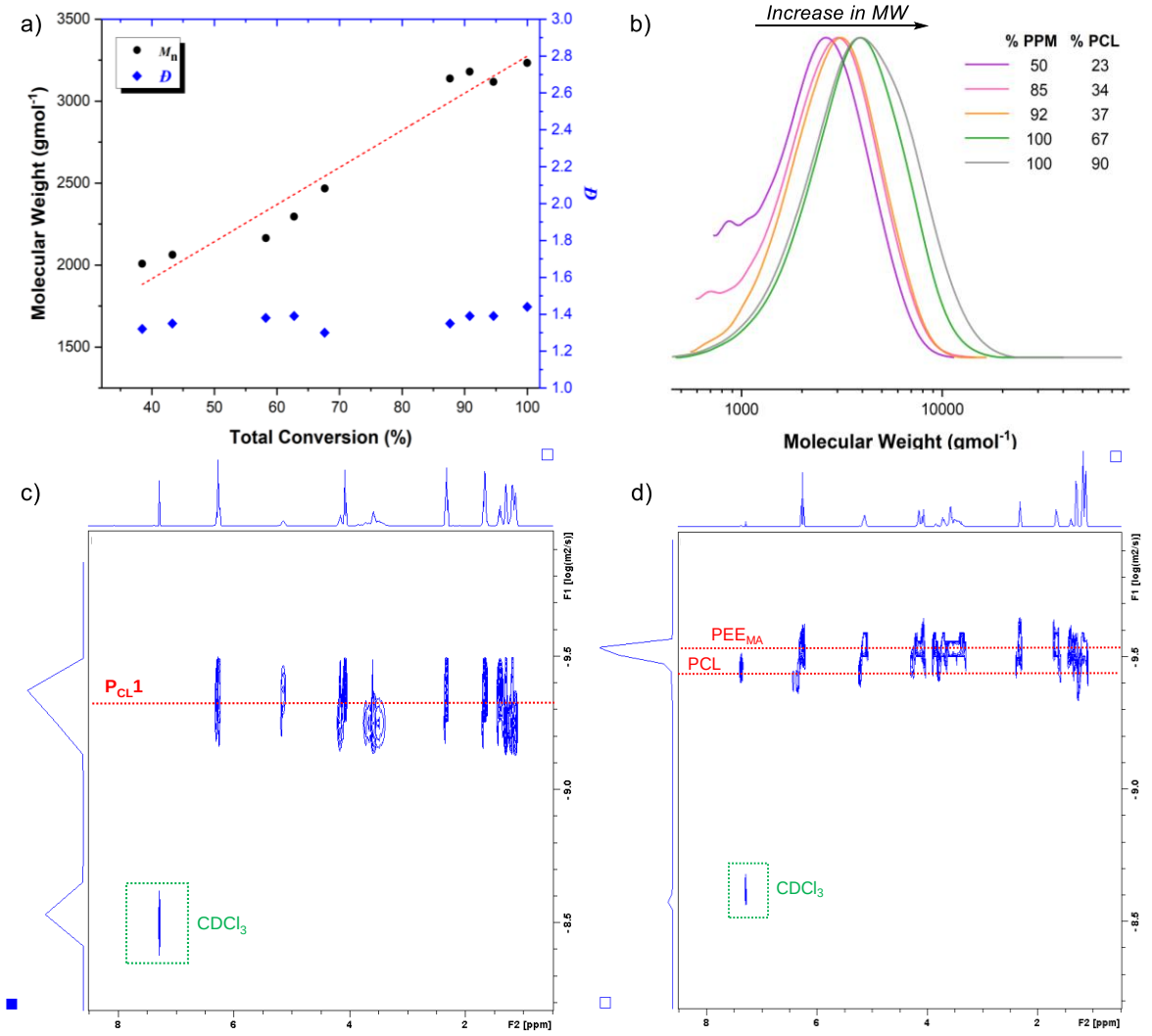



**Figure 5.8.** a) Plot of $M_n$ against percent conversion, b) SEC traces of selected aliquots from the PO, MA, and $\varepsilon$-CL one-pot polymerisation, $^1$H DOSY NMR spectra of c) **P$_{CL}$1**, and d) the PEE$_{MA}$ and PCL blend.

Polymer molar masses were identified using SEC (Figures 5.8a and b) and the isolated **P$_{CL}$1** showed a low $M_n$ of 3,200 g mol$^{-1}$. In addition, the polymer molar mass increased linearly with percent conversion, while $Đ$ remained consistently narrow, suggesting the formation of copolymer (Figure 5.8a and b). A single diffusion coefficient for the **P$_{CL}$1** was observed in the $^1$H DOSY NMR spectrum, unlike in the PEE$_{MA}$ and PCL blend where two different diffusion coefficients were obtained (Figure 5.8c and d), again confirming copolymer formation. The thermal properties of the isolated **P$_{CL}$1** were analysed by DSC and TGA measurements. DSC analysis suggested a $T_g$ of –37 °C and $T_m$ of 38 °C, suggesting some

microphase separation of the two polymers (Figure 5.6b). It is worth mentioning that both the $T_g$ and $T_m$ values observed for **$P_{CL}$1** are different to the constituent polymers ($T_g$ for $PEE_{MA}$ = –19 °C and $T_m$ for PCL = 52 °C) which may either be a symptom of the low molar masses and/or due to partial miscibility of the blocks. A single decomposition was observed, with $T_{d5}$ of 239 °C (Figure A3.40b).

## 5.4. Application of $P_{LA}$1 in toughening PLLA

### 5.4.1. Effect of additive amount

PLA is an important biodegradable thermoplastic which is utilised in many applications.[27-29] One drawback is its low toughness which has limited uses, including in screws and plates for fracture fixation, automotive plastics and durable goods, as well as in some rigid plastics applications.[25, 30] Strategies to toughen PLA have included the copolymerisation of PLA with other polymers and/or blending with plasticisers.[30] In terms of plasticisers the following factors are important to consider: I) The plasticiser should be softer than PLA (have a lower $T_g$) and II) It should be partially miscible with PLA.[30] Since the DSC analysis revealed a low $T_g$ for **$P_{LA}$1**, it could act as such a compatible soft material and because of the presence of the PLLA segment in **$P_{LA}$1**, the tapered copolymer should be partially miscible with PLLA. Therefore, we envisioned that **$P_{LA}$1** could be used to toughen PLLA.

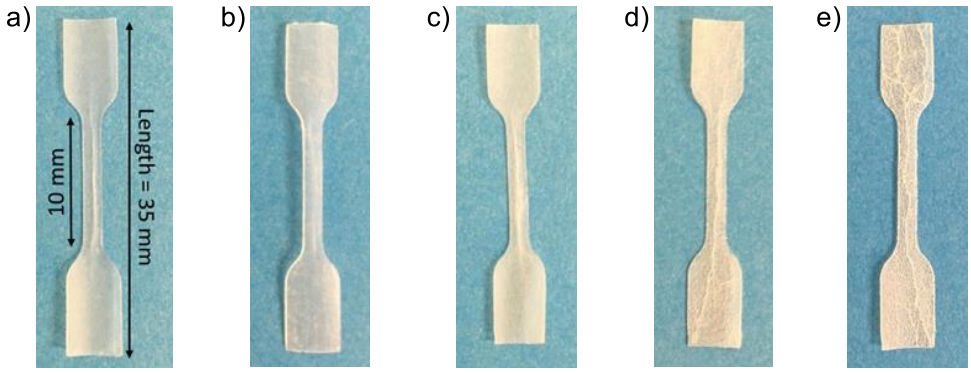



**Figure 5.9.** Dumbbell shaped PLLA samples containing different wt. % of **$P_{LA}$1**: a) 0 wt. % b) 2 wt. %, c) 5 wt. %, d) 10 wt. %, and e) 20 wt. %.

**Table 5.4.** Tensile testing data for PLLA specimens containing different amounts of **$P_{LA}$1**.

| Additive (weight %) | Young's Modulus (MPa) | Tensile Strength (MPa) | Elongation at Break (%) | Tensile Toughness (MJ $m^{-3}$) [a] |
|---|---|---|---|---|
| 0 wt. % | 1612.8 ± 26.3 | 53.1 ± 3.04 | 6.6 ± 1.15 | 2.1 ± 0.49 |
| 2 wt.% | 1610.4 ± 20.1 | 45.0 ± 1.53 | 14.7 ± 0.55 | 6.4 ± 0.44 |
| 5 wt.% | 1506.9 ± 32.2 | 44.2 ± 1.51 | 13.3 ± 0.61 | 5.6 ± 0.35 |
| 10 wt.% | 1054.2 ± 14.2 | 34.4 ± 0.99 | 6.5 ± 0.23 | 1.6 ± 0.12 |
| 20 wt.% | 1117.6 ± 15.0 | 23.8 ± 0.52 | 2.94 ± 0.12 | 0.39 ± 0.03 |

[a] calculated form the peak area under the plot between stress (y axis) and strain (x axis).

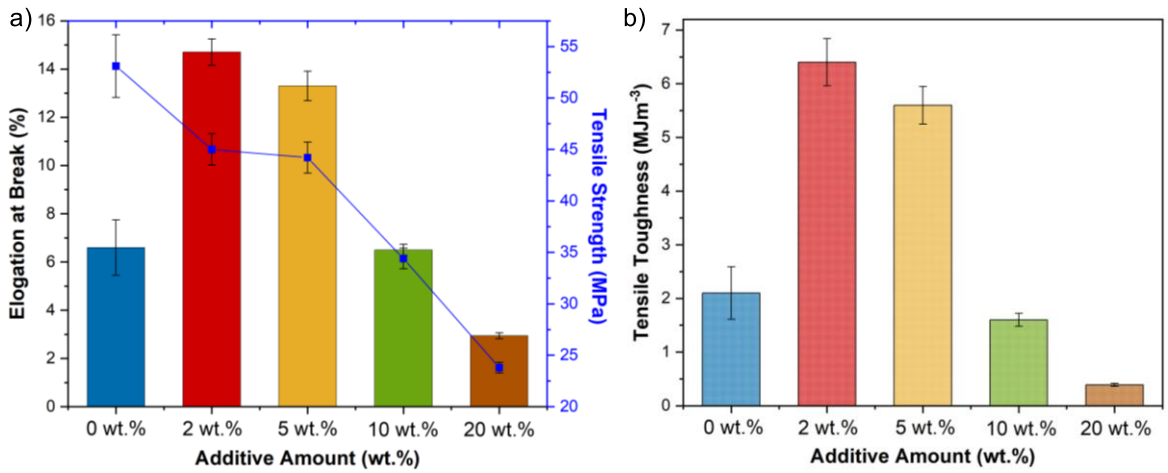



**Figure 5.10.** Mechanical properties of PLLA–**$P_{LA}$1** (0–20 wt. %) blends: a) elongation at break and tensile strength and b) tensile toughness.

The effect of blending different amounts of **$P_{LA}$1** with PLLA ($M_{n,SEC}$ (corrected with a correction factor of 0.58)[22] = 54,600 g $mol^{-1}$, $Đ$ = 1.73) was studied over the range 2–20 wt. % (Table 5.4 and Figure 5.10). Polymer films were prepared *via* solvent casting from $CHCl_3$. To ensure that individual polymer films were dry, the material was analysed by both $^1$H NMR spectroscopy (using DCM-$d_2$ as an NMR solvent) (Figures A3.31–A3.35) and TGA (Figure A3.41). It is worth noting that all polymer films were obtained as colourless materials and form transparent films, clearly important for any application. Dried polymer films were cut into dumbbell shaped specimens with a specific length of 35 mm, gauge length of 10 mm, and width of 2 mm (Figure 5.9). Tensile measurements of each specimen was conducted to measure mechanical properties including the Young's modulus (MPa),

tensile strength (MPa), and elongation at break (%) (Figures A3.42–A3.44). Tensile toughness (MJ $m^{-3}$) was calculated based on the area under the stress-strain plots (Table 5.4). Compared to neat PLLA material, an increase in percent elongation at break was observed when 2 and 5 wt. % of **$P_{LA}$1** was introduced and this results in an improvement to the tensile toughness of the PLLA films (Figure 5.10). For the PLLA specimen containing 2 wt. % of **$P_{LA}$1**, about 2 times increased elongation at break and therefore 3 times higher tensile toughness was observed compared to neat PLLA. Importantly, a similar Young's modulus to the neat PLLA specimen was observed at this loading – *i.e.* there was no compromise in mechanical strength. A similar result was seen for the 5 wt. % of **$P_{LA}$1** blend (tensile toughness = 5.6 ± 0.35 MJ $m^{-3}$). In this case, a slightly lower Young's modulus compared to the neat PLLA specimen was obtained and only a slightly lower tensile strength compared with neat PLLA specimen. In contrast, a dramatic decrease in tensile strength, Young's modulus, and elongation at break was seen when higher **$P_{LA}$1** (10 wt. % and 20 wt. %) loadings were used. Interestingly, the sample containing as little as 2 wt. % showed the highest toughness which is in contrast to other reported plasticisers where 10–30 wt. % is generally required to toughen the materials. For example, Sinclair reported the use of LA monomer and found that by adding 17.3 % LA, an increase in the strain at break around 50 times can be obtained, which can be increased further with further LA addition. However, a drastic decrease in tensile strength (*i.e.* 300 – 400 % reduction) was observed in all cases.[31] McCarthy and co-workers showed that the elongation at break of PLA can be improved by the addition of various citrate esters. The highest elongation at break value was 610 %, which is significantly higher than neat PLA (elongation at break = 75 %), achieved at 30 wt. % triethyl citrate. However, a seven-fold reduction of tensile strength compared to neat PLA film was seen which is a major down-side and essentially renders the improvement in elongation at break rather useless (Tensile strength of 7.2 *vs.* 51.7 MPa).[32] Averous and co-

workers demonstrated that polyethylene glycol (PEG) and oligomeric lactic acid (OLA) can be utilised as plasticisers for PLA. The addition of 20 wt. % of either PEG or OLA into PLA films resulted in an improvement of elongation at break to 160 % and 200 %, respectively (elongation at break of neat PLA = 9 %). However, a considerable reduction of tensile strength to 31 MPa (for PEG plasticiser) and 22 MPa (for OLA plasticiser) was observed.[33]

### 5.4.2. Exploring the chemistry of the additive – Cross-linking through alkene groups

Due to the presence of olefin functional groups in the polymer backbone of **P$_{LA}$1**, cross-linking reactions were explored as a strategy to further improve toughening in PLA blends. The thiol-ene reaction was explored using 2,2´-azobis(2-methylpropionitrole) (AIBN) as an initiator and conducting reactions under high temperature conditions, following a literature procedure.[34] Trimethylolpropane tris(3-mercaptopropionate) was used as the thiol, as it has been previously reported to allow for a high degree of cross-linking.[8] The molar ratio of SH to olefin functional groups was varied from [C=C]:[SH] = 1:1, 1:3 and 1:6, to obtain cross-linked samples denoted **P$_{LA}$2**, **P$_{LA}$3**, and **P$_{LA}$4**, respectively. Cross-linking conversion was monitored by $^{1}$H NMR spectroscopy (Figure A3.36). In the case of [C=C]:[SH] = 1:1, ≥ 96 % of cross-linking was observed with no further change in resonances even over prolonged reaction time (over 2 days). To ensure that cross-linking is not limited by the deactivation of AIBN, excess AIBN was added but similar cross-linking conversions were observed. The finding of a small quantity of residual olefin might be due to the limited flexibility of the polymer structure once a high cross-linking degree was achieved, meaning the final few olefin groups do not react with the residual SH functional groups. In the case of [C=C]:[SH] = 1:3 and 1:6, full cross-linking was seen, as evidenced by the lack of $^{1}$H NMR resonance for alkene or maleate ester functional groups. The cross-linked polymers were then purified by precipitation (three times) in hexane. DSC analysis of each cross-linked polymer sample was conducted (Figure 5.11a). In the case of **P$_{LA}$2**, a $T_g$ of –8 °C was

seen, which is similar to the uncross-linked sample (–5 °C for **$P_{LA}$1**). For **$P_{LA}$3** and **$P_{LA}$4**, lower $T_g$ values were observed (–15 °C and–32 °C, respectively) (Figure 5.11a). This apparent increase in chain mobility could be due to unreacted SH groups in the polymers and has been previously observed by other research groups studying thiol-ene reactions using these conditions (loadings of this thiol).[35] Raman spectroscopic analysis of each isolated cross-linked material was recorded to corroborate this hypothesis (Figures 5.11b and A3.37). A mixture of the precursor polymer and the thiol, trimethylolpropane tris(3-mercaptopropionate), was used for comparison. The free SH group resonates at 2580 $cm^{-1}$ and was clearly observed in the sample of **$P_{LA}$4**, but was absent for **$P_{LA}$2** and **$P_{LA}$3** samples. Any remaining SH groups for the latter two samples fall below the detection limit for Raman spectroscopy.

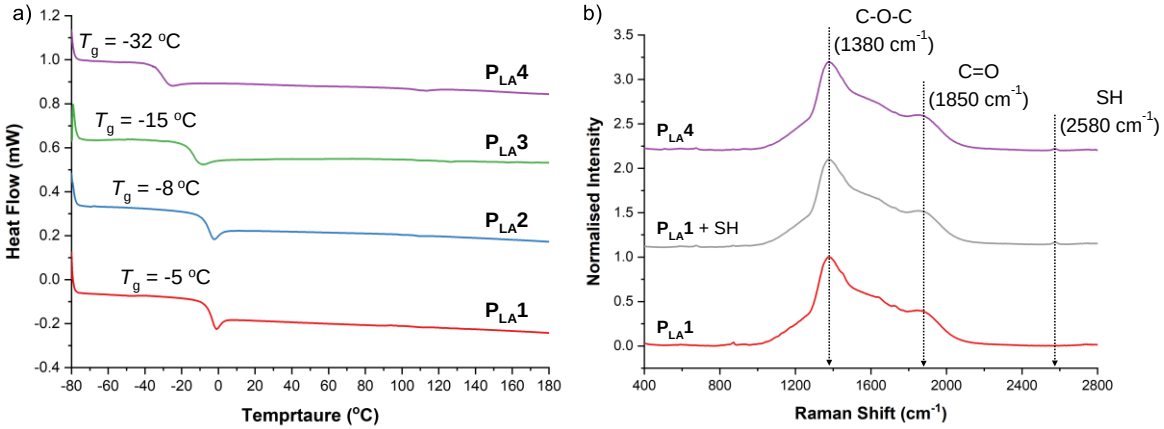



**Figure 5.11.** a) Stacks of DSC thermograms of isolated uncross-linked and cross-linked $PEE_{MA}$-PLLA tapered copolymers and b) stacks of Raman spectra of **$P_{LA}$1**, **$P_{LA}$1**+SH, and **$P_{LA}$4**.

Isolated cross-linked polymers were then investigated as additives for PLLA (Table 5.5 and Figure 5.12). Since the specimen containing 2 wt. % of **$P_{LA}$1** previously exhibited the best mechanical properties, the same content was used for the cross-linked copolymers (see previous section). PLLA films containing 2 wt. % of **$P_{LA}$2**– **$P_{LA}$4** were prepared following the same procedure discussed above. Tensile analysis results are listed in Table 5.5

**Table 5.5.** Tensile testing data for PLLA, containing 2 wt. % of different additives.

| Additive type | Young's Modulus (MPa) | Tensile Strength (MPa) | Elongation at Break (%) | Tensile Toughness (MJ $m^{-3}$) [a] |
|---|---|---|---|---|
| none | 1612.8 ± 26.3 | 53.1 ± 3.04 | 6.6 ± 1.15 | 2.1 ± 0.49 |
| **$P_{LA}1$** | 1610.4 ± 20.1 | 45.0 ± 1.53 | 14.7 ± 0.55 | 6.4 ± 0.44 |
| **$P_{LA}2$** | 2271.6 ± 169.3 | 54.3 ± 0.99 | 8.9 ± 0.49 | 4.1 ± 0.27 |
| **$P_{LA}3$** | 1620.8 ± 22.6 | 53.4 ± 2.53 | 15.3 ± 1.81 | 7.7 ± 0.95 |
| **$P_{LA}4$** | 1723.0 ± 126.0 | 43.0 ± 0.39 | 24.7 ± 1.14 | 11.1 ± 0.49 |

[a] calculated form the peak area under the plot between stress (y axis) and strain (x axis).

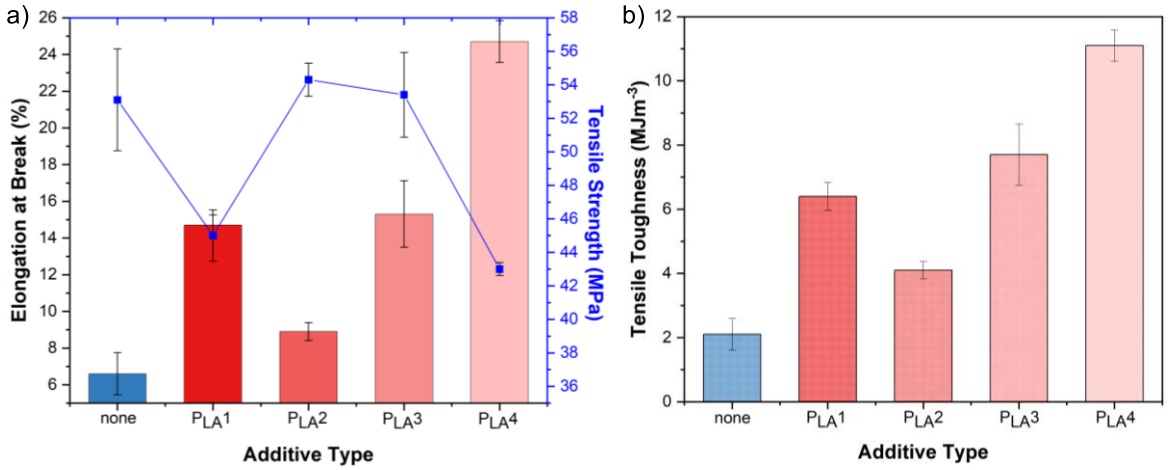



**Figure 5.12.** Mechanical properties of PLLA – different additives (2 wt. %) blends: a) elongation at break and tensile strength and b) tensile toughness.

Using **$P_{LA}2$** led to an increase in Young's modulus of the material specimen compared to using **$P_{LA}1$**, whilst similar Young's moduli were observed in the cases of **$P_{LA}3$**, and **$P_{LA}4$**. An improvement in tensile strength relative to using **$P_{LA}1$** was seen when **$P_{LA}2$**, or **$P_{LA}3$** were used (Figure 5.12a). As expected from its low $T_g$, the addition of **$P_{LA}4$** resulted in a drastically increased percent elongation at break and this further improved the material toughness. In the case of **$P_{LA}3$**, only a slight improvement in elongation at break and tensile toughness was observed. In contrast, a reduction in both elongation at break and material toughness was seen when **$P_{LA}2$** was used.

### 5.4.3. Effect of PLLA molar mass

**Table 5.6.** Tensile testing data for high molar mass PLLA, containing 2 wt. % of different additives.

| Additive type | Young's Modulus (MPa) | Tensile Strength (MPa) | Elongation at Break (%) | Tensile Toughness (MJ $m^{-3}$) [a] |
|---|---|---|---|---|
| none | 2197.9 ± 40.0 | 63.8 ± 0.86 | 8.7 ± 0.49 | 4.4 ± 0.22 |
| **$P_{LA}$1** | 2196.3 ± 91.6 | 56.5 ± 1.54 | 10.9 ± 0.55 | 5.7 ± 0.49 |
| **$P_{LA}$4** | 1987.7 ± 37.1 | 49.6 ± 0.72 | 35.5 ± 0.86 | 17.7 ± 0.21 |

[a] calculated form the peak area under the plot between stress (y axis) and strain (x axis).

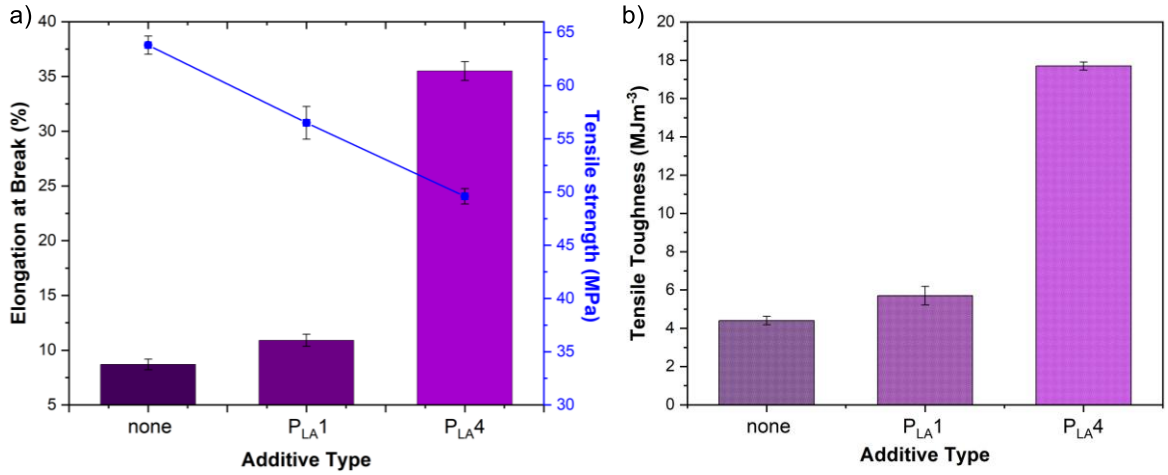



**Figure 5.13.** Mechanical properties of high molar mass PLLA – different additives (2 wt. %) blends: a) elongation at break and tensile strength and b) tensile toughness.

The effect of the PLLA molar mass was then investigated and a sample of high molar mass PLLA ($M_{n,SEC}$ (corrected with a correction factor of 0.58)[22] = 129,000 g $mol^{-1}$, $Đ$ = 1.41, PURASORB® PL 24, contributed by Corbion) was used to prepare the samples for mechanical testing. **$P_{LA}$4** was used as a representative additive since it gave the best mechanical properties when blended with the lower molar mass PLLA (see above). Neat PLLA films and PLLA with 2 wt. % of **$P_{LA}$1** were prepared for comparison. Table 5.6 and Figure 5.13 summarise the tensile measurements for each material. In all cases, a higher Young's modulus and tensile strength than that of lower molar mass material (see Table 5.5 for more detail) were observed irrespective of the additive added. In the case of elongation

at break, both neat PLLA and PLLA with 2 wt. % of **$P_{LA}$4** showed an improvement, whilst a slightly lower value than that of lower molar mass PLLA was observed when **$P_{LA}$1** was added. Again, PLLA, containing 2 wt. % of **$P_{LA}$4** exhibited the highest toughness of 17.7 ± 0.21 MJ $m^{-3}$ which is more than 4 times higher than neat PLLA.

## 5.5. Conclusion and Outlook

### 5.5.1. Conclusion

This chapter demonstrated the use of Sn(II)$(OMe)_2$, an industrially relevant catalyst, as an effective catalyst for the ROCOP of propylene oxide and various cyclic anhydrides (MA, PA, and SA) for the formation of novel polyester-*co*-ether materials. One-pot polymerisation of PO, MA, and lactone resulted the formation of copolymers with different structures, depending on the type of lactone. In the case of LA, a tapered copolymer was obtained, whilst a gradient copolymer was observed when *ε*-CL was used. This is due to the different polymerisation kinetics of the lactones. Several analytical techniques were used to confirm the polymer structures. Additionally, a block copolymer between $PEE_{MA}$ and PLA can be obtained from sequential monomer addition methods. Blending the two resultant block polymers of $PEE_{MA}$-*b*-PLLA or $PEE_{MA}$-*b*-PDLA allows for the formation of a stereocomplex between the PLA segments, which was confirmed by DSC analysis where an elevated $T_m$ (202 °C) was observed.

The resultant tapered copolymer (**$P_{LA}$1)** can be further used as an efficient additive to toughen PLLA. The effects of additive content were examined, and it was observed that blending in as little as 2 wt. % of **$P_{LA}$1** resulted in a doubling of the material's elongation at break and a tripling in PLLA toughness. Additionally, the cross-linking of $PEE_{MA}$ segments of the additive using multifunctional thiols can further enhance material toughness. Utilising **$P_{LA}$4** leads to a 4 fold increase in both percent elongation at break and tensile toughness

relative to neat PLLA. These improvements to the mechanical properties of PLLA are significant since the quantities of material added are low and would fall within specifications allowing the product to be labelled as PLLA.

### 5.5.2. Outlook

There are three clear areas for future investigation: 1) Expanding the scope of monomers used in polymerisation, 2) Accessing polymers with more complex structures and architectures, and 3) Investigating the effect of monomer concentration in the one-pot reactions to bias reactions towards particular polymer structures.

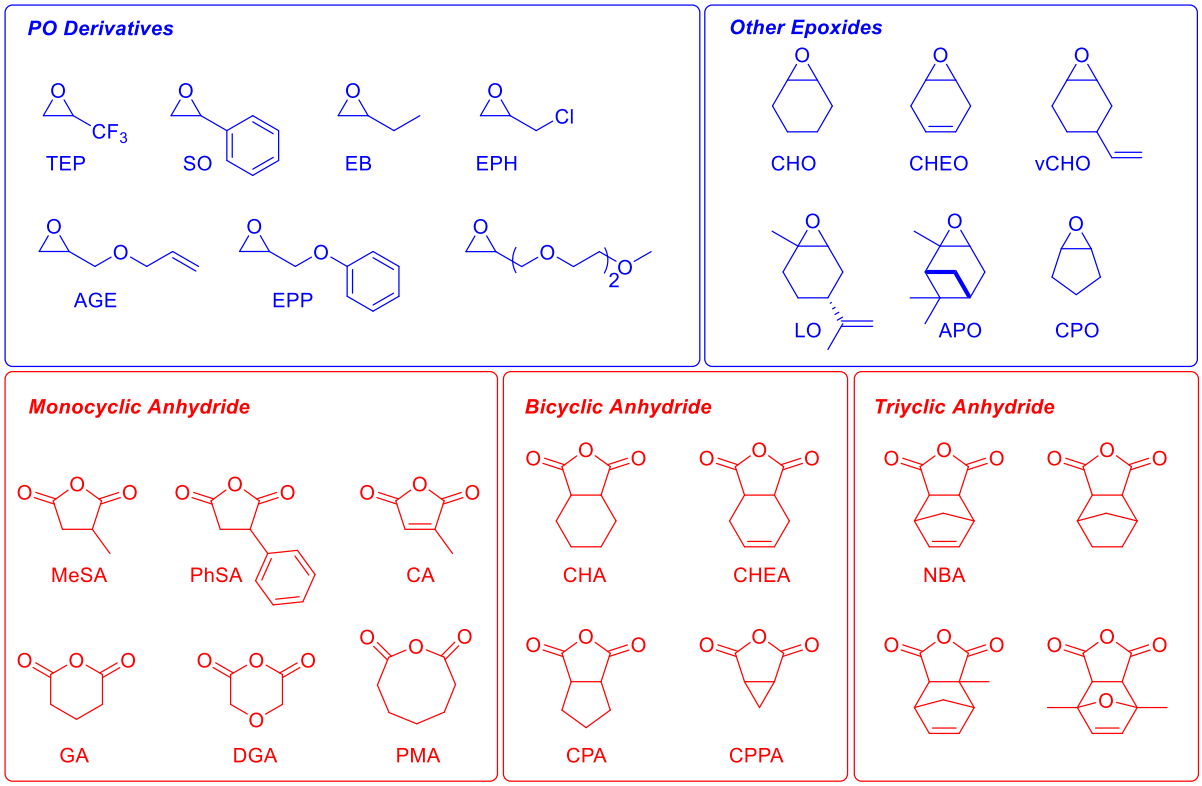
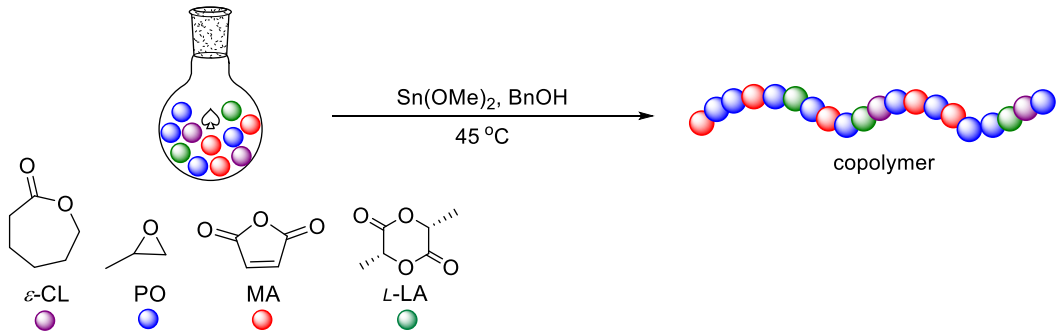



**Figure 5.14.** Examples of potential cyclic anhydride and epoxide monomers.

Given the promising results from ROCOP of PO and CAs, it is interesting to investigate a full range of epoxide and anhydride monomers and it is recommended that such a study begin with those which are commercially available (*e.g.* CHO, CPO, LO as examples for epoxides and GA, DGA, NBA as examples for anhydrides). It is obvious that polymer

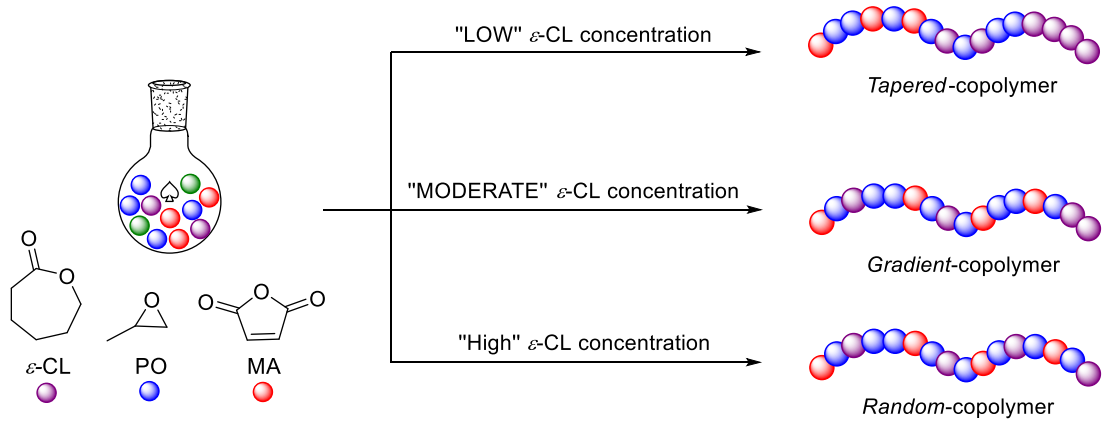
thermal and mechanical properties ($T_g$, $T_m$, $T_d$) depend strongly on the monomers incorporated into the polymer backbone. By expanding the range of monomers, it should be possible to offer materials which are rigid plastics (*e.g.* using cyclohexene oxide/tricyclic anhydride ROCOP) or flexible elastomers (*e.g.* using propene oxide/diglycolic anhydride). It is important firstly to work out which materials are accessible and also to qualify the properties for those new polymers. Figure 5.14 illustrates examples of potential epoxides and cyclic anhydrides which could be investigated in the future.




**Scheme 5.5.** One-pot polymerisation of PO, MA, LA and CL to access better additive for PLLA.

One means to access copolymers with more complex structures is to increase the number of monomers involved in polymerisations. PCL possesses a low $T_g$ but it is semi-crystalline and so provided its crystallinity can be suppressed, it is an interesting elastomeric component to the copolymers. Previous studies have demonstrated the copolymerisation of CL with LA, with the resulting products acting as plasticisers/additives to enhance the mechanical properties of PLA.[30] In our work, the softest plasticiser **P$_{LA}$4** resulted in the greatest improvement in PLA mechanical properties. A copolymerisation using 4 different monomers (LA, CL, PO, and MA) is an important target as it may allow further reduction in the $T_g$ values, whilst retaining the high miscibility with PLLA which is essential to reduce the additive loading in the eventual plastic (Scheme 5.5). By adopting such a strategy, using

commercially available monomers, it is important to keep targeting improvements to the mechanical properties of PLLA in terms of enhancing its elongation at break and toughness.




**Scheme 5.6.** Proposed $PEE_{MA}$-*co*-PCL with different architecture depending on CL concentration.

This chapter established that the one-pot polymerisation of PO, MA, and CL, using $Sn(OMe)_2$ as a catalyst, is feasible and appears to follow, at least in part, some of the rules of switchable catalysis. The polymerisation kinetics are first order in both CL and MA concentrations, in contrast to previous reports of switchable catalysts where zero order in MA and first order in CL are more commonly observed.[11, 12, 14, 15, 36] This finding suggests that the concentration of CL (or MA) may play a role in controlling the architecture of the polymer. In this thesis, only one set of loadings/conditions was used for the one-pot polymerisations where the concentration of CL is equal to the concentration of MA. Under these conditions, a gradient copolymer was obtained. A clear next stage investigation would be to change the CL concentration, and by aiming for higher CL concentrations it may be possible to make even more randomised structures, whereas targeting lower concentrations should allow access to greater block lengths in both the PEE and PCL portions (Scheme 5.6).

## 5.6. References


(1) Dove, A. P., Organic Catalysis for Ring-Opening Polymerization. *ACS Macro Lett.* **2012,** *1* (12), 1409–1412.

(2) Kamber, N. E.; Jeong, W.; Waymouth, R. M.; Pratt, R. C.; Lohmeijer, B. G. G.; Hedrick, J. L., Organocatalytic Ring-Opening Polymerization. *Chem. Rev.* **2007,** *107* (12), 5813–5840.

(3) O'Keefe, B. J.; Hillmyer, M. A.; Tolman, W. B., Polymerization of lactide and related cyclic esters by discrete metal complexes. *J. Chem. Soc. Dalton Trans.* **2001,** (15), 2215–2224.

(4) Robert, C.; de Montigny, F.; Thomas, C. M., Tandem synthesis of alternating polyesters from renewable resources. *Nat. Commun.* **2011,** *2* (1), 586.

(5) Longo, J. M.; Sanford, M. J.; Coates, G. W., Ring-Opening Copolymerization of Epoxides and Cyclic Anhydrides with Discrete Metal Complexes: Structure–Property Relationships. *Chem. Rev.* **2016,** *116* (24), 15167–15197.

(6) Paul, S.; Zhu, Y.; Romain, C.; Brooks, R.; Saini, P. K.; Williams, C. K., Ring-opening copolymerization (ROCOP): synthesis and properties of polyesters and polycarbonates. *Chem. Commun.* **2015,** *51* (30), 6459–6479.

(7) Chen, T. T. D.; Zhu, Y.; Williams, C. K., Pentablock Copolymer from Tetracomponent Monomer Mixture Using a Switchable Dizinc Catalyst. *Macromolecules* **2018,** *51* (14), 5346–5351.

(8) Stößer, T.; Li, C.; Unruangsri, J.; Saini, P. K.; Sablong, R. J.; Meier, M. A. R.; Williams, C. K.; Koning, C., Bio-derived polymers for coating applications: comparing poly(limonene carbonate) and poly(cyclohexadiene carbonate). *Polym. Chem.* **2017,** *8* (39), 6099–6105.

(9) Yi, N.; Chen, T. T. D.; Unruangsri, J.; Zhu, Y.; Williams, C. K., Orthogonal functionalization of alternating polyesters: selective patterning of (AB)n sequences. *Chem. Sci.* **2019,** *10* (43), 9974–9980.

(10) Ruzette, A.-V.; Leibler, L., Block copolymers in tomorrow's plastics. *Nat. Mat.* **2005,** *4* (1), 19–31.

(11) Stößer, T.; Chen, T. T. D.; Zhu, Y.; Williams, C. K., 'Switch' catalysis: from monomer mixtures to sequence-controlled block copolymers. *Phil. Trans. R. Soc. A* **2018,** *376* (2110), 20170066.

(12) Stößer, T.; Mulryan, D.; Williams, C. K., Switch Catalysis To Deliver Multi-Block Polyesters from Mixtures of Propene Oxide, Lactide, and Phthalic Anhydride. *Angew. Chem. Int. Ed.* **2018,** *57* (51), 16893–16897.

(13) Ji, H.-Y.; Wang, B.; Pan, L.; Li, Y.-S., One-Step Access to Sequence-Controlled Block Copolymers by Self-Switchable Organocatalytic Multicomponent Polymerization. *Angew. Chem. Int. Ed.* **2018,** *57* (51), 16888–16892.

(14) Stößer, T.; Sulley, G. S.; Gregory, G. L.; Williams, C. K., Easy access to oxygenated block polymers via switchable catalysis. *Nat. Commun.* **2019,** *10* (1), 2668.

(15) Stößer, T.; Williams, C. K., Selective Polymerization Catalysis from Monomer Mixtures: Using a Commercial Cr-Salen Catalyst To Access ABA Block Polyesters. *Angew. Chem. Int. Ed.* **2018,** *57* (21), 6337–6341.

(16) Drumright, R. E.; Gruber, P. R.; Henton, D. E., Polylactic Acid Technology. *Adv. Mat.* **2000,** *12* (23), 1841–1846.

(17) Aubrecht, K. B.; Hillmyer, M. A.; Tolman, W. B., Polymerization of Lactide by Monomeric Sn(II) Alkoxide Complexes. *Macromolecules* **2002,** *35* (3), 644–650.

(18) Dechy-Cabaret, O.; Martin-Vaca, B.; Bourissou, D., Controlled Ring-Opening Polymerization of Lactide and Glycolide. *Chem. Rev.* **2004,** *104* (12), 6147–6176.

(19) Dove, A. P.; Gibson, V. C.; Marshall, E. L.; White, A. J. P.; Williams, D. J., A well defined tin(ii) initiator for the living polymerisation of lactide. *Chem. Commun.* **2001,** (3), 283–284.

(20) Pound-Lana, G.; Rabanel, J.-M.; Hildgen, P.; Mosqueira, V. C. F., Functional polylactide via ring-opening copolymerisation with allyl, benzyl and propargyl glycidyl ethers. *Eur. Polym. J.* **2017,** *90*, 344–353.

(21) Ye, H.; Zhang, K.; Kai, D.; Li, Z.; Loh, X. J., Polyester elastomers for soft tissue engineering. *Chem. Soc. Rev.* **2018,** *47* (12), 4545–4580.

(22) Kowalski, A.; Duda, A.; Penczek, S., Polymerization of l,l-Lactide Initiated by Aluminum Isopropoxide Trimer or Tetramer. *Macromolecules* **1998,** *31* (7), 2114–2122.

(23) Anastasaki, A.; Waldron, C.; Wilson, P.; Boyer, C.; Zetterlund, P. B.; Whittaker, M. R.; Haddleton, D., High Molecular Weight Block Copolymers by Sequential Monomer Addition via Cu(0)-Mediated Living Radical Polymerization (SET-LRP): An Optimized Approach. *ACS Macro Lett.* **2013,** *2* (10), 896–900.

(24) Szwarc, M.; Levy, M.; Milkovich, R., Polymerization initiated by electron transfer to monomer. a new method of formation of block polymers. *J. Am. Chem. Soc.* **1956,** *78* (11), 2656–2657.

(25) Bandelli, D.; Alex, J.; Weber, C.; Schubert, U. S., Polyester Stereocomplexes Beyond PLA: Could Synthetic Opportunities Revolutionize Established Material Blending? *Macromol. Rapid Commun.* **2020,** *41* (1), 1900560.

(26) Stanford, M. J.; Dove, A. P., Stereocontrolled ring-opening polymerisation of lactide. *Chem. Soc. Rev.* **2010,** *39* (2), 486–494.

(27) Jamshidian, M.; Tehrany, E. A.; Imran, M.; Jacquot, M.; Desobry, S., Poly-Lactic Acid: Production, Applications, Nanocomposites, and Release Studies. *Compr. Rev. Food Sci. Food Saf.* **2010,** *9* (5), 552–571.

(28) Jem, K. J.; Tan, B., The development and challenges of poly (lactic acid) and poly (glycolic acid). *Adv. Ind. Eng. Polym. Res.* **2020,** *3* (2), 60–70.

(29) Madhavan Nampoothiri, K.; Nair, N. R.; John, R. P., An overview of the recent developments in polylactide (PLA) research. *Bioresour. Technol.* **2010,** *101* (22), 8493–8501.

(30) Anderson, K. S.; Schreck, K. M.; Hillmyer, M. A., Toughening Polylactide. *Polym. Rev.* **2008,** *48* (1), 85–108.

(31) Sinclair, R. G., The Case for Polylactic Acid as a Commodity Packaging Plastic. *J. Macromol. Sci. A* **1996,** *33* (5), 585–597.

(32) Labrecque, L. V.; Kumar, R. A.; Davé, V.; Gross, R. A.; McCarthy, S. P., Citrate esters as plasticizers for poly(lactic acid). *J. Appl. Polym. Sci.* **1997,** *66* (8), 1507–1513.

(33) Martin, O.; Avérous, L., Poly(lactic acid): plasticization and properties of biodegradable multiphase systems. *Polymer* **2001,** *42* (14), 6209–6219.

(34) Martín, C.; Kleij, A. W., Terpolymers Derived from Limonene Oxide and Carbon Dioxide: Access to Cross-Linked Polycarbonates with Improved Thermal Properties. *Macromolecules* **2016,** *49* (17), 6285–6295.

(35) Durand, P.-L.; Chollet, G.; Grau, E.; Cramail, H., Versatile cross-linked fatty acid-based polycarbonate networks obtained by thiol–ene coupling reaction. *RSC Adv.* **2019,** *9* (1), 145–150.

(36) Romain, C.; Williams, C. K., Chemoselective Polymerization Control: From Mixed-Monomer Feedstock to Copolymers. *Angew. Chem. Int. Ed.* **2014,** *53* (6), 1607–1610.

# *Chapter 6*

## *Conclusion, Challenges, and Future Work*

*Success is the sum of small efforts repeated day in and day out...*

*~ Robert Collier ~*

## 6.1. Conclusion

This thesis presents a range of new In(III), Ti(IV), and Zr(IV) phosphasalen catalysts for the production of polyesters, and the use of an industrially relevant Sn(II)$(OMe)_2$ catalyst to prepare new polyester-ether copolymers. All complexes, except the commercially available Sn(II) catalyst, were characterised using a range of spectroscopic and analytical techniques. These have included multinuclear NMR spectroscopy, elemental analysis, high resolution mass spectroscopy, and if applicable single crystal X-ray diffraction. The catalytic performances of all complexes in ROP, ROCOP or `Switch´ catalysis were investigated.

The catalytic activities of phosphasalen indium(III) complexes toward the ROP of *rac*-lactide were examined to understand the effect of the diamine backbone and influence of the phosphorous substituents on catalyst activity and stereoselectivity. The nature of the diamine backbone plays a key role in both catalyst activity and stereoselectivity. Complex **3.1**, featuring a $C_2$ diamine backbone, showed the highest activity, followed by complex **3.2**, containing $C_3$ diamine bridge. Complex **3.3**, possessing a $C_3Me_2$ diamine linker, exhibited the lowest polymerisation activity. The activity follows the order **3.1** > **3.2** > **3.3**. A different trend was seen for catalyst stereoselectivity, with complex **3.3** being the highest iso-selective catalyst followed by **3.1** and then **3.2**. Additionally, the phosphorus substituents have a crucial role in catalyst stereoselectivity. Replacing one phenyl phosphine substituent on complex **3.1** with a bulkier *tert*-butyl group to form indium complex **3.4** resulted in a significant enhancement in catalyst stereoselectivity. As a result, complex **3.4** produced highly isotactic PLA with $P_i$ up to 0.92 (T = 278 K). A kinetic study, in combination with isolation of the key intermediate during the ROP propagation step, was used to understand stereocontrol and a chain-end control mechanism is operative. The polymerisation of various lactones, including $\varepsilon$-CL, $\beta$-BL, $\varepsilon$-DL, and $\delta$-HL, was also feasible using the indium catalysts with activity values depending on the nature of both the lactone substrate and initiator.

Phosphasalen titanium(IV) and zirconium(IV) complexes were studied as initiators for the ring-opening copolymerisation of epoxides and cyclic anhydrides, as well as for ethylene polymerisations. Investigation of structure-activity and selectivity relationships highlighted the influence of the diamine backbone and coordination mode of the $^{i}$PrO co-ligands. Phosphasalen and salen titanium(IV) complexes containing a $C_2$ backbone (complexes **4.1** and **4.4**) showed higher catalytic activities and selectivities than those possessing $C_3Me_2$ or Ph linkers. Phosphasalen titanium(IV) complexes showed faster polymerisation rates and higher selectivities than their salen and salalen analogues. The introduction of the larger radii zirconium(IV) into the best performing phosphasalen ligand scaffold resulted in a drastic decrease in catalytic activity and selectivity. A mechanism was proposed for this catalyst system based on kinetic experiments and isolation of the propagating intermediate during the ROCOP. Additionally, all titanium(IV) complexes were active initiators in ethylene polymerisations. The polymerisations were carried out using cationic species and without sMAO. The activity order is **4.3** > **4.1** > **4.4** > **4.6** > **4.5** > **4.2**. Ultra high molar mass polyethylenes with molar masses up to 4 million g mol$^{-1}$ were produced.

$Sn(OMe)_2$ was also used for the first time in the ROCOP of PO and various cyclic anhydrides to produce new poly(ester-*ran*-ether) copolymers. In addition, its use in `Switch´ catalysis with exposure to mixtures of lactones, epoxides and anhydrides to make a range of different copolymer structures was explored. Polyester-ether copolymers with different microstructures including block-, tapered-, and gradient-copolymers were produced. By using *L*-LA, PO, and MA, a tapered polyester-ether copolymer was obtained, whilst using $\varepsilon$-CL, PO and MA, produced a gradient copolymer. Blending $PEE_{MA}$-*b*-PLLA and $PEE_{MA}$-*b*-PDLA allowed the formation of stereocomplexes of PLA segments and resulted in significant enhancement of the melting temperature. The tapered copolymers were efficient toughening agents for PLLA. Blending as little as 2 wt. % of the tapered copolymers, or its

cross-linked derivatives, into PLLA films resulted in an improved engineering strain whilst maintaining a high mechanical strength. As a result, overall, the toughness was enhanced by up to 400 %.

### 6.2. Challenges and Future Work

The developments in each chapter improve upon the performances of current catalysts for lactone ROP and ROCOP of epoxides and cyclic anhydrides. Specifically, the thesis shows the importance of systematic modification of both the ligand and the metal centre, although it also highlights the remaining challenges of rationalising which site to modify for the best effect. In addition, many of these catalysts are effective in `Switch´ catalysis using mixtures of lactone, epoxide and anhydride to access more complex copolymers and this allows overcoming of known material challenges, for example the toughening of the bio-plastic PLLA. The thesis also highlights remaining challenges which could be addressed by further research.

For LA polymerisation catalysis, the future focus could be to maximise both catalyst activity and iso-selectivity to facilitate the formation of stereocomplex PLA from the one-step ROP of *rac*-LA. This could be achieved either by ligand modification or metal centre alteration (Figure 6.1). Polymerisation results, presented in Chapter 3, indicated the importance of phosphorous substituents. Using complexes featuring asymmetric *tert*-butyl and phenyl phosphorous substituents allowed the production of highly isotactic PLA ($P_i$ up to 0.92, T = 278 K). Previous work by Myers *et al.* also investigated the chemistry of phenoxide substituents. Complexes possessing cumyl groups on the phenoxide rings showed high activity and iso-selectivity ($P_i$ up to 0.92, T = 258 K).[1]

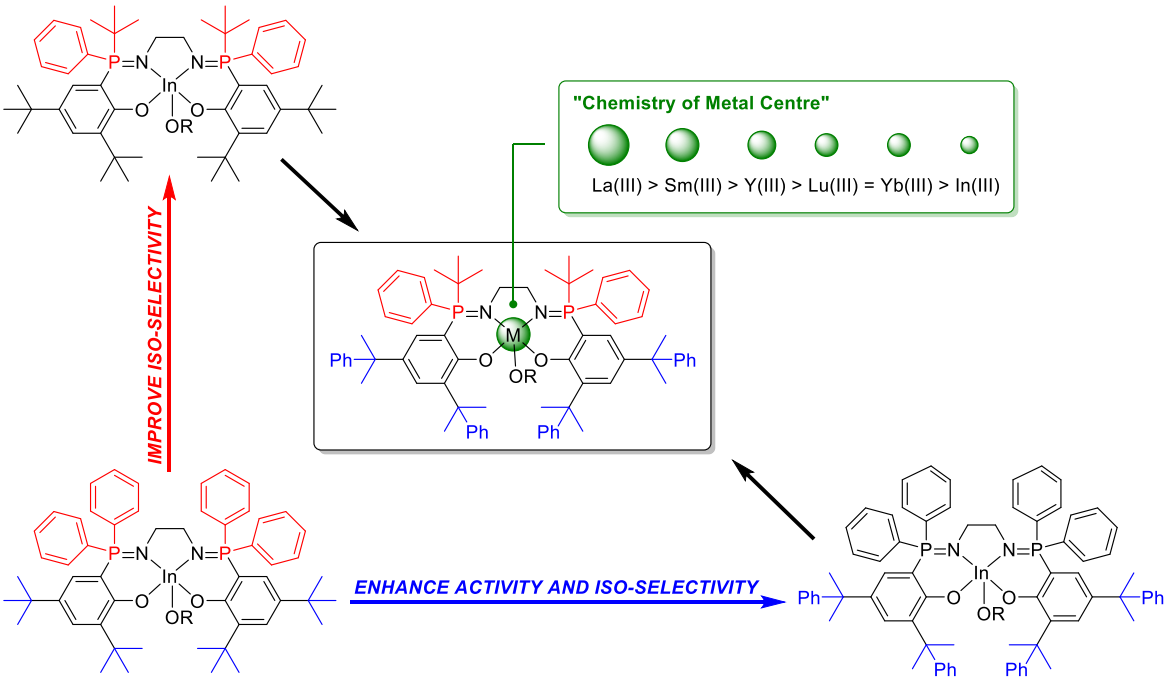



**Figure 6.1.** Structures of proposed phosphasalen complexes.

Future complexes could be designed by employing these two important findings (see complex structures in Figure 6.1). The structure-activity and structure-stereoselectivity relationships of future target complexes would also be worth studying. Additionally, the chemistry of different metal centres with the new ligand scaffolds would be interesting to investigate. The use of larger radii metal centers may allow access to complexes with higher catalytic activity due to rapid monomer coordination.[2]

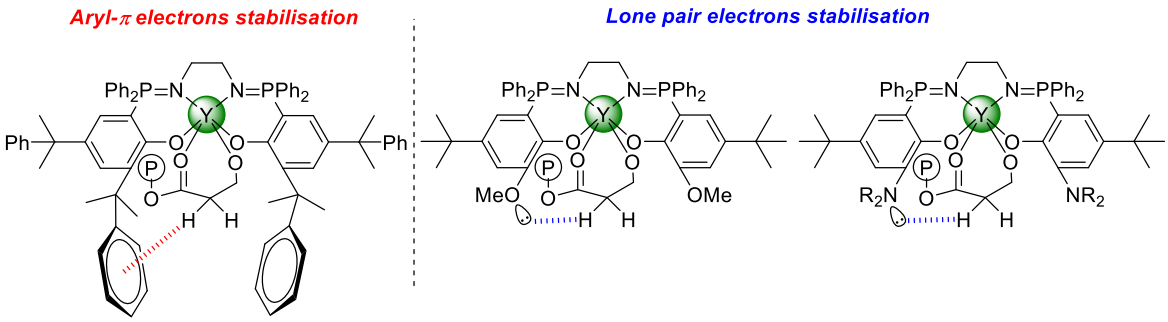



**Figure 6.2.** Proposed phosphasalen yttrium complexes for stereoselective *β*-BL polymerisations.

Exploration of complexes exhibiting high stereoselectivity for LA ROP using with more challenging lactones (*e.g.* $\beta$-butyrolactone) is a future target. Some of these polymerisations were explored in Chapter 3. Unfortunately, the complexes only showed low stereoselectivities and produced atactic polyhydroxy butyrates. Carpentier and co-workers showed that high stereoselectivity for $\beta$-BL polymerisations could be achieved by employing yttrium amino-phenolate complexes, containing aryl functional groups on the phenolate rings.[3-8] The introduction of aryl containing substituents was proven to help stabilise the last inserted monomer *via* interactions between H atoms and π electrons and improve catalyst stereoselectivities. Future target complexes could be designed based on this ground breaking study (Figure 6.2). The first target complex would involve the use of yttrium phosphasalen complex, possessing cumyl phenoxide substituents which may show similar effect to Carpenteir discovery and produce high stereoselective polymers from $\beta$-BL. The next generations will explore the chemistry of other stabilisation groups (*e.g.* OMe or $NR_2$). Employing OMe or $NR_2$ may allow access to complexes with stronger lactate stabilisation through H-bonding interactions. It would be interesting to explore whether such stabilisations might be used to direct lactide enantiomer enchainment, and hence stereochemistry.

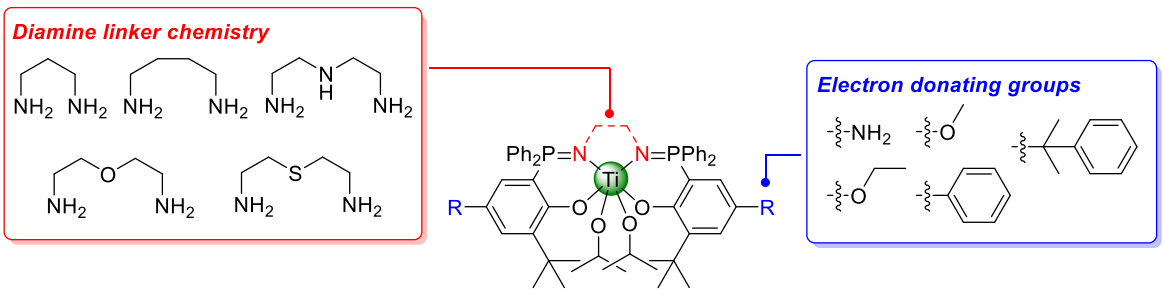



**Figure 6.3.** Structures of titanium(IV) salen or phosphasalen complexes.

For epoxide and anhydride ROCOP, most current catalysts require co-catalysts. However, the presence of a co-catalyst often leads to the formation of polymers with low end group

fidelities and low molar masses.[9, 10] The development of highly active and selective single component catalysts remains highly desirable, as does accessing lower catalyst loadings to maximise the resulting polyester molar mass. The titanium catalysts shown in Chapter 4 represent an interesting class for further investigation, as they were able to operate without co-catalyst and showed high selectivities. However, their low catalytic activities and the need for high catalyst loading are still challenges which warrant further investigations. One future target will be to maximise catalyst activity and to make catalysts with better tolerance at low loadings by means of exploring changes to the (para) phenoxide substituents, as well as diamine backbone chemistries. The introduction of electron donating groups at the para phenoxide sites may enhance the lability of metal-alkoxide or metal-carboxylate intermediates and thereby accelerate catalysis (*i.e.* enhancing polymerisation rate) (Figure 6.3). Similarly, the use of diamine linkers possessing heteroatoms (*e.g.* O, S, N) might allow access to similar effects and improvements in catalytic activity. Chapter 4 studies also suggested that the use of a highly rigid backbone (*e.g.* phenylene diamine) directed the formation of complexes with *cis*-coordination of alkoxide co-ligands which then hampered activity. The next generation of complexes should focus on complexes with *trans*-coordination of alkoxide initiating groups. The more flexible diamine linkers (*e.g.* C3, C4) would be interesting targets since they may allow the production of complexes with alkoxide *trans*-coordination.

Additionally, the full empirical rate law of the ROCOP using the titanium complexes should be investigated, since it will give insight into the polymerisation mechanism and which step to optimise in terms of structure-activity relationships (*e.g.* monometallic, bimetallic, bicomponent mechanisms). The results presented in Chapter 4 only pin pointed the polymerisation order in anhydride concentration. The polymerisation order in catalyst and

epoxide concentrations must be determined to establish a full rate law. This would ensure appropriate design for future ligands and complexes.

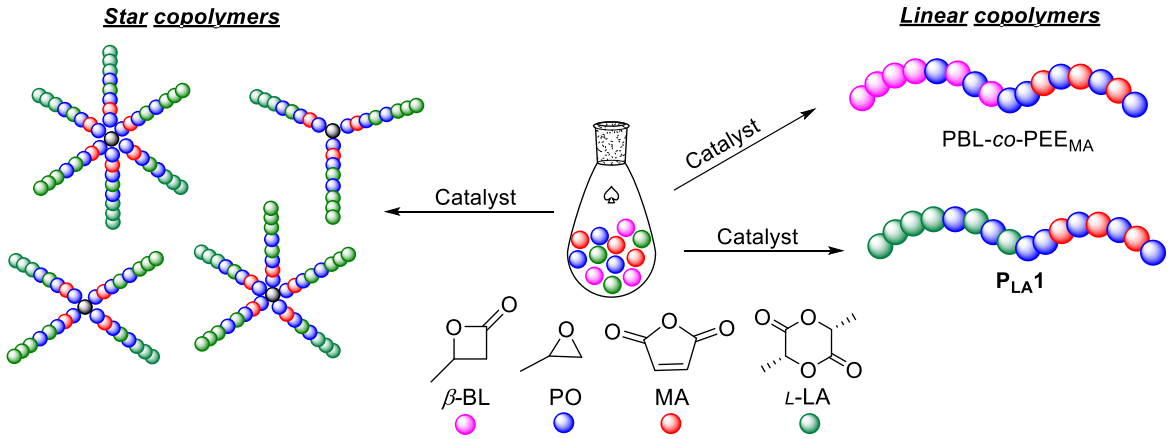



**Figure 6.4.** Switch catalyses for the synthesis of copolymers with various architectures.

Future work based on results presented in Chapter 5 could be to further investigate material (PLLA + additives) mechanical properties (*e.g.* impact strength, toughness) using Charpy or Notched Izod tests. Both tests would allow a better understanding of material impact strength and toughness. The testing results could be compared against reported tensile data for PLA-plasticiser/additive blends to understand the relevance of the results in the broader context of PLA chemistry. In addition, the *in situ* cross-linking of the additive polymers in PLLA could be carried out, rather than blending the cross-linked derivatives with PLLA which was carried out in Chapter 5. This may allow better understanding of polymer structure-properties relationships. The understanding of polymer micro/macro structures could also be a focus of future research. This includes the study of the material morphology, polymer rheology, and PLLA crystallisation kinetics. It would also be interesting to examine the degradation rates of the materials as well as the additives to evaluate their end-of-life profiles. A range of characterisation techniques such as NMR spectroscopy, mass spectrometry, and liquid chromatography could be performed to identify the nature of degradation products.

In addition, the study in Chapter 5 only concerned the use of linear polymers. To gain further understanding of polymer architecture-property relationships, the synthesis of tapered copolymers with various architectures (*e.g.* star polymers) could be performed (Figure 6.4). The target copolymers could then be studied as additives for PLLA toughening to establish a library of these copolymer properties. Star copolymers may be even more effective toughening agents *vs.* linear polymers since they provide a higher crosslink density and accelerate formation of networked materials. Copolymers between PO, MA and other lactones (*e.g.* $\beta$-BL) would also be interesting to investigate as it may allow access to bespoke toughening agents for other highly brittle bioplastics, *e.g.* PHB or PHA (Figure 6.4).

## 6.3. References

(1) Myers, D.; White, A. J. P.; Forsyth, C. M.; Bown, M.; Williams, C. K., Phosphasalen Indium Complexes Showing High Rates and Isoselectivities in *rac*-Lactide Polymerizations. *Angew. Chem. Int. Ed.,* **2017,** *56* (19), 5277–5282.

(2) Bakewell, C.; White, A. J. P.; Long, N. J.; Williams, C. K., Metal-Size Influence in Iso-Selective Lactide Polymerization. *Angew. Chem. Int. Ed.,* **2014,** *53* (35), 9226–9230.

(3) Ajellal, N.; Bouyahyi, M.; Amgoune, A.; Thomas, C. M.; Bondon, A.; Pillin, I.; Grohens, Y.; Carpentier, J.-F., Syndiotactic-Enriched Poly(3-hydroxybutyrate)s via Stereoselective Ring-Opening Polymerization of Racemic *β*-Butyrolactone with Discrete Yttrium Catalysts. *Macromolecules*, **2009,** *42* (4), 987–993.

(4) Amgoune, A.; Thomas, C. M.; Ilinca, S.; Roisnel, T.; Carpentier, J.-F., Highly Active, Productive, and Syndiospecific Yttrium Initiators for the Polymerization of Racemic *β*-Butyrolactone. *Angew. Chem. Int. Ed.,* **2006,** *45* (17), 2782–2784.

(5) Bouyahyi, M.; Ajellal, N.; Kirillov, E.; Thomas, C. M.; Carpentier, J.-F., Exploring Electronic versus Steric Effects in Stereoselective Ring-Opening Polymerization of Lactide and *β*-Butyrolactone with Amino-alkoxy-bis(phenolate)–Yttrium Complexes. *Chem. Eur. J.,* **2011,** *17* (6), 1872–1883.

(6) Klitzke, J. S.; Roisnel, T.; Kirillov, E.; Casagrande, O. d. L.; Carpentier, J.-F., Yttrium– and Aluminum–Bis(phenolate)pyridine Complexes: Catalysts and Model Compounds of the Intermediates for the Stereoselective Ring-Opening Polymerization of Racemic Lactide and *β*-Butyrolactone. *Organometallics*, **2014,** *33* (1), 309–321.

(7) Klitzke, J. S.; Roisnel, T.; Kirillov, E.; Casagrande, O. d. L.; Carpentier, J.-F., Discrete O-Lactate and *β*-Alkoxybutyrate Aluminum Pyridine–Bis(naphtholate) Complexes: Models for Mechanistic Investigations in the Ring-Opening Polymerization of Lactides and *β*-Lactones. *Organometallics,* **2014,** *33* (20), 5693–5707.

(8) Ligny, R.; Hänninen, M. M.; Guillaume, S. M.; Carpentier, J.-F., Steric vs. electronic stereocontrol in syndio- or iso-selective ROP of functional chiral β-lactones mediated by achiral yttrium-bisphenolate complexes. *Chem. Commun.,* **2018,** *54* (58), 8024–8031.

(9) Longo, J. M.; Sanford, M. J.; Coates, G. W., Ring-Opening Copolymerization of Epoxides and Cyclic Anhydrides with Discrete Metal Complexes: Structure–Property Relationships. *Chem. Rev.*, **2016,** *116* (24), 15167-15197.

(10) Paul, S.; Zhu, Y.; Romain, C.; Brooks, R.; Saini, P. K.; Williams, C. K., Ring-opening copolymerization (ROCOP): synthesis and properties of polyesters and polycarbonates. *Chem. Commun.* **2015,** *51* (30),, 6459-6479.

# *Chapter 7*

# *Experimental*

*Thesis writing always seems impossible until it's done...*

*~ Nattawut Yuntawattana ~*

## 7.1. General procedures

### 7.1.1. Material and methods

All chemical reagents were obtained from commercial sources (Aldrich, Fisher and Fluorochem) and used as received unless stated otherwise. All solvents used in the reactions were collected from an MBraun solvent purification system (SPS) and degassed three times by freeze-pump-thaw before use. Tetrahydrofuran was distilled over Na/benzophenone under nitrogen atmosphere and degassed three times before use. Benzene-$d_6$, toluene-$d_8$, and chloroform-$d_3$ were distilled over $CaH_2$ and stored over activated molecular sieves under nitrogen. THF-$d_8$ was degassed three times and stored over activated molecular sieves under nitrogen. Lactide monomers were recrystallised from hot anhydrous toluene and sublimed three times before use. $\varepsilon$-Caprolactone, $\varepsilon$-decalactone, $\delta$-hexalactone, and $\beta$-butyrolactone were distilled over $CaH_2$ and degassed three times before use. Cyclohexene oxide, propylene oxide, and vinyl cyclohexene oxide were first distilled over $CaH_2$, followed by the second distillation over NaH/MeI and degassed three times prior to use. Styrene oxide and *tert*-butyl glycidyl ether were distilled over $CaH_2$ and degassed before used. Phthalic anhydride was dissolved in anhydrous benzene and filtered to remove trace amount of phthalic acid. The phthalic anhydride monomer was then recrystallised in anhydrous chloroform and sublimed before use. Succinic anhydride and maleic anhydride were recrystallised from hot anhydrous benzene and sublimed before use. Glutaric anhydride and diglycolic anhydride were sublimed before used.

All reactions were carried out under dry nitrogen atmosphere using standard Schlenk techniques. The complexation reactions and polymerisations were performed in an MBraun glovebox ($O_2$ and water levels below 0.1 ppm) unless stated otherwise.

### 7.1.2. Measurements

**NMR spectroscopy**: NMR spectra were recorded on Bruker Avance III HD Nanobay 400 MHz, Bruker Avance III 500 MHz and Bruker Avance III 500 MHz (with $^{13}C$ cryoprobe) NMR spectrometers. The following abbreviations are used in the report of spectra: s, singlet; bs, broad singlet; d, doublet, dd: doublet of doublets; t, triplet; q, quartet; quin; quintet; sex, sextet; sept, septet; m, multiplet.

**Size exclusion chromatography**: The molar masses and dispersities of highly isotactic polylactides were recorded on an Agilent PL GPC-50 instrument, with HPLC grade $CHCl_3$ as the eluent at a flow rate of 1.0 mL $min^{-1}$ at 40 °C. In the case of other polyesters, SEC data were obtained using a Shimadzu LC-20AD instrument with HPLC grade THF as the eluent flowing at 1.0 mL $min^{-1}$ at 30 °C. Two Polymer Labs Mixed-D columns were used in series. Narrow dispersity polystyrene standards were used to calibrate the instruments. The polyesters were dissolved in HPLC grade THF or $CHCl_3$ and filtered prior to analysis (200 µm PTFE filter). In the case of polyethylene samples, chlorobenzene was used as an eluent and SEC were recorded at 160 °C. The molar mass of the resultant PLA was corrected by a factor of 0.58 and a correction factor of 0.56 was used to correct the molar mass of resultant PCL.[1] Other polymer samples, polymer molar masses were reported as determined by the analysis software.

**Differential scanning calorimetry**: DSC data were recorded on DSC3+ (Mettler Toledo, Ltd). A sealed empty crucible was used as a reference, and the DSC was calibrated using indium and zinc standards. For PLA sample, samples were heated from room temperature to 200 °C, at a rate of 5 °C $min^{-1}$, under $N_2$ flow (100 mL $min^{-1}$). Subsequently, the samples were cooled to –20 °C, at a rate of 5 °C $min^{-1}$, followed by a heating procedure from –20 °C to 200 °C, at a rate of 5 °C $min^{-1}$. Each sample was run for two heating−cooling cycles. The

glass transition ($T_g$) and melting ($T_m$) temperatures reported are taken from the second heating cycle.

For other polyester samples, samples were heated to 190 °C, at a heating rate of 10 °C $min^{-1}$, under $N_2$ flow (100 ml $min^{-1}$). Subsequently, the samples were cooled to –80 °C, at a rate of 10 °C $min^{-1}$, followed by a heating procedure from –80 °C to 190 °C, at a rate of 10 °C $min^{-1}$. Each sample was run for two heating–cooling cycles. The glass transition temperatures ($T_g$) reported are taken from the second heating cycle.

For polyethylene sample, samples were heated from room temperature to 200 °C, at a rate of 10 °C $min^{-1}$, under $N_2$ flow (100 mL $min^{-1}$). Subsequently, the samples were cooled to 25 °C, at a rate of 10 °C $min^{-1}$, followed by a heating procedure from 25 °C to 200 °C, at a rate of 10 °C $min^{-1}$. Each sample was run for three heating−cooling cycles. The melting temperatures ($T_m$) reported are taken from the third heating cycle

**Tensile measurements:** Dumbbell specimens were cut according to ISO 527-2, specimen type 5B with Zwick ZCP020 cutting press (length = 35 mm, gauge length = 10 mm, width = 2 mm). Monotonic uniaxial extension experiments were carried out on a Shimadzu EZ-LZ Universal testing instrument at an extension rate of 10 mm $min^{-1}$. An external camera was used to calculate the Young's Modulus, $E$ within the 0.025–0.25% strain region. 3 specimens were tested for each sample.

**Thermal Gravimetric Analysis (TGA):** Measured on Mettler-Toledo Ltd TGA/DSC 1 system. Powder polymer samples were heated from 30 to 500 °C at a rate of 5 °C $min^{-1}$, under $N_2$ flow (100 mL $min^{-1}$).

**X-ray diffraction**: Data collection was carried out with an Oxford Diffraction Supernova diffractometer using, Cu Kα (λ = 1.5417 Å) radiation. The resulting raw data was processed

using CrysAlisPro. All the X-ray single crystal structures were solved using SHELXT and Full-matrix least-squares refinements, based on $F^2$, were performed in SHELXL-14,[2] as incorporated in the WinGX package[3] by Dr. Christopher B. Durr, Dr. Kirsten E. Christensen, and Dr. Andreas Phanopoulos.

**Elemental analysis**: EA analyses (C,H,N) were performed by Mr Stephen Boyer at London Metropolitan University.

**High-resolution mass spectrometry**: HRMS were performed on an Agilent 7200 quadrupole time of flight (Q-ToF) instrument equipped with a direct insertion probe (Scientific Instrument Manufacturer (SIM) GmbH) using electron ionisation (EI) as an ionisation technique. Instrument control and data processing were performed using Agilent MassHunter software.

## 7.2. Typical polymerisation procedures for Chapter 3

### 7.2.1. Lactide polymerisation

All LA polymerisations (except low temperature polymerisations) were manipulated in a nitrogen filled glove box at room temperature. The polymerisation vessels were charged with LA (0.288 g, 2 mmol) and dissolved in THF (1.5 mL). A stock solution of catalyst (0.5 mL, 0.008 M) was then injected to a solution of monomer such that the [LA] = 1 M and [In] = 2 mM. Aliquots were withdrawn from the reaction mixture at predetermined times and quenched with hexane (~ 1 mL). The aliquots were then removed from the glovebox and left to evaporate. The crude products were analysed by $^1$H NMR and $^1$H{$^1$H} NMR (where applicable) spectroscopies and SEC. The tacticity ($P_i$ or $P_s$) was determined by the integration of the tetrad levels in $^1$H{$^1$H} NMR spectrum using Bernoulian statistics.[4] In some cases, the high conversion polymers were purified and analysed by DSC to determine their thermal properties.

In the case of low temperature LA polymerisations, the polymerisations were prepared in a nitrogen filled glove box by keeping the same concentrations of LA and catalyst as the ambient temperature polymerisations. The polymerisation ampoules were closed properly and removed from the glove box. The reaction vessels were then cooled to 278 K in a prepared cooling bath. Aliquots were then taken at specific times and analysed by $^{1}$H NMR spectroscopy and SEC.

### 7.2.2. $\varepsilon$-Caprolactone polymerisation.

In a glove box, a polymerisation vessel was loaded with catalyst (0.5 mL taken from a stock solution at 5 mM stock solution in THF, 2.5 $\mu$mol), THF (0.61 mL), and $\varepsilon$-CL (0.14 mL, 1.25 mmol). The reaction vessel was sealed and allowed to stir at room temperature. At predetermined reaction times, aliquots were withdrawn and quenched by addition of wet $CDCl_3$. The crude products were then characterised by NMR spectroscopy. Molar masses of the crude products were analysed using SEC in THF against narrow polystyrene standard.

### 7.2.3. $\beta$-Butyrolactone polymerisation.

In a glove box, a polymerisation vessel was charged with catalyst (0.55 mL taken from a stock solution at 5.45 mM stock solution in THF, 3 $\mu$mol) and $\beta$-BL (49 $\mu$L, 0.6 mmol). The reaction vessel was sealed and allowed to stir at room temperature. At predetermined reaction times, aliquots were withdrawn and quenched directly into wet $CDCl_3$. The crude products were then characterised by NMR analysis. Molar masses of the crude products were analysed using SEC in THF against narrow polystyrene standard.

### 7.2.4. $\varepsilon$-Decalactone polymerisation.

In a glove box, a polymerisation vessel was loaded with catalyst (0.5 mL taken from a stock solution at 6 mM stock solution in THF, 3 $\mu$mol) and $\varepsilon$-DL (105 $\mu$L, 0.6 mmol). The reaction vessel was sealed and allowed to stir at room temperature. At predetermined reaction times,

aliquots were withdrawn and quenched directly into wet $CDCl_3$. The crude products were then analysed by NMR. Molar masses of the crude products were determined using SEC in THF against narrow polystyrene standard.

### 7.2.5. δ-Hexalactone polymerisation.

In a glove box, a polymerisation vessel was charged with catalyst (0.11 mL taken from a stock solution at 22.7 mM stock solution in THF, 2.5 μmol) and δ-HL (0.14 mL, 1.25 mmol). The reaction vessel was sealed and allowed to stir at room temperature. At predetermined reaction times, aliquots were withdrawn and quenched directly into wet $CDCl_3$. The crude products were then characterised by NMR spectroscopy. Molar masses of the crude products were analysed using SEC in THF against narrow polystyrene standard.

### 7.2.6. Polymer purification

The crude polymer mixture was dissolved in $CHCl_3$ (~5 mL) and dropwise added into a solution of methanol (~40 mL) to precipitate the polymer. The mixture was filtered and the polymer was then dried. The polymer was dissolved in $CHCl_3$ (~5 mL) and rapidly filtered through a small pad of silica to remove a trace amount of indium complex. The crude polymer was precipitated in methanol 3 times. The solvent was removed in *vacuo* and the product dried both under vacuum and in a 40 °C vacuum oven.

### 7.2.7. Determination of stereocontrol degree of polymers

In the case of polylactide, the microstructure of a polymer was determined from its $^1H\{^1H\}$ NMR spectrum. The $^1H\{^1H\}$ NMR spectra exhibited up to five peaks which belong to each tetrad probability and reflect the stereochemistry along the polymer chain. Peak deconvolution was carried out using MestReNova v.11.0.2, and was used to calculate the tetrad integrals. The $P_i$ values, the probability of isotactic enchainment, were calculated from each of tetrad integrals using Bernoulian statistical equations as shown below.[4]

$$[iii] = P_i^2 + P_iP_s/2 \quad \textbf{(1)}$$

$$[iis] = P_iP_s/2 \quad \textbf{(2)}$$

$$[sii] = P_iP_s/2 \quad \textbf{(3)}$$

$$[sis] = P_s^2/2 \quad \textbf{(4)}$$

$$[isi] = (P_s^2 + P_iP_s)/2 \quad \textbf{(5)}$$

## 7.3. Typical polymerisation procedures for Chapter 4

### 7.3.1. Polymerisation procedure for ROCOP of epoxide and cyclic anhydride.

In a glove box, a pre-dried polymerisation vessel was charged with anhydride (0.25 mmol) and catalyst (2.5 mM). Epoxide (0.31 mmol) and toluene were then added to a reaction mixture such that [anhydride] = 5 M, [epoxide] = 6.25 M and total reaction volume is 0.5 mL. The polymerisation vessel was sealed with PVC tape, removed from the glove box, and heated on the preheated aluminium block at 80 °C. Aliquots were withdrawn from the reaction mixture and quenched with wet $CDCl_3$. The crude product was analysed by $^1$H NMR spectroscopy to determine the conversion and selectivity of polyester formation. Molar masses were determined by SEC in THF at a flow rate of 1 ml min$^{-1}$ against polystyrene standards.

### 7.3.2. Polymerisation procedure for *in situ* IR study.

In a glove box, a pre-dried Schlenk tube was charged with phthalic anhydride (1.33 g, 9.0 mmol), cyclohexene oxide (1.14 mL, 11.55 mmol) and toluene 1.36 mL. A stock solution of titanium catalyst in toluene (0.18 M, 0.50 mL) was then injected to the reaction mixture such that [anhydride] = 3 M, [epoxide] = 3.75 M and the total volume of reaction mixture of 3 mL. The Schlenk tube was then sealed, removed from the glove box and heated in a preheated oil bath at 80 °C. The IR signal of the polyester (at 1727 cm$^{-1}$) was recorded at appropriate time intervals. Once the polymerisation reached full consumption of phthalic anhydride, the reaction mixture was quenched using wet $CDCl_3$. The conversion and selectivity of polyester formation were analysed by $^1$H NMR spectroscopy.

### 7.3.3. Ethylene polymerisation using sMAO as a co-catalyst procedure.

The pre-activated titanium catalyst (10.0 mg), tri-*iso*-butyl aluminium scavenger (150 mg), and hexane (50 mL) were added to a high-pressure Rotaflo ampoule. Ethylene gas was fed into the polymerisation vessel at 2 bar over-pressure at 80 °C. The polymerisation was carried out for 1 h and stopped by removing the ampoule from the heating bath and degassing under vacuum. The polymer was isolated and washed with hexane, three times, before drying in a vacuum oven at 40 °C for 48 h.

### 7.3.4. Ethylene polymerisation procedure by cationic complex.

In a glove box, a high-pressure Rotaflo ampoule, equipped with a stir bar was charged with a titanium or zirconium catalyst (0.010 mmol) and toluene (20 mL). A solution of tri-*iso*-butyl aluminium (0.10 mL, 0.40 mmol) in toluene (10 mL) was then dropwise added. The reaction mixture was allowed to stir at room temperature for 30 min. Trityl tetrakis(pentafluoro)borate (10.15 mg, 0.011 mmol) and toluene (20 mL) were then added. The ampoule was sealed and removed from the glovebox. Ethylene gas was fed into the reaction vessel at 2 bar over-pressure at 40 °C and allowed to react for 1 h. The reaction was stopped by removing from heating bath and degassing. The polymer was isolated and washed with hexane before drying in a vacuum oven at 40 °C for 48 h.

### 7.3.5. Polymer purification

All resultant polyesters were purified prior to DSC analysis. The crude polyester sample was dissolved in $CH_2Cl_2$ (~ 2 mL) and dropwise added into a hexane solution (~ 30 mL) to precipitate the polymer. The precipitation was then repeated three times before a pure polymer sample was isolated. The sample was then dried using a vacuum oven at 40 °C for 48 h.

In the case of polyethylene, after the polymer was isolated from reaction mixture, polyethylene was washed with a hexane solution three times and then dried in a vacuum oven at 40 °C for 48 h.

### 7.4. Typical polymerisation procedures for Chapter 5.

#### 7.4.1. Polymerisation procedure for ROCOP of PO and cyclic anhydride.

The polymerisation vessels were charged with cyclic anhydride (7.15 mmol) and $Sn(OMe)_2$ (12.90 mg, 0.071 mmol). BnOH (14.75 μL, 0.14 mmol) was then added to a reaction mixture followed by propylene oxide (5 mL, 71.5 mmol) such that the [anhydride] = 1.43 M and [Sn] = 14.27 mM. The polymerisation vessel was sealed with PVC tape and removed from the glovebox and heated at 45 °C on a preheated aluminium block. Aliquots were withdrawn from the reaction mixture at desired times and quenched with wet $CDCl_3$ (~ 0.6 mL). Monomer conversion and the percentage ester linkages were analysed by $^1$H NMR spectroscopy. Polymer molar masses were analysed by SEC.

#### 7.4.2. Polymerisation procedure for ROP of *L*-LA or *ε*-CL.

A pre-died polymerisation vessel, equipped with a stir bar was charged with *L*-LA (1.03 g, 7.15 mmol) or *ε*-CL (0.79 mL, 7.15 mmol) and $Sn(OMe)_2$ (12.90 mg, 0.071 mmol). BnOH (14.75 μL, 0.14 mmol) was then added to a reaction mixture followed by propylene oxide (5 mL, 71.5 mmol). The polymerisation vessel was sealed with PVC tape and removed from the glovebox and heated at 45 °C on a preheated aluminium block. Aliquots were withdrawn from the reaction mixture at desired times and quenched with wet $CDCl_3$ (~ 0.6 mL). Monomer conversion and the percentage ester linkages were determined by $^1$H NMR spectroscopy. Polymer molar masses were analysed by SEC.

### 7.4.3. One-pot polymerisation of PO, MA, and *L*-LA procedure.

A pre-dried 22 mL glass vial with a PTFE-lined thermoset cap, equipped with a stir bar was charged with MA (0.98 g, 9.99 mmol), *L*-LA (1.44 g, 9.99 mmol) and $Sn(OMe)_2$ (18.06 mg, 0.10 mmol). BnOH (20.67 μL, 0.20 mmol) and PO (7 mL, 99.91 mmol) were then added to the reaction mixture followed by the addition of the internal standard mesitylene (0.69 mL, 5.0 mmol). The reaction vessel was sealed with PVC tape, removed from the glovebox and heated to 45 °C in a preheated silicone bath. Aliquots were withdrawn from the reaction at desired times and quenched with wet $CDCl_3$. The crude product was then analysed by $^1H$ NMR spectroscopy and the polymer molar mass was determined by SEC.

### 7.4.4. PO, MA, *L*-LA one-pot polymerisation procedure: *in situ* $^1H$ NMR study.

A pre-dried J. Young valve NMR tube was charged with MA (0.07 g, 0.71 mmol), *L*-LA (0.10 g, 0.71 mmol) and $Sn(OMe)_2$ (4.30 mg, 0.02 mmol). BnOH (4.92 μL, 0.05 mmol) and the internal standard mesitylene (49.6 μL, 0.36 mmol) were then added using a Hamilton glass syringe. PO (0.50 mL, 7.14 mmol) and $CDCl_3$ (2.29 mL) were added to the reaction mixture such that [MA] = [LA] = 0.25 M and [PO] = 2.5 M). The reaction was then heated at 45 °C and NMR signals were recorded on the Bruker Avance III HD Nanobay 400 MHz NMR instrument. The collected data was then analysed and the conversion of individual monomers were calculated against the internal standard.

### 7.4.5. One-pot polymerisation of PO, MA, and ε-CL procedure.

A pre-dried 22 mL glass vial with PTFE-lined thermoset cap was charged with MA (0.98 g, 9.99 mmol), ε-CL (1.11 mL, 9.99 mmol), and $Sn(OMe)_2$ (18.06 mg, 0.10 mmol). BnOH (20.67 μL, 0.20 mmol) and PO (7 mL, 99.91 mmol) were then added to the reaction mixture followed by the addition of the internal standard mesitylene (0.69 mL, 4.996 mmol). The reaction vessel was sealed with PVC tape, removed from the glovebox and heated to 45 °C in a preheated silicone bath. Aliquots were withdrawn from the reaction at desired times and

quenched with wet $CDCl_3$. The crude product was then analysed by $^1H$ NMR spectroscopy and the polymer molar mass was determined by SEC.

### 7.4.6. Polymer purification

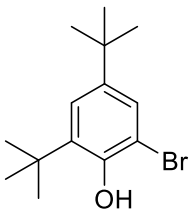
The crude polymer mixture was dissolved in $CH_2Cl_2$ and dropwise added into a hexane solution to precipitate the polymer. The mixture was filtered and the polymer was then dried. The polymer was dissolved in $CH_2Cl_2$ and rapidly filtered through a small pad of silica. The crude polymer was precipitated in hexane three times. The polymer was then dried in a vacuum oven at 40 °C for 48 h.

### 7.4.7. Preparation of polymer film for tensile testing.

For all polymer films the total amount of polymer used was 1.54 g. The polymer was dissolved in $CHCl_3$ (52 mL) and allowed to stir at room temperature for 4 h or until all polymer was fully dissolved. The polymer solution was then transferred into a PTFE mould. The PTFE mould was covered by aluminium foil and left at room temperature for 16–18 h for solvent to evaporate. The polymer film was then removed from the mould and dried in a vacuum oven at 40 °C for 72–96 h. The remaining solvent residue in materials was checked by $^1H$ NMR spectroscopy and thermogravimetric analysis before the tensile measurement was conducted.

## 7.5. Typical synthetic procedures for starting materials for ligand synthesis

### 7.5.1. Synthesis of 2-bromo-4,6-di-*tert*-butylphenol [5]




To a solution of 2,4-di-*tert*-butylphenol (20.00 g, 96.93 mmol) in acetonitrile (300 mL) at 0 °C was slowly added *N*-bromosuccinimide (17.25 g, 96.93 mmol), affording a clear yellow solution. The reaction mixture was then warmed up to ambient temperature and allowed to stir overnight. The reaction was washed with a 1 M solution of $Na_2SO_3$ (10 mL) after which the

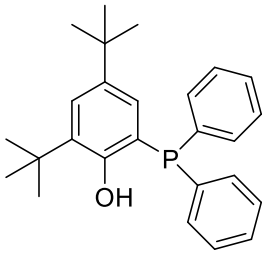
solvent was removed under vacuum to give a pale-orange solid as the product in good yield (21.84 g, 79 %).

$^{1}$H NMR (400 MHz, $CDCl_3$): δ 7.32 (1H, d, $^{4}J_{HH}$ = 2.3 Hz, Ar***H***), 7.24 (1H, d, $^{4}J_{HH}$ = 2.3 Hz, Ar***H***), 5.65 (1H, s, O***H***), 1.41 (9H, s, Ar***H***), 1.29 (9H, s, Ar***H***).

$^{13}$C{$^{1}$H} NMR (125 MHz, $CDCl_3$): δ 148.0 (Ar***C***Br), 143.7 (Ar***C***O), 136.7 (Ar***C***), 126.2 (Ar***C***H), 123.7 (Ar***C***H), 111.9 (Ar***C***), 35.6 (***C***$(CH_3)_3$), 34.4 (***C***$(CH_3)_3$), 31.4 (C(***C***$H_3)_3$), 29.4 (C(***C***$H_3)_3$).

Anal. Calc. ($C_{14}H_{21}BrO$): C, 58.95; H, 7.42 Found C, 58.87; H, 7.54

### 7.5.2. Synthesis of 2-(diphenylphosphaneyl)-4,6-di-*tert*-butyl-phenol (S2) [6]




Under nitrogen atmosphere, to a stirred solution of 2-bromo-4,6-di-*tert*-butylphenol (4.00 g, 14.02 mmol) in diethyl ether (50 mL) at –78 °C was slowly added $^{n}$BuLi (1.6 M in hexane, 18.41 mL, 29.45 mmol), affording a pale-yellow suspension. The reaction mixture was allowed to stir at ambient temperature for 1 hour, generating a clear pale-yellow solution. The cold bath was then reapplied. To the reaction mixture was slowly added chlorodiphenylphosphine (2.59 mL, 14.02 mmol). The reaction mixture was warmed to room temperature and allowed to stir overnight during which a white suspension was formed. The white suspension was then washed with a 1 M solution of $KH_2PO_4$ (120 mL). The organic layer was then dried with $MgSO_4$ and the solvent was removed under vacuum to isolate the product in moderate yield (7.44 g, 45 %).

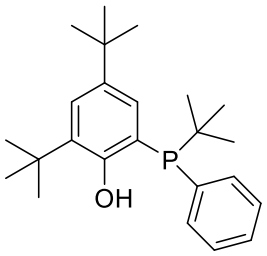
$^{1}$H NMR (400 MHz, $CDCl_3$): δ 7.31-7.22 (10H, m, Ar***H***), 6.80 (1H, dd, $^{3}J_{HH}$ = 5.8 Hz, $^{4}J_{HH}$ = 2.4 Hz, Ar***H***), 6.58 (1H, d, $^{3}J_{PH}$ = 10.0 Hz, Ar***H***), 1.34 (9H, s, C***H***$_3$), 1.07 (9H, s, C***H***$_3$).

$^{13}C\{^{1}H\}$ NMR (125 MHz, $CDCl_3$): δ 155.9 (d, $^{2}J_{PC}$ = 19.9 Hz, Ar***C***O), 142.2 (d, $^{3}J_{PC}$ = 2.8 Hz, Ar***C***), 135.4 (d, $^{3}J_{PC}$ = 3.8 Hz, Ar***C***), 135.2 (d, $^{1}J_{PC}$ = 1.8 Hz, Ar***C***), 133.4 (Ar***C***H), 133.2 (Ar***C***H), 129.2 (Ar***C***H), 128.8 (Ar***C***H), 128.6 (d, $^{1}J_{PC}$ = 3.8 Hz, Ar***C***), 128.5 (Ar***C***H), 126.2 (Ar***C***H), 119.9 (Ar***C***H), 35.1 (***C***$(CH_3)_3$), 34.4 (***C***$(CH_3)_3$), 31.4 (C(***C***$H_3)_3$), 29.6 (C(***C***$H_3)_3$).

$^{31}P\{^{1}H\}$ NMR (162 MHz, $CDCl_3$): δ –30.0 (s, ***P***)

Anal. Calc. ($C_{26}H_{31}OP$): C, 79.97; H, 8.00 found C, 80.11; H, 8.11

### 7.5.3. Synthesis of 2-(*tert*-butyl-phenylphosphaneyl)-4,6-di-*tert*-butyl-phenol (S3)




Compound **S3** was synthesised according to the synthesis of **S2**. Chloro(*tert*-butyl)phenylphosphine (0.99 mL, 3.50 mmol) was used instead of chlorodiphenylphosphine. The product was obtained as colourless crystals in moderate (0.91g, 47 %).

$^{1}H$ NMR (400 MHz, $CDCl_3$): δ 7.61-7.54 (2H, m, Ar***H***), 7.37-7.28 (5H, m, Ar***H***), 1.41 (9H, s, C(C***H***$_3)_3$), 1.28 (9H, s, C(C***H***$_3)_3$), 1.19 (9H, d, $^{3}J_{PH}$ = 13.7 Hz, C(C***H***$_3)_3$).

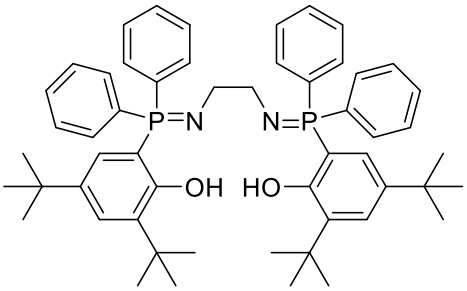
$^{13}C\{^{1}H\}$ NMR (125 MHz, $CDCl_3$): δ 157.3 (d, $^{2}J_{PC}$ = 20.7 Hz, Ar***C***O), 140.8 (Ar***C***), 135.1 (d, $^{1}J_{PC}$ = 9.1 Hz, Ar***C***), 134.8 (Ar***C***), 133.6 (d, $^{2}J_{PC}$ = 16.9 Hz, Ar***C***H), 129.2 (Ar***C***H), 128.2 (Ar***C***), 128.1 (d, $^{2}J_{PC}$ = 8.0 Hz, Ar***C***H), 125.9 (Ar***C***H), 118.3 (Ar***C***H), 35.1 (***C***$(CH_3)_3$), 34.3 (***C***$(CH_3)_3$), 31.6 (C(***C***$H_3)_3$), 31.4 (d, $^{1}J_{PC}$ = 7.8 Hz, ***C***$(CH_3)_3$), 29.5 (C(***C***$H_3)_3$), 28.6 (d, $^{2}J_{PC}$ = 14.4 Hz, C(***C***$H_3)_3$).

$^{31}P\{^{1}H\}$ NMR (162 MHz, $CDCl_3$): δ –19.2 (s, ***P***).

HRMS (EI) Calc. ($C_{24}H_{35}OP$): m/z: 370.2420 Found: m/z 370.2414

## 7.6. Synthesis of phosphasalen, and salen ligands

### 7.6.1. Synthesis of phosphasalen ligand $^{P\text{-}salen}L^1H_2$ [7]




Ligand $^{P\text{-}salen}L^1H_2$ was prepared following the literature method.[7] Under a nitrogen atmosphere, liquid bromine (0.26 mL, 5.12 mmol) was slowly added to a stirred solution of **S1** (2.00 g, 5.12 mmol) in dichloromethane (60 mL) at –78 °C, affording a clear yellow solution. The reaction mixture was then allowed to stir at room temperature for 2 hours. The reaction mixture was cooled down again. Tributylamine (0.61 mL, 2.56 mmol) and ethylenediamine (0.17 mL, 2.56 mmol) were then slowly added to the reaction mixture, affording a pale-yellow solution. The reaction mixture was allowed to stir at ambient temperature overnight during which a pale-yellow suspension was formed. The reaction mixture was then filtered and the filtrate dried under vacuum to give a yellow oil. The crude oil was vigorously stirred in THF (10 mL) for 20 minutes during which a white solid formed. The white solid was then filtered and the brominium salt removed by $Al_2O_3$ column chromatography (DCM:EtOH = 40:1). The organic solvent was removed under vacuum to give a pale-yellow powder as the product in low yield (0.46 g, 11 %).

$^1$H NMR (400 MHz, $CDCl_3$): δ 7.66-7.50 (12H, m, Ar***H***), 7.45-7.37 (8H, m, Ar***H***), 7.36 (2H, d, $^4J_{HH}$ = 2.6 Hz, Ar***H***), 6.21 (2H, dd, $^4J_{HH}$ = 2.6 Hz, $^3J_{PH}$ = 15.7 Hz, Ar***H***), 5.29 (2H, s, O***H***), 3.21-3.10 (4H, m, C***H***$_2$), 1.39 (18H, s, C***H***$_3$), 1.07 (18H, s, C***H***$_3$).

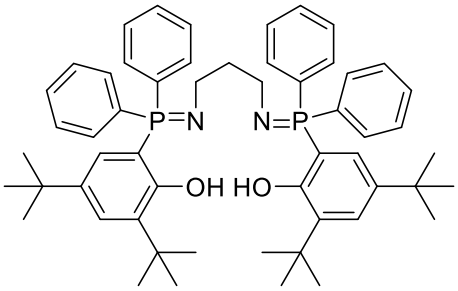
$^{13}$C{$^1$H} NMR (125 MHz, $CDCl_3$): δ 173.5 (Ar***C***O), 140.2 (d, $^3J_{PC}$ = 9.4 Hz, Ar***C***), 133.4 (d, $^1J_{PC}$ = 10.3 Hz, Ar***C***), 132.7 (d, $^3J_{PC}$ = 2.6 Hz, Ar***C***), 129.9 (Ar***C***H), 129.0 (d, $^3J_{PC}$ = 12.2 Hz, Ar***C***H), 126.4 (Ar***C***H), 126.2 (d, $^2J_{PC}$ = 14.4 Hz, Ar***C***H), 125.6 (Ar***C***H), 101.3 (d, $^1J_{PC}$

= 112.5 Hz, Ar***C***), 44.0 (dd. $^{2}J_{PC}$ = 10.3 Hz, $^{3}J_{PC}$ = 3.5 Hz, ***C***$H_2$), 35.3 (d, $^{4}J_{PC}$ = 2.0 Hz, ***C***$(CH_3)_3$), 33.9 (d, $^{4}J_{PC}$ = 1.1 Hz, ***C***$(CH_3)_3$), 31.5 (C(***C***$H_3)_3$), 29.3 (C(***C***$H_3)_3$).

$^{31}P\{^{1}H\}$ NMR (162 MHz, $CDCl_3$): δ 41.8 (s, ***P***)

Anal. Calc. ($C_{54}H_{66}N_2O_2P_2$): C, 77.48; H, 7.95; N, 3.35 found C, 77.35; H, 8.01; N, 3.42

### 7.6.2. Synthesis of phosphasalen ligand $^{P\text{-}salen}L^{2}H_2$ [8]




Ligand $^{P\text{-}salen}L^{2}H_2$ was synthesised according to the procedure used in preparation of $^{P\text{-}salen}L^{1}H_2$. 1,3-Diaminopropane (0.21 mL, 2.56 mmol) was used instead of ethylenediamine. The product was isolated as a yellow solid after $Al_2O_3$ column chromatography (DCM:EtOH = 40:1) in reasonable yield (0.98 g, 22 %)

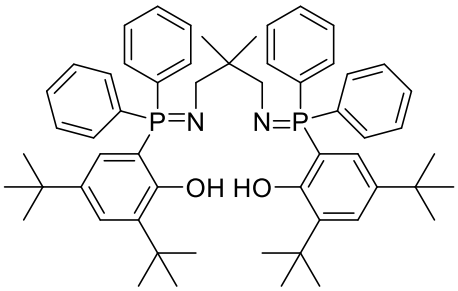
$^{1}H$ NMR (400 MHz, $CDCl_3$): δ 7.69-7.48 (12H, m, Ar***H***), 7.48-7.31 (10H, m, Ar***H***), 6.23 (2H, d, $^{4}J_{HH}$ = 16.2 Hz, Ar***H***), 2.96 (4H, bs, C***H***$_2$), 1.75 (2H, bs, C***H***$_2$), 1.41 (18H, s, C(C***H***$_3)_3$), 1.07 (18H, s, C(C***H***$_3)_3$).

$^{13}C\{^{1}H\}$ NMR (125 MHz, $CDCl_3$): δ 173.6 (Ar***C***O), 140.4 (d, $^{3}J_{PC}$ = 9.6 Hz, Ar***C***), 133.5 (d, $^{1}J_{PC}$ = 10.3 Hz, Ar***C***), 132.9 (d, $^{3}J_{PC}$ = 2.5 Hz, Ar***C***), 129.7 (Ar***C***H), 129.0 (d, $^{3}J_{PC}$ = 12.2 Hz, Ar***C***H), 125.8 (Ar***C***H), 125.6 (d, $^{2}J_{PC}$ = 14.2 Hz, Ar***C***H), 125.0 (Ar***C***H), 100.4 (d, $^{1}J_{PC}$ = 113.5 Hz, Ar***C***), 40.2 (d, $^{2/3}J_{PC}$ = 4.4 Hz, ***C***$H_2$), 35.4 (d, $^{4}J_{PC}$ = 1.9 Hz, ***C***$(CH_3)_3$), 33.9 (d, $^{4}J_{PC}$ = 1.2 Hz, ***C***$(CH_3)_3$), 31.5 (C(***C***$H)_3)_3$), 29.3 (C(***C***$H_3)_3$).

$^{31}P\{^{1}H\}$ NMR (162 MHz, $CDCl_3$): δ 41.8 (s, ***P***)

Anal. Calc. ($C_{55}H_{68}N_2O_2P_2$): C, 77.62; H, 8.05; N, 3.19 Found C, 77.70; H, 8.14; N, 3.22

### 7.6.3. Synthesis of phosphasalen ligand $^{P\text{-}salen}L^3H_2$ [8]




Ligand $^{P\text{-}salen}L^3H_2$ was synthesised according to the procedure used in preparation of $^{P\text{-}salen}L^1H_2$. 2,2-Dimethyl-1,3-propanediamine (0.31 mL, 2.56 mmol) was used instead of ethylenediamine. The product was isolated as a yellow solid after $Al_2O_3$ column chromatography (DCM:EtOH = 40:1) in low yield (0.64 g, 14 %).

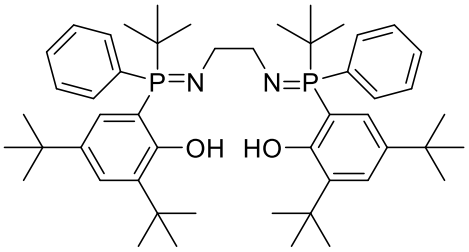
$^1$H NMR (400 MHz, $CDCl_3$): δ 7.69-7.60 (8H, m, Ar***H***), 7.60-7.52 (4H, m, Ar***H***), 7.45-7.35 (10H, m, Ar***H***), 6.25 (2H, dd, $^4J_{HH}$ = 2.6 Hz, $^3J_{PH}$ = 16.1 Hz, Ar***H***), 5.30 (2H, s, O***H***), 2.78 (4H, d, $^2J_{HH}$ = 6.8 Hz, C***H***$_2$), 1.41 (18H, s, C(C***H***$_3$)$_3$), 1.06 (18H, s, C(C***H***$_3$)$_3$), 0.91 (6H, s, C***H***$_3$).

$^{13}$C{$^1$H} NMR (125 MHz, $CDCl_3$): δ 173.0 (d, $^2J_{PC}$ = 4.2 Hz, Ar***C***O), 140.3 (d, $^3J_{PC}$ = 9.3 Hz, Ar***C***), 133.7 (d, $^1J_{PC}$ = 10.0 Hz, Ar***C***), 132.9 (d, $^3J_{PC}$ = 2.6 Hz, Ar***C***), 129.5 (Ar***C***H), 129.0 (d, $^3J_{PC}$ = 11.9 Hz, Ar***C***H), 125.8 (Ar***C***H), 125.6 (d, $^2J_{PC}$ = 13.9 Hz, Ar***C***H), 125.1 (Ar***C***H), 100.8 (d, $^1J_{PC}$ = 113.4 Hz, Ar***C***), 51.1 (d, $^2J_{PC}$ = 5.8 Hz, ***C***H$_2$), 37.2 (t, $^3J_{PC}$ = 12.3 Hz, (***C***(CH$_3$)$_2$), 35.4 (d, $^4J_{PC}$ = 2.0 Hz, ***C***(CH$_3$)$_3$), 33.9 (d, $^4J_{PC}$ = 1.1 Hz, ***C***(CH$_3$)$_3$), 31.5 (C(***C***H$_3$)$_3$), 29.4 (C(***C***H$_3$)$_3$), 23.6 (C(***C***H$_3$)$_2$).

$^{31}$P{$^1$H} NMR (162 MHz, $CDCl_3$): δ 41.6 (s, ***P***)

Anal. Calc. ($C_{57}H_{72}N_2O_2P_2$): C, 77.87; H, 8.26; N, 3.19 Found C, 77.84; H, 8.36; N, 3.25

### 7.6.4. Synthesis of phosphasalen ligand $^{P\text{-}salen}L^4H_2$




Ligand $^{P\text{-}salen}L^4H_2$ was synthesised according to the procedure used in preparation of $^{P\text{-}salen}L^1H_2$. **S3** (1.00 g, 2.70 mmol) was used instead of **S2**. After $Al_2O_3$ column chromatography, a crude pink oil was isolated. The crude oil product was then recrystallised from pentane to give pale-pink crystals as the product in low yield (0.22 g, 10%).

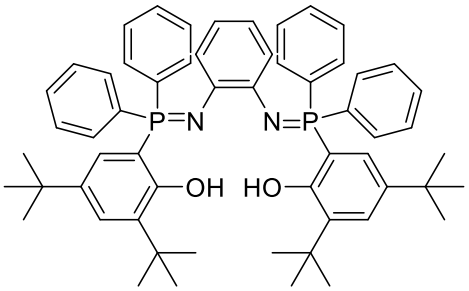
$^1$H NMR (400 MHz, $CDCl_3$): δ 7.97-7.88 (4H, m, Ar***H***), 7.57-7.50 (2H, m, Ar***H***), 7.48-7.40 (4H, m, Ar***H***), 7.33 (2H, d, $^4J_{HH}$ = 2.6 Hz, Ar***H***), 6.80 (2H, dd, $^4J_{HH}$ = 2.6 Hz, $^3J_{PH}$ = 13.7 Hz, Ar***H***), 3.08-2.83 (4H, m, C***H***$_2$), 1.42 (9H, s, C(C***H***$_3$)$_3$), 1.30 (9H, d, $^3J_{PH}$= 15.5 Hz, C(C***H***$_3$)$_3$), 1.16 (9H, s, C(C***H***$_3$)$_3$).

$^{13}$C{$^1$H} NMR (125 MHz, $CDCl_3$): δ 173.8 (weak, Ar***C***O), 140.6 (d, $^1J_{PC}$ = 8.4 Hz, Ar***C***), 133.4 (d, $^3J_{PC}$ = 8.6 Hz, Ar***C***H), 131.8 (d, $^4J_{PC}$ = 2.8 Hz, Ar***C***H), 130.7 (d, $^1J_{PC}$ = 11.0 Hz, Ar***C***), 128.9 (Ar***C***H), 128.2 (d, $^2J_{PC}$ = 11.4 Hz, Ar***C***H), 127.4 (d, $^2J_{PC}$ = 12.9 Hz, Ar***C***H), 125.8 (Ar***C***), 124.8 (Ar***C***), 43.2 (dd, $^3J_{PC}$ = 2.6 Hz, $^2J_{PC}$ = 8.0 Hz, ***C***H$_2$), 36.1 (***C***(CH$_3$)$_3$), 35.4 (d, $^1J_{PC}$ = 27.2 Hz, ***C***(CH$_3$)$_3$), 33.9 (***C***(CH$_3$)$_3$), 31.6 (C(***C***H$_3$)$_3$), 29.2 (C(***C***H$_3$)$_3$), 26.7 (C(***C***H$_3$)$_3$).

$^{31}$P{$^1$H} NMR (162 MHz, $CDCl_3$): δ 55.9 (s, ***P***)

Anal. Calc. ($C_{50}H_{74}N_2O_2P_2$): C, 75.34; H, 9.36; N, 3.51 Found C, 75.42; H, 9.50; N, 3.54

### 7.6.5. Synthesis of phosphasalen ligand $^{P\text{-}salen}L^5H_2$ [8]




Ligand $^{P\text{-}salen}L^5H_2$ was synthesised according to the procedure used in preparation of $^{P\text{-}salen}L^1H_2$. *o*-phenylenediamine (0.21 g, 1.92 mmol) and 1,4-diazabicyclo[2.2.2]octane (0.22 g, 1.92 mmol) were used instead of ethylendiamine and tributylamine, respectively. After the reaction mixture was allowed to stir at ambient temperature overnight, the solution mixture was filtered and organic solvent was removed under vacuum to give a pale-yellow crude oil. The crude oil was vigorously stirred in THF (30 mL) to remove trace amount of 1,4-diazabicyclo[2.2.2]octane. The reaction mixture was then filtered and the filtrate dried in *vacuo*. The crude oil product was then vigorously stirred in $Et_2O$ (80 mL) during which a white powder product was formed. The product was isolated as a yellow solid after purification by $Al_2O_3$ column chromatography (DCM:EtOH = 40:1) in reasonable yield (0.4 g, 24 %)

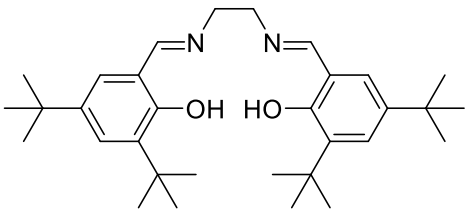
$^1$H NMR (400 MHz, $CDCl_3$): δ 7.92-7.77 (8H, m, Ar***H***), 7.55-7.46 (4H, m, Ar***H***), 7.45-7.36 (8H, m, Ar***H***), 7.30 (2H, $^4J_{HH}$ = 2.4 Hz, Ar***H***), 6.84 (dd, $^3J_{PH}$ = 16.3 Hz, $^4J_{HH}$ = 2.4 Hz, Ar***H***), 6.48-6.40 (2H, m, Ar***H***), 6.40-6.32 (2H, m, Ar***H***), 1.15 (18H, s, C(C***H***$_3$)$_3$), 1.12 (18H, s, C(C***H***$_3$)$_3$).

$^{13}$C{$^1$H} NMR (125 MHz, $CDCl_3$): δ 163.8 (Ar***C***O), 141.7 (d, $^2J_{PC}$ = 14.8 Hz, Ar***C***), 138.1 (d, $^1J_{PC}$ = 9.7 Hz, Ar***C***), 133.2 (d, $^2J_{PC}$ = 10.1 Hz, Ar***C***H), 131.8 (d, $^4J_{PC}$ = 2.5 Hz, Ar***C***H), 131.5 (Ar***C***), 130.8 (Ar***C***), 128.5 (d, $^3J_{PC}$ = 11.4 Hz, Ar***C***H), 128.0 (Ar***C***H), 125.9 (d, $^2J_{PC}$ = 13.4 Hz, Ar***C***), 120.8 (d, $^3J_{PC}$ = 8.7 Hz, Ar***C***H), 119.2 (Ar***C***H), 105.9 (d, $^2J_{PC}$ = 127.1 Hz, Ar***C***H), 35.2 (d, $^4J_{PC}$ = 1.4 Hz, ***C***(CH$_3$)$_3$), 34.2 (***C***(CH$_3$)$_3$), 31.5 (C(***C***H$_3$)$_3$), 29.4 (C(***C***H$_3$)$_3$).

$^{31}$P{$^1$H} NMR (162 MHz, $CDCl_3$): δ 19.2 (s, ***P***)

Anal. Calc. ($C_{55}H_{68}N_2O_2P_2$): C, 78.70; H, 7.52; N, 3.16 Found C, 78.61; H, 7.77; N, 3.25

### 7.6.6. Synthesis of salen ligand $^{salen}L^1H_2$ [9]

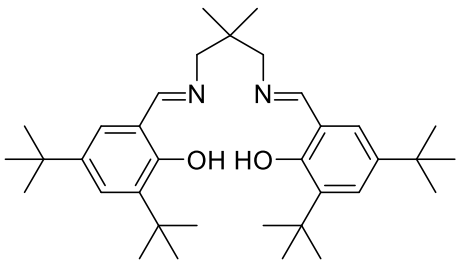



To a stirred solution of 3,5-di-*tert*-butyl-2-hydroxybenzaldehyde (2.0 g, 8.53 mmol) at 70 °C in ethanol (40 mL) was dropwise added a solution of ethylenediamine (0.28 mL, 4.26 mmol) in ethanol (10 mL). A catalytic amount of formic acid was then added. The solution mixture was allowed to stir at 70 °C for 6 h during the time which yellow crystals formed as the product in almost quantitative yield (1.89 g, 90 %).

$^1$H NMR (400 MHz, $CDCl_3$): δ 13.58 (2H, bs, O***H***), 8.40 (2H, s, NC***H***), 7.37 (2H, d, $^4J_{HH}$ = 2.3 Hz, Ar***H***), 7.08 (2H, d, $^4J_{HH}$ = 2.4 Hz, Ar***H***), 3.93 (4H, s, C***H***$_2$), 1.43 (18H, s, C(C***H***$_3$)$_3$), 1.28 (18H, s, C(C***H***$_3$)$_3$).

$^{13}$C{$^1$H} NMR (125 MHz, $CDCl_3$): δ 167.7 (N***C***H), 158.2 (Ar***C***O), 140.2 (Ar***C***), 136.7 (Ar***C***), 127.2 (Ar***C***H), 126.2 (Ar***C***H), 117.9 (Ar***C***), 59.8 (***C***H$_2$), 35.2 (***C***(CH$_3$)$_3$), 34.2 (***C***(CH$_3$)$_3$), 31.6 (C(***C***H$_3$)$_3$), 29.6 (C(***C***H$_3$)$_3$).

### 7.6.7. Synthesis of salen ligand $^{salen}L^2H_2$

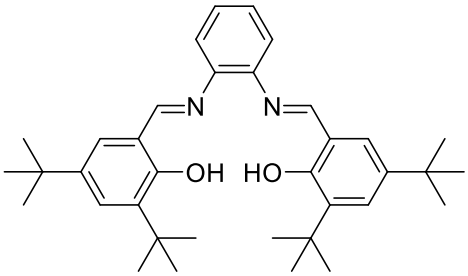



Ligand $^{salen}L^2H_2$ was synthesised according to the procedure used in $^{salen}L^1H_2$ preparation. 2,2-di-methyl-1,3-propanediamine (0.51 mL, 4.26 mmol) was used instead of ethylenediamine. The product was isolated as yellow crystals in almost quantitative yield (2.09 g, 92 %).

$^{1}$H NMR (400 MHz, $CDCl_3$): δ 13.82 (2H, bs, O***H***), 8.37 (2H, s, NC***H***), 7.39 (2H, d, $^{4}J_{HH}$ = 2.3 Hz, Ar***H***), 7.11 (2H, d, $^{4}J_{HH}$ = 2.3 Hz, Ar***H***), 3.48 (4H, s, C***H***$_2$), 1.47 (18H, s, C(C***H***$_3$)$_3$), 1.31 (18h, s, C(C***H***$_3$)$_3$), 1.10 (6H, s, C(C***H***$_3$)$_2$).

$^{13}$C{$^{1}$H} NMR (125 MHz, $CDCl_3$): δ 166.9 (N***C***H), 158.3 (Ar***C***O), 140.1 (Ar***C***), 136.8 (Ar***C***), 127.0 (Ar***C***H), 126.1 (Ar***C***H), 118.0 (Ar***C***), 68.4 (***C***H$_2$), 36.5 (***C***(CH$_3$)$_2$), 35.2 (***C***(CH$_3$)$_3$), 34.3 (***C***(CH$_3$)$_3$), 31.6 (C(***C***H$_3$)$_3$), 29.6 (C(***C***H$_3$)$_3$), 24.7 (C(***C***H$_3$)$_2$).

### 7.6.8. Synthesis of salen ligand $^{salen}$L$^{3}$H$_2$




Ligand $^{salen}$**L$^{3}$H$_2$** was synthesised according to the procedure used in $^{salen}$**L$^{1}$H$_2$** preparation. *O*-phenylenediamine (0.46 g, 4.26 mmol) was used instead of ethylenediamine. The product was isolated as yellow crystals in high yield (2.02 g, 88 %).

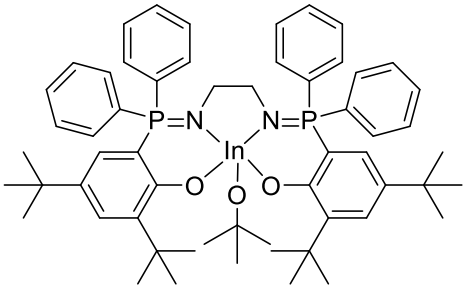
$^{1}$H NMR (400 MHz, $CDCl_3$): δ 8.67 (2H, s, NC***H***), 7.44 (2H, d, $^{4}J_{HH}$ = 2.3 Hz, Ar***H***), 7.35-7.29 (2H, m, Ar***H***), 7.27-7.23 (2H, m, Ar***H***), 7.22 (2H, d, $^{4}J_{HH}$ = 2.3 Hz, Ar***H***), 1.44 (18H, s, C(C***H***$_3$)$_3$), 1.32 (18H, s, C(C***H***$_3$)$_3$).

$^{13}$C{$^{1}$H} NMR (125 MHz, $CDCl_3$): δ 164.9 (N***C***H), 158.7 (Ar***C***O), 142.9 (Ar***C***), 140.4 (Ar***C***), 137.3 (Ar***C***), 128.3 (Ar***C***H), 127.4 (Ar***C***H), 126.9 (Ar***C***H), 119.9 (Ar***C***H), 118.5 (Ar***C***), 35.3 (***C***(CH$_3$)$_3$), 34.3 (***C***(CH$_3$)$_3$), 31.6 (C(***C***H$_3$)$_3$), 29.6 (C(***C***H$_3$)$_3$).

Anal. Calc. ($C_{36}H_{48}N_2O_2$): C, 79.96; H, 8.95; N, 5.18 Found C, 79.85; H, 8.83; N, 5.36

## 7.7. Synthesis of Indium Complexes

### 7.7.1. Synthesis of indium complex 3.1 [10]




A solution of potassium *bis*(trimethylsilyl)amide (0.14 g, 0.72 mmol) in THF (3 mL) was added into a suspension of ligand $^{\text{P-salen}}\mathbf{L}^{1}\mathbf{H}_2$ (0.30 g, 0.36 mmol) in THF (8 mL). The reaction mixture was allowed to stir at room temperature for 2 hours. An aliquot was then taken and analysed with $^{31}P\{^{1}H\}$ NMR spectroscopy. $InCl_3$ (0.08 g, 0.72 mmol) was then added to the reaction mixture. The reaction was allowed to stir at room temperature for 2 hours. An aliquot was then taken and analysed with $^{31}P\{^{1}H\}$ NMR spectroscopy before addition of KO$^t$Bu (0.04 g, 0.36 mmol). The reaction mixture was then allowed to stir at room temperature overnight. The suspension was then centrifuged to remove the KCl salt. The solvent layer was then separated, filtered and dried under vacuum to yield a white solid as the product in good yield (0.28 g, 76 %).

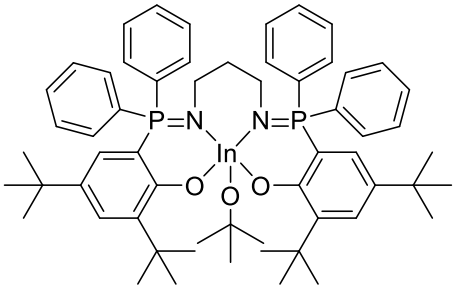
$^{1}H$ NMR (400 MHz, THF-$d_8$): δ 7.81-7.72 (4H, m, Ar***H***), 7.67-7.53 (6H, m, Ar***H***), 7.52-7.43 (6H, m, Ar***H***), 7.38-7.29 (6H, m, Ar***H***), 6.34 (2H, dd, $^{4}J_{HH}$ = 2.2 Hz, $^{3}J_{PH}$ = 17.2 Hz, Ar***H***), 3.13-2.81 (4H, m, C***H***$_2$), 1.51 (18H, s, C(C***H***$_3$)$_3$), 1.06-0.92 (27H, m, C***H***$_3$)

$^{13}C\{^{1}H\}$ NMR (125 MHz, THF-$d_8$): δ 171.2 (d, $^{2}J_{PC}$ = 2.8 Hz, Ar***C***O), 142.7 (d, $^{3}J_{PC}$ = 9.7 Hz, Ar***C***), 135.0 (d, $^{3}J_{PC}$ = 8.70 Hz, Ar***C***), 133.5 (d, $^{2}J_{PC}$ = 9.7 Hz, Ar***C***H), 132.8 (d, $^{1}J_{PC}$ = 97.1 Hz, Ar***C***), 129.6 (d, $^{4}J_{PC}$ = 11.7 Hz, Ar***C***H), 129.4 (d, $^{3}J_{PC}$ = 10.7 Hz, Ar***C***H), 129.1 (Ar***C***H), 127.3 (d, $^{2}J_{PC}$ = 13.7 Hz, Ar***C***H), 108.6 (d, $^{1}J_{PC}$ = 118.6 Hz, Ar***C***), 69.1 (O***C***(CH$_3$)$_3$), 47.0 (d, $^{2}J_{PC}$ = 8.5 Hz, ***C***H$_2$), 36.7 (***C***(CH$_3$)$_3$), 34.5 ( **C**(CH$_3$)$_3$), 31.8 (C(***C***H$_3$)$_3$), 31.0 (C(***C***H$_3$)$_3$) 30.8 (OC(***C***H$_3$)$_3$),.

$^{31}P\{^{1}H\}$ NMR (162 MHz, THF-$d_8$): δ 40.2 (s, ***P***)

Anal. Calc. ($C_{58}H_{73}InN_2O_3P_2$): C, 68.10; H, 7.19; N, 2.74 Found C, 68.18; H, 7.30; N, 2.62

### 7.7.2. Synthesis of indium complex 3.2



Complex **3.2** was synthesised according to the preparation of complex **3.1**. $^{\text{P-salen}}\mathbf{L^2H_2}$ (0.30 g, 0.35 mmol) was used instead of $^{\text{P-salen}}\mathbf{L^1H_2}$. The product was isolated as a white powder after washing with hexane in moderate yield (0.16 g, 44 %).

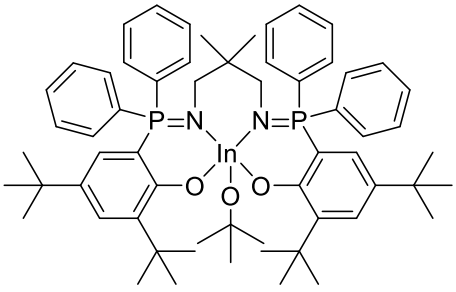
$^1$H NMR (400 MHz, THF-$d_8$): δ 7.77-7.62 (8H, m, Ar***H***), 7.62-7.33 (12H, m, Ar***H***), 7.31 (2H, d, $^4J_{HH}$ = 2.4 Hz, Ar***H***), 6.42 (2H, dd, $^3J_{PH}$ = 16.5 Hz, $^4J_{HH}$ = 2.4 Hz, Ar***H***), 3.49-2.95 (6H, bs, C***H***$_2$), 1.30 (18H, s, C(C***H***$_3$)$_3$), 1.06 (18H, s, C(C***H***$_3$)$_3$), 1.04 (9H, s, C(C***H***$_3$)$_3$).

$^{13}$C{$^1$H} NMR (125 MHz, THF-$d_8$): δ 171.0 (d, $^2J_{PC}$ = 2.7 Hz, Ar***C***O), 142.4 (d, $^3J_{PC}$ = 10.2 Hz, Ar***C***), 135.2 (d, $^3J_{PC}$ = 14.5 Hz, Ar***C***), 134.4 (bs, Ar***C***H), 132.7 (bs, Ar***C***), 129.4 (d, $^{3/4}J_{PC}$ = 10.9 Hz, Ar***C***H), 129.0 (Ar***C***H), 127.3 (d, $^2J_{PC}$ = 12.8 Hz, Ar***C***H), 109.6 (d, $^1J_{PC}$ = 113.8 Hz, Ar***C***), 69.2 (O***C***(CH$_3$)$_3$), 46.5 (***C***H$_2$), 44.4 (CH$_2$***C***H$_2$CH$_2$), 36.4 (***C***(CH$_3$)$_3$), 34.6 (***C***(CH$_3$)$_3$), 31.9 (C(***C***H$_3$)$_3$), 30.8 (C(***C***H$_3$)$_3$), 30.5 (OC(***C***H$_3$)$_3$).

$^{31}$P{$^1$H} NMR (162 MHz, THF-$d_8$): δ 40.3 (s, ***P***)

Anal. Calc. ($C_{59}H_{75}InN_2O_3P_2$): C, 68.33; H, 7.29; N, 2.70 Found C, 67.81; H, 6.90; N, 2.78.

### 7.7.3. Synthesis of indium complex 3.3



Complex **3.3** was synthesised according to the preparation of complex **3.1**. $^{\text{P-salen}}\mathbf{L^3H_2}$ (0.13 g, 0.14 mmol) was used instead of $^{\text{P-salen}}\mathbf{L^1H_2}$. The product was isolated as a white powder after washing with hexane in moderate yield (0.07 g, 43 %).

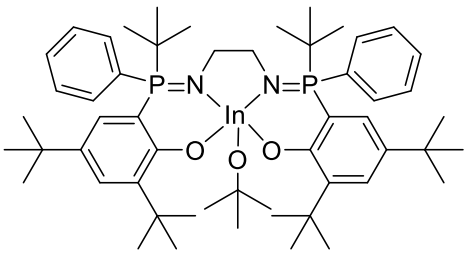
$^{1}$H NMR (400 MHz, THF-$d_8$): δ 7.99-7.88 (4H, m, Ar***H***), 7.67-7.44 (12H, m, Ar***H***), 7.43-7.34 (4H, m, Ar***H***), 7.33 (2H, d, $^{4}J_{HH}$ = 2.6 Hz, Ar***H***), 6.58 (2H, dd, $^{4}J_{HH}$ = 2.5 Hz, $^{3}J_{PH}$ = 16.2 Hz, Ar***H***), 3.41-3.26 (2H, m, C***H***$_2$), 2.93-2.80 (2H, m, C***H***$_2$), 1.33 (18H, s, C***H***$_3$), 1.11-1.05 (27H, m, C***H***$_3$), 0.60 (3H, s, C***H***$_3$), 0.13 (3H, s, C***H***$_3$)

$^{13}$C{$^{1}$H} NMR (125 MHz, THF-$d_8$): δ 171.4 (d, $^{2}J_{PC}$ = 3.8 Hz, Ar***C***O), 142.3 (d, $^{3}J_{PC}$ = 9.9 Hz, Ar***C***), 135.4 (d, $^{4}J_{PC}$ = 15.0 Hz, Ar***C***H), 135.1 (d, $^{2/3}J_{PC}$ = 9.9 Hz, Ar***C***H), 134.7 (d, $^{2/3}J_{PC}$ = 9.5 Hz, Ar***C***H), 132.7 (d. $^{2/3}J_{PC}$ = 10.4 Hz, Ar***C***H), 131.7 (d, $^{1}J_{PC}$ = 92.3, Ar***C***), 130.3 (d, $^{1}J_{PC}$ = 88.5 Hz, Ar***C***), 129.1 (d, $^{2/3}J_{PC}$ = 11.5 Hz, Ar***C***H), 128.9 (Ar***C***H), 127.6 (d, $^{2}J_{PC}$ = 13.2 Hz, Ar***C***H), 109.2 (d, $^{1}J_{PC}$ = 114.7 Hz, Ar***C***), 69.6 (***C***(CH$_3$)$_3$), 57.1 (d, $^{2}J_{PC}$ = 7.8 Hz, ***C***H$_2$), 37.6 (d, $^{3}J_{PC}$ = 10.0 Hz, ***C***(CH$_3$)$_2$), 36.5 (***C***(CH$_3$)$_3$), 35.3 (C(***C***H$_3$)$_3$), 34.6 (***C***(CH$_3$)$_3$), 31.8 (C(***C***H$_3$)$_3$), 30.8 (C(***C***H$_3$)$_3$), 26.4 (C(***C***H$_3$)$_2$), 25.9 (C(***C***H$_3$)$_2$).

$^{31}$P{$^{1}$H} NMR (162 MHz, THF-$d_8$): δ 40.6 (s, ***P***)

Anal. Calc. ($C_{61}H_{79}InN_2O_3P_2$): C, 68.79; H, 7.48; N, 2.63 Found C, 68.90; H, 7.62; N, 2.45

### 7.7.4. Synthesis of indium complex 3.4




Complex **3.4** was synthesised according to the preparation of complex **3.1**. **$^{P\text{-salen}}$L$^{4}$H$_2$** (0.12 g, 0.15 mmol) was used instead of **$^{P\text{-salen}}$L$^{1}$H$_2$**. The product was isolated as a white powder after washing with hexane in moderate yield (0.01 g, 64%).

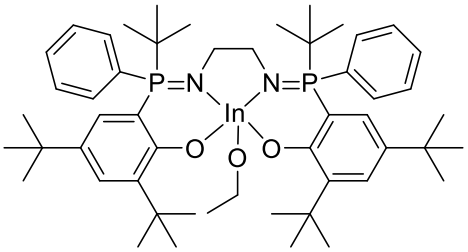
$^{1}$H NMR (400 MHz, THF-$d_8$): δ 8.27-8.16 (4H, m, Ar***H***), 7.64-7.52 (6H, m, Ar***H***), 7.31 (2H, d, $^{4}J_{HH}$ = 2.4 Hz, Ar***H***), 6.22 (2H, dd, $^{3}J_{PH}$ = 16.7 Hz, $^{4}J_{HH}$ = 2.6 Hz, Ar***H***), 5.51 (2H, s, O***H***), 3.13-2.85 (4H, m, C***H***$_2$), 1.54 (18H, s, C(C***H***$_3$)$_3$), 1.43 (18H, d, $^{3}J_{PH}$ = 14.5 Hz, C(C***H***$_3$)$_3$), 1.02 (18H, s, C(C***H***$_3$)$_3$), 0.99 (9H, s, C(C***H***$_3$)$_3$).

$^{13}C\{^{1}H\}$ NMR (125 MHz, THF-$d_8$): δ 171.3 (d, $^{3}J_{PC}$ = 3.8 Hz, Ar***C***O), 142.6 (d, $^{4}J_{PC}$ = 10.4 Hz, Ar***C***), 134.9 (d, $^{2}J_{PC}$ = 7.9 Hz, Ar***C***H), 134.5 (d, $^{1}J_{PC}$ = 14.3 Hz, Ar***C***), 132.7 (d, $^{4}J_{PC}$ = 2.6 Hz, Ar***C***H), 130.4 (Ar***C***), 129.5 (d, $^{3}J_{PC}$ = 10.4 Hz, Ar***C***H), 128.8 (d, $^{2}J_{PC}$ = 13.3 Hz, Ar***C***H), 128.2 (d, $^{4}J_{PC}$ = 2.5 Hz, Ar***C***H), 106.9 (d, $^{1}J_{PC}$ = 105.8, Ar***C***), 68.9 (O***C***$(CH_3)_3$), 48.6 (dd, $^{3}J_{PC}$ = 5.0 Hz, $^{2}J_{PC}$= 12.5 Hz, ***C***$H_2$), 38.8 (***C***$(CH_3)_3$), 36.7 (d, $^{4}J_{PC}$ = 1.7 Hz, ***C***$(CH_3)_3$), 35.5 (C(***C***$H_3)_3$), 34.4 (***C***$(CH_3)_3$), 31.7 (C(***C***$H_3)_3$), 31.1 (C(***C***$H_3)_3$), 28.0 (C(***C***$H_3)_3$)

$^{31}P\{^{1}H\}$ NMR (162 MHz, THF-$d_8$): δ 56.4 (s, ***P***)

Anal. Calc. ($C_{54}H_{81}InN_2O_3P_2$): C, 65.98; H, 8.31; N, 2.85 Found C, 65.85; H, 8.16; N, 2.97

### 7.7.5. Synthesis of indium complex 3.5




Complex **3.5** was synthesised according to the procedure used for preparation of complex **3.1** but, used ligand $^{\text{P-salen}}\mathbf{L^4H_2}$ instead of $^{\text{P-salen}}\mathbf{L^1H_2}$ and KOEt (0.02 g, 0.26 mmol) instead of KO$^{t}$Bu. After work up, colourless crystals were obtained as the product in moderate yield (0.08 g, 41 %).

$^{1}H$ NMR (400 MHz, THF-$d_8$): δ 8.21-8.13 (4H, m, Ar***H***), 7.64-7.54 (6H, m, Ar***H***), 7.31 (2H, $^{4}J_{HH}$ = 2.5 Hz, Ar***H***), 6.33 (2H, dd, $^{3}J_{PH}$ = 16.6 Hz, $^{4}J_{HH}$ = 2.6 Hz, Ar***H***), 3.70 (2H, q, $^{3}J_{HH}$ = 6.2 Hz, OC***H***$_2$CH$_3$), 3.11-2.83 (4H, m, C***H***$_2$), 1.53 (18H, s, C***H***$_3$), 1.44 (18H, d, $^{3}J_{PH}$ = 14.6 Hz, C***H***$_3$), 1.02 (18H, s, C***H***$_3$), 0.82 (3H, t, $^{3}J_{HH}$ = 6.3 Hz, OCH$_2$C***H***$_3$).

$^{13}C\{^{1}H\}$ NMR (125 MHz, THF-$d_8$): δ 171.3 (d, $^{3}J_{PC}$ = 3.4 Hz, Ar***C***O), 142.5 (d, $^{1}J_{PC}$ = 9.9 Hz, Ar***C***), 134.8 (d, $^{2}J_{PC}$ = 7.9 Hz, Ar***C***H), 132.8 (d, $^{4}J_{PC}$ = 2.5 Hz, Ar***C***H), 130.3 (Ar***C***), 129.6 (d, $^{3}J_{PC}$ = 10.3 Hz, Ar***C***H), 129.0 (d, $^{2}J_{PC}$ = 13.3 Hz, Ar***C***H), 128.3 (d, $^{4}J_{PC}$ = 1.9 Hz, Ar***C***H), 107.7 (Ar***C***), 106.8 (Ar***C***), 62.2 (O***C***H$_2$CH$_3$), 48.9 (dd, $^{3}J_{PC}$ = 4.1 Hz, $^{2}J_{PC}$ = 11.3

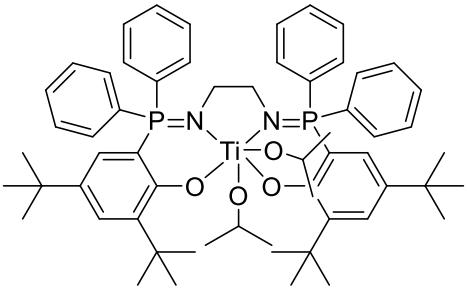
Hz, ***C***$H_2$), 38.8 (d, $^1J_{PC}$ = 57.1 Hz, ***C***$(CH_3)_3$), 36.7 (d, $^4J_{PC}$ = 1.7 Hz, ***C***$(CH_3)_3$), 34.4 (***C***$(CH_3)_3$), 31.8 (C(***C***$H_3)_3$), 30.9 (C(***C***$H_3)_3$), 28.0 (C(***C***$H_3)_3$), 22.8 ($OCH_2$***C***$H_3$).

$^{31}P\{^1H\}$ NMR (162 MHz, THF-$d_8$): δ 56.9 (s, ***P***)

Anal. Calc. ($C_{54}H_{81}InN_2O_3P_2$): C, 65.40; H, 8.25; N, 2.93 Found C, 65.52; H, 8.25; N, 2.72

### 7.8. Synthesis of phosphasalen and salen titanium complexes

#### 7.8.1. Synthesis of phosphasalen titanium complex 4.1




To a stirred suspension of **$^{P\text{-salen}}$L$^1$H$_2$** (0.70 g, 0.84 mmol) in toluene (30 mL) at 5 °C was dropwise added a solution of Ti($O^i$Pr)$_4$ (0.24 g, 0.85 mmol) in toluene (20 mL). The solution mixture was then slowly warmed to ambient temperature and allowed to stir for 16 hours. An aliquot was then withdrawn and diluted in toluene-$d_8$. $^{31}P\{^1H\}$ NMR spectroscopy was performed to check the completion of reaction. The solvent residue was then removed under vacuum to give a yellow oil as the crude product. The product was then recrystallised by a layer-by-layer of toluene and hexane mixture. The product was isolated as a pale-yellow crystal in high yield (0.77 g, 92 %).

$^1$H NMR (400 MHz, toluene-$d_8$): δ 8.26-8.15 (2H, m, *cis*-Ar***H***), 7.88-7.79 (2H, m, *cis*-Ar***H***), 7.79-7.60 (20H, m, *trans*-Ar***H***), 7.42-7.33 (2H, m, *cis*-Ar***H***), 7.32-7.24 (2H, m, *cis*-Ar***H***), 7.24-7.19 (2H, m, *trans*-Ar***H***), 7.15-6.86 (16H, m, *cis*-Ar***H***), 6.75 (2H, dd, $^3J_{PH}$ = 15.8 Hz, $^4J_{HH}$ = 2.2 Hz, *trans*-Ar***H***), 5.29 (1H, sept, $^3J_{HH}$ = 6.0 Hz, *cis*-C***H***$(CH_3)_2$), 4.62 (2H, sept, $^3J_{HH}$ = 6.0 Hz, *trans*-C***H***$(CH_3)_2$), 4.20-3.98 (1H, m, *cis*-C***H***$_2$), 3.48-3.29 (4H, m, *trans*-C***H***$_2$), 2.97-2.76 (3H, m, *cis*-C***H***$_2$), 1.88 (9H, s, *cis*-C(C***H***$_3)_3$), 1.81 (18H, s, *trans*-C(C***H***$_3)_3$), 1.59 (18H, s, *trans*-C(C***H***$_3)_3$), 1.40 (3H, d, $^3J_{HH}$ = 6.0 Hz, *cis*-CH(C***H***$_3)_2$), 1.22 (3H, d, $^3J_{HH}$ =5.7 Hz, *cis*-CH(C***H***$_3)_2$), 1.20 (9H, s, *cis*-C(C***H***$_3)_3$), 1.16 (18H, s, *cis*-C(C***H***$_3)_3$), 1.08 (3H, d, $^3J_{HH}$

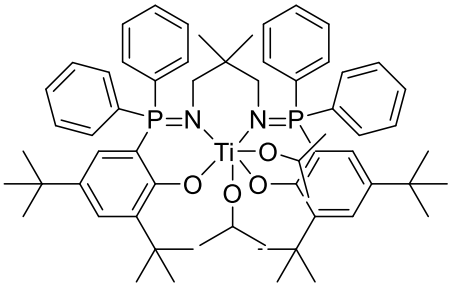
= 6.0 Hz, *cis*-CH(C***H***$_3$)$_2$), 0.93-0.90 (3H, d, $^3J_{HH}$ =6.0 Hz, *cis*-CH(C***H***$_3$)$_2$), 0.83 (12H, d, $^3J_{HH}$ = 6.0 Hz, *trans*-CH(C***H***$_3$)$_2$).

$^{13}$C{$^1$H} NMR (125 MHz, toluene-$d_8$): δ 172.0 (d, $^2J_{PC}$ = 3.7 Hz, *cis*-Ar***C***O), 170.0 (d, $^2J_{PC}$ = 2.4 Hz, *trans*-Ar***C***O), 168.3 (d, $^2J_{PC}$ = 2.4 Hz, *cis*-Ar***C***O), 149.4 (d, Ar***C*** or Ar***C***H), 138.7 (d, Ar***C*** or Ar***C***H), 138.2 (d, Ar***C*** or Ar***C***H), 136.9 (d, Ar***C*** or Ar***C***H), 136.7 (d, Ar***C*** or Ar***C***H), 134.4-133.9 (m, *cis*-Ar***C***H), 133.6 (d, *trans*-Ar***C***H), 133.4 (d, *trans*-Ar***C***H), 132.6 (Ar***C*** or Ar***C***H), 132.2 (Ar***C*** or Ar***C***H), 132.0 (Ar***C*** or Ar***C***H), 131.9-131.8 (m, Ar***C*** or Ar***C***H), 131.6 (d, Ar***C*** or Ar***C***H), 131.6 (Ar***C*** or Ar***C***H), 131.5 (Ar***C*** or Ar***C***H), 131.4-131.3 (Ar***C*** or Ar***C***H), 131.2 (Ar***C*** or Ar***C***H), 131.0 (Ar***C*** or Ar***C***H), 130.8 (Ar***C*** or Ar***C***H), 127.2 (Ar***C*** or Ar***C***H), 126.8 (Ar***C*** or Ar***C***H), 111.2 (d, $^2J_{PC}$ = 123.3 Hz, *trans*-Ar***C***H), 111.2 (d, $^2J_{PC}$ = 120.4 Hz, *cis*-Ar***C***H), 107.7 (d, $^2J_{PC}$ = 112.7 Hz, *cis*-Ar***C***H), 76.3 (*cis*-***C***H(CH$_3$)$_2$), 72.2 (*trans*-***C***H(CH$_3$)$_2$), 53.4 (*trans*-***C***H$_2$), 52.6 (d, $^2J_{PC}$ = 3.4 Hz, *cis*-***C***H$_2$), 52.5 (d, $^2J_{PC}$ = 3.4 Hz, *cis*-***C***H$_2$), 36.4 (d, $^4J_{PC}$ = 1.4 Hz, *cis*-***C***(CH$_3$)$_3$), 36.1 (d, $^4J_{PC}$ = 1.7 Hz, *trans*-***C***(CH$_3$)$_3$), 35.9 (d, $^4J_{PC}$ = 1.7 Hz, *trans*-***C***(CH$_3$)$_3$), 34.2 (*cis*-***C***(CH$_3$)$_3$), 34.1 (*cis*-***C***(CH$_3$)$_3$), 32.0 (*cis*-***C***(CH$_3$)$_3$), 31.7 (*cis*-C(***C***H$_3$)$_3$), 31.6 (*cis*-C(***C***H$_3$)$_3$), 31.6 (*cis*-C(***C***H$_3$)$_3$), 30.9 (*trans*-C(***C***H$_3$)$_3$), 30.8 (*cis*-C(***C***H$_3$)$_3$), 27.1 (*cis*-CH(***C***H$_3$)$_2$), 27.1 (*trans*-CH(***C***H$_3$)$_2$), 26.7 (*cis*-CH(***C***H$_3$)$_2$), 26.5 (*cis*-CH(***C***H$_3$)$_2$), 26.0 (*cis*-CH(***C***H$_3$)$_2$).

$^{31}$P{$^1$H} NMR (162 MHz, toluene-$d_8$): δ 30.3 (s, ***P***), 29.8 (s, ***P***), 28,5 (s, ***P***).

Anal. Calc. ($C_{60}H_{78}TiN_2O_4P_2$): C, 71.99; H, 7.85; N, 2.80 Found C, 72.27; H, 7.93; N, 2.75

### 7.8.2. Synthesis of phosphasalen titanium complex 4.2




Complex **4.2** was synthesised according to the procedure used in the preparation of **4.1**. $^{\text{P-salen}}\mathbf{L}^{\mathbf{3}}\mathbf{H_2}$ (0.10 g, 0.11 mmol) was used instead of $^{\text{P-salen}}\mathbf{L}^{\mathbf{1}}\mathbf{H_2}$. The product was isolated as yellow crystals after crystallisation in near-quantitative yield (0.11 g, 96 %).

$^{1}$H NMR (400 MHz, toluene-$d_8$): δ 8.35-8.20 (2H, m, Ar***H***), 8.11-7.98 (2H, m, Ar***H***), 7.90-7.80 (2H, m, Ar***H***), 7.59 (2H, dd, $^{3}J_{PH}$ = 24.6 Hz, $^{4}J_{HH}$ = 2.2 Hz, Ar***H***), 7.38-7.28 (2H, m, Ar***H***), 7.28-6.87 (12H, m, Ar***H***), 6.87-6.76 (2H, m, Ar***H***), 5.50 (1H, sept, $^{3}J_{HH}$ = 5.7 Hz, C***H***$(CH_3)_2$), 4.16 (1H, sept, $^{3}J_{HH}$ = 6.0 Hz, C***H***$(CH_3)_2$), 4.03 (1H, t, $^{4}J_{HH}$ = 13.0 Hz, C***H***$_2$), 3.45 (1H, $^{4}J_{HH}$ = 11.4 Hz, C***H***$_2$), 3.04 (1H, dd, $^{2}J_{HH}$ = 20.5 Hz, $^{4}J_{HH}$ = 11.6 Hz, C***H***$_2$), 2.79 (1H, dd, $^{2}J_{HH}$ = 25.8 Hz, $^{4}J_{HH}$ = 12.5 Hz, C***H***$_2$), 1.68 (9H, s, C(C***H***$_3)_3$), 1.56 (3H, d, $^{3}J_{HH}$ = 5.6 Hz, CH(C***H***$_3)_2$), 1.51 (9H, s, C(C***H***$_3)_3$), 1.42 (3H, d, $^{3}J_{HH}$ = 5.6 Hz, CH(C***H***$_3)_2$), 1.23 (9H, s, C(C***H***$_3)_3$), 1.22 (9H, s, C(C***H***$_3)_3$), 0.94 (3H, d, $^{3}J_{HH}$ = 5.8 Hz, CH(C***H***$_3)_2$), 0.74 (3H, d, $^{3}J_{HH}$ = 6.0 Hz, CH(C***H***$_3)_2$), 0.43 (3H, s, C(C***H***$_3)_2$), 0.08 (3H, s, C(C***H***$_3)_2$).

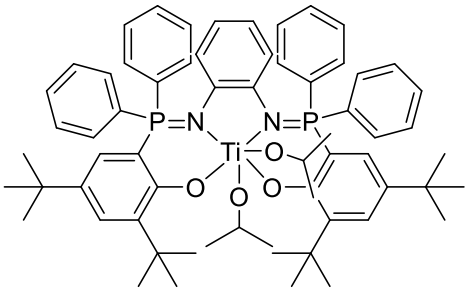
$^{13}$C{$^{1}$H} NMR (125 MHz, toluene-$d_8$): δ 171.4 (d, $^{2}J_{PC}$ = 2.5 Hz, Ar***C***O), 169.1 (d, $^{2}J_{PC}$ = 1.8 Hz, Ar***C***O), 140.0 (d, Ar***C*** or Ar***C***H), 137.9 (d, Ar***C*** or Ar***C***H), 135.0 (d, Ar***C*** or Ar***C***H), 134.7 (d, Ar***C*** or Ar***C***H), 134.6 (d, Ar***C*** or Ar***C***H), 134.4 (d, Ar***C*** or Ar***C***H), 134.1 (d, Ar***C*** or Ar***C***H), 133.9 (Ar***C*** or Ar***C***H), 133.4 (Ar***C*** or Ar***C***H), 132.7 (Ar***C*** or Ar***C***H), 131.8 (Ar***C*** or Ar***C***H), 131.6-131.4 (m, Ar***C*** or Ar***C***H), 131.3 (d, Ar***C*** or Ar***C***H), 131.0 (Ar***C*** or Ar***C***H), 139.8 (d, Ar***C*** or Ar***C***H), 130.2 (Ar***C*** or Ar***C***H), 126.7 (dd, Ar***C*** or Ar***C***H), 112.9 (d, $^{2}J_{PC}$ = 119.7 Hz, Ar***C***H), 107.0 (d, $^{2}J_{PC}$ = 121.2 Hz, Ar***C***H), 76.9 (***C***H$(CH_3)_2$), 76.5 (***C***H$(CH_3)_2$), 60.5 (d, $^{2}J_{PC}$ = 4.0 Hz, ***C***H$_2$), 59.9 (d, $^{2}J_{PC}$ = 4.4 Hz, ***C***H$_2$), 36.7 (dd, $^{3}J_{PC}$ = 5.6 Hz, ***C***$(CH_3)_2$), 35.8 (d, $^{4}J_{PC}$ = 1.9 Hz, ***C***$(CH_3)_3$), 35.5 (d, $^{4}J_{PC}$ = 1.8 Hz, ***C***$(CH_3)_3$), 34.3 (***C***$(CH_3)_3$), 34.1 (***C***$(CH_3)_3$), 32.0 (C(***C***$H_3)_3$), 31.7 (C(***C***$H_3)_3$), 30.9 (C(***C***$H_3)_3$), 30.8 (C(***C***$H_3)_3$), 27.5

($CH(\boldsymbol{C}H_3)_2$), 27.4 ($CH(\boldsymbol{C}H_3)_2$), 26.7 ($CH(\boldsymbol{C}H_3)_2$), 26.2 ($C(\boldsymbol{C}H_3)_2$), 25.8 ($CH(\boldsymbol{C}H_3)_2$), 24.4 ($C(\boldsymbol{C}H_3)_2$).

$^{31}P\{^1H\}$ NMR (162 MHz, toluene-$d_8$): δ 31.0 (s, ***P***), 30.0 (s, ***P***).

Anal. Calc. ($C_{63}H_{84}TiN_2O_4P_2$): C, 72.54; H, 8.12; N, 2.69 Found C, 72.39; H, 8.36; N, 2.58

### 7.8.3. Synthesis of phosphasalen titanium complex 4.3




Complex **4.3** was synthesised according to the procedure used in the preparation of **4.1**. $^{\text{P-salen}}\mathbf{L}^{5}\mathbf{H}_2$ (0.30 g, 0.34 mmol) was used instead of $^{\text{P-salen}}\mathbf{L}^{1}\mathbf{H}_2$. The product was isolated as yellow crystals after crystallisation in high yield (0.30 g, 85 %).

$^1H$ NMR (400 MHz, toluene-$d_8$): δ 8.37-8.20 (2H, m, Ar***H***), 8.04-7.82 (4H, m, Ar***H***), 7.57 (2H, dd, $^3J_{PH}$ = 7.9 Hz, $^4J_{HH}$ =2.1 Hz, Ar***H***), 7.36-7.15 (6H, m, Ar***H***), 7.15-6.93 (4H, m, Ar***H***), 6.92-6.71 (6H, m, Ar***H***), 6.50-6.18 (4H, m, Ar***H***), 5.10 (1H, sept, $^3J_{HH}$ = 6.0 Hz, C***H***$(CH_3)_2$), 4.25 (1H, sept, $^3J_{HH}$ = 6.3 Hz, C***H***$(CH_3)_2$), 1.64 (9H, s, $C(C\boldsymbol{H}_3)_3$), 1.38-1.30 (12H, m, $C(C\boldsymbol{H}_3)_3$+$CH(C\boldsymbol{H}_3)_2$), 1.29-1.20 (12H, m, $C(C\boldsymbol{H}_3)_3$+$CH(C\boldsymbol{H}_3)_2$), 1.15 (9H, s, $C(C\boldsymbol{H}_3)_3$), 0.94 (3H, d, $^3J_{HH}$ = 6.2 Hz, $CH(C\boldsymbol{H}_3)_2$), 0.80 (3H, d, $^3J_{HH}$ = 6.0 Hz, $CH(C\boldsymbol{H}_3)_2$).

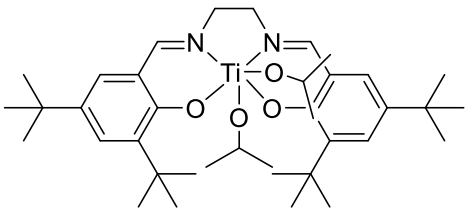
$^{13}C\{^1H\}$ NMR (125 MHz, toluene-$d_8$): δ 170.9 (d, $^2J_{PC}$ = 2.3 Hz, Ar***C***O), 167.2 (Ar***C***O), 147.2 (dd, Ar***C***), 145.4 (dd, Ar***C***), 140.2 (d, Ar***C***), 138.4 (d, Ar***C***), 134.7 (d, Ar***C***), 134.4-133.7 (m, Ar***C***H), 132.2-132.0 (Ar***C***H), 131.7 (Ar***C***H), 131.4 (Ar***C***H), 131.4 (Ar***C***H), 131.2 (Ar***C***H), 130.6 (Ar***C***H), 126.9 (d, Ar***C***H), 125.9 (d, Ar***C***H), 121.5 (d, Ar***C***H), 121.2 (Ar***C***H), 118.4 (d, Ar***C***H), 118.1 (Ar***C***H), 113.6 (d, $^2J_{PC}$ = 124.5 Hz, Ar***C***H), 108.0 (d, $^2J_{PC}$ = 115.8 Hz, Ar***C***H), 77.2 (***C***H$(CH_3)_2$), 76.5 (***C***H$(CH_3)_2$), 36.0 (d, $^4J_{PC}$ = 1.2 Hz, ***C***$(CH_3)_3$), 35.4 (d,

$^{4}J_{PC}$ = 1.6 Hz, ***C***$(CH_3)_3$), 34.3 (***C***$(CH_3)_3$), 34.0 (***C***$(CH_3)_3$), 31.8 (C(***C***$H_3)_3$), 31.6 (C(***C***$H_3)_3$), 30.8 (C(***C***$H_3)_3$), 26.9 (CH(***C***$H_3)_2$), 26.9 (CH(***C***$H_3)_2$), 26.4 (CH(***C***$H_3)_2$), 26.2 (CH(***C***$H_3)_2$).

$^{31}P\{^{1}H\}$ NMR (162 MHz, toluene-$d_8$): δ 24.8 (s, ***P***), 19.9 (s, ***P***).

Anal. Calc. ($C_{64}H_{78Ti}N_2O_4P_2$): C, 73.27; H, 7.49; N, 2.67 Found C, 73.16; H, 7.58; N, 2.61

### 7.8.4. Synthesis of salen titanium complex 4.4 [9]



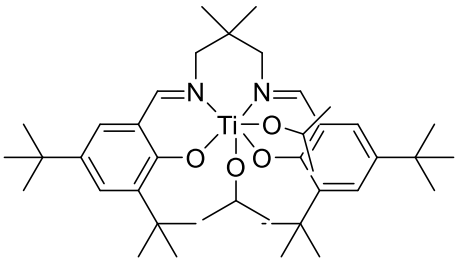

To a vigorously stirred solution of Ti(O$^{i}$Pr)$_4$ (0.29 g, 1.04 mmol) in anhydrous toluene (30 mL) at 5 °C was slowly added a solution of **$^{salen}$L$^{1}$H$_2$** (0.50 g, 1.01 mmol) in toluene (20 mL). The reaction mixture was slowly warmed to room temperature and allowed to stir at ambient temperature for 16 h. The volatile organic solvent was then removed in *vacuo* to give the crude product as an oil. The crude product was washed with hexane. The solvent residue was then removed under vacuum to give a yellow powder as the product in good yield (0.48 g, 72 %).

$^{1}H$ NMR (400 MHz, $CDCl_3$): δ 8.27 (2H, s, NC***H***), 7.48 (2H, d, $^{4}J_{HH}$ = 2.5 Hz, Ar***H***), 7.16 (2H, $^{4}J_{HH}$ = 2.5 Hz, Ar***H***), 4.13 (2H, sept, $^{3}J_{HH}$ = 6.0 Hz, C***H***$(CH_3)_2$), 3.96 (4H, s, C***H***$_2$), 1.49 (18H, s, C(C***H***$_3)_3$), 1.32 (18H, s, C(C***H***$_3)_3$), 0.66 (12H, d, $^{3}J_{HH}$ = 6.0 Hz, CH(C***H***$_3)_2$).

$^{13}C\{^{1}H\}$ NMR (125 MHz, $CDCl_3$): δ 163.6 (N***C***H), 163.5 (Ar***C***O), 138.3 (Ar***C***), 137.3 (Ar***C***), 129.8 (Ar***C***H), 127.7 (Ar***C***), 122.0 (Ar***C***H), 72.6 (***C***H$(CH_3)_2$), 58.6 (***C***H$_2$), 35.6 (***C***$(CH_3)_3$), 34.2 (***C***$(CH_3)_3$), 31.7 (C(***C***$H_3)_3$), 29.8 (C(***C***$H_3)_3$), 26.0 (CH(***C***$H_3)_2$).

Anal. Calc. ($C_{38}H_{60}N_2O_4Ti$): C, 69.49; H, 9.21; N, 4.27 Found C, 69.56; H, 9.37; N, 4.38

### 7.8.5. Synthesis of salen titanium complex 4.5



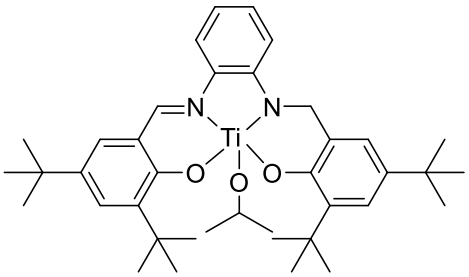
Complex **4.5** was synthesised according to the procedure used in the preparation of **4.4**. $^{salen}\mathbf{L^2H_2}$ (0.08 g, 0.22 mmol) was used instead of $^{salen}\mathbf{L^1H_2}$. The product was isolated as a yellow powder in high yield (0.73 g, 80 %).

$^1$H NMR (400 MHz, $CDCl_3$): δ 7.98 (1H, s, NC***H***), 7.93 (1H, s, NC***H***), 7.43 (1H, d, $^4J_{HH}$ = 2.6 Hz, Ar***H***), 7.28 (1H, d, $^4J_{HH}$ = 2.6 Hz, Ar***H***), 7.09 (1H, d, $^4J_{HH}$ = 2.6 Hz, Ar***H***), 7.02 (1H, d, $^4J_{HH}$ = 2.6 Hz, Ar***H***), 4.91-4.76 (2H, m, C***H***$(CH_3)_2$ + C***H***$_2$), 4.36 (1H, sept, $^3J_{HH}$ = 6.0 Hz, C***H***$(CH_3)_2$), 3.93 (1H, d, $^4J_{HH}$ = 12.2 Hz, C***H***$_2$), 3.16 (1H, d, $^4J_{HH}$ = 12.2 Hz, C***H***$_2$), 3.08 (1H, d, $^4J_{HH}$ = 10.2 Hz, C***H***$_2$), 1.45 (9H, s, C(C***H***$_3)_3$), 1.31 (9H, s, C(C***H***$_3)_3$), 1.25 (9H, s, C(C***H***$_3)_3$), 1.17 (3H, d, $^3J_{HH}$ = 6.0 Hz, CH(C***H***$_3)_2$), 1.14 (3H, d, $^3J_{HH}$ = 6.0 Hz, CH(C***H***$_3)_2$), 1.06 (3H, s, C(C***H***$_3)_2$), 0.99 (9H, s, C(C***H***$_3)_3$), 0.80 (3H, d, $^3J_{HH}$ = 6.10 Hz, CH(C***H***$_3)_2$), 0.72 (3H, d, $^3J_{HH}$ = 6.10 Hz, CH(C***H***$_3)_2$), 0.68 (3H, s, C(C***H***$_3)_2$).

$^{13}$C{$^1$H} NMR (125 MHz, $CDCl_3$): δ 165.1 (N***C***H), 164.4 (Ar***C***O), 163.8 (Ar***C***O), 161.4 (N***C***H), 138,7 (Ar***C***), 138.4 (Ar***C***), 136.7 (Ar***C***), 136.6 (Ar***C***), 128.9 (Ar***C***H), 128.6 (Ar***C***H), 127.2 (Ar***C***), 126.0 (Ar***C***), 123.2 (Ar***C***H), 121.4 (Ar***C***H), 73.5 (***C***H$(CH_3)_2$), 72.8 (***C***H$(CH_3)_2$), 37.2 (***C***H$_2$), 35.5 (***C***$(CH_3)_3$), 34.8 (***C***$(CH_3)_3$), 34.2 (***C***$(CH_3)_3$), 34.0 (***C***$(CH_3)_3$), 31.7 (C(***C***H$_3)_3$), 31.5 (C(***C***H$_3)_3$), 30.1 (C(***C***H$_3)_3$), 29.7 (C(***C***H$_3)_3$), 26.8 (C(***C***H$_3)_2$), 26.4 (C(***C***H$_3)_2$), 25.7 (CH(***C***H$_3)_2$), 25.7 (CH(***C***H$_3)_2$), 23.7 (***C***$(CH_3)_2$).

Anal. Calc. ($C_{41}H_{66}TiN_2O_4$): C, 70.47; H, 9.52; N, 4.01 Found C, 70.44; H, 9.47; N, 4.09

### 7.8.6. Synthesis of salalen titanium complex 4.6



Complex **4.6** was synthesised according to the procedure used in the preparation of **4.1**. $^{salen}\mathbf{L}^{3}\mathbf{H}_{2}$ (0.50 g, 0.92 mmol) was used instead of $^{salen}\mathbf{L}^{1}\mathbf{H}_{2}$. The product was isolated as a dark brown solid in near-quantitative yield (0.55 g, 92 %).

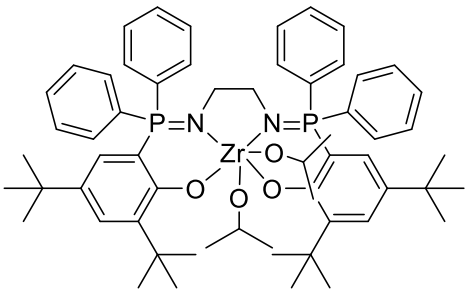
$^{1}$H NMR (400 MHz, $CDCl_3$): δ 9.09 (1H, s, NC***H***), 7.58 (1H, d, $^{4}J_{HH}$ = 2.3 Hz, Ar***H***), 7.55 (1H, dd, $^{4}J_{HH}$ = 1.1 Hz, $^{3}J_{HH}$ = 8.1 Hz, Ar***H***), 7.41 (1H, d, $^{4}J_{HH}$ = 2.4 Hz, Ar***H***), 7.25-7.13 (3H, m, Ar***H***), 6.77 (1H, d, $^{3}J_{HH}$ = 8.1 Hz, Ar*H*), 6.73-6.65 (1H, m, Ar*H*), 4.79 (2H, quart, $^{2}J_{HH}$ = 16.1 Hz, NC$\boldsymbol{H}_2$), 4.17 (1H, sept, $^{3}J_{HH}$ = 6.0 Hz, C***H***$(CH_3)_2$), 1.52 (9H, s, C(C***H***$_3)_3$), 1.49 (9H, s, C(C***H***$_3)_3$), 1.31 (9H, s, C(C***H***$_3)_3$), 1.27 (9H, s, C(C***H***$_3)_3$), 0.81 (3H, d, $^{3}$*J*HH = 6.0 Hz, CH(C***H***$_3)_2$), 0.79 (3H, d, $^{3}$*J*HH = 6.0 Hz, CH(C***H***$_3)_2$).

$^{13}$C{$^{1}$H} NMR (175 MHz, $CDCl_3$): δ 163.7 (H***C***N), 157.8 (Ar***C***O), 156.5 (Ar***C***O), 154.6 (Ar***C***), 142.3 (Ar***C***), 141.6 (Ar***C***), 138.2 (Ar***C***), 136.4 (Ar***C***), 135.1 (Ar***C***), 130.9 (Ar***C***H), 129.5 (Ar***C***H), 129.0 (Ar***C***), 127.8 (Ar***C***H), 122.7 (Ar***C***H), 122.4 (Ar***C***). 122.1 (Ar***C***H), 116.4 (Ar***C***H), 113.7 (Ar***C***H), 108.9 (Ar***C***H), 80.9 (***C***H$(CH_3)_2$), 54.2 (N***C***$H_2$), 35.8 (***C***$(CH_3)_3$), 35.6 (***C***$(CH_3)_3$), 34.5 (C(***C***$H_3)_3$), 34.5 (C(***C***$H_3)_3$), 31.9 (C(***C***$H_3)_3$), 31.6 (C(***C***$H_3)_3$), 30.6 (C(***C***$H_3)_3$), 30.0 (C(***C***$H_3)_3$), 26.2 (CH(***C***$H_3)_2$), 26.2 (CH(***C***$H_3)_2$).

Anal. Calc. ($C_{39}H_{54}TiN_2O_3$): C, 72.43; H, 8.42; N, 4.33 Found C, 72.36; H, 8.49; N, 4.25

## 7.9. Synthesis of phosphasalen zirconium complex

### 7.9.1. Synthesis of phosphasalen zirconium complex 4.7



Complex **4.7** was synthesised according to the procedure used in the preparation of **4.1**. $Zr(O^iPr)_4 \cdot {}^iPrOH$ (0.23 g, 0.60 mmol) was used instead of $Ti(O^iPr)_4$. The product was isolated as a white powder after washing with hexane in near-quantitative yield (0.59 g, 94 %)

$^1$H NMR (500 MHz, toluene-$d_8$): 8.08 (3H, bs, Ar***H***), 7.98-7.89 (1H, m, Ar***H***), 7.81 (2H, bs, Ar***H***), 7.76-754 (8H, m, Ar***H***), 7.39 (3H, bs, Ar***H***), 7.28-7.15 (5H, m, Ar***H***), 6.73-6.64 (2H, m, Ar***H***), 4.11 (2H, sept, $^3J_{HH}$ = 5.8 Hz, C***H***$(CH_3)_2$), 3.36-3.24 (4H, m, C***H***$_2$), 1.81 (18H, s, C(C***H***$_3)_3$), 1.16 (18H, s, C(C***H***$_3)_3$), 0.90 (12H, d, $^3J_{HH}$ = 5.8 Hz, CH(C***H***$_3)_2$).

$^{13}$C{$^1$H} NMR (125 MHz, toluene-$d_8$): δ 168.7 (d, $^2J_{PC}$ = 2.4 Hz, Ar***C***O), 138.9 (d, Ar***C***H), 136.4 (Ar***C***H), 133.6 (d, Ar***C***H), 131.7 (d, Ar***C***H), 130.8 (Ar***C***), 130.0 (Ar***C***), 127.2 (d, Ar***C***), 126.5 (d, Ar***C***), 113.0 (d, $^2J_{PC}$ = 123.9 Hz, Ar***C***H), 68.4 (***C***H$(CH_3)_2$), 52.5 (dd, $^2J_{PC}$ = 4.2 Hz, $^3J_{PC}$ = 14.5 Hz, ***C***H$_2$), 36.0 (***C***$(CH_3)_3$), 34.2 (***C***$(CH_3)_3$), 31.7 (C(***C***H$_3)_3$), 30.6 (C(***C***H$_3)_3$), 27.6 (CH(***C***H$_3)_2$).

$^{31}$P{$^1$H} NMR (162 MHz, toluene-$d_8$): δ 32.9 (s, ***P***)

Anal. Calc. ($C_{60}H_{78}ZrN_2O_4P_2$): C, 69.00; H, 7.53; N, 2.68 Found C, 68.86; H, 7.60; N, 2.64

## 7.10. References


(1) Kowalski, A.; Duda, A.; Penczek, S., Polymerization of l,l-Lactide Initiated by Aluminum Isopropoxide Trimer or Tetramer. *Macromolecules,* **1998,** *31* (7), 2114–2122.

(2) Sheldrick, G., A short history of SHELX. *Acta Cryst. A,* **2008,** *64* (1), 112–122.

(3) Farrugia, L., WinGX and ORTEP for Windows: an update. *J. Appl. Crystallogr.* **2012,** *45* (4), 849–854.

(4) Coudane, J.; Ustariz-Peyret, C.; Schwach, G.; Vert, M., More about the stereodependence of DD and LL pair linkages during the ring-opening polymerization of racemic lactide. *J. Polym. Sci., Part A: Polym. Chem.,* **1997,** *35* (9), 1651–1658.

(5) Kavala, V.; Naik, S.; Patel, B. K., A New Recyclable Ditribromide Reagent for Efficient Bromination under Solvent Free Condition. *J. Org. Chem.,* **2005,** *70* (11), 4267–4271.

(6) He, L.-P.; Hong, M.; Li, B.-X.; Liu, J.-Y.; Li, Y.-S., Ethylene/hexene living copolymerization and ethylene/methyl 10-undecenoate copolymerization by titanium complexes bearing phenoxy-phosphine or thiophenoxy-phosphine ligands. *Polymer,* **2010,** *51* (19), 4336–4339.

(7) Bakewell, C.; Cao, T.-P.-A.; Long, N.; Le Goff, X. F.; Auffrant, A.; Williams, C. K., Yttrium Phosphasalen Initiators for *rac*-Lactide Polymerization: Excellent Rates and High Iso-Selectivities. *J. Am. Chem. Soc.,* **2012,** *134* (51), 20577–20580.

(8) Bakewell, C.; Cao, T.-P.-A.; Le Goff, X. F.; Long, N. J.; Auffrant, A.; Williams, C. K., Yttrium Phosphasalen Initiators for *rac*-Lactide Polymerization. *Organometallics,* **2013,** *32* (5), 1475–1483.

(9) Gregson, C. K. A.; Blackmore, I. J.; Gibson, V. C.; Long, N. J.; Marshall, E. L.; White, A. J. P., Titanium–salen complexes as initiators for the ring opening polymerisation of *rac*-lactide. *Dalton Trans.,* **2006,** (25), 3134–3140.

(10) Myers, D.; White, A. J. P.; Forsyth, C. M.; Bown, M.; Williams, C. K., Phosphasalen Indium Complexes Showing High Rates and Isoselectivities in *rac*-Lactide Polymerizations. *Angew. Chem. Int. Ed.,* **2017,** *56* (19), 5277–5282.

# *Appendices*

*We cannot become what we want by remaining what we are...*

*~ Max Depree ~*

# A1. Chapter 3

## A1.1. Spectral characterisation for ligands $^{P\text{-salen}}L^1H_2$–$^{P\text{-salen}}L^4H_2$

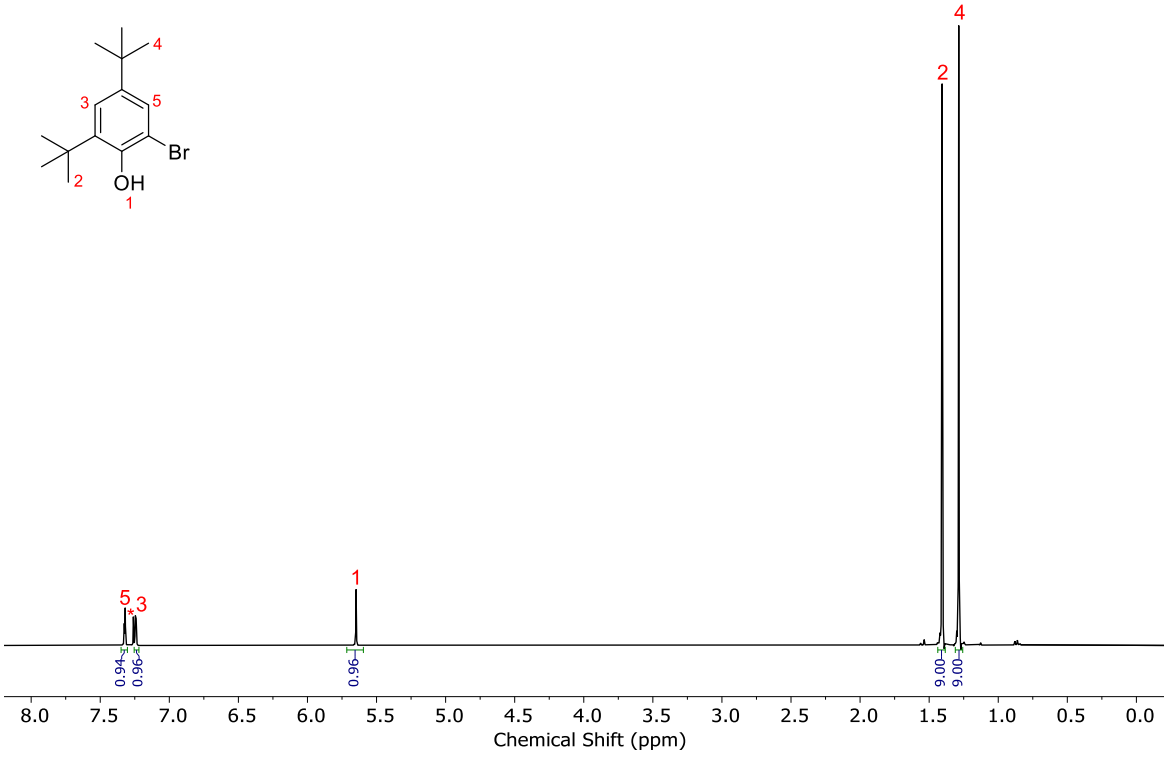



**Figure A1.1.** $^1$H NMR spectrum of 2-bromo-4,6-di-tert-butylphenol in $CDCl_3$.

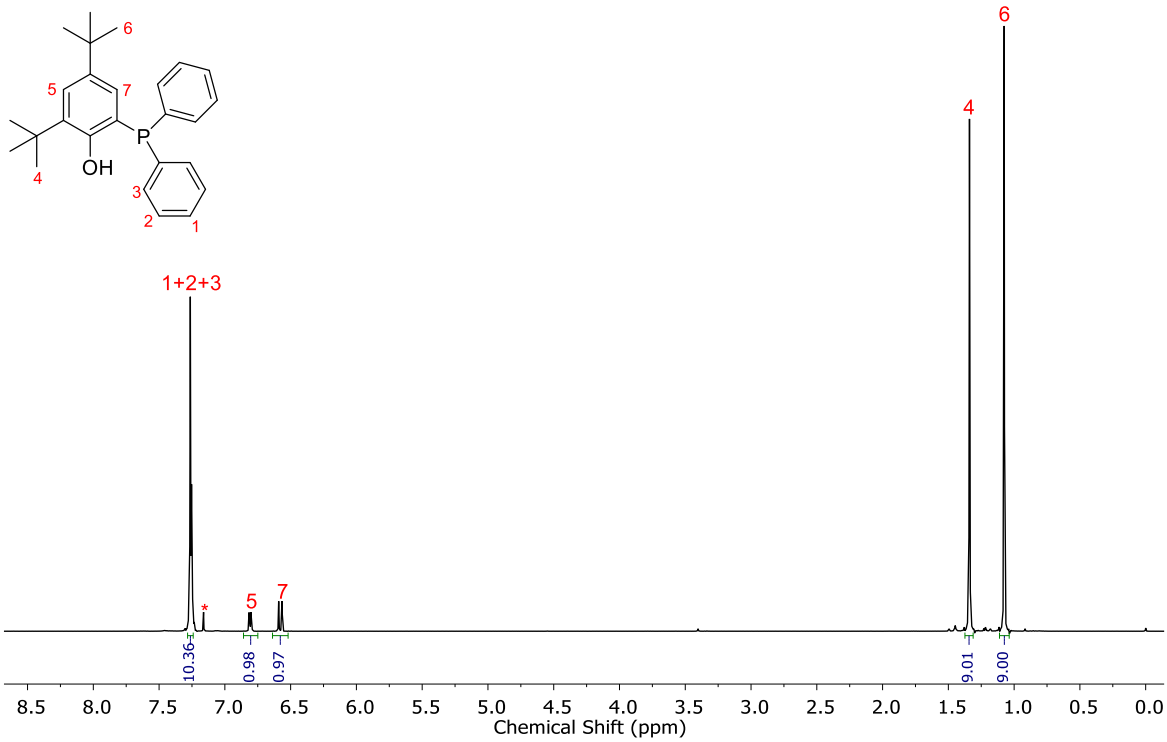



**Figure A1.2.** $^1$H NMR spectrum of **S2** in $CDCl_3$.

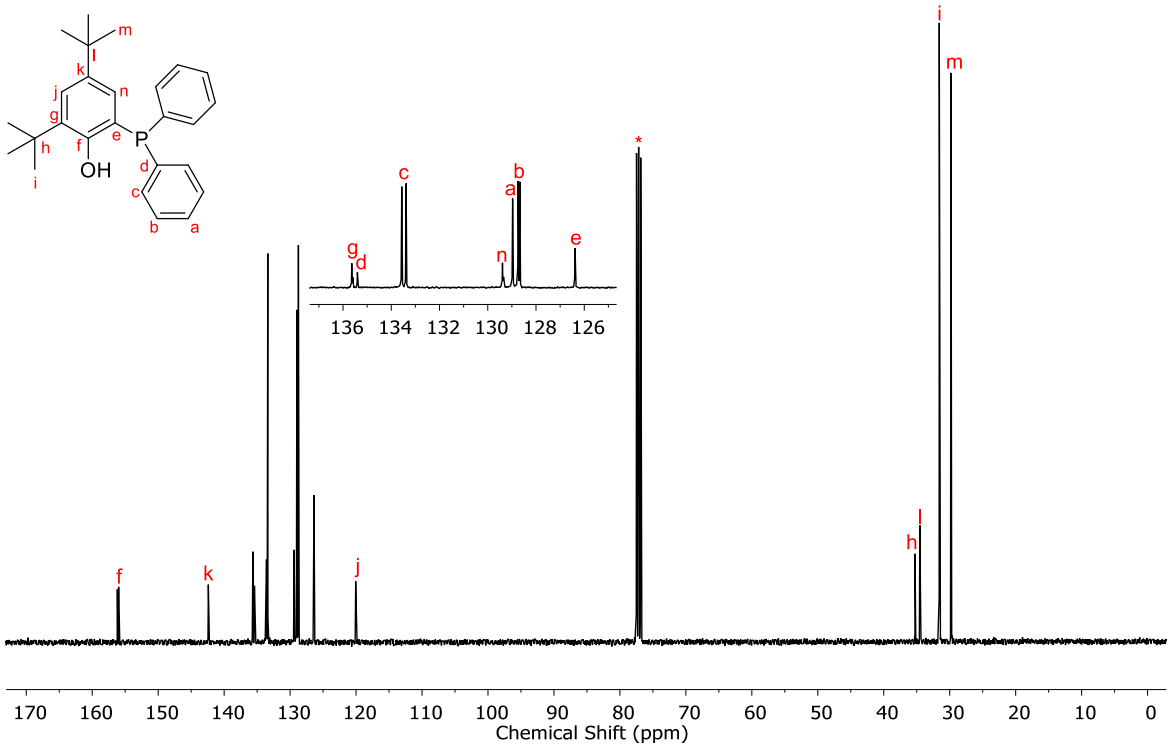



**Figure A1.3.** $^{13}C\{^{1}H\}$ NMR spectrum of **S2** in $CDCl_3$.

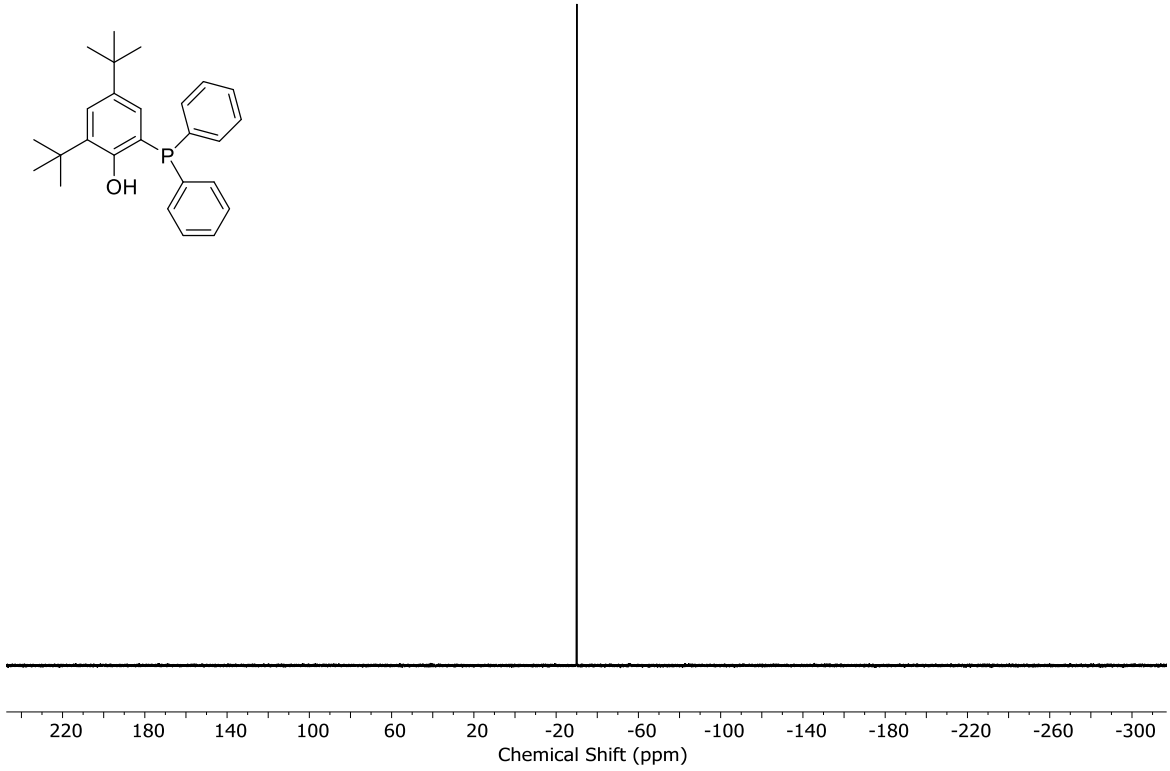



**Figure A1.4.** $^{31}P\{^{1}H\}$ NMR spectrum of **S2** in $CDCl_3$.

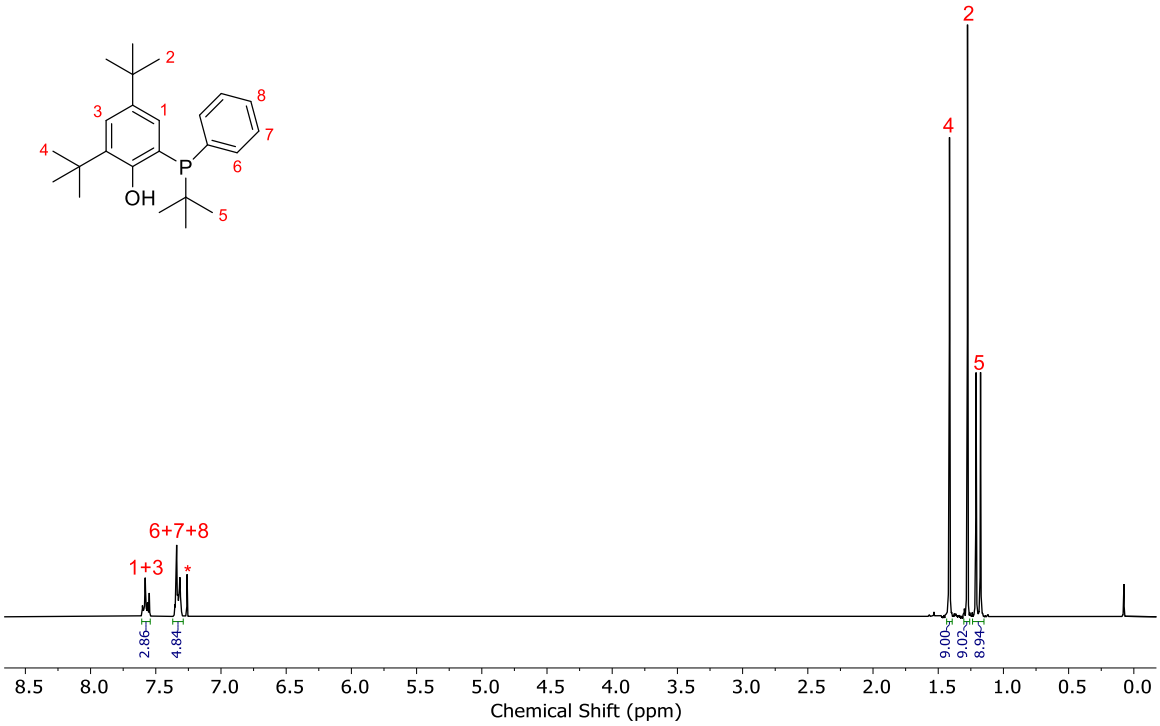



**Figure A1.5.** $^{1}H$ NMR spectrum of **S3** in $CDCl_3$.

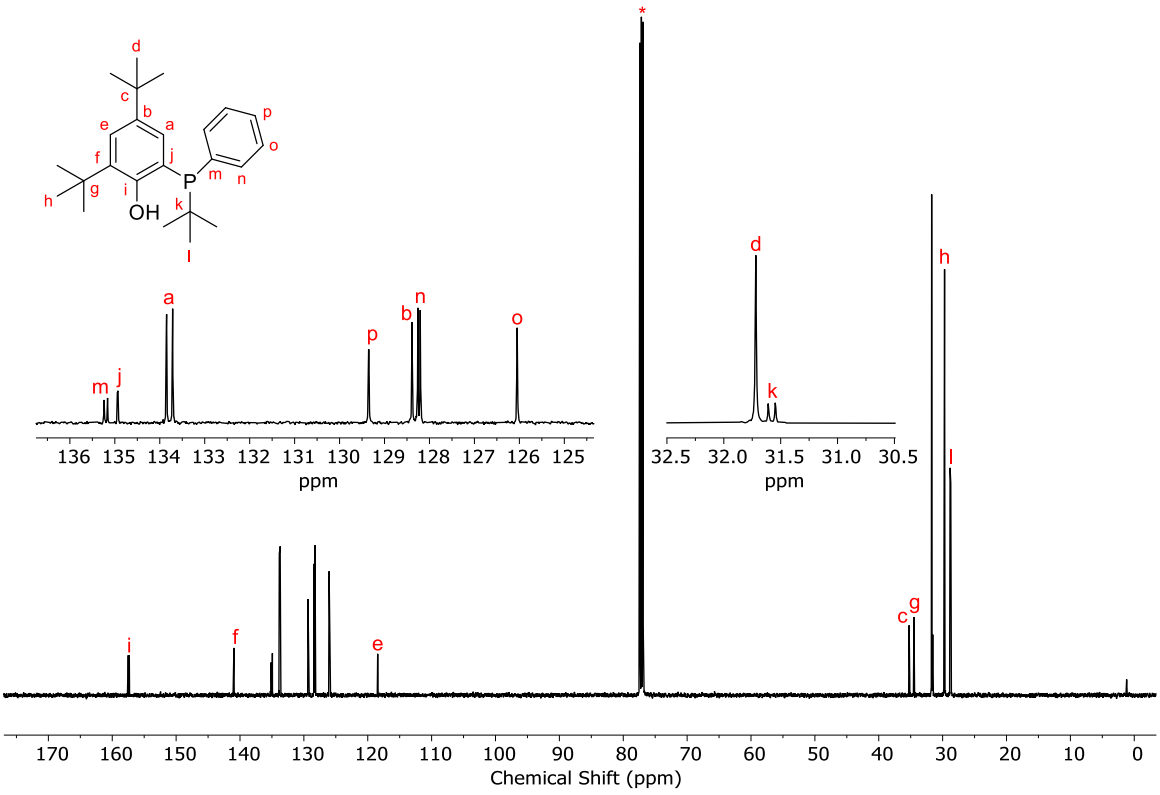



**Figure A1.6.** $^{13}C\{^{1}H\}$ NMR spectrum of **S3** in $CDCl_3$.

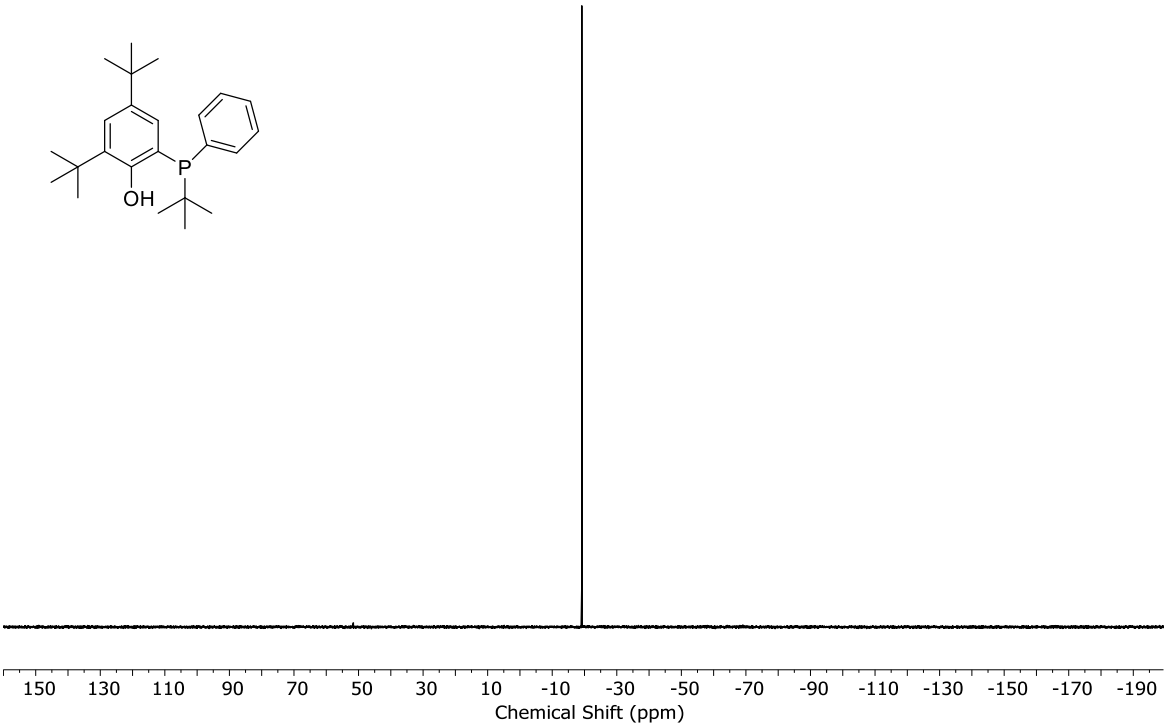



**Figure A1.7.** $^{31}P\{^{1}H\}$ NMR spectrum of **S3** in $CDCl_3$.

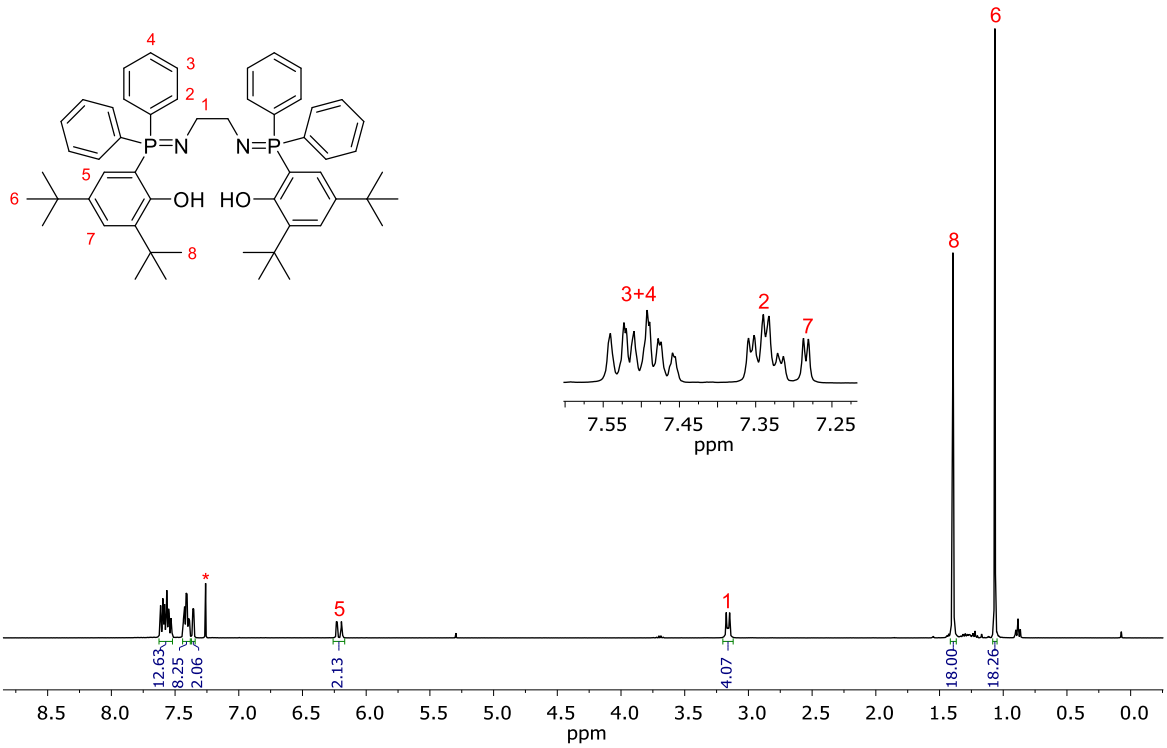



**Figure A1.8.** $^{1}H$ NMR spectrum of ligand $^{\textbf{P-salen}}\textbf{L}^{1}\textbf{H}_2$ in $CDCl_3$.

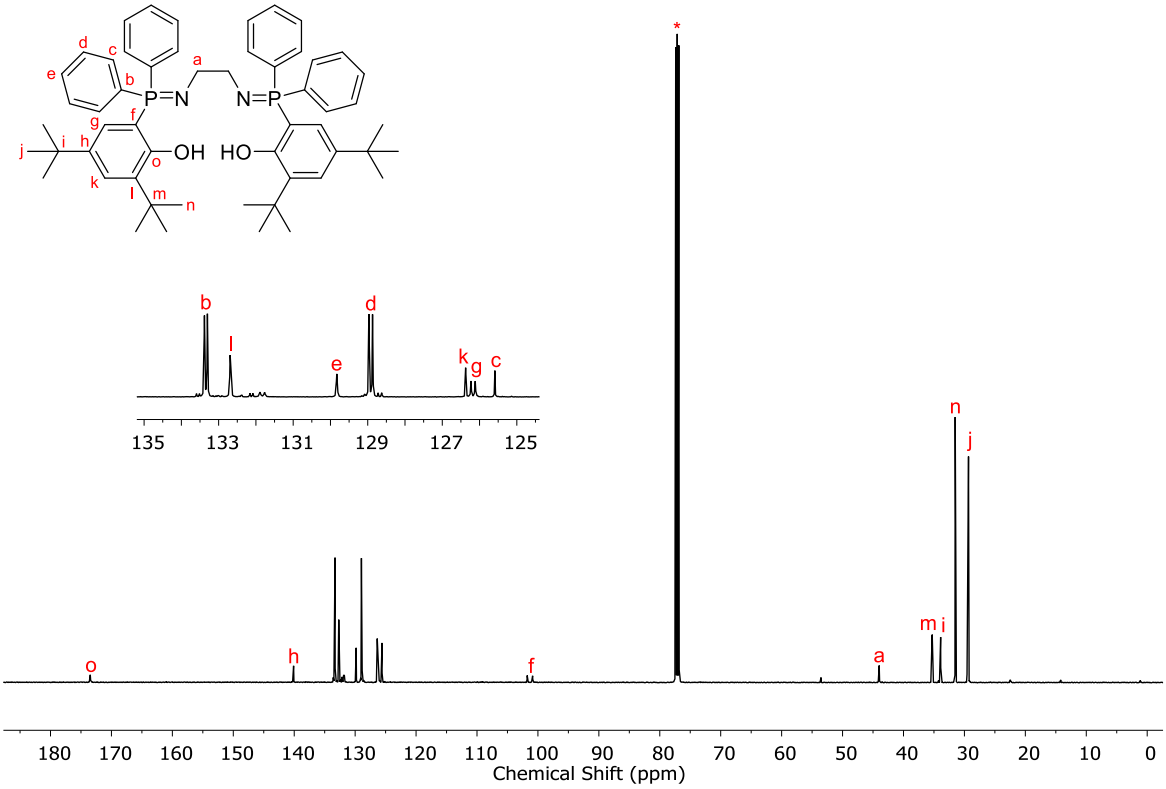



**Figure A1.9.** $^{13}C\{^{1}H\}$ NMR spectrum of ligand $^{\text{P-salen}}\mathbf{L^{1}H_{2}}$ in $CDCl_3$.

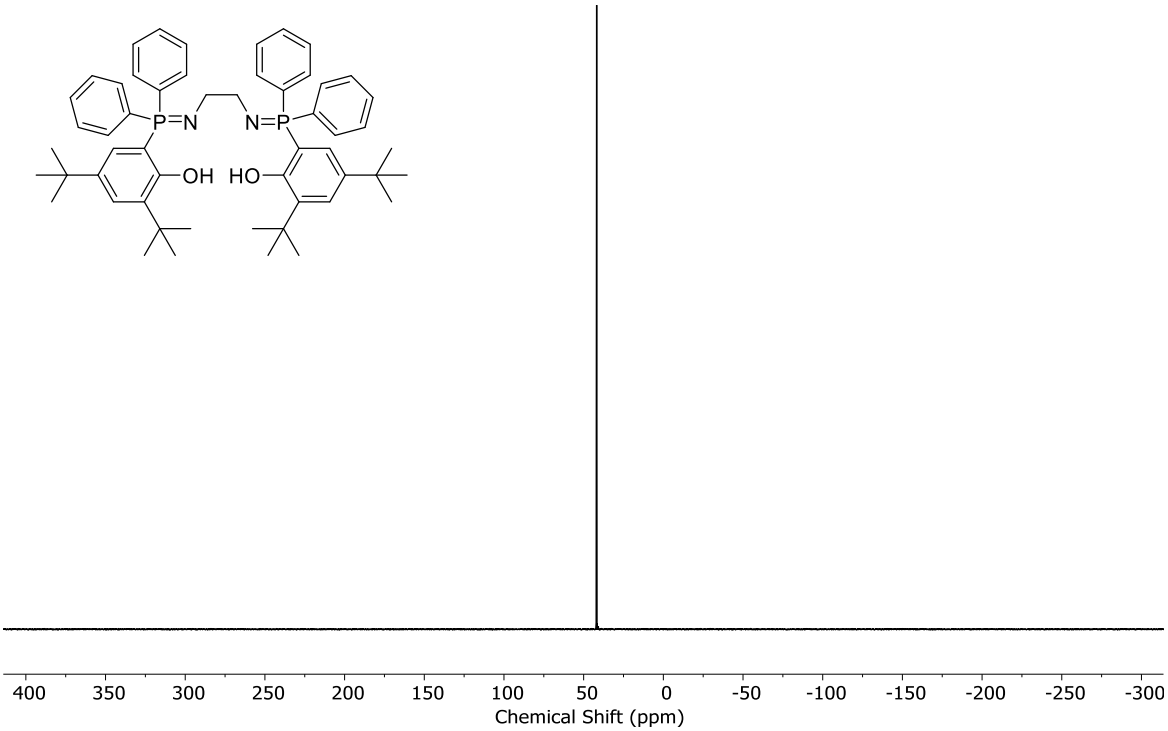



**Figure A1.10.** $^{31}P\{^{1}H\}$ NMR spectrum of ligand $^{\text{P-salen}}\mathbf{L^{1}H_{2}}$ in $CDCl_3$.

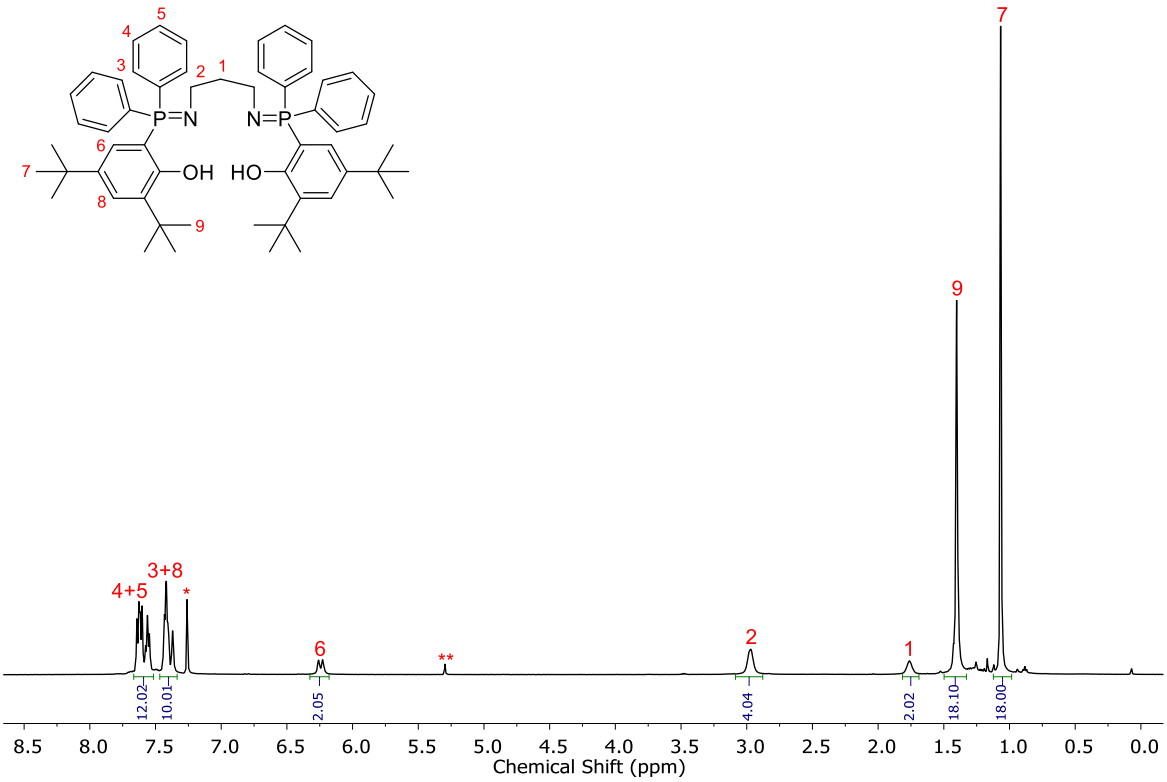



**Figure A1.11.** $^{1}$H NMR spectrum of ligand $^{\mathbf{P\text{-}salen}}\mathbf{L}^{\mathbf{2}}\mathbf{H_2}$ in $CDCl_3$.

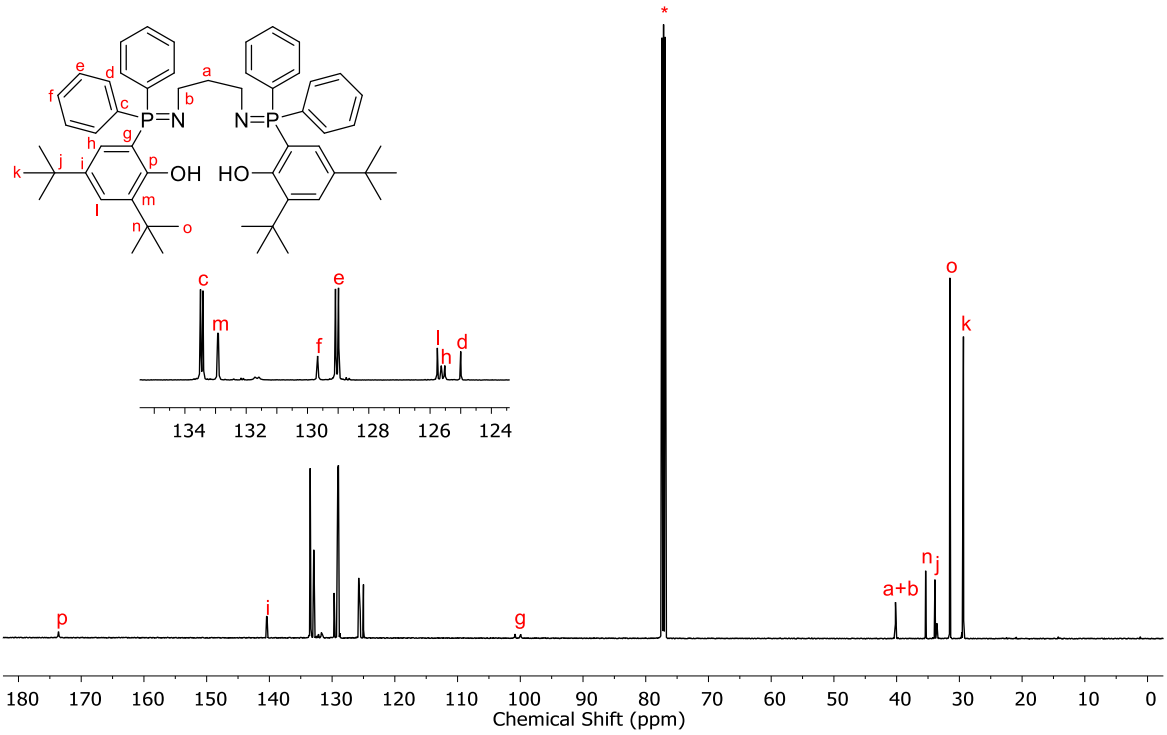



**Figure A1.12.** $^{13}$C{$^{1}$H} NMR spectrum of ligand $^{\mathbf{P\text{-}salen}}\mathbf{L}^{\mathbf{2}}\mathbf{H_2}$ in $CDCl_3$.

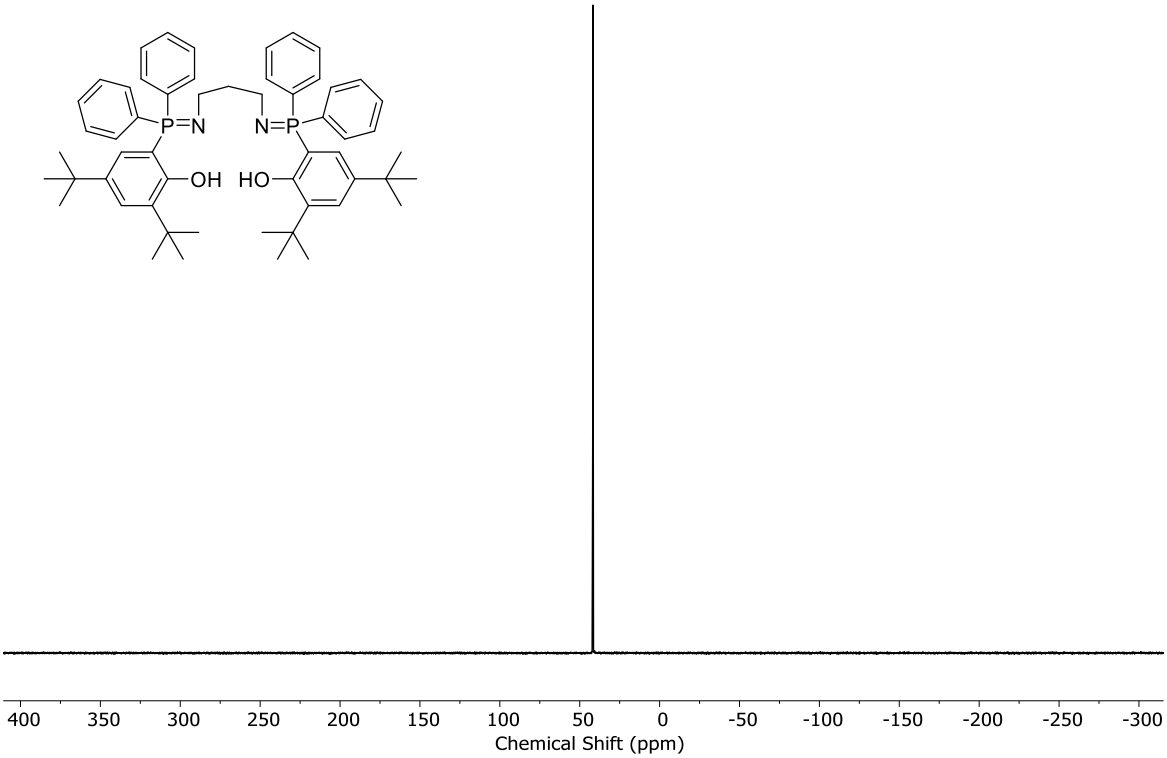



**Figure A1.13.** $^{31}P\{^{1}H\}$ NMR spectrum of ligand $^{\textbf{P-salen}}\textbf{L}^{\textbf{2}}\textbf{H}_{\textbf{2}}$ in $CDCl_3$.

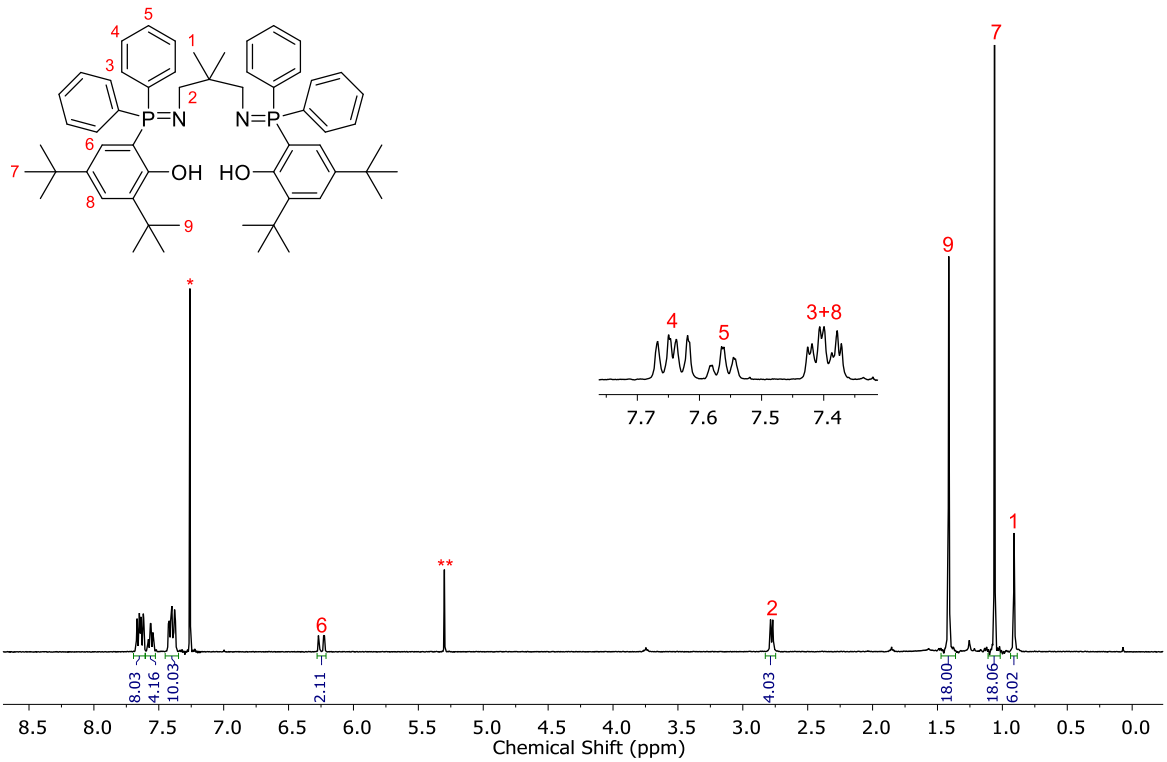



**Figure A1.14.** $^{1}H$ NMR spectrum of ligand $^{\textbf{P-salen}}\textbf{L}^{\textbf{3}}\textbf{H}_{\textbf{2}}$ in $CDCl_3$.

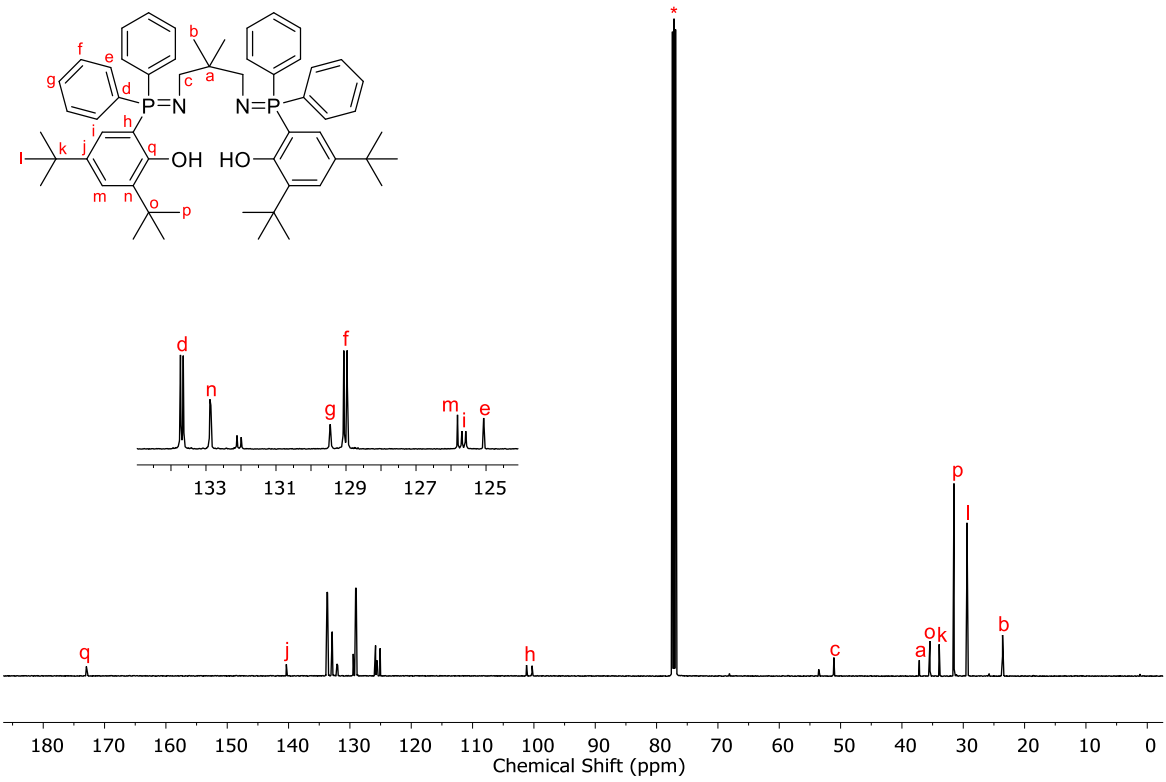



**Figure A1.15.** $^{13}C\{^{1}H\}$ NMR spectrum of ligand $^{\textbf{P-salen}}\textbf{L}^{3}\textbf{H}_2$ in $CDCl_3$.

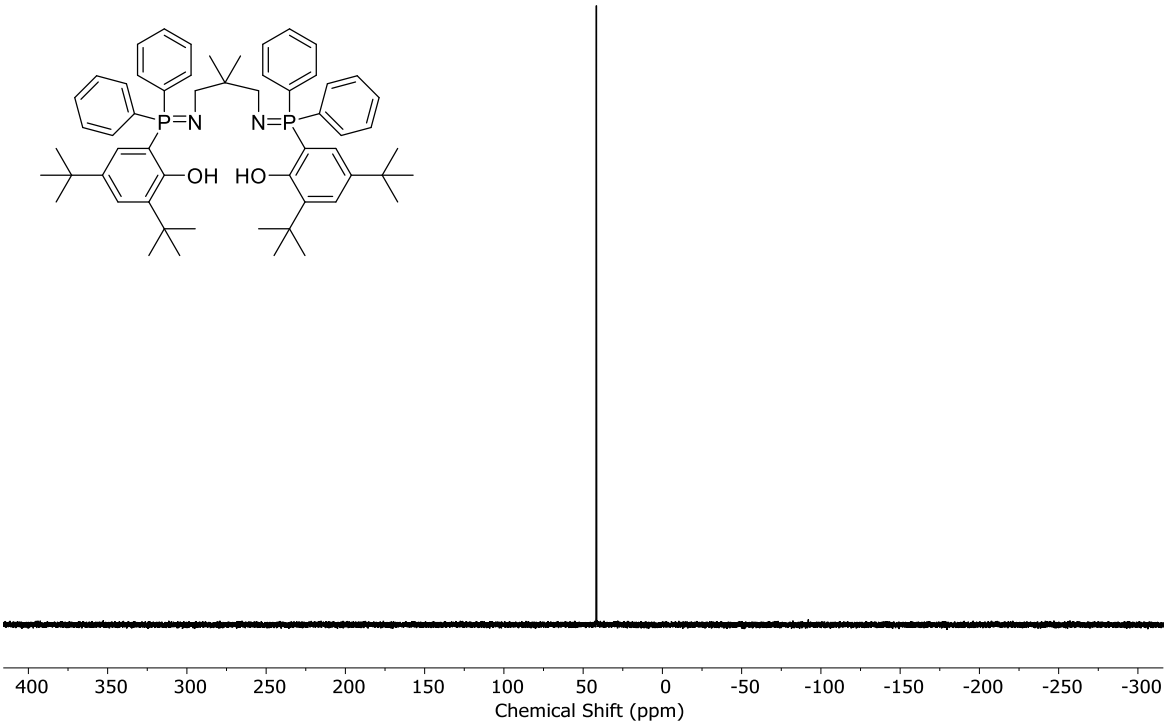



**Figure A1.16.** $^{31}P\{^{1}H\}$ NMR spectrum of ligand $^{\textbf{P-salen}}\textbf{L}^{3}\textbf{H}_2$ in $CDCl_3$.

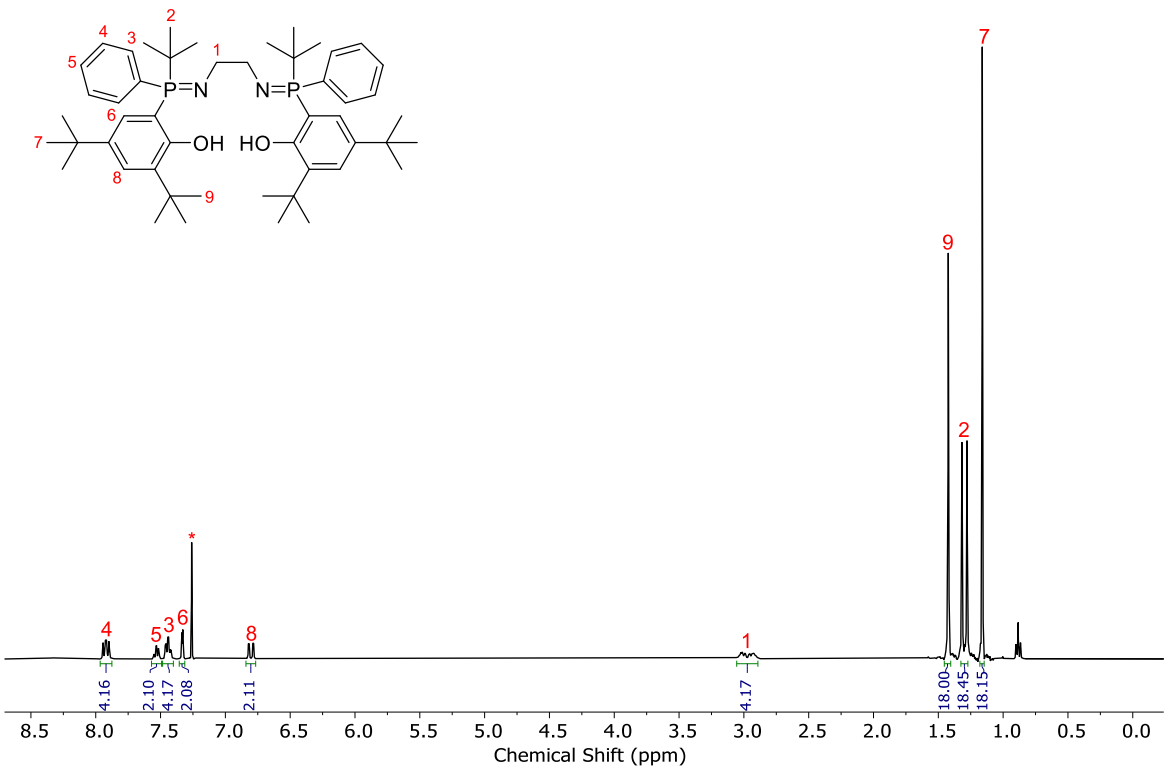



**Figure A1.17.** $^{1}$H NMR spectrum of ligand $^{\text{P-salen}}\mathbf{L}^{4}\mathbf{H}_2$ in $CDCl_3$.

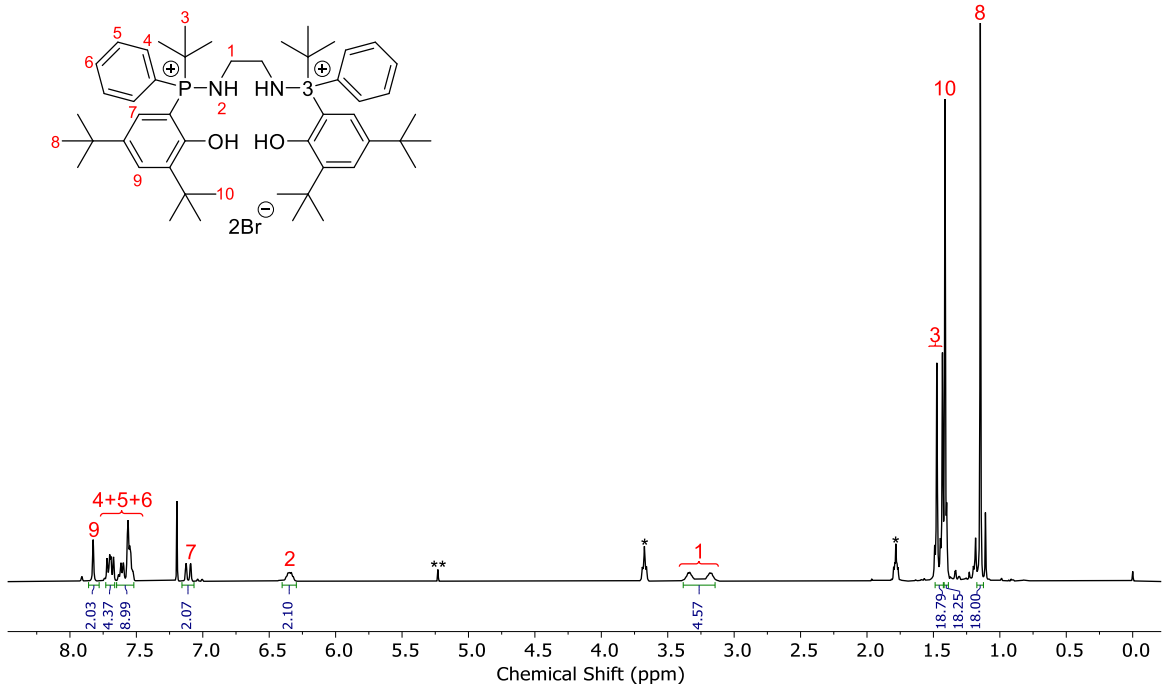



**Figure A1.18.** $^{1}$H NMR spectrum of ligand $^{\text{P-salen}}\mathbf{L}^{4}\mathbf{H}_2$ in $CDCl_3$ (prior to purification by column chromatography).

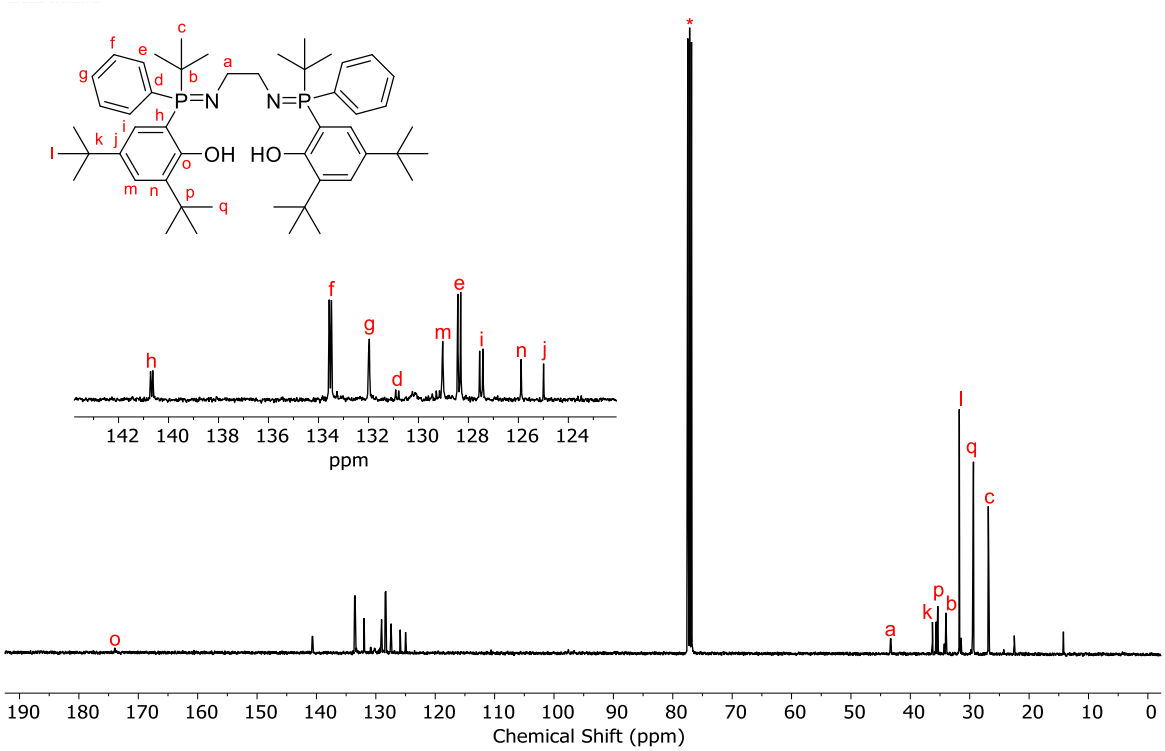



**Figure A1.19.** $^{13}C\{^{1}H\}$ NMR spectrum of ligand $^{\text{P-salen}}\mathbf{L^4H_2}$ in $CDCl_3$.

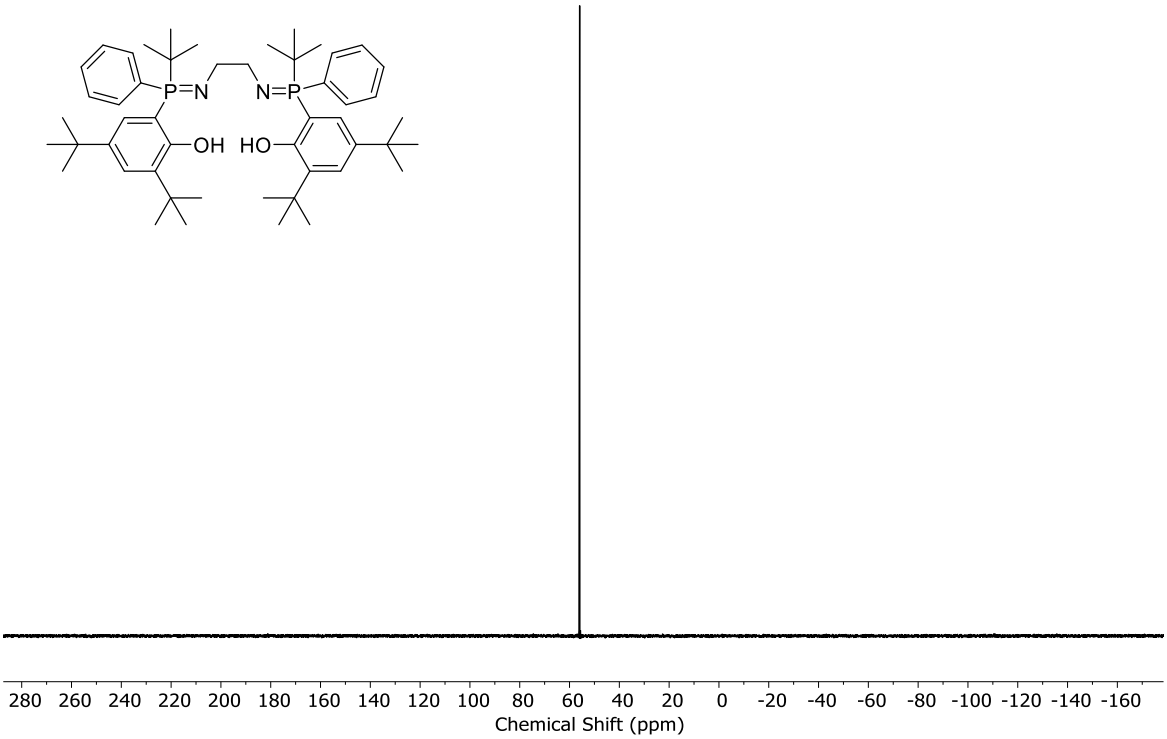



**Figure A1.20.** $^{31}P\{^{1}H\}$ NMR spectrum of ligand $^{\text{P-salen}}\mathbf{L^4H_2}$ in $CDCl_3$.

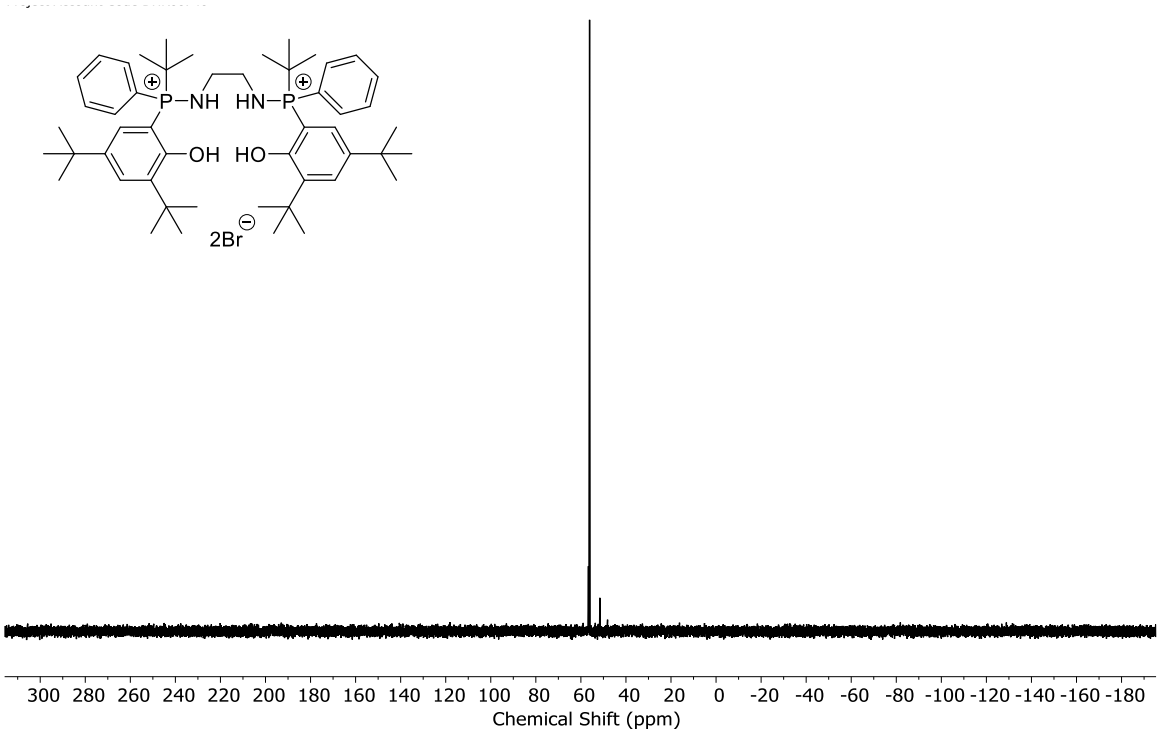



**Figure A1.21.** $^{31}P\{^{1}H\}$ NMR spectrum of ligand $^{\mathbf{P\text{-}salen}}\mathbf{L^4H_2}$ in $CDCl_3$ (prior to purification by column chromatography).

## A1.2. Spectral characterisation for indium complexes 3.1–3.5

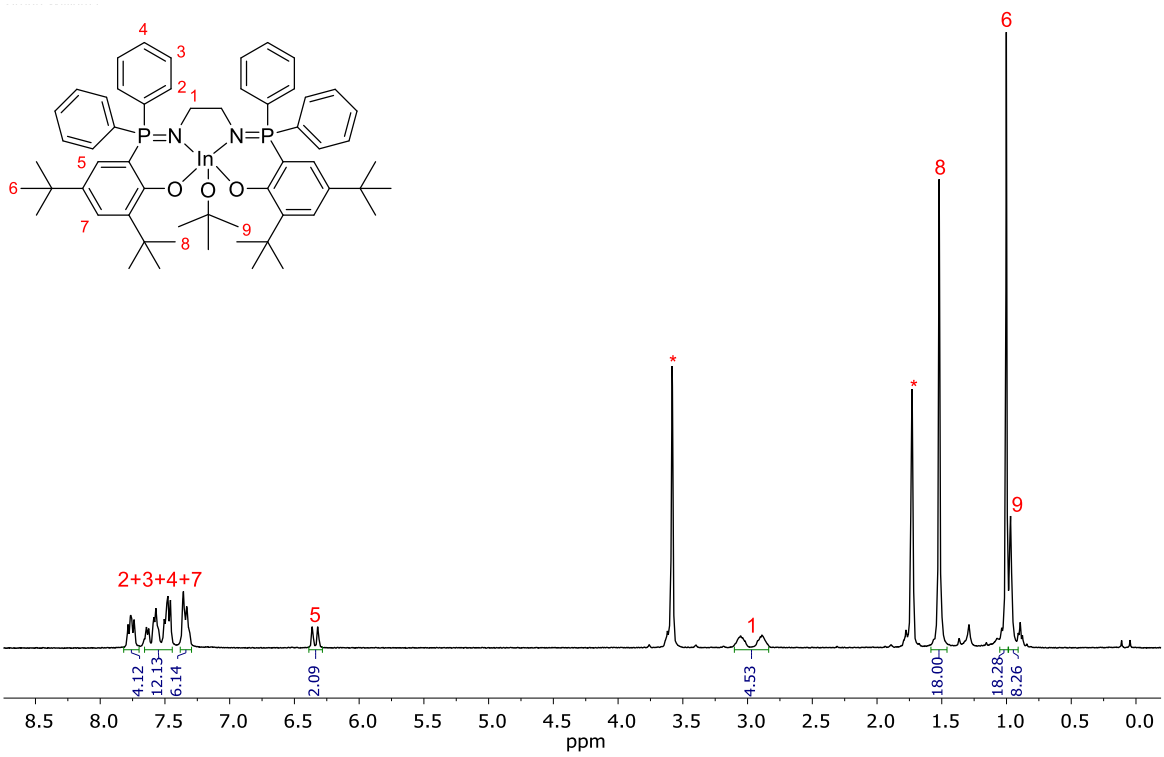



**Figure A1.22.** $^{1}$H NMR spectrum of complex **3.1** in THF-$d_8$.

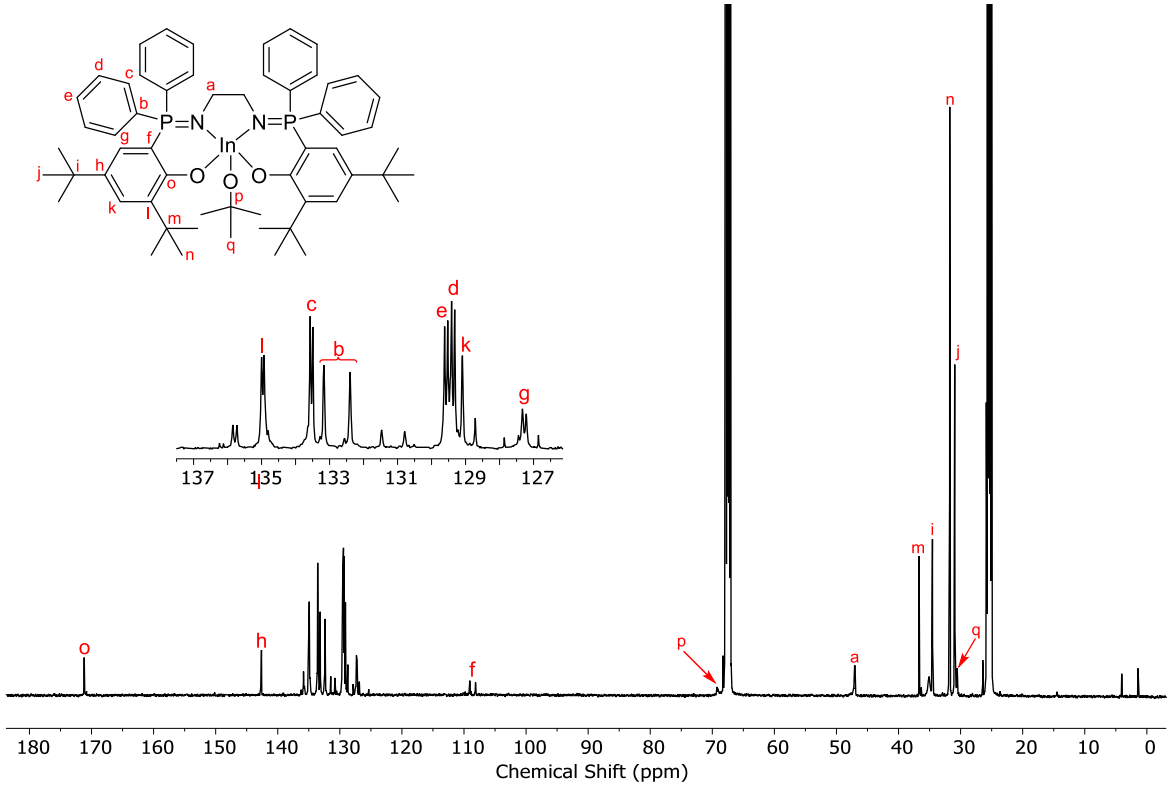



**Figure A1.23.** $^{13}$C{$^{1}$H} NMR spectrum of complex **3.1** in THF-$d_8$.

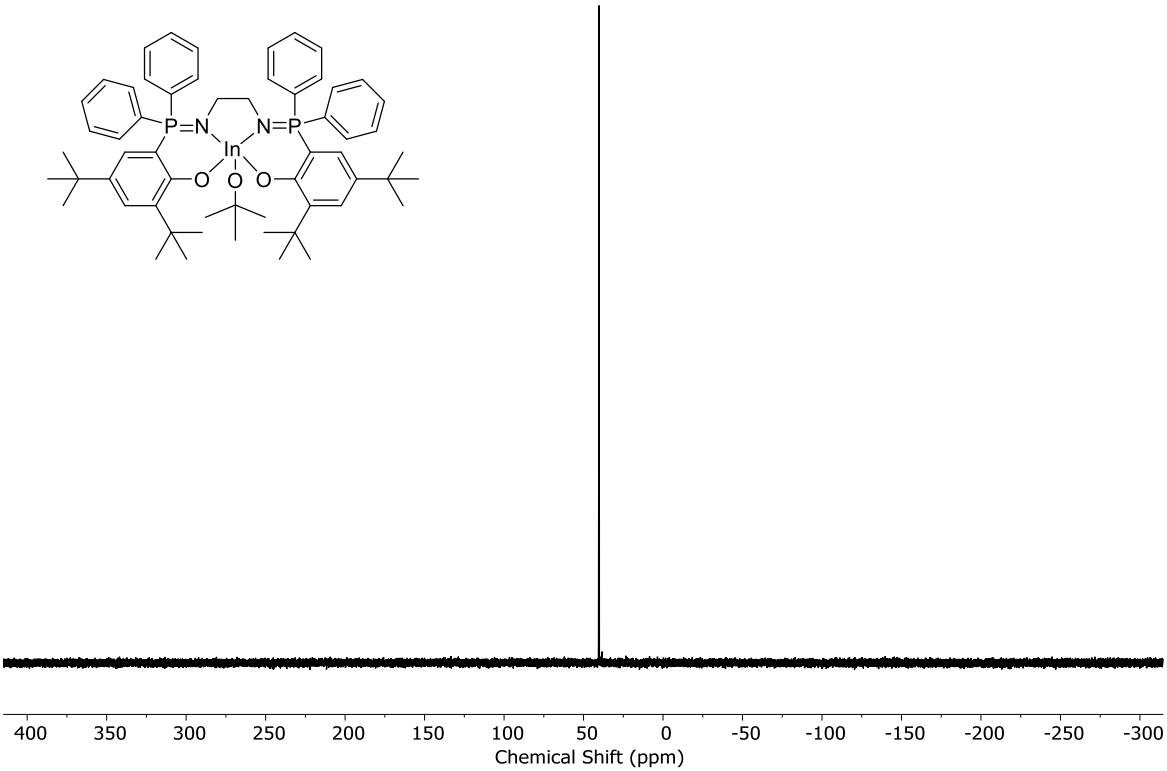



**Figure A1.24.** $^{31}P\{^{1}H\}$ NMR spectrum of complex **3.1** in THF-$d_8$.

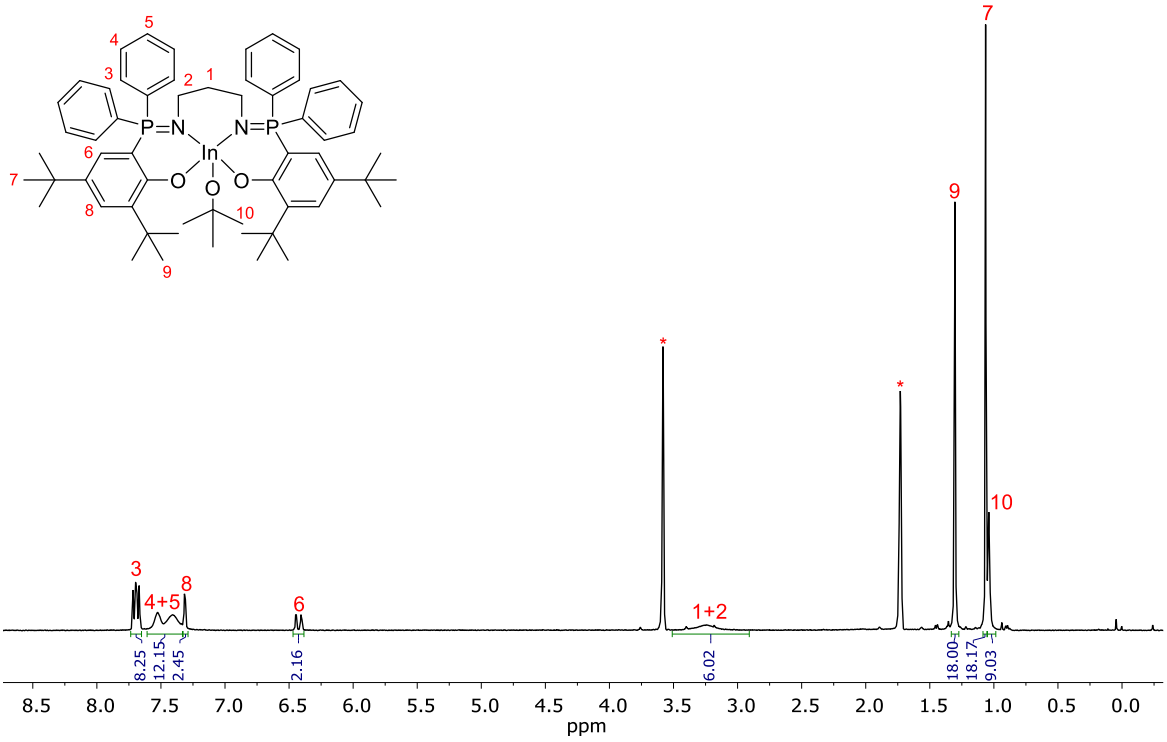



**Figure A1.25.** $^{1}H$ NMR spectrum of complex **3.2** in THF-$d_8$.

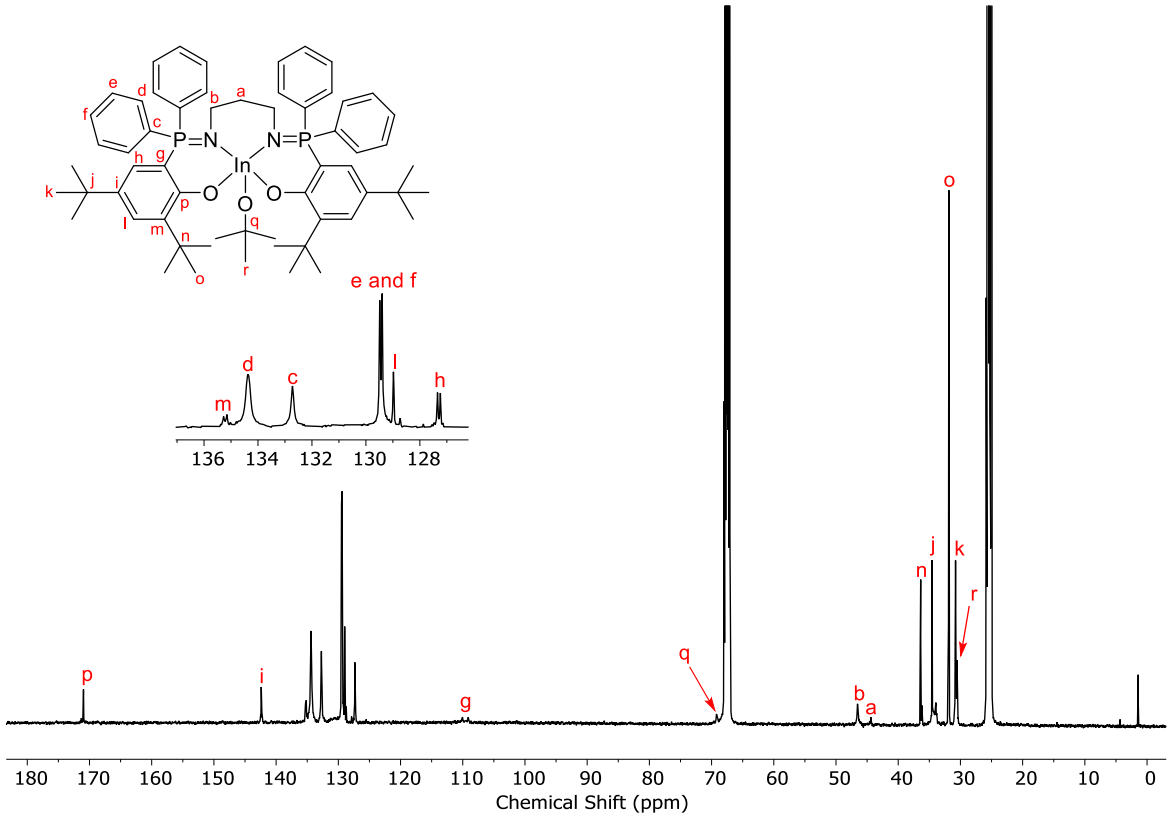



**Figure A1.26.** $^{13}C\{^{1}H\}$ NMR spectrum of complex **3.2** in THF-$d_8$.

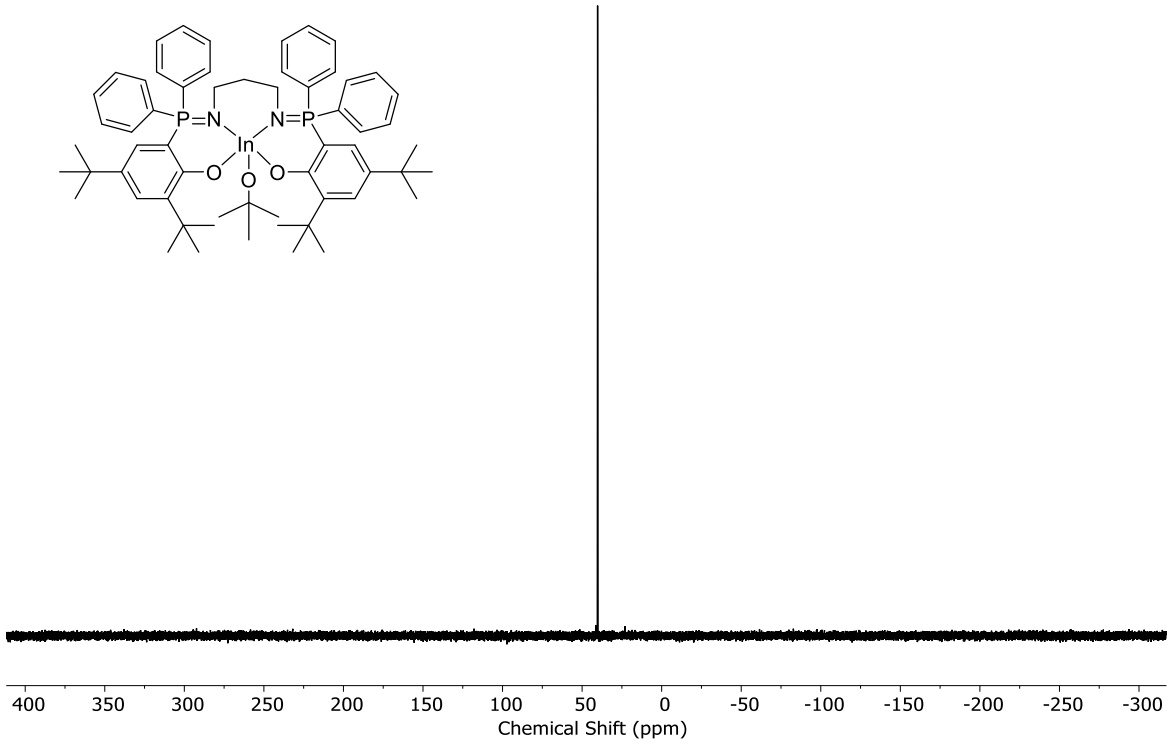



**Figure A1.27.** $^{31}P\{^{1}H\}$ NMR spectrum of complex **3.2** in THF-$d_8$.

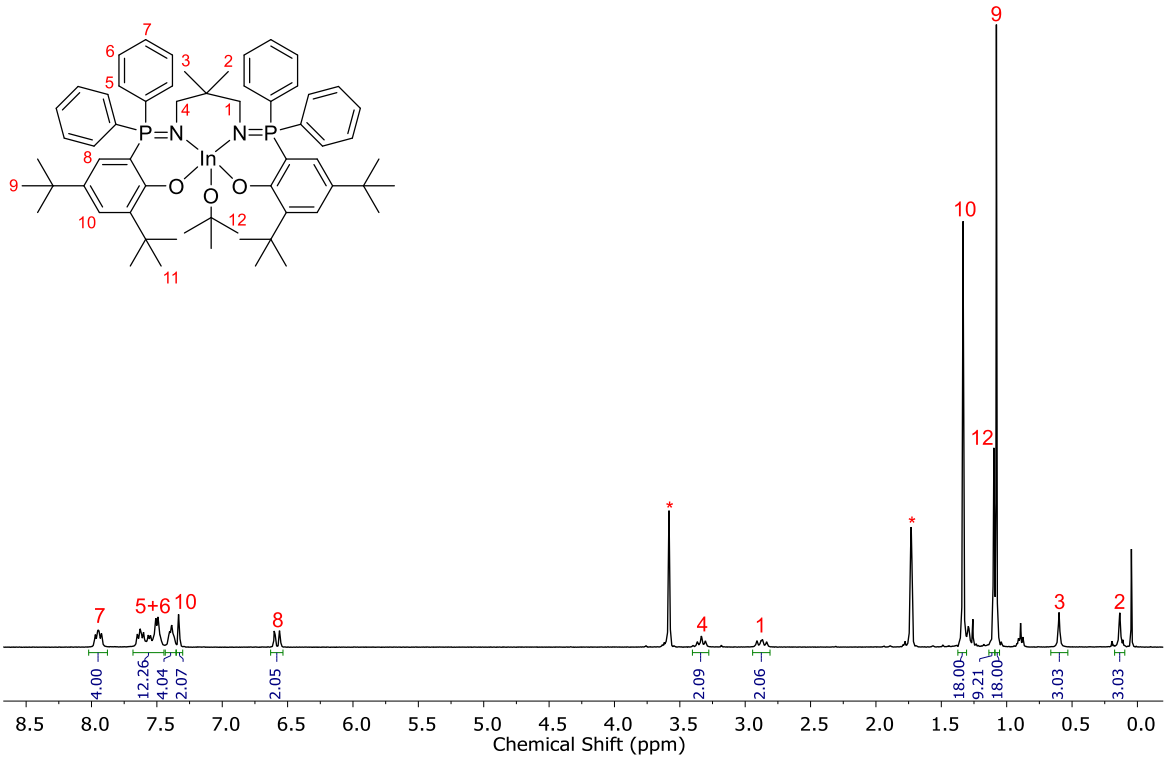



**Figure A1.28.** $^{1}$H NMR spectrum of complex **3.3** in THF-$d_8$.

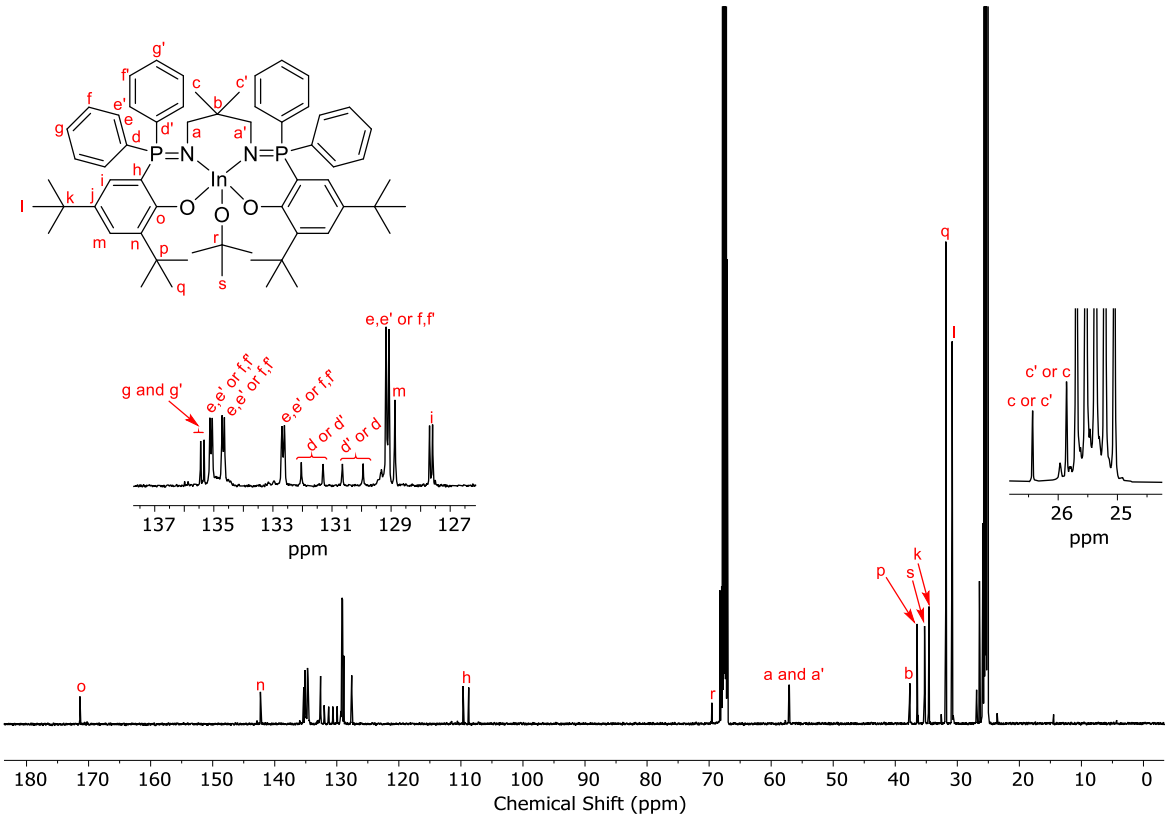



**Figure A1.29.** $^{13}$C{$^{1}$H} NMR spectrum of complex **3.3** in THF-$d_8$.

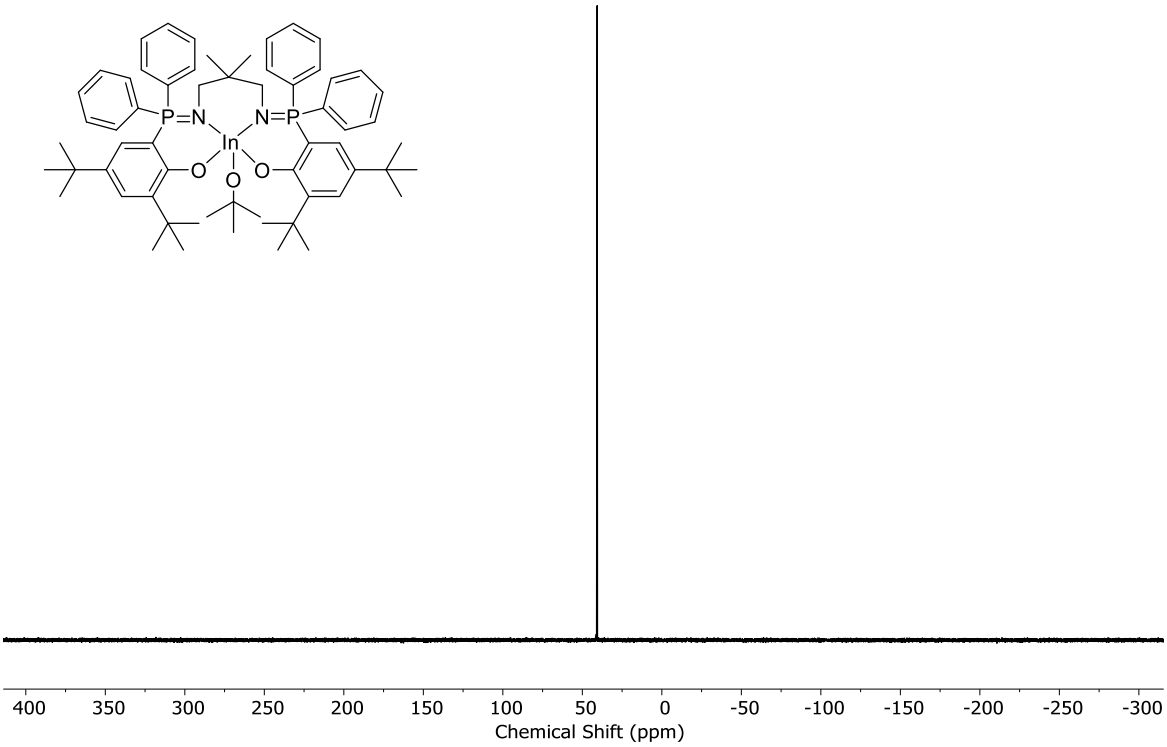



**Figure A1.30.** $^{31}P\{^{1}H\}$ NMR spectrum of complex **3.3** in THF-$d_8$.

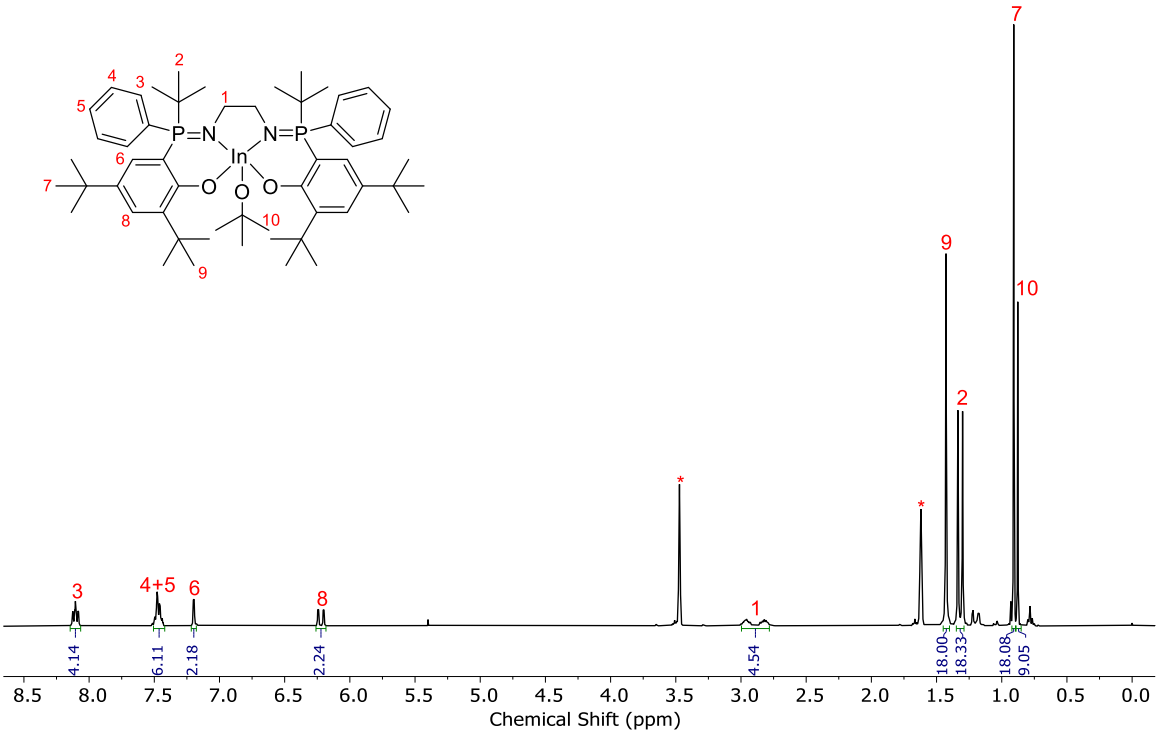



**Figure A1.31.** $^{1}H$ NMR spectrum of complex **3.4** in THF-$d_8$.

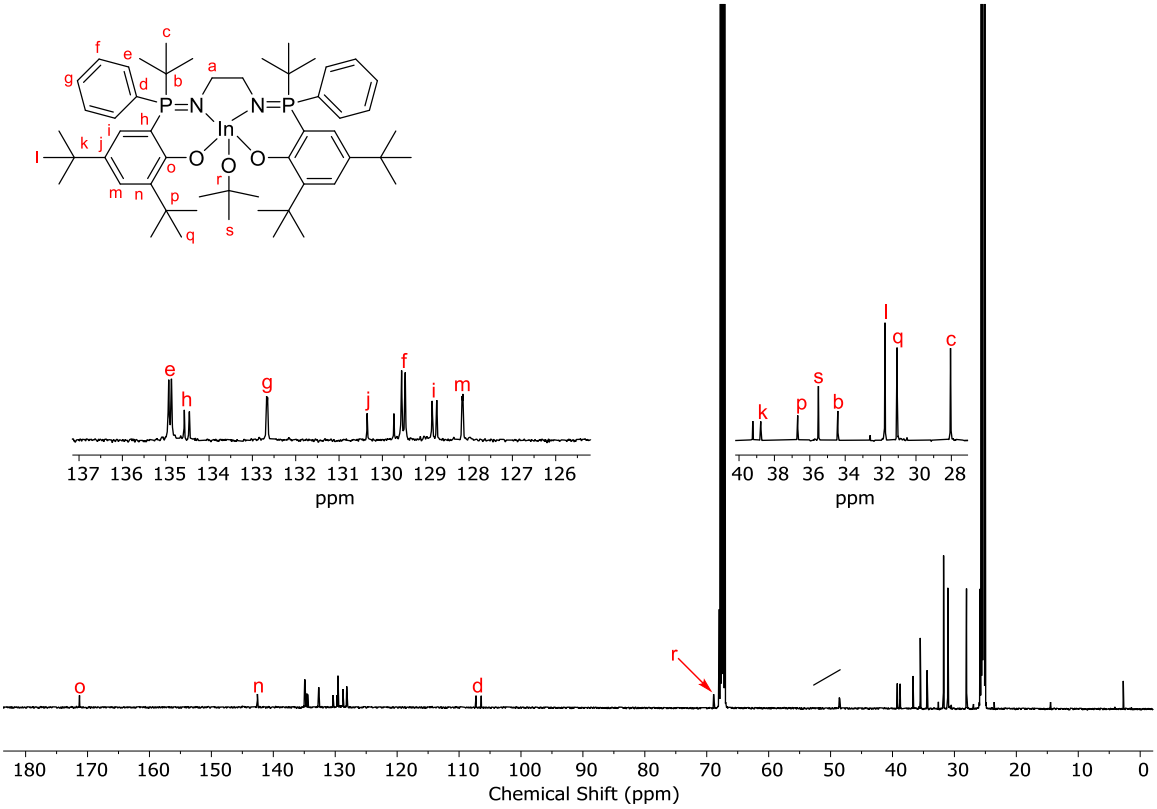



**Figure A1.32.** $^{13}C\{^{1}H\}$ NMR spectrum of complex **3.4** in THF-$d_8$.

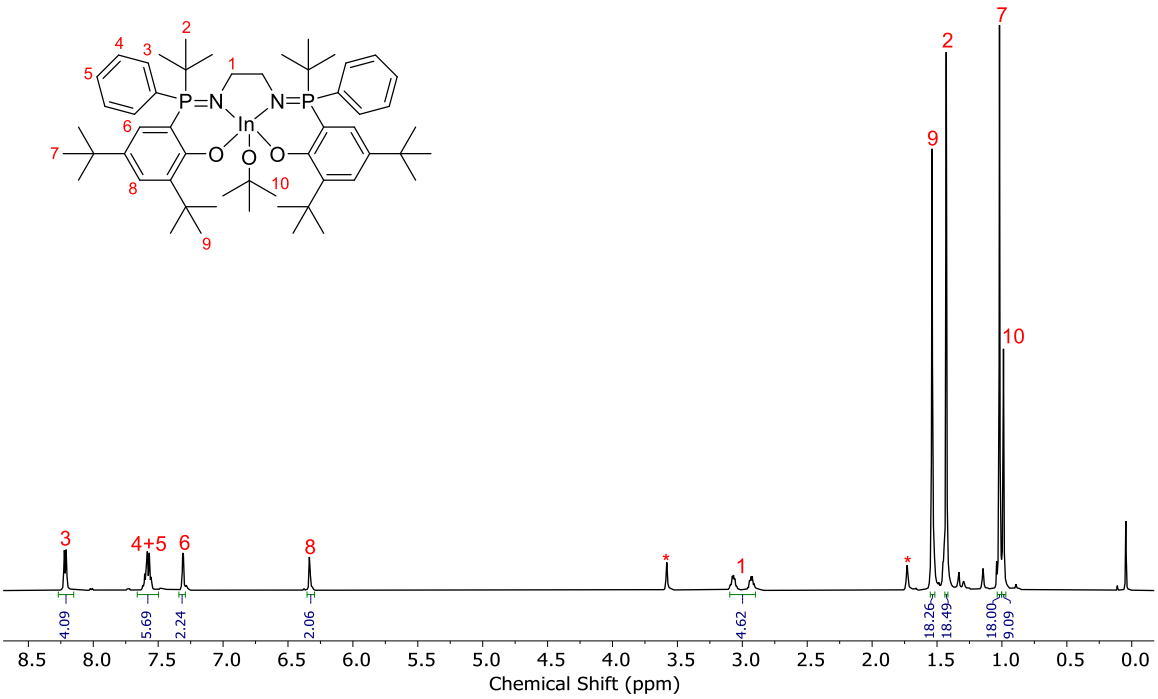



**Figure A1.33.** $^{1}H\{^{31}P\}$ NMR spectrum of complex **3.4** in THF-$d_8$.

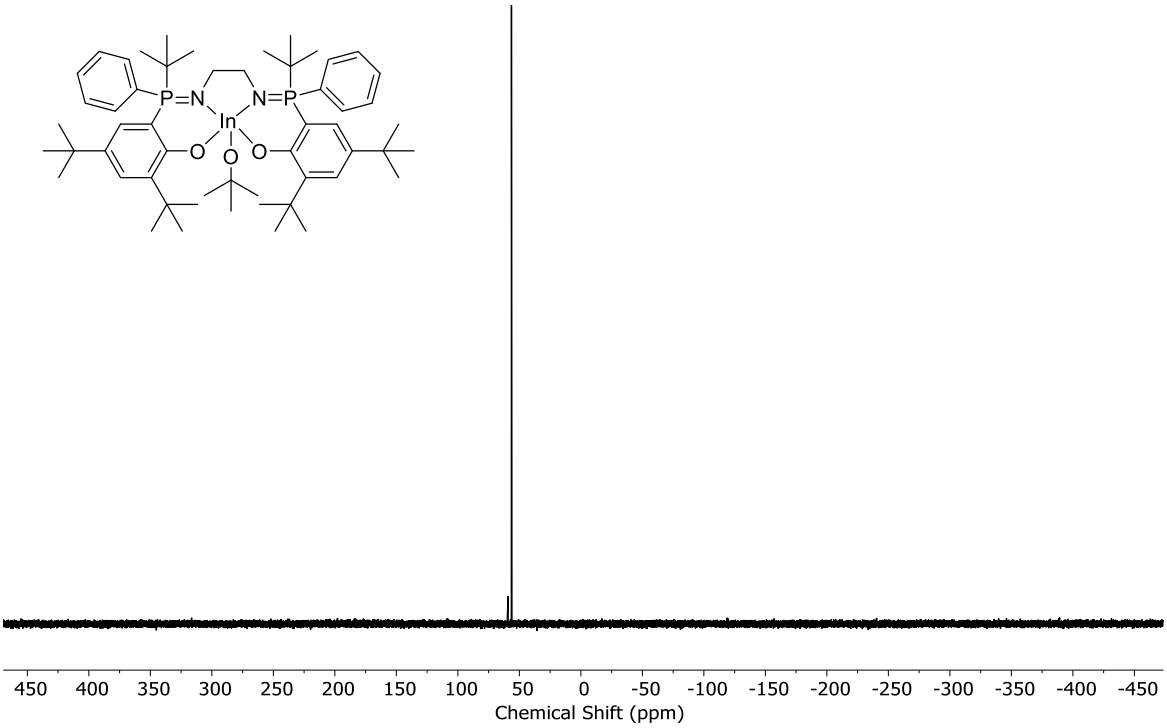



**Figure A1.34.** $^{31}P\{^{1}H\}$ NMR spectrum of complex **3.4** in THF-$d_8$.

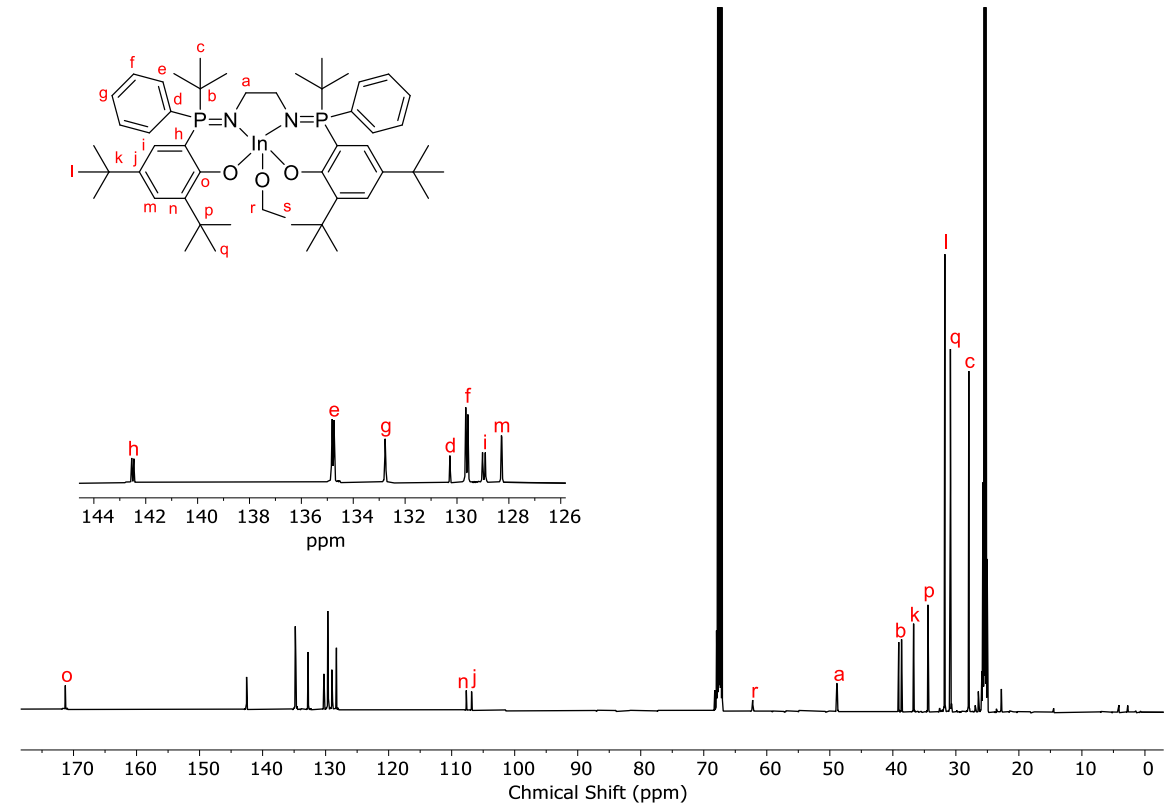



**Figure A1.35.** $^{13}C\{^{1}H\}$ NMR spectrum of complex **3.5** in THF-$d_8$.

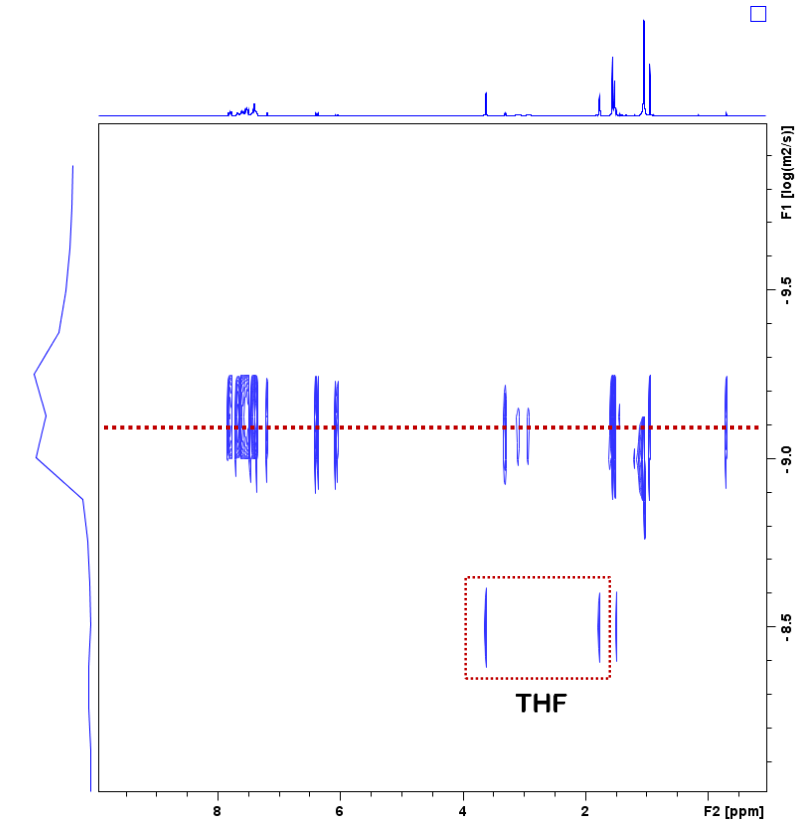



**Figure A1.36.** $^{1}$H DOSY NMR spectrum of complex **3.1** in THF-$d_8$.

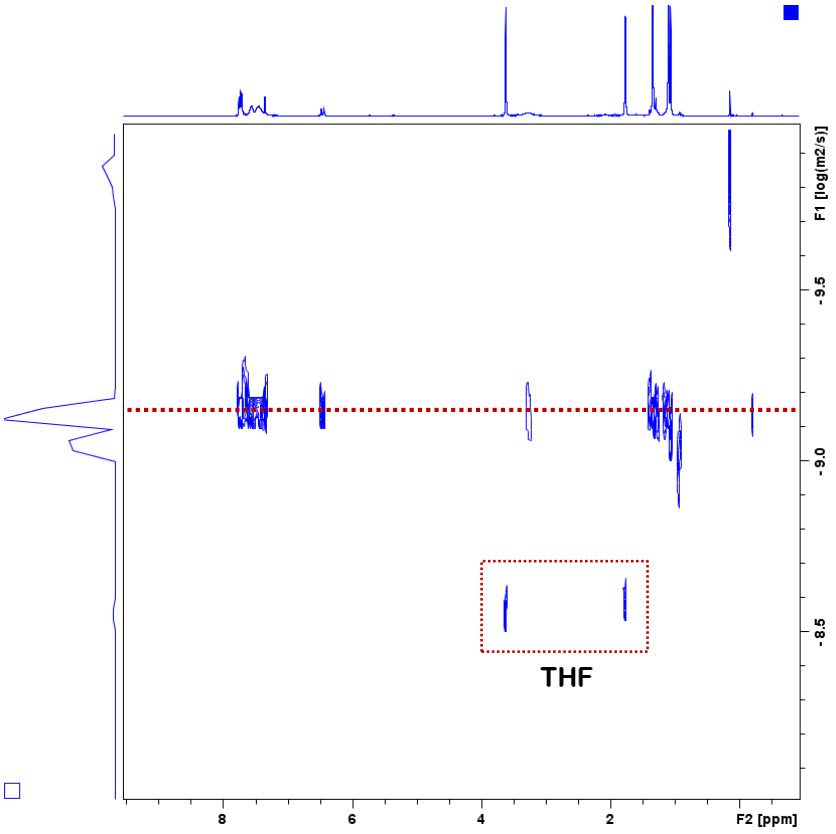



**Figure A1.37.** $^{1}$H DOSY NMR spectrum of complex **3.2** in THF-$d_8$.

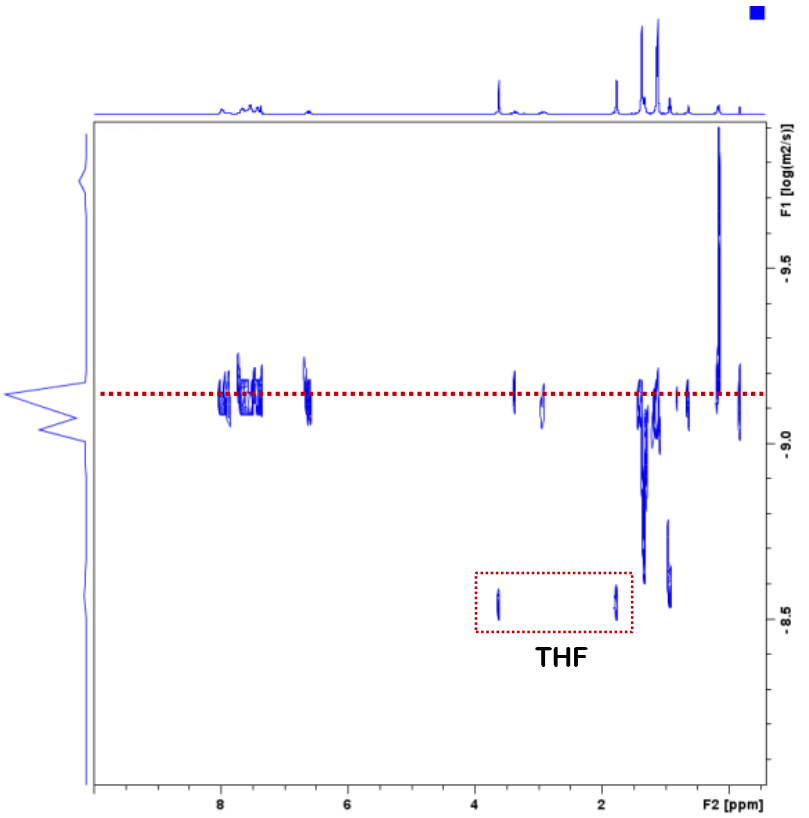



**Figure A1.38.** $^{1}$H DOSY NMR spectrum of complex **3.3** in THF-$d_8$.

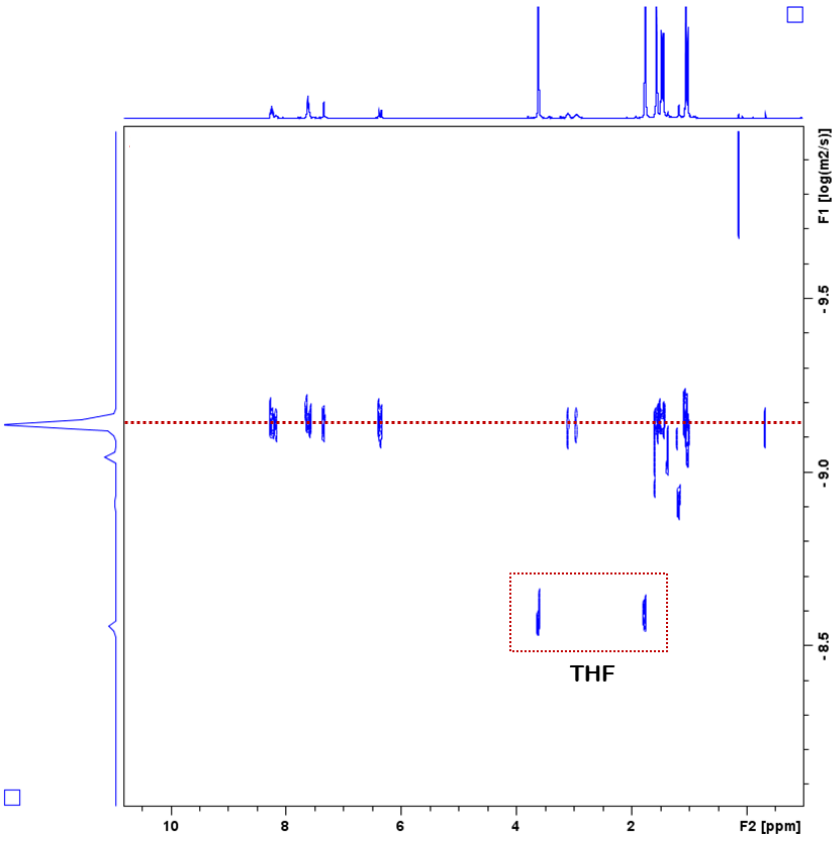



**Figure A1.39.** $^{1}$H DOSY NMR spectrum of complex **3.4** in THF-$d_8$.

### A1.3. Additional crystallographic data for ligand $^{P\text{-}salen}L^4H_2$

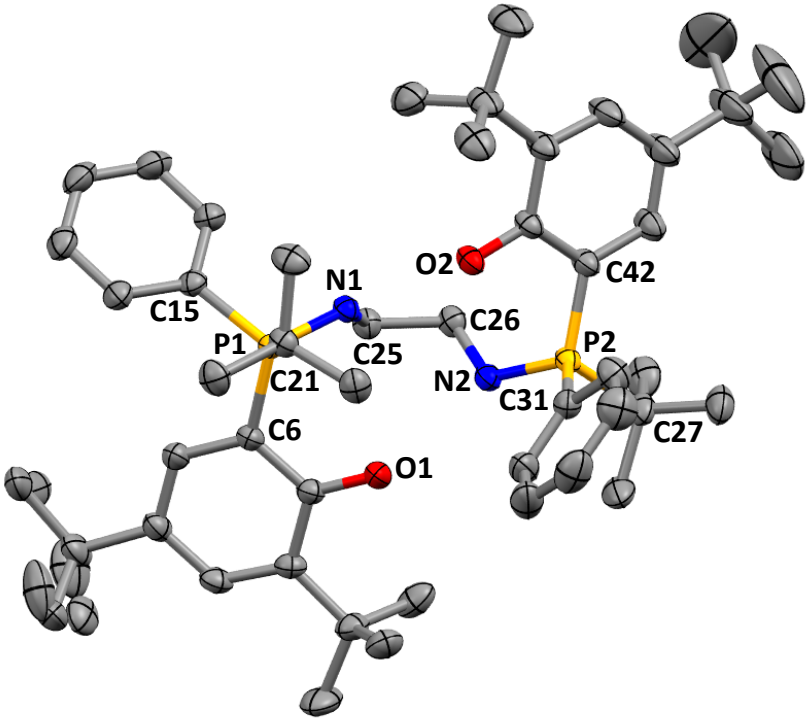



**Figure A1.40.** Representation of the molecular structure of ligand $^{P\text{-}salen}L^4H_2$.

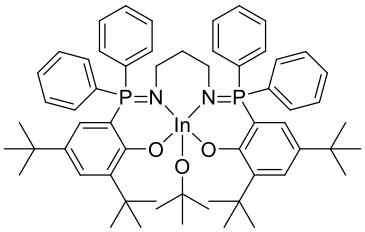
**Table A1.1.** Selected bond lengths (Å) of ligand $^{P\text{-}salen}L^4H_2$.

| Bond length (Å) for $H_2L^4$ | |
|---|---|
| P(1)-N(1) | 1.629(1) |
| P(1)-C(6) | 1.783(1) |
| P(1)-C(15) | 1.826(1) |
| P(1)-C(21) | 1.849(2) |
| P(2)-N(2) | 1.639(1) |
| P(2)-C(27) | 1.856(2) |
| P(2)-C(31) | 1.803(2) |
| P(2)-C(42) | 1.766(1) |
| N(1)-C(25) | 1.466(2) |
| N(2)-C(26) | 1.464(2) |

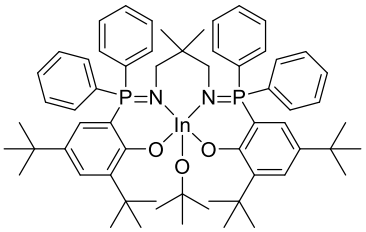
**Table A1.2.** Summary of crystallographic refinement data for ligand $^{P\text{-salen}}L^4H_2$.

| Compound | Complex $H_2L^4$ |
|---|---|
| Empirical Formula | $C_{50}H_{74}N_2O_2P_2$ |
| Formula weight ($gmol^{-1}$) | 797.05 |
| Crystal system | Triclinic |
| a (Å) | 11.4385(4) |
| b (Å) | 15.3688(5) |
| c (Å) | 15.4343(5) |
| α (°) | 84.413(3) |
| β (°) | 78.850(3) |
| γ (°) | 78.526(3) |
| Unit cell volume ($Å^3$) | 2600.66(16) |
| No. of formula units per unit cell | 2 |
| Space group | P-1 |
| Density (calculated) ($Mg\ m^{-3}$) | 1.018 |
| Diffractometer wavelength (Å) | 1.54184 |
| Temperature (K) | 150(2) |
| Absorption coefficient ($mm^{-1}$) | 1.020 |
| No. of reflections collected | 27304 |
| No. of unique reflections | 10793 |
| $R_{int}$ | 0.0301 |
| Final $R_1$ values ($I > 2\sigma I$) | 0.0451 |
| Final $wR_2$ values ($I > 2\sigma I$) | 0.1199 |
| $R_1$ values (all data) | 0.0548 |
| $wR_2$ values (all data) | 0.1289 |
| Goodness of fit on $F^2$ | 1.027 |

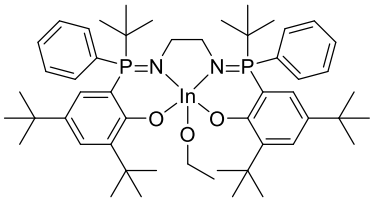
## A1.4. Additional crystallographic data for complexes 3.1–3.5 and intermediate 3.4′




3.2



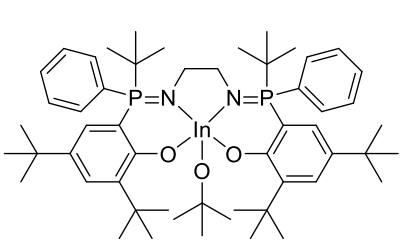

3.3



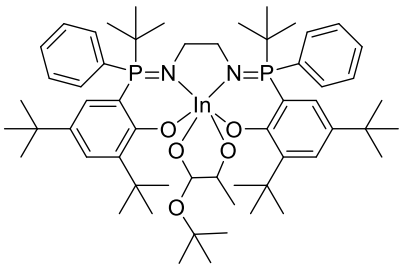

3.5

**Table A1.3.** Summary of crystallographic refinement data for complexes **3.1**–**3.5**.

| Compound | Complex 3.2 | Complex 3.3 | Complex 3.5 |
|---|---|---|---|
| Empirical Formula | $C_{65}H_{89}InN_2O_3P_2$ | $C_{65}H_{87}InN_2O_4P_2$ | $C_{52}H_{77}InN_2O_3P_2$ |
| Formula weight ($gmol^{-1}$) | 1123.14 | 1137.12 | 954.91 |
| Crystal system | Monoclinic | Orthorhombic | Triclinic |
| a (Å) | 15.1464(2) | 20.6809(2) | 14.2993(6) |
| b (Å) | 16.9612(2) | 18.5748(2) | 14.3196(6) |
| c (Å) | 26.1549(2) | 15.7154(2) | 17.8201(6) |
| α (°) | 90 | 90 | 105.160(4) |
| β (°) | 103.9430(10) | 90 | 107.065(4) |
| γ (°) | 90 | 90 | 96.826(4) |
| Unit cell volume | 6521.25(13) | 6036.97(12) | 3290.3(2) |
| No. of formula units per unit cell | 4 | 4 | 2 |
| Space group | $P2_1/c$ | $Pna2_1$ | P-1 |
| Density (calculated) ($Mg\ m^{-3}$) | 1.144 | 1.251 | 0.964 |
| Diffractometer wavelength | 1.54184 | 1.54184 | 1.54184 |
| Temperature (K) | 150(2) | 150(2) | 150(2) |
| Absorption coefficient ($mm^{-1}$) | 3.675 | 3.990 | 3.571 |
| No. of reflections collected | 77110 | 36488 | 36127 |
| No. of unique reflections | 13587 | 11541 | 13579 |
| $R_{int}$ | 0.0327 | 0.0311 | 0.0892 |
| Final $R_1$ values ($I > 2\sigma I$) | 0.0275 | 0.0270 | 0.0671 |
| Final $wR_2$ values ($I > 2\sigma I$) | 0.0699 | 0.0692 | 0.1656 |
| $R_1$ values (all data) | 0.0312 | 0.0291 | 0.0887 |
| $wR_2$ values (all data) | 0.0722 | 0.0707 | 0.1842 |
| Goodness of fit on $F^2$ | 1.025 | 1.067 | 0.987 |




**3.4**




**3.4'**

**Table A1.4.** Summary of crystallographic refinement data for compounds **3.4** and **3.4′**.

| **Compound** | **Complex 3.4** | **Intermediate 3.4′** |
|---|---|---|
| Empirical Formula | $C_{63}H_{102}InN_2O_3P_2$ | $C_{57}H_{85}InN_2O_5P_2$ |
| Formula weight ($gmol^{-1}$) | 1112.22 | 1055.02 |
| Crystal system | Monoclinic | Orthorhombic |
| a (Å) | 10.9894(2) | 11.12800(10) |
| b (Å) | 28.7519(10) | 18.2363(2) |
| c (Å) | 19.8100(4) | 30.9376(4) |
| α (°) | 90 | 90 |
| β (°) | 91.214(2) | 90 |
| γ (°) | 90 | 90 |
| Unit cell volume ($Å^3$) | 6257.9(3) | 6278.28(12) |
| No. of formula units per unit cell | 4 | 4 |
| Space group | $P2_1/n$ | $P2_12_12_1$ |
| Density (calculated) ($Mg\ m^{-3}$) | 1.181 | 1.116 |
| Diffractometer wavelength (Å) | 1.54184 | 1.54184 |
| Temperature (K) | 150(2) | 150(2) |
| Absorption coefficient ($mm^{-1}$) | 3.819 | 3.810 |
| No. of reflections collected | 52665 | 39863 |
| No. of unique reflections | 12991 | 13004 |
| $R_{int}$ | 0.0633 | 0.0396 |
| Final $R_1$ values ($I > 2\sigma I$) | 0.0584 | 0.0255 |
| Final $wR_2$ values ($I > 2\sigma I$) | 0.1442 | 0.0615 |
| $R_1$ values (all data) | 0.0803 | 0.0281 |
| $wR_2$ values (all data) | 0.1581 | 0.0628 |
| Goodness of fit on $F^2$ | 1.026 | 1.031 |

## A1.5. Additional polymerisation data

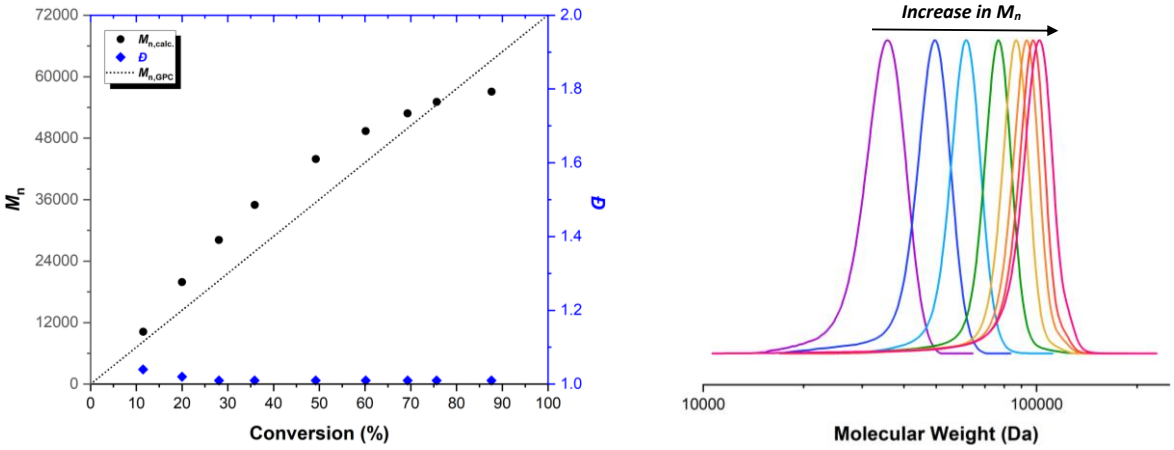



**Figure A1.41.** Plots of $M_n$ (●), theoretical $M_n$ (…) and $Đ$ (♦) against percentage conversion (left) and overlay of SEC traces for the polymerisation of *rac*-lactide initiated by complex **3.1** (right).

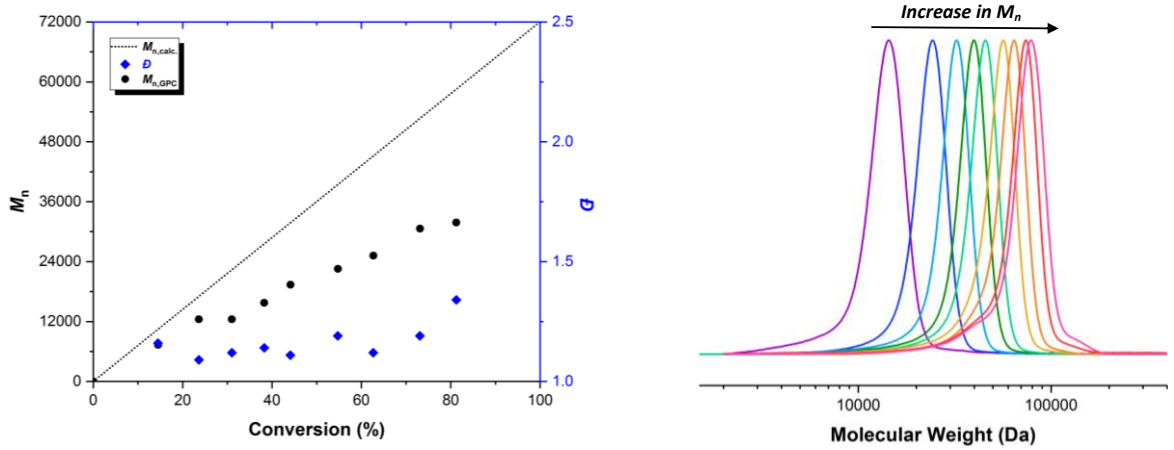



**Figure A1.42.** Plots of $M_n$ (●), theoretical $M_n$ (…) and $Đ$ (♦) against percentage conversion (left) and overlay of SEC traces for the polymerisation of *rac*-lactide initiated by complex **3.2** (right).

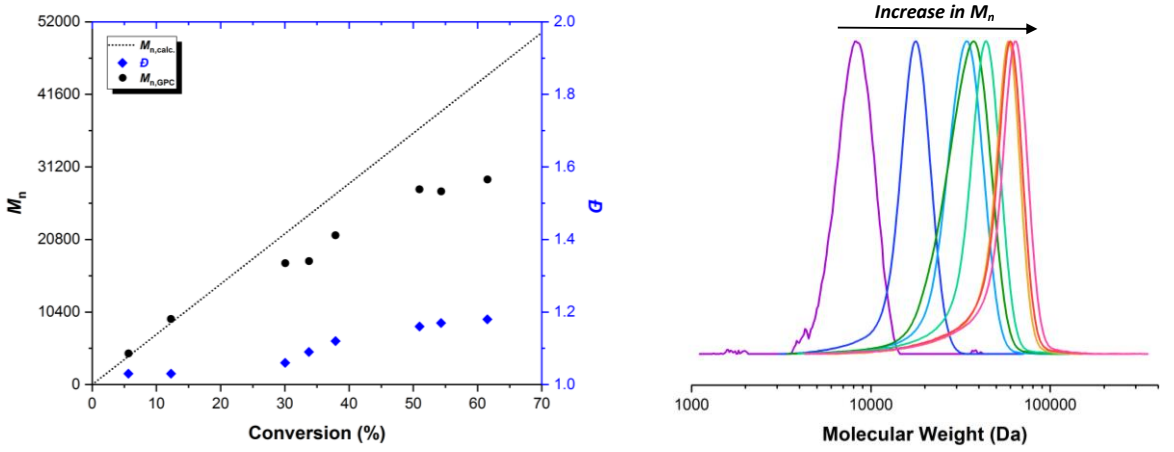



**Figure A1.43.** Plots of $M_n$ (●), theoretical $M_n$ (…) and $Đ$ (♦) against percentage conversion (left) and overlay of SEC traces for the polymerisation of *rac*-lactide initiated by complex **3.3** (right).

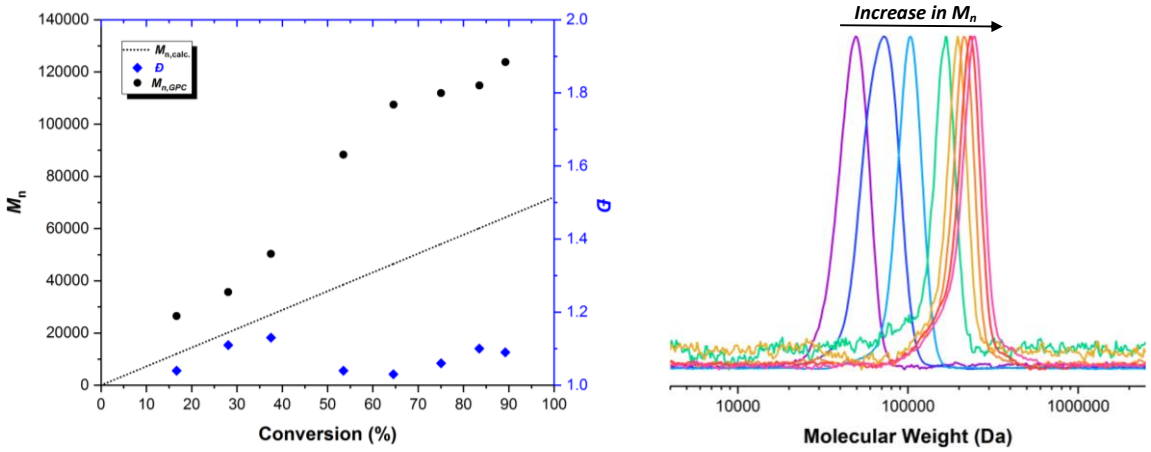



**Figure A1.44.** Plots of $M_n$ (●), theoretical $M_n$ (…) and $Đ$ (♦) against percentage conversion (left) and overlay of SEC traces for the polymerisation of *rac*-lactide initiated by complex **3.4** (right).

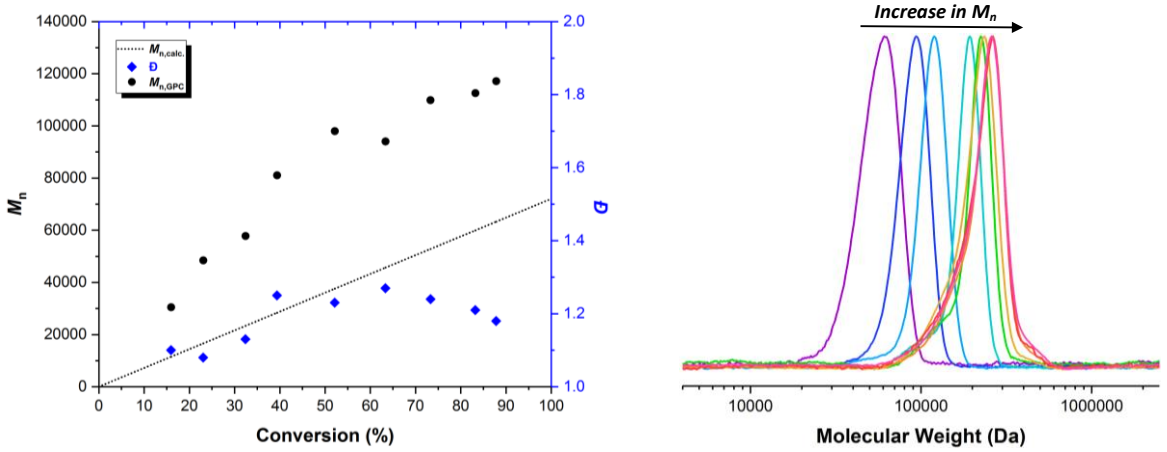



**Figure A1.45.** Plots of $M_n$ (●), theoretical $M_n$ (…) and $Đ$ (♦) against percentage conversion (left) and overlay of SEC traces for the polymerisation of *D*-lactide initiated by complex **3.4** (right).

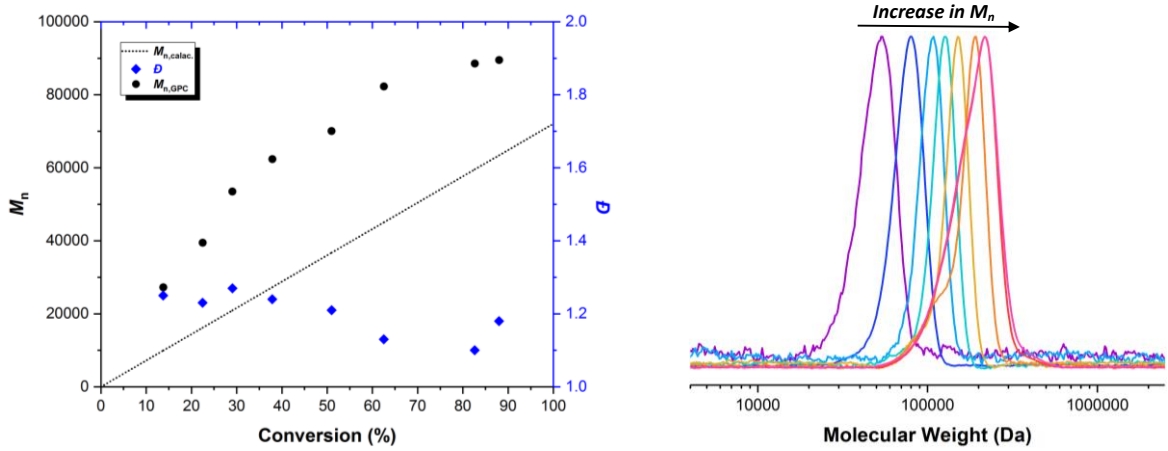



**Figure A1.46.** Plots of $M_n$ (●), theoretical $M_n$ (…) and $Đ$ (♦) against percentage conversion (left) and overlay of SEC traces for the polymerisation of *L*-lactide initiated by complex **3.4** (right).

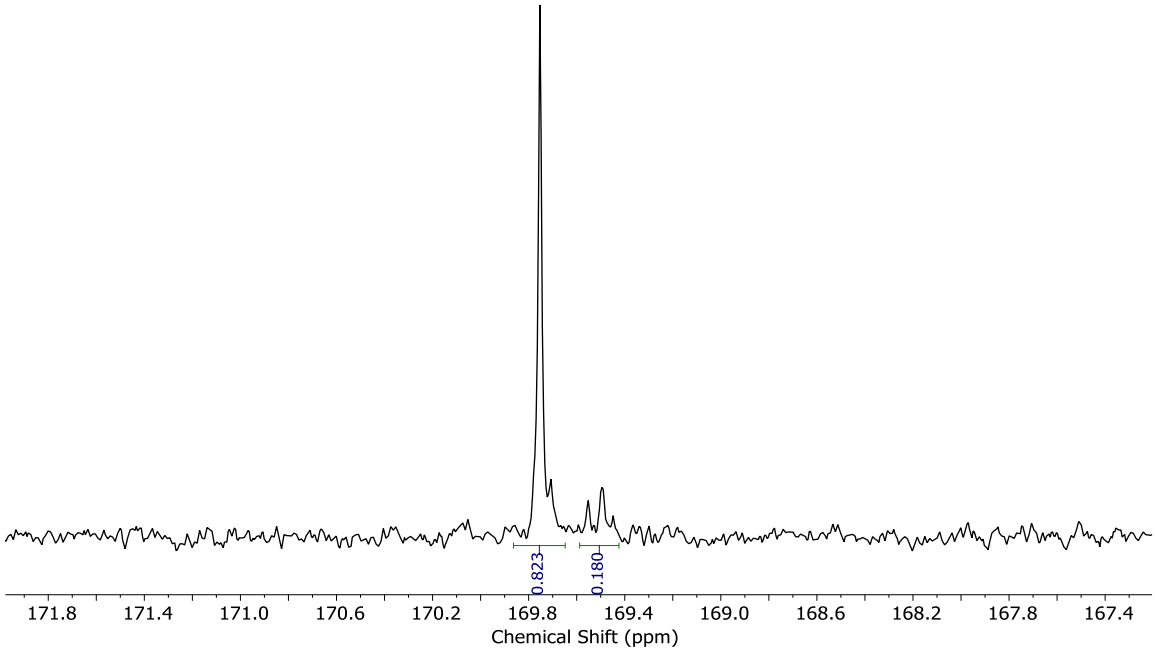



**Figure A1.47.** $^{13}C\{^{1}H\}$ NMR spectrum of PLA2 in $CDCl_3$ showing carbonyl region (δ 169.8 ppm for iso-rich hexad and δ 169.6-169.4 ppm for racemic-rich hexad).

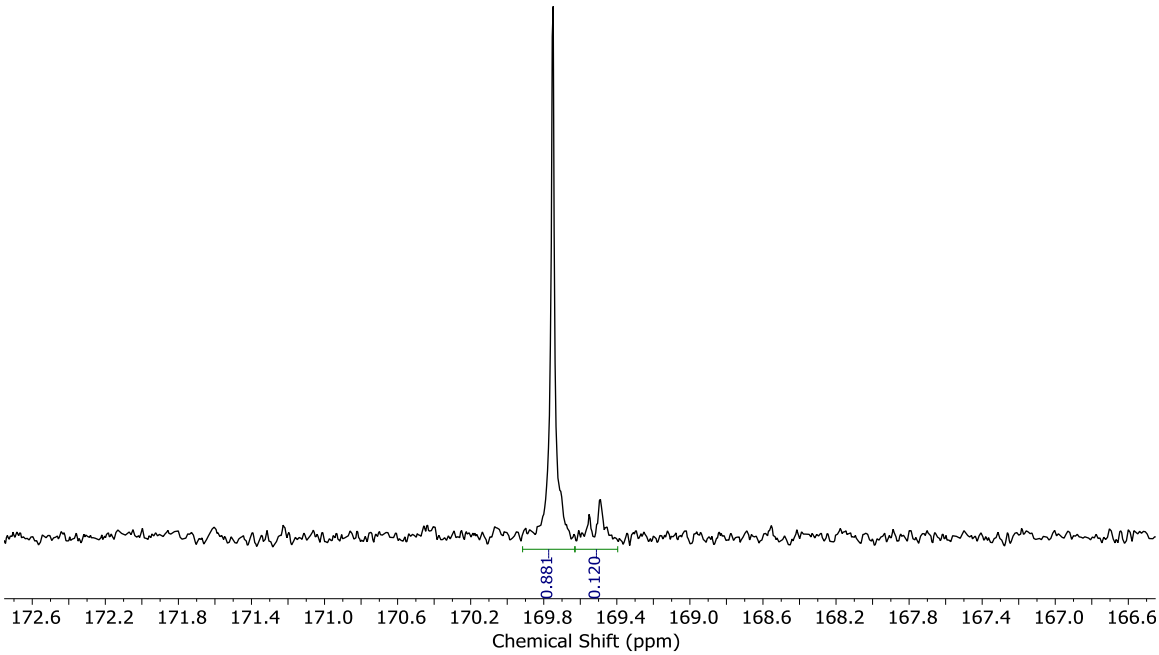



**Figure A1.48.** $^{13}C\{^{1}H\}$ NMR spectrum of PLA3 in $CDCl_3$ showing carbonyl region (δ 169.8 ppm for iso-rich hexad and δ 169.6-169.4 ppm for racemic-rich hexad).

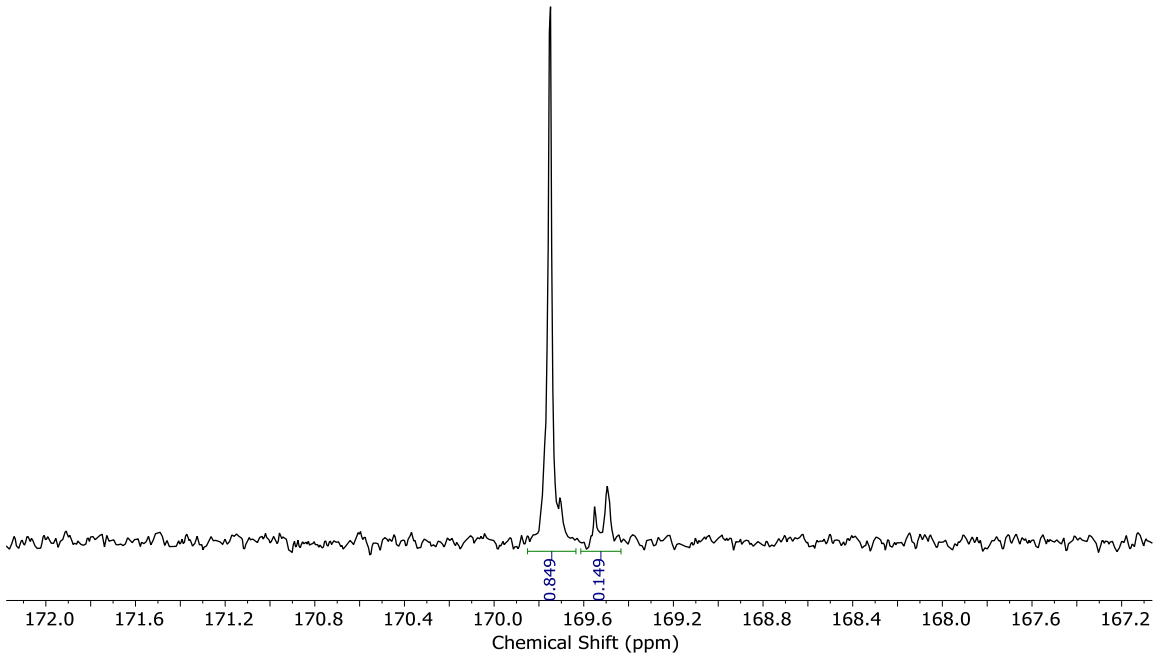



**Figure A1.49.** $^{13}C\{^{1}H\}$ NMR spectrum of PLA4 in $CDCl_3$ showing carbonyl region (δ 169.8 ppm for iso-rich hexad and δ 169.6-169.4 ppm for racemic-rich hexad).

| Tetrad | Integration | $P_i$ |
|---|---|---|
| sis | 0.03 | 0.77 |
| sii/iis | 0.11 | 0.65 |
| iis/sii | 0.04 | 0.91 |
| iii | 0.66 | 0.75 |
| isi | 0.16 | 0.68 |
| **Average** | | **0.75 ± 0.07** |

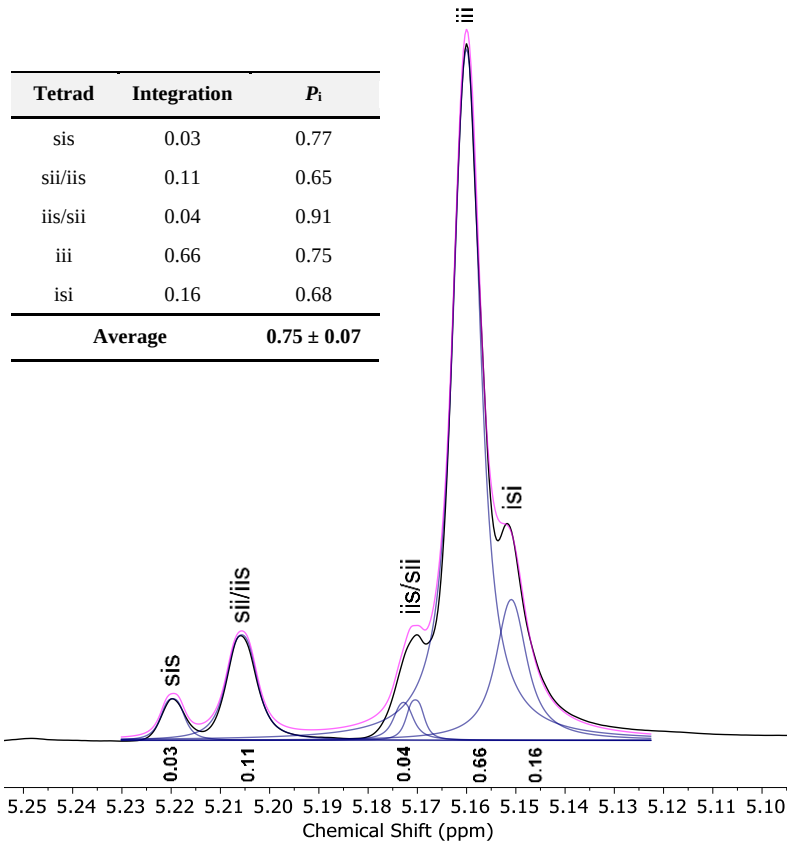



**Figure A1.50.** $^{1}H\{^{1}H\}$ NMR spectrum of the resultant PLA initiated by complex **3.1**. Condition: [LA]:[**3.1**] = 500, [LA] = 1 M, THF, 298 K.

| Tetrad | Integration | $P_i$ |
|---|---|---|
| sis | 0.05 | 0.67 |
| sii/iis | 0.10 | 0.73 |
| iis/sii | 0.11 | 0.67 |
| iii | 0.58 | 0.68 |
| isi | 0.16 | 0.68 |
| **Average** | | **0.69 ± 0.02** |

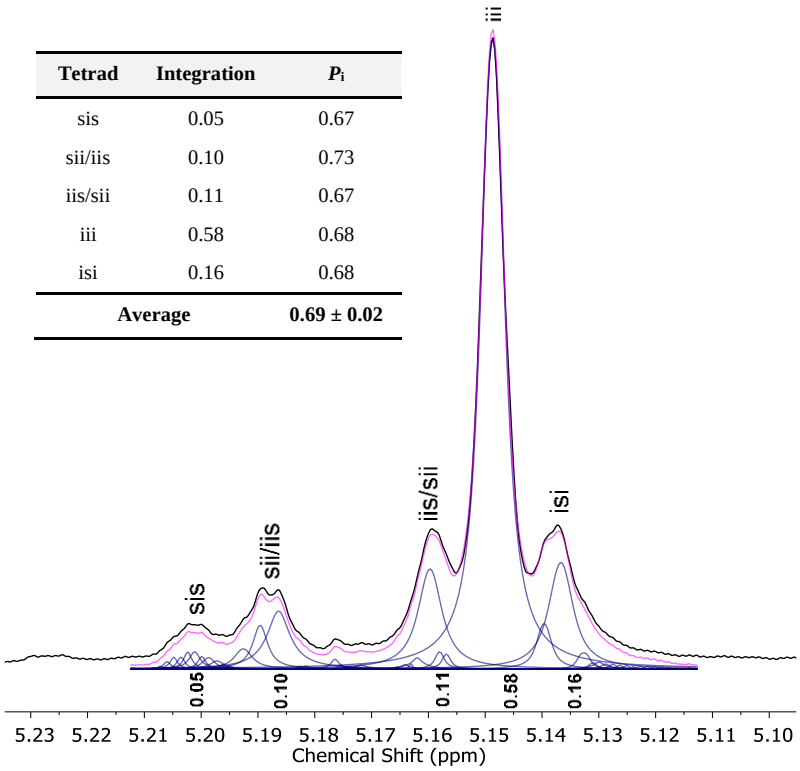



**Figure A1.51.** $^{1}H\{^{1}H\}$ NMR spectrum of the resultant PLA initiated by complex **3.2**. Condition: [LA]:[**3.2**] = 500, [LA] = 1 M, THF, 298 K.

| Tetrad | Integration | $P_i$ |
|---|---|---|
| sis | 0.03 | 0.77 |
| sii/iis | 0.04 | 0.92 |
| iis/sii | 0.08 | 0.80 |
| iii | 0.78 | 0.85 |
| isi | 0.07 | 0.85 |
| **Average** | | **0.84 ± 0.04** |

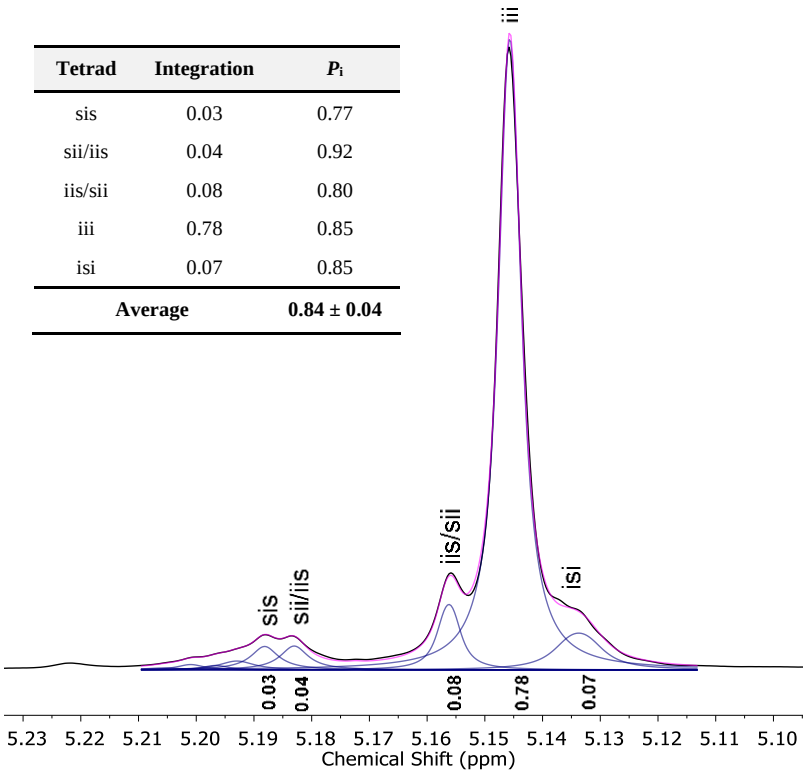



**Figure A1.52.** $^{1}H\{^{1}H\}$ NMR spectrum of the resultant PLA initiated by complex **3.3**. Condition: [LA]:[**3.3**] = 500, [LA] = 1 M, THF, 298 K.

| Tetrad | Integration | $P_i$ |
|---|---|---|
| sis | 0.02 | 0.80 |
| sii/iis | 0.01 | 0.97 |
| iis/sii | 0.03 | 0.93 |
| iii | 0.91 | 0.94 |
| isi | 0.03 | 0.95 |
| **Average** | | **0.92 ± 0.04** |

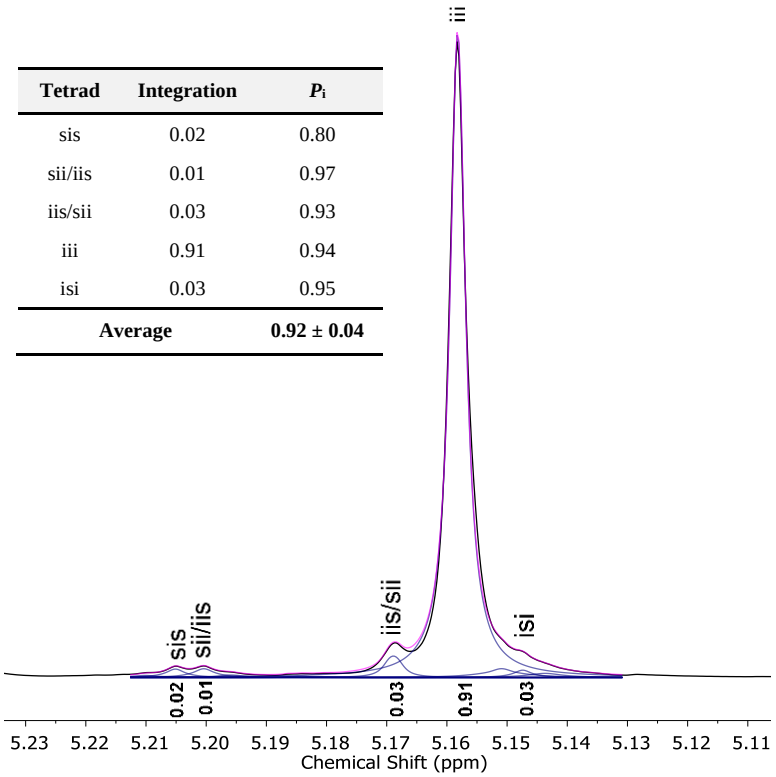



**Figure A1.53.** $^{1}H\{^{1}H\}$ NMR spectrum of the resultant PLA initiated by complex **3.4**. Condition: [LA]:[**3.4**] = 500, [LA] = 1 M, THF, 278 K.

| Tetrad | Integration | $P_i$ |
|---|---|---|
| sis | 0.02 | 0.77 |
| sii/iis | 0.02 | 0.95 |
| iis/sii | 0.03 | 0.93 |
| iii | 0.88 | 0.92 |
| isi | 0.04 | 0.92 |
| **Average** | | **0.90 ± 0.05** |

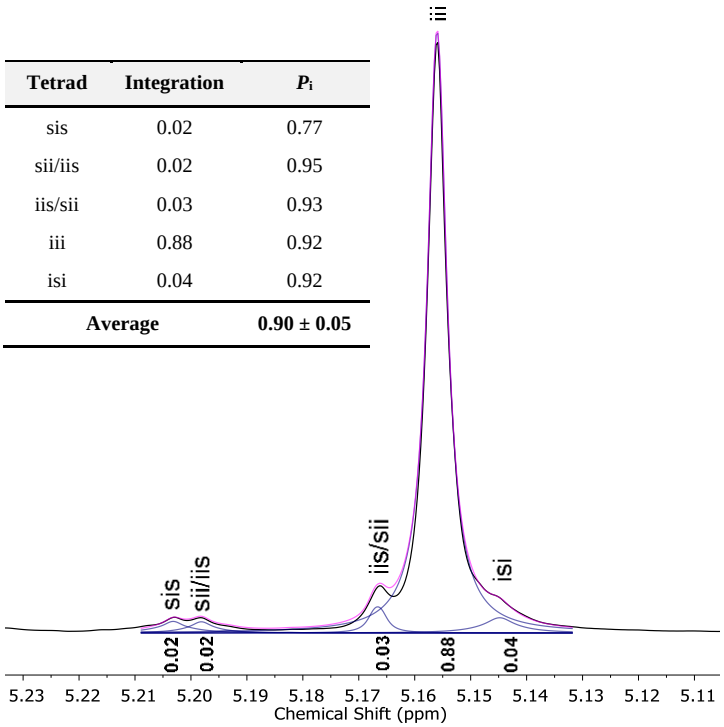



**Figure A1.54.** $^{1}H\{^{1}H\}$ NMR spectrum of the resultant PLA initiated by complex **3.5**. Condition: [LA]:[**3.5**] = 500, [LA] = 1 M, THF, 298 K.

| Tetrad | Integration | $P_i$ |
|---|---|---|
| sis | 0.01 | 0.88 |
| sii/iis | 0.06 | 0.86 |
| iis/sii | 0.01 | 0.98 |
| iii | 0.89 | 0.93 |
| isi | 0.03 | 0.95 |
| **Average** | | **0.92 ± 0.04** |

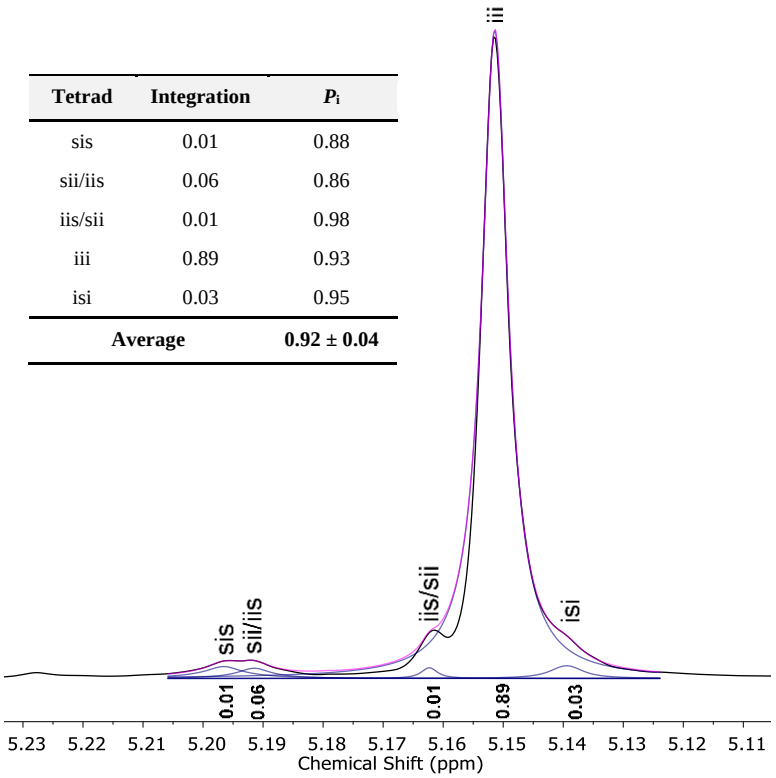



**Figure A1.55.** $^{1}H\{^{1}H\}$ NMR spectrum of the resultant PLA initiated by complex **3.5**. Condition: [LA]:[**3.5**] = 1500, [LA] = 1 M, THF, 298 K.

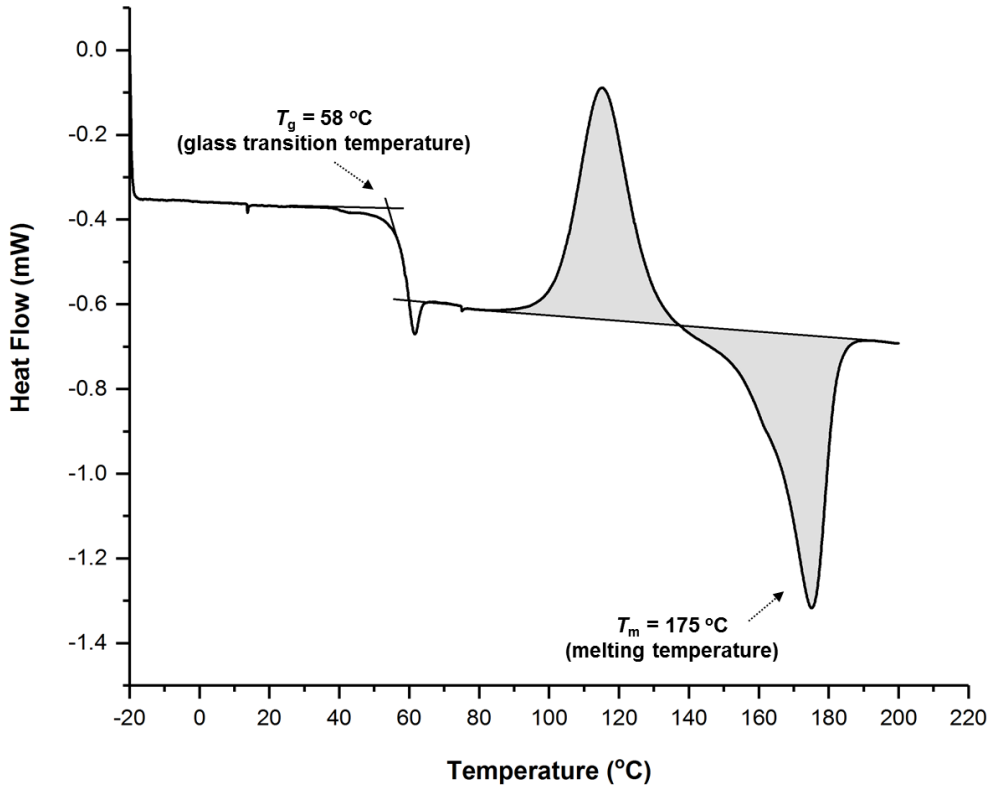



**Figure A1.56.** DSC thermogram of the resultant PLA initiated by complex **3.4** at 298 K.

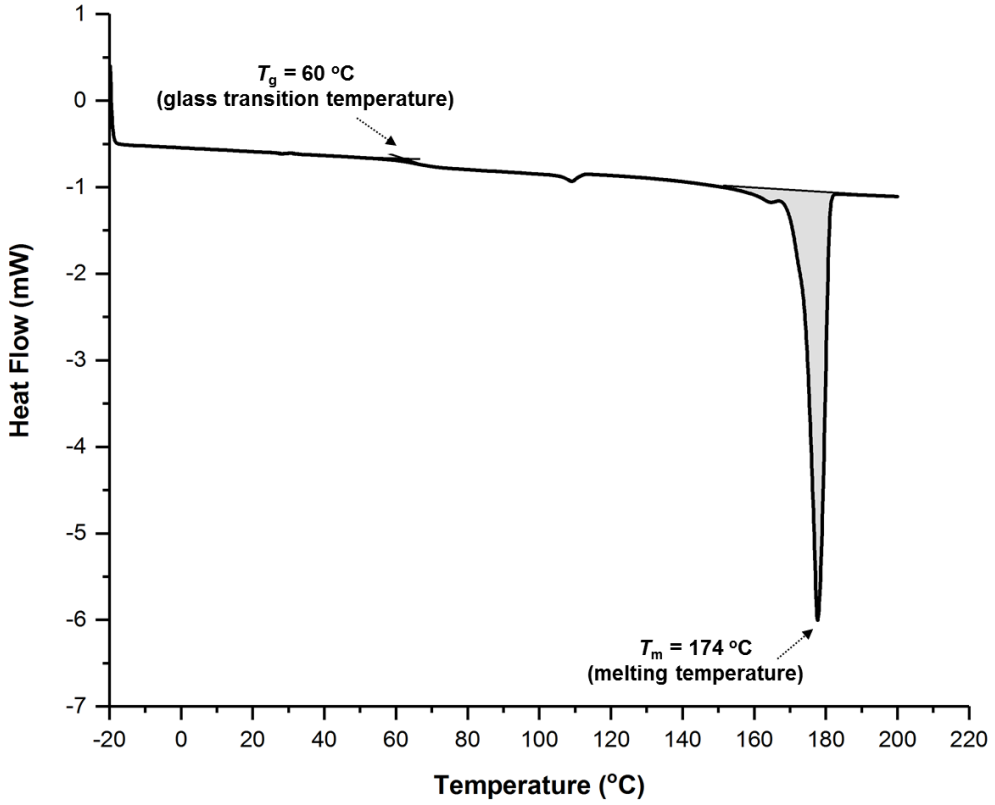



**Figure A1.57.** DSC thermogram of the resultant PDLA initiated by complex **3.4** at 298 K.

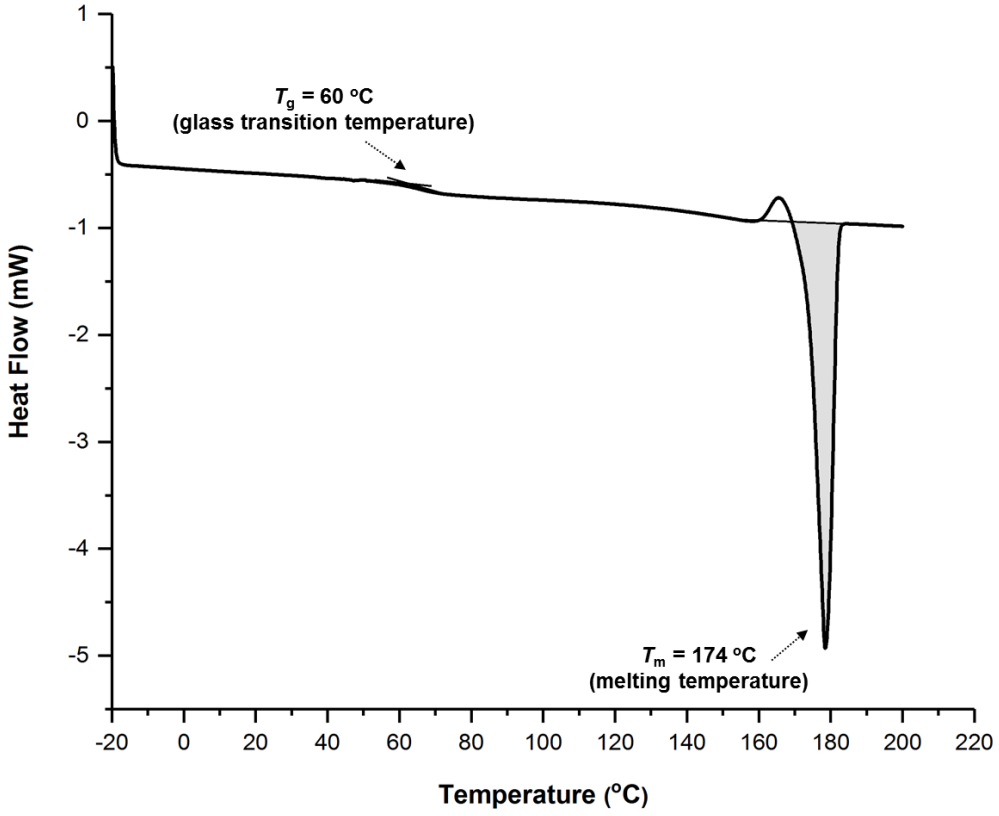



**Figure A1.58.** DSC thermogram of the resultant PLLA initiated by complex **3.4** at 298 K.

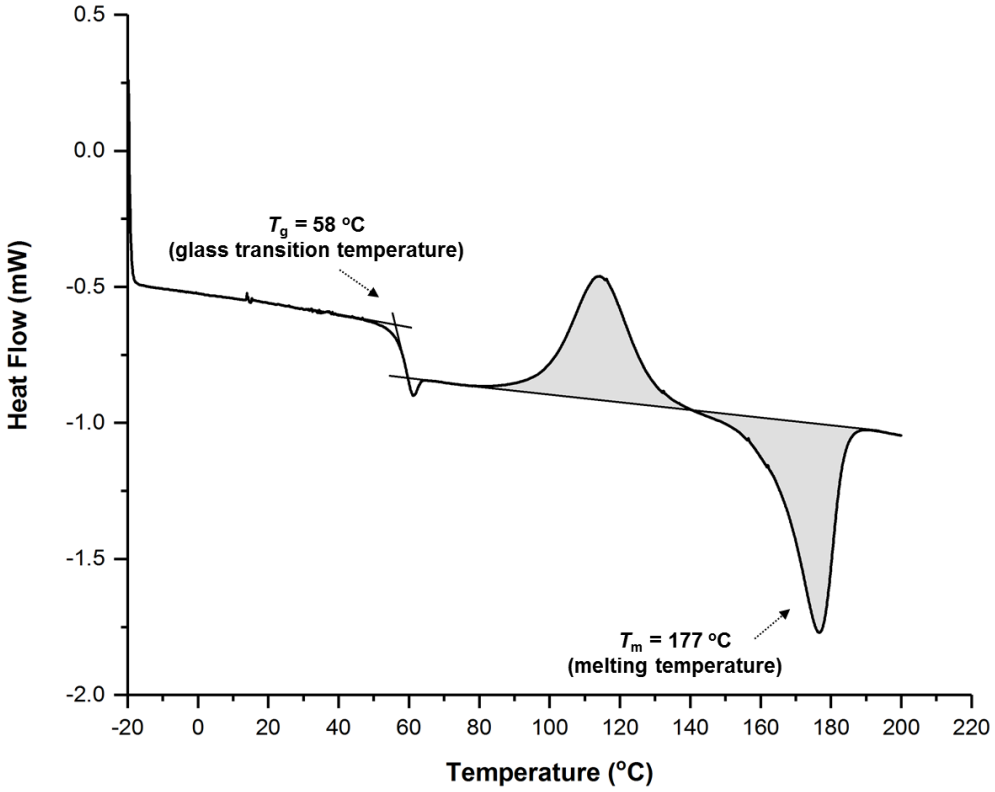



**Figure A1.59.** DSC thermogram of the resultant PLA initiated by complex **3.5** at 298 K.

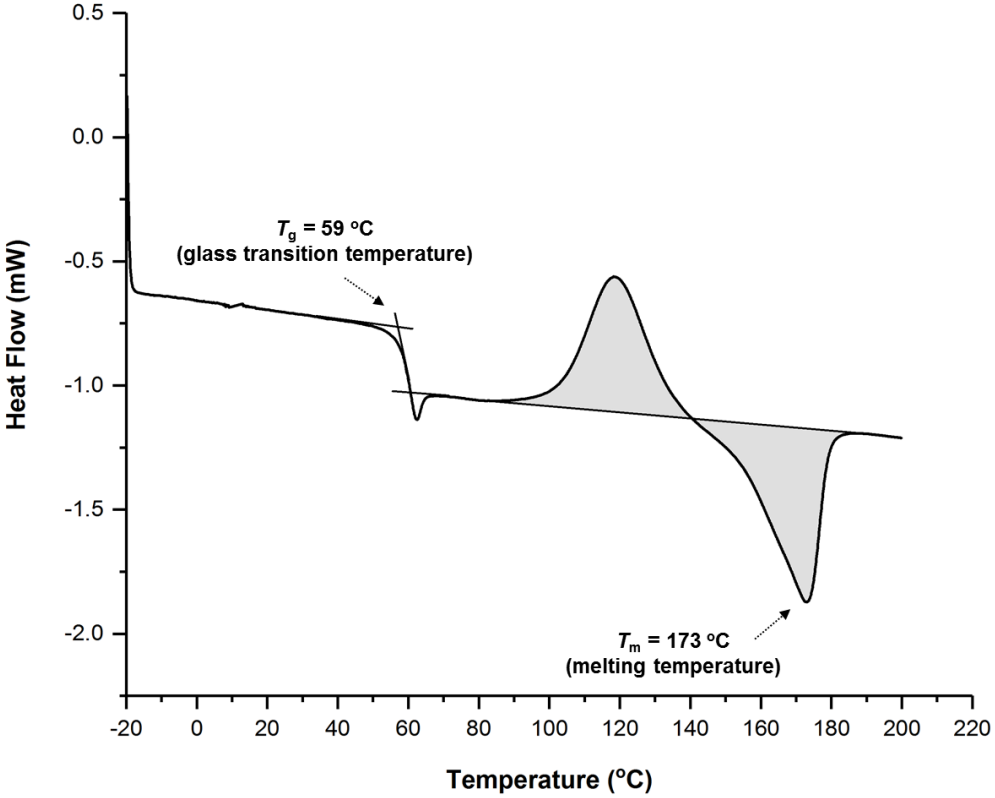



**Figure A1.60.** DSC thermogram of the resultant PLA initiated by complex **3.5** at 298 K (PLA4)

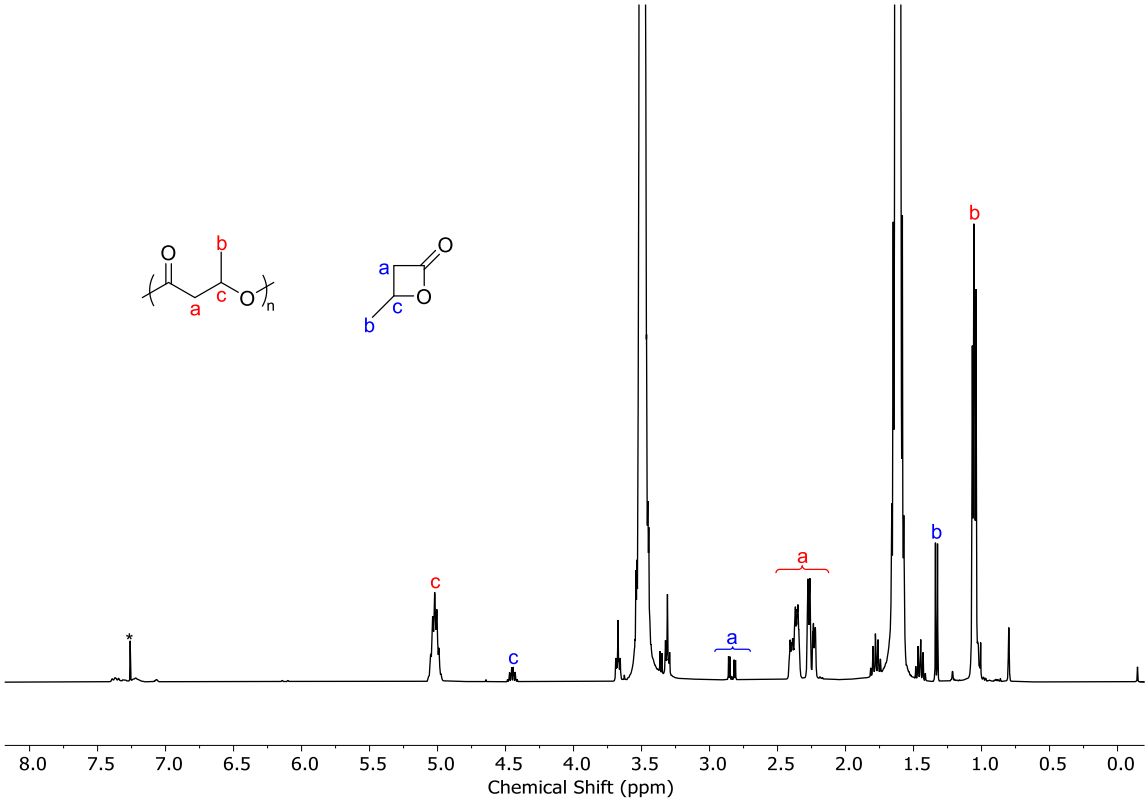



**Figure A1.61.** $^{1}$H NMR spectrum of crude PBL, initiated by complex **3.2** in $CDCl_3$.

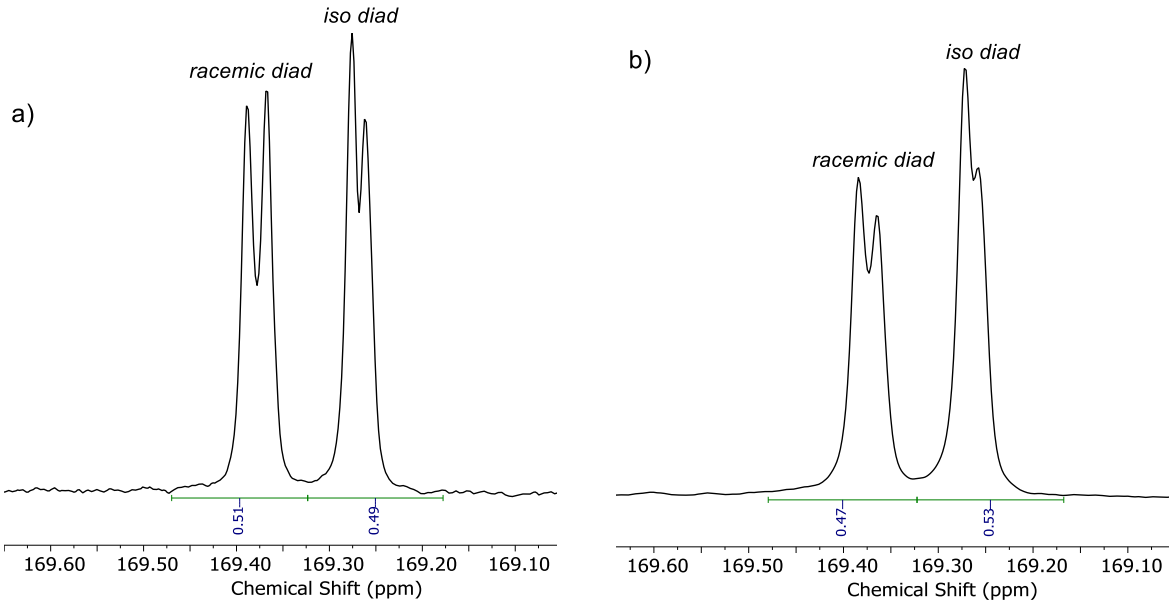



**Figure A1.62.** Carbonyl region of $^{13}C\{^{1}H\}$ NMR spectra of PHB prepared by a) complex **3.1** and b) complex **3.2**.

# A2. Chapter 4

## A2.1. Spectral characterisation data for ligand $^{P\text{-}salen}L^5H_2$ and $^{salen}L^1H_2$–$^{salen}L3H_2$

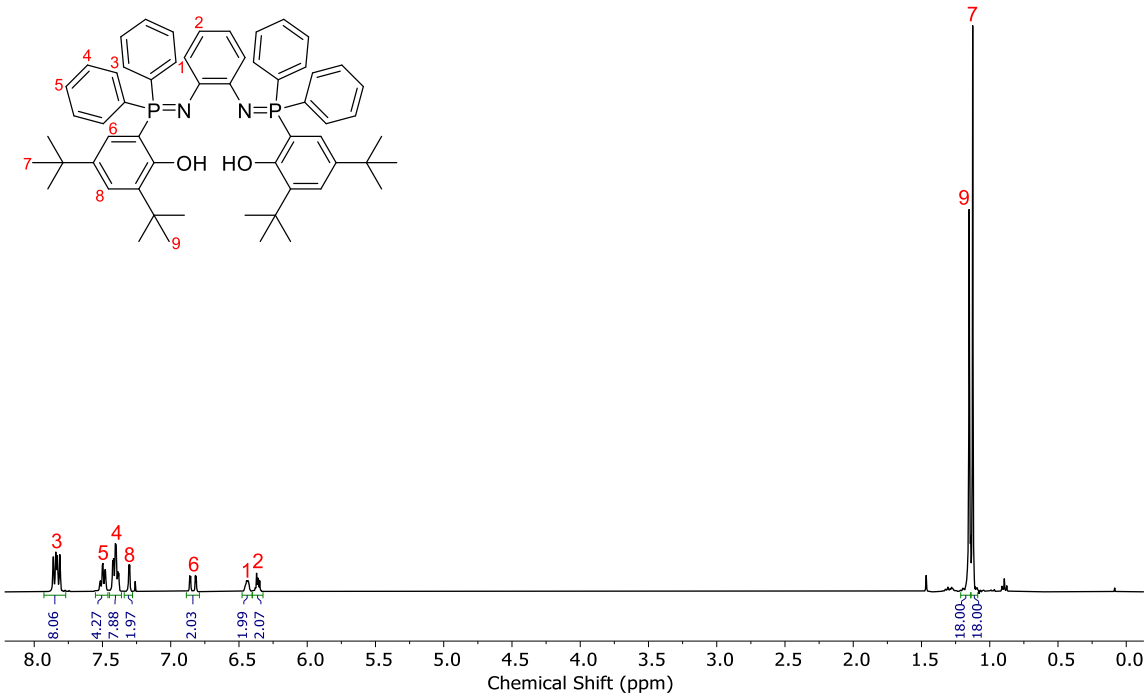



**Figure A2.1.** $^{1}$H NMR spectrum of ligand $^{P\text{-}salen}L^5H_2$ in $CDCl_3$.

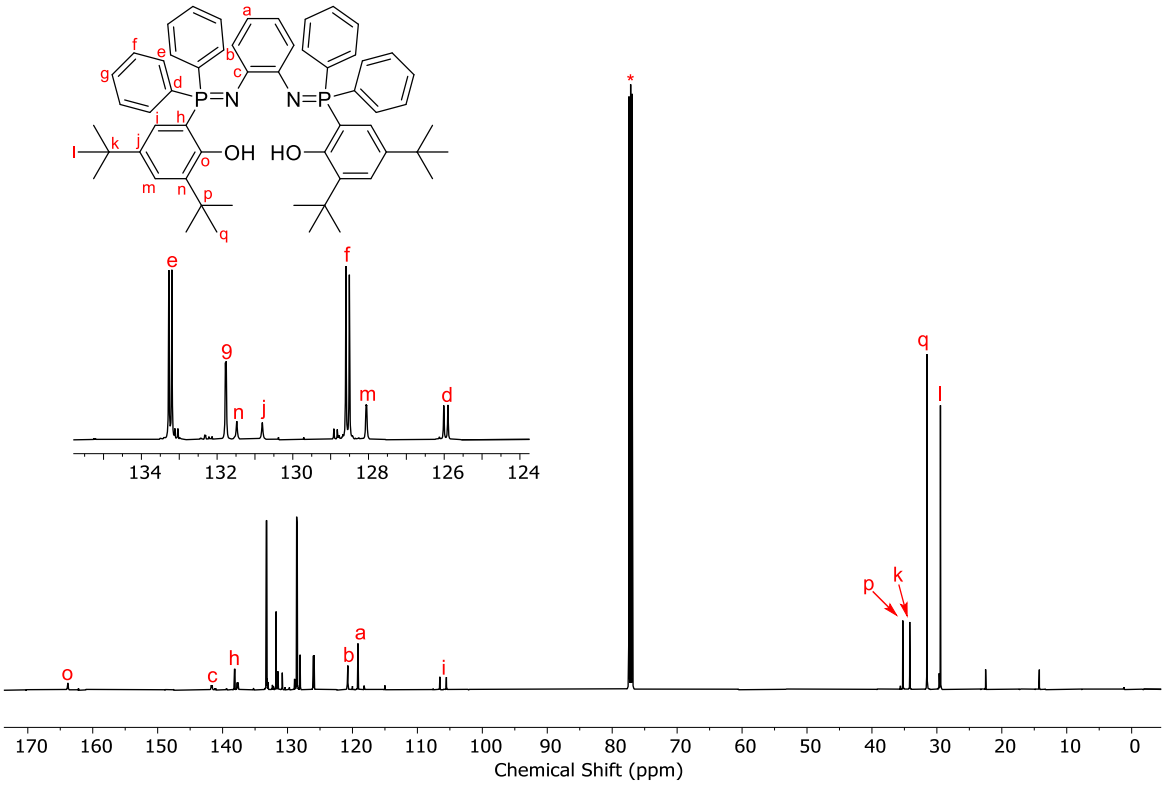



**Figure A2.2.** $^{13}C\{^{1}H\}$ NMR spectrum of ligand $^{P\text{-}salen}L^5H_2$ in $CDCl_3$.

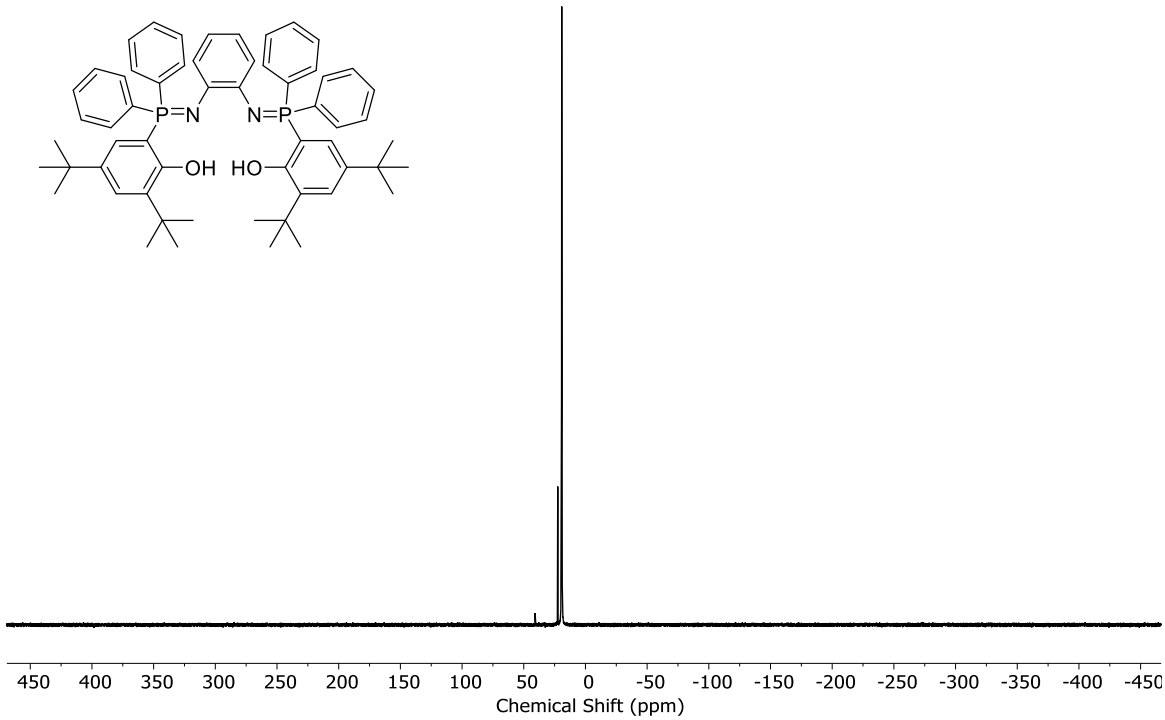



**Figure A2.3.** $^{31}P\{^{1}H\}$ NMR spectrum of ligand $^{\text{P-salen}}\mathbf{L}^{5}\mathbf{H_2}$ in $CDCl_3$.

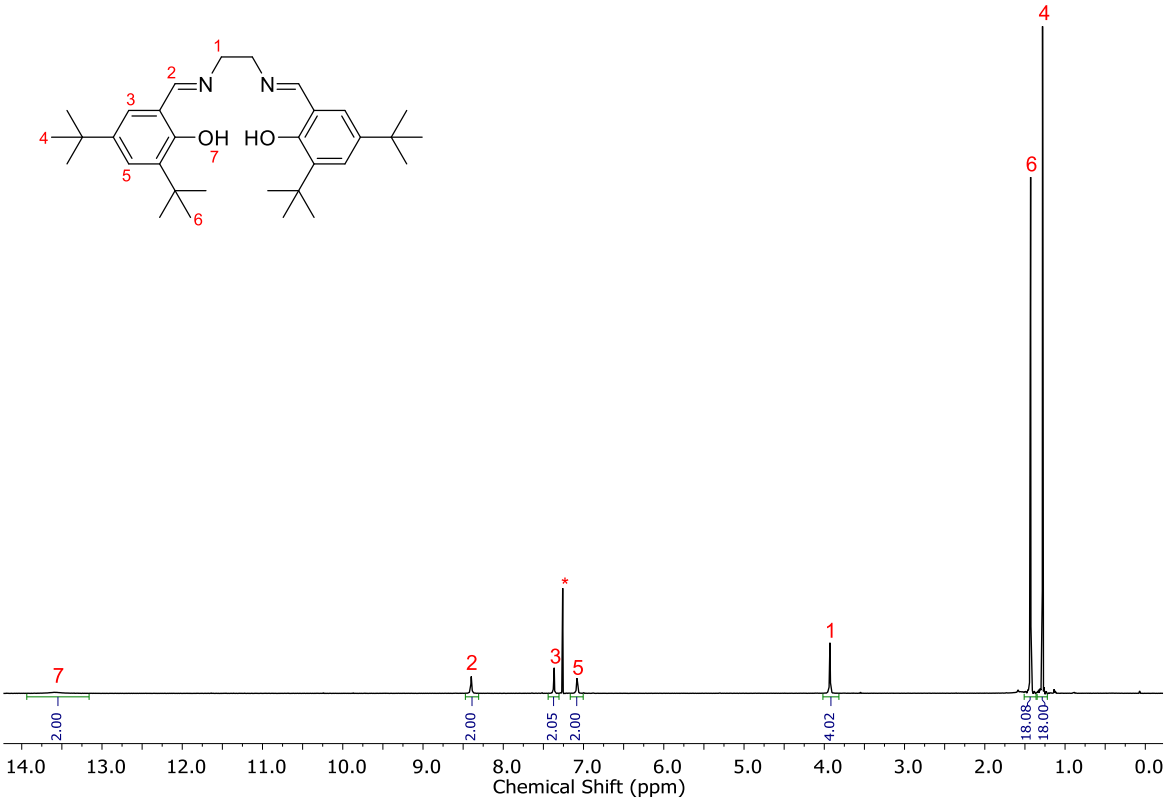



**Figure A2.4.** $^{1}H$ NMR spectrum of ligand $^{\text{salen}}\mathbf{L}^{1}\mathbf{H_2}$ in $CDCl_3$.

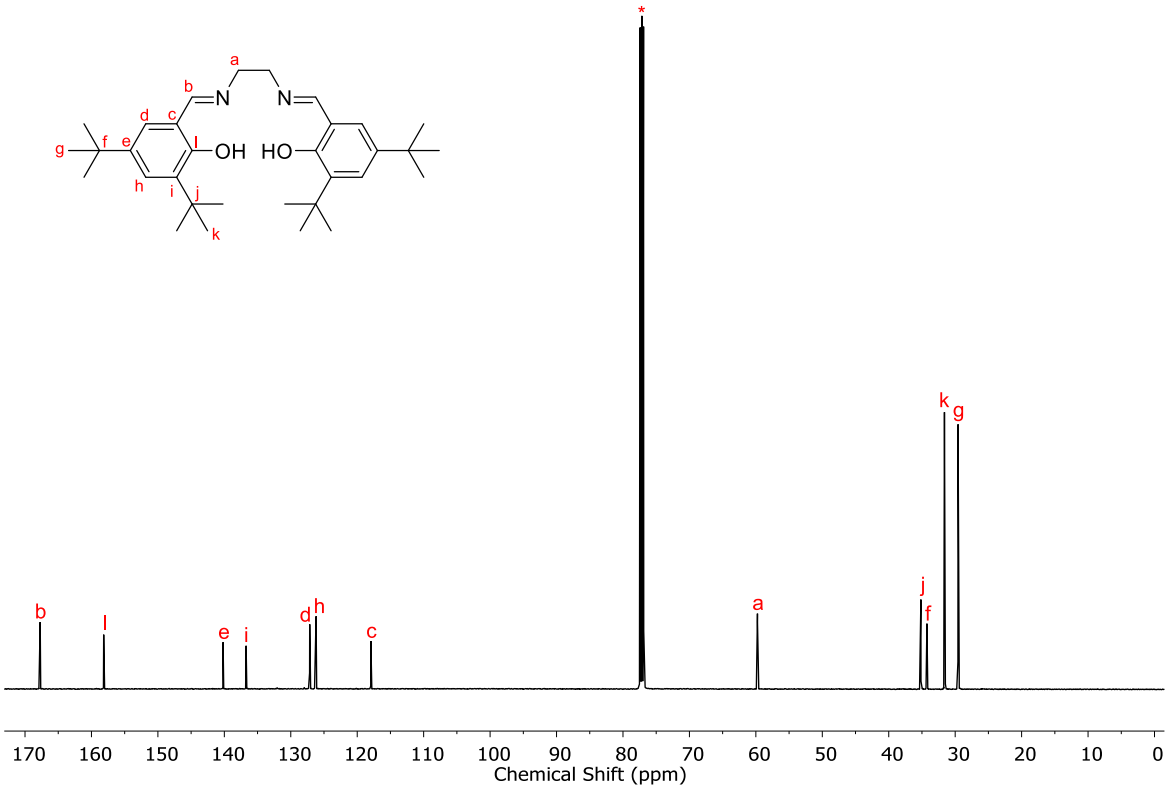



**Figure A2.5.** $^{13}C\{^{1}H\}$ NMR spectrum of ligand $^{salen}\mathbf{L^1H_2}$ in $CDCl_3$.

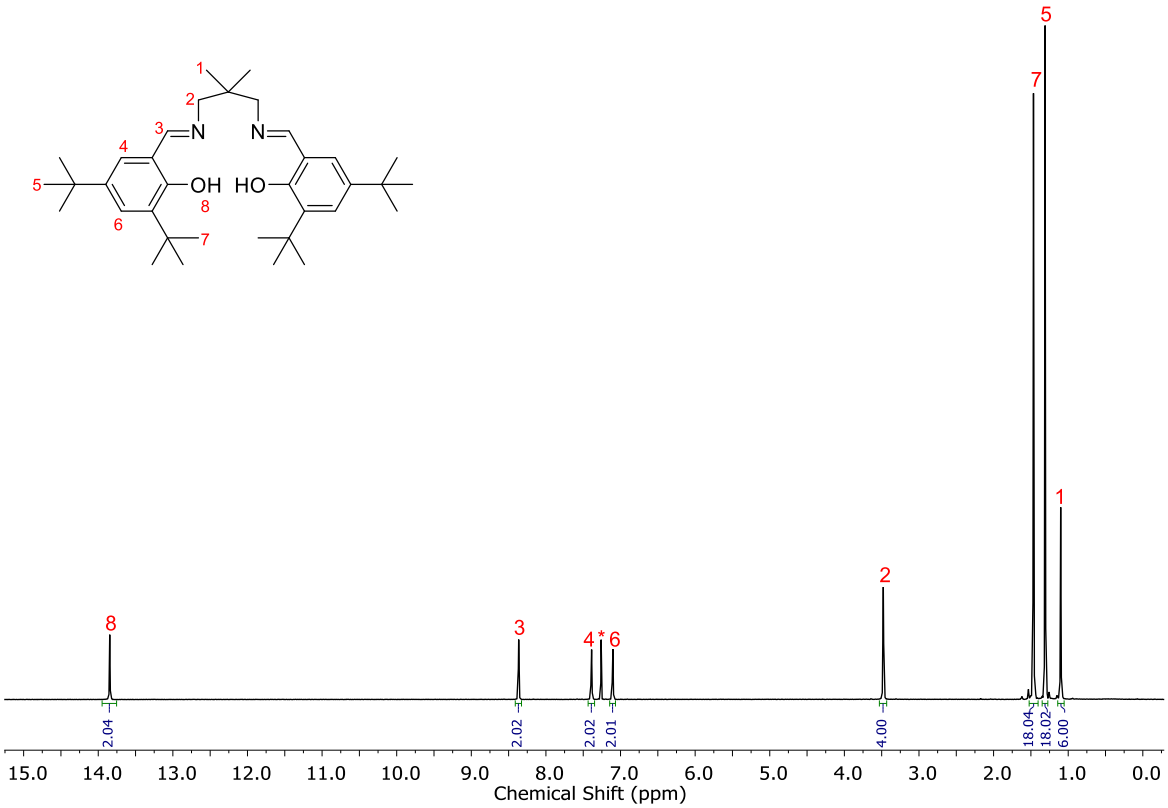



**Figure A2.6.** $^{1}H$ NMR spectrum of ligand $^{salen}\mathbf{L^2H_2}$ in $CDCl_3$.

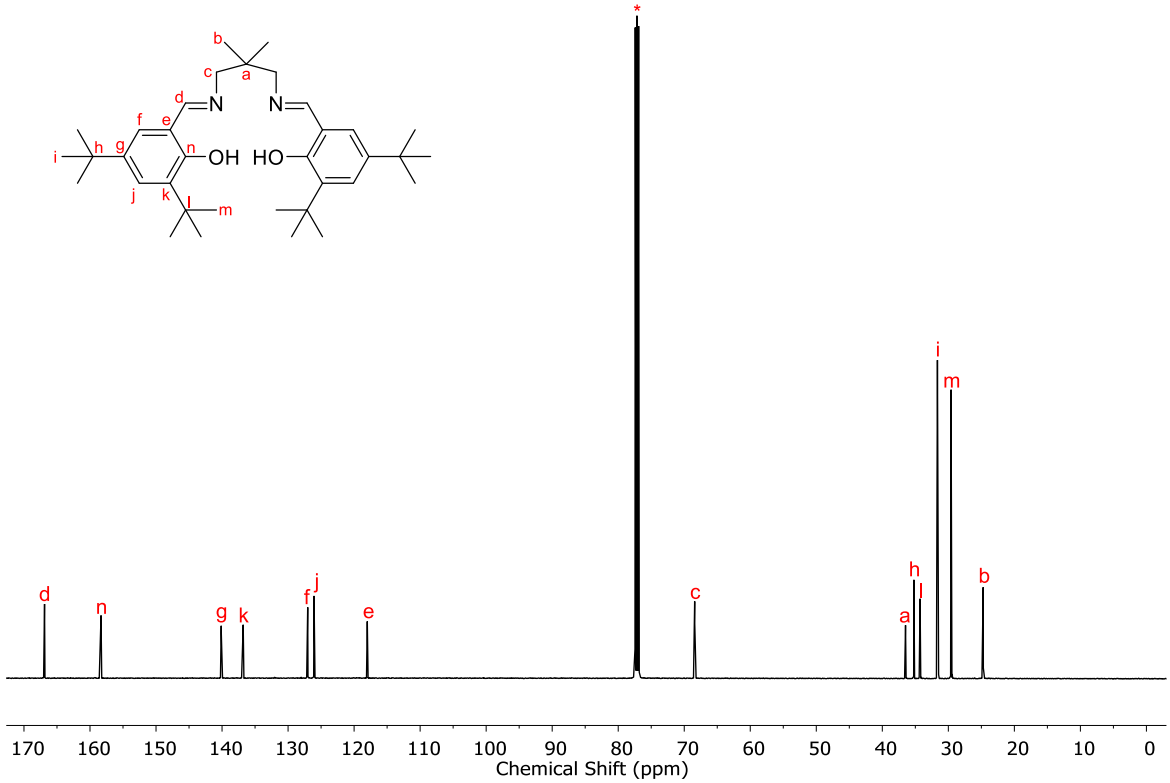



**Figure A2.7.** $^{13}C\{^{1}H\}$ NMR spectrum of ligand $^{salen}\mathbf{L^{2}H_{2}}$ in $CDCl_3$.

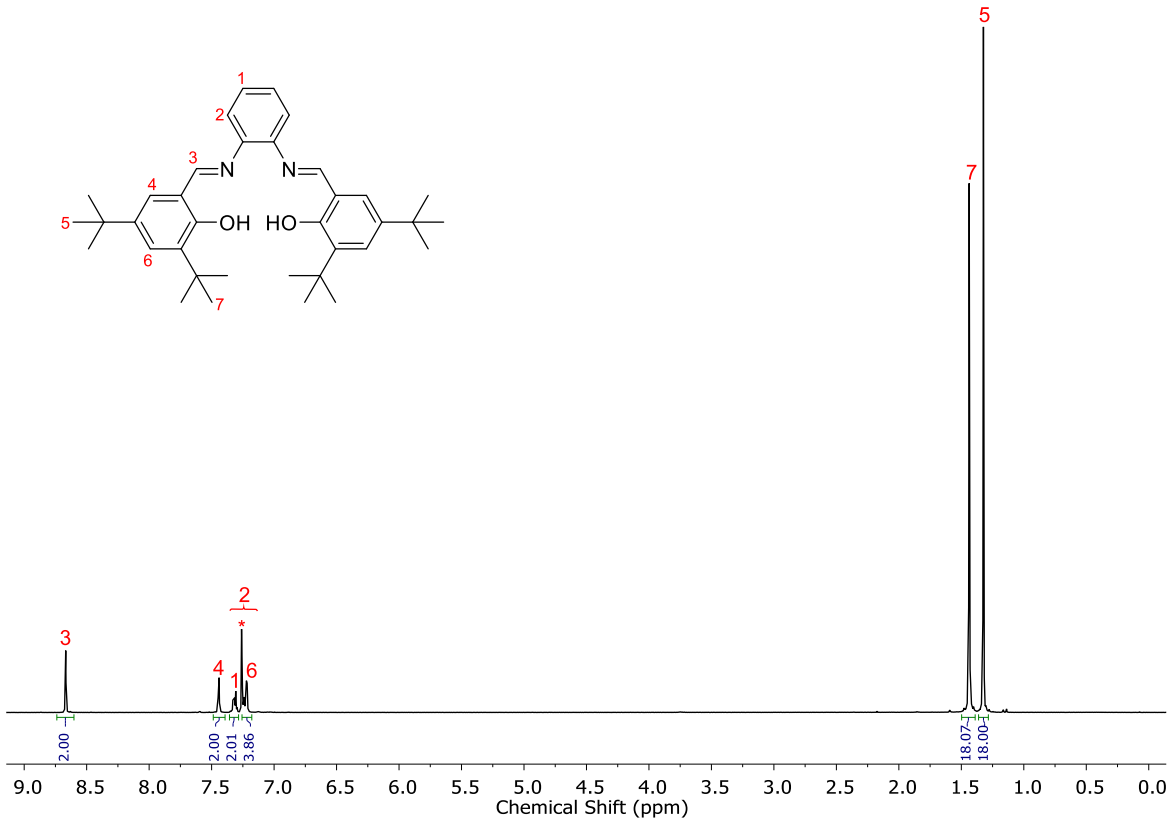



**Figure A2.8.** $^{1}H$ NMR spectrum of ligand $^{salen}\mathbf{L^{3}H_{2}}$ in $CDCl_3$.

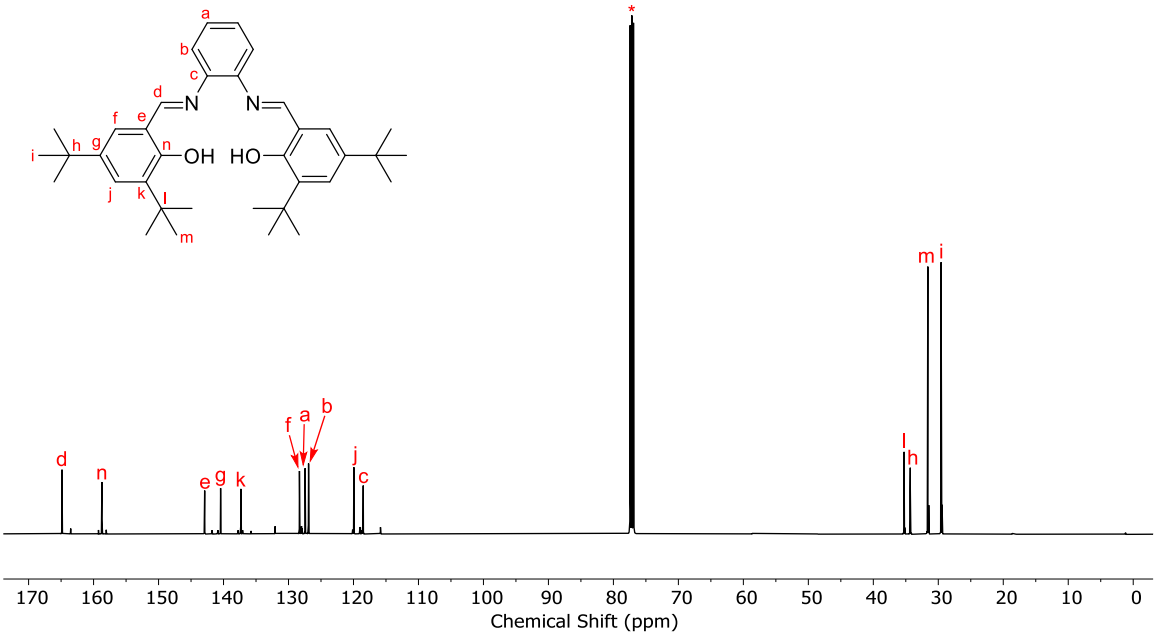



**Figure A2.9.** $^{13}C\{^{1}H\}$ NMR spectrum of ligand $^{salen}L^{3}H_2$ in $CDCl_3$.

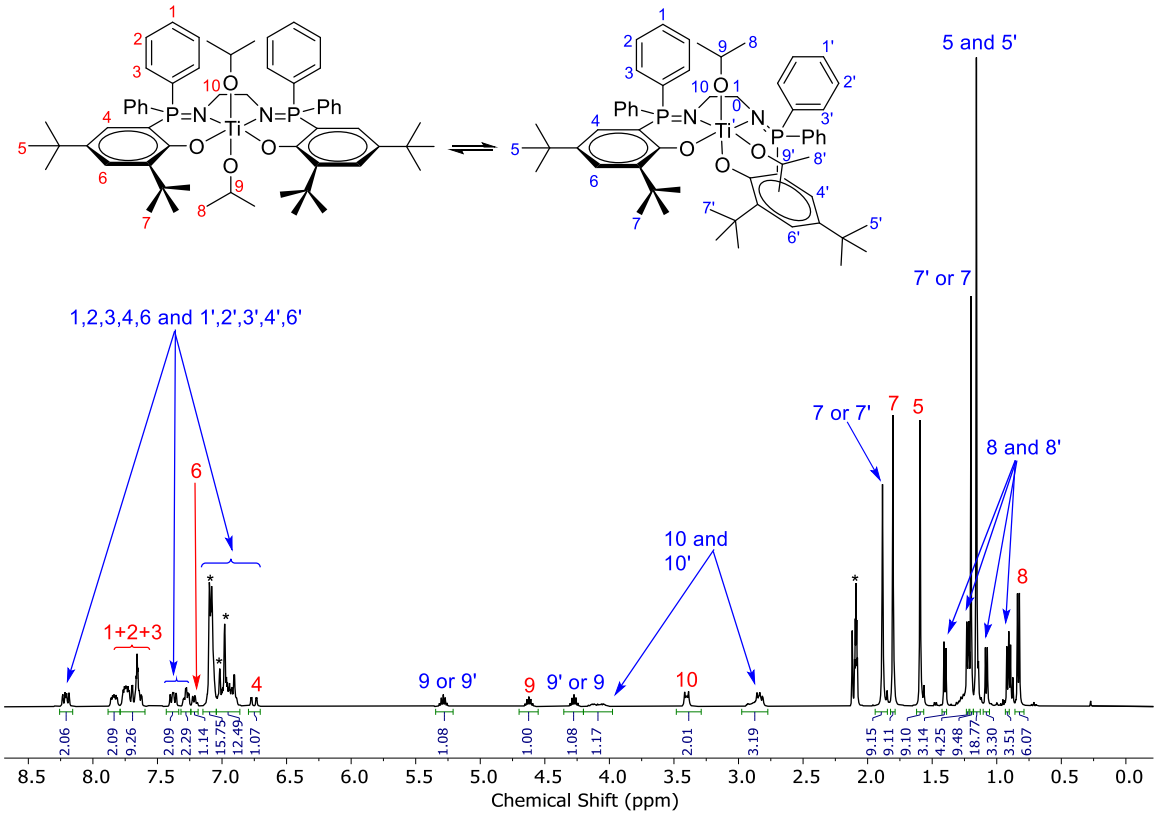



**Figure A2.10.** $^{1}H$ NMR spectrum of complex **4.1** in toluene-$d_8$.

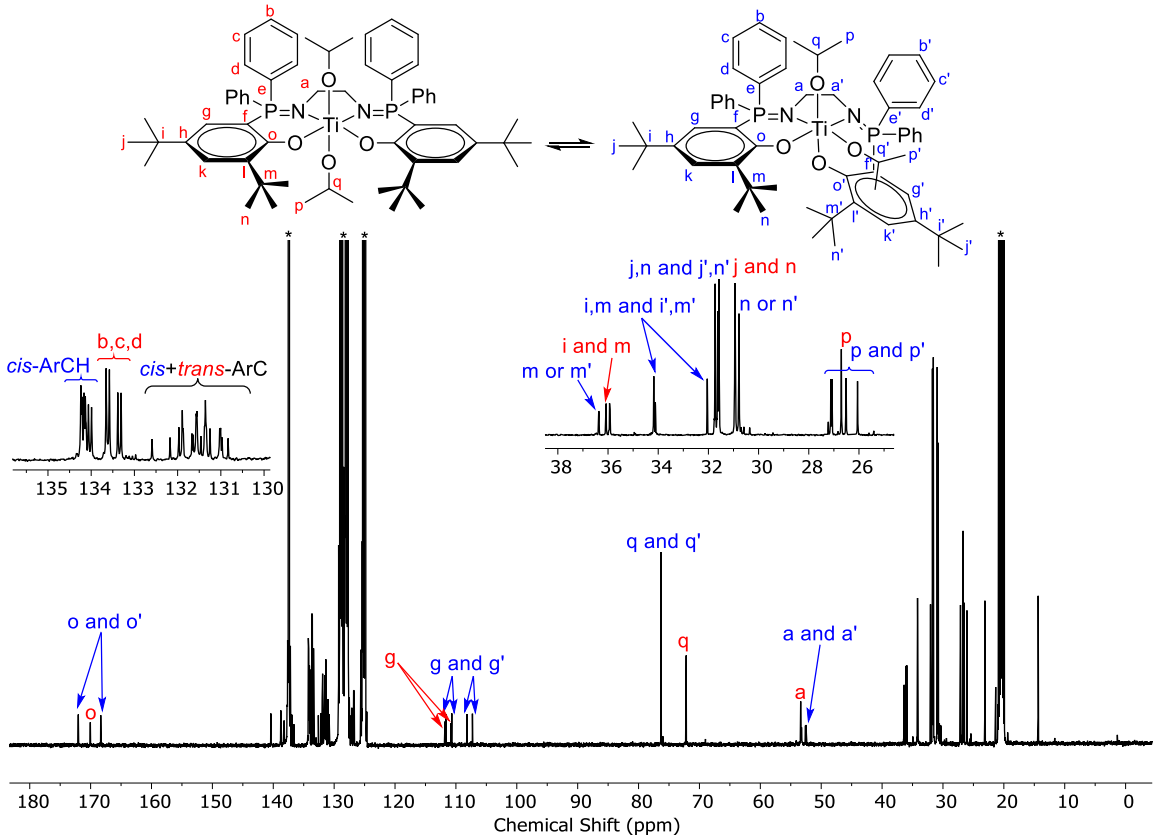



**Figure A2.11.** $^{13}C\{^{1}H\}$ NMR spectrum of complex **4.1** in toluene-$d_8$.

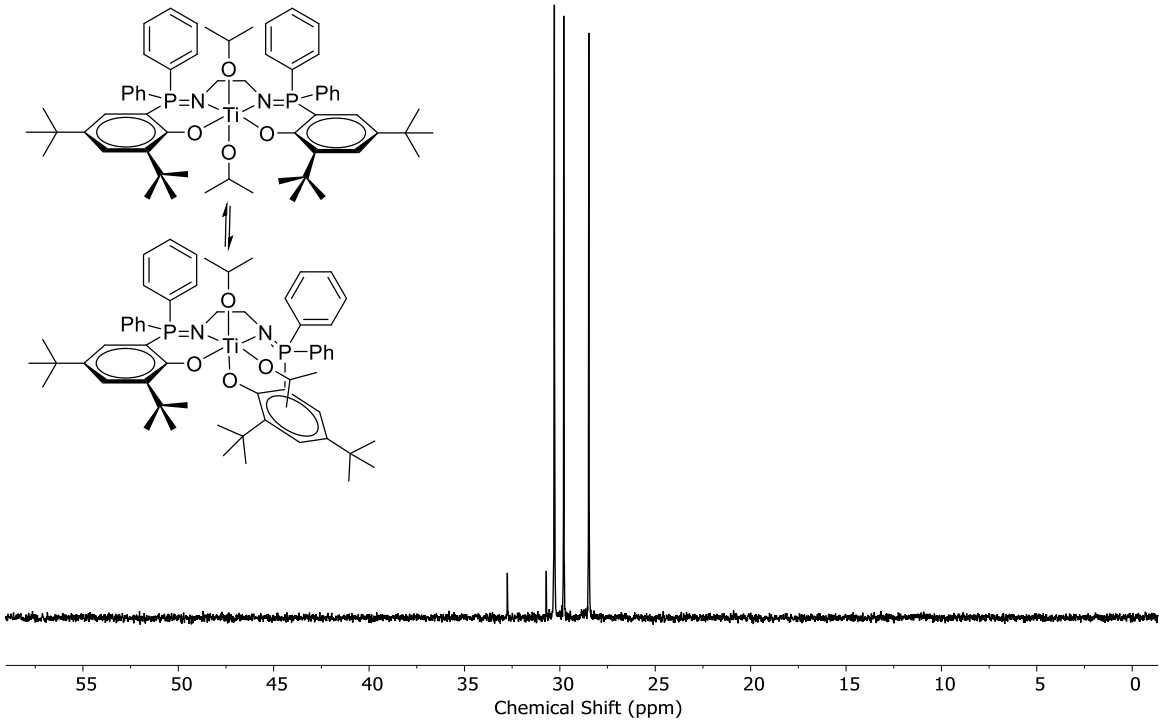



**Figure A2.12.** $^{31}P\{^{1}H\}$ NMR spectrum of complex **4.1** in toluene-$d_8$.

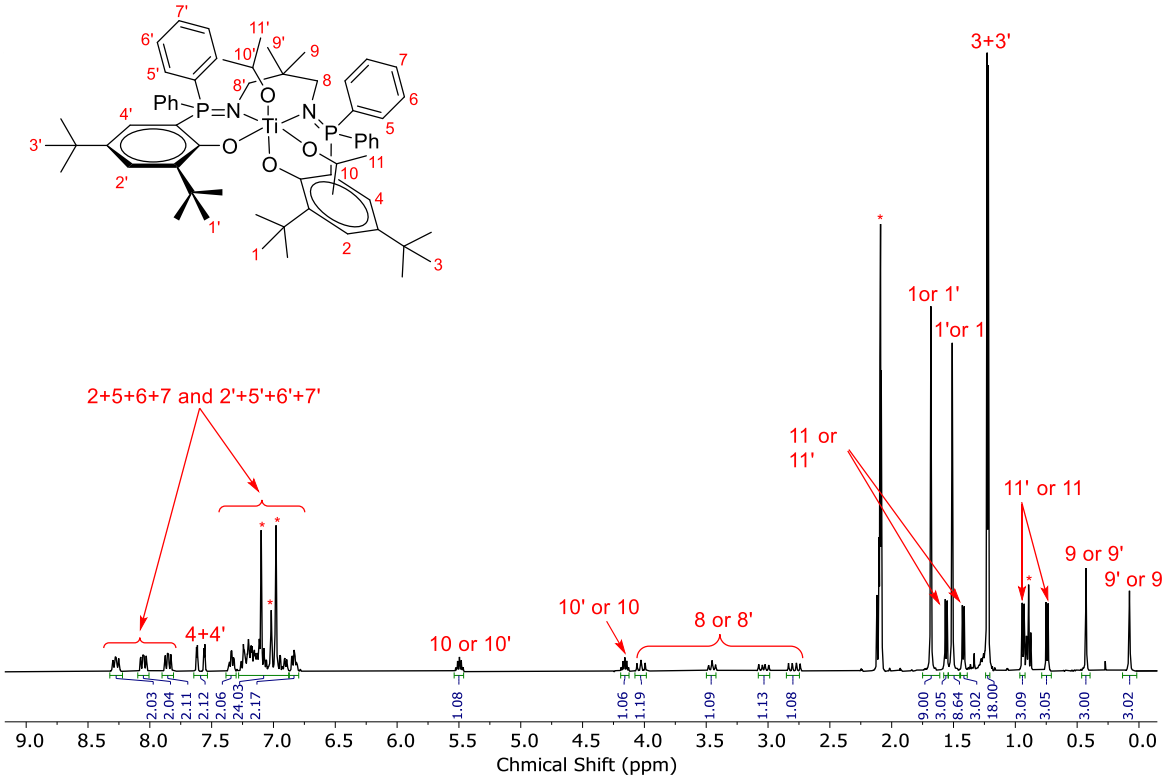



**Figure A2.13.** $^{1}$H NMR spectrum of complex **4.2** in toluene-$d_8$.

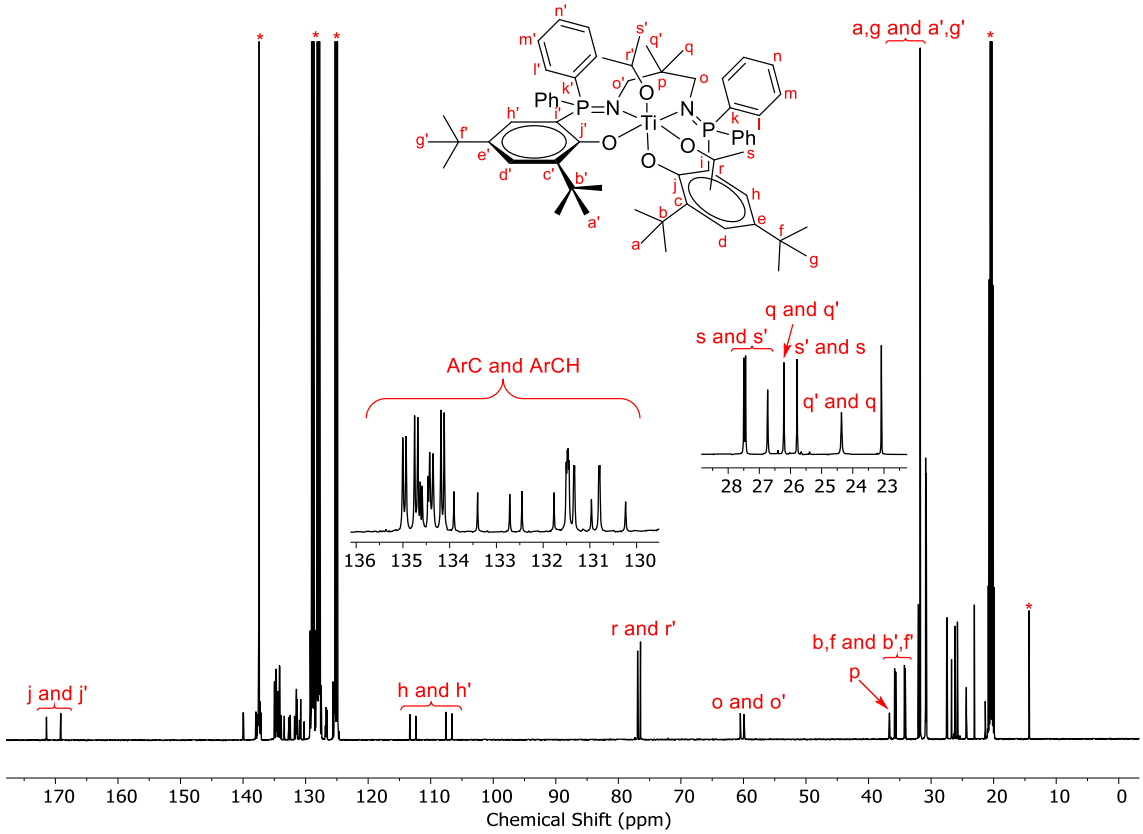



**Figure A2.14.** $^{13}$C{$^{1}$H} NMR spectrum of complex **4.2** in toluene-$d_8$.

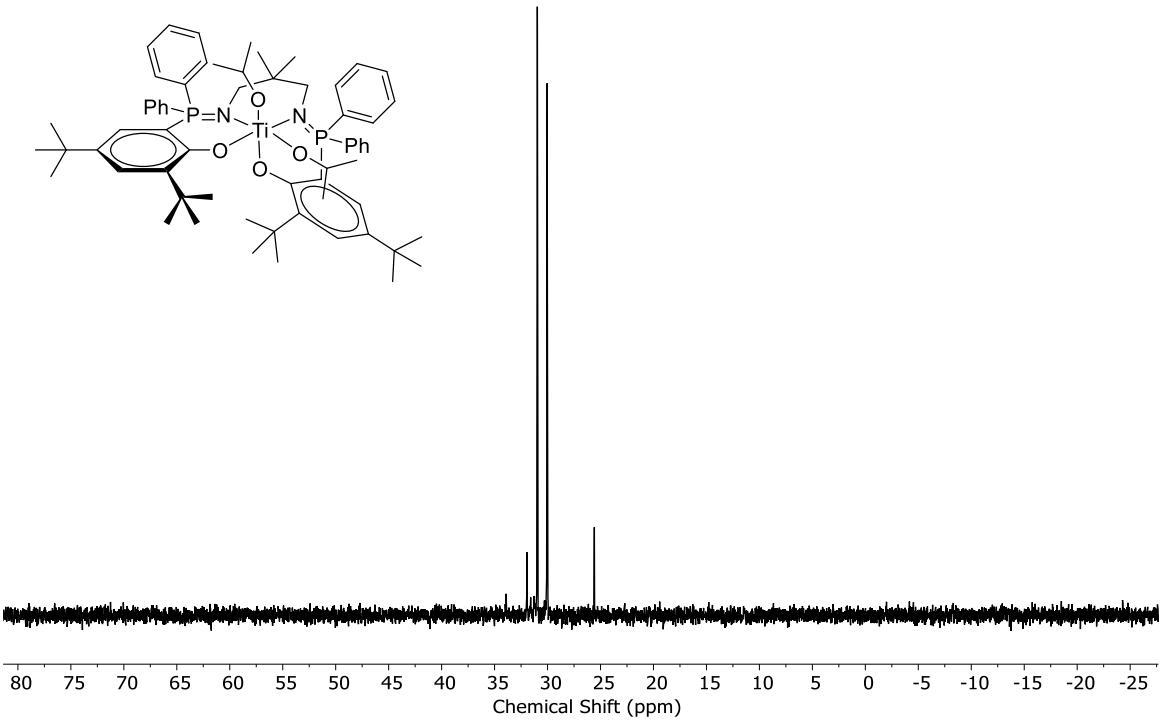



**Figure A2.15.** $^{31}P\{^{1}H\}$ NMR spectrum of complex **4.2** in toluene-$d_8$.

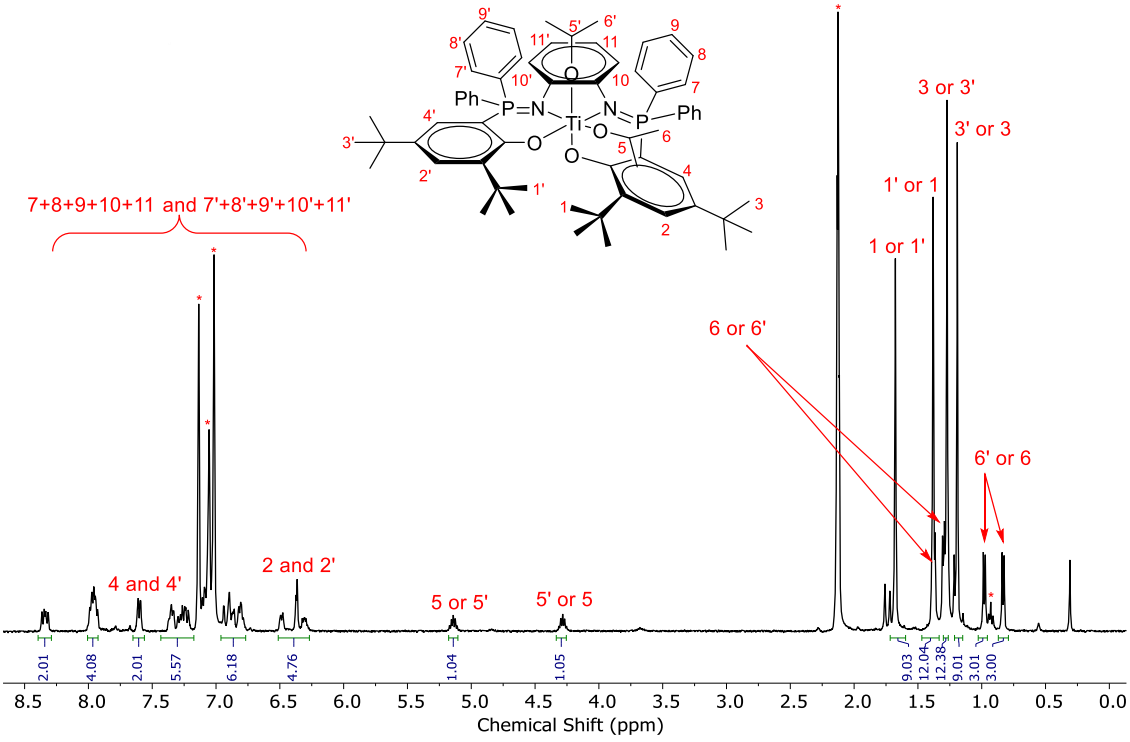



**Figure A2.16.** $^{1}H$ NMR spectrum of complex **4.3** in toluene-$d_8$.

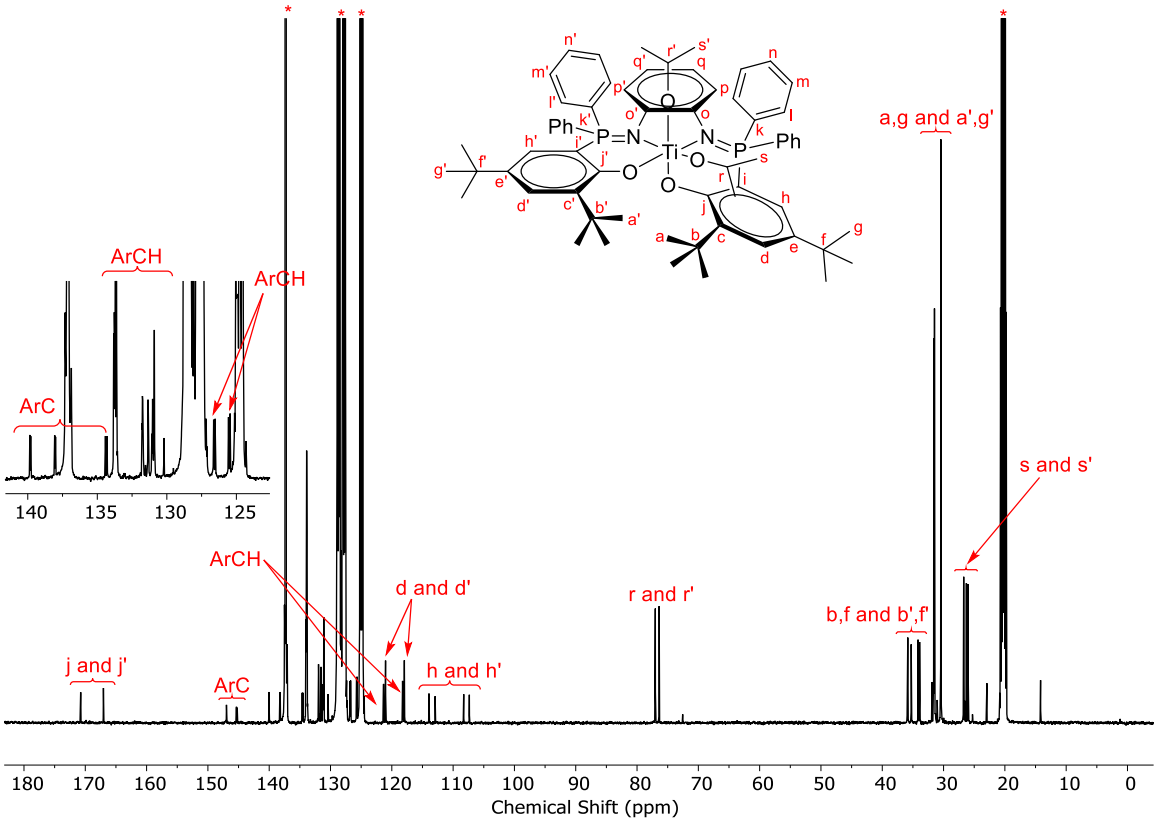



**Figure A2.17.** $^{13}C\{^{1}H\}$ NMR spectrum of complex **4.3** in toluene-$d_8$.

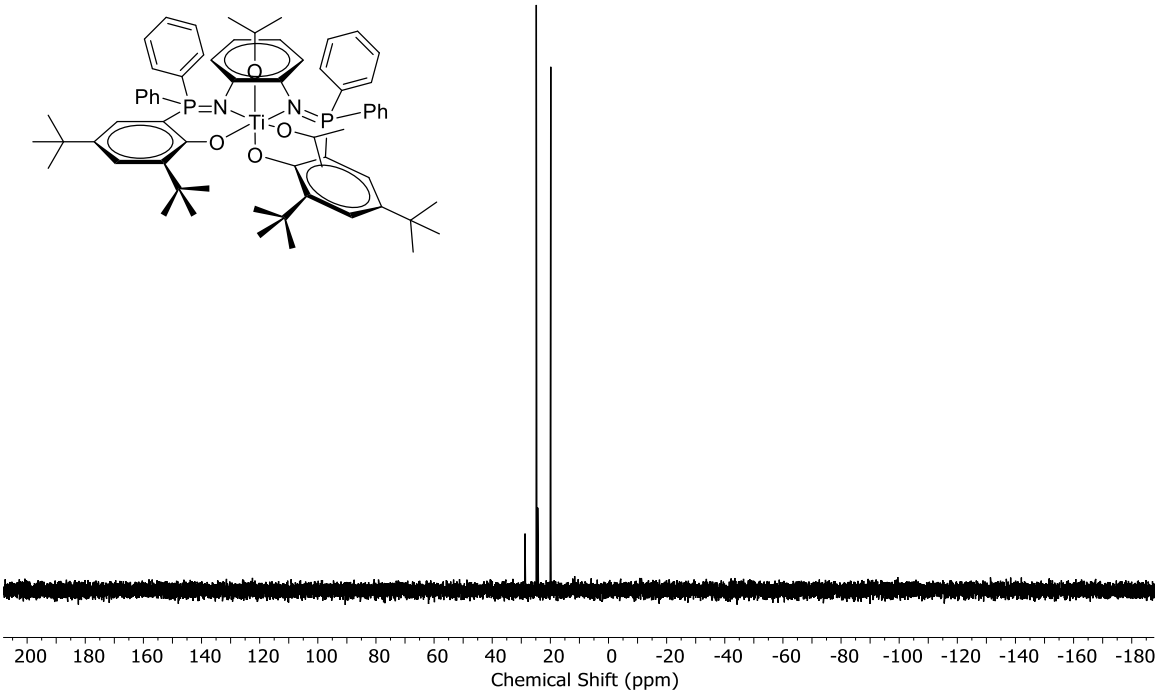



**Figure A2.18.** $^{31}P\{^{1}H\}$ NMR spectrum of complex **4.3** in toluene-$d_8$.

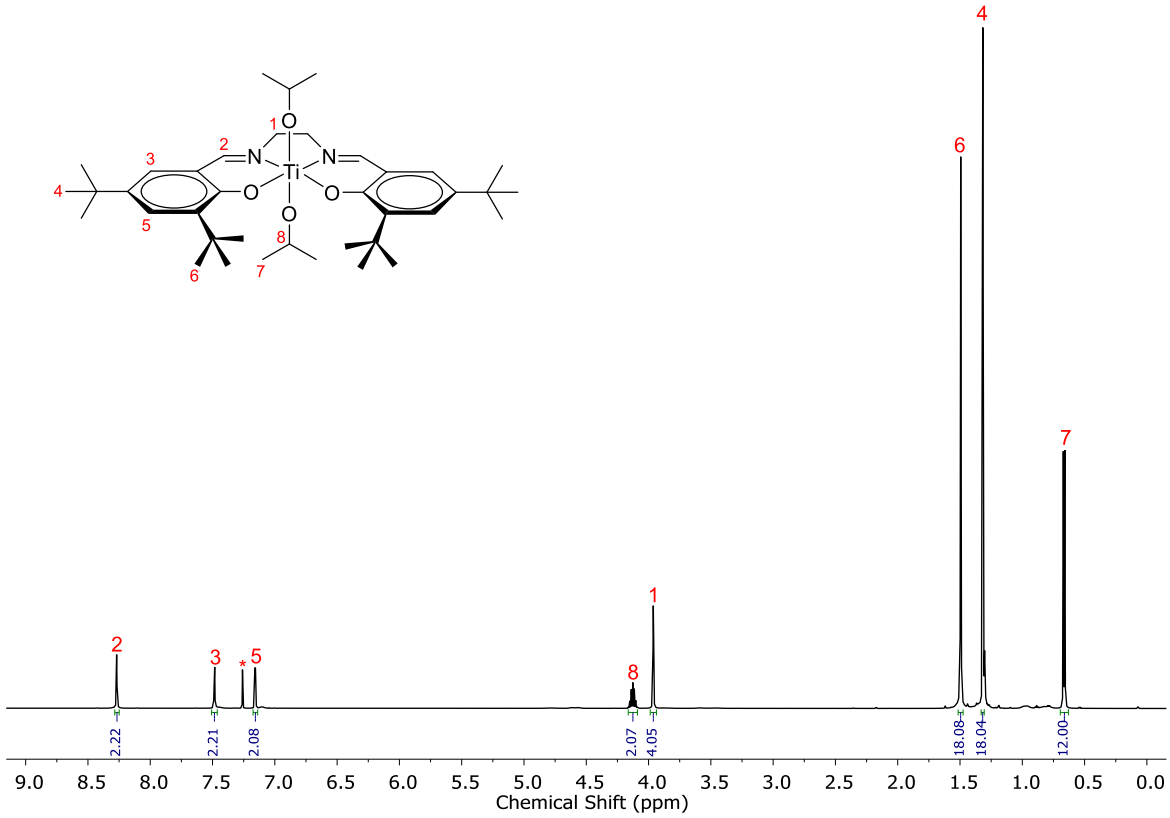



**Figure A2.19.** $^{1}$H NMR spectrum of complex **4.4** in $CDCl_3$.

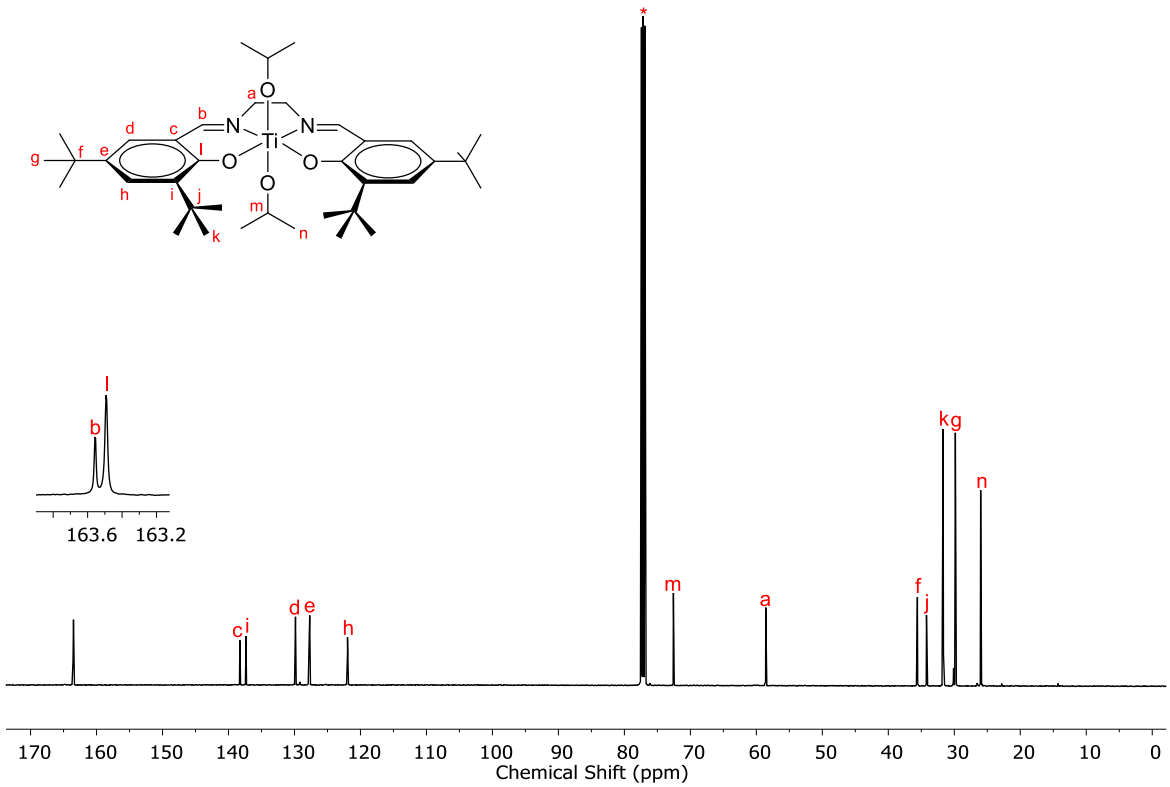



**Figure A2.20.** $^{13}C\{^{1}H\}$ NMR spectrum of complex **4.4** in $CDCl_3$.

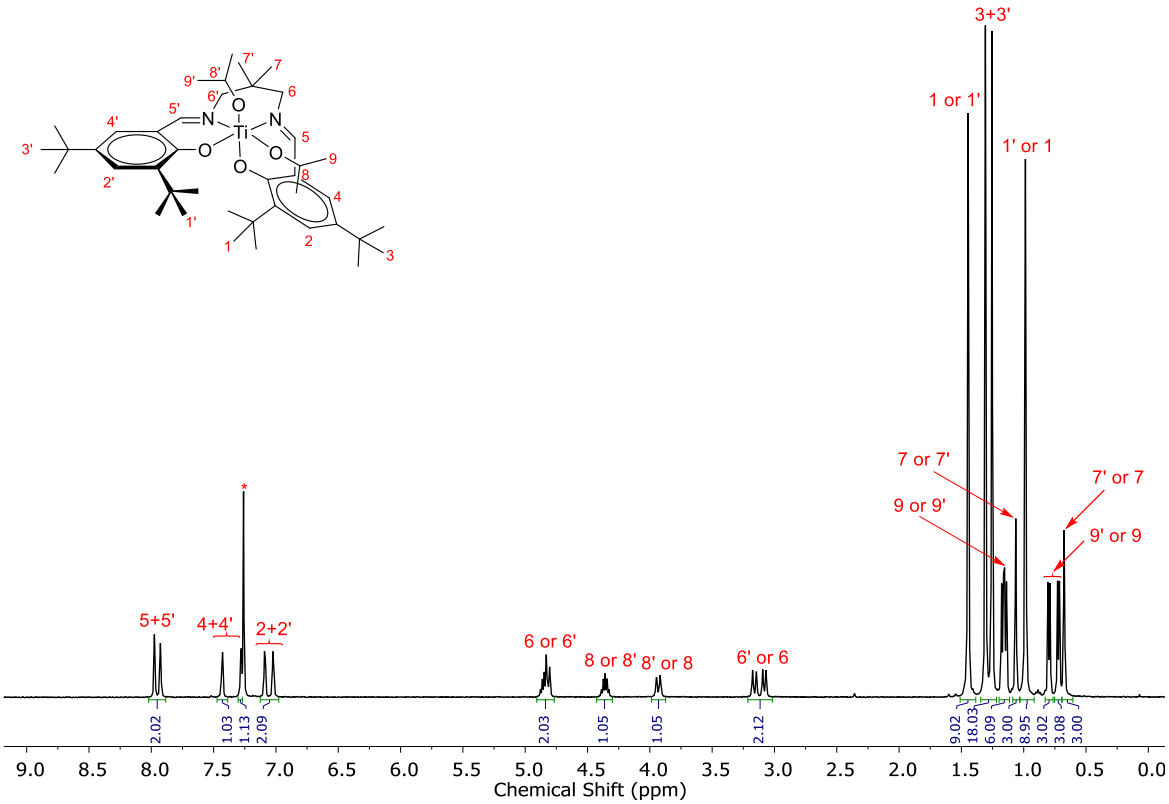



**Figure A2.21.** $^{1}$H NMR spectrum of complex **4.5** in $CDCl_3$.

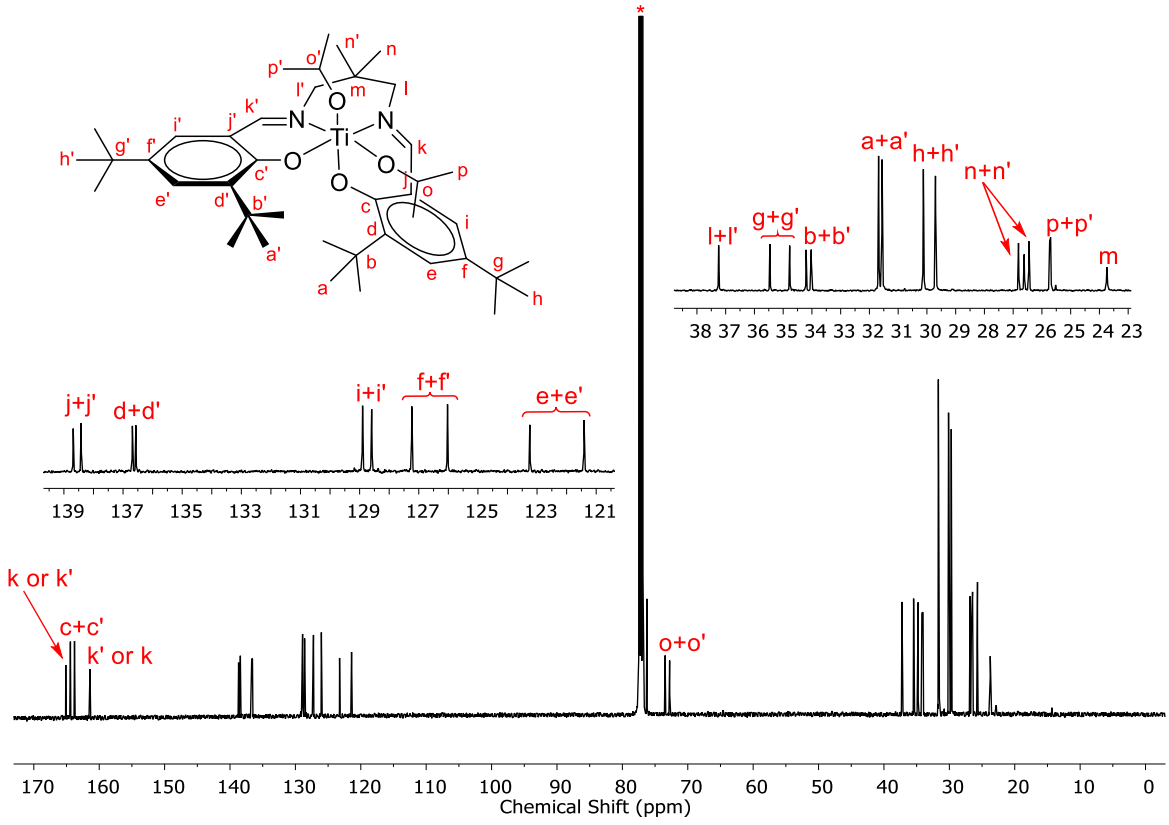



**Figure A2.22.** $^{13}$C{$^{1}$H} NMR spectrum of complex **4.5** in $CDCl_3$.

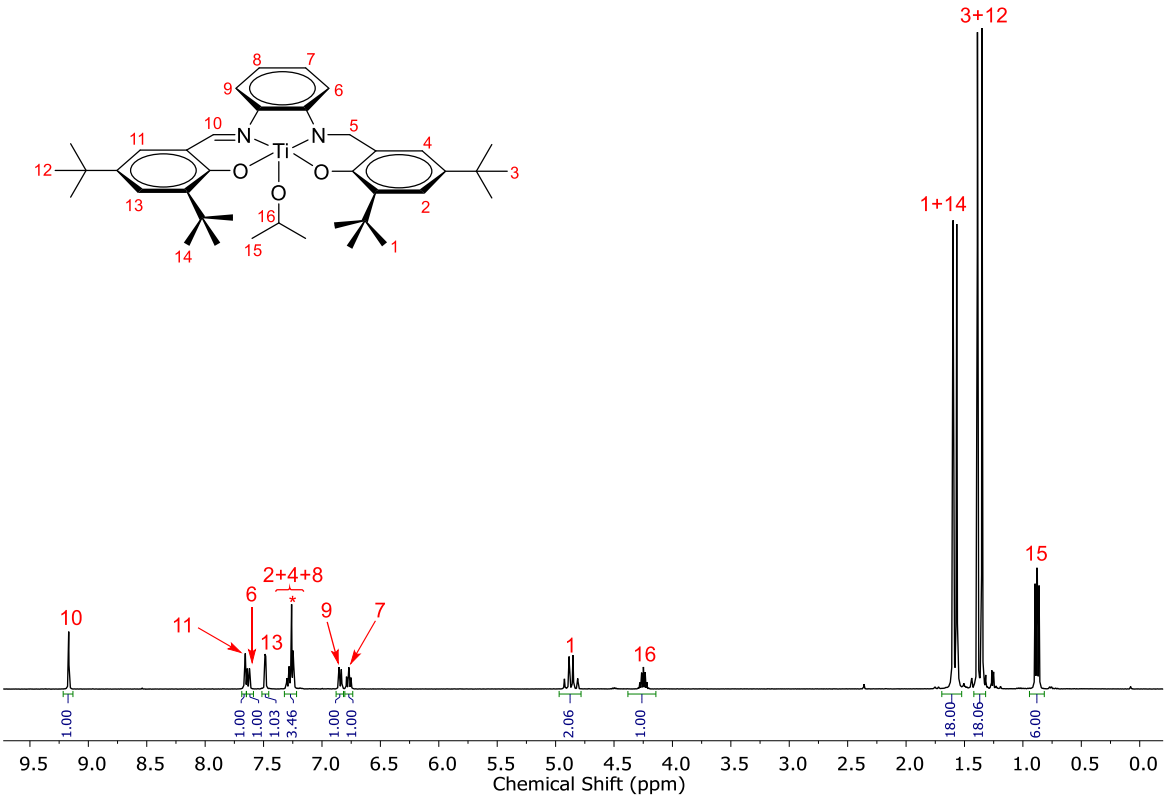



**Figure A2.23.** $^{1}$H NMR spectrum of complex **4.6** in $CDCl_3$.

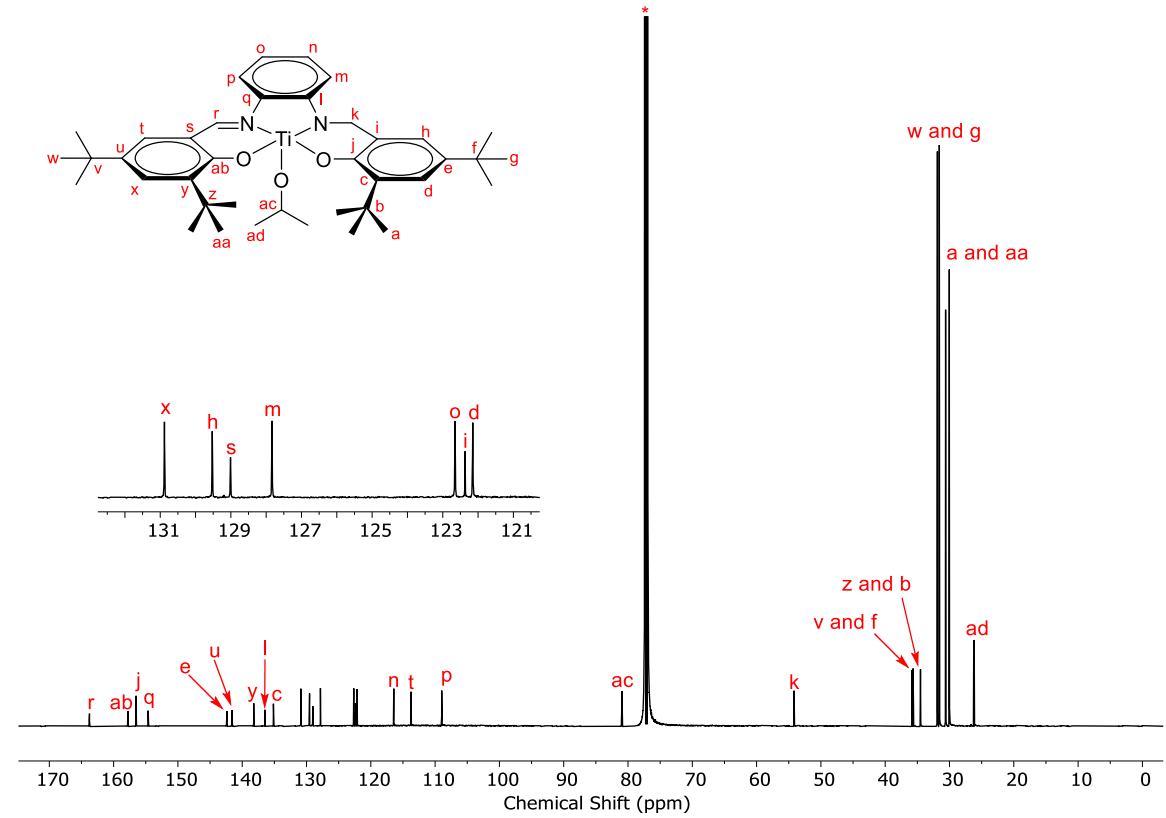



**Figure A2.24.** $^{13}$C{$^{1}$H} NMR spectrum of complex **4.6** in $CDCl_3$.

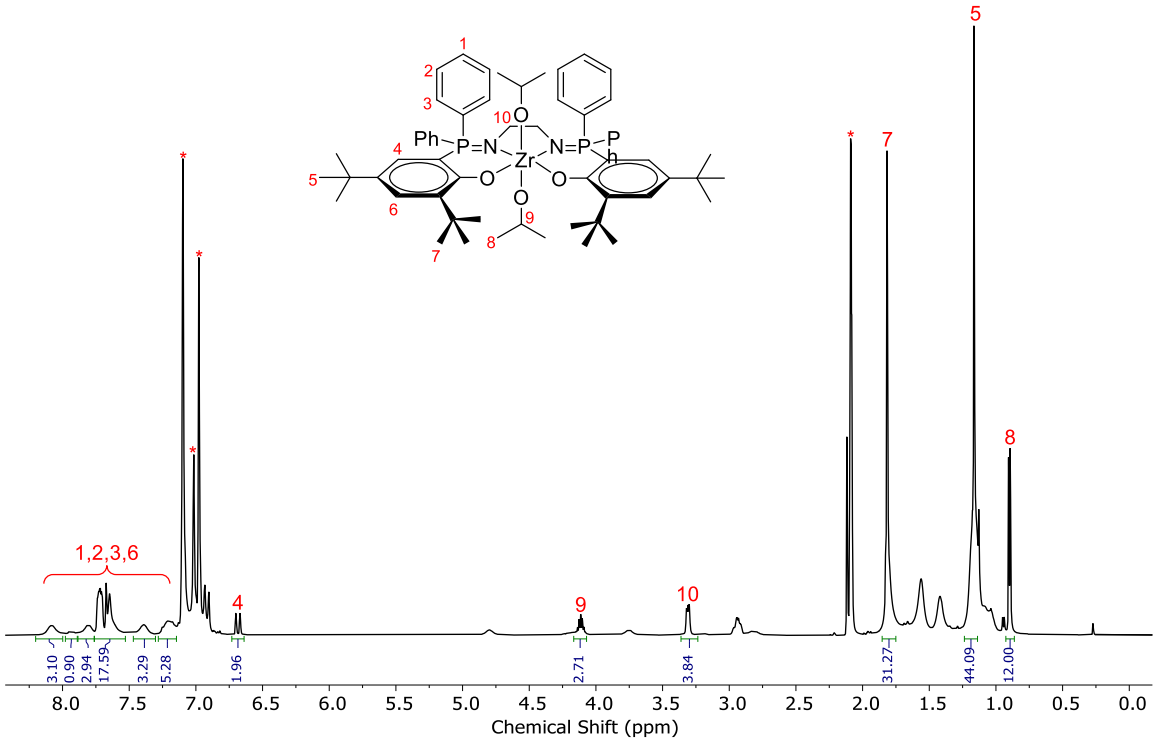



**Figure A2.25.** $^{1}$H NMR spectrum of complex **4.7** in toluene-$d_8$.

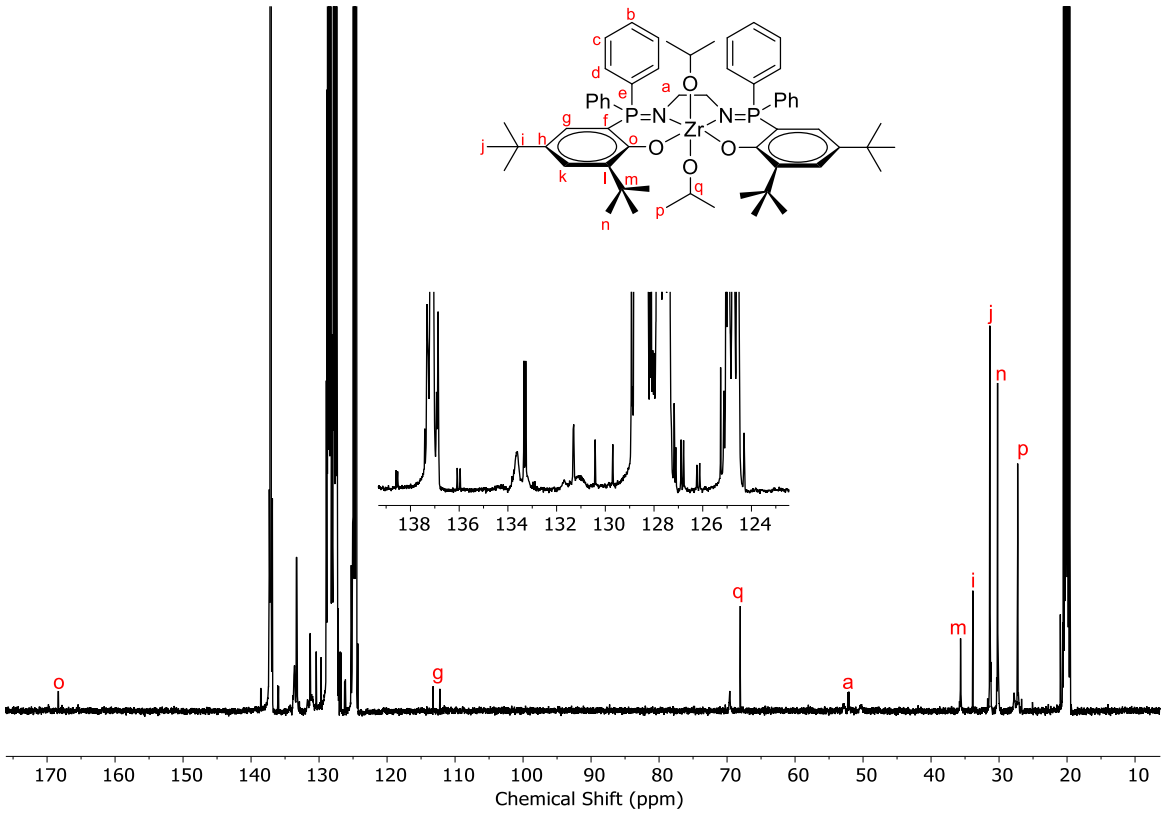



**Figure A2.26.** $^{13}$C{$^{1}$H} NMR spectrum of complex **4.7** in toluene-$d_8$.

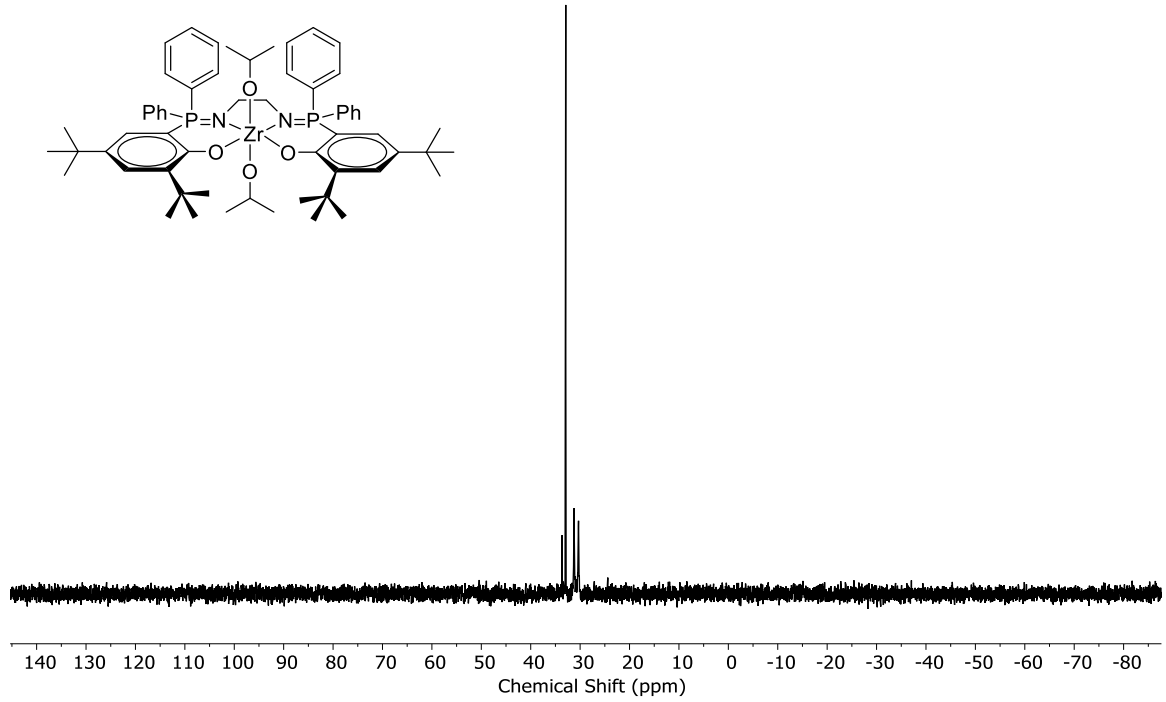



**Figure A2.27.** $^{31}P\{^{1}H\}$ NMR spectrum of **complex 4.7** in toluene-$d_8$.

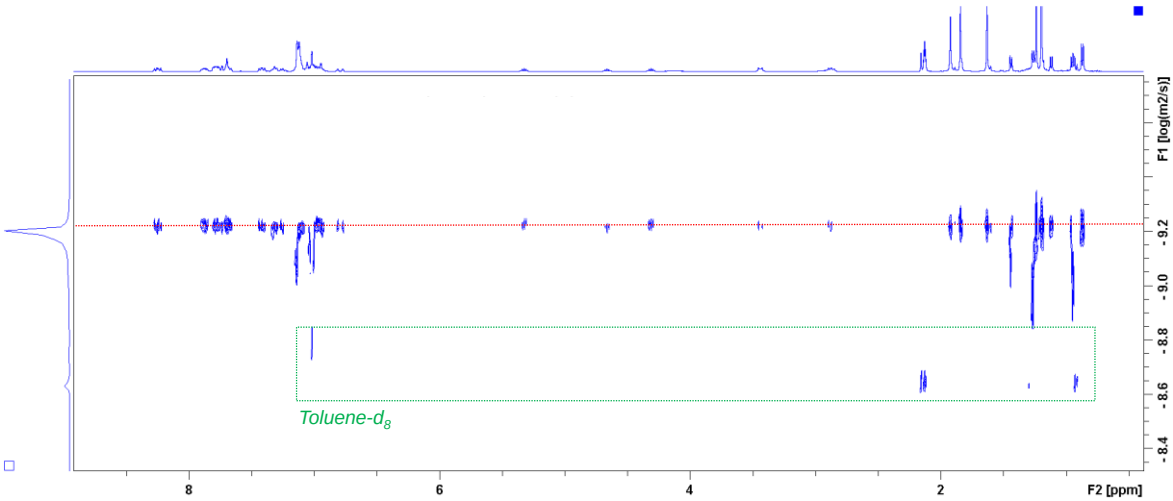



**Figure A2.28.** $^{1}H$ DOSY NMR spectrum of complex **4.1** in toluene-$d_8$.

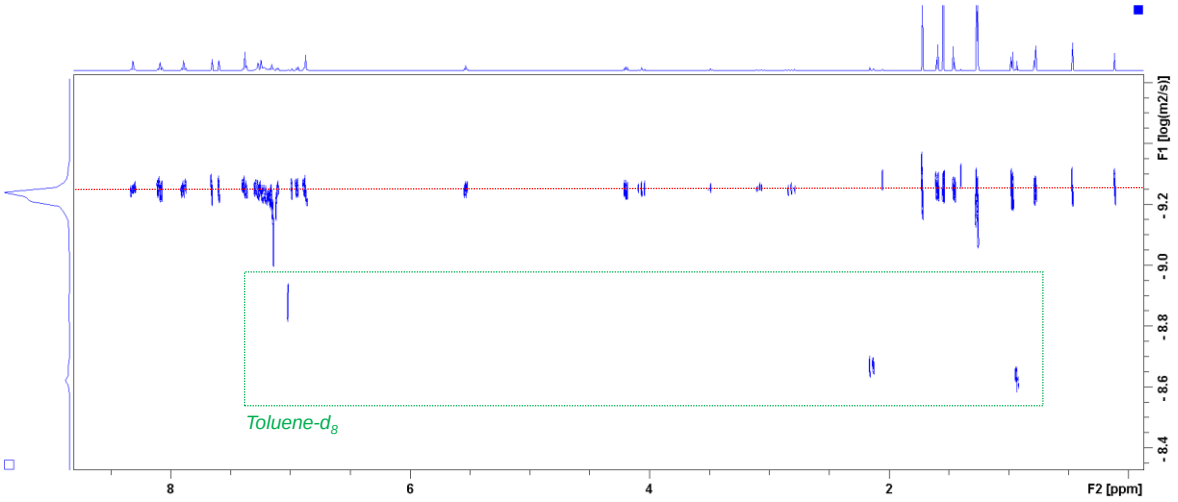



**Figure A2.29.** $^{1}$H DOSY NMR spectrum of complex **4.2** in toluene-$d_8$.

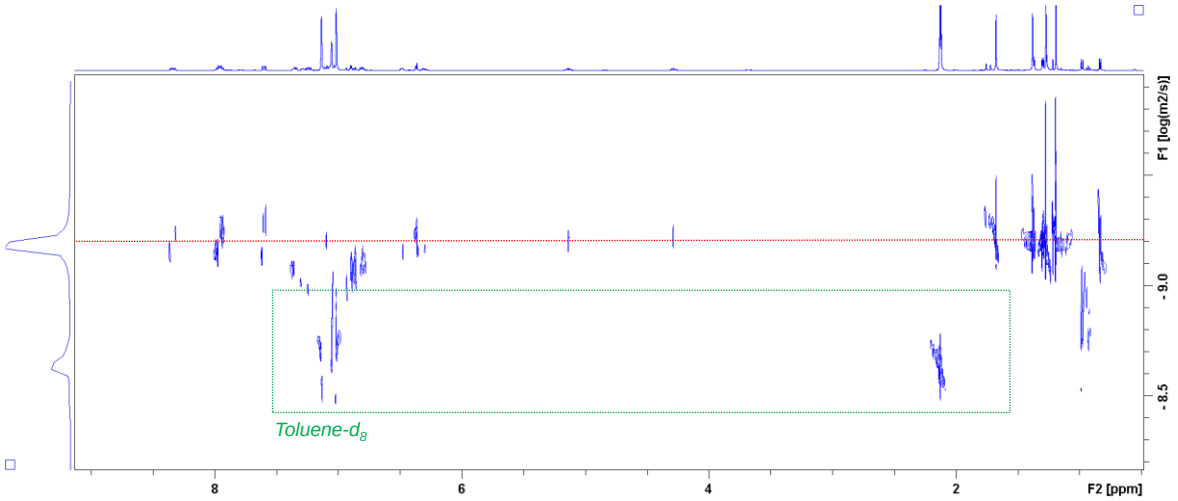



**Figure A2.30.** $^{1}$H DOSY NMR spectrum of complex **4.3** in toluene-$d_8$.

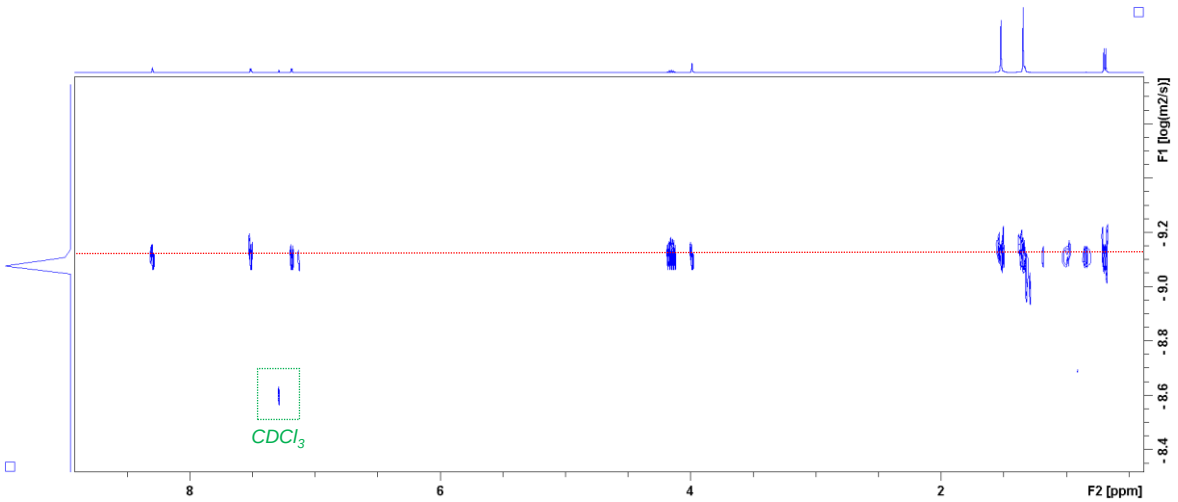



**Figure A2.31.** $^{1}$H DOSY NMR spectrum of complex **4.4** in $CDCl_3$.

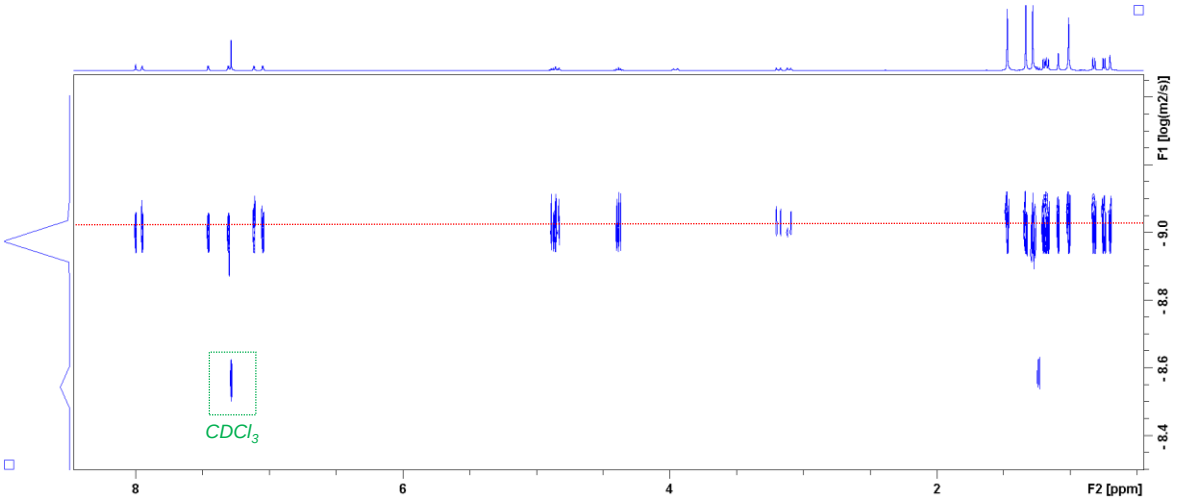



**Figure A2.32.** $^{1}$H DOSY NMR spectrum of complex **4.5** in $CDCl_3$.

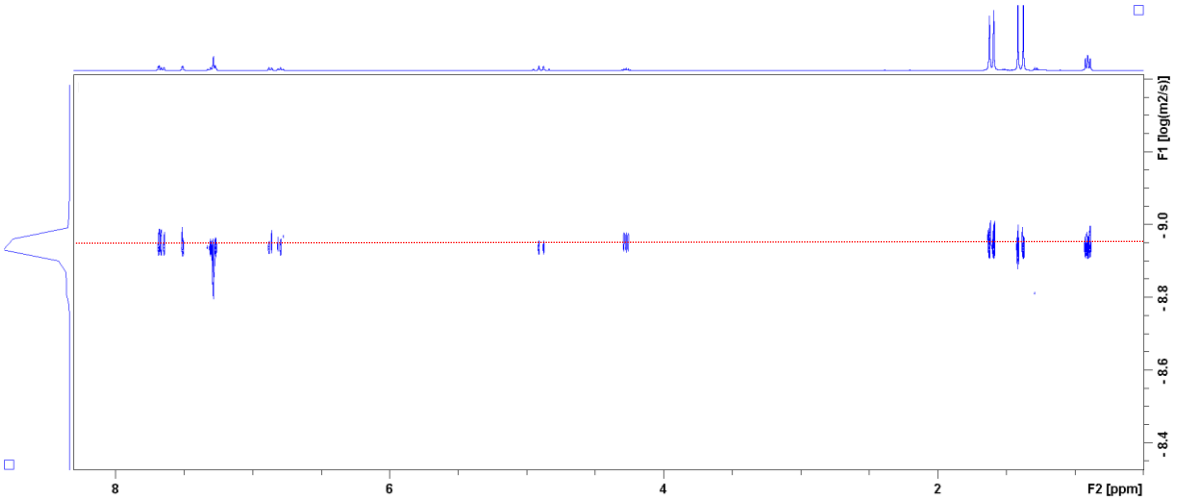



**Figure A2.33.** $^{1}$H DOSY NMR spectrum of complex **4.6** in $CDCl_3$.

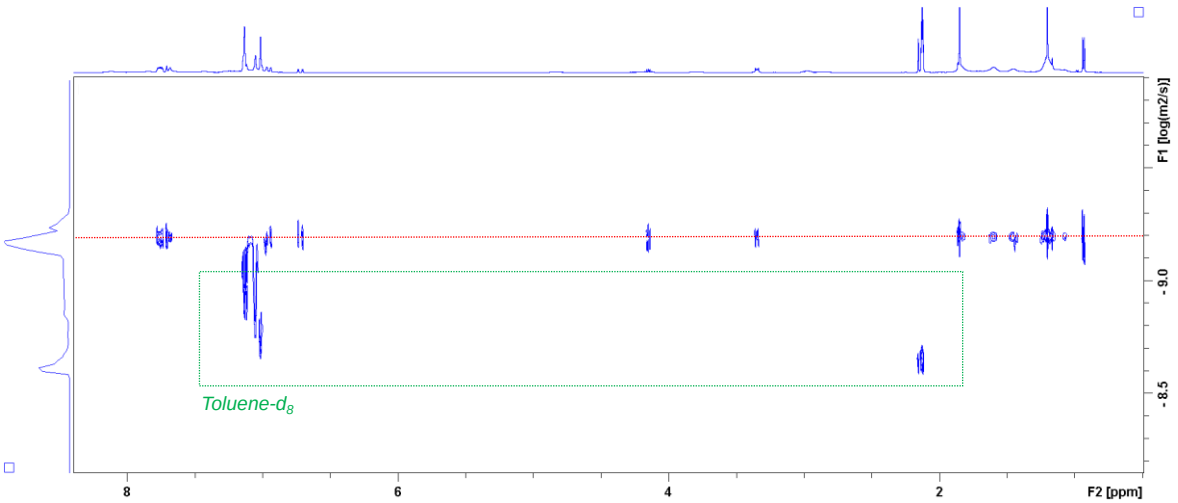
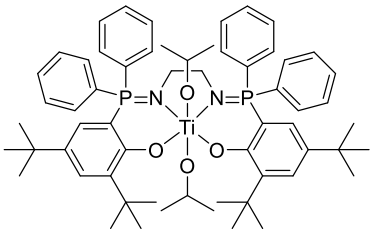
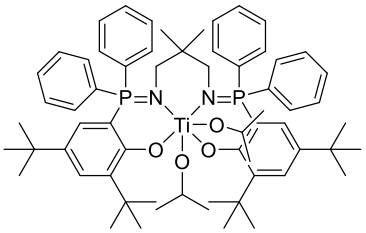



**Figure A2.34.** $^{1}$H DOSY NMR spectrum of complex **4.7** in toluene-$d_8$.

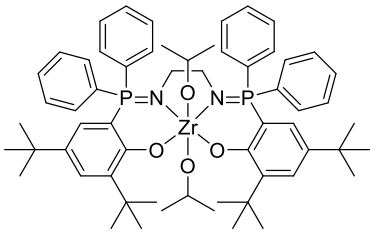
## A2.2. Additional crystallographic data for complexes 4.1–4.7 and intermediate 4.3″




4.1



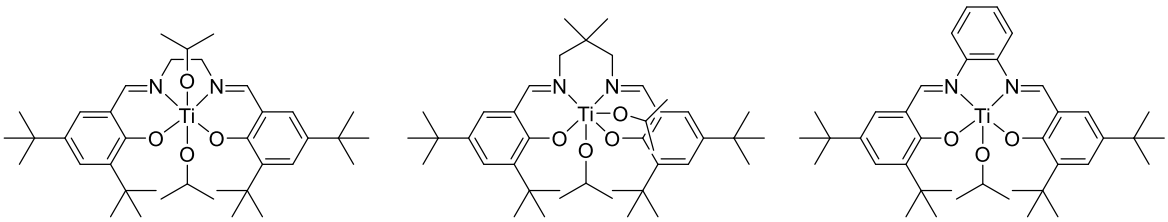

4.2




4.7

**Table A2.1.** Summary of crystallographic refinement data for complexes **4.1**, **4.2**, and **4.7**.

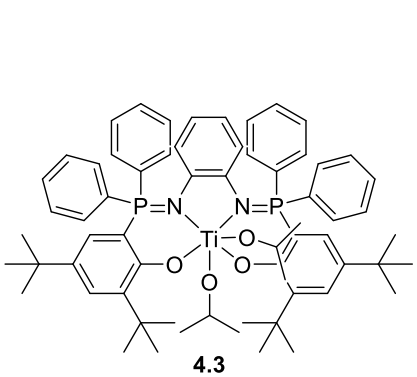
| Compound | Complex 4.1 | Complex 4.2 | Complex 4.7 |
|---|---|---|---|
| Empirical Formula | $C_{67}H_{86}TiN_2O_4P_2$ | $C_{63}H_{84}TiN_2O_4P_2$ | $C_{60}H_{78}ZrN_2O_4P_2$ |
| Formula weight ($gmol^{-1}$) | 1093.21 | 1043.22 | 1044.46 |
| Crystal system | Monoclinic | Triclinic | Monoclinic |
| a (Å) | 15.3383(3) | 14.5274(2) | 15.07820(10) |
| b (Å) | 20.8558(3) | 14.8686(2) | 21.41630(10) |
| c (Å) | 19.4083(3) | 15.5396(2) | 19.40710(10) |
| α (°) | 90 | 97.3203(13) | 90 |
| β (°) | 96.593(2) | 96.0734(13) | 95.3804(6) |
| γ (°) | 90 | 100.4151(13) | 90 |
| Unit cell volume | 6167.51(18) | 3245.69(8) | 6239.31(6) |
| No. of formula units per unit cell | 4 | 2 | 4 |
| Space group | $P2_1/n$ | P-1 | $P2_1/n$ |
| Density (calculated) ($Mg\ m^{-3}$) | 1.177 | 1.067 | 1.112 |
| Diffractometer wavelength | 1.54184 | 1.54184 | 1.54184 |
| Temperature (K) | 150(2) | 150(2) | 150(2) |
| Absorption coefficient ($mm^{-1}$) | 2.030 | 1.907 | 2.248 |
| No. of reflections collected | 35819 | 84601 | 48356 |
| No. of unique reflections | 12723 | 13489 | 12911 |
| $R_{int}$ | 0.0494 | 0.028 | 0.031 |
| Final $R_1$ values ($I > 2\sigma I$) | 0.0552 | 0.0326 | 0.0281 |
| Final $wR_2$ values ($I > 2\sigma I$) | 0.1427 | 0.0879 | 0.0699 |
| $R_1$ values (all data) | 0.0759 | 0.0346 | 0.0328 |
| $wR_2$ values (all data) | 0.1586 | 0.0899 | 0.0738 |
| Goodness of fit on $F^2$ | 1.037 | 0.9966 | 0.9969 |



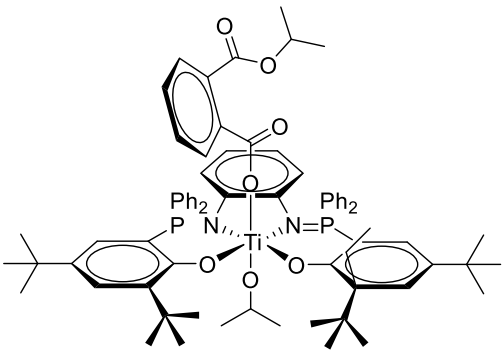
4.4 4.5 4.6

**Table A2.2.** Summary of crystallographic refinement data complexes **4.4**–**4.6**.

| Compound | Complex 4.4 | Complex 4.5 | Complex 4.6 |
|---|---|---|---|
| Empirical Formula | $C_{38}H_{60}TiN_2O_4$ | $C_{41}H_{66}TiN_2O_4$ | $C_{39}H_{54}TiN_2O_3$ |
| Formula weight ($gmol^{-1}$) | 656.80 | 698.89 | 646.77 |
| Crystal system | Orthorhombic | Triclinic | Triclinic |
| a (Å) | 25.1534(2) | 15.2962(4) | 11.1346(6) |
| b (Å) | 11.89210(10) | 16.4385(5) | 12.9611(5) |
| c (Å) | 26.0750(2) | 19.1764(6) | 12.9914(6) |
| α (°) | 90 | 99.780(3) | 91.345(3) |
| β (°) | 90 | 105.094(2) | 103.628(4) |
| γ (°) | 90 | 97.604(2) | 92.513(3) |
| Unit cell volume | 7799.73(11) | 4508.1(2) | 1819.23(15) |
| No. of formula units per unit cell | 8 | 4 | 2 |
| Space group | P b c a | P-1 | P-1 |
| Density (calculated) ($Mg\ m^{-3}$) | 1.119 | 1.030 | 1.181 |
| Diffractometer wavelength | 1.54184 | 1.54180 | 1.54184 |
| Temperature (K) | 150(2) | 150(2) | 150(2) |
| Absorption coefficient ($mm^{-1}$) | 2.145 | 1.880 | 2.276 |
| No. of reflections collected | 77634 | 50633 | 18294 |
| No. of unique reflections | 8135 | 18624 | 7505 |
| $R_{int}$ | 0.036 | 0.052 | 0.034 |
| Final $R_1$ values ($I > 2\sigma I$) | 0.0313 | 0.0824 | 0.0483 |
| Final $wR_2$ values ($I > 2\sigma I$) | 0.0859 | 0.2378 | 0.1247 |
| $R_1$ values (all data) | 0.0352 | 0.0943 | 0.0533 |
| $wR_2$ values (all data) | 0.0911 | 0.2532 | 0.1305 |
| Goodness of fit on $F^2$ | 1.0007 | 0.9953 | 1.0081 |




4.3




4.3''

**Table A2.3.** Summary of crystallographic refinement data for complex **4.3** and intermediate **4.3′′**.

| Compound | Complex 4.3 | Intermediate 4.3′′ |
|---|---|---|
| Empirical Formula | $C_{64}H_{78}TiN_2O_4P_2$ | $C_{80}H_{86}TiN_2O_{10}P_2$ |
| Formula weight ($gmol^{-1}$) | 1049.18 | 1345.42 |
| Crystal system | Monoclinic | Triclinic |
| a (Å) | 21.8079(5) | 12.2878(11) |
| b (Å) | 11.2637(3) | 13.7412(8) |
| c (Å) | 24.6704(7) | 24.6789(11) |
| α (°) | 90 | 80.691(4) |
| β (°) | 108.285(3) | 84.730(5) |
| γ (°) | 90 | 81.841(6) |
| Unit cell volume | 5754.0(3) | 4060.4(5) |
| No. of formula units per unit cell | 4 | 2 |
| Space group | P21/n | P-1 |
| Density (calculated) ($Mg\ m^{-3}$) | 1.211 | 1.100 |
| Diffractometer wavelength | 1.54184 | 1.54184 |
| Temperature (K) | 150(2) | 150(2) |
| Absorption coefficient ($mm^{-1}$) | 2.157 | 1.689 |
| No. of reflections collected | 33905 | 29507 |
| No. of unique reflections | 11873 | 14574 |
| $R_{int}$ | 0.071 | 0.061 |
| Final $R_1$ values ($I > 2\sigma I$) | 0.0496 | 0.0643 |
| Final $wR_2$ values ($I > 2\sigma I$) | 0.1084 | 0.1412 |
| $R_1$ values (all data) | 0.0726 | 0.1120 |
| $wR_2$ values (all data) | 0.1225 | 0.1788 |
| Goodness of fit on $F^2$ | 1.0173 | 0.9990 |

## A2.3. Additional polymerisation data

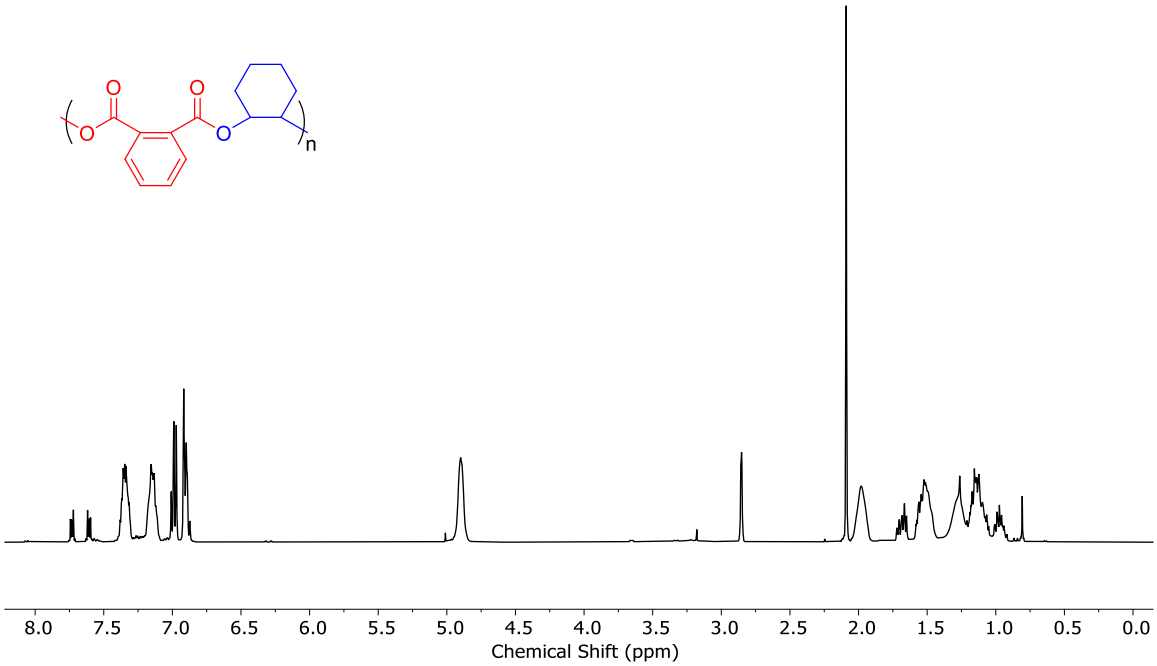



**Figure A2.35.** $^{1}$H NMR spectrum of crude poly(CHO-*alt*-PA), prepared by **4.1** in $CDCl_3$.

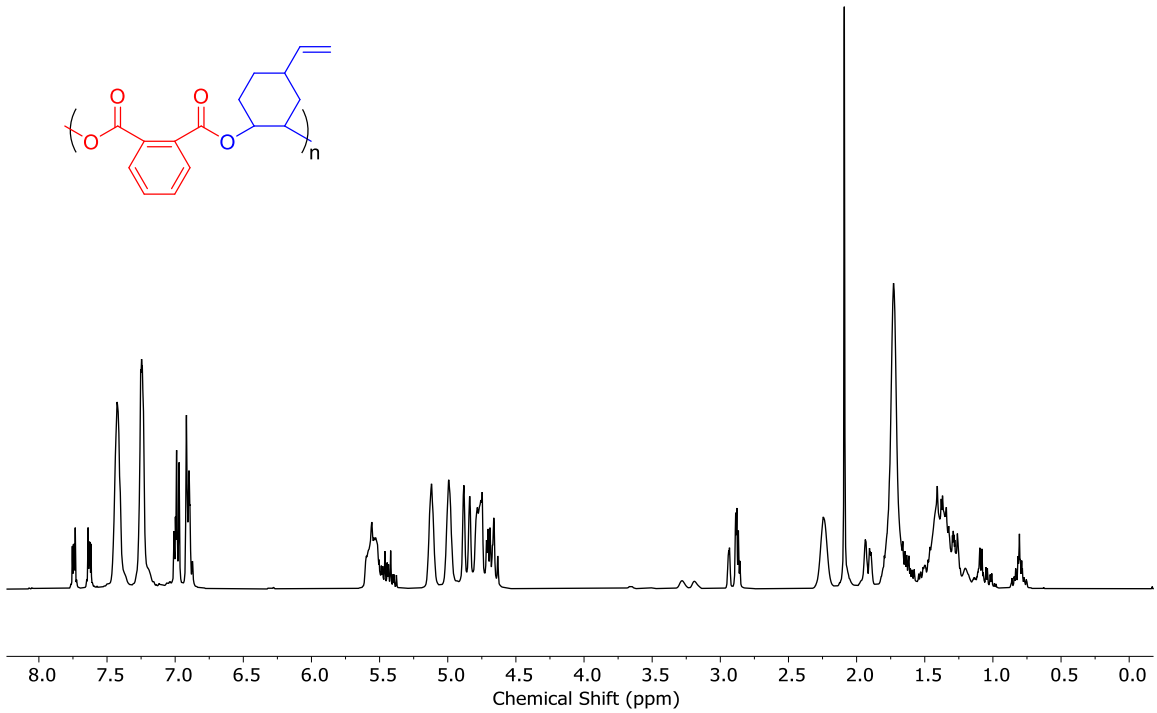



**Figure A2.36.** $^{1}$H NMR spectrum of crude poly(vCHO-*alt*-PA) , prepared by **4.1** in $CDCl_3$.

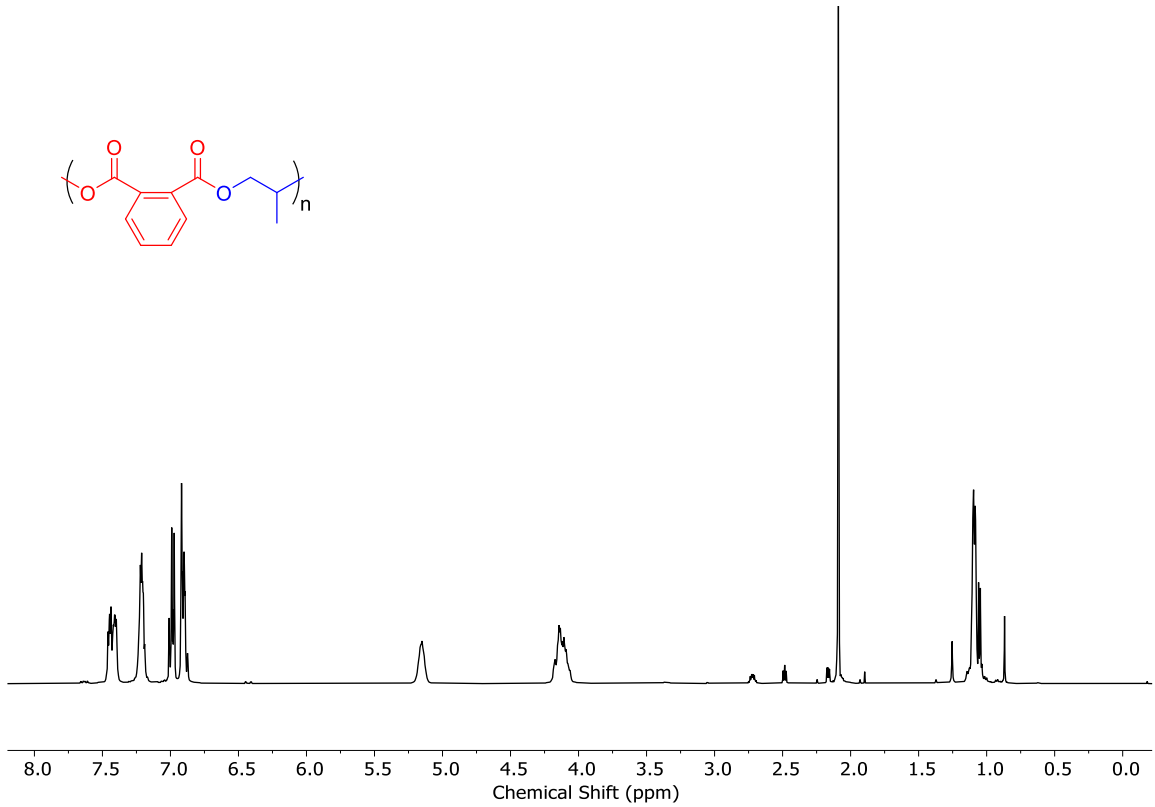



**Figure A2.37.** $^{1}$H NMR spectrum of crude poly(PO-*alt*-PA), prepared by **4.1** in $CDCl_3$.

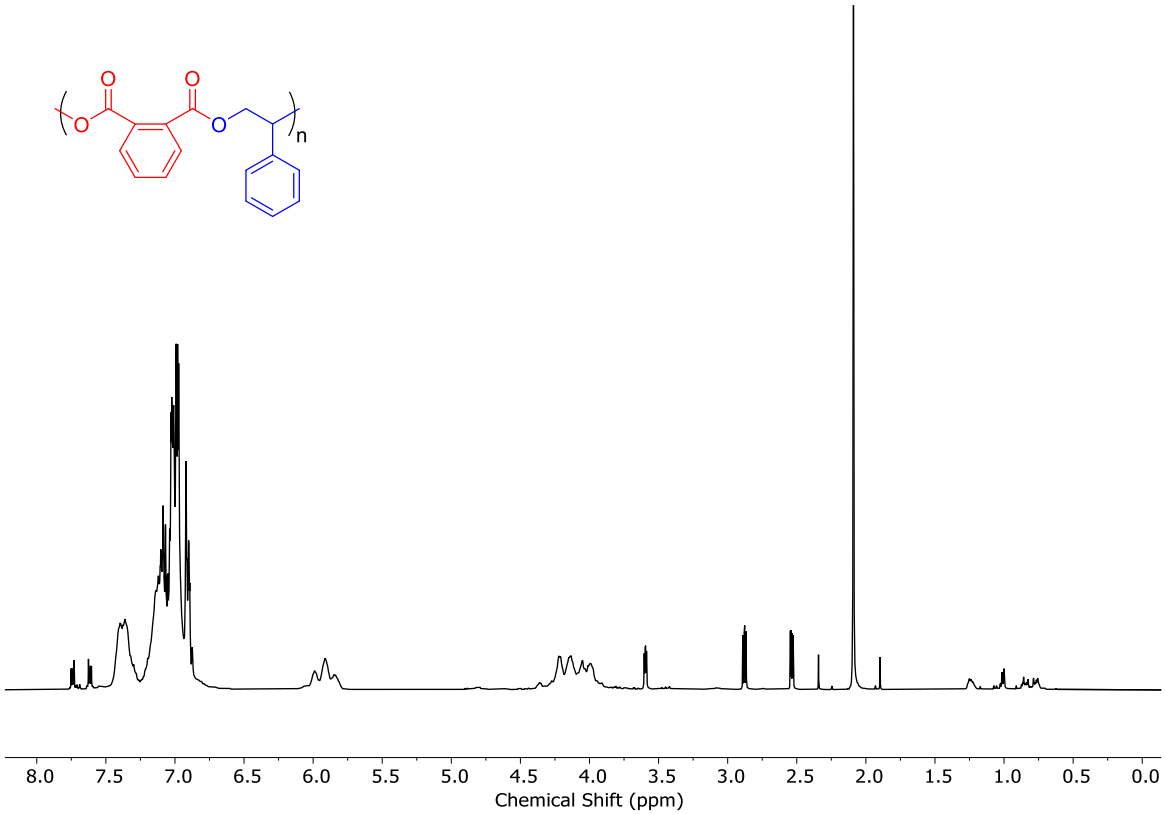



**Figure A2.38.** $^{1}$H NMR spectrum of crude poly(SO-*alt*-PA), prepared by **4.1** in $CDCl_3$.

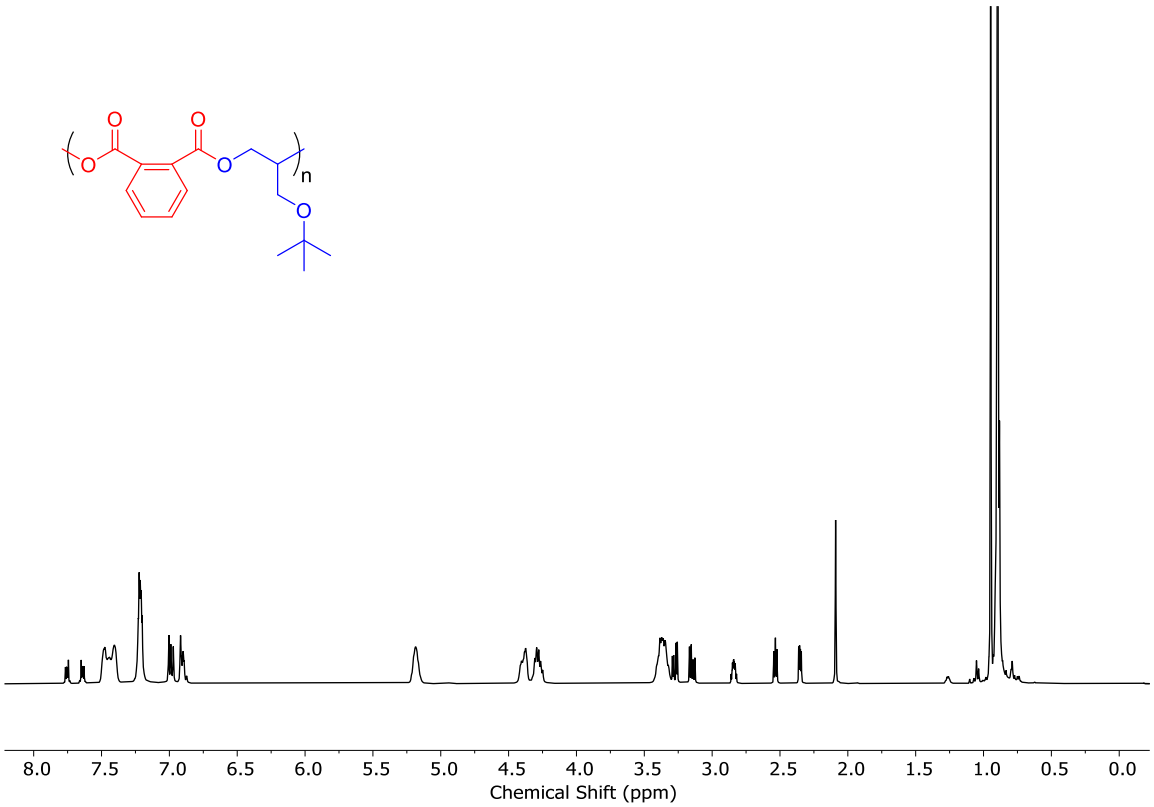



**Figure A2.39.** $^{1}$H NMR spectrum of crude poly($^{t}$BGE-*alt*-PA), prepared by **4.1** in $CDCl_3$.

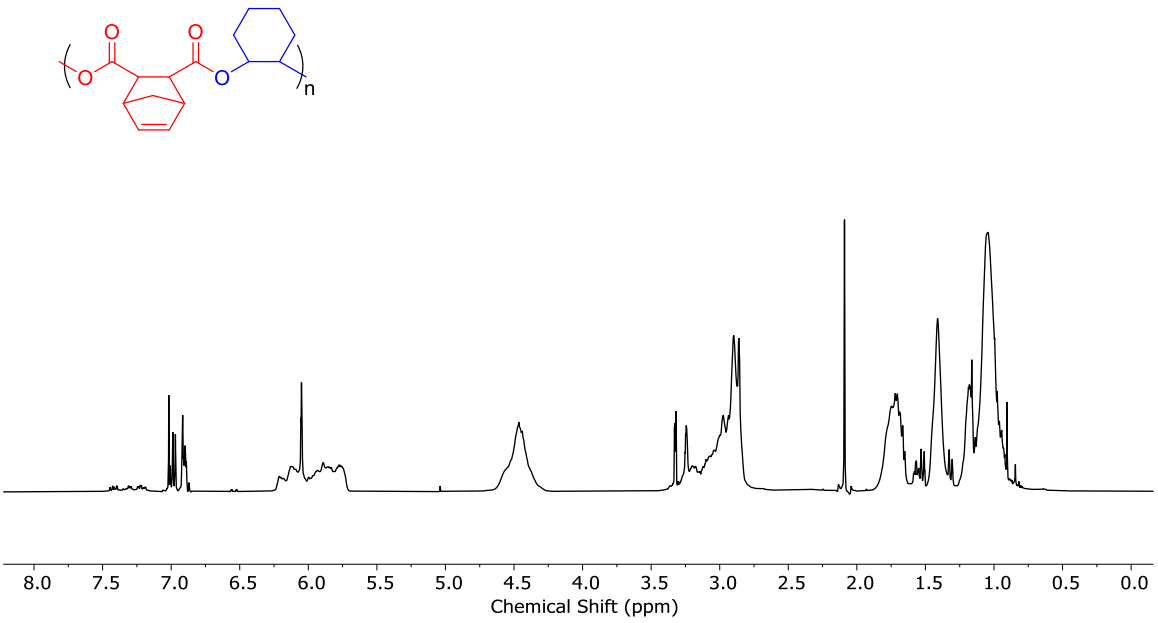



**Figure A2.40.** $^{1}$H NMR spectrum of crude poly(CHO-*alt*-NBA), prepared by **4.1** in $CDCl_3$.

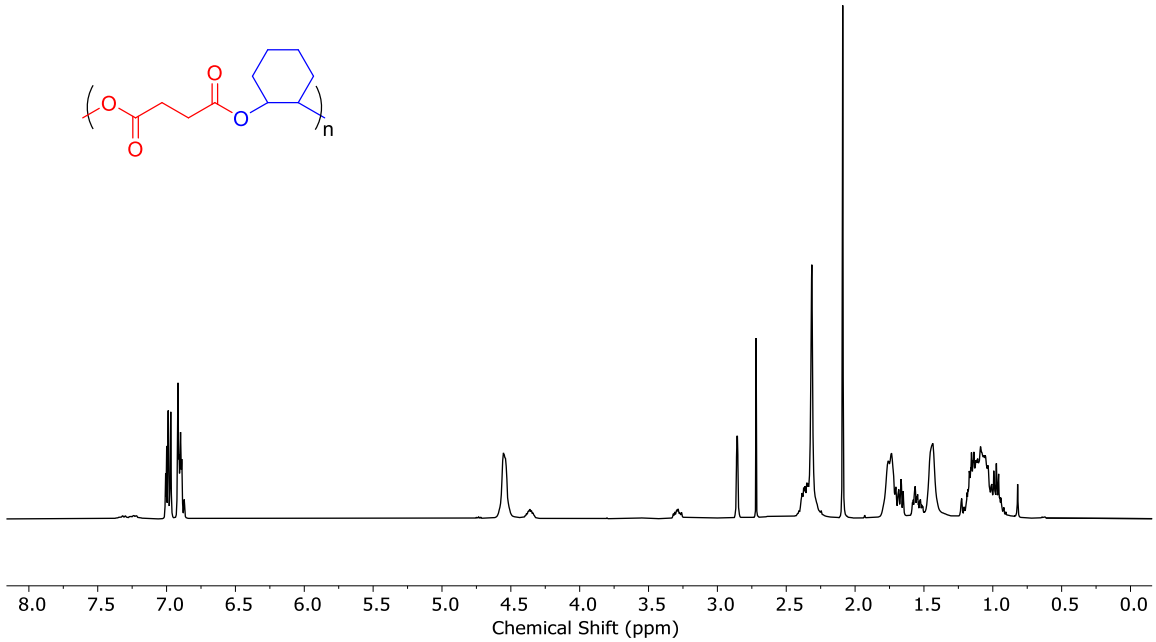



**Figure A2.41.** $^{1}$H NMR spectrum of crude poly(CHO-*alt*-SA), prepared by **4.1** in $CDCl_3$.

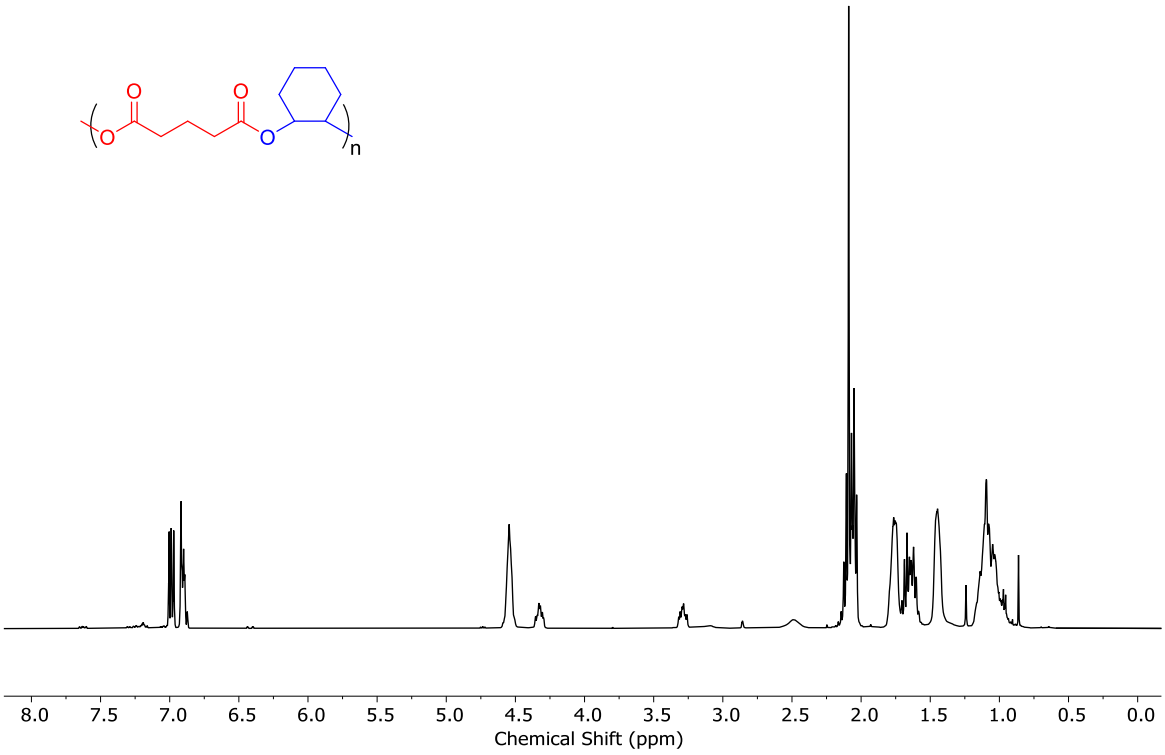



**Figure A2.42.** $^{1}$H NMR spectrum of crude poly(CHO-*alt*-GA), prepared by **4.1** in $CDCl_3$.

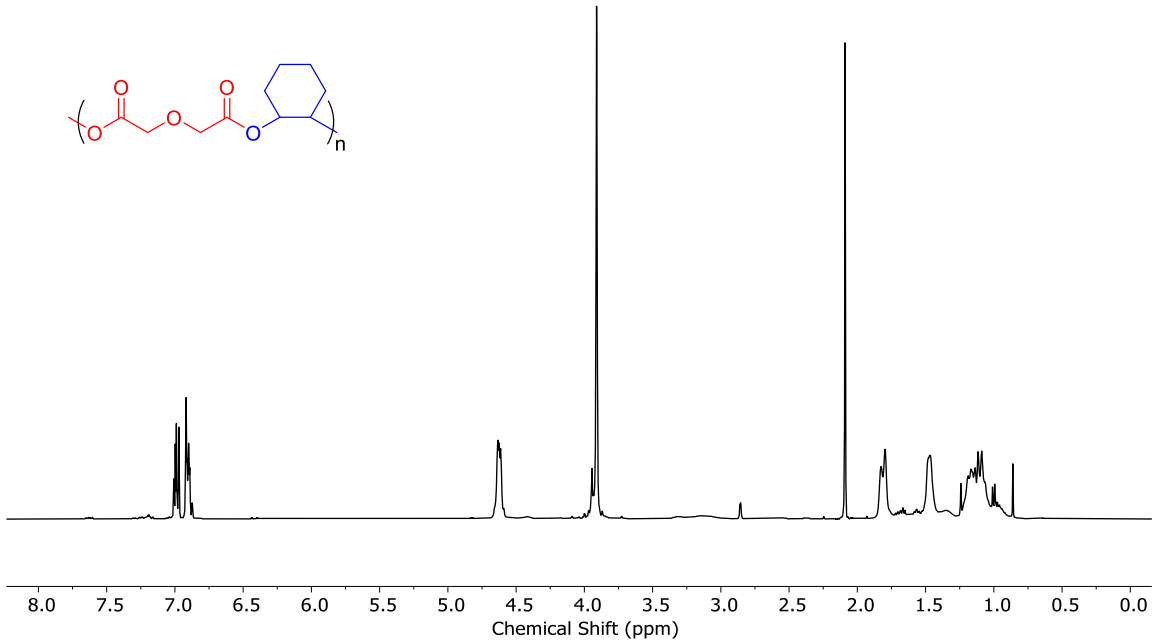



**Figure A2.43.** $^{1}$H NMR spectrum of crude poly(CHO-*alt*-DGA), prepared by **4.1** in $CDCl_3$.

# A3. Chapter 5

## A3.1. Additional polymerisation data

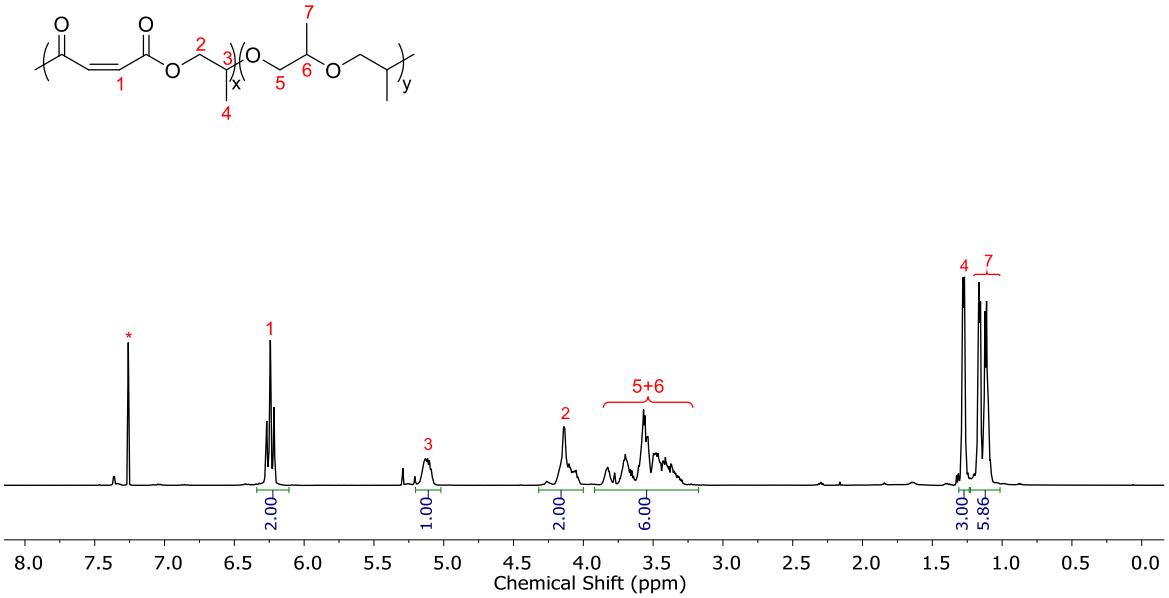



**Figure A3.1.** $^{1}H$ NMR spectrum of $PEE_{MA}$ in $CDCl_3$.

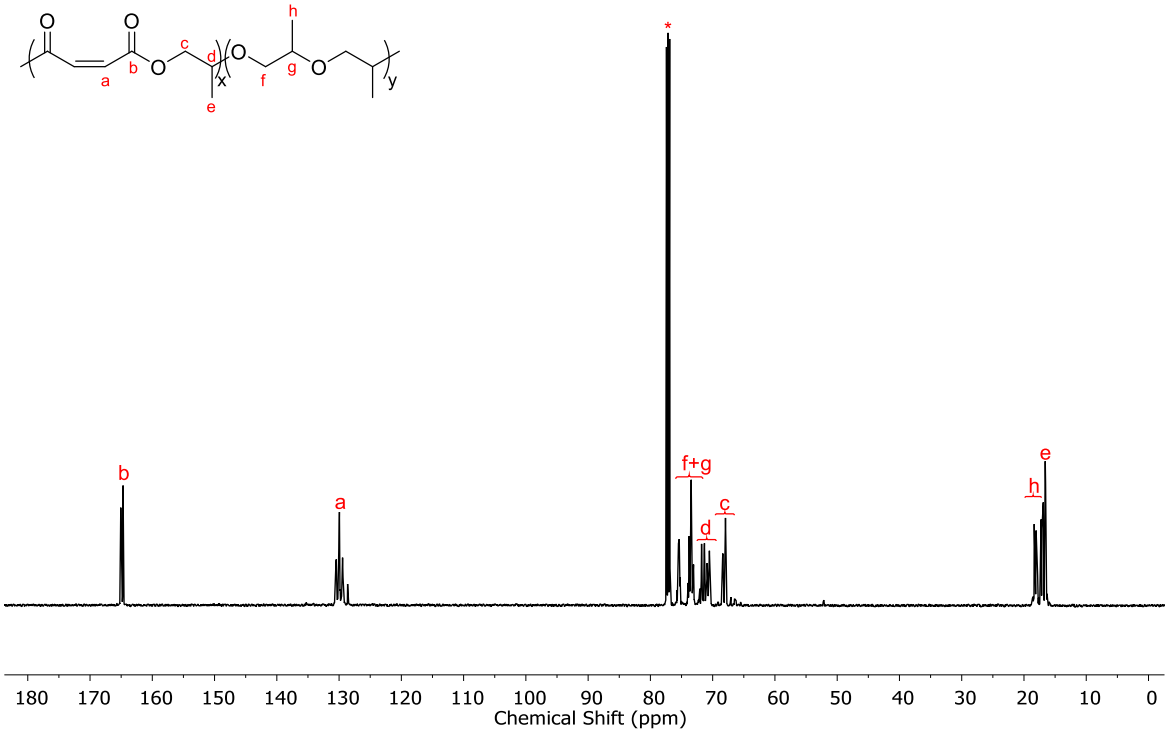



**Figure A3.2.** $^{13}C\{^{1}H\}$ NMR spectrum of $PEE_{MA}$ in $CDCl_3$.

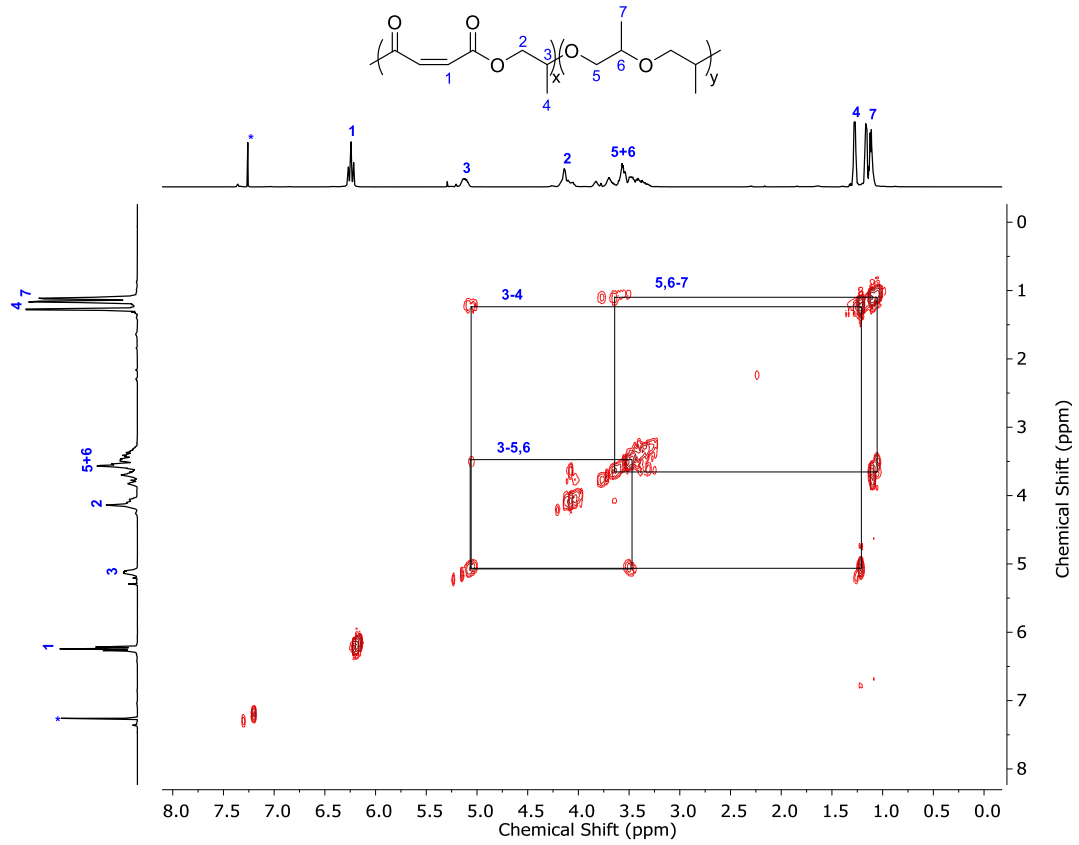



**Figure A3.3.** $^{1}$H-$^{1}$H COSY NMR spectrum of $PEE_{MA}$ in $CDCl_3$.

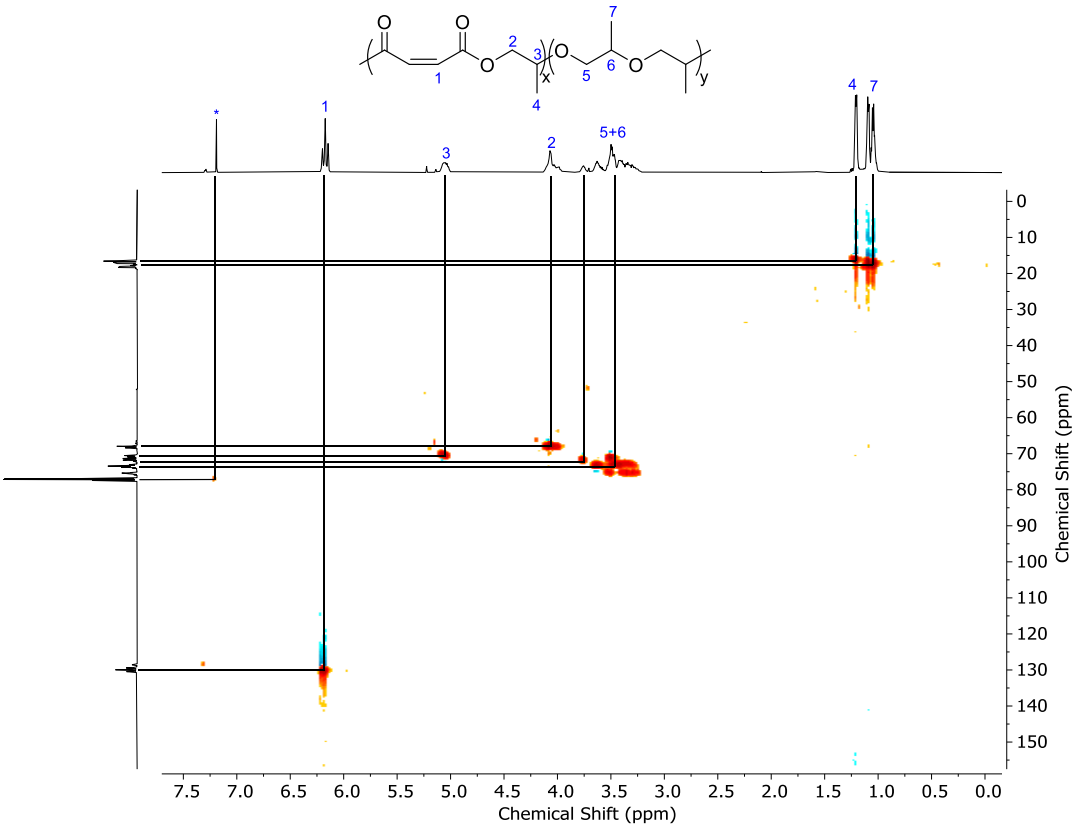



**Figure A3.4.** $^{1}$H-$^{13}$C HSQC NMR spectrum of $PEE_{MA}$ in $CDCl_3$.

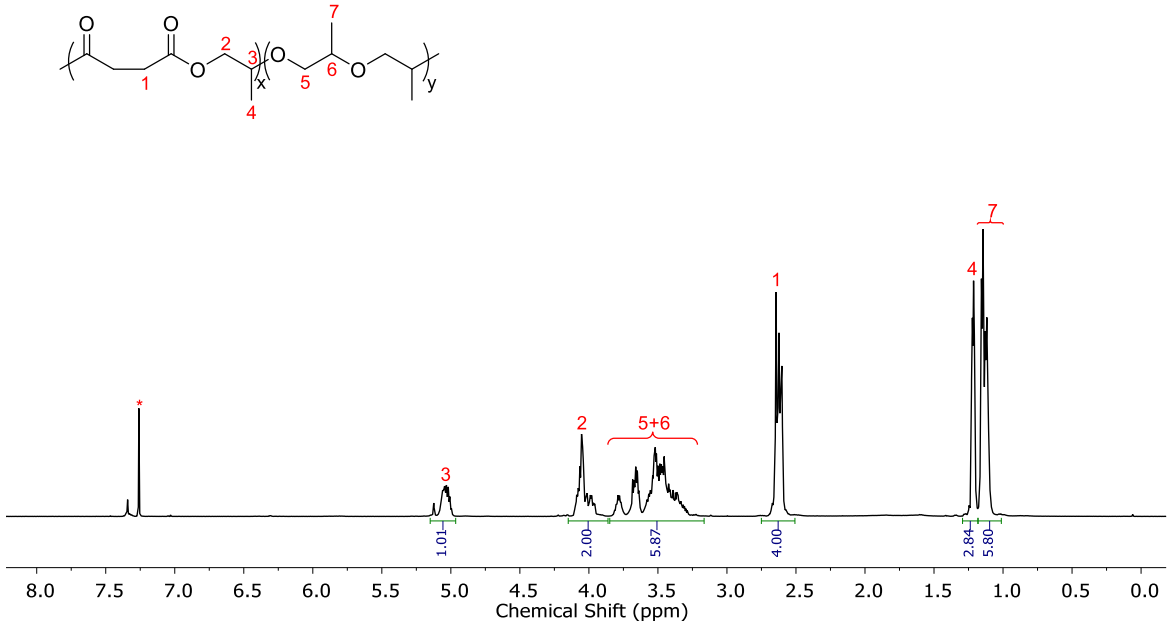



**Figure A3.5.** $^{1}H$ NMR spectrum of $PEE_{SA}$ in $CDCl_3$.

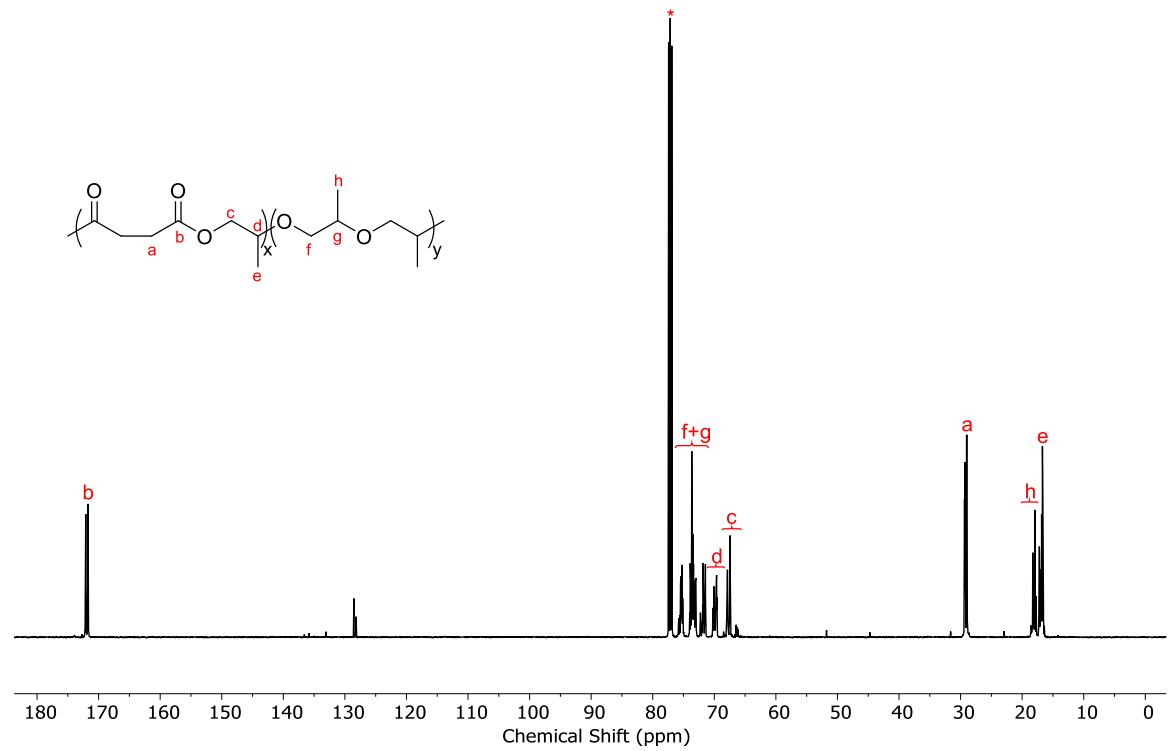



**Figure A3.6.** $^{13}C\{^{1}H\}$ NMR spectrum of $PEE_{SA}$ in $CDCl_3$.

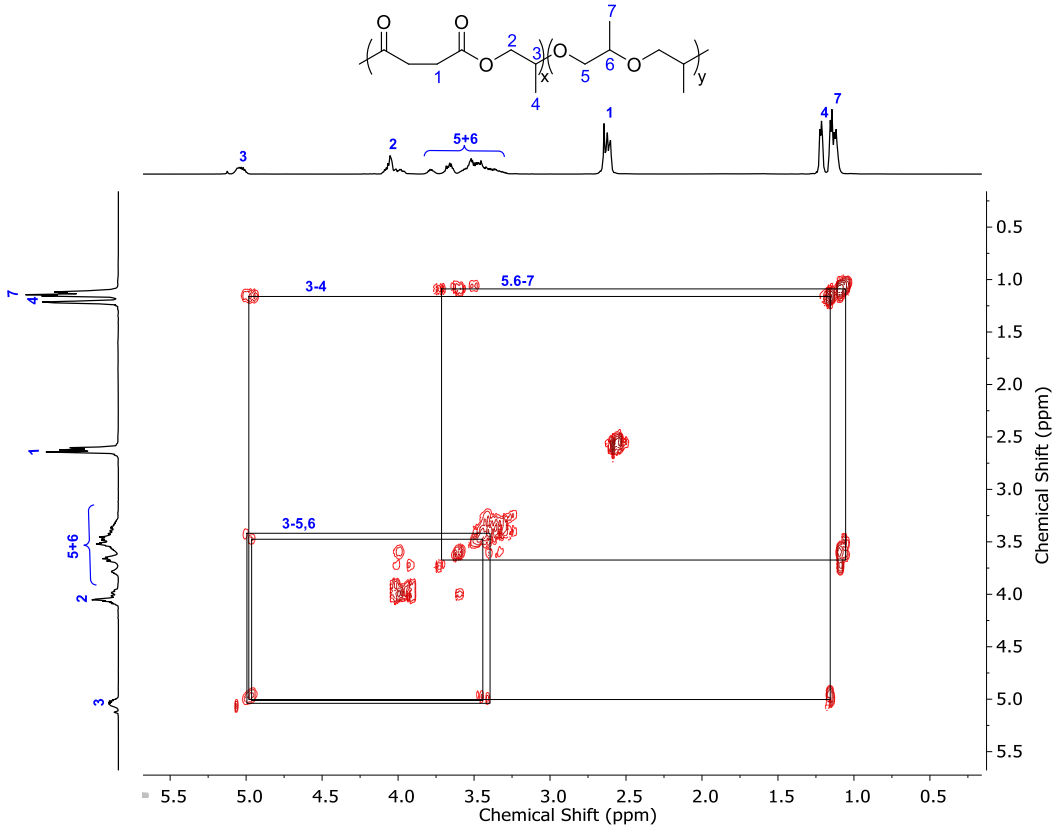



**Figure A3.7.** $^{1}H$-$^{1}H$ COSY NMR spectrum of $PEE_{SA}$ in $CDCl_3$.

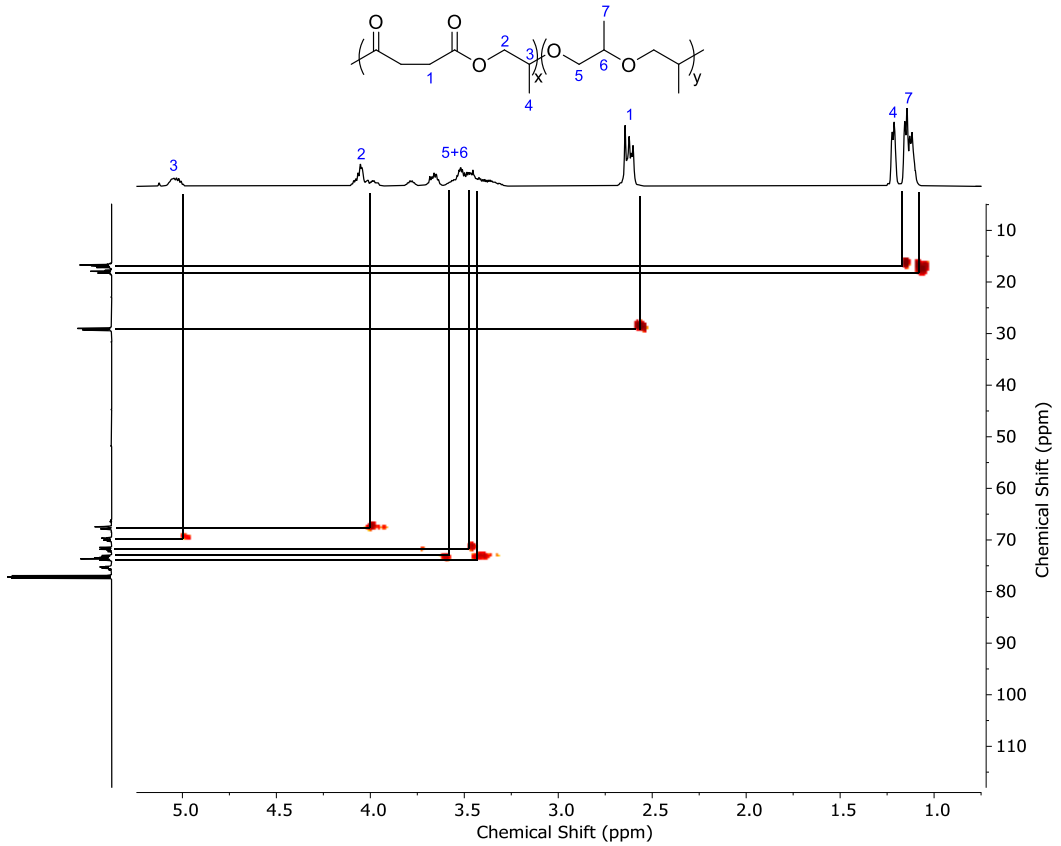



**Figure A3.8.** $^{1}H$-$^{13}C$ HSQC NMR spectrum of $PEE_{SA}$ in $CDCl_3$.

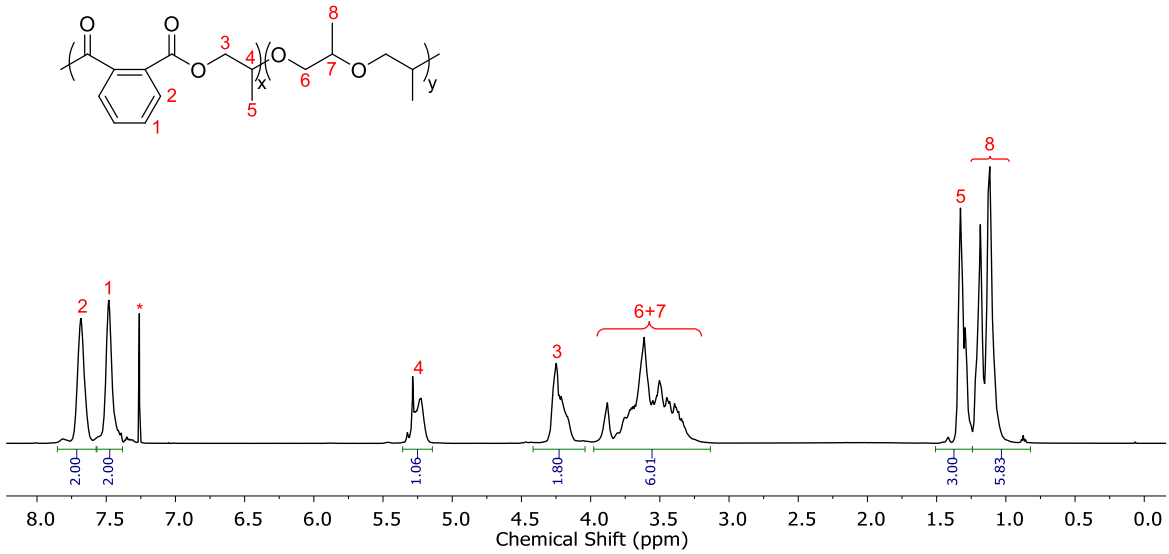



**Figure A3.9.** $^{1}H$ NMR spectrum of $PEE_{PA}$ in $CDCl_3$.

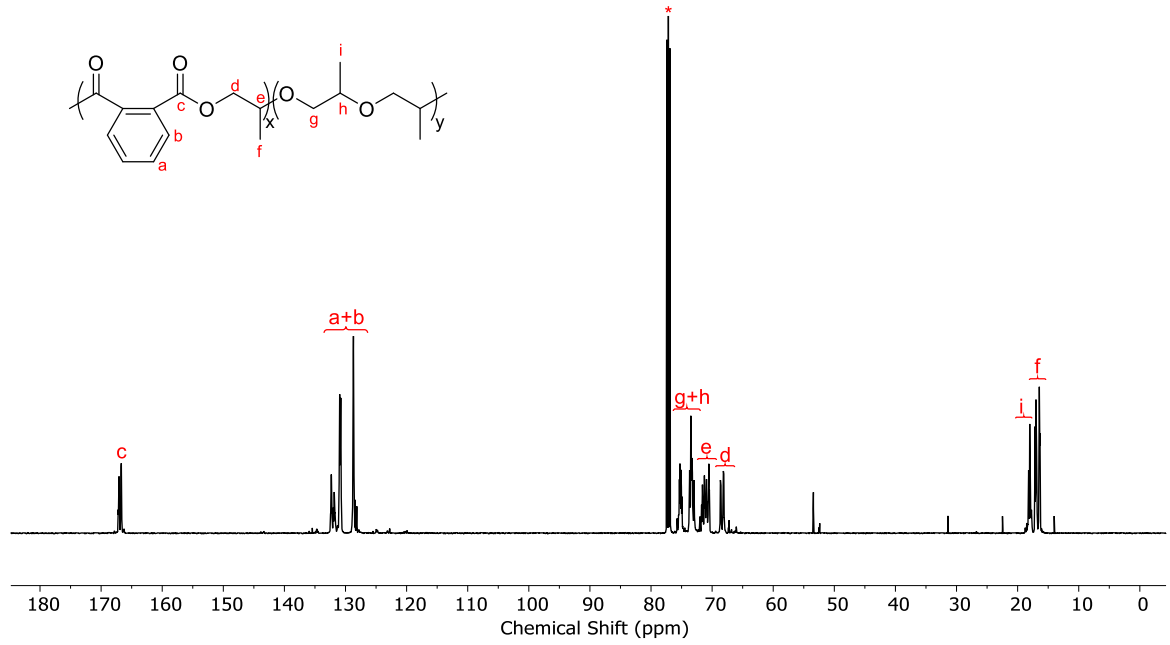



**Figure A3.10.** $^{13}C\{^{1}H\}$ NMR spectrum of $PEE_{PA}$ in $CDCl_3$.

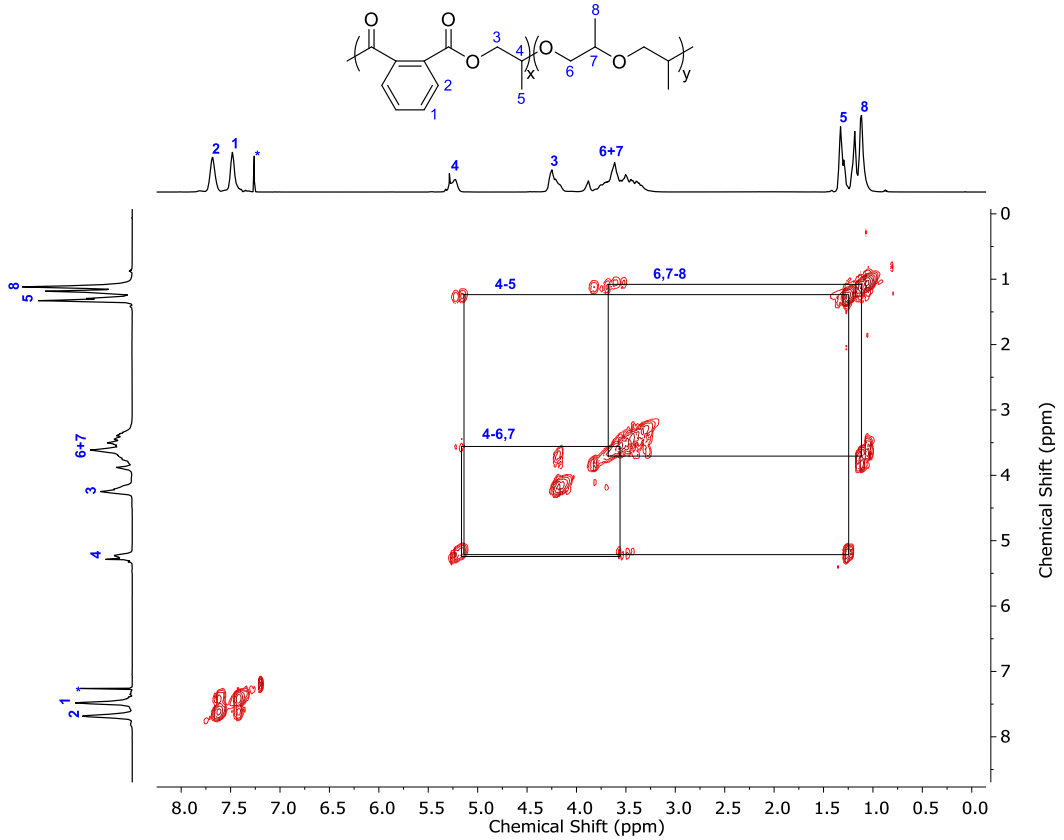



**Figure A3.11.** $^{1}H$-$^{1}H$ COSY NMR spectrum of $PEE_{PA}$ in $CDCl_3$.

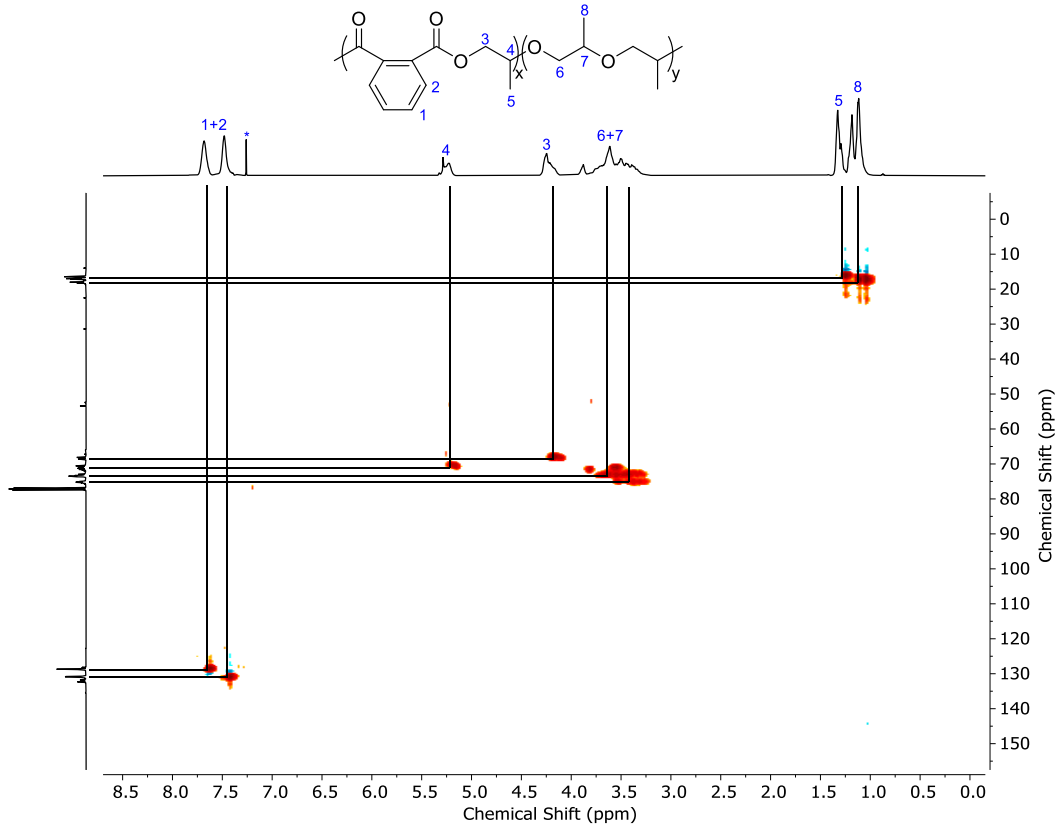



**Figure A3.12.** $^{1}H$-$^{13}C$ HSQC NMR spectrum of $PEE_{PA}$ in $CDCl_3$.

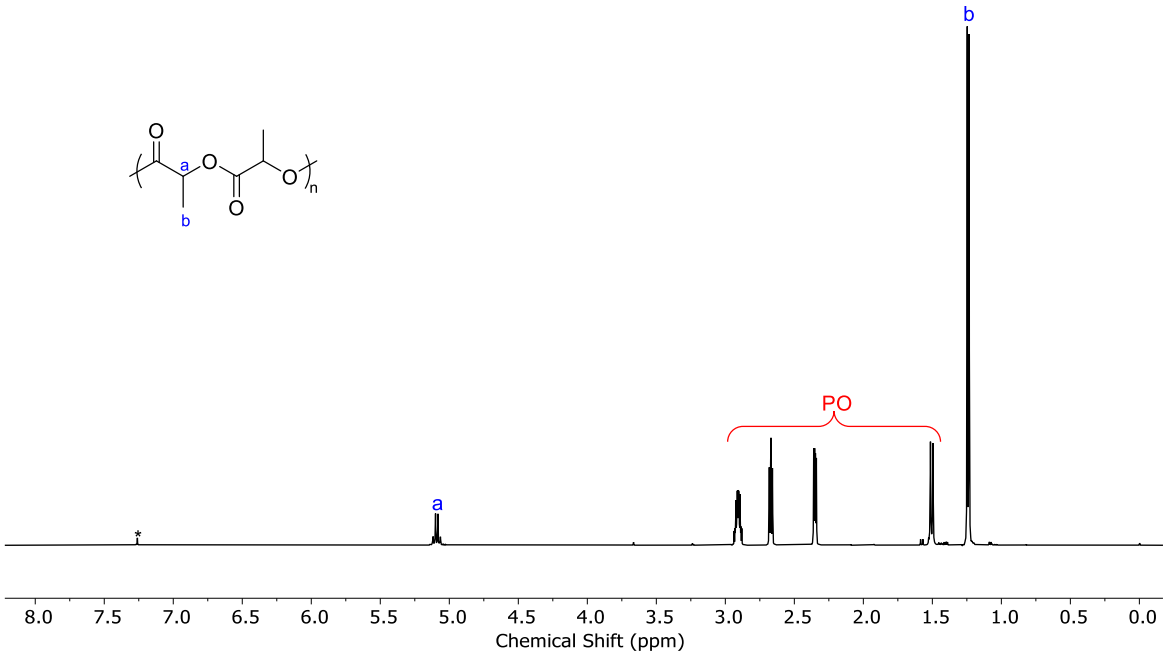



**Figure A3.13.** $^{1}$H NMR spectrum of crude PLLA in $CDCl_3$.

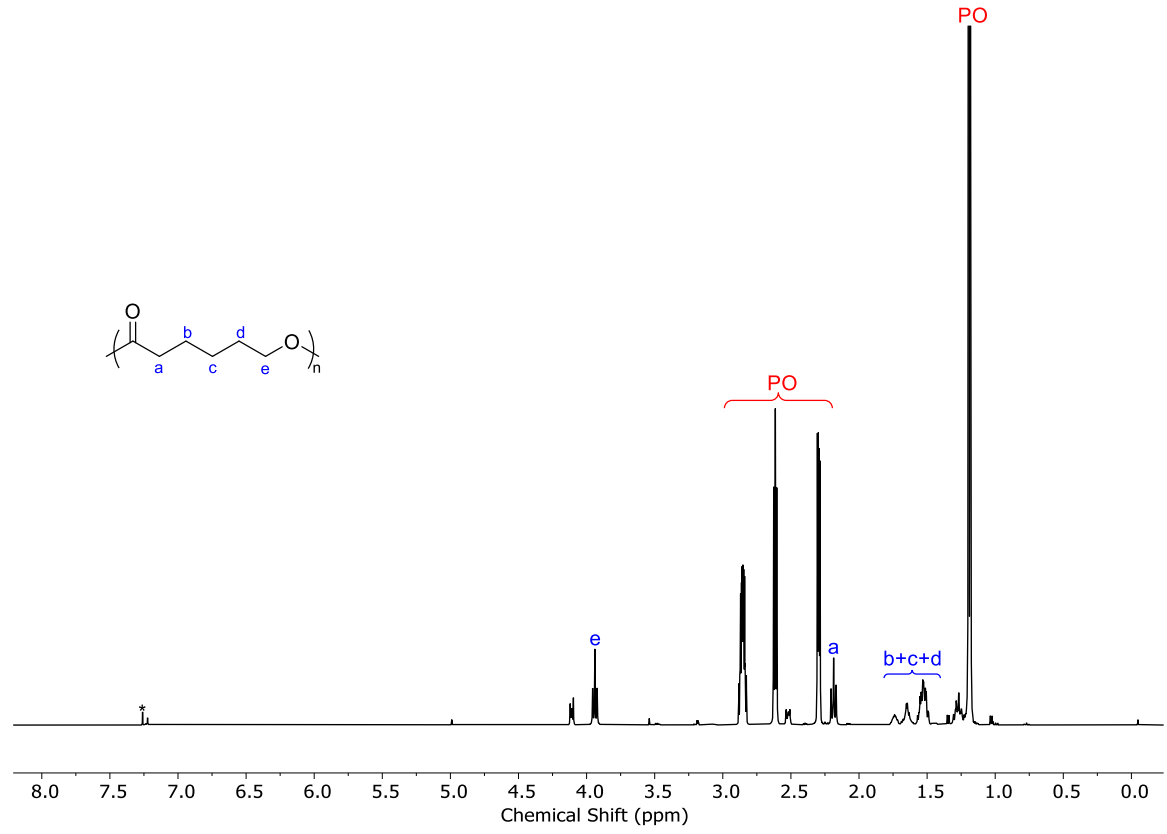



**Figure A3.14.** $^{1}$H NMR spectrum of crude PCL in $CDCl_3$.

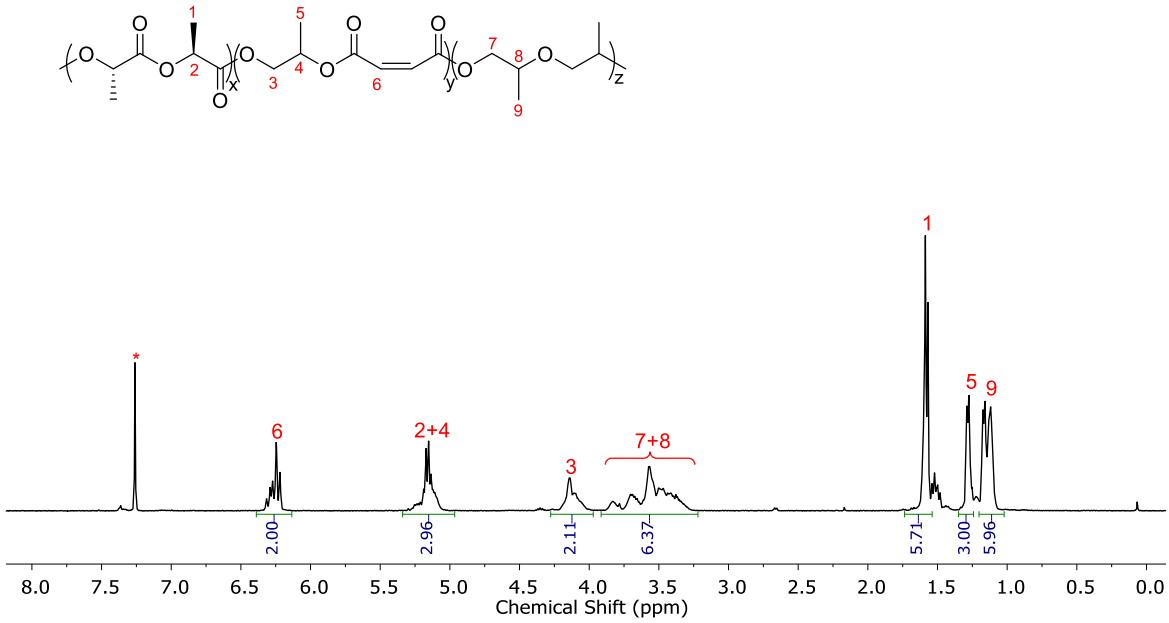



**Figure A3.15.** $^{1}$H NMR spectrum of **PLA1** in $CDCl_3$.

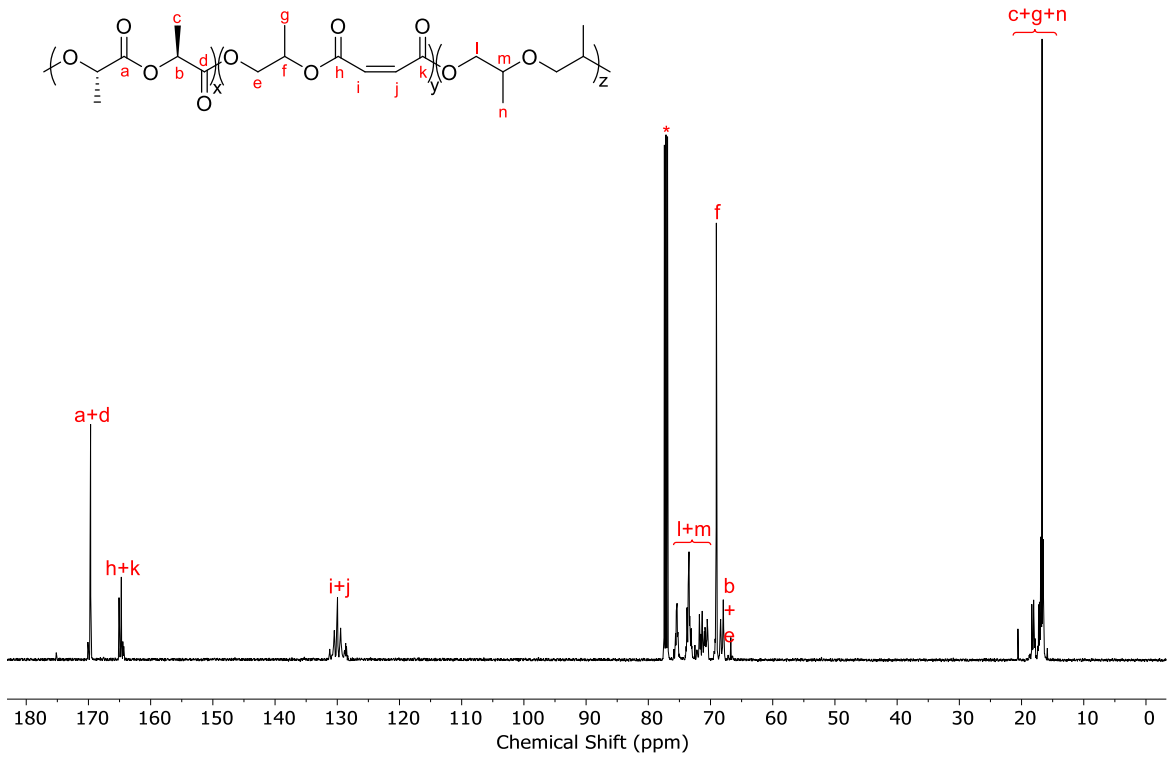



**Figure A3.16.** $^{13}$C{$^{1}$H} NMR spectrum of **PLA1** in $CDCl_3$.

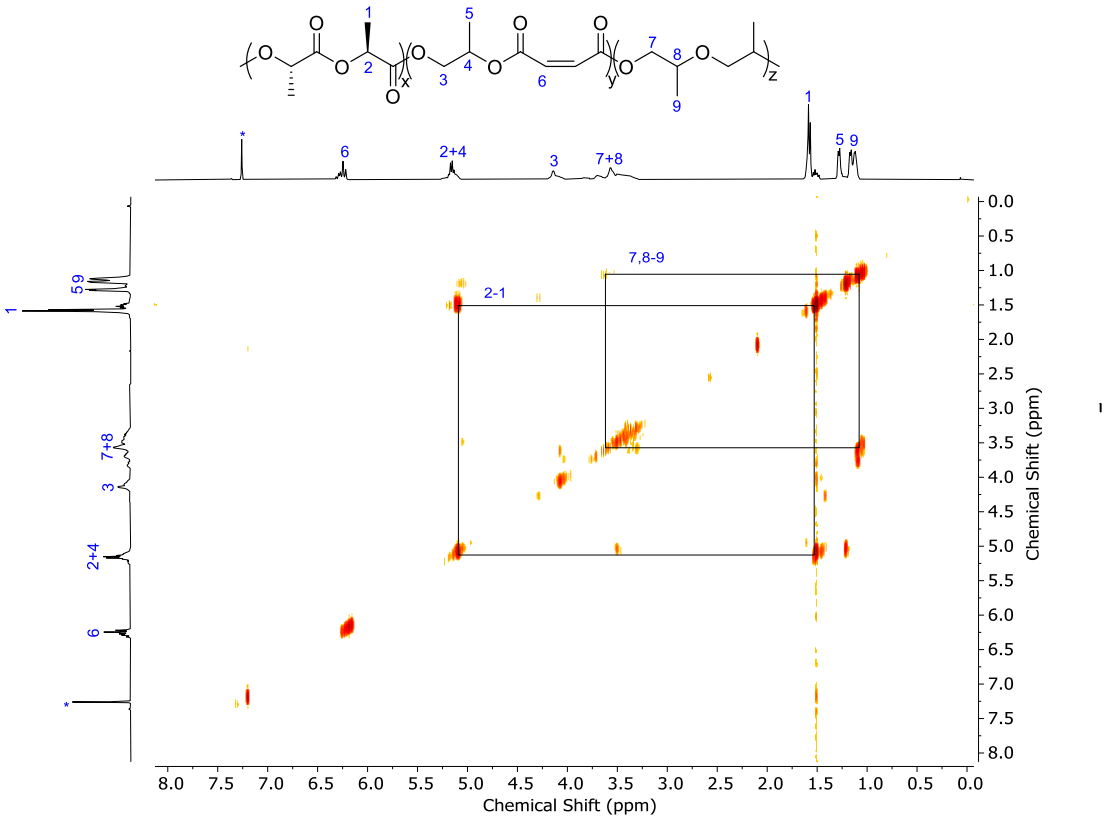



**Figure A3.17.** $^{1}$H-$^{1}$H COSY NMR spectrum of **P$_{LA}$1** in $CDCl_3$.

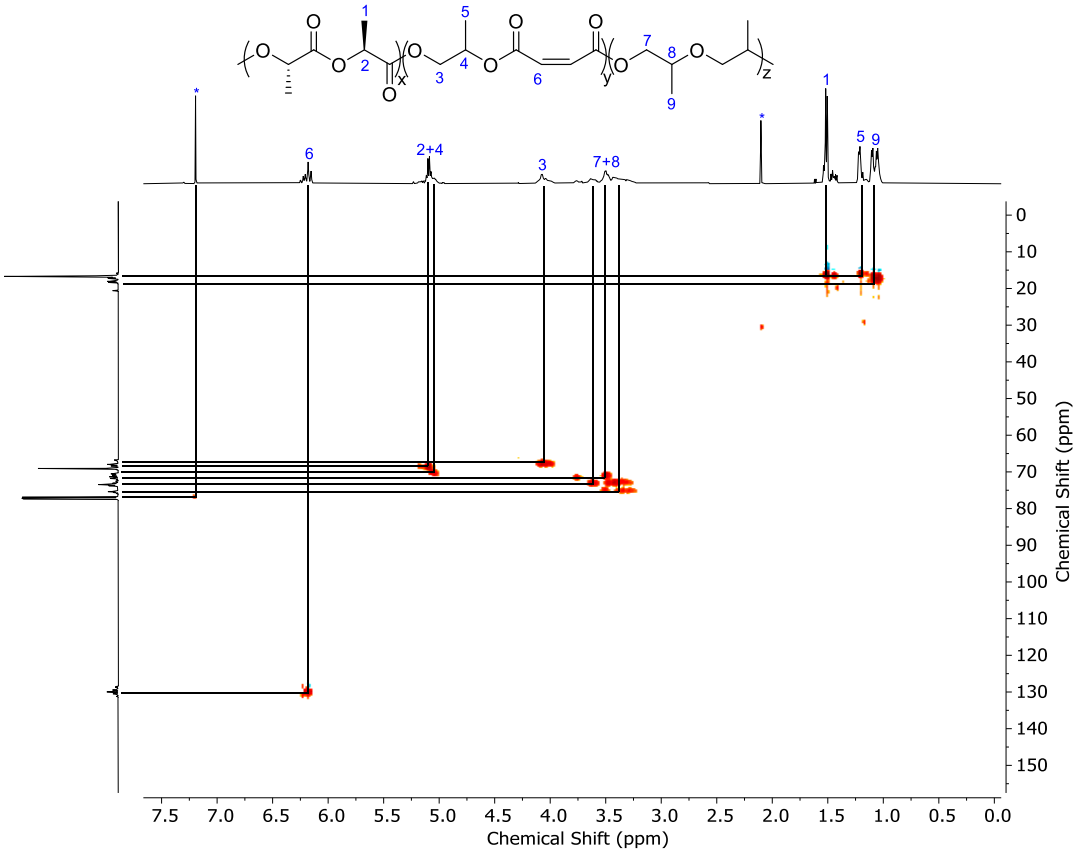



**Figure A3.18.** $^{1}$H-$^{13}$C HSQC NMR spectrum of **P$_{LA}$1** in $CDCl_3$.

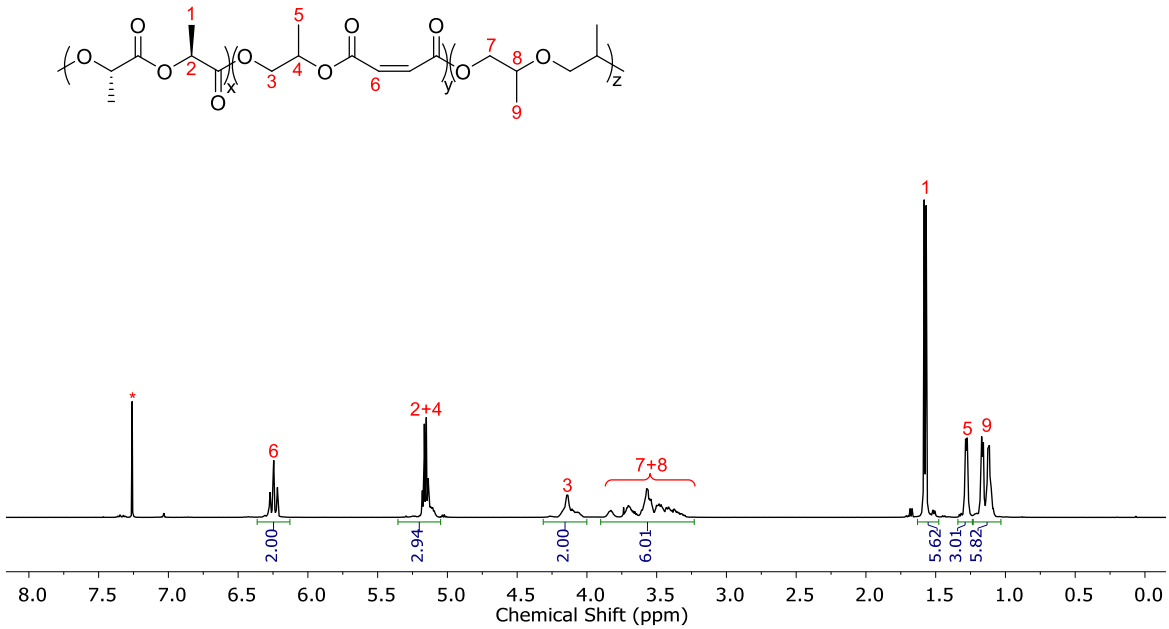



**Figure A3.19.** $^{1}$H NMR spectrum of PEE$_{MA}$-*b*-PLLA in $CDCl_3$.

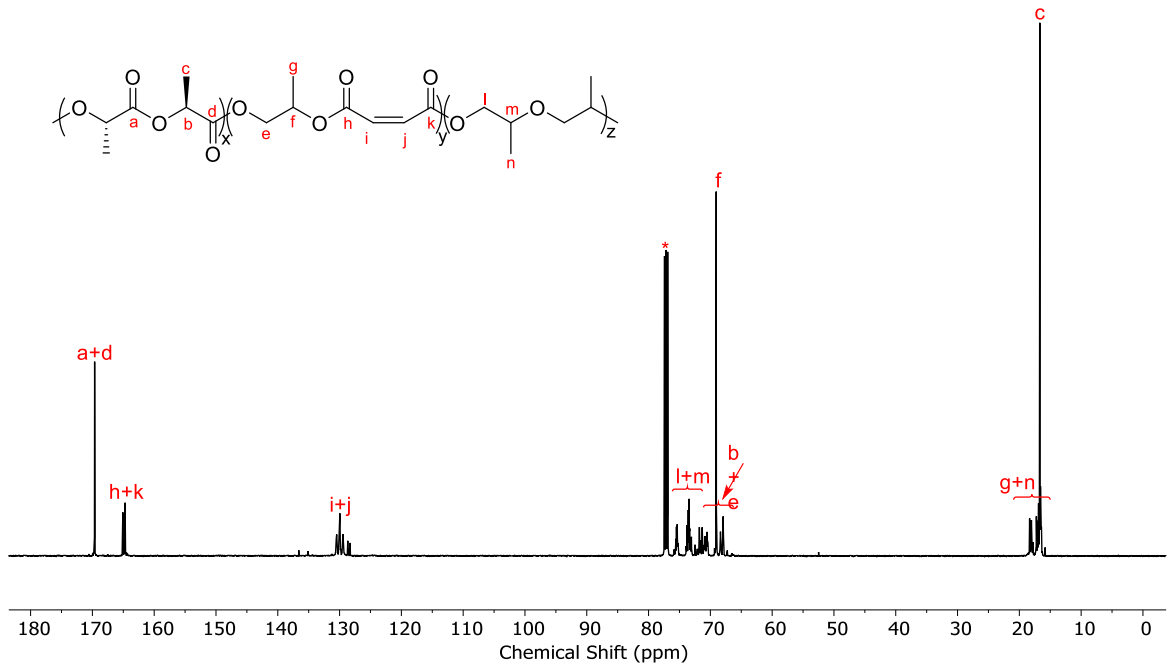



**Figure A3.20.** $^{13}$C{$^{1}$H} NMR spectrum of EE$_{MA}$-*b*-PLLA in $CDCl_3$.

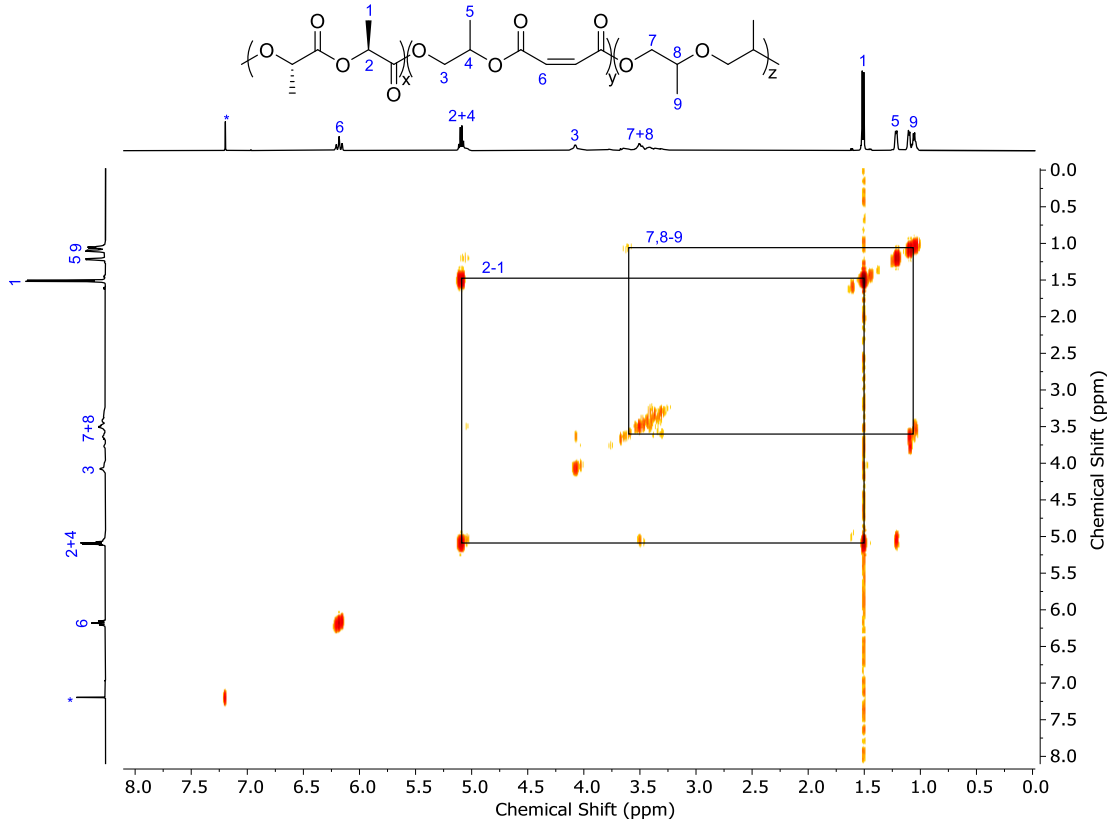



**Figure A3.21.** $^{1}H$-$^{1}H$ COSY NMR spectrum of $PEE_{MA}$-*b*-PLLA in $CDCl_3$.

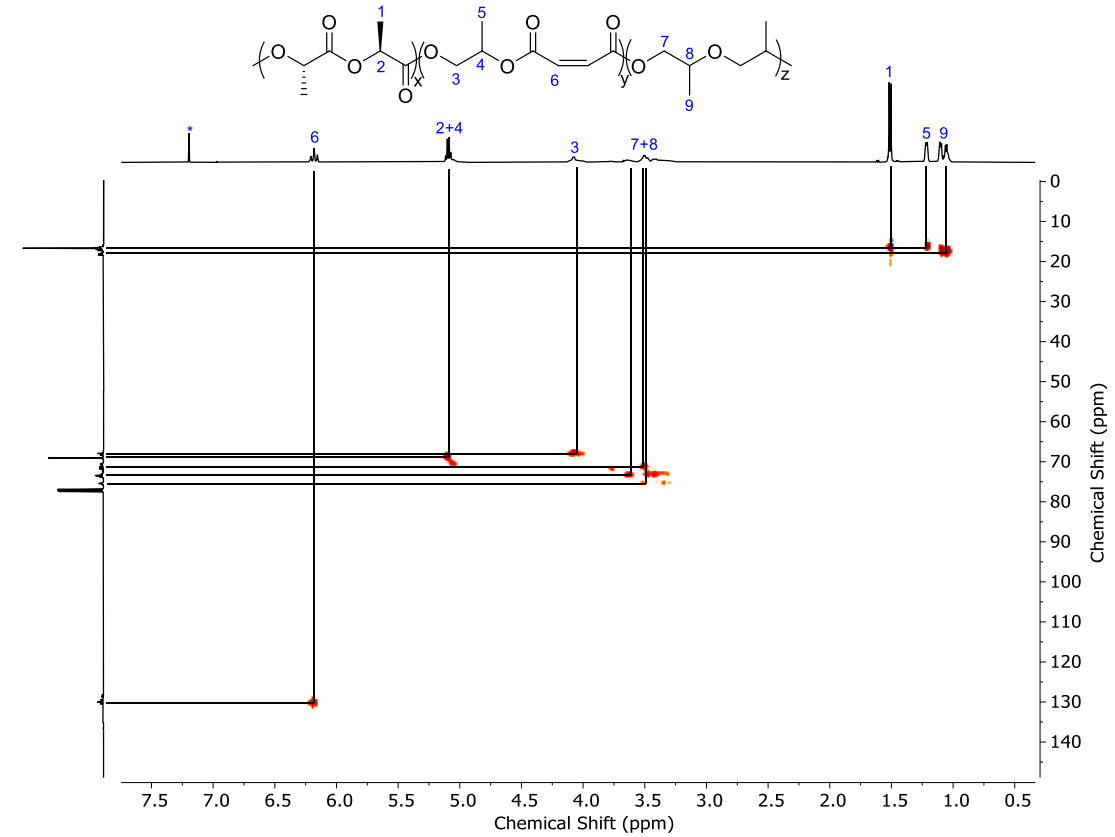



**Figure A3.22.** $^{1}H$-$^{13}C$ HSQC NMR spectrum of $PEE_{MA}$-*b*-PLLA in $CDCl_3$.

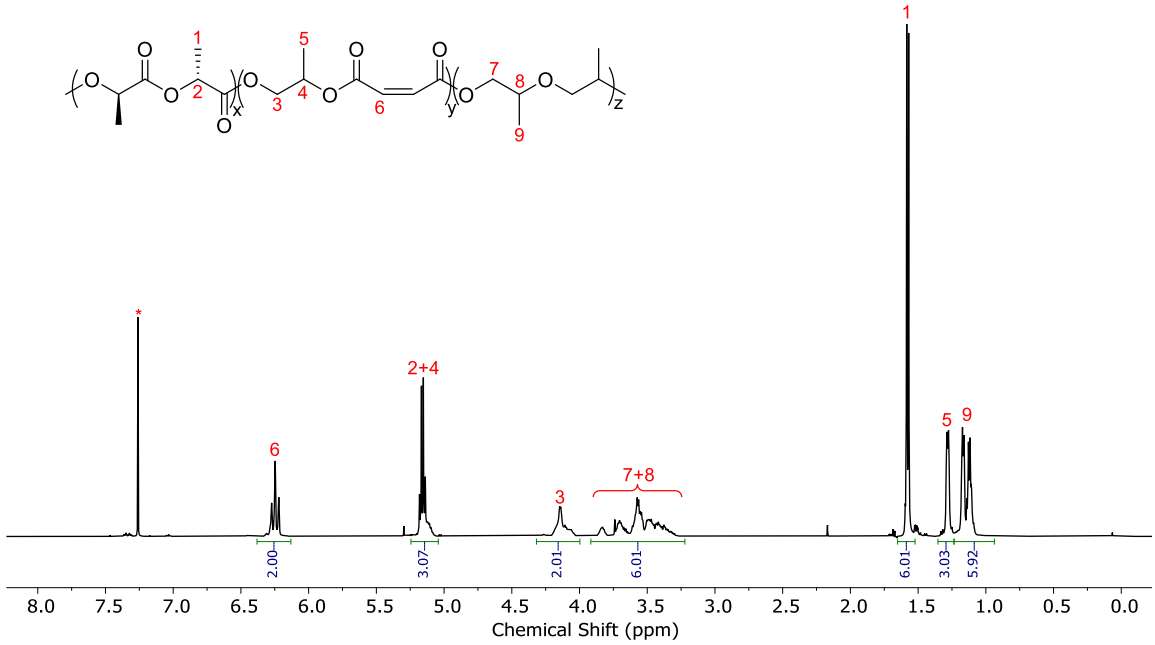



**Figure A3.23.** $^{1}$H NMR spectrum of PEE$_{MA}$-*b*-PDLA in $CDCl_3$.

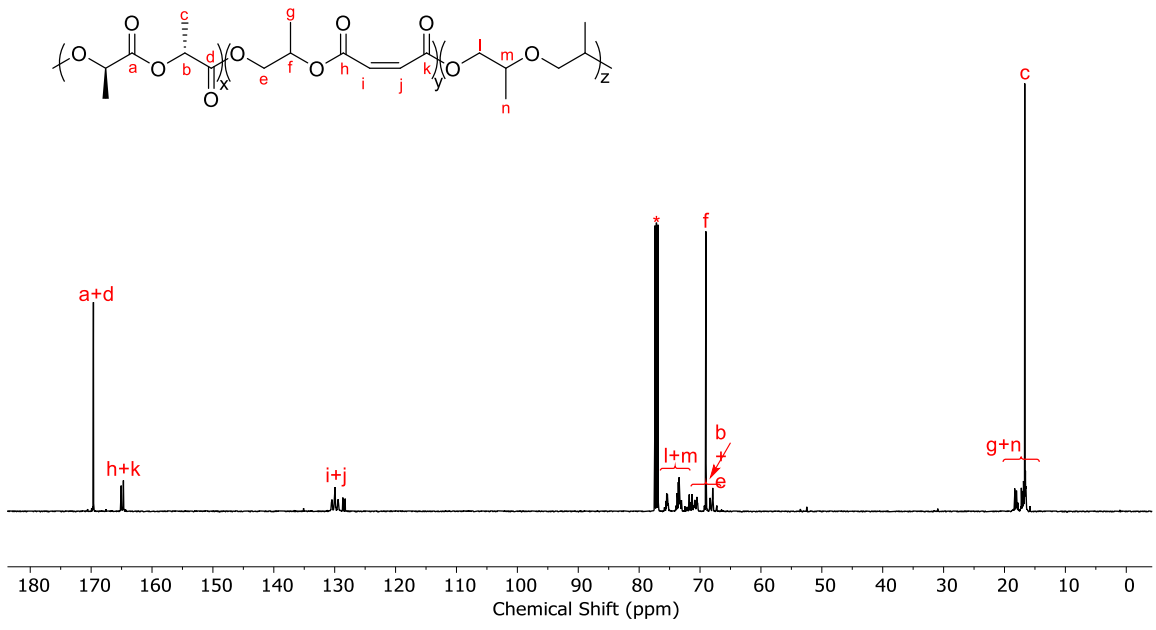



**Figure A3.24.** $^{13}$C{$^{1}$H} NMR spectrum of EE$_{MA}$-*b*-PDLA in $CDCl_3$.

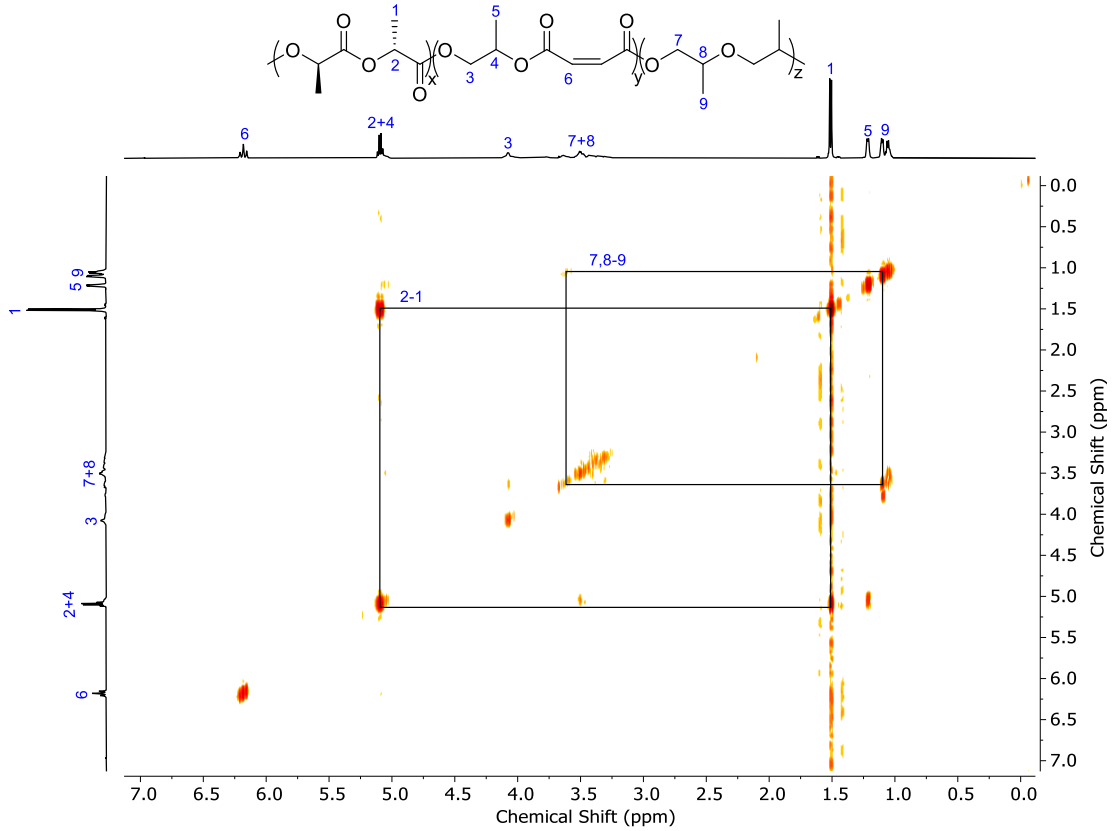



**Figure A3.25.** $^{1}H$-$^{1}H$ COSY NMR spectrum of $PEE_{MA}$-*b*-PDLA in $CDCl_3$.

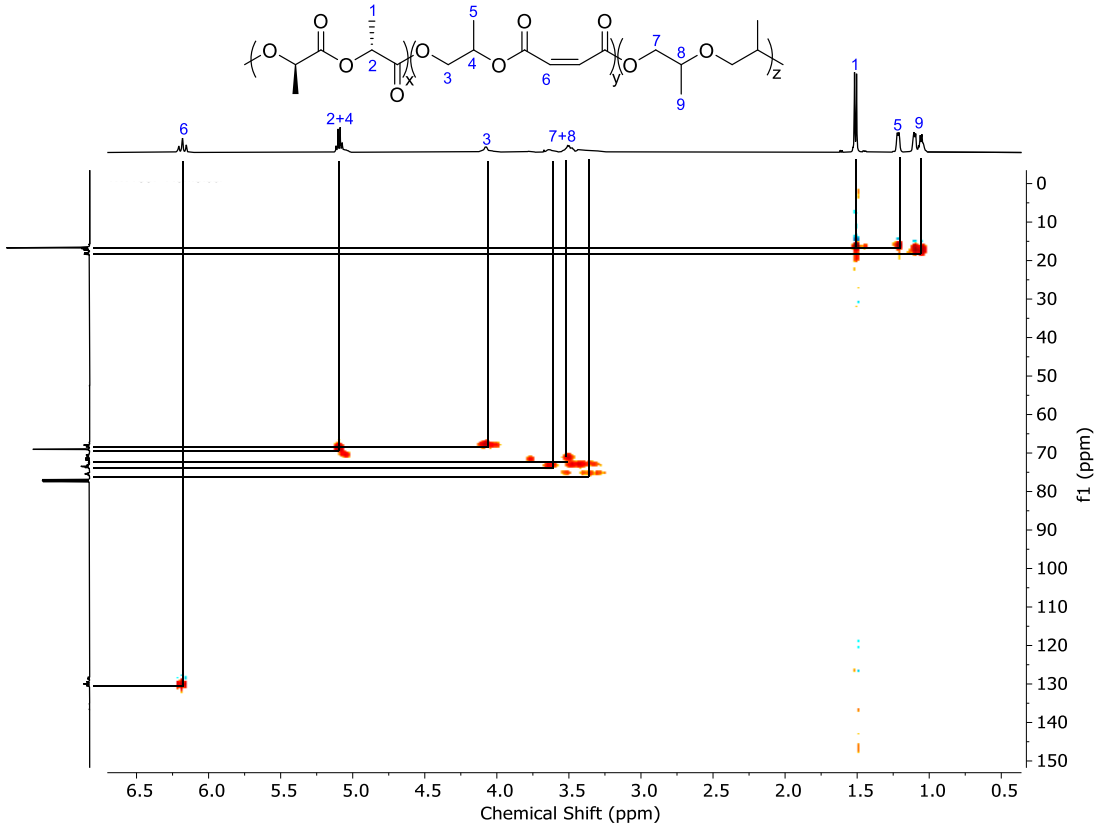



**Figure A3.26.** $^{1}H$-$^{13}C$ HSQC NMR spectrum of $PEE_{MA}$-*b*-PDLA in $CDCl_3$.

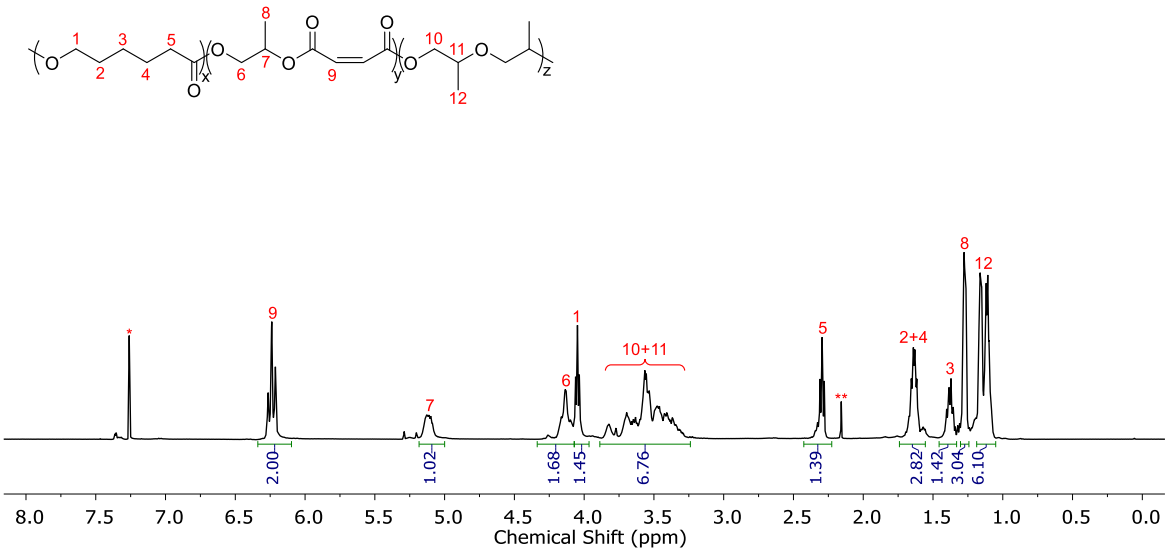



**Figure A3.27.** $^{1}$H NMR spectrum of **$P_{CL}$1** in $CDCl_3$.

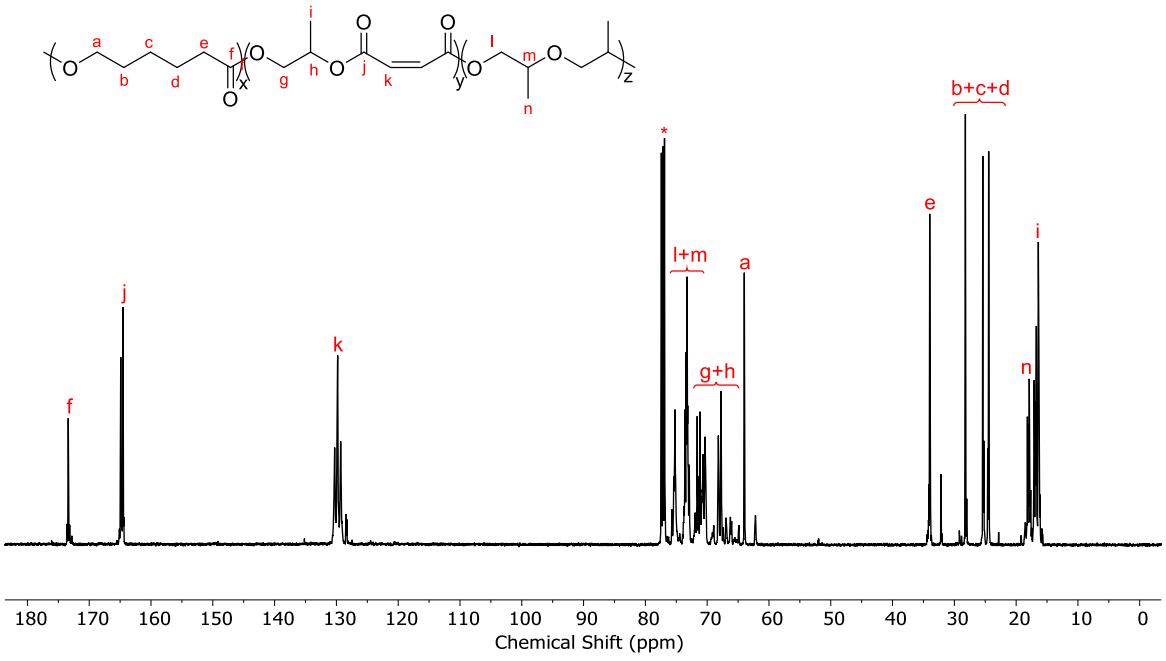



**Figure A3.28.** $^{13}C\{^{1}H\}$ NMR spectrum of **$P_{CL}$1** in $CDCl_3$.

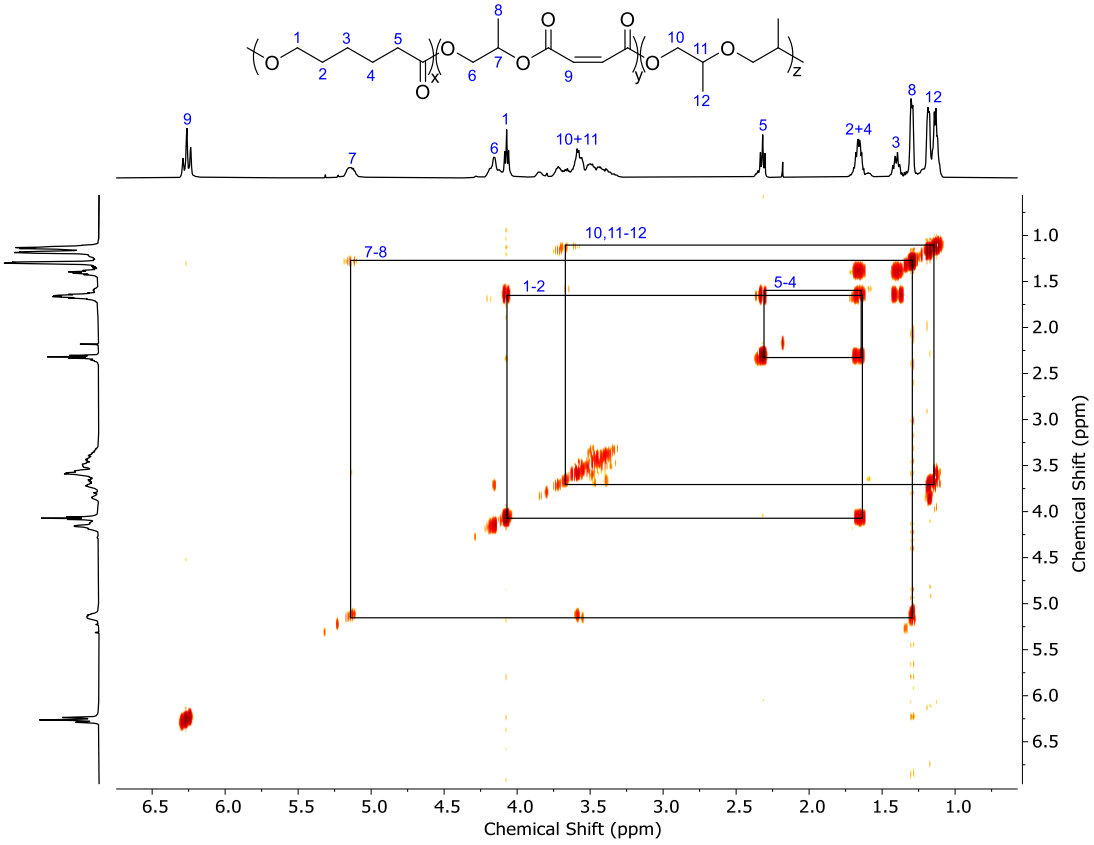



**Figure A3.29.** $^{1}$H-$^{1}$H COSY NMR spectrum of **$P_{CL}$1** in $CDCl_3$.

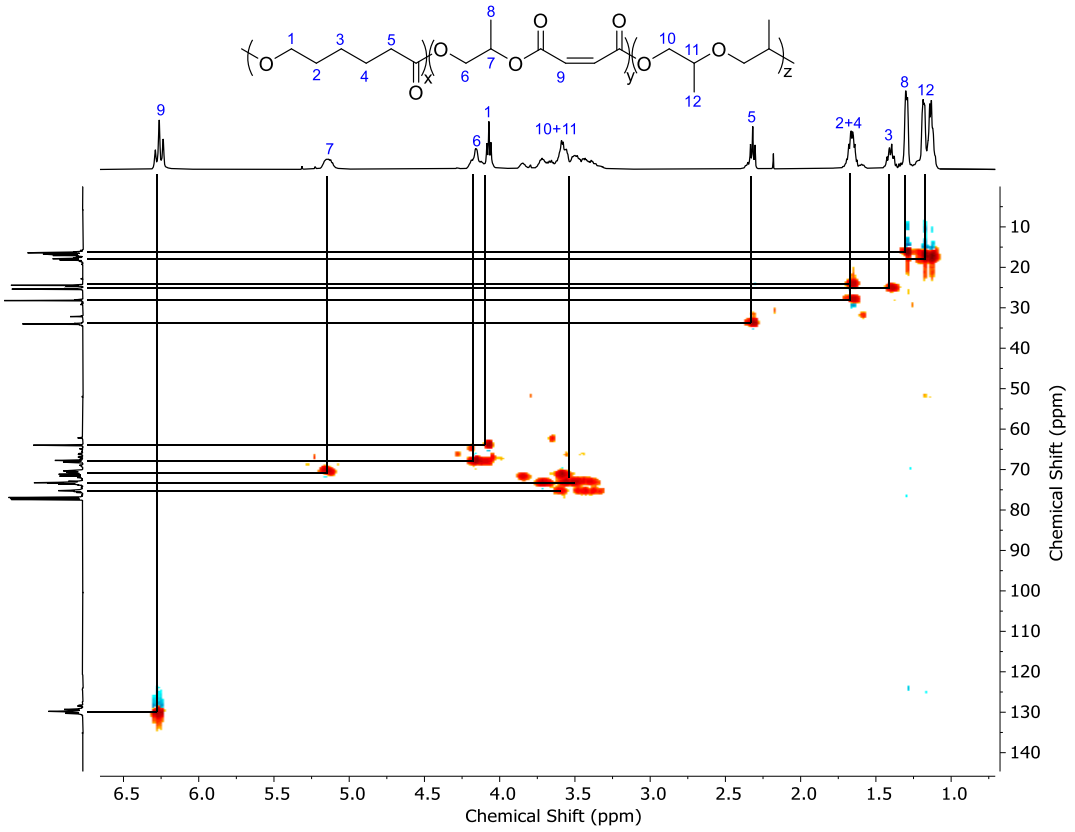



**Figure A3.30.** $^{1}$H-$^{13}$C HSQC NMR spectrum of **$P_{CL}$1** in $CDCl_3$.

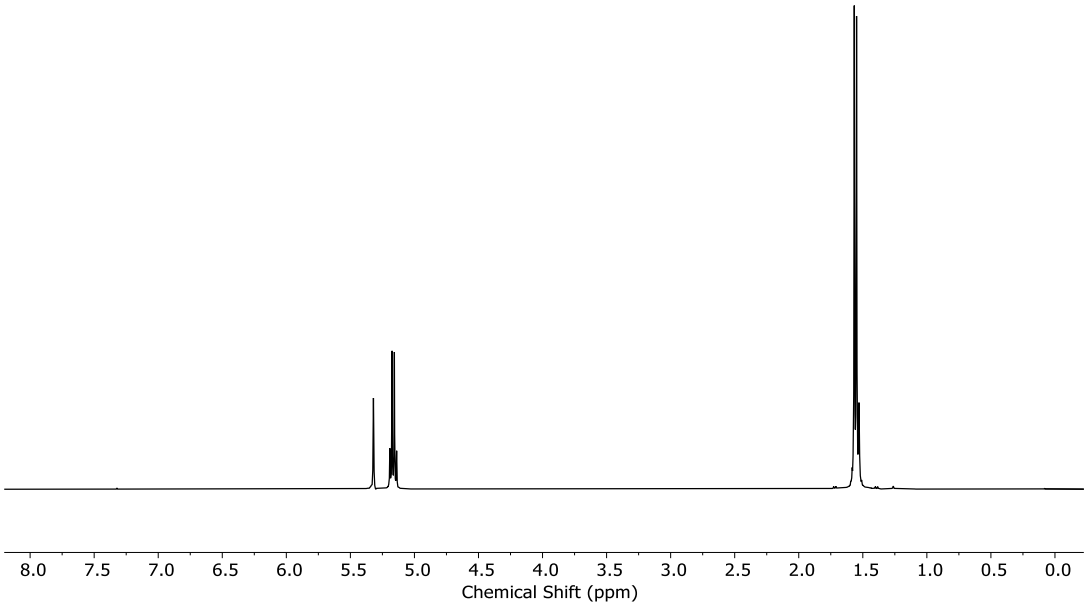



**Figure A3.31.** $^{1}$H NMR spectrum of neat PLLA sample in $CD_2Cl_2$.

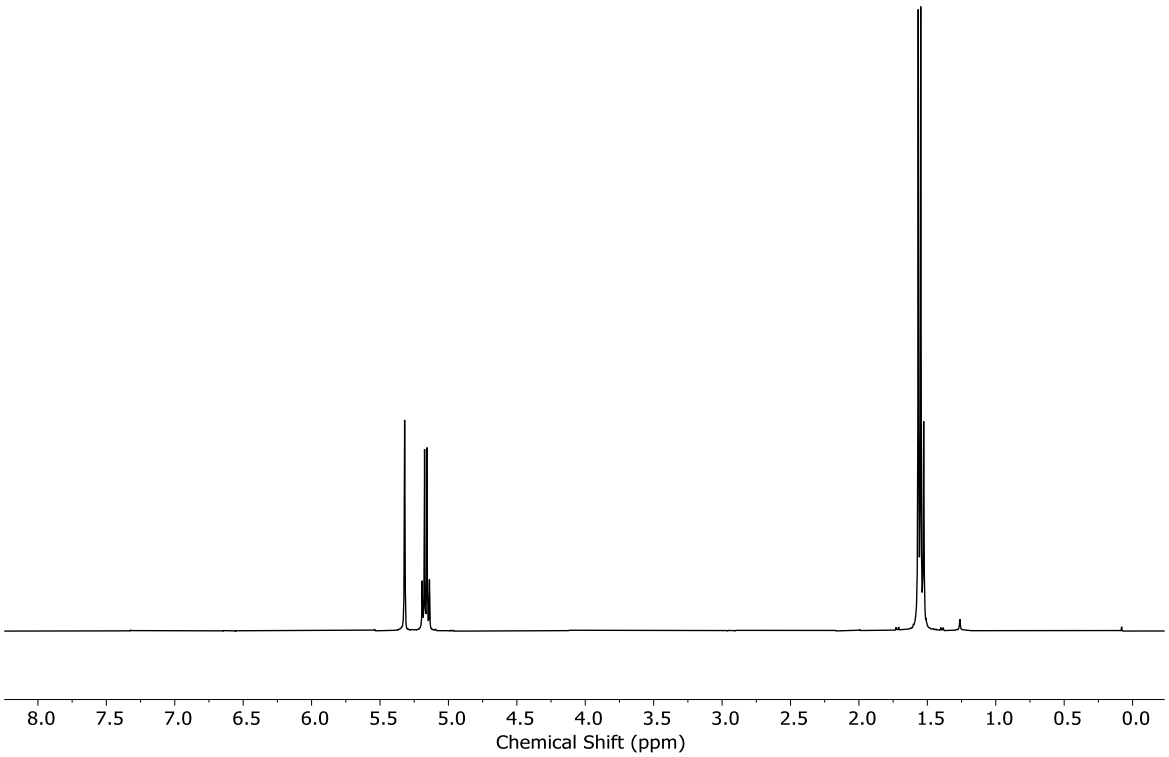



**Figure A3.32.** $^{1}$H NMR spectrum of PLLA sample + 2 wt. % of $\mathbf{P_{LA}1}$ in $CD_2Cl_2$.

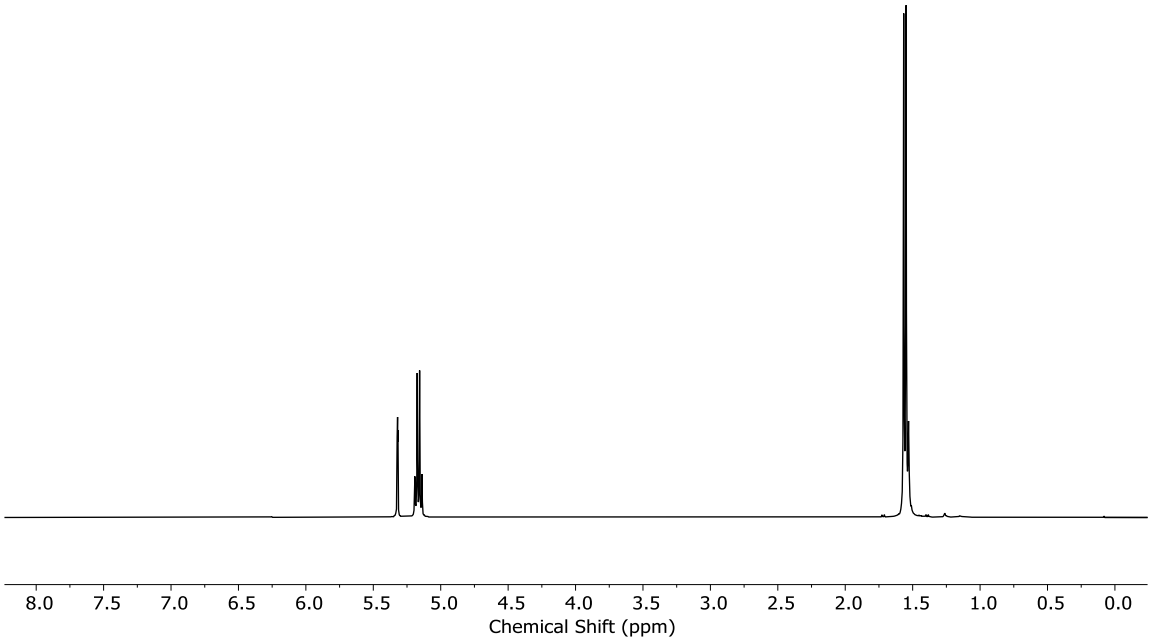



**Figure A3.33.** $^{1}$H NMR spectrum of PLLA sample + 5 wt. % of $\mathbf{P_{LA}1}$ in $CD_2Cl_2$.

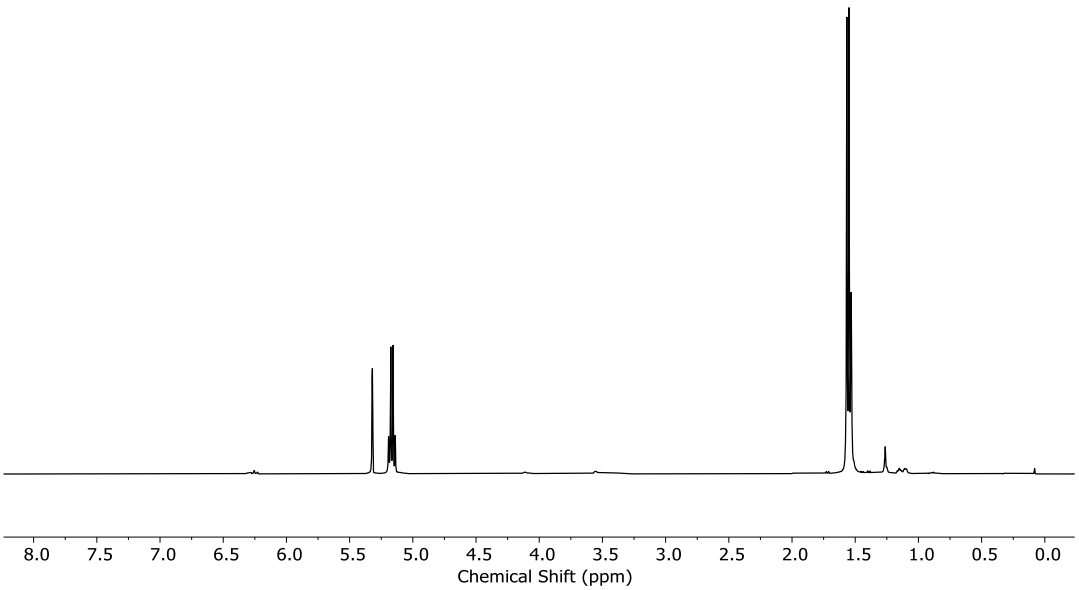



**Figure A3.34.** $^{1}$H NMR spectrum of PLLA sample + 10 wt. % of $\mathbf{P_{LA}1}$ in $CD_2Cl_2$.

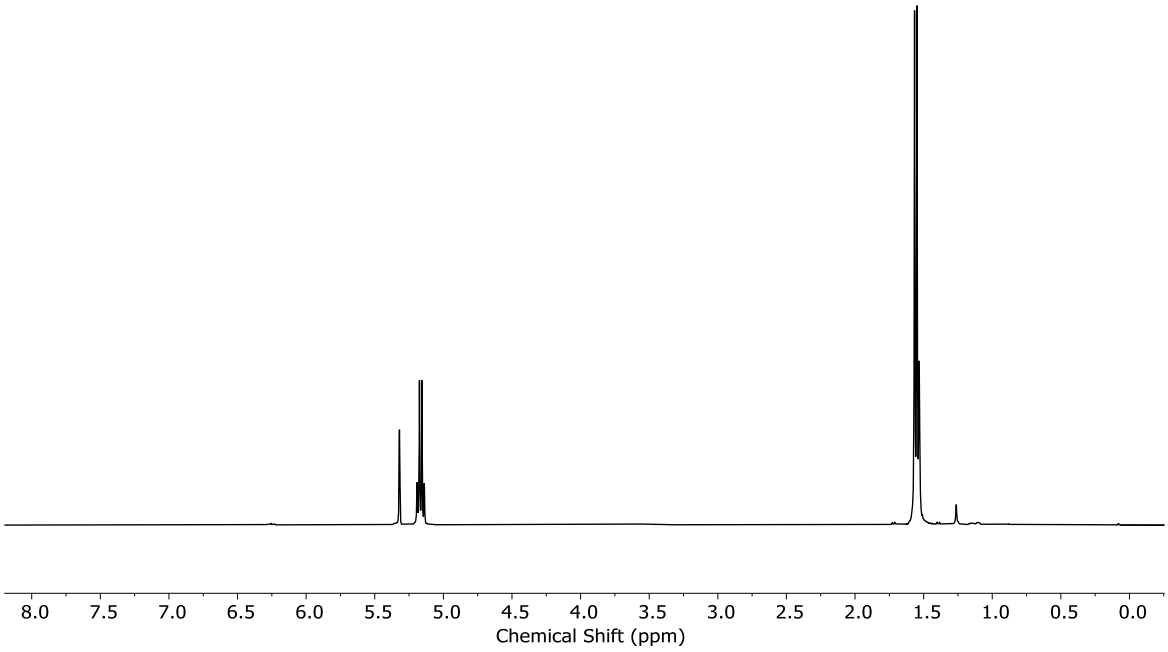



**Figure A3.35.** $^{1}$H NMR spectrum of PLLA sample + 20 wt. % of **PLA1** in $CD_2Cl_2$.

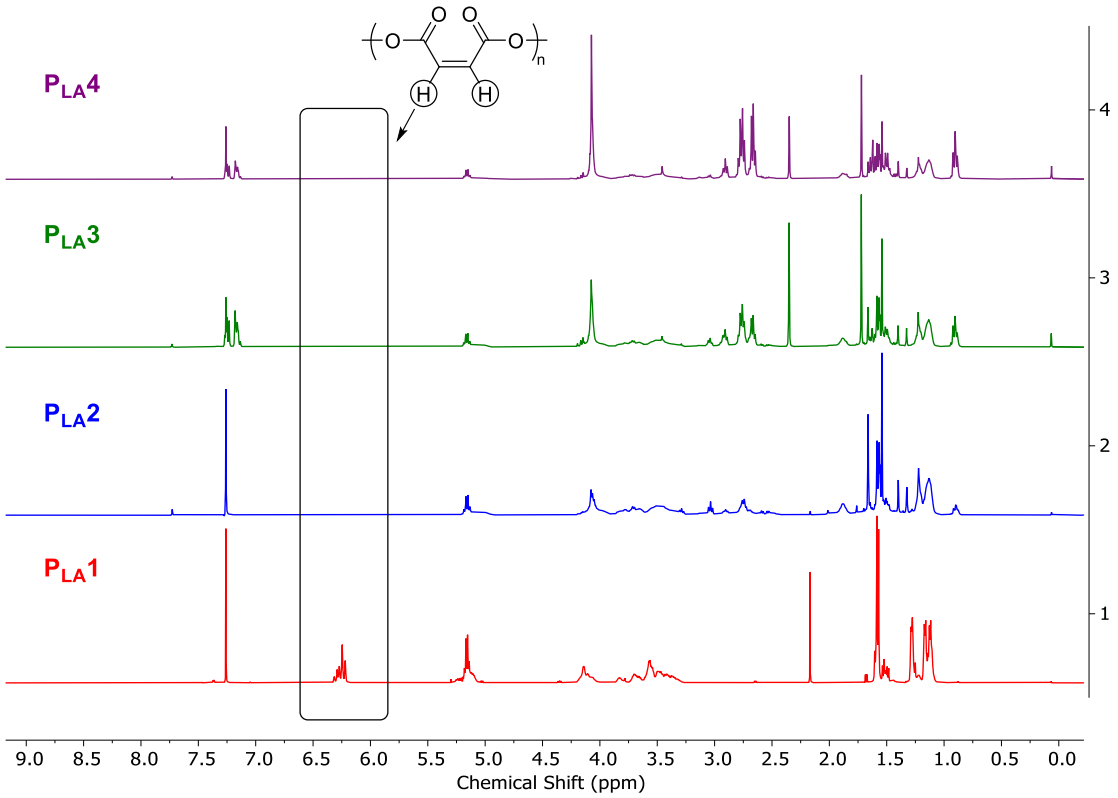



**Figure A3.36.** Stacked $^{1}$H NMR spectra of **PLA1** (red), **PLA2** (blue), **PLA3** (green), **PLA4** (violet) in $CDCl_3$.

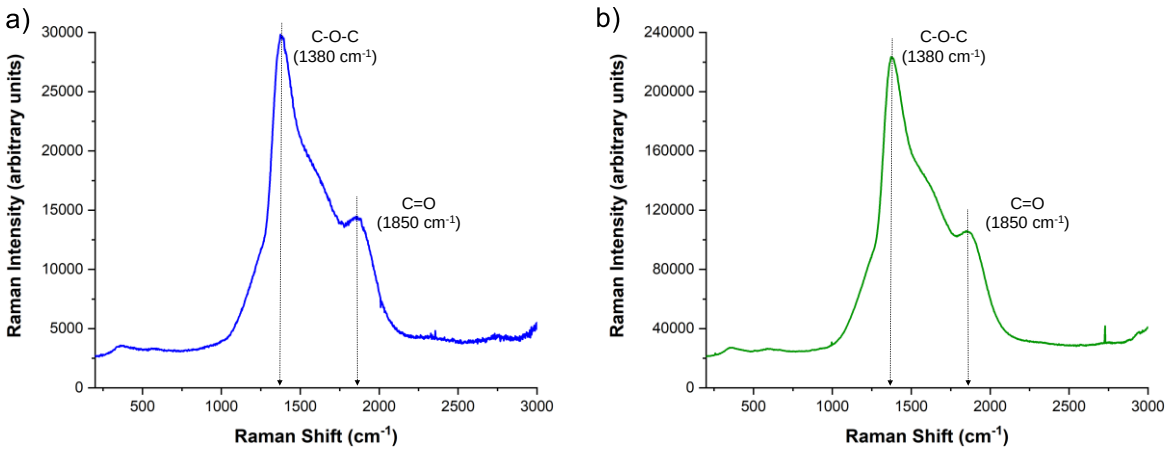



**Figure A3.37.** Raman spectra of of a) **PLA2** (blue) and **PLA3** (green).

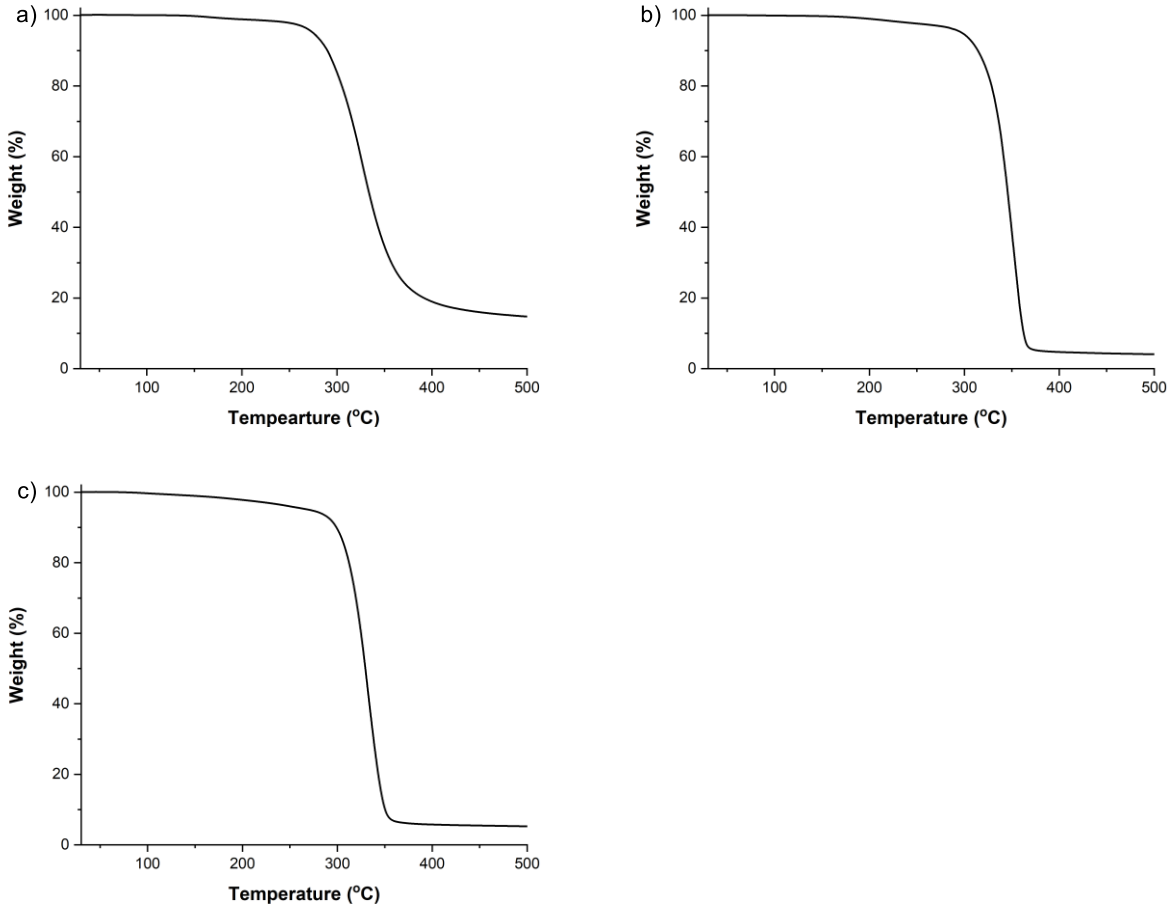



**Figure A3.38.** TGA thermograms of a) $PEE_{MA}$, b) $PEE_{SA}$, and c) $PEE_{PA}$.

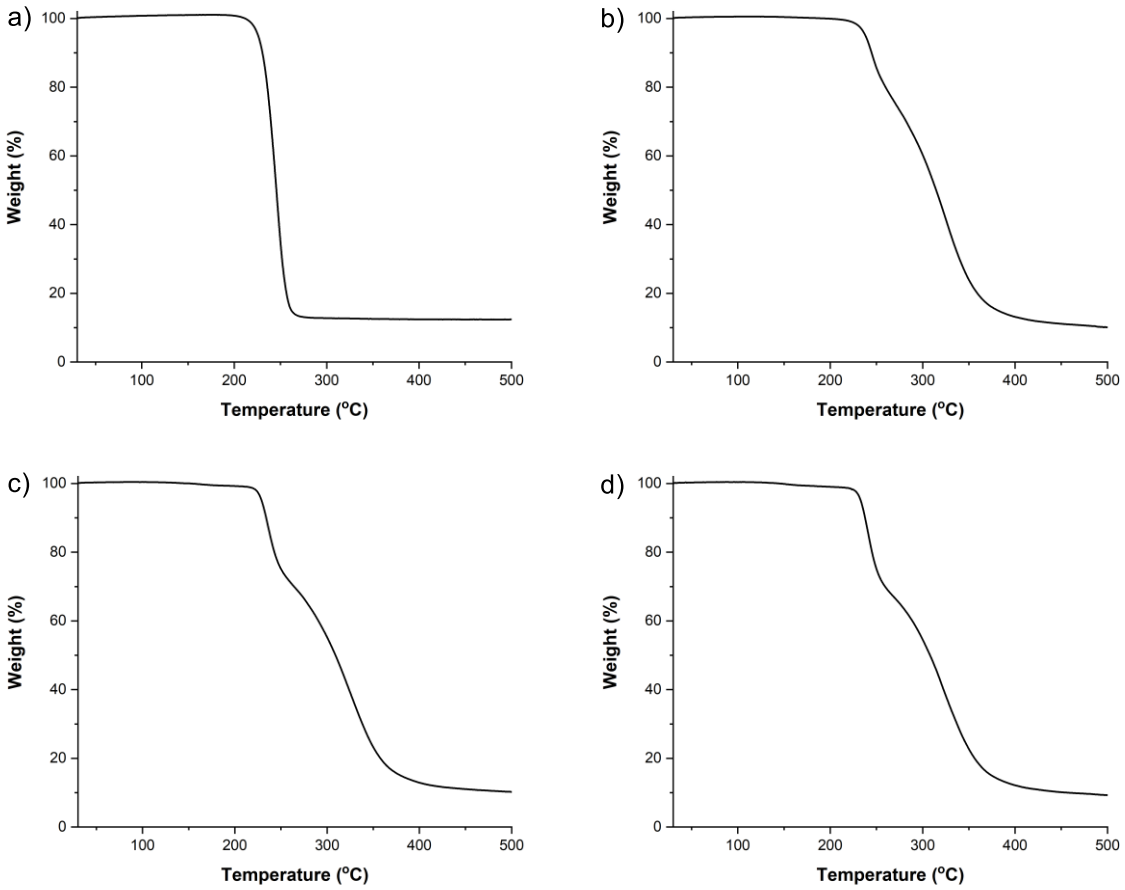



**Figure A3.39.** TGA thermograms of a) PLLA, b) $\mathbf{P_{LA}1}$, c) $PEE_{MA}$-*b*-PLLA, and d) in $PEE_{MA}$-*b*-$PLA_{stereocomplex}$ $CDCl_3$.

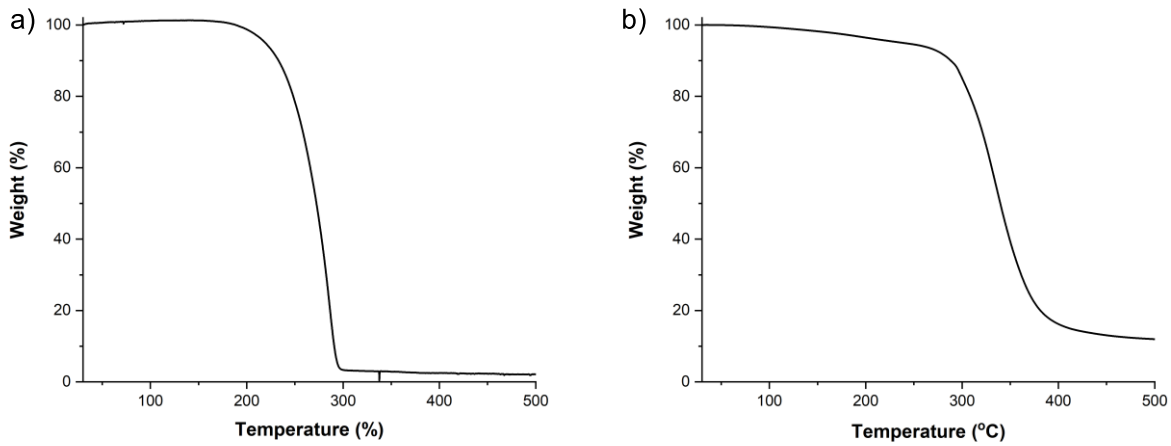



**Figure A3.40.** TGA thermograms of a) PCL and b) $\mathbf{P_{CL}1}$.

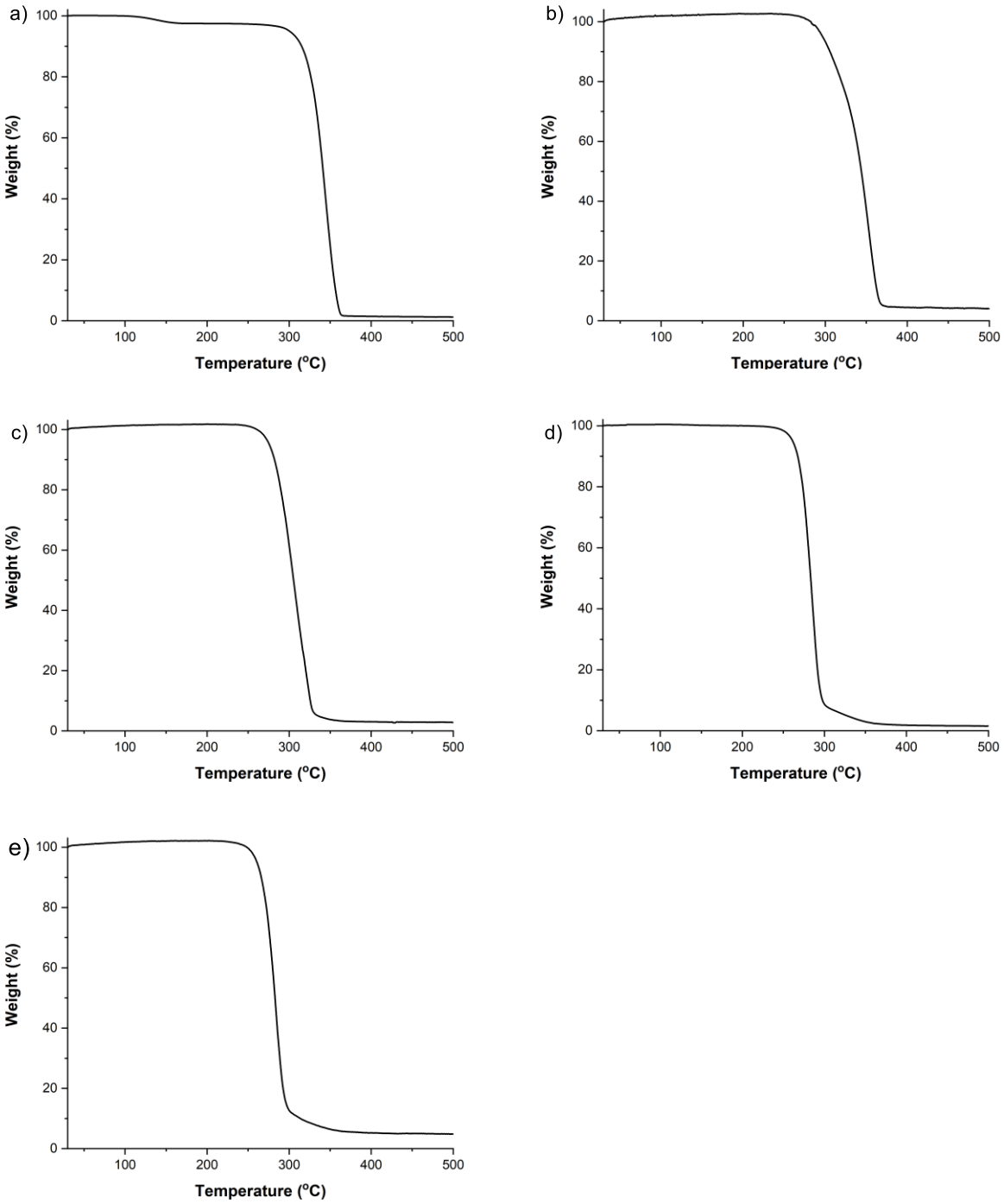



**Figure A3.41.** TGA thermograms of a) neat PLLA, b) PLLA + 2 wt. % of PLA1, c) PLLA + 5 wt. % of PLA1, d) PLLA + 10 wt. % of PLA1, and PLLA + 20 wt. % of PLA1.

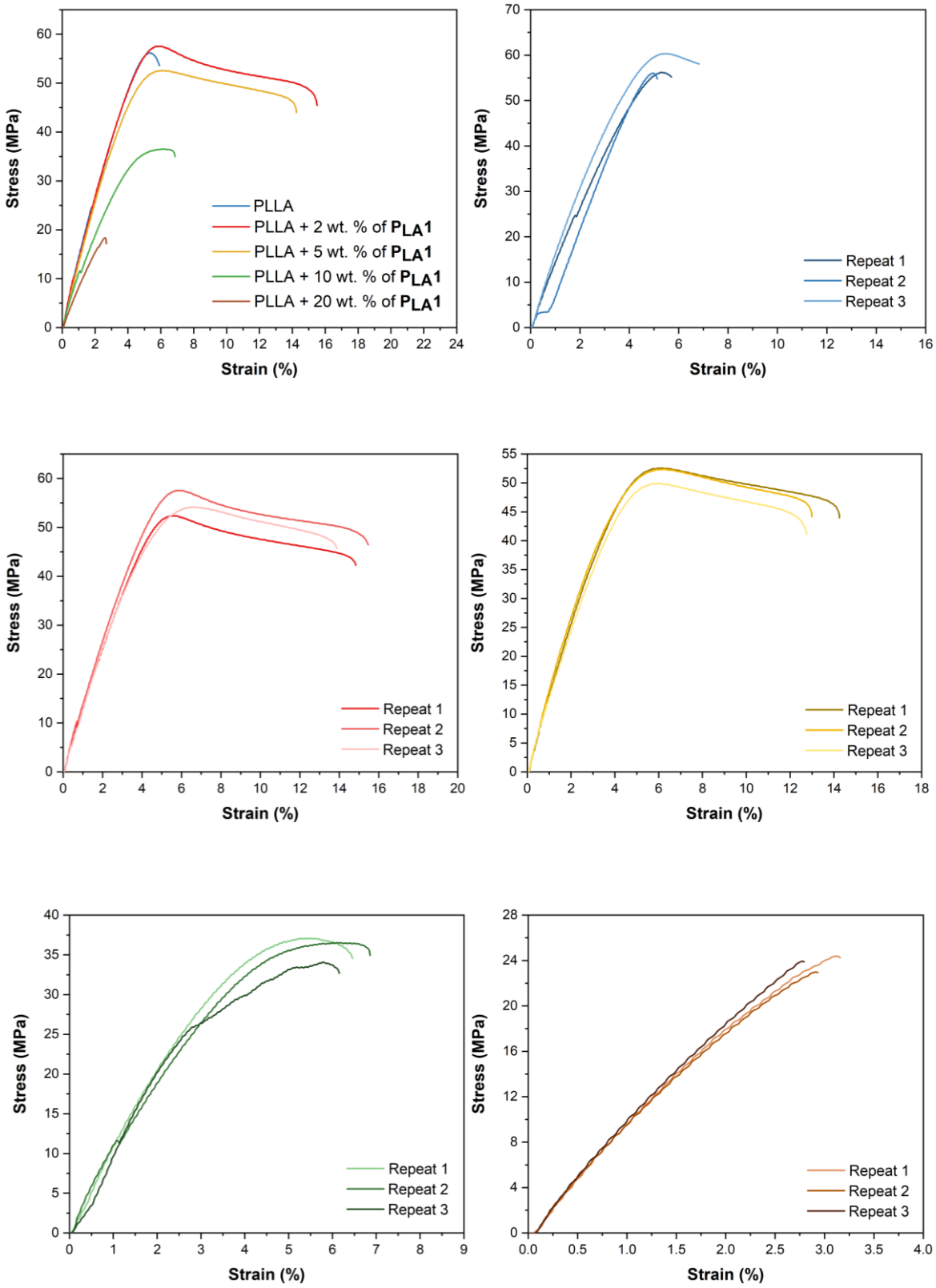



**Figure A3.42.** Plots of Stress aginst strain curver for PLLA films, containing different amount of additive **$P_{LA}$1**.

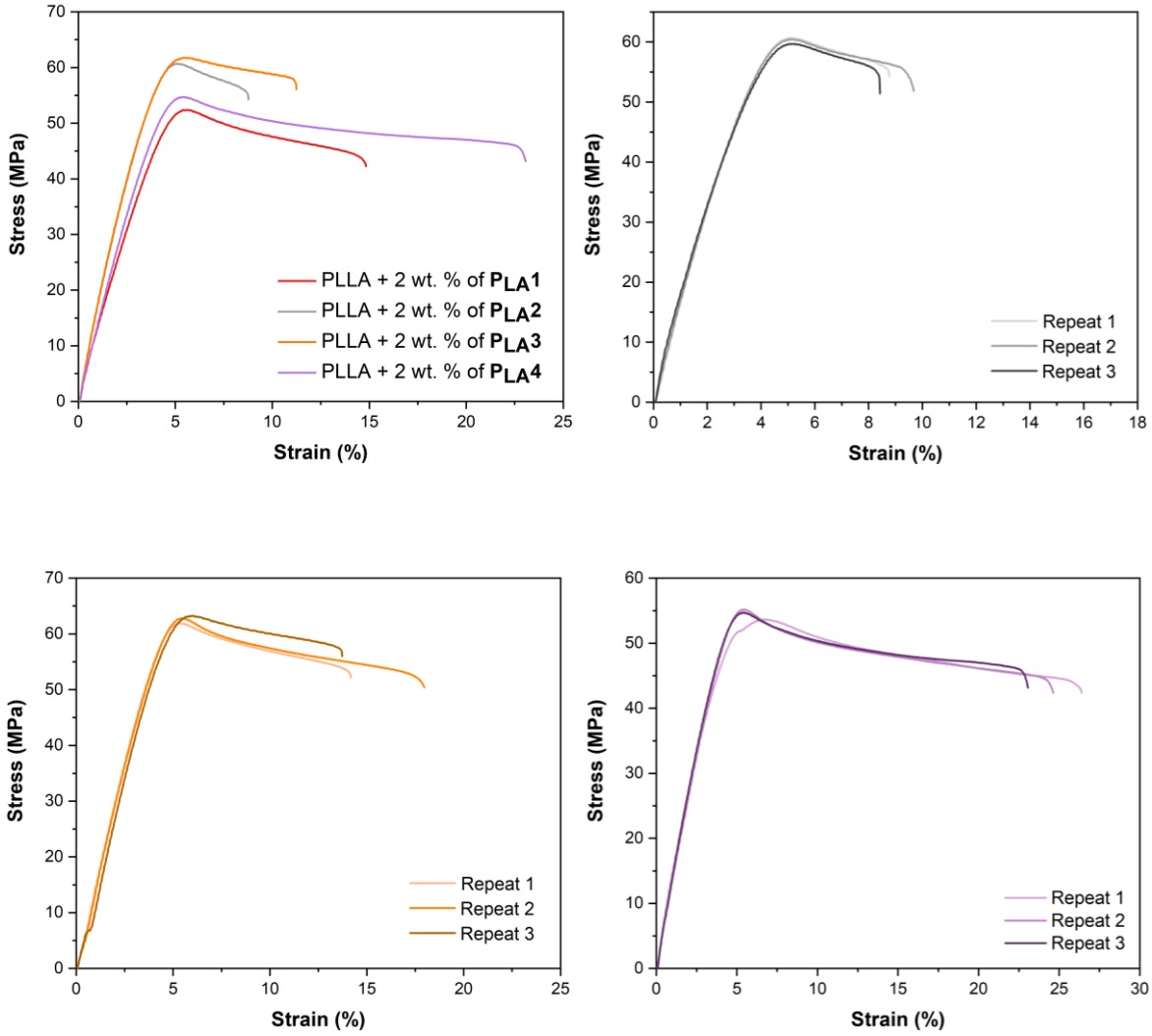



**Figure A3.43.** Plots of Stress aginst strain curver for PLLA films, containing 2 wt. % of different additives.

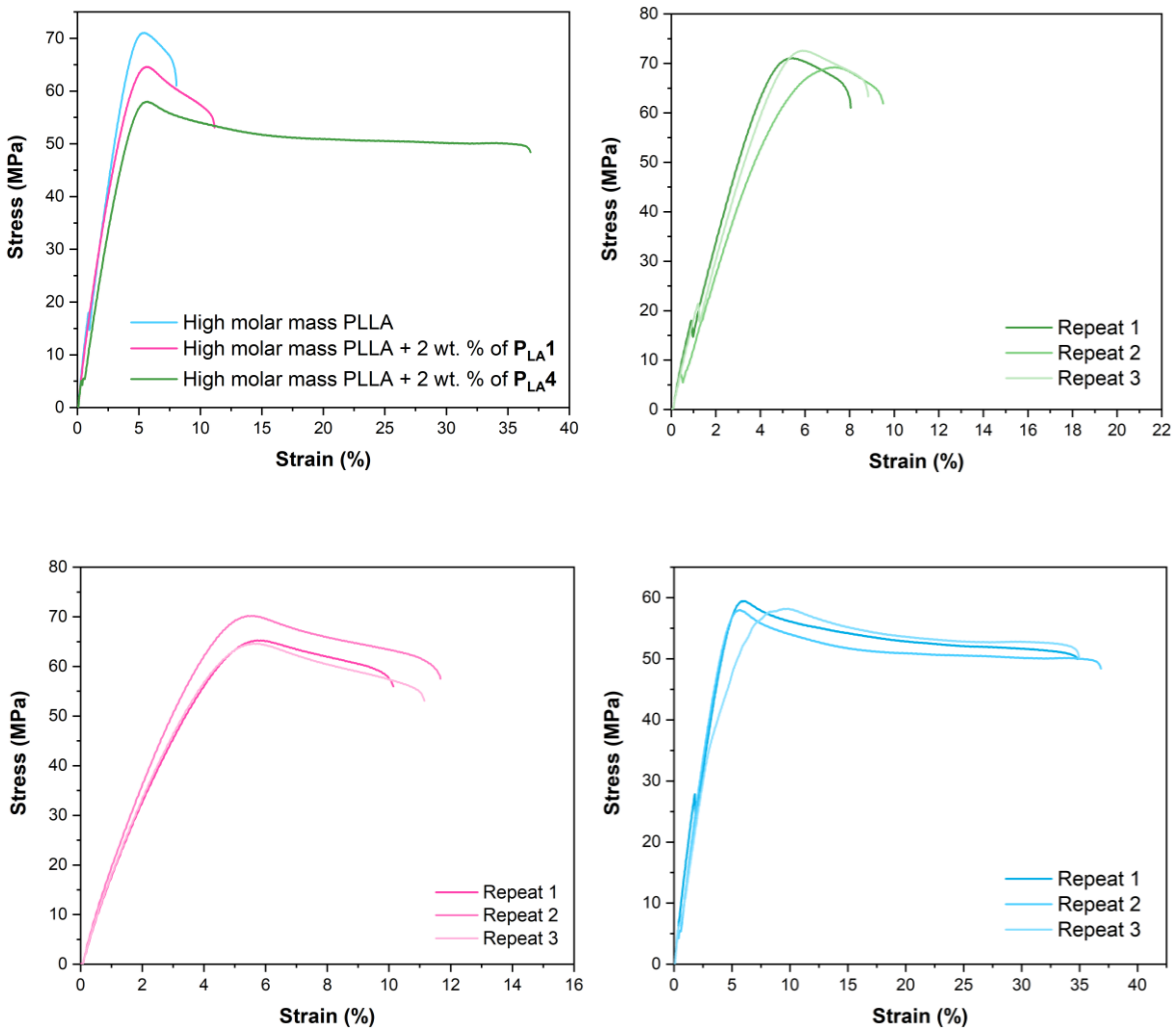



**Figure A3.44.** Plots of Stress aginst strain curver for high molar mass PLLA films, containing 2 wt. % of different additives.